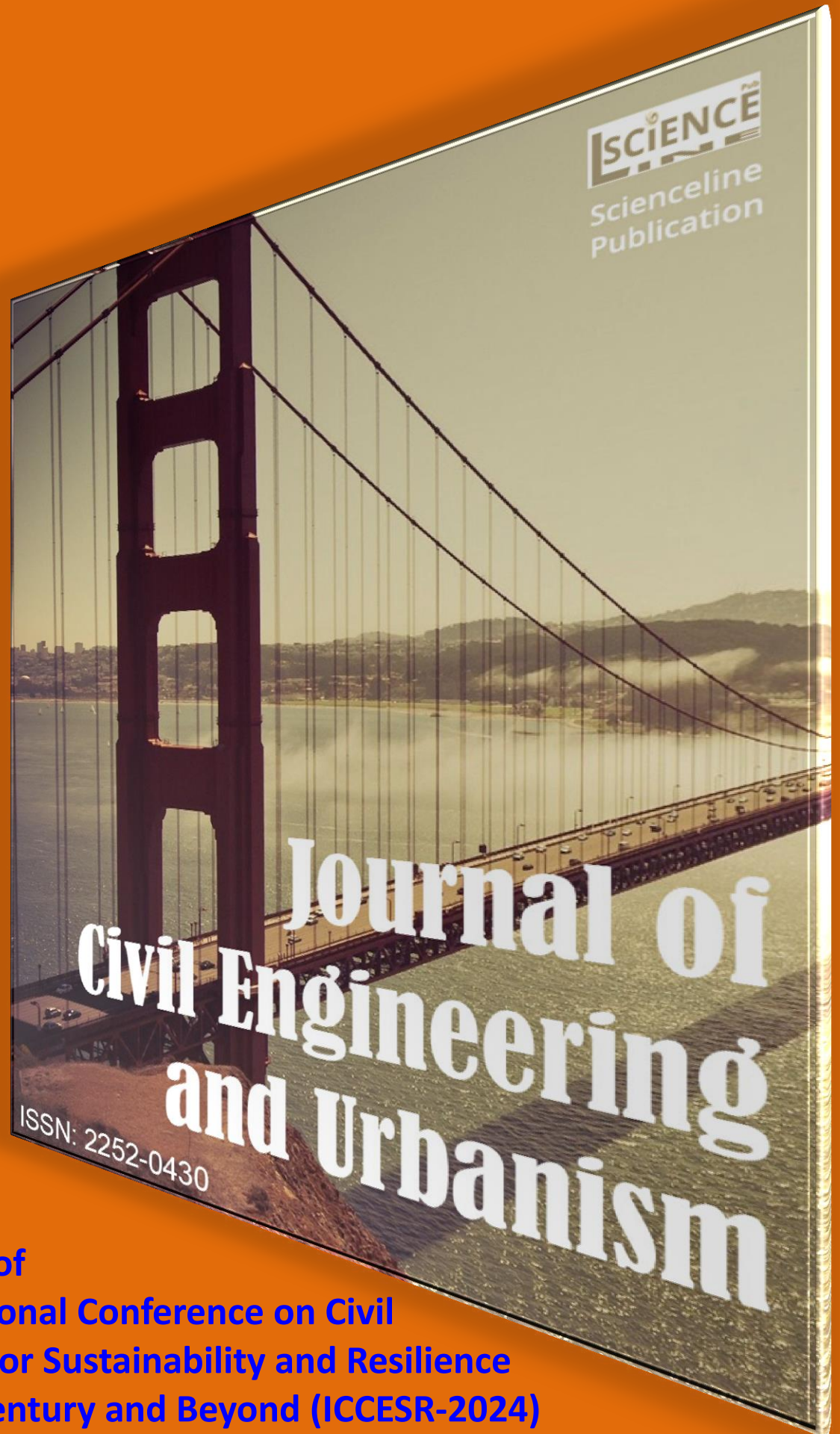




BOOKLET



Proceedings of
The International Conference on Civil
Engineering for Sustainability and Resilience
in the 21st Century and Beyond (ICCESR-2024)

Volume 14, Issue 3, September 15, 2024

Proceedings of The International Conference on Civil Engineering for Sustainability and Resilience in the 21st Century and Beyond (ICCESR-2024)



International Conference
on Civil Engineering for Sustainability and Resilience in the 21st Century and Beyond
(ICCESR-2024)

June 25 - 26, 2024
Venue of Conference: Virtual (Gaborone, Botswana)

University of Botswana, Gaborone, Botswana,

25–26 June, 2024

The International Conference on Civil Engineering for Sustainability and Resilience in the 21st Century and Beyond (ICCESR-2024), organized by the Department of Civil Engineering at the University of Botswana, brought together academia, practitioners, researchers, policy makers and regulators to discuss emerging and pertinent issues relating to sustainability and resilience in Civil Engineering and related disciplines. The conference thematic areas encompassed developments and improvements in innovative designs, construction and smart technologies and the formulation of appropriate policies in the face of climate change to ensure sustainability and resilience.

This Special Issue of the Journal of Civil Engineering and Urbanism is a compilation of the proceedings of the ICCESR-2024 conference.

ICCESR-2024 has been held as authorized partner for the Scienceline International journal (Journal of Civil Engineering and Urbanism).

Dr. Damilola Oyejobi

Secretary, ICCESR-2024 Organizing committee

<https://conferences.ub.bw/index.php/ICCESR/ICCESR-2024>

Email: Oyejobido@ub.ac.bw; iccesr-2024@ub.ac.bw

Prof. Dr. Yashon Ouma

CONGRESS CHAIRMAN

Email: Oumay@ub.ac.bw

Guest Editors

Prof. Dr. Yashon Ouma

Department of Civil Engineering, Faculty of Engineering and Technology, Private Bag UB 0061, University of Botswana, Gaborone, Botswana

Prof. Dr. Ssegawa, Joseph

Department of Civil Engineering, Faculty of Engineering and Technology, Private Bag UB 0061, University of Botswana, Gaborone, Botswana

Dr. Damilola Oyewumi Oyejobi

Department of Civil Engineering, Faculty of Engineering and Technology, Private Bag UB 0061, University of Botswana, Gaborone, Botswana

Dr. Ali A Firoozi

Department of Civil Engineering, Faculty of Engineering and Technology, Private Bag UB 0061, University of Botswana, Gaborone, Botswana

Selected Reviewers

Prof. Dr. Mohammed Jameel

King Khalid University, Saudi Arabia

Prof. Dr. Modupe Jimoh

Department of Civil Engineering, University of Warwick, United Kingdom

Prof. Dr. Bolanle Ikotun

University of South Africa, UNISA, South Africa

Prof. Dr. Abdulkadir Taofeeq Sholagberu

Department of Water Resources and Environmental Engineering, University of Ilorin, Ilorin, Nigeria

Dr. Ajibola Ibrahim Quadri

Federal University of Technology, Akure, Ondo State, Nigeria

Dr. Daniel Oguntayo

Department of Civil Engineering, Landmark University, Omu-Aran, Kwara State, Nigeria

Mr. Lawrence Zahemen Tuleun

Department of Water Resources and Environmental Engineering, University of Ilorin, Ilorin, Nigeria

Dr. B. Madzikigwa

Department of Civil Engineering, University of Botswana, Gaborone, Botswana

Dr. B. Wilson

Department of Civil Engineering, University of Botswana, Gaborone, Botswana

Dr. Lopang Maphale

Department of Civil Engineering, University of Botswana, Gaborone, Botswana

Dr. B. Nkwae

Department of Civil Engineering, University of Botswana, Gaborone, Botswana

Editorial Team of Journal of Civil Engineering and Urbanism

Editors-in-Chief

Heydar Dehghanpour; PhD of Civil Engineering, Construction Materials, Istanbul Aydin University, Faculty of Engineering and Architecture, Department of Civil Engineering, Besyol, Kucukcekmece/Istanbul, **TÜRKİYE**; ([Scopus ID](#), [WoS Metrics](#), [Google Scholar](#), [LinkedIn](#), [Email: haydardehgan@aydin.edu.tr](#))

Kianoush Zaker Haghghi; PhD of Urban Planning, Islamic Azad University, Hamedan, **IRAN**; ([Google Scholar](#), [ORCID](#); [Emails k.zakerhaghghi@gmail.com](#))

Managing editor

Ali Akbar Firoozi; PhD, Civil and Structural Engineering, Universiti Kebangsaan, **MALAYSIA**; Assistant Professor at the Faculty of Engineering and Technology, University of Botswana, Gaborone, **Botswana**; ([Scopus ID](#), [Google Scholar](#), [ORCID](#), [Website](#), [Email: a.firoozi@gmail.com](#))

Section Editors

Amir Ghatefar; PhD, Structural Engineering, [Research Associate at SIMTReC](#), University of Manitoba, Winnipeg, Manitoba,, **CANADA**; [Email: ghatefar@gmail.com](#)

Biao Hu; PhD, Assistant Prof at the School of Civil and Transportation Engineering, Shenzhen University, Shenzhen, 518060, **CHINA** ([Scopus ID](#), [Google Scholar](#), [ORCID](#), [Emails: biaohu3-c@szu.edu.cn or, biaohu3-c@my.cityu.edu.hk](#))

N. Vivekanandan (M.Sc. in Mathematics, M.Phil. in Mathematics, M.E. in Hydrology, MBA in Human Resources, M.A. in Public Administration, M.A. in Sociology, PGDH, PGDCA, PGDOR, PGDSMA, PGDSBSA, PGDPM&IR), Scientist, Hydrometeorology Division, Central Water and Power Research Station, Pune 411024, Maharashtra, **INDIA**; ([Scopus ID](#), [Google Scholar](#), [ORCID](#), [Email: anandaan@rediffmail.com](#))

Language Editor

Mehrdad Ehsani-Zad, MA in TEFL, Takestan, Islamic Azad University, **IRAN** ([Email: mehrdad.ehsanizad@yahoo.com](#))

Statistical Editor

Heydar Dehghanpour; PhD of Civil Engineering, Construction Materials, Istanbul Aydin University, Istanbul, **TÜRKİYE**

Technical Editor

N. Vivekanandan (M.Sc. in Mathematics, M.Phil. in Mathematics, M.E. in Hydrology, MBA in Human Resources, M.A. in Public Administration, M.A. in Sociology, PGDH, PGDCA, PGDOR, PGDSMA, PGDSBSA, PGDPM&IR), Scientist, Hydrometeorology Division, Central Water and Power Research Station, Pune 411024, Maharashtra, **INDIA**; ([Scopus ID](#), [Google Scholar](#), [ORCID](#), [Email: anandaan@rediffmail.com](#))

Editorial Team

Ahmad Maleki; PhD, Assistant Prof., Civil Engineering, Islamic Azad University of Maragheh, **IRAN**; [Email: maleki_civil@yahoo.com](#)

Ali Sadr Momtazi; PhD, Associate Prof., Structural Engineering, Guilan University, Guilan, **IRAN;** Email: sadrmomtazi@yahoo.com

Ali Soltani; Associate Prof., Urban Planning, Shiraz University, Shiraz, **IRAN;** Emails: ali_soltani54@yahoo.com; soltani@shirazu.ac.ir

Ali Mashhadizadeh Roveshti; PhD; Urban and Regional Planning, Gazi University, Ankara, **TÜRKİYE;** Email: mashhadizadeh54@gmail.com

Ayda Rastiemadabadi; Ph.D., in Urban and Regional Planning, Polytechnic University of Catalonia, ETSAB Barcelona School of Architecture, Department of Urbanism, Territory and Landscape, Barcelona, **SPAIN;** Lecturer in Department of Urban and Regional Planning, Faculty of Architecture, Ondokuz Mayıs University, **TÜRKİYE;** Email: ayda.rastiemadabadi@upc.edu

Egbuna Chukwuemeka Kingsley; PhD, Hydrogeology and Environmental Engineering, University of Bristol, Bristol, **UK;** Email: C.Egbuna1@uni.brighton.ac.uk

Golrokh Daneshgar; PhD, Assistant Prof., Architecture, Islamic Azad University, Hamedan, **IRAN;** Email: daneshgar.golrokh@gmail.com

Babak Alinejad; PhD, Assistant Prof., Civil Engineering, University of Maragheh, Maragheh, **IRAN;** Email: alinejad.science@gmail.com

Biao Hu; PhD, Assistant Prof at the School of Civil and Transportation Engineering, Shenzhen University, Shenzhen, 518060, CHINA ([Scopus ID](#), [Google Scholar](#), Emails: biaohu3-c@szu.edu.cn or, biaohu3-c@my.cityu.edu.hk

Hossein Showkati; PhD, Associate Prof., Civil Engineering, Urmia University, Urmia, **IRAN;** Email: h.showkati@urmia.ac.ir

Jianfei Zhu; PhD, Associate Prof., Architecture, Melbourne University, **AUSTRALIA**
Justyna Karakiewicz; PhD, Associate Prof., Urban Design, Melbourne University, **AUSTRALIA;** Email: justynak@unimelb.edu.au

Mahnaz Mahmoody; PhD, Assistant Prof., Architecture, Islamic Azad University, Qazvin, **IRAN;** Email: mahnaz_mahmoody@yahoo.com

Mahdi Shirdel; PhD, Department of of Civil Engineering, Faculty of Engineering, Kharazmi University, Tehran, **IRAN;** Email: m.shirdel.eng@gmail.com

Melanie L. Sattler; PhD, Associate Prof., Environmental Engineering & Earth Sciences Program, University of Texas at Arlington, **USA,** Email: msattler@uta.edu

Miles Lewis; PhD, Professor, Architecture, Melbourne University, **AUSTRALIA**

Mojtaba Emamzadeh; MSc of Structural-Earthquake Engineering, Islamic Azad University of Maragheh, **IRAN;** Email: mojtabaemamzadeh@gmail.com

Mona Hashemi Yazdi; Master of Art in Urban Design, Tehran University of Art, Tehran, **IRAN;** Email: yazdi_ma@yahoo.com

Morteza Chekaniazar; MSc; Department of Art and Architecture, Faculty of Urban Planning, Islamic Azad University, Hamedan, **IRAN;** ([Google Scholar](#), Email: mchekaniazar@yahoo.com)

Mukhallad Mohammed Mawlood Al-Mashhadani; Civil Engineering Department, Engineering & Architectural Faculty, Istanbul Gelişim University, **TÜRKİYE;** [Website](#); Email: mashhadani@gelisim.edu.tr

Orhan Canpolat; PhD, Professor in material science; Yıldız Teknik Üniversitesi. İstanbul, **TÜRKİYE;** Email: canpolat@yildiz.edu.tr

Prasenjit Chatterjee; PhD, Associate Professor and Head of the Dept. of Mechanical Eng. (areas of interests: multi-criteria decision-making, urban transport management, multi-objective optimization etc.), MCKV Institute of Engineering, West Bengal, **INDIA;** Email: prasenjit2007@gmail.com

Rasoul Khodayari; PhD, Structural- Earthquake Engineering, Science and Research Branch, Islamic Azad University, Tehran, **IRAN;** Email: rasoolkhodayari@gmail.com

Stephen P. Mattingly; PhD, Associate Prof., Transportation Engineering, University of Texas at Arlington, **USA**

Advisory Board

Hossein Showkati; PhD, Associate Prof., Civil Engineering, Urmia University, Urmia, **IRAN;** Email: h.showkati@urmia.ac.ir

Mohammad Arif Kamal; PhD, Associate Prof., Architecture & Environmental Design, Aligarh Muslim University, **INDIA;** Email: architectarif@gmail.com

Volume 14 (3S); 15 Sep, 2024 [ICCESR-2024]

Research Paper

Comparison of Concrete Strengthened with Carbon Fibre-Reinforced Polymer (CFRP) and Carbon Textile-Reinforced Mortar (CTRM)

Wang X, Lin X, and Xu S.

J. Civil Eng. Urban., 14(3s): 102-106, 2024; pii:S225204302400008-14

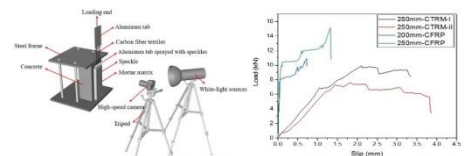
DOI: <https://dx.doi.org/10.54203/jceu.2024.8>

Abstract

Applying new composite material for strengthening and repairing existing structures is an important research topic. Carbon Fiber Reinforced Polymer/Plastics (CFRP) and Carbon Textile Reinforced Mortar (CTRM) are two common structural external reinforcement materials. 18 concrete specimens strengthened with CFRP and CTRM are prepared in this study. The quasi-static single-sided shear tests combined with the Digital Image Correlation (DIC) method is applied. The results show that the interface bonding strength of CFRP strengthening (0.76-0.96 MPa) is 65.0% to 74.8% higher than the CTRM-concrete interface (0.43-0.63 MPa). The ductility and energy dissipation capacity of CTRM strengthening is better than that of CFRP strengthening, and the effective bonding length is 125 to 300 mm. In practical work, CFRP is preferred for improving the strength of concrete components, while CTRM is preferred for improving ductility and seismic resistance.

Keywords: Carbon fibre-reinforced composites (CFRP); Carbon textile-reinforced mortar (CTRM); Digital image correlation method (DIC); Single-sided shear test

[Full text-PDF] [[Crossref Metadata](#)] [Export from [ePrints](#)]



The comparison of the bond behaviour and strengthening effect of Carbon Fibre-Reinforced Polymer (CFRP) and Carbon Textile-Reinforced Mortar (CTRM) to the concrete element is conducted by performing a single-sided shear test.

Key-Word: Wang X, Lin X, and Xu S. (2024). Comparison of Concrete Strengthened With Carbon Fibre-Reinforced Polymer (CFRP) and Carbon Textile-Reinforced Mortar (CTRM). *J. Civil Eng. Urban.*, 14(3S): 102-106. DOI: <https://dx.doi.org/10.54203/jceu.2024.8>

Research Paper

Effects of Blended Portland-Fly Ash Cement on Compressive Strength of Seawater Mixed and Cured Lateritic Concrete

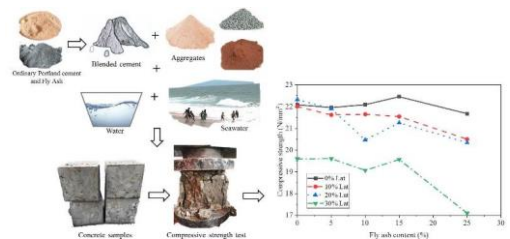
Alabi SA, Arum C, Akande AR, Mahachi J, and Afolayan JO.

J. Civil Eng. Urban., 14(3s): 107-112, 2024; pii:S225204302400009-14

DOI: <https://dx.doi.org/10.54203/jceu.2024.9>

Abstract

The use of cement in the construction industry is accompanied by the release of greenhouse gases (GHGs) into the ecosystem, and freshwater usage is on the rise globally, putting the world in a potential freshwater scarcity. This study investigated the effects of blended Portland-fly ash cement on the compressive strength of seawater-mixed and cured lateritic concrete by partially replacing the concrete materials: cement with fly ash at 0%, 5%, 10%, 15%, and 25%; fine aggregate, with laterite at 0%, 10%, 20%, and 30%. A concrete mix ratio of 1:1.5:3 was used in the production of concrete cubes with an expected target compressive strength of 20 N/mm². The compressive strength of the cubes was measured at 7, 28, and 56 days using standard testing procedures. Cubes cast with and cured in seawater (SW-SW) had strength values relatively higher than those cast with and cured in freshwater (FW-FW) at 28 days of curing. At 28 days, SW-SW cubes gave 22.44 N/mm² while FW-FW cubes gave 21.80 N/mm² as the highest strength values at 10% Lat and 10% FA. However, the FW-FW cubes had strength values higher than those of seawater mixed and cured concrete (SW-SW) at 56 days. FW-FW cubes gave 26.82 N/mm² while SW-SW cubes gave 26.34 N/mm² as their highest strength values at 10% Lat and 10% FA. Generally, an increase in fly ash and laterite content significantly reduces the compressive strength of concrete. Overall, seawater is recommended for curing and mixing, especially in non-reinforcing



Alabi SA, Arum C, Akande AR, Mahachi J, and Afolayan JO. (2024). Effects of Blended Portland-Fly Ash Cement on Compressive Strength of Seawater Mixed and Cured Lateritic Concrete. *J. Civil Eng. Urban.*, 14(3S): 107-112. DOI: <https://dx.doi.org/10.54203/jceu.2024.9>

concrete. 10% fly ash and 10% laterite are also recommended for use in blended Portland cement-fly ash concrete as they give the highest strength values.

Keywords: Concrete, Fly Ash, Laterite, Seawater, Compressive strength

[Full text-[PDF](#)] [[Crossref Metadata](#)] [Export from [ePrints](#)]

Research Paper

Statistical Evaluation of the Geometric Properties Steel Bars for Reinforced Concrete in Botswana

Adewuyi AP, and Eric GB.

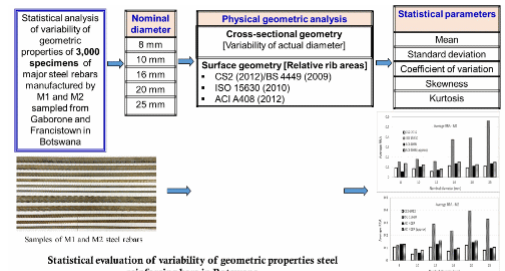
J. Civil Eng. Urban., 14(3s): 113-122, 2024; pii:S225204302400010-14

DOI: <https://dx.doi.org/10.54203/jceu.2024.10>

Abstract

Uncertainties in construction materials, especially steel reinforcing bars, have multiplying adverse impacts on the integrity and reliability of constructed facilities from construction to service life stages. Botswana depends on importation of rebars to meet the ever-increasing demands for buildings and reinforced concrete civil infrastructure. The study assessed the mass and geometric properties of the two most utilized steel reinforcing bars, designated as M1 and M2, in Botswana. With the aid of digital analytical balance and Vernier calipers, measurements of mass per unit length and the relative rib area (RRA), which depends on nominal diameter, rib height, rib spacing, and longitudinal rib or gap thickness were made from 3000 standard bars each of nominal sizes from 8 mm to 25 mm randomly sampled at the suppliers' depots/warehouses and various construction sites in Gaborone and Francistown. The RRA is a measure of the surface geometry for interfacial bonding between steel reinforcing bar and the surrounding concrete. The geometric properties of each steel bar type of the nominal sizes were characterized in terms of the statistical parameters and compared for compliance with standard specifications such as CS2 (2012), ISO 15630, ACI A408. The actual mass and diameter of bars were within the tolerance of $\pm 1\%$ of the respective nominal size which satisfied all the standard requirements. Only the 8 mm diameter M2 bars did not have longitudinal ribs/gaps. ACI specifies a range of 0.10 to 0.14 for RRA, while CS2/ISO 15630 only specifies for the minimum RRA values of 0.040 for 8 to 12 mm bars and 0.056 for 16 to 25 mm bars. M2 bars of 10 mm dia. bars did not satisfy CS2/ISO 15630 requirements. However, M1 (8 mm and 12 mm) and M2 (10, 16 and 25 mm) bar sizes are below the minimum and M2 bars of 20 mm diameter are above the recommended RRA values of ACI A408. These would reduce the load carrying capacity of RC members reinforced with the unsatisfactory bar sizes.

Keywords: Surface geometry, reinforcing bars, relative rib area, interfacial bonding, statistical indices, load carrying capacity.



Adewuyi AP and Eric GB (2024). Statistical Evaluation of the Geometric Properties Steel Bars for Reinforced Concrete in Botswana. *J. Civil Eng. Urban.* 14(3s): 113-122. DOI: <https://dx.doi.org/10.54203/jceu.2024.10>

[Full text-[PDF](#)] [[Crossref Metadata](#)] [Export from [ePrints](#)]

Research Paper

Enhancing Structural Application: Assessing the Suitability of Sawn and Glue Laminated *Albizia zygia* (Ayunre) Timber for Sustainable Construction

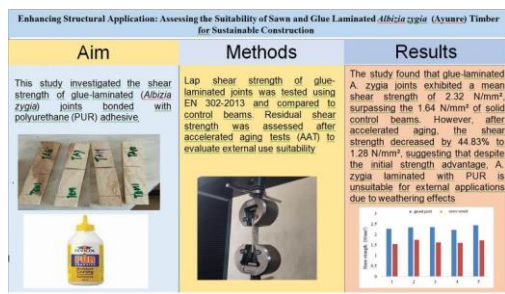
Ekundayo OO, Arum C, and Shittu LT.

J. Civil Eng. Urban., 14(3s): 123-131, 2024; pii:S225204302400011-14

DOI: <https://dx.doi.org/10.54203/jceu.2024.11>

Abstract

Leading economies are moving towards a bio-based economy for sustainability, but Africa struggles to utilize its bio-resource such as timber for advanced engineering application due to its natural limitations. Nevertheless, glue lamination (glulam) is promising for enhancing wood for structural application. Hence, this study investigated the shear strength of glue laminated (glulam) joints of *Albizia zygia* (*A. zygia*) timber species bonded with polyurethane (PUR) adhesive and other essential physical and mechanical properties in line with relevant standards. Briefly state the methodology before results to ensure flow. The results showed that the mean density of the wood species is 519 at a mean moisture content of 12%. The wood recorded a mean volumetric shrinkage and volumetric swelling of 1.17% and 6.52% respectively. Other properties include mean bending strength at 53.89, mean stiffness at 6106 N/mm², compressive strength parallel to grain at 32.70 and mean tensile strength at 33.61. Furthermore, the lap shear strength for glue laminated joints was tested according to EN 302-2013 standard and compared to control solid beams. The mean



Ekundayo OO, Arum C, and Shittu LT (2024). Enhancing Structural Application: Assessing the Suitability of Sawn and Glue Laminated *Albizia zygia* (Ayunre) Timber for Sustainable Construction. *J. Civil Eng. Urban.*, 14 (3s): 123-131. DOI: <https://dx.doi.org/10.54203/jceu.2024.11>

shear strength for glulam was 2.32 while it was 1.64 for the control beams. Thus, the glued joints performed better in shear than the control specimen. Finally, the residual shear strength of the joints was a mean value of 1.28 after subjecting them to accelerated aging tests (AAT). This is equivalent to 44.83% decrease of the shear strength in the dry use state. Hence, glue laminated *A. zygia* using PUR is not suitable for external use due to weathering effects on its shear strength. Based on the findings in this study, *A. zygia* is a moderately dense wood suitable for structural use but for interior application when laminated with PUR. It is shown that locally sourced *A. zygia* can be enhanced through glue lamination for structural joints in service class 2 according to Eurocode 5.

Keywords: Glued joints, adhesives, Polyurethane, Tensile shear strength and *Albizia zygia*

[Full text-[PDF](#)] [[Crossref Metadata](#)] [Export from [ePrints](#)]

Research Paper

The Integration of Geographic Information Systems and Building Information Modelling to Sustainably Manage Development Sites in Gaborone, Botswana

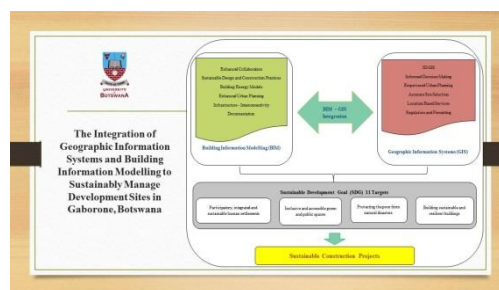
Moreri K, Segobye M, Maphale L and Onneng B.

J. Civil Eng. Urban., 14(3s): 132-141, 2024; pii:S225204302400012-14

DOI: <https://dx.doi.org/10.54203/jceu.2024.12>

Abstract

For many years, site development professionals and urban planners have worked in silos, yet they share a similar objective of providing a better built and natural environment. Moreover, there seems to be a stereotype in terms of focus areas; with urban planners more on the macroscale while their site development counterparts are more on the micro end. The two professional groups speak in different languages and use different instruments. For example, urban planners have introduced Geographic Information Systems (GIS) while site development professionals like architects, engineers, contractors, and facility managers advocate for Building Information Modelling (BIM). The increasing complexity of site development, their related environmental, geographical, and surrounding infrastructure is highly desired to support informed decision-making. Advancements in computer science and data technologies can make this integration easier. However, the understanding of GIS and BIM integration is still in its infancy, as innovative applications of their fusion is yet to be explored comprehensively. Therefore, this study investigates how GIS and BIM can be integrated to derive big data to support site development in Gaborone, Botswana. It will further propose a conceptual framework for integrating BIM and GIS for better site development and sustainable urban management in Gaborone.



Keywords: Building Information Modelling, Geographic Information Systems, Sustainable Urban Management, Sustainable Construction Projects, BIM-GIS Integration, Conceptual Framework

[Full text-[PDF](#)] [[Crossref Metadata](#)] [Export from [ePrints](#)]

Research Paper

Comparative Analysis of Statistical Models for Predicting the Properties of Agricultural Waste-Enhanced Sandcrete Blocks

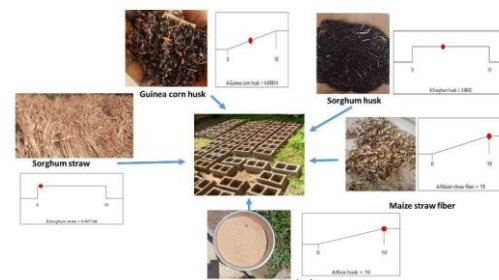
Odeyemi SO, Adisa MO, Kenku KO, Yusuf SA, Amuda MA, and Oladejo SO.

J. Civil Eng. Urban., 14(3s): 142-148, 2024; pii:S225204302400013-14

DOI: <https://dx.doi.org/10.54203/jceu.2024.13>

Abstract

Sandcrete blocks represent an indispensable building material, primarily composed of sand, water, and cement as a binding agent. Given the significant cost associated with cement, there is a need to produce low-cement blocks that are economically viable and cost-effective. This challenge has prompted the exploration of alternative materials to reduce cement content, simultaneously addressing environmental pollution and health risks associated with agricultural waste in rural areas. Notable examples of such alternative materials include various agricultural waste components. The primary objective of this research is to establish statistical models for predicting the compressive strength of blocks reinforced with rice husk, guinea corn husk, maize straw, and a combination of sorghum husk and straw. The research findings indicate that the density of fibre-reinforced blocks decreased as the quantity of fibre increased. Furthermore, the compressive strength of the sandcrete blocks decreased as the fibre content increased. However, compressive strengths



Odeyemi SO, Adisa MO, Kenku KO, Yusuf SA, Amuda MA, and Oladejo SO. (2024). Comparative Analysis of Statistical Models for Predicting the Properties of Agricultural Waste-Enhanced Sandcrete Blocks. *J. Civil Eng. Urban.*, 14(3s): 142-148. DOI: <https://dx.doi.org/10.54203/jceu.2024.13>

of 2.41 N/mm², 1.90, 2.40 N/mm², and 3.01 N/mm² were achieved for rice husk, guinea corn husk, maize-straw, and a combination of sorghum husk and straw-reinforced sandcrete blocks, respectively. Only sandcrete blocks with sorghum husk and straw met the Nigerian Industrial Standard specifications (NIS 87:2000). A water-binder ratio of 0.4 was determined as optimal for all the blocks under investigation. Four models with precision values higher than 4.0 were generated to predict the compressive strengths of the blocks. This research represents a valuable contribution to developing environmentally friendly building materials for the construction industry.

Keywords: Agricultural waste; Sandcrete blocks; Statistical models; Straw.

[Full text-[PDF](#)] [[Crossref Metadata](#)] [Export from [ePrints](#)]

Mapping Buildings from Semi-Informal Settlements Using Non-Parametric Classifiers: A Case of Old Naledi

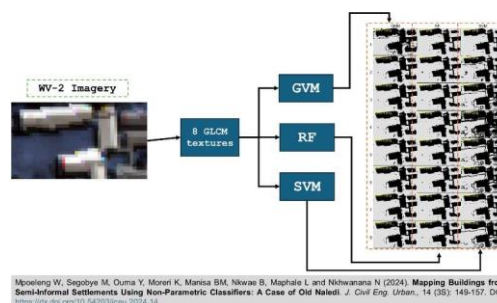
Mpoeleng W, Segobye M, Ouma Y, Moreri K, Manisa BM, Nkwae B, Maphale L and Nkhwanana N.

J. Civil Eng. Urban., 14(3s): 149-157, 2024; pii:S225204302400014-14

DOI: <https://dx.doi.org/10.54203/jceu.2024.14>

Abstract

Building footprints are essential for planning and designing new infrastructure like water reticulation, electricity transmission, sewer, and road networks. They are also necessary for delivery, census, and disaster management. It is therefore important to have up-to-date maps and GIS databases for service provision. However, mapping building of footprints in semi-informal settlements is problematic because of the spatial heterogeneity of settlements. This study evaluates three non-parametric machine learning algorithms for extracting building footprints from WorldView-2 (WV2) satellite imagery in a semi-informal settlement. WV2 satellite imagery data was fused with gray-level co-occurrence matrices (GLCM) to enhance building extraction. The algorithms used include the Gaussian Mixture Model (GMM), Random Forest (RF), and Support Vector Machine (SVM). The results indicate that GLCM does not improve the detection of buildings when using the GMM algorithm, but it increases building detection with RF and SVM. The GMM algorithm achieved the highest average accuracy of 92% for building detection. However, SVM and RF have an overall accuracy of 79% and 70% respectively. Though RF did not perform very well in identifying individual buildings, its overall accuracy was high. The outcome indicates that machine learning algorithms can adequately map building footprints from high-resolution satellite imagery.



Keywords: Building detection, WorldView-2, machine learning, Gray-Level Co-Occurrence Matrix (GLCM)

[Full text-[PDF](#)] [[Crossref Metadata](#)] [Export from [ePrints](#)]

Research Paper

Fluoride Concentration in Selected Water Sources of Ngamiland and Boteti Districts: Risk of Dental Fluorosis

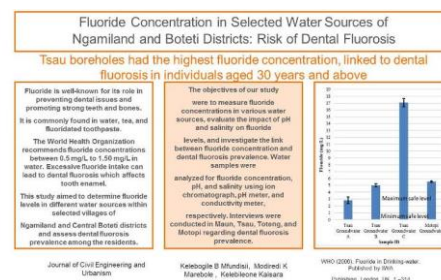
Mfundisi KB, Marebole MK, and Kaisara K.

J. Civil Eng. Urban., 14(3s): 158-163, 2024; pii:S225204302400015-14

DOI: <https://dx.doi.org/10.54203/jceu.2024.15>

Abstract

Fluoride is well-known for its role in preventing dental issues and promoting strong teeth and bones. It is commonly found in water, tea, and fluoridated toothpaste. The World Health Organisation recommends fluoride concentrations between 0.5 mg/L to 1.50 mg/L in water. Excessive fluoride intake can lead to dental fluorosis which affects tooth enamel. This study aimed to investigate fluoride levels in different water sources within selected villages of Ngamiland and Central Boteti districts and assess dental fluorosis prevalence among the residents. Our objectives were to measure fluoride concentrations in various water sources, evaluate the impact of pH and salinity on fluoride levels, and determine the link between fluoride concentration and dental fluorosis prevalence. Water samples were analyzed for fluoride concentration, pH, and salinity using ion chromatograph, pH meter, and conductivity meter, respectively. Interviews were conducted in Maun, Tsau, Toteng, and Motopi regarding dental fluorosis prevalence. Results showed that groundwater in Motopi and Tsau had fluoride concentrations ranging from 2.81 – 17.05 mg/L, while Toteng tap and standpipe water had fluoride concentrations of 0.78 and 0.83 mg/L. Maun tap and



standpipe water, as well as Motopi surface water, yielded fluoride concentrations ranging from 0.16 – 0.37 mg/L. Salinity and pH showed no significant relationship with fluoride concentration, with correlation coefficients of 0.09 and 0.46, respectively. In conclusion, Tsau boreholes had the highest fluoride concentration, linked to dental fluorosis in individuals aged 30 years and above. Maun tap and standpipe water, alongside Motopi tap and surface water, exhibited low fluoride concentrations, while Toteng tap, and standpipe water revealed appropriate fluoride levels. The study revealed that Salinity and pH do not influence fluoride concentration in water.

Keywords: Dental Fluorosis Risk, Groundwater Management, Surface Water Management, Ngamiland and Central Boteti Districts

[Full text-[PDF](#)] [[Crossref Metadata](#)] [Export from [ePrints](#)]

Moment Gradient Factor Verification for Selected Monosymmetric Beams under Linear Moment Gradients

Mudenda K.

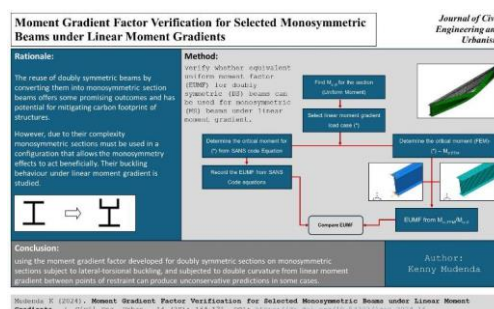
J. Civil Eng. Urban., 14(3s): 164-171, 2024; pii:S225204302400016-14

DOI: <https://dx.doi.org/10.54203/jceu.2024.16>

Abstract

The reuse of doubly symmetric beams by converting them into monosymmetric section beams offers some promising outcomes and has potential for mitigating carbon footprint of structures. However, due to their complexity monosymmetric sections must be used in a configuration that allows the monosymmetry effects to act beneficially. Although the South African design standard for hot-rolled steel does not provide any guidance on the design of monosymmetric beams, the Southern African steel construction handbook provides a formula for determining the critical elastic buckling moment for monosymmetric beams. This guidance implies that the moment gradient factor used for doubly symmetric sections can be used on monosymmetric sections as well. The aim of the study was to verify the validity of this approach of extending the moment gradient factor used for doubly symmetric beams to monosymmetric beams for two specific types of monosymmetric sections. It was found that although this approach appears to be justified for monosymmetric members in single curvature bending it may produce unconservative values of the critical buckling load in double curvature bending between restraint points. The level of un-conservatism also varies for different spans of the same member. This makes it difficult to specify a single moment modification factor value for these cases. The sensitivity in terms of load reduction observed for double curvature bending case was different for the two members examined with this attributed to differences in how the shear centre moves relative to the centroid. It is recommended that the critical buckling load for monosymmetric sections be determined on a case specific basis for members in double curvature from linear moment gradients. Under single curvature bending the moment gradient factor for doubly symmetric members appears to give acceptable predictions of the critical load.

Keywords: Steel beam, Monosymmetric, Lateral-torsional buckling, Moment gradient factor



[Full text-[PDF](#)] [[Crossref Metadata](#)] [Export from [ePrints](#)]

Research Paper

Experiences Encountered while Using Construction Contracts during Project Delivery in Botswana

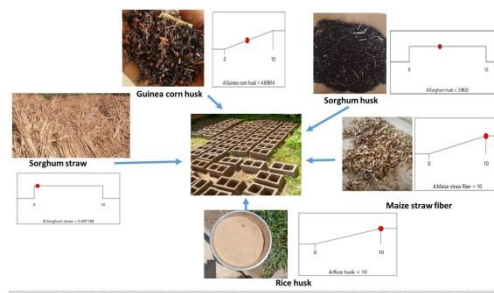
Ssegawa JK, Ntshwene K, and Kamaruddeen AM.

J. Civil Eng. Urban., 14(3s): 172-181, 2024; pii:S225204302400017-14

DOI: <https://dx.doi.org/10.54203/jceu.2024.17>

Abstract

Various forms of contracts guide the construction project delivery processes across the world. To make procurement more accessible and faster, various institutions have developed what is known as standard forms of contracts (SfOC). These institutions believe that SfOCs could be used in an adopted or adapted mode to reduce the burden of writing contracts every time a project is procured. This article discusses the results of a study that investigated the effectiveness of identified SfOCs and the experiences encountered by key stakeholders in using the contracts during construction project delivery. Study participants were drawn from contractor, consulting and client organisations and completed



Odeyemi SO, Adisa MO, Kenku KD, Yusuf SA, Amuda MA, and Olatodjo SO. (2024). Comparative Analysis of Statistical Models for Predicting the Properties of Agricultural Waste-Enhanced Sandcrete Blocks. *J. Civil Eng. Urban.*, 14(3s): 142-148. DOI: <https://dx.doi.org/10.54203/jceu.2024.17>

a questionnaire with both closed and open-ended questions. 11 attributes synthesised from literature were used to measure the effectiveness of a contract. Three major SFoCs were identified as being used in Botswana: the Joint Contract Tribunal (JCT), the New Engineering Contract (NEC) and International Federation of Consulting Engineers (FIDIC). The FIDIC has a long history of use, but in recent years, the NEC entered the arena. Due to the low usage of the JCT, the discussion centred on the NEC and FIDIC contracts. Some insights were drawn from the study. Respondents did not find a big difference in the effectiveness of the two contracts (WME for NEC =3.3 and FIDIC =3.1). However, there were a few attributes for which the NEC seemed to be a better contract. These were a) simple and non-legalistic language with self-contained clauses and b) a communicative and proactive risk management regime, which respondents identified with a propensity to reduce or avoid disputes. The study had the limitations of having used a small (38) sample of respondents and the fact that NEC has not been used in the country for the length of time as the FIDIC contract.

Keywords: Construction contract, Standard forms of contract, Contract Administration, Construction industry, Botswana

[Full text-[PDF](#)] [[Crossref Metadata](#)] [Export from [ePrints](#)]

Research Paper

Fixed-Bed Adsorption Dynamics of Total Organic Carbon from Gamodubu Landfill Leachate Using Biochar Derived From Gaborone Wastewater Treatment Plant Sewage Sludge

Tshenyego LD, Odirile PT and Gaboutloeloe GK.

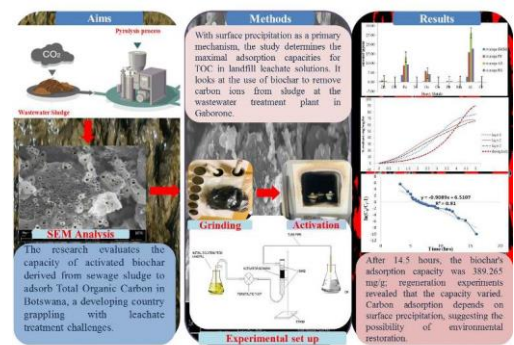
J. Civil Eng. Urban., 14(3s): 182-189, 2024; pii:S225204302400018-14

DOI: <https://dx.doi.org/10.54203/jceu.2024.18>

Abstract

In developing countries like Botswana, addressing leachate treatment presents considerable difficulties, especially regarding the management of sewage sludge (SS). This research evaluated the capacity of activated biochar, derived from sewage sludge, to adsorb Total Organic Carbon (TOC). Biochar was produced under conditions with limited oxygen, by placing approximately 50 grams of dried sewage sludge in sealed porcelain crucibles and heating them at a rate of 10°C per minute to 400°C for four hours. The resulting biochar (WWSBC400) was then stored in plastic bags in a dry environment. The pyrolysis yield was calculated as the ratio of the weight of the produced biochar to the initial weight of the dry sewage sludge. The study identified the maximum adsorption capacities (qm) for TOC in landfill leachate solutions, highlighting surface precipitation as a key adsorption mechanism for WWSBC400. Additionally, the removal of carbon ions using biochar produced from sludge at Gaborone's wastewater treatment facility was investigated. Continuous adsorption columns were utilized to demonstrate TOC solution adsorption, with performance evaluated in a fixed-bed column through model simulation. The Thomas model was used to compare experimental kinetic data, with the experimental data generally aligning well with the Thomas model, achieving a correlation coefficient (R^2) of 0.9114 for the first round of activated biochar removal. The adsorption capacity of the biochar was recorded at 389.265 mg/g after 14.5 hours of column adsorption, with regeneration studies showing varying adsorption capacities of 742.82 mg/g, 875.47 mg/g, 682.13 mg/g, and 735.21 mg/g for successive rounds. Surface precipitation was found to be a vital process for carbon adsorption onto WWSBC400. In conclusion, using sewage sludge biochar for co-contaminated soil shows potential for heavy metal immobilization, presenting a viable option for environmental rehabilitation.

Keywords: Biochar Adsorption kinetic models; Fixed-bed column, Total Organic Carbon, sewage sludge, environmental remediation.



Tshenyego LD, Odirile PT and Gaboutloeloe GK (2024). Fixed-Bed Adsorption Dynamics of Total Organic Carbon from Gamodubu Landfill Leachate Using Biochar Derived From Gaborone Wastewater Treatment Plant Sewage Sludge. *J. Civil Eng. Urban.*, 14 (3s): 182-189. DOI: <https://dx.doi.org/10.54203/jceu.2024.18>

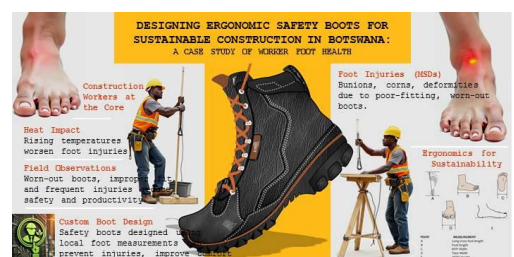
[Full text-[PDF](#)] [[Crossref Metadata](#)] [Export from [ePrints](#)]

Designing Ergonomic Safety Boots for Sustainable Construction in Botswana: A Case Study of Worker Foot Health

Botshabelo K, Sealetsa O, Setlhatlhanyo K, Moalosi R, Rapitsenyane Y, and Dichabeng P.

J. Civil Eng. Urban., 14(3s): 191-198, 2024; pii:S225204302400019-14

DOI: <https://dx.doi.org/10.54203/jceu.2024.19>



Botshabelo K, Sealetsa O, Setlhatlhanyo K, Moalosi R, Rapitsenyane Y, and Dichabeng P (2024). Designing Ergonomic Safety Boots for Sustainable Construction in Botswana: A Case Study of Worker Foot Health. *J. Civil Eng. Urban.*, 14 (3s): 191-198. DOI: <https://dx.doi.org/10.54203/jceu.2024.19>

Abstract

The most essential asset in every construction work is the workers. In this regard, sustainability in construction must include and be centred on this vital resource. However, research indicates that civil engineers and construction workers often advocate for sustainability in infrastructural developments. This critical asset in construction often needs more consideration when people are engaged in construction work despite the many ergonomics challenges widely reported in the industry. This leads to workers in this industry being grossly afflicted by injuries such as musculoskeletal disorders, particularly of the foot. In addition, changes in global temperatures, attributed to global warming, situate civil engineers and construction workers, as they often work in open and challenging terrains, at risk of heat-related illnesses such as heat hyperpyrexia and heat exhaustion, which may also aggravate these musculoskeletal disorders conditions. However, it is pretty disturbing to notice that such illnesses are less investigated, particularly musculoskeletal disorders of the feet, which may be exasperated by the dire heat conditions noticeable in Botswana. This is because there is often a need for more knowledge and understanding of the risks associated with musculoskeletal disorders (MSDs). Furthermore, expertise in ergonomics is limited to assisting in the design of work as well as its conditions. This bequeaths both civil engineers and construction workers to operate under very challenging conditions despite pursuance of sustainability. Therefore, this case study investigated the prevalence of musculoskeletal disorders of the feet in the construction industry in Botswana with the purpose of designing a safety boot that matches the anthropometric measurements of the construction workers' feet. The research culminates in the design of a safety boot that is based on the workers' anthropometric measurements to prevent the occurrence of MSDs. The results of the study indicate that workers in this industry suffer from toe bunions, cons, toe deformities, smelly feet, etc. The study additionally indicates foot size differences across Botswana's tribes. These differences may have severe implications for the use of safety boots and the development of ergonomics illnesses, mainly since the current safety boots used are imported from elsewhere with no modification to address the anthropometric feet measurements of Batswana. It is anticipated that the research will provide the necessary awareness that can help civil engineers explore sustainability not only from the context of infrastructural development (objects) but also from the perspective of workers (humans). This underscores the need for further research and action in this critical area.

Keywords: Construction Worker Ergonomics, Musculoskeletal Disorders, Safety Boot Design, Anthropometric Measurements, Heat-related Illnesses, Sustainable Construction Practices

[Full text-[PDF](#)] [[Crossref Metadata](#)] [Export from [ePrints](#)]

Effects of Resampled DEM on Watershed Characteristics and Prediction of Sediment Load in Oyun Watershed, Kwara, Nigeria

Adeogun AG, Mansur AW and Mohammed AA.

J. Civil Eng. Urban., 14(3s): 199-205, 2024; pii:S225204302400020-14

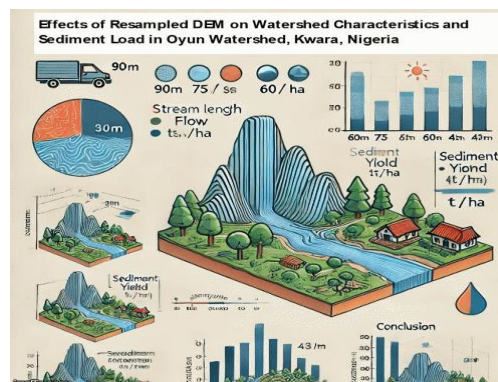
DOI: <https://dx.doi.org/10.54203/jceu.2024.20>

Abstract

Understanding the terrain and its impact on watershed characteristics, streamflow, and sediment loading is crucial for effective water resource management. This study investigates the influence of resampled Digital Elevation Models (DEM) on the prediction of watershed characteristics, streamflow, and sediment loading upstream of Oyun River Watershed, Nigeria. Various DEM resolutions, ranging from 30-meter to 90-meter, were analysed to assess their effects on hydrological predictions. To delineate the watershed, a DEM of 90-meter resolution was sourced from the space Shuttle Radar Topography Mission (SRTM), and the ASTER global DEM data sources. The 90-meter resolution was resampled to four different resolutions which are 75-meter, 60-meter, 45-meter, and 30-meter resolutions. The watershed and streamline were delineated, and the hydrologic simulation was performed using Soil and Water Assessment Tool (SWAT). The research findings revealed that changes in DEM resolution had a negligible impact on streamflow predictions within the Oyun River Watershed. However, a noticeable impact was observed in the prediction of sediment concentration. The 90-meter resolution DEM yielded the lowest predicted sediment concentration, measuring 2.28 mg/l, while the 30-meter resampled DEM produced the highest value at 5.21mg/l. Similarly, the sediment yield (SYLD t/ha) exhibited considerable variation across the different DEM resolutions, with the 90-meter DEM demonstrating the lowest value of approximately 528.90 t/ha, and the 30-meter DEM registering the highest at 2145.57 t/ha. Overall, this research highlights the necessity of careful DEM selection in hydrological modelling to ensure a comprehensive understanding of watershed dynamics, particularly in regions where sediment transport and water quality are of paramount concern.

Keywords: DEM, Hydrological Modelling, Nigeria, Sediment Loads, Watershed

[Full text-[PDF](#)] [[Crossref Metadata](#)] [Export from [ePrints](#)]



Stakeholders Influence on Construction Project Success

Mwakamui HK, Ntshwene K.

J. Civil Eng. Urban., 14(3s): 206-211, 2024; pii:S225204302400021-14

DOI: <https://dx.doi.org/10.54203/jceu.2024.21>

Abstract

For the past decade Botswana's construction industry has been embroiled in a lot of controversies based on construction project constraints. These are characterized by construction project delays, budget overruns as well as scope creep and some of these construction projects have been deemed unsuccessful by different stakeholders. To find a mitigating factor for these problems, construction project constraints must be investigated beyond just the triple constraints to provide a solution for the Botswana construction industry. Therefore, the overall purpose of this study was to investigate how construction project constraints and stakeholders influence the outcome of a project. The study adopted a qualitative approach through face-to-face interviews with selected stakeholders such as construction professionals, clients and other beneficiaries in the Gaborone and greater Gaborone areas. Thematic analysis was used to analyze data. The findings of the study established that the success of a construction project is subjective and is based on who is being asked, the construction professionals, the client and other beneficiaries had different perspectives on success of a project. The study revealed that initial constraints in a construction project tend to be carried along to the final stages of a construction project. However new few construction project constraints also emerge at the final stages of a construction project. The study found that stakeholders such as the client and other beneficiaries have a significant impact on construction projects due to their influence both positive and negative depending on the level of engagement.

Keywords: Factors of project success, Project constraints, Stakeholders, Triple constraints

[Full text-[PDF](#)] [[Crossref Metadata](#)] [Export from [ePrints](#)]

Stakeholders Influence on Construction Project Success

A qualitative study exploring construction project constraints and stakeholder influence in Botswana's construction industry.

Problem: Construction Constraints
- Delays
- Budget Overruns
- Scope Creep

Approach: Qualitative Study
- Interviews with Stakeholders
- Thematic Analysis

Findings: Stakeholder Influence
- Success is Subjective
- Initial Constraints Persist
- Stakeholders Play a Major Role

Mwakamui HK, and Ntshwene K (2024). Stakeholders Influence on Construction Project Success. *J. Civil Eng. Urban.*, 14 (3S): 206-211. DOI: <https://dx.doi.org/10.54203/jceu.2024.21>

Research Paper

Integrating Prophet Forecasting with Gaussian Mixture Model- Hidden Markov Model (GMM-HMM) for Early Warning System in Dam Deformation Monitoring

Tshireletso T, and Moyo P.

J. Civil Eng. Urban., 14(3s): 212-219, 2024; pii:S225204302400022-14

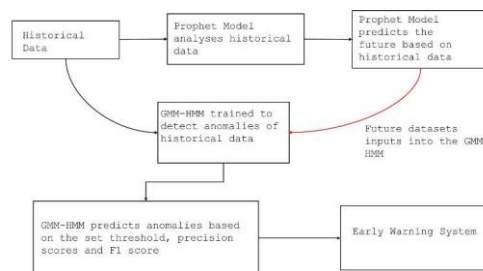
DOI: <https://dx.doi.org/10.54203/jceu.2024.22>

Abstract

Ensuring dam safety requires a monitoring system that can predict deformations and detect anomalies in real-time. This study combines the forecasting capabilities of the Prophet model with the real-time anomaly detection of a Gaussian Mixture Model-Hidden Markov Model (GMM-HMM) framework. The Prophet model analyses historical deformation data to forecast future deformations, enabling early issue identification. The GMM-HMM framework continuously monitors incoming data to detect deviations from predictions. Results shows that the GMM-HMM, with 10 components and a Mahalanobis distance threshold of 0.1, achieved a precision of 0.602, recall of 1.0, and F-1 score of 0.751, ensuring high sensitivity and accurate anomaly detection on. The GMM-HMM was then used to detect anomalies on Prophet forecasted radial deformations. Anomalies were detected on upper limit and lower limit deformations. This combined approach enhances dam safety by integrating predictive and real-time monitoring capabilities, offering a comprehensive early warning system for dam infrastructure.

Keywords: Gaussian Mixture Model, Hidden Markov Model, Prophet Model, Dam Deformation Forecasting

[Full text-[PDF](#)] [[Crossref Metadata](#)] [Export from [ePrints](#)]



Tshireletso T, and Moyo P (2024). Integrating Prophet Forecasting with Gaussian Mixture Model-Hidden Markov Model (GMM-HMM) for Early Warning System in Dam Deformation Monitoring. *J. Civil Eng. Urban.*, 14 (3S): 212-219. DOI: <https://dx.doi.org/10.54203/jceu.2024.22>

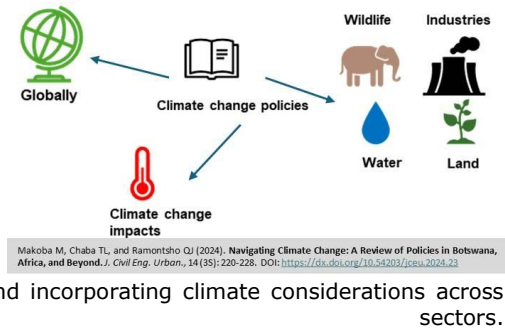
Navigating Climate Change: A Review of Policies in Botswana, Africa, and Beyond

Makoba M, Chaba TL, and Ramontsho QJ.

DOI: <https://dx.doi.org/10.54203/jceu.2024.23>

Abstract

This paper is an insightful perspective analysis of Botswana climate change policies in an effort to establish their effectiveness in relation to regional and international initiatives. For a critical review of both mitigation and adaptation efforts by different countries, the effectiveness is analysed, including their strengths and inadequacies noted, and recommendations made towards enhancing policy coherence and effectiveness. It examines the steps Botswana and other countries have taken to cut greenhouse gas emissions, improve energy efficiency, support the use of renewable energy sources, and implement sustainable land management practices. The paper also delves into Botswana's efforts to build climate resilience, such as creating a National Adaptation Plan and incorporating climate considerations across various



Keywords: Climate change policies, Policy review, International agreements, Sustainable development, Botswana

[Full text-PDF] [[Crossref Metadata](#)] [Export from [ePrints](#)]

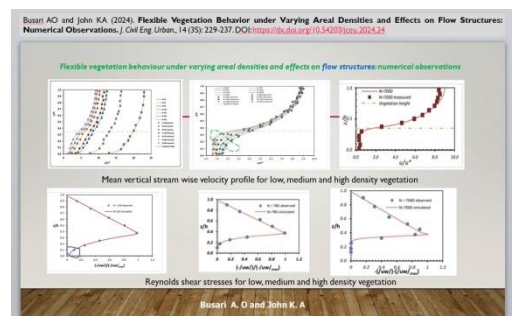
Flexible Vegetation Behavior under Varying Areal Densities and Effects on Flow Structures: Numerical Observations

Busari AO and John KA.

DOI: <https://dx.doi.org/10.54203/jceu.2024.24>

Abstract

This study carried out extensive numerical studies on a refined "One dimensional (1-D) Reynolds Averaging Navier-Stokes (RANS) Model" for vegetated open channel flow. In the 1-D RANS model, the Spalart Allmaras closure model was used to model the turbulence caused by eddies within the vegetation zone and the interface between the top of the vegetation and the clear water zone. In this work, numerical simulations using 1-D RANS model are carried out using dataset obtained from the laboratory under different hydraulic conditions of varying areal vegetation densities. Three classes of highly flexible vegetation densities were simulated: low, medium and highly dense vegetation. The model predictions in terms of mean vertical stream-wise velocity profile and Reynolds Shear Stresses were compared with the laboratory flume experimental results. The 1-D RANS model performances were satisfactory for low and medium densities. However, discrepancies were seen in the model prediction for highly dense vegetation. Hence, the hydraulic roughness parameters in the numerical model has been modified for model re-calibration to capture the position of zero-displacement of velocities. Using the modified parameters, the velocity profiles and the Reynolds Shear Stresses were predicted with very low uncertainty.



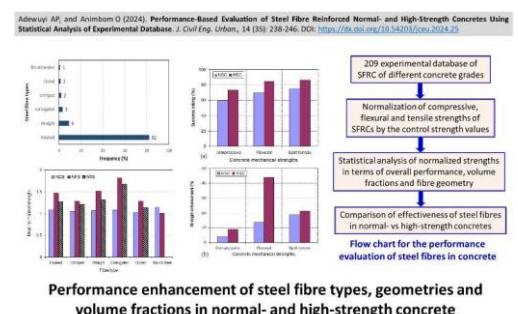
Keywords: Zero-displacement parameter, 1-D RANS model, Reynolds shear stresses, areal density, flexible vegetation

[Full text-PDF] [[Crossref Metadata](#)] [Export from [ePrints](#)]

Performance-Based Evaluation of Steel Fibre Reinforced Normal- and High-Strength Concretes Using Statistical Analysis of Experimental Database

Adewuyi AP, and Animbom O.

DOI: <https://dx.doi.org/10.54203/jceu.2024.25>



Abstract

The widespread acceptance of concrete can be attributed to its unique characteristics, despite inherent drawbacks such as brittleness and weak tensile strength. The study was aimed at evaluating the optimal content and characterization of steel fibres required to impede crack propagation and enhance overall strength of concrete. The influence of critical factors like fibre content, length, diameter, and volume fraction on the performance of steel fibre reinforced concretes (SFRC) through statistical analysis of 209 experimental data. The influence of these factors on the compressive, flexural, and tensile strengths of concrete was analyzed as a function of the mean and coefficient of variation of the normalized strength values. The study found that steel fibres in concrete produced success rates of 67.9% (7.1% average strength improvement = ASI) in compressive strength, 78.5% (38.2% ASI) in flexural strength and 84.2% (23.8% ASI) in tensile strength. The study further separately examined the impact of steel fibres on both normal strength concretes (NSC) and high strength concretes (HSC). The findings indicated an overall success rate of 60% (6.97% ASI), 69.9% (38.36% ASI), and 75.6% (23.59% ASI) for compressive, flexural, and split tensile strength, respectively, in NSC. However, higher degree of strength enhancement of 74.0% (7.16% ASI), 84.8% (39.21% ASI), and 86.6% (23.51% ASI) were recorded for compressive, flexural, and split tensile strength, respectively in HSC. The research underscores the effectiveness of incorporating steel fibres as a reinforcement strategy in enhancing various strength aspects of concrete.

Keywords: Fibre reinforced concrete, steel fibres, compressive strength, tensile strength, flexural strength, normalized strength, average strength improvement.

[Full text-[PDF](#)] [[Crossref Metadata](#)] [Export from [ePrints](#)]

Empirical Scrutiny of Geopolymer Concrete Containing Locally-produced Superplasticizer under Varied Temperatures

Agashua LO, Arum C, Oluyemi-Ayibiowu BD, and Ikumapayi CM.

J. Civil Eng. Urban., 14(3s): 247-262, 2024; pii:S225204302400026-14

DOI: <https://dx.doi.org/10.54203/jceu.2024.26>

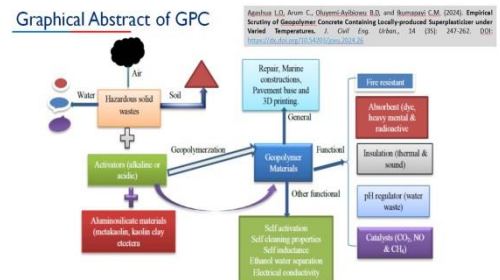
Abstract

Cement manufacturing companies contribute greatly to carbon-dioxide emission during production, hence there is need for novel eco-friendly or biodegradable cementitious material, which has the same strength and also durable. Geopolymers which are eco-friendly waste materials, which can also reduce construction cost are therefore considered for this purpose. The geopolymer stabilizing materials, fly ash (FA), kaolin clays powder (KCP), rice husk ash (RHA), and alkaline activator (procured sodium silicate, waste-created sodium silicate and sodium hydroxide) were added at 0, 2.5, 5, 7.5, and 10%, to the naturally created superplasticizer geopolymer concrete (GPC), so as to solve the problem of workability and efflorescence associated with fly ash based GPC. FTIR results shows major absorbance band at the region between 950 and 3250 cm^{-1} . It means that addition of the naturally made superplasticizer to the geopolymer concrete lowered the viscosity and increased the flow behavior of concrete. The geopolymer concrete consists of super plasticizer (1.5%) and optimum of various binders i.e. 5% FA + 7.5% KC + 10% RHA + aggregate + water. At temperature above 70°C both compressive strength and weight decreases, for naturally made and purchased sodium silicate. The optimal geopolymer product showed substantial strength and durability enhancements at 70°C temperatures, with strength and durability values decline above 70°C, indicating material deterioration. A positive correlation between hot-state temperature, strength and durability properties was also established. The R² of the Feret on the test set reaches 0.967, indicating its excellent predictive performance.

Keywords: Rice Husk, Fourier Transform Infrared Spectroscopy, Waste-created sodium silicate, Superplasticizer; Eco-friendly

[Full text-[PDF](#)] [[Crossref Metadata](#)] [Export from [ePrints](#)]

Graphical Abstract of GPC



Research Paper

An Analysis of Water Demand of the Rural Population within the Iishana System, Namibia

Eino J, Katte VY, Busari AO, Pires EES, Johannes P, Fahrenberg M, Reinhardt CI, Jüpner R and Schulte A.

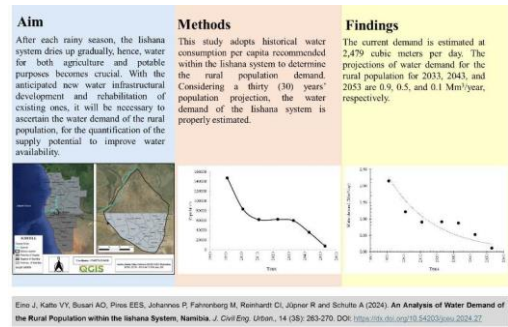
J. Civil Eng. Urban., 14(3s): 263-270, 2024; pii:S225204302400027-14

DOI: <https://dx.doi.org/10.54203/jceu.2024.27>

Abstract

The Namibian people, particularly, those living within the Iishana system, which is a subset of the Cuvelai Basin, often encounter recurrent floods and droughts. After each rainy season, the Iishana system dries up gradually, hence, water for both agriculture and potable purposes becomes crucial. With the anticipated new water infrastructural development and rehabilitation of existing ones, it will be necessary to ascertain the water demand of the rural population, for the quantification of the supply potential to improve water availability. This study adopts historical water consumption per capita recommended within the Iishana system to determine the rural population demand. Considering a thirty years' population projection, the water demand of the Iishana system is properly estimated. Moreover, the historical hydrological dataset daily data for the period 2012-2021 was used for the analysis. The current demand is estimated at 2,479 cubic meters per day. The projections of water demand for the rural population for 2033, 2043, and 2053 are 0.9, 0.5, and 0.1 Mm³/year, respectively. More so, the surface water resource potential of the system is estimated at an average of 300 mm/year. The region loses more water through evaporation than it receives in the wet season. Around 2500 mm of water evaporates from the surface annually, giving a water deficit of 2200 mm/year. The region's flat, shallow landscape, high evaporation rate, and the inadequacy of infrastructure have made the area vulnerable in terms of water security for both agricultural and potable purposes, resulting in droughts after the rainy season. With these findings, it is recommended to build water infrastructures within the region to improve the well-being and livelihood of rural communities.

Keywords: Water demand, water supply, rural population, per capita demand, Iishana system, Namibia



[Full text-PDF] [[Crossref Metadata](#)] [Export from [ePrints](#)]

Meeting the Sustainability Emergency in Built Environment Curricula through Tripartite Pedagogy Quasi-Experimentation

Ewurum NI, Aguome NM, Kelobonye K, Emoh FI.

J. Civil Eng. Urban., 14(3s): 271-277, 2024; pii:S225204302400028-14

DOI: <https://dx.doi.org/10.54203/jceu.2024.28>

Abstract

This study evaluates the effectiveness of a tripartite pedagogy framework integrating specialized tracks, optional minors, and experiential learning to enhance sustainability education in built environment curricula. Employing a mixed-methods quasi-experimental design, the research assessed 239 industrial training students in Enugu, Nigeria. Results from the t-test demonstrate significant improvements in sustainability knowledge post-intervention and high interest in optional sustainability courses. Repeated measures of ANOVA revealed substantial enhancements in students' ability to apply sustainability concepts over time. Qualitative data highlighted practical challenges in experiential learning, including resource constraints. The findings provide empirical support for the tripartite approach, extending previous research by quantifying impacts on practical skills development. This study contributes to the limited body of evidence on integrated sustainability education interventions in the Global South, demonstrating significant improvements in students' sustainability knowledge and application skills through a tripartite pedagogy framework. The findings highlight the potential of specialized tracks, optional minors, and experiential learning to bridge the gap between academic preparation and industry needs. It is recommended that educational institutions prioritize these integrative approaches and address resource constraints to enhance the effectiveness and scalability of sustainability education in built environment curricula.

Keywords: Building Research Establishment Environmental Assessment Methodology, Built environment curricula, Experiential learning, Optional minors, Specialized tracks, Sustainability competencies



[Full text-PDF] [[Crossref Metadata](#)] [Export from ePrints]

Enhancing Water Level Prediction through a Hybrid Feature Selection Approach

Tshireletso T, Ouma Y, Moalafhi D, and Anderson G.

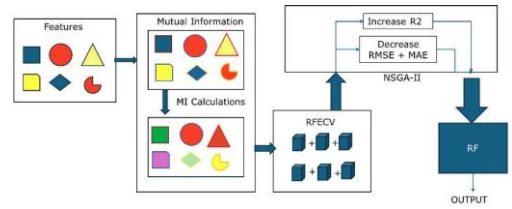
J. Civil Eng. Urban., 14(3s): 278-282, 2024; pii:S225204302400029-14

DOI: <https://dx.doi.org/10.54203/jceu.2024.29>

Abstract

Accurate prediction of water levels (WL) is essential for various applications, from flood management to environmental monitoring. In this study, an enhanced approach to feature selection tailored for water level prediction models is presented. Our method integrates Mutual Information and Recursive Feature Elimination with Cross-Validation (RFECV), augmented by the Non-Dominated Sorting Genetic Algorithm II (NSGA-II), to systematically evaluate and refine subsets of features. Mutual Information facilitates the identification of relevant feature dependencies, while RFECV iteratively eliminates less informative features to optimize predictive accuracy. The inclusion of NSGA-II further enhances the selection process by considering multiple conflicting objectives simultaneously, such as maximizing R2 score and minimizing the number of selected features, RMSE, and MAE. Through extensive experimentation and validation on real-world datasets, we demonstrate the effectiveness of our hybrid feature selection approach in capturing intricate relationships within the data, leading to significantly improved predictive performance in water level prediction models.

Keywords: Mutual Information, Recursive Feature Elimination with Cross validation, Non-Dominated Sorting Genetic Algorithm II



Tshireletso T, Ouma Y, Moalafi D, and Anderson G (2024). Enhancing Water Level Prediction through a Hybrid Feature Selection Approach. *J. Civil Eng. Urban.*, 14 (3S): 278-282. DOI: <https://dx.doi.org/10.54203/jceu.2024.29>

[Full text-PDF] [[Crossref Metadata](#)] [Export from ePrints]

Investigation of Performance of Copper Slag and Ore Tailings Novel Trial Self-compacting Concrete Mixtures

Fidler A and. Oyejobi DO.

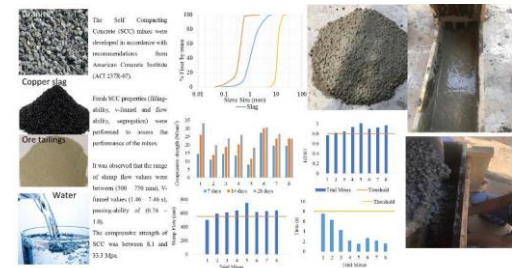
J. Civil Eng. Urban., 14(3s): 283-288, 2024; pii:S225204302400030-14

DOI: <https://dx.doi.org/10.54203/jceu.2024.30>

Abstract

A non-conventional concrete with the properties of flow-ability, filling-ability, and passing-ability without any need for mechanical compaction but flow under self-weight is known as self-compacting concrete. This study developed trial mixtures for self-compacting concrete (SCC) using locally available waste products. The copper slag and ore tailings from Bamangwato Concessions Limited Mine in Selebi-Phikwe, Botswana were used as source of fine aggregate, and fines substitute. Eight mix proportions were developed with the quantities of cement, granite, copper slag, ore tailings and water-cement ratio as variables. The mix proportions were developed in accordance with recommendations from American Concrete Institute (ACI 237R-07) and fresh SCC properties (flow ability, passing ability, filling-ability, and segregation) were performed to assess the performance of the mixes. It was observed that the range of slump flow values were between (500 – 750 mm), V-funnel values (1.46 – 7.46 s), passing-ability of (0.76 – 1.0). The hardened properties of SCC (strength and density) were between 8.1 and 33.3 MPa, and 2093 to 2406 kg/m³ respectively. It could be concluded that SCC produced from mine wastes (copper slag and ore tailings) is found suitable for the use in unreinforced and normal concrete applications.

Keywords: Self-compacting concrete, filling-ability, flow-ability, passing-ability, slump flow, segregation and compressive strength.



Fidler A and. Oyejobi DO. (2024). Investigation of Performance of Copper Slag and Ore Tailings Novel Trial Self-compacting Concrete Mixtures. *J. Civil Eng. Urban.*, 14 (3S): 283-288. DOI: <https://dx.doi.org/10.54203/jceu.2024.30>

[Full text-PDF] [[Crossref Metadata](#)] [Export from ePrints]

Efficacy of Direct SPT-Based Pile Design Methods in Residual Soils of Southern Africa

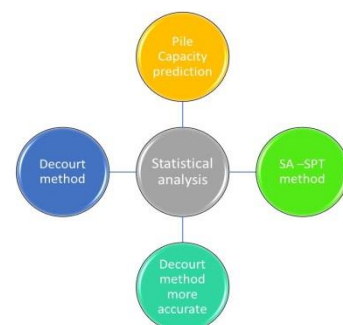
Masilo T and Dithinde M.

J. Civil Eng. Urban., 14(3s): 289-294, 2024; pii:S225204302400031-14

DOI: <https://dx.doi.org/10.54203/jceu.2024.31>

Abstract

Direct SPT-based pile design methods are very popular these days despite the fact that many of such methods are based on small databases of pile load tests. Due to the dependence of soil behaviour on geological setting and site specific conditions, it is possible that some of the methods do not produce good prediction of pile capacity. Accordingly



Masilo T and Dithinde M. (2024). Efficacy of Direct SPT-Based Pile Design Methods in Residual Soils of Southern Africa. *J. Civil Eng. Urban.*, 14 (3S): 289-294. DOI: <https://dx.doi.org/10.54203/jceu.2024.31>

this paper presents the evaluation of two SPT-based pile design methods in residual soils against a pile load test database from the Southern African region. The methods include the (i) Franki-SA method reported in Byrne et al. (1995) and (ii) Decourt Method (1995). The pile load tests consist of 26 cases of bored piles in residual soil with each case accompanied by SPT measurements. The SPT measurements were used to calculate the predicted capacity in accordance with the procedure for each of the two methods while the pile load tests were used to determine the measured capacity. The findings of the evaluation indicate that the Decourt method is more reliable and accurate than the SA method. The poor performance of the SA methods suggests further studies to develop specific calculation factors for base and shaft capacities in residual soils.

Keywords: SPT-based pile methods, Load Bearing Capacity, Pile Load Test, Chin extrapolation method, Terzaghi's 10% criteria, Rank Index.

[Full text-PDF] [Crossref Metadata] [Export from ePrints]

Behaviour of Fly-Ash Geopolymer Mortar in Simulated Environments

Oyejobi DO.

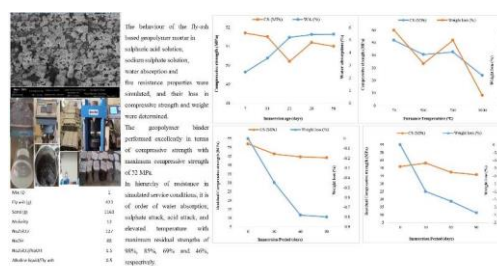
J. Civil Eng. Urban., 14(3s): 295-301, 2024; pii:S225204302400032-14

DOI: <https://dx.doi.org/10.54203/jceu.2024.32>

Abstract

Concrete and mortar usually found themselves in normal and harsh environments. The environment has great influence on the mechanical and durability behaviours of the concrete. In this study, fly ash was processed using circular economy concept and subsequently used as precursor for geopolymer mortar. The fly ash from Morupule power plant station has previously been characterized for its physical, chemical, and microstructural properties. Based on its suitability, the fresh and mechanical properties of the geopolymer mortar were carried out, and afterward, the durability behaviour is investigated in this study. The geopolymer mortar was formulated from the mixture of fly ash, sand and alkaline activators and cured thermally at 70°C. The behaviour of the geopolymer mortar in sulphuric acid solution, sodium sulphate solution, water absorption and fire resistance properties were simulated, and their loss in compressive strength and weight were determined. The laboratory experiment indicated that geopolymer mortars are highly resistant to sulphate attack, water absorption with moderate resistance against sulfuric acid and fire resistance. The effects of varying other parameters on the performance of concrete can be looked into in the future studies.

Keywords: Geopolymer mortar, environment, durability, mechanical, fly ash, circular economy



Behaviour of Fly-Ash Geopolymer Mortar in Simulated Environments
Oyejobi DO (2024). *J. Civil Eng. Urban.*, 14 (3s): 295-301. DOI: <https://dx.doi.org/10.54203/jceu.2024.32>

[Full text-PDF] [Crossref Metadata] [Export from ePrints]

Flexural Behaviour of Concrete Beams Reinforced With Major Steel Bars under Normal and Corrosive Operational Conditions

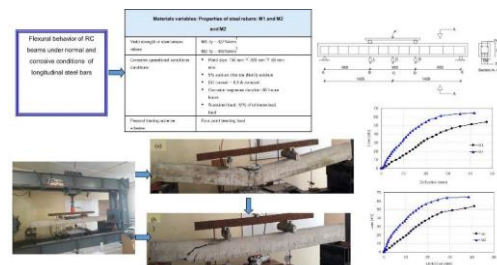
Adeyuyi AP and Eric GB.

J. Civil Eng. Urban., 14(3s): 302-310, 2024; pii:S225204302400033-14

DOI: <https://dx.doi.org/10.54203/jceu.2024.33>

Abstract

Quality assurance of construction materials is very fundamental for structural safety, reliability, serviceability, and durability of constructed civil infrastructure. Inflow of defective or substandard building and construction materials into the industry, particularly reinforcing steel bars, is responsible for many structurally deficient constructed facilities which often lead to failure or ultimate collapse of reinforced concrete (RC) structures. Characterization of steel rebars from two major manufacturers into Botswana construction industry, designated herein as M1 and M2, were conducted as a basis for the evaluation of the quality assurance and control of the products. The flexural behaviour of their respective RC beams, designated herein as B-M1 and B-M2, of dimension 150 × 200 × 3000 mm and subject to four-point loading tests were determined under normal and artificially induced corrosion conditions to assess the influence of steel rebars M1 and M2 on the stiffness and load-carrying capacity. The average yield strengths of steel reinforcing bars were 427 N/mm² for M1 and 459 N/mm² for M2. The moduli of elasticity for M1 and M2 were 203 GPa and 205 GPa, respectively. The percentage elongation was found to be 7.93% for M1 and 7.24% for M2. The flexural strength of beams reinforced with M1 was 7% and 16.5% lower than RC beam with M2 under normal and accelerated corrosion of 5% of NaCl solution for 60 hours condition, respectively. The flexural behaviour of RC beams reinforced with



Flexural behaviour of RC beams with M1 and M2 tension rebars under normal and corrosive conditions
Adeyuyi AP and Eric GB (2024). *J. Civil Eng. Urban.*, 14 (3s): 302-310. DOI: <https://dx.doi.org/10.54203/jceu.2024.33>

B-M1 had a lower flexural strength under both normal and corrosive environmental conditions as compared to B-M2. The flexural strength of B-M1 had reduced from 48.5 N/mm² to 41.0 N/mm², while B-M2 reduced from 52.2 N/mm² to 49.2 N/mm². This represented loss of load-carrying capacity of 15.4% and 5.8% for B-M1 and B-M2 respectively due to exposure to corrosive environment. The findings revealed disparity in bending capacity due to the low interfacial bonding due to reduced relative rib areas. A more intensive quality control of imported steel should be ensured at the ports of entry by relevant regulatory agencies.

Keywords: Flexural capacity, Stiffness, Reinforcing bars, Relative rib area, Interfacial bonding, Accelerated corrosion, Ultimate load.

[Full text-[PDF](#)] [[Crossref Metadata](#)] [Export from ePrints]

The Use of Machine Learning Approach to Predict Pile Capacity in Non-Cohesive Soils

Palalane L and Dithinde M.

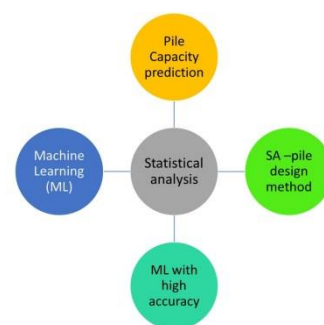
J. Civil Eng. Urban., 14(3s): 311-317, 2024; pii:S225204302400034-14

DOI: <https://dx.doi.org/10.54203/jceu.2024.34>

Abstract

Existing theoretical and empirical pile design methods cannot accurately model the complex interaction between piles and soil. Consequently, there is a growing trend towards utilizing machine learning techniques to better capture the nonlinear soil-pile interaction. This paper aims to predict the capacity of bored piles in cohesionless soils using a machine learning approach. The machine learning algorithm was trained using a database of 18 bored pile cases in non-cohesive soils and validated with a separate dataset of 8 bored piles in cohesionless soil. Moreover, the performance of the machine learning method was compared with that of a traditional pile design method (i.e., SA-SPT method) in Southern Africa. The evaluation was based on the ratio of measured capacity to predicted capacity (Q_m/Q_p) statistics and the coefficient of determination (R^2). The results showed an R^2 of 0.89 for the machine learning method compared to 0.85 for the SA-SPT method, indicating the superior accuracy of the machine learning approach in predicting pile capacity.

Keywords: Machine learning, SPT-based pile methods, Load Bearing Capacity, Full-scale Load Test, Chin extrapolation method, Terzaghi's 10% criteria.



Palalane L and Dithinde M (2024). The Use of Machine Learning Approach to Predict Pile Capacity in Non-Cohesive Soils. *J. Civil Eng. Urban.*, 14 (3s): 311-317. DOI: <https://dx.doi.org/10.54203/jceu.2024.34>

[Full text-[PDF](#)] [[Crossref Metadata](#)] [Export from ePrints]

Geotechnical characterization of the Manyana black cotton soils in Botswana

Marumo MN, Lebitsa G, Malumbela G.

J. Civil Eng. Urban., 14(3s): 318-324, 2024; pii:S225204302400035-14

DOI: <https://dx.doi.org/10.54203/jceu.2024.35>

Abstract

The Manyana Village is divided into two types of soils. The center of the village is covered with sand that overlays clays from weathered dolerite whilst the eastern side is covered with exposed clays. Houses constructed on the eastern side of the village are prone to severe cracking attributed to the black cotton soils. The paper hints at shrink-swell mechanism of black cotton soils as a possible explanation for the cracking observed on the houses. Three laboratory methods of identifying and characterizing expansive soils are discussed followed by use of Dynamic Cone Penetration (DCP) in field-testing as well as use of indicator tests and particle sizing in the laboratory. The experimental results have shown a high field moisture content of (18 to 27%) in the eastern part of the village which was three times larger than moisture content at the village center. The clays had a plasticity index range of 12% to 30% with a clay content of 21% to 47% whilst the sandy areas were non-plastic with a clay content of at most 4%. The clay minerals identified from the samples tested were vermiculite, illite, kaolinite and montmorillonite. The soil samples from the village had low potential expansiveness whilst most samples on black cotton soil had a medium to high potential of expansiveness. The bearing capacity estimated from DCP data at depths of 1m throughout the village were 72 kPa to 275 kPa under dry conditions. A draft plasticity index map of Manyana village was produced based on the results of the investigation, the next step is to investigate the effectiveness of different soil stabilization methods for this area and taking in to consideration cost, durability and environmental impact.

Keywords: Black cotton soil, Cracking, Moisture content, Plasticity index, Bearing capacity.

[Full text-[PDF](#)] [[Crossref Metadata](#)] [Export from ePrints]

Evaluation of the Compressive Strength and Sorptivity of Pozzolanic Concrete Containing Calcined Termite Mound

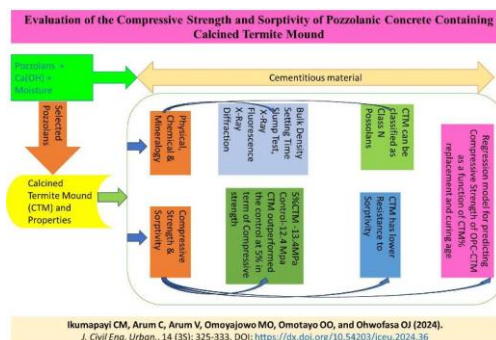
Ikumapayi CM, Arum C, Arum V, Omoyajowo MO, Omotayo OO, and Ohwofasa OJ.
J. Civil Eng. Urban., 14(3s): 325-333, 2024; pii:S225204302400036-14
DOI: <https://dx.doi.org/10.54203/jceu.2024.36>

Abstract

Pozzolans have long been established as viable materials for the partial replacement of cement in concrete. However, the extent to which they can be used is still under investigation. Pozzolans do not in themselves have cementitious value but can react chemically with calcium hydroxide and moisture to produce cementitious compounds. Pozzolanic concretes have been reported to have varied properties in term of compressive strength and durability properties which need to be ascertained. This research focuses on Calcined Termite Mound (CTM) and its influence on the compressive strength and sorptivity of concrete. Several tests were carried out to ascertain the physical, chemical, and mineralogical properties of CTM and conventional concrete constituents. Some of these tests include bulk density, setting time, aggregate crushing value (ACV), aggregate impact value (AIV), slump test, X-Ray Fluorescence (XRF), X-Ray Diffraction (XRD), sorptivity, and compressive strength tests. Compressive strength tests results for concrete containing Ordinary Portland Cement (OPC) and CTM cement blends show that CTM has higher silica content compared to OPC and can be classified as Class-N pozzolans. It is also richer in calcium oxide. The study also reveals that CTM has an optimum replacement level of 5% with strength of 13.4 MPa at 28 days, which is higher than the 12.4 MPa of control concrete. Also, the result of sorptivity test for OPC-CTM blended concrete gave lower resistance to sorptivity. Regression models were developed to predict the compressive strengths of OPC-CTM concrete as a function of % replacement level and curing age.

Keywords: Calcine termite mound; Compressive strength; Pozzolanic concrete; Sorptivity.

[Full text-PDF] [Crossref Metadata] [Export from ePrints]



Estimation of Water Demand for the Rural Population in the Angolan Part of the Iishana System

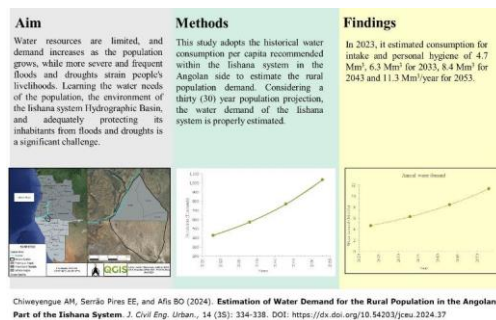
Chiweyengue AM, Serrão Pires EE, and Afis BO.
J. Civil Eng. Urban., 14(3s): 334-338, 2024; pii:S225204302400037-14
DOI: <https://dx.doi.org/10.54203/jceu.2024.37>

Abstract

The Iishana is a shallow, low-slope channel system located in the Cuvelai basin (Southern Angola and Northern Namibia), characterised by drought and flood cycles due to erratic climate variability. The knowledge gap regarding the actual water needs in the area, the number of residents within the system, the seasonal influence of cattle migration, and poor socio-economic conditions, make the population even more vulnerable to droughts. The main objective of this study is to estimate the water demand by the rural population on the Angolan side of the Iishana system, attempting to fill the knowledge gap. To reach the demand estimates, a mathematical procedure within a GIS environment was used, in QGIS 3.32.2 software, relating population gridded and meteorological data to make the necessary calculations. In 2023, it estimated consumption for intake and personal hygiene of 4.7 Mm³, 6.3 Mm³ for 2033, 8.4 Mm³ for 2043 and 11.3 Mm³/year for 2053. In recent years there have been rainfall records throughout the Iishana system, at an average of 518 mm/annum, but high temperatures accelerate water evaporation. Due to the topographical conditions, the waters are drained by gravity to the south of the basin (Republic of Namibia), causing a greater shortage in the dry season on the Angolan side, the study targets the estimation of water demand and the concept of rainwater harvest and sustainable water infrastructure to supply safe drinking water to equalise water demand and reduce vulnerability to climate change. These early findings may provide a basis for developing sustainable water infrastructure and use plans to improve the livelihoods of the resident population within the basin.

Keywords: Water demand, Water supply, Iishana system, Cuvelai Basin, Water infrastructure.

[Full text-PDF] [Crossref Metadata] [Export from ePrints]



<Previous issue | [Next issue](#) | [Archive](#)

This work is licensed under a [Creative Commons Attribution 4.0 International License \(CC BY 4.0\)](https://creativecommons.org/licenses/by/4.0/).



Comparison of Concrete Strengthened with Carbon Fibre-Reinforced Polymer (CFRP) and Carbon Textile-Reinforced Mortar (CTRM)

Xuan Wang¹  , Xinyue Lin² , and Shunbi Xu² 

¹School of Civil & Environmental Engineering and Geography Science, Ningbo University, Ningbo, China

²Pan Tianshou College of Architecture, Art and Design, Ningbo University, Ningbo, China

✉Corresponding author's Email: wangxuan@nbu.edu.cn

ABSTRACT

Applying new composite material for strengthening and repairing existing structures is an important research topic. Carbon Fiber Reinforced Polymer/Plastics (CFRP) and Carbon Textile Reinforced Mortar (CTRM) are two common structural external reinforcement materials. 18 concrete specimens strengthened with CFRP and CTRM are prepared in this study. The quasi-static single-sided shear tests combined with the Digital Image Correlation (DIC) method is applied. The results show that the interface bonding strength of CFRP strengthening (0.76-0.96 MPa) is 65.0% to 74.8% higher than the CTRM-concrete interface (0.43-0.63 MPa). The ductility and energy dissipation capacity of CTRM strengthening is better than that of CFRP strengthening, and the effective bonding length is 125 to 300 mm. In practical work, CFRP is preferred for improving the strength of concrete components, while CTRM is preferred for improving ductility and seismic resistance.

Keywords: Carbon fibre-reinforced composites (CFRP); Carbon textile-reinforced mortar (CTRM); Digital image correlation method (DIC); Single-sided shear test

INTRODUCTION

The global building stock comprises many historic constructions that require repair and structural strengthening. This requirement arises from the need to improve the original performance of these structures under existing loads or to increase their load-bearing capacity to satisfy changes in use and increase their service life. Applying new composite material for strengthening and repairing existing structures is an important research topic. Carbon fibre-reinforced polymer (CFRP) and carbon textile-reinforced mortar (CTRM) have recently been applied in structural strengthening (Koutas, 2019; Zampieri, 2018). CTRM comprises carbon textiles combined with an inorganic mortar matrix. CFRP comprises CFRP sheet and epoxy resin. The mechanical behaviour of TRM depends on the material properties of the fibre and the bond behaviour between the fibre and the substrate (Raouf, 2006). The FRP/TRM-concrete bond performance is critical for ensuring the safety and efficiency of the strengthening (Yuan, 2004; Yao, 2007; Ueda, 2005; Su, 2021). The single shear pull-out test (Oliveira, 2010; Zhou, 2020; Yang, 2017) has been widely

used in the laboratory to characterise the FRP-concrete bond behaviour, which adequately reproduces the loading conditions in service.

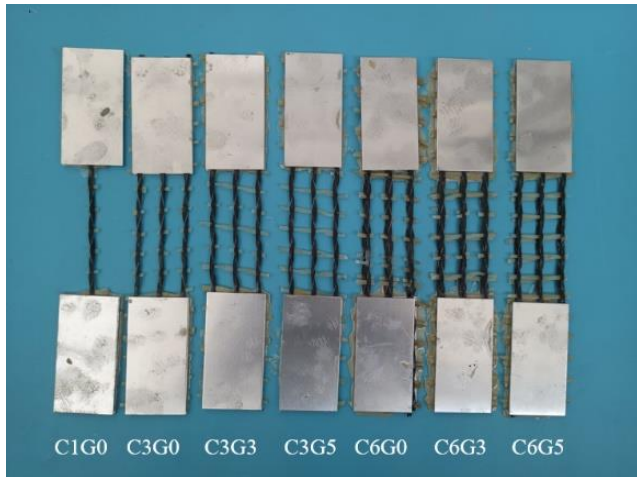
The typical failure modes of composite strengthened concrete have been identified in the literature (De Felice, 2018): (1) damage of the substrate, (2) debonding at the fiber-substrate interface, and (3) fibre rupture. However, a comparison of the bond behaviour of CFRP and CTRM is still lacking (Wang, 2020; Wang, 2023). In this study, the bond behaviour of CFRP and CTRM to concrete was investigated experimentally by using single-sided shear tests.

MATERIALS AND METHODS

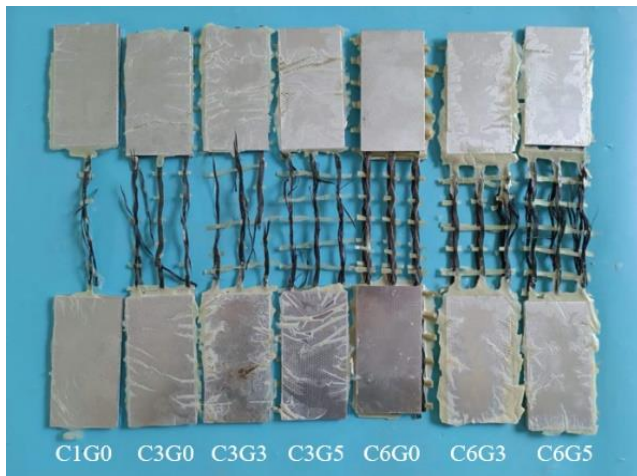
Carbon textile and CFRP

Five carbon textile and CFRP sheet samples are prepared for mechanical characterisation tests. The length and width of the sample are 230 mm and 50 mm, respectively. Each sample is bonded and gripped with two aluminium taps of 50 mm in length. The failure patterns are shown in Figures 1 and 2. The test results are listed in Table 1.

RESEARCH ARTICLE
 PII: S225204302400008-14
 Received: June 25, 2024
 Revised: September 02, 2024
 Accepted: September 05, 2024



(a) Sample preparation



(b) Failure pattern

Figure 1. Tensile sample of carbon textile



(a) Sample preparation



(b) Failure pattern

Figure 2. Tensile sample of CFRP sheet

Table 1. Tensile mechanical properties of carbon textile and CFRP sheet

Specimen No.	Peak load (kN)	Tensile stress (MPa)	Peak strain (%)	Elastic modulus (GPa)
C1G0	2.30 (0.02)	1121.96	1.3 (0.05)	121 (5.7)
C3G0	6.34 (0.16)	1124.63	1.6 (0.05)	76 (2.2)
C3G3	6.70 (0.05)	1188.73	1.8 (0.06)	81 (2.1)
C3G5	6.66 (0.22)	1180.73	1.8 (0.05)	77 (1.5)
C6G0	9.57 (0.27)	848.36	2.0 (0.05)	58 (0.9)
C6G3	9.81 (0.65)	869.49	2.3 (0.12)	53 (1.5)
C6G5	9.51 (0.28)	842.90	2.1 (0.03)	55 (1.1)
CFRP sheet	6.045 (0.05)	3630	/	/

Coefficients of variation (CoV) in brackets

Preparation of specimen

Figure 3 shows the procedure for preparing a CTRM strengthened concrete specimen. The concrete block dimensions are 300 mm or 400 mm × 100 mm × 100 mm, the corresponding bond length is 250 mm or 350 mm, and the width is 50 mm. Pre-cut carbon textiles were laid onto the first layer of mortar, and finally, another layer of mortar was applied to the textile to finish the process (Figure 3). The total thickness of the CTRM is 15 mm.





Figure 3. Preparation of CTRM strengthened concrete specimen

Test setup

The single-lap shear bond test (Zhang, 2023) was applied to the wet lay-up unidirectional CFRP and CTRM strengthened concrete elements. Figure 4 shows a test setup of the single-lap pull-out tests, according to the recommendation of RILEM Technical Committee 250-CSM (De Felice, 2018). The loading was applied from the unembedded textile to the CTRM and concrete. The unembedded textile was pulled out monotonically by the testing machine. The digital image correlation measures the surface displacement and strain distribution of the test specimen.

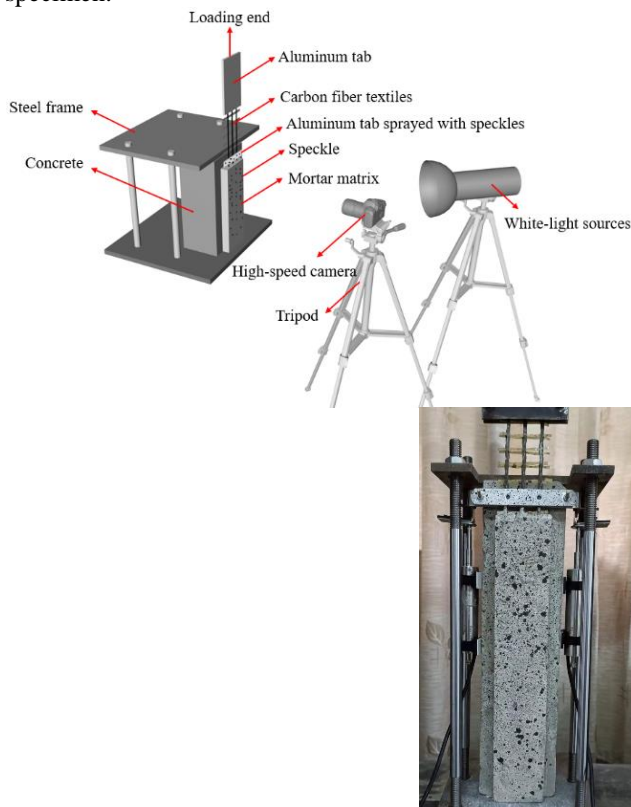


Figure 4. Test setup.

RESULTS AND DISCUSSION

Test results for each specimen are listed in Table 2 and Table 3. For the CTRM strengthened concrete, the average initial cracking and peak loads at the loading end were 8.11 kN and 9.01 kN, respectively. For the CFRP strengthened concrete, the average initial cracking load and peak load at the loading end were 12.87 kN and 15.13 kN, respectively. The failure mode of TRM strengthened concrete was a mixed damage failure with matrix crack and textile rupture. The bond strength of 6 specimens of Type I (T2I and T3I) is relatively higher than that of 6 specimens of Type II (T2II and T3II), indicating that its bonding length is greater than the effective bonding length. This is because the protective layer of Type I is thicker, which makes its effective bonding length shorter.

In contrast, the failure mode of 6 specimens of CFRP strengthened concrete (F2 and F3) was a debonding failure, as shown in Figure 5. The results show that the interface bonding strength of CFRP strengthening (0.76-0.96 MPa) is 65.0% to 74.8% higher than the CTRM-concrete interface (0.43-0.63 MPa), indicating that the bond of CFRP is stronger than that of CTRM.

Figure 6 compares the experimental load-slip responses of CTRM and CFRP-strengthened concrete. The load-slip curves show that CTRM strengthening has better ductility and energy dissipation capacity than CFRP strengthening. Figure 7 shows the strain contours obtained by DIC of the specimens at different load levels, P_u is the peak load. The length of failure was conducted from the DIC results, which is the length of strain distribution at peak load. The strain contours show that the effective bonding length is 125 to 300 mm.

Table 2. Test results of CTRM strengthened concrete

No.	FL (mm)	FM	CL (kN)	PL (kN)	BS (MPa)
T2 I -1	128	Mixed failure	6.86	9.89	0.66
T2 I -2	120		6.08	9.39	0.63
T2 I -3	125		7.76	9.16	0.61
T3 I -1	126	Mixed failure	7.68	9.42	0.45
T3 I -2	131		9.11	10.13	0.48
T3 I -3	129		9.37	9.37	0.45
T2 II -1	250	Mixed failure	7.32	7.37	0.49
T2 II -2	250		7.99	7.99	0.53
T2 II -3	250		8.07	8.07	0.54
T3 II -1	302	Mixed failure	9.12	9.12	0.43
T3 II -2	296		8.79	8.79	0.42
T3 II -3	306		9.19	9.40	0.45

FL, FM, CL, PL BS are failure length, failure mode, crack load, peak load, and bond strength.

Table 3. Test results of CFRP strengthened concrete

No.	FL (mm)	FM	CL (kN)	PL (kN)	BS (MPa)
F2-1	250	CFRP debond	12.13	14.35	0.96
F2-2	250		12.06	15.18	1.01
F2-3	250		11.85	13.51	0.90
F3-1	350	CFRP debond	13.22	14.56	0.69
F3-2	350		14.68	17.55	0.84
F3-3	350		13.29	15.61	0.74

FL, FM, CL, PL BS are failure length, failure mode, crack load, peak load, and bond strength.



(a) CTRM strengthened concrete



(b) CFRP strengthened concrete

Figure 5. Failure mode

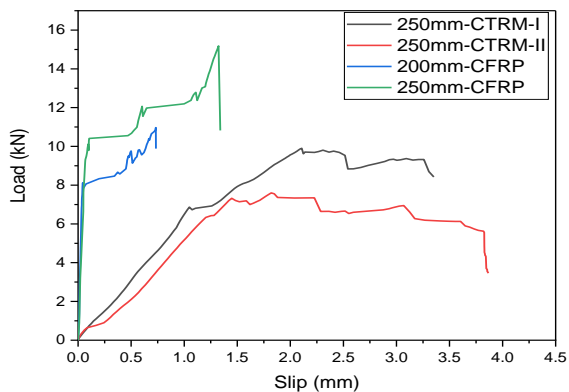
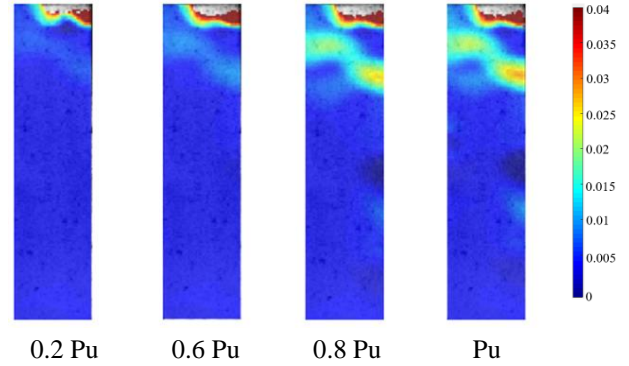
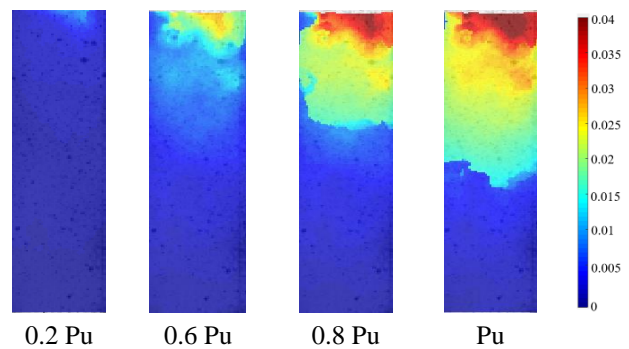


Figure 6. Comparison of the experimental load-slip curves



(a) CTRM strengthened concrete



(b) CFRP strengthened concrete

Figure 7. Strain contours at different load levels (DIC)

CONCLUSIONS

This study conducted 18 quasi-static single-sided shear tests on concrete specimens strengthened with CFRP and CTRM, combined with the Digital Image Correlation (DIC) method. The results show that the interface bonding strength of CFRP strengthening (0.76-0.96 MPa) is 65.0% to 74.8% higher than the CTRM-concrete interface (0.43-0.63 MPa). The ductility and energy dissipation capacity of CTRM strengthening is better than that of CFRP strengthening, and the effective bonding length is 125 to 300 mm. In practical work, CFRP is preferred for improving the strength of concrete components, while CTRM is preferred for improving ductility and seismic resistance.

DECLARATIONS

Corresponding Author

Correspondence and requests for materials should be addressed to Xuan Wang; E-mail: Email: wangxuan@nbu.edu.cn; 0000-0002-7833-9317

Data availability

The datasets used and/or analysed during the current study available from the corresponding author on reasonable request.

Acknowledgements

The authors would like to acknowledge the Science and Technology Innovation 2025 Major Project of Ningbo (Grant No. 2021Z104) to supported this research.

Authors' contribution

First Author performed the experiments, analysed the data obtained and wrote the manuscript. Second and Third Author designed the experimental process and revised the manuscript. Both authors read and approved the final manuscript

Competing interests

The authors declare no competing interests in this research and publication.

REFERENCES

- Koutas LN, Tetta Z, Bournas DA, Triantafillou TC (2019). Strengthening of concrete structures with textile reinforced mortars: State-of-the-art review. *Journal of Composites for Construction*, 23, 03118001. [https://doi.org/10.1061/\(ASCE\)CC.1943-5614.0000882](https://doi.org/10.1061/(ASCE)CC.1943-5614.0000882)
- Zampieri P, Simoncello N, Tetougueni CD, Pellegrino C (2018). A review of methods for strengthening of masonry arches with composite materials. *Engineering Structures*, 171, 154-69. <https://doi.org/10.1016/j.engstruct.2018.05.070>
- Raof SM, Koutas LN, Bournas DA (2016). Bond between textile-reinforced mortar (TRM) and concrete substrates: Experimental investigation. *Composites Part B: Engineering*, 98, 350-61. <https://doi.org/10.1016/j.compositesb.2016.05.041>
- Yuan H, Teng JG, Seracino R, Wu ZS, Yao J (2004). Full-range behavior of FRP-to-concrete bonded joints. *Eng Struct*. 26, (5) 553-565. <https://doi.org/10.1016/j.engstruct.2003.11.006>
- Yao J, Teng JG (2007). Plate end debonding in FRP-plated RC beams-I: Experiments. *Eng Struct* 29:2457-71. <https://doi.org/10.1016/j.engstruct.2006.11.022>
- Ueda T, Dai J (2005). Interface bond between FRP sheets and concrete substrates: properties, numerical modeling and roles in member behaviour. *Prog Struct Eng Mater.*, 7:27-43. <https://doi.org/10.1002/pse.187>
- Su M, Zhong Q, Peng H, Li S (2021). Selected machine learning approaches for predicting the interfacial bond strength between FRPs and concrete. *Constr Build Mater*. 270:121456. <https://doi.org/10.1016/j.conbuildmat.2020.121456>
- Oliveira DV, Basilio I, Lourenço PB (2010). Experimental bond behavior of FRP sheets glued on brick masonry. *J Compos Constr* 15, (1) 32-41. [https://doi.org/10.1061/\(ASCE\)CC.1943-5614.0000086](https://doi.org/10.1061/(ASCE)CC.1943-5614.0000086)
- Zhou Y, Zheng S, Huang Z, Sui L, Chen Y (2020). Explicit neural network model for predicting FRP-concrete interfacial bond strength based on a large database. *Compos Struct*;240. <https://doi.org/10.1016/j.compstruct.2020.111998>
- Yang S, Liu Y, Xu X, Gong J, Yang C (2017). Determination of boundary effect on mode II fracture energy of FRP sheet-to-concrete bonded joints. *Eng Fract Mech* 181:130-42. <https://doi.org/10.1016/j.engfracmech.2017.07.006>
- De Felice G, Aiello MA, Caggegi C, Ceroni F, De Santis S, Garbin E et al., (2018). Recommendation of RILEM Technical Committee 250-CSM: Test method for Textile Reinforced Mortar to substrate bond characterisation. *Materials and Structures*, 51, 1-9. <https://doi.org/10.1617/s11527-018-1216-x>

Publisher's note: [Scienceline Publication](#) Ltd. remains neutral with regard to jurisdictional claims in published maps and institutional affiliations.



Open Access: This article is licensed under a Creative Commons Attribution 4.0 International License, which permits use, sharing, adaptation, distribution and reproduction in any medium or format, as long as you give appropriate credit to the original author(s) and the source, provide a link to the Creative Commons licence, and indicate if changes were made. The images or other third party material in this article are included in the article's Creative Commons licence, unless indicated otherwise in a credit line to the material. If material is not included in the article's Creative Commons licence and your intended use is not permitted by statutory regulation or exceeds the permitted use, you will need to obtain permission directly from the copyright holder. To view a copy of this licence, visit <https://creativecommons.org/licenses/by/4.0/>.

Effects of Blended Portland-Fly Ash Cement on Compressive Strength of Seawater Mixed and Cured Lateritic Concrete

Stephen Adeyemi Alabi^{1,2,3,✉} , Chinwuba Arum^{2,4} , Adebisi R. Akande² , Jeffrey Mahachi³ , and Joseph Olasehinde Afolayan² 

¹Department of Civil Engineering, University of Botswana, Gaborone, Botswana

²Department of Civil and Environmental Engineering, Federal University of Technology, Akure, Nigeria

³Department of Civil Engineering Technology, University of Johannesburg, Doornfontein, Johannesburg, South Africa

⁴Department of Civil and Environmental Engineering, University of Namibia, Eng. José Eduardo dos Santos (JEDS) Campus, Namibia

✉Corresponding author's Email: alabisa@ub.ac.bw

ABSTRACT

The use of cement in the construction industry is accompanied by the release of greenhouse gases (GHGs) into the ecosystem, and freshwater usage is on the rise globally, putting the world in a potential freshwater scarcity. This study investigated the effects of blended Portland-fly ash cement on the compressive strength of seawater-mixed and cured lateritic concrete by partially replacing the concrete materials: cement with fly ash at 0%, 5%, 10%, 15%, and 25%; fine aggregate, with laterite at 0%, 10%, 20%, and 30%. A concrete mix ratio of 1:1.5:3 was used in the production of concrete cubes with an expected target compressive strength of 20 N/mm². The compressive strength of the cubes was measured at 7, 28, and 56 days using standard testing procedures. Cubes cast with and cured in seawater (SW-SW) had strength values relatively higher than those cast with and cured in freshwater (FW-FW) at 28 days of curing. At 28 days, SW-SW cubes gave 22.44 N/mm² while FW-FW cubes gave 21.80 N/mm² as the highest strength values at 10% Lat and 10% FA. However, the FW-FW cubes had strength values higher than those of seawater mixed and cured concrete (SW-SW) at 56 days. FW-FW cubes gave 26.82 N/mm² while SW-SW cubes gave 26.34 N/mm² as their highest strength values at 10% Lat and 10% FA. Generally, an increase in fly ash and laterite content significantly reduces the compressive strength of concrete. Overall, seawater is recommended for curing and mixing, especially in non-reinforcing concrete. 10% fly ash and 10% laterite are also recommended for use in blended Portland cement-fly ash concrete as they give the highest strength values.

Keywords: Concrete, Fly Ash, Laterite, Seawater, Compressive strength

INTRODUCTION

Concrete has been extensively used as a construction material ever since it was introduced to the construction industry (Basavana et al., 2015). Concrete is used for numerous purposes in the construction industry, such as the construction of buildings, foundations, parking structures, pipes, dams, pools, and other similar structures (Ogunjiofor, 2020). The average annual production is approximately 1 ton of concrete per human being in the world (Marie and Quiasrawi, 2012). The need to prevent the depletion of non-renewable materials and make concrete construction sustainable led to the replacement of the constituent materials of concrete with alternative ones. The partial replacement of sand with laterite resulted in lateritized concrete (Folagbade and Aluko, 2019).

Over two billion tons of freshwater is consumed every year, which is approximately 9% of the global industrial

water demand (Monteiro and Miller, 2017; Miller et al., 2016). Predictions show that in 2050, 75% of the water demand for concrete production will occur in regions most likely to experience water shortages (Miller et al., 2018).

Given the increase in freshwater usage globally which may lead to a potential freshwater shortage, seawater becomes plausible as an alternative mixing water for concrete (Mekonnen and Hoekstra, 2016; Miller et al., 2015). Although the use of seawater in concrete mixtures is currently prohibited because of its high chloride contents that promote corrosion of reinforcing steel (El-Reedy, 2017), the issue can be addressed by using non-corrosive reinforcement such as fibre-reinforced polymer (FRP) bars (Younis et al., 2018).

Several works have been carried out on the possibility of using seawater for mixing and curing concrete. Khatib and Bayasi (2003) studied the strength and durability of

RESEARCH ARTICLE
 PII: S225204302400009-14
 Received: June 25, 2024
 Revised: September 02, 2024
 Accepted: September 05, 2024

seawater-mixed concrete and concluded that the compressive strength of seawater (SW)-mixed concrete was slightly lower than that of freshwater (FW)-mixed concrete but the difference was not significant. Lee *et al.*, (2008) also investigated the influence of curing in SW on the properties of concrete and showed from the study that the compressive strength of concrete cured in FW was slightly higher than that of concrete cured in SW but the difference was not significant.

Attempts have been made to also partially replace the cement content of lateritized concrete with pozzolanic materials such as fly ash, cassava peel ash and volcanic ash, among others (Ogunbode, 2010; Al-Ani and Hughes, 1989).

Azad *et al.*, (2016) studied the effects of fly ash on the mechanical properties of concrete and found that the addition of fly ash to concrete can increase its compressive strength, tensile strength and flexural strength. Kishore *et al.*, (2017) however found that the compressive strength and flexural strength of concrete reduce with an increase in fly ash content.

The scope of this study included casting and curing blended Portland fly ash lateritic concrete made with fly ash in FW and SW. In this study, fly ash was used as a partial replacement for cement at 0%, 5%, 10%, 15%, and 25% levels, and laterite for sand at 0%, 10%, 20%, and 30% replacement levels in the concrete mix. The effects of the laterite and fly ash on the compressive strength of the concrete were studied and compared with that of ordinary Portland cement (OPC) concrete mixed and cured with FW as a control.

MATERIALS AND METHODS

Sources and preparation of materials

The materials used for this study were sourced locally and tested to ensure that they meet all the necessary standards. Lafarge Portland cement, grade 42.5, type 1 general-purpose cement as per the ASTM C150, (2012) was used in this study as shown in Figure 1a.

Fly ash sample was obtained from the Olokwu coal mining site, Omala Local Government, Kogi State, Northcentral Nigeria. The specific gravity test was carried out following BS EN 12620:2002 as well as X-ray Fluorescence (XRF) analysis, and X-ray diffraction (XRD) were carried out to examine the chemical composition and the mineralogical composition of the fly ash. It is light brown in colour (Figure 1 b). The results of other physical properties of the binders are shown in Table 1.

Laterite was sourced from a laterite quarry within the Akure metropolis, Southwestern Nigeria (Figure 1 c). Physical properties such as specific gravity test was carried out on the laterite samples. Clean and dry fine river sand (Akure pit sand, APS) that was well-graded was used for casting all the specimens. They were sourced from Akure, Southwestern Nigeria, and kept clean and dry to prevent bulking of aggregates. Crushed granite stones with a maximum size of 20 mm conforming to the requirements of ASTM C33/C33 M and BS 882 (1992) were used. A sieve analysis test and specific gravity test were carried out following BS EN 12620:2002 on both the fine and coarse aggregates.

Potable water and seawater following the requirements of BS EN 1008:2002, were used for the mixing and curing of concrete cubes. The water samples were tested to have pH values of 6.03 and 7.14 for the FW and the SW, respectively.

The freshwater and seawater used for the mixing and curing of the concrete cubes were tested at the Department of Chemistry, Federal University of Technology, Akure, Nigeria, for several chemical properties and physical properties. The freshwater was found weakly acidic/neutral while the seawater was very neutral. As expected, the seawater used had very high content, 22.465 mg/L of Na⁺ of and 76.205 mg/L of K⁺ compared to the 2.017 mg/L and 5.621 mg/L respectively for freshwater.

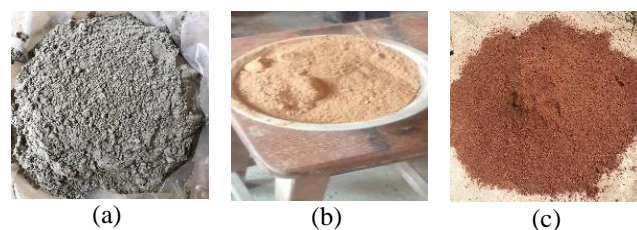


Figure 1. Materials used (a) ordinary Portland cement (OPC) (b) fly ash (FA) (c) Lateritic soil.

Table 1. Properties of the binders

Properties / Parameters	OPC	FA
Specific gravity (kg/m ³)	3.02	2.35
Initial setting time (minutes)	75	-
Final setting time (minutes)	270	-
Normal consistency (%)	26	-
Moisture content (%)	-	16.35
Dry density (g/cm ³)	-	0.458

Methods

The constituents of concrete were batched by weight based on the mix ratio of 1:1.5:3 with a target strength of 20 N/mm² at 28 days of curing.

Fly ash was added as a partial substitute for cement at 0%, 5%, 10%, 15%, and 25%, while laterite was used to replace fine aggregate at 0%, 10%, 20%, and 30%. Fine aggregate and binders (cement and fly ash) were first thoroughly mixed before coarse aggregates were added. A water-binder ratio of 0.55 was adopted, and a slump test was carried out. The freshly mixed concrete was filled into moulds in three layers of approximately 50 mm before compacting with 25 strokes of the tamping rod. Four different types of combinations were made with a total of 360 cubes. The first mixture included mixing the constituents with freshwater and curing the cubes in freshwater. This served as the control mix. Two other combinations included mixing with freshwater and curing in seawater, and vice-versa. The last mix had seawater as both the mixing and curing water.

A total of 360 cubes were cast and tested for compressive strength at 28 days of curing. The compressive strength test was carried out on cubes with a size of 150 mm x 150 mm x 150 mm in accordance with BS EN 12390-2. An ELE Compression Testing Machine with a loading capacity set to 2000 kN was used to determine the strength. Concrete specimens of size 200 mm x 50 mm x 50 mm were tested according to BS 812-120: 1989. They were cast and demoulded after 24 hours and placed in air to cure for the shrinkage to be monitored.

RESULTS AND DISCUSSION

Physical properties of materials used

The specific gravity test was carried out on fine aggregate, coarse aggregate, fly ash, and laterite. The results were 2.74, 2.63, 2.35, and 2.63, respectively. All the values conform to the required standard as specified in ASTM C127 (2015), so they can be used in concrete works. The sieve analysis test was carried out following BS EN 12620:2002. The result of the test carried out on Akure Pit Sand (APS) and laterite is shown in Figure 2. The sand was well graded with coefficients of uniformity (C_u) and coefficient of gradation (C_c) of 1.71 and 1.04 respectively. The laterite used was a silt-clay material, as 50.18% of its sample passed through sieve No. 200 (0.075mm). The sand was fine sand, with 92.67% passing the 75 mm sieve size and retaining the 2 mm sieve size. For the crushed granite stones used, they were purely grave material.

The fly ash used for the preparation of concrete specimens was characterized using X-ray fluorescence (XRF) analysis. The results, as shown in Figure 3 show that it contains a high percentage of SiO₂. The oxide composition test also indicated that the fly ash contained a SiO₂ content of 57.35% which is more than the 25% recommended by BS EN 197-1 (2011) for pozzolans. It was also a class F pozzolan (SiO₂ + Al₂O₃ + Fe₂O₃ > 70%) according to ASTM C618-12a, so it was suitable for replacing cement (see Figure 2).

The setting times of cement were determined using freshwater and seawater. The initial and final setting times were 148 minutes and 205 minutes for freshwater, and 106 minutes and 128 minutes when seawater was used. These values are in line with Ghalehnovi et al., 2010 and Uzoh et al., 2017. They also conform to the limit set by BS EN 197-1:2011 for grade 42.5N cement. The fineness value for the cement was 1.77%. The average water absorption for fine aggregate and coarse aggregate are 0.55% and 0.71% respectively. The bulk density of crushed granite stone was 1.71 g/cm³.

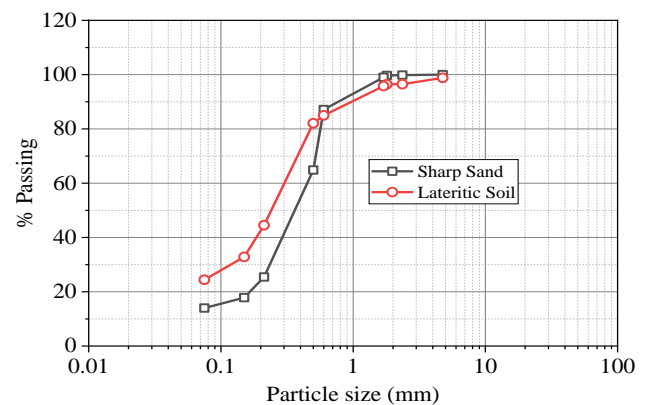


Figure 2. The grain size distribution of sand and lateritic soil.

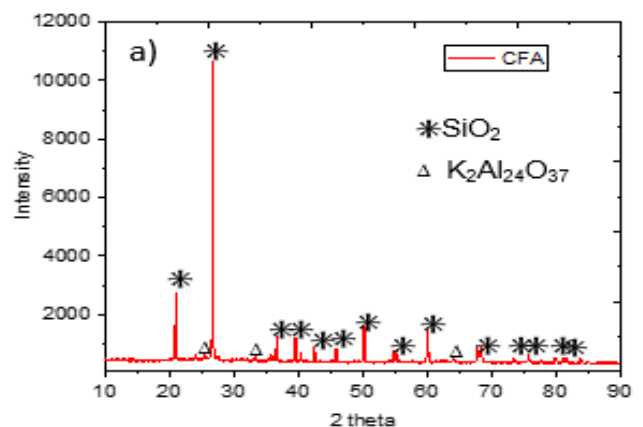


Figure 3. X-ray Diffraction (XRD) pattern of coal fly ash.

Table 2. Chemical and physical properties of OPC and FA.

Oxide (%)	CaO	SiO ₂	Al ₂ O ₃	Fe ₂ O ₃	MgO	K ₂ O	SO ₃
FA	1.72	57.2	28.6	6.58	1.78	2.81	0.02

Compressive strength

The strength values for the four different environments are presented in Figures 4, 5, 6 and 7. The compressive strength for the different concrete cube samples generally increases with an increase in curing days. This agrees with the findings of Sata *et al.* (2007). It is evident that all the conventional concrete produced from the control had a higher strength than the blended Portland cement-fly ash lateritized concrete at 28 days of curing. At 28 days of curing, the SW-SW cubes gave the best strength values: 22.38 N/mm², 22.53 N/mm², 22.67 N/mm², 22.62 N/mm², and 22.16 N/mm² for 0%FA/0% Lat., 5% FA/0% Lat. 10% FA/0% Lat., 15% FA/0% Lat., and 25% FA/0% Lat., respectively. These values were found to be higher than 21.91 N/mm², 21.87 N/mm², 21.85 N/mm², 21.88 N/mm², and 21.85 N/mm² obtained for corresponding FW-FW cubes at 28 days of curing.

However, at 56 days, FW-FW cubes gave the highest strength values of 26.59 N/mm², 26.79 N/m², 27.47 N/mm², 26.82 N/mm² and 27.79 N/mm² for 25% FA/0% Lat., 15% FA/0% Lat., 10% FA/0% Lat., 5% FA/0% Lat., and 0% FA/0% Lat., respectively which exceeded the target strength of 20N/mm².

Cubes produced with 10% fly ash and 10% laterite generally gave the highest strength of 26.82 N/mm² in terms of replacement, next to the control mix.

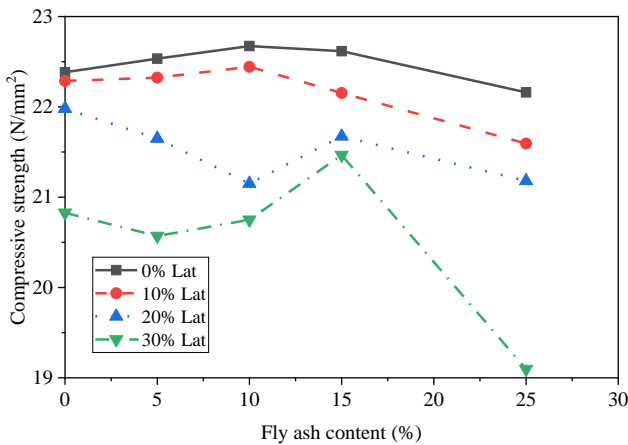


Figure 4. Compressive strength (N/mm²) against % of fly ash for SW-SW cubes at 28 days.

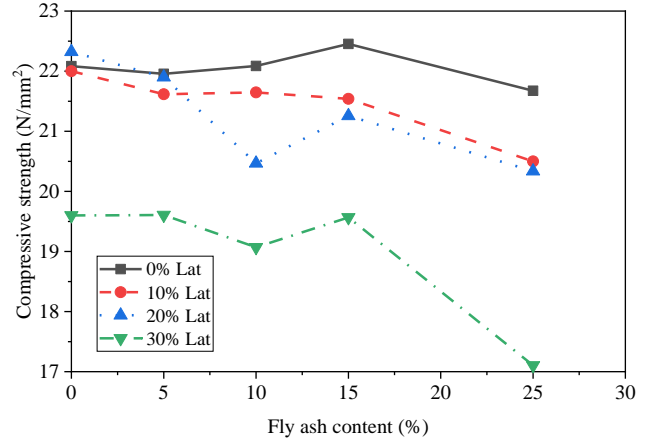


Figure 5. Compressive strength (N/mm²) against % of fly ash for SW-FW cubes at 28 days.

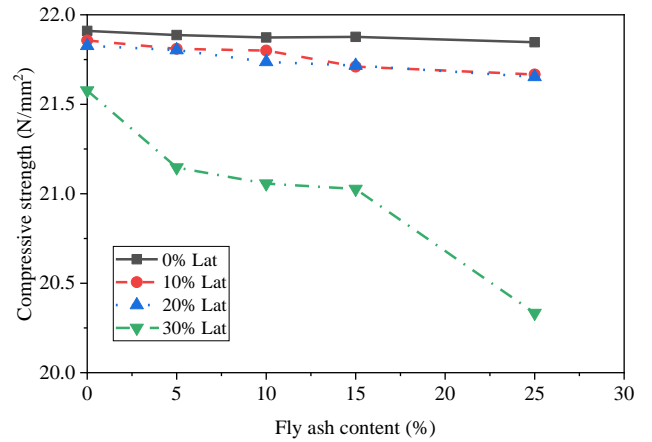


Figure 6. Compressive strength (N/mm²) against % of fly ash for FW-FW cubes at 28 days.

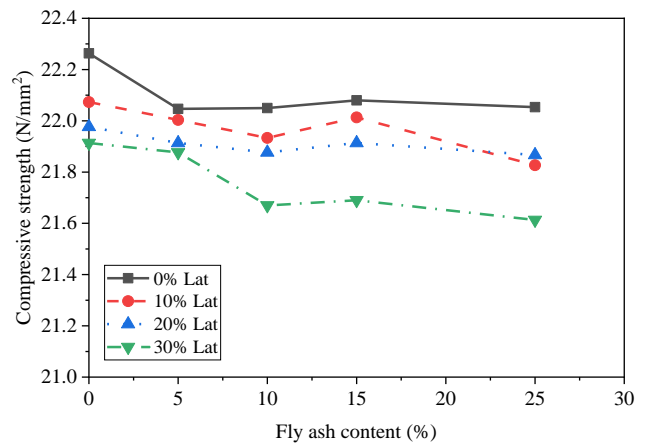


Figure 7. Compressive strength (N/mm²) against % of fly ash for FW-SW cubes at 28 days.

CONCLUSION

A study on the effects of Blended Portland-Fly Ash Cement on Compressive Strength of Seawater Mixed and Cured Lateritic Concrete and the following conclusions can be drawn:

(1) Fly ash possesses pozzolanic properties and can therefore be used as a cementitious material in concrete. Drying shrinkage and compressive strength of concrete reduce with an increase in fly ash content. Curing periods had a significant effect on the strength development of blended Portland cement-fly ash lateritized concrete, as there was strength gain with increasing curing age for all fly ash and laterite replacement levels.

(2) The strength of the control mix was generally slightly higher than that of the blended Portland cement-fly ash seawater-mixed and cured lateritized concrete. Though the strength compared well.

(3) 10% fly Ash and 10% laterite are recommended for the replacement of cement and sand, respectively, in plain concrete works. Recycling activities for wastes like fly ash should be encouraged by all institutions. Technology should be developed for the production of fly ash and other pozzolans so they can be readily available for concrete work.

Finally, seawater can be used for mixing and curing plain concrete in place of freshwater and for reinforced concrete if the reinforcing material is non-corroding.

DECLARATIONS

Corresponding Author

Correspondence and requests for materials should be addressed to Stephen Adeyemi Alabi; E-mail: alabisa@ub.ac.bw; ORCID: 0000-0001-8731-6961

Data availability

The datasets used and/or analysed during the current study available from the corresponding author on reasonable request.

Acknowledgements

The authors would like to acknowledge the Office of Research and Development (ORD), University of Botswana for sponsoring the presentation of these findings at the International Conference on Civil Engineering for Sustainability and Resilience in the 21st Century and Beyond (ICCESR 2024) at the University of Botswana and the Federal University of Technology, Akure, Nigeria,

for creating a conducive environment to conduct this research.

Authors' contribution

SA Alabi developed the concept for the research and designed the experimental process. C Arum and AR Akande assisted in the design of the experimental process of writing the manuscript. SA Alabi, J Mahachi and JO Afolayan carried out the bench work and wrote the draft manuscript. All the authors read and approved the final manuscript

Competing interests

The authors declare no competing interests in this research and publication.

REFERENCES

- Al-Ani, M. and Hughes, B. (1989). Pulverized-fuel ash and its uses in concrete, *Magazine of Concrete Research*. 41 (147), 55-63. DOI: <https://doi.org/10.1680/macr.1989.41.147.63>
- ASTM C127-15 (2015). Standard Test Method for Density, Relative Density and Absorption of Coarse Aggregate. ASTM International.
- ASTM C33-18 (2018). Standard Specification for concrete aggregates. ASTM International.
- ASTM C618-12a (2012). Standard Specification for Coal Fly Ash and Raw or Calcined Natural Pozzolan for Use in Concrete. ASTM International
- Azad, A. K., Rokanuzzaman, M. and Hossain, M. M. (2016). Effect of fly ash on the mechanical properties of concrete. *International Journal of Engineering and Technology*. 8 (2), 1017-1024. <https://doi.org/10.2478/jaes-2018-0016>.
- Basavana, S. N., Gowda, C., Rajasekaranb and Subhash C. Yaragal. (2015). Significance of processing laterite on strength characteristics of lateritized concrete, *IOP Conference Series: Materials Science and Engineering*, 431 082003, DOI: <https://doi.org/10.1088/1757-899X/431/8/082003>
- BS 882 (1992). Specification for aggregates From natural sources for concrete. British Standard Institution, London, United Kingdom
- BS EN 1008 (2002). Mixing water for concrete – Specification for sampling, testing and assessing the suitability of water, including water recovered from processes in the concrete industry, as mixing water for concrete. BSI, London, UK.
- BS EN 12620. (2002). Aggregates for Concrete. (AMD Corrigendum 15333)
- BS EN 197-1. (2011). Cement Composition, specifications and conformity criteria for common cements. European Standard Specifications
- El-Reedy, M. A. (2017). *Steel-Reinforced Concrete Structures: Assessment and Repair of Corrosion*, CRC Press. DOI: <https://doi.org/10.1201/b22237>
- Folagbade, S. O. and Aluko, O. (2019). Permeation Resistance of Sawdust Ash Blended Cement Lateritized Concrete. *Civil*

- Engineering Dimension. 21(2), 76-83. DOI: <https://doi.org/10.9744/ced.21.2.76-83>
- Ghalehnovi, S.S., Kadir, R.A. and Behbahani, H. (2010). Evaluation of Setting Time of Concrete Containing High Volume Fly Ash. *International Journal of Civil Engineering*. 8(2), 94-101.
- Khatib, J. M. and Bayasi, Z. H. (2003). Strength and durability of seawater-mixed concrete. *Cement and Concrete Research*. 33(10), 1565-1570.
- Kishore, K. S. K., Ravindra, G., and Rao, M. C. (2017). An experimental study on the effect of fly ash on the compressive strength of concrete. *International Journal of Innovative Research in Science, Engineering and Technology*. 6(8), 16584-16591.
- Kumar, A. (2017). *Effect of Curing and Mixing Concrete Proportion on Drying Shrinkage of concrete*. Master's thesis. Texas, A&M University.
- Lee, H. S., Moon, J. and Cho, S. W. (2008). Influence of curing in seawater on the properties of concrete. *Cement and Concrete Research*. 38(6), 840-846.
- Marie, I. & Quiasrawi, H. (2012). Closed loop recycling of recycled concrete aggregates. *Journal of Cleaner Production*, 37, 243-248. DOI: <https://doi.org/10.1016/j.jclepro.2012.07.020>
- Mekonnen, M. M., & Hoekstra, A. Y. (2016). Four billion people facing severe water scarcity. *Science Advances*. 2(2), e1500323. DOI: <https://doi.org/10.1126/sciadv.1500323>
- Miller, S. A., Horvarth, A., & Monteiro, P. J. M. (2016). Readily Implementable techniques can cut annual CO₂ emissions from the production of concrete by over 20%. *Environ. Res. Lett.* 11(7), 74029. DOI: <https://doi.org/10.1088/1748-9326/11/7/074029>
- Miller, S. A., Horvarth, A., & Monteiro, P. J. M. (2018). Impacts of booming concrete production on water resources worldwide. *Nat. Sustain.* 1, 69-76. DOI: <https://doi.org/10.1038/s41893-017-0009-5>
- Miller, S., Shemer, H., & Semiat, R. (2015). "Energy and environmental issues in desalination." *Desalination*, 366, 2–8. DOI: <https://doi.org/10.1016/j.desal.2014.11.034>
- Monteiro, P. J. M. & Miller, S. A. (2017). Towards Sustainable Concrete. *Nat. Water*. 16, 698-699. DOI: <https://doi.org/10.1038/nmat4930>
- Ogunbode, E. B. (2010). *Performance characteristic of Fly ash/OPC Laterized Concrete*, M.Sc. Thesis, Department of Building, University of Jos.
- Ogunjiofor, E. I. (2020). Possibility of Usage of Seawater for Mixing and Curing of Concrete in Salty Water Localities. *Journal of Engineering Research and Reports*. 2, 19–27. DOI: <https://doi.org/10.9734/jerr/2020/v19i317234>
- Sata, V., Chai, J. and Kraiwood, K. (2007). "Influence of pozzolan from various by-product materials on mechanical properties of high-strength concrete". *Construction and Building Materials*. 21, 1589 – 1598. DOI: <https://doi.org/10.1016/j.conbuildmat.2005.09.011>
- Uzoh, O.C., Nwachukwu, P.C. and Unadi, E.U. (2017). Evaluation of Setting Time and Compressive Strength of Concrete with Rice Husk Ash. *Journal of Materials Science and Engineering*, 5(1), 29-35.
- Younis, A., Ebead, U., Suraneni, P. & Nanni, A. (2018). Fresh and hardened properties of seawater-mixed concrete. *Construction and Building Materials*. 190, 276–286. DOI: <https://doi.org/10.1016/j.conbuildmat.2018.09.126>

Publisher's note: [Scienceline Publication](#) Ltd. remains neutral with regard to jurisdictional claims in published maps and institutional affiliations.



Open Access: This article is licensed under a Creative Commons Attribution 4.0 International License, which permits use, sharing, adaptation, distribution and reproduction in any medium or format, as long as you give appropriate credit to the original author(s) and the source, provide a link to the Creative Commons licence, and indicate if changes were made. The images or other third party material in this article are included in the article's Creative Commons licence, unless indicated otherwise in a credit line to the material. If material is not included in the article's Creative Commons licence and your intended use is not permitted by statutory regulation or exceeds the permitted use, you will need to obtain permission directly from the copyright holder. To view a copy of this licence, visit <https://creativecommons.org/licenses/by/4.0/>.

Statistical Evaluation of the Geometric Properties Steel Bars for Reinforced Concrete in Botswana

Adekunle P. Adewuyi , and Gaolatlhe B. Eric 

Department of Civil Engineering, University of Botswana, Gaborone, Botswana

Corresponding author's Email: AdewuyiA@ub.ac.bw

ABSTRACT

Uncertainties in construction materials, especially steel reinforcing bars, have multiplying adverse impacts on the integrity and reliability of constructed facilities from construction to service life stages. Botswana depends on importation of rebars to meet the ever-increasing demands for buildings and reinforced concrete civil infrastructure. The study assessed the mass and geometric properties of the two most utilized steel reinforcing bars, designated as M1 and M2, in Botswana. With the aid of digital analytical balance and Vernier calipers, measurements of mass per unit length and the relative rib area (RRA), which depends on nominal diameter, rib height, rib spacing, and longitudinal rib or gap thickness were made from 3000 standard bars each of nominal sizes from 8 mm to 25 mm randomly sampled at the suppliers' depots/warehouses and various construction sites in Gaborone and Francistown. The RRA is a measure of the surface geometry for interfacial bonding between steel reinforcing bar and the surrounding concrete. The geometric properties of each steel bar type of the nominal sizes were characterized in terms of the statistical parameters and compared for compliance with standard specifications such as CS2 (2012), ISO 15630, ACI A408. The actual mass and diameter of bars were within the tolerance of $\pm 1\%$ of the respective nominal size which satisfied all the standard requirements. Only the 8 mm diameter M2 bars did not have longitudinal ribs/gaps. ACI specifies a range of 0.10 to 0.14 for RRA, while CS2/ISO 15630 only specifies for the minimum RRA values of 0.040 for 8 to 12 mm bars and 0.056 for 16 to 25 mm bars. M2 bars of 10 mm dia. bars did not satisfy CS2/ISO 15630 requirements. However, M1 (8 mm and 12 mm) and M2 (10, 16 and 25 mm) bar sizes are below the minimum and M2 bars of 20 mm diameter are above the recommended RRA values of ACI A408. These would reduce the load carrying capacity of RC members reinforced with the unsatisfactory bar sizes.

Keywords: Surface geometry, reinforcing bars, relative rib area, interfacial bonding, statistical indices, load carrying capacity.

INTRODUCTION

Steel reinforced concrete has been used for decades as the construction material of choice because it is economical and versatile (Rabi et al., 2022; van Damme, 2018; Otieno, 2008; Jumaat et al., 2006). The embedded steel rebar has a good interfacial bonding with the surrounding concrete and an excellent tensile strength. It can still be bent or shaped for almost any concrete construction application (Sulaiman et al., 2017; Metelli and Plizzari, 2014; Zuo and Darwin, 2000a). The effectiveness of reinforcing bars in concrete is directly connected to the quality of the steel bars and the strength of concrete is good in compression, but weak in tension and flexure. The quality assurance of steel reinforcement in reinforced concrete (RC) infrastructure has not received considerable attention as the compressive strength of concrete at both the design and construction stages. This quality is an aggregation of

the physical, chemical and mechanical properties which are often determined from laboratory experimental and field testing (Bame et al., 2023). The use of sub-standard reinforcing steel bars causes structural defects, failures or ultimate collapse, which could result in loss of lives, properties, infrastructure and economic investments. Therefore, it is imperative to test the properties of steel bars to ensure their compliance with standard specifications, which are necessary to satisfy the ultimate and serviceability limit states (Alexander and Beushausen, 2019).

Efficient and effective transfer of force between reinforcement and concrete is required for optimal design of reinforced concrete structures. Three basic mechanics are required to effectively transfer force or stresses from a deformed reinforcing bar to the surrounding concrete. These are (1) the chemical adhesion between the reinforcing bar and the surrounding concrete; (2) the

RESEARCH ARTICLE
 PII: S225204302400010-14
 Received: June 25, 2024
 Revised: September 02, 2024
 Accepted: September 05, 2024

frictional forces arising from the roughness of the interface, forces transverse to the bar surface, and relative slip between the bar and the surrounding concrete; and (3) the mechanical anchorage or bearing of the ribs against the concrete surface (ACI 408R-03, 2012). Although the physical, chemical and mechanical properties of steel bars are critical for these three mechanics, they are most influenced by the cross-sectional and surface geometries.

Hence, for safety, reliability and durability of RC structures, compliance of the cross-section and surface geometries of steel rebars with relevant standards is fundamental both during construction and in service life. The conformity of the cross-section with the specification is a function of the agreement between the nominal and the actual diameter of bars, which determines the tensile strength of the member (Metelli and Plizzari, 2014; Zuo and Darwin, 2000a). On the other hand, the relative rib area, as a major parameter of the surface geometry, measure the adhesion, frictional forces and the interfacial bonding between steel and the surrounding concrete. This guarantees sufficient concrete-steel shear adhesion to prevent slippage of reinforcement in concrete (Sun et al. 2018; Barsic et al., 2012). The combination of the two is a measure of the load-carrying capacity of RC structural members in tension, compression or flexure. The geometric rib features of bars include the shape, width, height, spacing and inclination with respect to the longitudinal axis of the rods (Leramo et al., 2018). The relative rib area rather than the minimum rib height or the maximum rib spacing controls the bond strength between reinforcing steel and concrete (Metelli and Plizzari, 2014; Zuo and Darwin, 2000a; Zuo and Darwin, 2000b). This was based on a maximum average rib spacing equivalent to 70% of the nominal diameter of the bar and a minimum height of deformations equal to 4% for bars with a nominal diameter.

The purpose of this study was to assess the cross-sectional and surface geometries of steel reinforcing bars used in the import dependent Botswana construction industry. The study highlights the uncertainties that characterize the geometric properties of two most common reinforcing bars sampled from major suppliers and distributors spread over Gaborone and Francistown and the environs using ISO 15630, CS2 and ACI A408R Standards.

Theoretical Background for Relative Rib Area

a) CS2 (2012) and BS 4449:2005+A2:2009

Construction Standard CS2 (2012) is the publication of the Standing Committee on Concrete Technology by

the Government of Hong Kong. It is an extract of Steel for the reinforcement of concrete (BS 4449:2005+A2:2009), a publication of British Standards Institution. CS2 (2012) and BS 4449 (2009) specify the relative rib area, for ribbed steel reinforcing bars using the Simpson’s rule formula as shown in Equation (1):

$$f_R = \frac{(2a_{1/4} + a_m + 2a_{3/4})(\pi d - \sum e_i)}{6\pi dc} \quad [1]$$

where $a_{1/4}$, a_m , $a_{3/4}$ are the height of transverse ribs at the quarter-point, mid-point, and three-quarters point respectively measured as the mean of at least three measurements in this position per row on different transverse ribs. $\sum e_i$ is the part of the circumference without ribs determined as the sum of the average gap (e) between each pair of two adjacent ribs. e is determined from at least three measurements. d is the nominal diameter of the bar and c is the average spacing of the transverse ribs.

A typical surface rib geometry with two rows in transverse ribs is shown in Figure 1. The recommended average rib height, h is 0.03d to 0.15d, the rib spacing c is 0.4d to 1.2d, and the transverse rib inclination angle, β is 35° to 75°. The minimum allowable relative rib area are 0.035, 0.040 and 0.056 for $d \leq 6$, $6 < d \leq 12$ and $d > 12$, respectively.

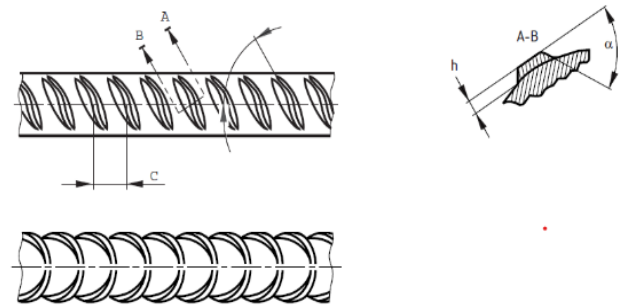


Fig. 1. Surface rib geometry with two rows of transverse ribs

b) ISO 15630-1-2010

The relative rib area specified by ISO 15630-1 (2010) is as expressed in Equation (2)

$$f_R = \frac{1}{\pi d} \sum_{i=1}^n \frac{\frac{1}{m} \sum_{j=1}^m F_{R,i,j} \sin \beta_{i,j}}{C_i} + \frac{1}{p} \sum_{k=1}^q a'_k \quad [2]$$

where n = number of rows of transverse ribs on the circumference, m = number of different transverse rib inclinations per row, q = number of longitudinal ribs for cold-twisted bars, p = pitch for cold-twisted bars determined as the mean of the distances between two consecutive corresponding points of a longitudinal rib on the same longitudinal line, for each longitudinal rib.

where $F_R = \sum_{i=1}^p (a_{s,i} \Delta l)$ is the area of the longitudinal section of one rib (Figure 2), where $a_{s,i}$ is the average height of a portion i of a rib subdivided into p parts of length Δl .

c) ACI 408R (2012)

According to ACI 408R (2012) defines the relative rib area as the ratio of the projected rib area normal to the bar axis to the product of the nominal bar perimeter and the

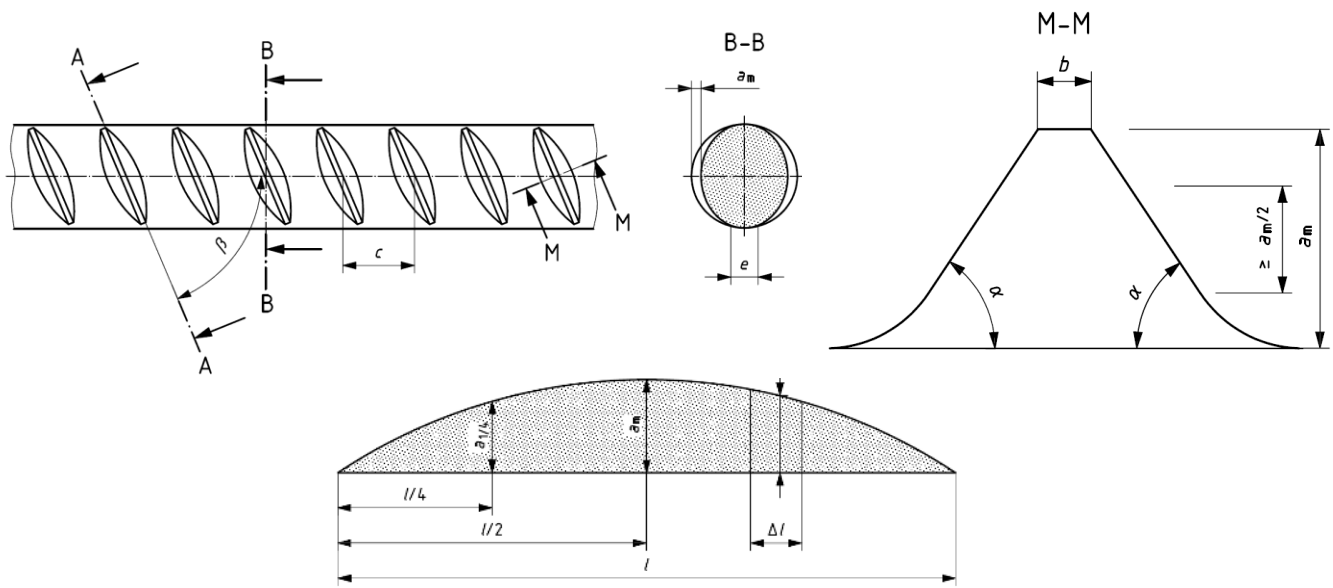
average centre-to-centre rib spacing as expressed in Equation (3).

$$R_r = \frac{h_r}{s_r} \left(1 + \frac{\sum \text{gaps}}{p} \right) \tag{3}$$

where h_r = average rib height, s_r = average rib spacing, $\sum \text{gaps}$ = sum of gaps between ends of transverse deformations, and p = actual perimeter.

For steel reinforcing bars with no gaps or longitudinal ribs, $\sum \text{gaps} = 0$, and R_r becomes

$$R_r = \frac{\text{Bearing area, } \pi d h_r}{\text{Shearing area, } \pi d h_r} = \frac{h_r}{s_r} \tag{4}$$



Section A-A is a flattened representation of a transverse rib.

Fig. 2. Determination of the rib flank inclination (α) and determination of the area of the longitudinal section of one rib (F_R)

MATERIALS AND METHODS

Assessment of reinforcing steel bars used in construction, specifically focusing on samples imported into the country from two major manufacturers designated as M1 and M2 was conducted. The assessment involved testing the physical and geometric properties of these steel bars, which were ribbed or deformed.

All 3000 random samples were sourced from various suppliers' warehouses, distributors' shops and various construction sites in Gaborone and Francistown and the environs. The samples of steel reinforcing bars from nominal diameter 8 mm to 25 mm of standard length 6 m are as shown in Figure 3.



Figure 3. Samples of M1 and M2 steel bars

1. **Random selection of samples:** Reinforcing steel bars were randomly selected from tonnes of imported material from major suppliers, distributors' storehouses and construction sites in Gaborone and Francistown and the surrounding areas for measurement. 3000 samples of each nominal bar sizes from 8 mm to 25 mm were considered for the study.

2. **Measurement parameters:** The measurements focused on four key geometric properties:

- Actual diameter was measured by placing the outside jaws of the electronic vernier caliper around a point between two transverse ribs, perpendicular to the longitudinal rib.
- Rib height was measured by positioning the knife-edge of the calipers over two adjacent ribs and extending the depth gauge until it contacts the bar.
- Rib spacing was measured by placing the outside jaws of the digital calipers between two adjacent transverse ribs.
- The gap due on the longitudinal rib was measured by placing the outside jaws of the calipers over the outer edge of the longitudinal rib.

This process ensures accurate measurement of the geometric properties of the reinforcing bars, which is crucial for quality control and compliance with standards as stated in ASTM A615 are shown in Fig. 4.

The following equations were used for statistical analysis of the results obtained for.

$$\text{Mean: } \bar{x} = \frac{\sum_{i=1}^n x_i}{n} \quad [5]$$

$$\text{Standard deviation: } s = \frac{\sum \sqrt{|x_i - \bar{x}|^2}}{n-1} \quad [6]$$

$$\text{Coefficient of variation, CoV} = \frac{s}{\bar{x}} \quad [7]$$

$$\text{Skewness, } s_k = \frac{n}{(n-1)(n-2)} \frac{\sum_{i=1}^n (x_i - \bar{x})^3}{s^3} \quad [8]$$

Kurtosis,

$$k_{ts} = \frac{n(n+1)}{(n-1)(n-2)(n-3)} \sum_{i=1}^n \left(\frac{(x_i - \bar{x})^4}{s^4} \frac{3(n-1)^2}{(n-2)(n-3)} \right) \quad [9]$$

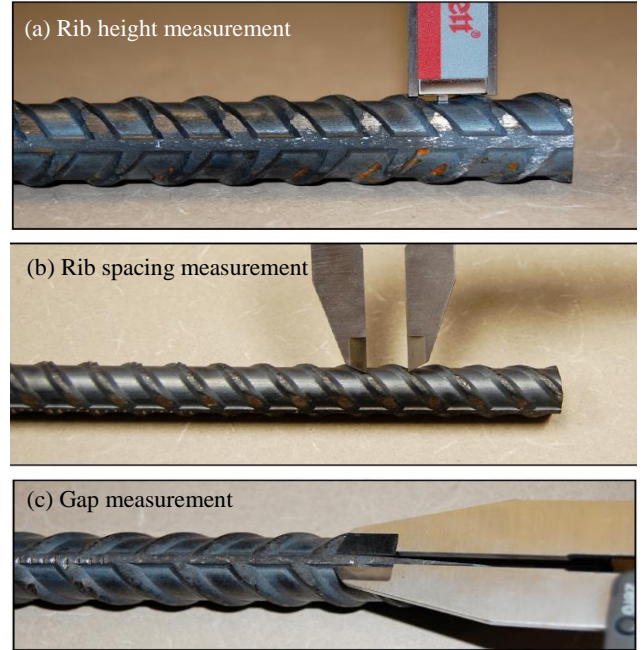


Figure 4. Measurement parameters for relative rib

RESULTS AND DISCUSSION

The average measurement data for the geometric properties of sampled 8 mm, 10 mm, 12 mm, 16 mm, 20 mm and 25 mm diameter steel reinforcing bars is summarized in Table 1 to provide a comprehensive overview of the experimental results and statistical analysis of the geometric properties of the sampled steel reinforcing bars. They are crucial for understanding the variability and quality of the bars tested, which is essential for ensuring compliance with standards and quality control in construction and engineering applications.

Actual mass per meter of steel reinforcing bars

The average mass per unit length (in kg/m) of 3000 samples for each nominal size of M1 and M2 were measured as shown on Table 1. The results showed that the measured samples from M1 and M2 are agreeable to as specified by mass per meter in BS 4449 (2005) for all diameter sizes. The standard deviations were all agreeable to the given tolerance. It has been noted that diameter 20 mm of M1 has the least uncertainties as it has the lowest coefficient of variation (CoV). The results shows that most of samples of 8 mm diameter were closer to the mean value as compared to other diameters.

Table 1. Average mass of steel reinforcing bars

Type	Statistical Analysis	Nominal bar diameter					
		8 mm	10 mm	12 mm	16 mm	20 mm	25 mm
M1	Average (kg/m)	0.397	0.618	0.885	1.577	2.469	3.857
	Standard deviation	0.020	0.026	0.037	0.064	0.095	0.155
	COV (%)	5.098	4.153	4.134	4.063	3.861	4.010
M2	Average (kg/m)	0.395	0.617	0.887	1.578	2.465	3.835
	Standard deviation	0.023	0.027	0.041	0.078	0.114	0.174
	COV (%)	5.745	4.343	4.615	4.941	4.638	4.543

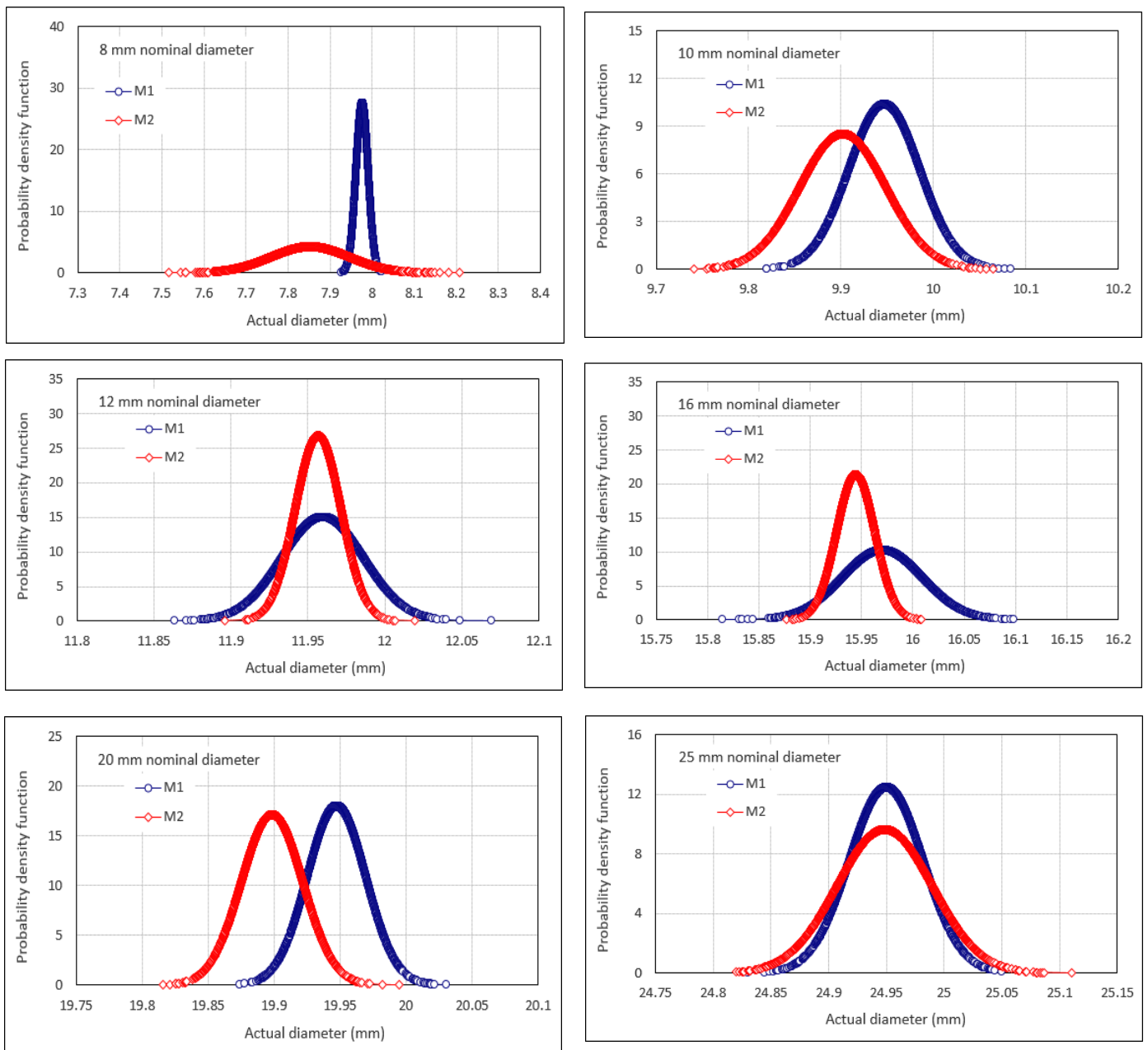


Figure 5. Probability density function curves of 8 mm to 25 mm nominal bar

Actual diameter of steel reinforcing bars

The statistical analysis and probability density function curves of actual diameters in Fig. 5 shows that the average actual diameters of M1 samples were slightly greater than average actual diameters of M2 with an exception to the actual diameters of 12 mm and 25 mm sizes which were the same for both M1 and M2. The median values of the measured samples shows that most of the samples from both M1 and M2 were close to the average diameter sizes from 8 mm to 25 mm.

Figure 6 presents the statistical parameters of the analysis of the 3000 random samples such as the standard deviation, CoV, skewness and kurtosis of all actual diameters bar sizes for the cross-sectional geometry. The standard deviation of M2 samples for diameter sizes 8 mm, 10 mm and 25 mm, high which brings about high CoV of those samples. The higher the CoV, the higher the variability of results obtained. For M1 samples, diameter

size of 16 mm showed a higher dispersion of results from the average value followed by 10 mm and 25 mm sizes in terms of standard deviation.

Skewness of the normal distribution curves were assessed to verify how symmetrical the curves were to the mean value while kurtosis was calculated to measure the risk or uncertainty of data obtained by classifying curves as peaked or flat. The criteria used was between -0.5 and 0.5, the data are fairly symmetrical, between -1 and -0.5 or between 0.5 and 1, the data are moderately skewed and lastly skewness less than -1 or greater than 1, the data are highly skewed. For kurtosis, the general guideline is that if the number is greater than +1, the distribution is too peaked while a kurtosis of less than -1 indicates a distribution that is too flat. The results shows that all diameters from M1 and M2 were fairly skewed and very low risk/uncertainty in terms of graphs being peaked or flat.

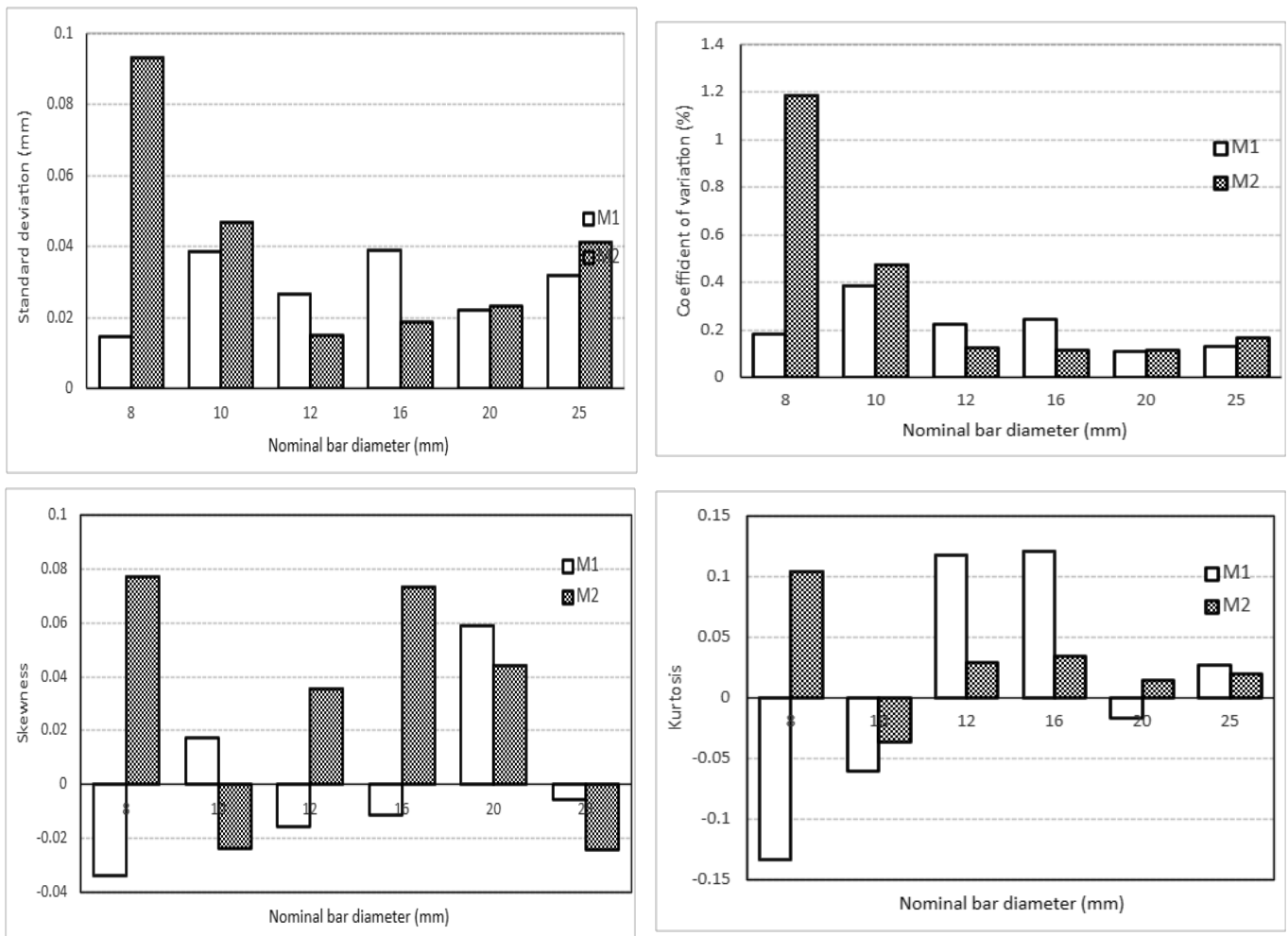


Figure 6. Statistical parameters of cross-sectional variability in bar sizes

Relative rib area

Average relative rib areas for all nominal bar size samples of both M1 and M2 are compared by bar graphs in Fig. 7. The results show that ISO 15630 (2010) produced the highest RRA values and was closely followed by ACI 408R (2012) and lastly CS2 (2012) which was comparative to BS 4449 (2005). With ISO 15630, RRA for M1 was very high for bar sizes 16 mm, 20 mm and 25 mm whereas for M2 is high in 12 mm, 20 mm and 25 mm bar sizes. The bars for M1 and M2 met requirements for RRA when using all standards except for few cases with ACI 408. M1 (8 mm and 12 mm) and M2 (10, 16 and 25 mm) bar sizes were below the minimum and M2 bars of 20 mm diameter were above the recommended RRA threshold values of ACI A408. Bond strength is strongly dependent on the relative rib area because an increase in relative rib area from 0.04 to 0.10 leads to an increase of bond strength of up to 40% (Metelli & Plizzari, 2014).

The fib Model Code (2010) which requires $RRA \geq 0.05$ reveals that the RRA values above 0.14 may develop higher bond stresses. Lower relative rib area and higher coefficient of variation increases uncertainties. The standard deviation of samples was low, but 10 mm diameter bars of M2 steel bars recorded high CoV values. Uncertainties are most likely where CoV was as high as evident with the actual diameter of 8 mm and 10 mm of M2. Diameter 8 mm of M2 had the highest values for skewness and kurtosis showing that it is highly skewed to the left and a highly peaked. A high positive kurtosis is considered as a risk because it is a leptokurtic distribution showing heavy tails on either side. They have large outliers as compared to all other diameter sizes. This concludes that M1 samples were preferred to M2 which are characterized by some relative rib area. The statistical summary of the measured diameters of bars for M1 and M2 reinforcing bars are summarized in Table 2, while

Table 3 to Table 6 present the statistical summary of the relative rib areas computed by different international and national models.

Studies have shown that relative rib area rather than the minimum rib height or the maximum rib spacing influences the bond stress between reinforcing steel and the surrounding concrete. In addition, high relative rib area of steel bars may enhance bond strength (Barbosa et al. 2008, Metelli & Plizzari, 2014).

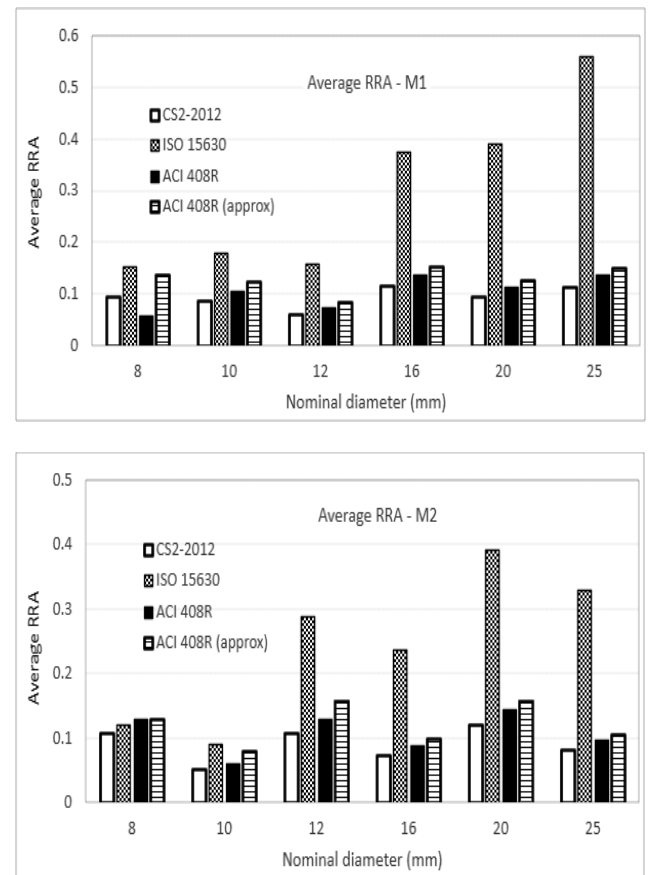


Figure 7. Relative rib areas of all nominal bar sizes for different standards

Table 2. Statistical summary of actual diameter of reinforcing bars

Bar size (mm)	8		10		12		16		20		25	
	M1	M2	M1	M2	M1	M2	M1	M2	M1	M2	M1	M2
Statistical parameters												
Average	7.98	7.85	9.95	9.90	11.96	11.96	15.97	15.94	19.95	19.90	24.95	24.95
COV (%)	0.18	1.19	0.39	0.47	0.22	0.12	0.24	0.12	0.11	0.12	0.13	0.17
Skewness	-0.03	0.08	0.02	-0.02	-0.02	0.04	-0.01	0.07	0.06	0.04	-0.01	-0.02
Kurtosis	-0.13	0.10	-0.06	-0.04	0.12	0.03	0.12	0.03	-0.02	0.02	0.03	0.02

Table 3. Statistical summary of relative rib areas computed by CS2 (2012)

Bar size (mm)	8		10		12		16		20		25	
Statistical Parameters	M1	M2	M1	M2	M1	M2	M1	M2	M1	M2	M1	M2
Average	0.094	0.107	0.087	0.051	0.061	0.107	0.115	0.074	0.094	0.121	0.114	0.081
COV (%)	2.66	2.66	2.81	12.23	2.07	0.78	1.36	0.96	1.25	4.20	1.49	3.15
Skewness	0.008	0.123	-0.001	0.105	0.011	-0.004	0.048	-0.045	0.025	0.131	0.024	0.006
Kurtosis	0.014	-0.047	0.021	0.004	0.064	0.023	-0.087	-0.038	-0.083	-0.014	-0.007	0.118

Table 4. Statistical summary of relative rib areas estimated by ISO 15630

Bar size (mm)	8		10		12		16		20		25	
Statistical Parameters	M1	M2	M1	M2	M1	M2	M1	M2	M1	M2	M1	M2
Average	0.154	0.121	0.179	0.091	0.157	0.289	0.376	0.238	0.392	0.392	0.561	0.329
COV (%)	5.25	7.27	6.14	19.83	3.55	1.27	2.24	2.11	2.28	11.07	7.97	10.83
Skewness	0.006	-0.117	-0.050	0.151	0.034	0.033	-0.201	-0.057	-0.007	-0.149	-1.356	-0.212
Kurtosis	-0.006	0.114	0.019	-0.010	-0.058	-0.024	0.146	-0.035	0.102	0.022	2.295	0.038

Table 5. Statistical summary of relative rib areas computed by ACI 408R-03

Bar size (mm)	8		10		12		16		20		25	
Statistical Parameters	M1	M2	M1	M2	M1	M2	M1	M2	M1	M2	M1	M2
Average	0.059	0.129	0.104	0.061	0.073	0.129	0.138	0.089	0.113	0.145	0.137	0.097
COV (%)	4.18	3.65	4.55	19.35	3.31	1.11	1.62	1.61	2.05	5.94	2.43	5.25
Skewness	0.070	0.077	0.060	0.094	0.030	0.027	0.071	-0.039	0.068	0.027	0.078	-0.012
Kurtosis	-0.119	-0.071	-0.025	-0.029	-0.062	-0.041	0.015	-0.006	-0.007	-0.039	-0.015	-0.154

Table 6. Statistical summary of relative rib areas estimated ACI 408R-03 (approx)

Bar size (mm)	8		10		12		16		20		25	
Statistical Parameters	M1	M2	M1	M2	M1	M2	M1	M2	M1	M2	M1	M2
Average	0.138	0.129	0.124	0.079	0.085	0.158	0.153	0.100	0.126	0.158	0.151	0.106
COV (%)	4.08	3.65	4.55	19.30	3.31	1.10	1.62	1.61	2.05	5.94	2.43	5.25
Skewness	0.055	0.077	0.063	0.088	0.031	0.024	0.073	-0.031	0.068	0.028	0.081	-0.014
Kurtosis	-0.158	-0.071	-0.026	-0.036	-0.053	-0.060	0.009	-0.001	-0.003	-0.036	-0.011	-0.154

CONCLUSIONS

The following salient conclusions can be drawn from the study. The average mass of steel reinforcing bar samples of M1 and M2 were almost the same for all diameters and met all standard requirements. However, the standard deviation and the CoV of nominal bar size 8 mm for M2 were evidently conspicuously high at 0.09 and 1.19% respectively, but still fell within the acceptable limit. The average actual diameters of M1 and M2 were slightly lower than all nominal diameters though fulfilled the requirement with their tolerance. M1 (8 mm and 12 mm) and M2 (10, 16 and 25 mm) bar sizes are below the minimum and M2 bars of 20 mm diameter are above the recommended RRA values of ACI A408. Relative rib area calculated using ISO 15630 and CS2 met the requirements. In conclusion, M1 have better properties as no risks were detected on actual diameters and relative rib areas, and as such enhances the interfacial bonding, tension and flexural capacity of RC structures.

DECLARATIONS

Corresponding author

Correspondence and requests for materials should be addressed to Adekunle P. Adewuyi; Email: AdewuyiA@ub.ac.bw; ORCID: 0000-0001-8190-7357

Data availability

The datasets used and/or analysed during the current study are available from the corresponding author on reasonable request.

Acknowledgements

The authors would like to acknowledge the Office of Research & Development of the University of Botswana for the internal funding for this research project R1207. The technical staff of the Structural Engineering Laboratory of the Department of Civil Engineering are also appreciated for their support and for creating a conducive environment to conduct this research.

Authors' contribution

AP Adewuyi initiated the research idea, identified the research gaps in the existing literature, designed the experimental process, verified the analyzed data obtained and partly wrote and revised the manuscript. GB Eric developed the proposal, conducted the field study designed, implemented the experimental plan, analyzed

the data and wrote the manuscript. Both authors read and approved the final manuscript.

Competing interests

The authors declare no competing interests in this research and publication.

REFERENCES

- ACI Committee 408R (2012). Splice and development length of high relative rib area reinforcing bars in tension (ACI 408.3R-09), Farmington Hills, Michigan: American Concrete Institute.
- Alexander, M., Beushausen, H. (2019). Durability, service life prediction, and modelling for reinforced concrete structures – review and critique. *Cement and Concrete Research*, 122, 17-29. <http://dx.doi.org/10.1016/j.cemconres.2019.04.018>
- Bame, P.C., Yamb, B.E., Ndigu, B. (2023), Assessment of deviation in quality of steel reinforcing bars used in some building sites in Cameroon, *World Journal of Engineering and Technology*, 11, 917-931. <http://dx.doi.org/10.4236/wjet.2023.114061>
- Barbosa, M.T.G., Filho, E.S.S., de Oliveira, T.M., dos Santos, W.J. (2008) Analysis of the relative rib area of reinforcing bars pull out tests, *Materials Research*, 11(4), 453-457. <http://dx.doi.org/10.1590/S1516-14392008000400013>
- Basic, G., Butkovic, I., Simunovic, V., Katic, M. (2012), Analysis of dimensional characteristics of the ribs on steel bars for reinforcement of concrete, *Annals of DAAAM for 2012 & Proceedings of the 23rd International DAAAM Symposium*, 23(1), 351 - 354.
- BS 4449:2005+A2 (2009), Steel for the reinforcement of concrete — Weldable reinforcing steel — Bar, coil and decoiled product — Specification, London, British Standards Institution.
- ISO 15630-1 (2010). Steel for the reinforcement and prestressing of concrete — Test methods — Part 1: Reinforcing bars, wire rod and wire, International Organization for Standardization, Geneva.
- Jumaat, M.Z., Kabir, M.H., Obaydullah, M. (2006), A review of the repair of reinforced concrete beams. *Journal of Applied Science Research*, 2(6): 317-326. <http://eprints.um.edu.my/id/eprint/6103>
- Leramo, R.O., Adekoya, L.O., Loto, C.A. (2018), Evaluation of surface geometries and physical properties of concrete reinforcement steel rods rolled in Nigeria, *Case Studies in Construction Materials*, 8, 150-159. <http://dx.doi.org/10.1016/j.cscm.2017.12.003>
- Metelli, G., Plizzar, G.A. (2014) Influence of the relative rib area on bond behaviour, *Magazine of Concrete Research*, 66(6), 277–294. <http://dx.doi.org/10.1680/macr.13.00198>
- Otieno, M. (2008), Corrosion propagation in cracked and uncracked concrete. Master Thesis: University of Cape

- Town, 153 pp. <https://open.uct.ac.za/items/e30803db-bfbc-407b-a82c-397d46297d29>
- Rabi, M., Shamass, R., Cashell, K.A. (2022), Structural performance of stainless steel reinforced concrete members: A review, *Construction and Building Materials*, 325, 126673. <http://dx.doi.org/10.1016/j.conbuildmat.2022.126673>
- Sulaiman, M.F., Ma.C.-K., Apandi, N.M., Chin, S., Awang, A.Z., Mansur, S.A., Omar, W. (2017), A review on bond and anchorage of confined high-strength concrete, *Structures*, 11(1), 97-109, <http://dx.doi.org/10.1016/j.istruc.2017.04.004>
- Sun, X., Kong, H., Wang H., Zhang, H. (2018). Evaluation of corrosion characteristics and corrosion effects on the mechanical properties of reinforcing steel bars based on three-dimensional scanning, *Corrosion Science*, 142, 284-294. <http://dx.doi.org/10.1016/j.corsci.2018.07.030>
- Van Damme, H. (2018), Concrete material science: Past, present, and future innovations. *Cement and Concrete Research*, 112: 5-24. <http://dx.doi.org/10.1016/j.cemconres.2018.05.002>
- Zuo, J. & Darwin, D. (2000a). Bond slip of high relative rib area bars under cyclic loading. *ACI Structural Journal*, 97(2), 331-335. <http://dx.doi.org/10.14359/864>
- Zuo, J., Darwin, D. (2000b) Splice strength of conventional and high relative rib area bars in normal and high-strength concrete, *ACI Structural Journal*, 97(4), 630-641. <http://dx.doi.org/10.14359/7428>

Publisher's note: [Scienceline Publication](#) Ltd. remains neutral with regard to jurisdictional claims in published maps and institutional affiliations.



Open Access: This article is licensed under a Creative Commons Attribution 4.0 International License, which permits use, sharing, adaptation, distribution and reproduction in any medium or format, as long as you give appropriate credit to the original author(s) and the source, provide a link to the Creative Commons licence, and indicate if changes were made. The images or other third party material in this article are included in the article's Creative Commons licence, unless indicated otherwise in a credit line to the material. If material is not included in the article's Creative Commons licence and your intended use is not permitted by statutory regulation or exceeds the permitted use, you will need to obtain permission directly from the copyright holder. To view a copy of this licence, visit <https://creativecommons.org/licenses/by/4.0/>.

Enhancing Structural Application: Assessing the Suitability of Sawn and Glue Laminated *Albizia zygia* (Ayunre) Timber for Sustainable Construction

Olurotimi Olusegun Ekundayo¹  , Chinwuba Arum^{2,3} , and Lovelt Temilola Shittu¹ 

¹Department of Building Technology, Federal University of Technology, Akure, Nigeira

²Department of Civil and Mining Engineering, JEDS Campus, University of Namibia, Namibia

³Department of Civil Engineering, Federal University of Technology, Akure, Nigeria

✉ Corresponding author's Email: oekundayo@futa.edu.ng

ABSTRACT

Leading economies are moving towards a bio-based economy for sustainability, but Africa struggles to utilize its bio- resource such as timber for advanced engineering application due to its natural limitations. Nevertheless, glue lamination (glulam) is promising for enhancing wood for structural application. Hence, this study investigated the shear strength of glue laminated (glulam) joints of *Albizia zygia* (*A. zygia*) timber species bonded with polyurethane (PUR) adhesive and other essential physical and mechanical properties in line with relevant standards. Briefly state the methodology before results to ensure flow. The results showed that the mean density of the wood species is 519 kg/m³ at a mean moisture content of 12%. The wood recorded a mean volumetric shrinkage and volumetric swelling of 1.17% and 6.52% respectively. Other properties include mean bending strength at 53.89N/mm², mean stiffness at 6106 N/mm², compressive strength parallel to grain at 32.70N/mm² and mean tensile strength at 33.61N/mm². Furthermore, the lap shear strength for glue laminated joints was tested according to EN 302-2013 standard and compared to control solid beams. The mean shear strength for glulam was 2.32N/mm² while it was 1.64N/mm² for the control beams. Thus, the glued joints performed better in shear than the control specimen. Finally, the residual shear strength of the joints was a mean value of 1.28N/mm² after subjecting them to accelerated aging tests (AAT). This is equivalent to 44.83% decrease of the shear strength in the dry use state. Hence, glue laminated *A. zygia* using PUR is not suitable for external use due to weathering effects on its shear strength. Based on the findings in this study, *A. zygia* is a moderately dense wood suitable for structural use but for interior application when laminated with PUR. It is shown that locally sourced *A. zygia* can be enhanced through glue lamination for structural joints in service class 2 according to Eurocode 5.

Keywords: Glued joints, adhesives, Polyurethane, Tensile shear strength and *Albizia zygia*

INTRODUCTION

In recent years, there has been an emergence of global sustainability campaign. The United Nations established Sustainable Development Goals (SDGs) in 2015 to achieve balance in economic, social, and environmental development by 2030 (Rosati and Faria, 2019). CO₂ emissions and environmental preservation have since then become the rallying points of social development (Wang and Wang, 2018). Wood is a preferred green building material because of its low carbon footprint (Martinez, 2015) and efficient strength-to-weight ratio (Ramage et al., 2017). However, biodegradability and dimension constraints limit its robust application. Hence, due to these limitations, technological solutions such as glue lamination have been developed. Wood is a lignocellulose polymer, adaptable for high quality engineered wood

products (EWP), such as glued laminated timber (glulam) (Ekundayo et al. 2022). Glulam, utilizing structural adhesives for lapped wood joints, offers superior strength compared to sawn timber (Nadir and Nagarajan, 2014). Structural adhesives have long been utilized to enhance the load-bearing capacity of wood products intended for structural use.

Glulam is not an entirely new endeavor in Nigeria, as some research efforts have explored adhesive use to enhance properties of local wood species (Adebayo, 2020; Ekundayo et al., 2021; Ekundayo et al. 2022). Furthermore, studies on hard wood species like *Albizia zygia* indicate its durability and diverse uses, including structural applications (Ogunwusi, 2012; Jimoh et al., 2017). However, despite significant interest in this wood species and its properties, its gluing capability for engineered wood products especially at joints is

RESEARCH ARTICLE
 PII: S225204302400011-14
 Received: June 25, 2024
 Revised: September 02, 2024
 Accepted: September 05, 2024

unreported. This study therefore aims to investigate the performance of glued joints using industry-standard adhesives like polyurethane (PUR) which is important for structural use. Successful stress transfer at joints using glue lamination is critical for engineered wood product as this offers flexibility in design, CO₂ mitigation, and efficient stress transfer without the typical failure modes common to other fastening methods such as bolts, staples, pins and dowels which can damage wood fibre extensively.

Furthermore, Polyurethane Resin (PUR) adhesive was selected for this study due to its availability, versatility, ease of application, and compatibility with various wood types, including hardwood, softwoods, and modified wood (Shirmohammadli et al., 2023; Sastri, 2022). Notably, it bonds well to untreated high-moisture wood and is formaldehyde-free, gaining traction in the engineered wood product industry (Lehringer and Gabriel, 2014; Shirmohammadli et al., 2023). Although optimal at low temperatures, its bond strength weakens above 150°C (Sastri, 2022). PUR adhesives produce durable bonds with solvent and chemical resistance, offering adaptability in curing shapes and penetration into wood bonding sites (Sastri, 2022). One-part PUR can penetrate active bonding sites in wood for polymerization and curing to around 9.5 mm limited only by moisture dispersion (Sastri, 2022). The use of wood in Nigeria is still largely rudimentary hence this research is an attempt at enhancing the mechanical performance of local wood species for what will be strategic in the transition to sustainable construction.

MATERIALS AND METHODS

Sample preparation

The two major materials used for this research work were *A. zygia* timber and polyurethane resin (PUR) adhesive. The timber specie was sourced and sawn from Igbara-oke town in Ondo state of Nigeria. The wood was gathered as planks with the dimensions 50 mm x 300 mm x 3600 mm and was inspected to ensure it was free of defects and rot. It was thereafter transported in a pick-up van to the building department workshop and also Forest and Wood Technology workshop of the Federal University of Technology, Akure which is the study area located at 7°15'0"N 5°11'42"E as shown Figure 1 (Bing images, 2024). The one-part polyurethane adhesive was sourced from Lagos, Nigeria as the bonding agent.

Wood samples of 20 mm × 20 mm × 60 mm were prepared for the determination of basic physical properties

(moisture content, density, volumetric shrinkage and swelling) and compressive strength test. The moisture content of the samples was determined by placing them in an electric oven at a temperature of 105°C for 24 hours. The weight measurements for calculating the density were taken using an electronic weighing balance that shows values up to 0.1 decimal place.

All the mechanical properties test were done on a universal testing machine equipped with a computerized data acquisition system at the Department of Agricultural Engineering, Federal University of Technology, Akure. Wood samples with dimensions 20 mm × 20 mm × 300 mm and 5 mm × 20 mm × 180 mm were prepared for bending strength and tensile strength tests respectively according to ASTM D143-21 (2021) Planks for producing glued laminated specimens were glued and clamped as shown in Figure 2 for 24 hours. After 24 hours, the samples were resized to 6 mm×20 mm×150 mm as shown in Figure 3 for evaluating lap shear strength.

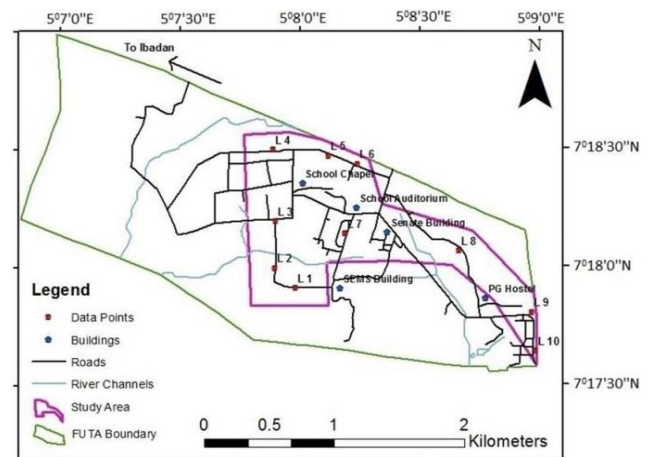


Figure 1. Map of the Federal University of Technology, Akure



Figure 2. Clamping of laminates



Figure 3. Resized, glued joints specimen.

Moisture content and density

Moisture content was determined according to (Eq.1) after subjecting the green samples to oven drying for 24 hours at $103 \pm 2^\circ\text{C}$.

$$MC = \frac{M_w - M_d}{M_d} \times 100 \quad (1)$$

Where; M_w is green weight in grams; M_d is dry weight in grams.

Also, the wood density was determined using (Eq.2):

$$\rho = \frac{M}{V} \quad (2)$$

where M is the mass of wood in kilograms; V is the volume of wood in cubic meter

Volumetric shrinkage and swelling

The volumetric shrinkage was determined according to (Eq.3) after subjecting the green samples to oven drying for 72 hours at $103 \pm 2^\circ\text{C}$.

$$S_s = \frac{V_w - V_{od}}{V_{od}} \times 100 \quad (3)$$

where S_s is the volumetric shrinkage value; V_{od} is the oven dried volume (final volume); V_w is the initial wet volume.

Similarly, the volumetric swelling was determined according to (Eq.4) after immersing dry wood samples in water for 72 hours.

$$S_w = \frac{V_w - V_{od}}{V_{od}} \times 100 \quad (4)$$

where S_w is the volumetric swelling value; V_{od} is the oven dried volume (initial volume)

V_w is the final wet volume

Bending strength

Bending strength, was determined for a total of nine (9) wood samples (Figure 4). The bending strength that is the modulus of rupture (MOR) was determined through a three-point test on a universal testing machine (Figure 5) and calculated using (Eq 5):

$$f_b = \frac{3 \times P_{max} \times L}{2 \times b \times h^2} \quad (5)$$

where: f_b is the bending strength; P_{max} is the maximum load; L is the loading span, b is the breadth; h is the thickness.



Figure 4: Samples after bending strength test

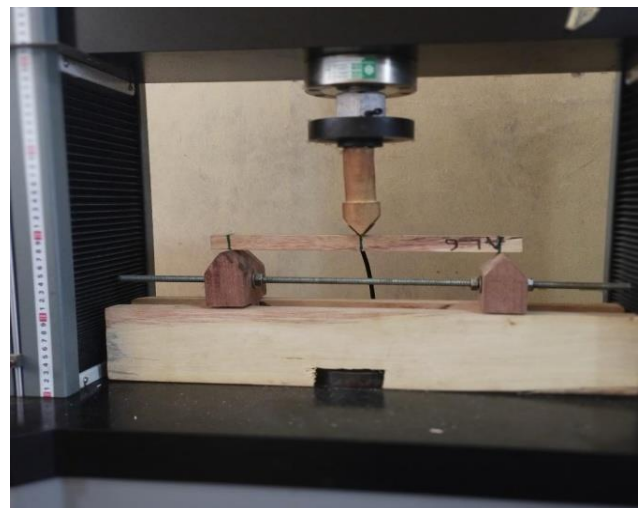


Figure 5: Bending strength sample on UTM

Modulus of elasticity (MOE)

Furthermore, modulus of elasticity in bending was determined for the wood species using (Eq 6):

$$MOE = \frac{PL^3}{4 \times \Delta \times b \times h^3} \quad (6)$$

where; P is maximum load within the limit of proportionality; L is span of the test specimen within the limit of proportionality; b is breadth of the test specimen; h is depth or mean thickness of the test specimen (mm); Δ is the deflection within the elastic limit.

Tensile strength

Tensile strength was determined on the wood sample using a universal testing machine. It is obtained using (Eq.7).

$$f_t = \frac{P}{A} \tag{7}$$

where: f_t is the tensile strength; P is the maximum tensile load; A is the cross-sectional area

Compressive strength

Compressive strength was determined on the wood sample using a universal testing machine. Compressive strength was determined using (Eq.8).

$$f_c = \frac{P}{A} \tag{8}$$

where: f_c is the compressive strength; P is the failure load; A is the cross-sectional area of the specimen

Lap shear strength

Lap shear test was determined on the wood specimens (Figure 6 and 7) using a universal testing machine, according to EN 302-1:2013. The cross-head displacement control rate was 1 mm/min. With F as the applied load and A as the bonded area (approximately 120 mm²), tensile shear strength was then determined as the maximum stress at the breaking point of the material, according to (Eq.9).

$$f_{st} = \frac{P}{A} \tag{9}$$

where: f_{st} is the tensile shear strength; P is the failure load in tension; A is the cross-sectional area



Figure 6. Samples on UTM.



Figure 7. Wood samples after testing

Accelerated aging tests (AAT)

Accelerated aging test was carried out on the glulam wood sample by boiling for two hours, and freezing for two hours in three repeated cycles for a total of twelve hours (six hours for boiling and six hours for freezing). Then, the shear strength of the glued lapped joints subjected to accelerated aged glulam was tested on the universal testing machine and calculated using (Eq. 9).

RESULTS AND DISCUSSION

Density

The mean density of *A. zygia* wood was 519 kg/m³ at a standard moisture content of 12%. Wood having density of between 500 kg/m³ and 650 kg/m³ is classified as moderately heavy (Panda., 2008). Therefore, *A. zygia* is found to be a moderately heavy wood.

Volumetric Shrinkage and Swelling

Table 1 shows the result for volumetric shrinkage and volumetric swelling for the wood samples. Dimensional stability behavior in timber is a critical design consideration especially for wood that is to be deployed for structural engineering application. Dimensional movements occur in timber because it is a hygroscopic material which responds to ambient moisture content within the environment. For *A. zygia*, the values of the mean shrinkage as a result of moisture loss were 1.17% for shrinkage and 6.52% for swelling. The swelling values obtained are smaller compared to hard wood species such as *Celtismildbraedii* (11.36 %), *Khayaivorensis* (10.46 %), *Meliceaeexcelsa* (10.12 %), *Afzeliaafricana* (7.5 %)

(Jamala et al., 2013). It is however similar to *Triplocyton scleroxylon* (6.44 %) and 9.57 %, 8.83 % and 7.74 % for the top, middle and basal portion of *Gmelina arborea* according to Owoyemi et al. (2015). Based on a similar study by Sadiku, (2018). *A. zygia* is grouped as a small movement wood species in terms of its dimensional stability and falls in the same class with wood species such *V. paradoxa*, *A. africana*, and *Ivorensis doka*

Table 1. Results of basic physical properties of sawn *A.zygia*

Specimen	Density (kg/m ³)	Volumetric Shrinkage (%)	Volumetric Swelling (%)
1	458.00	1.58	6.18
2	592.00	0.29	4.65
3	450.00	2.04	6.25
4	629.00	1.54	6.09
5	608.00	0.42	9.44
Mean	547.40	1.17	6.52

Bending strength of sawn *A. zygia*

The mean bending strength of *A. zygia* was 53.89 N/mm² at a mean moisture content of 12% is slightly lower than the existing range of 55.51- 86.00 N/mm² reported in literature (Adegoke et al., 2011). The mean bending strength complies with BS 5268 part 2 for D30 strength class. This implies that it is comparable to wood species such as Oak. The result is however lower than the Mozambiquan variant with an internationally published value of 69.75 N/mm² (Mepepe (*Albizia zygia*) | ITTO, n.d). This can be due to the effect a tree’s origin has on its growth in response to prevailing climatic conditions. Fréjavielle et al. (2019) observed that the environment in which a tree grows impacts on the tree’s phenotype thus leading to variations in properties, such as wood quality. Similarly, Munalula et al. 2016 also highlighted that wood quality is influenced by variations in climatic conditions (which also vary between different regions) affecting the growth of the parent tree.

The relationship between the MOR values and density at 12% moisture content is shown in Figure 8. From the graph, it can be deduced that the higher the density, the higher the bending strength of wood.

Modulus of elasticity of sawn *A.zygia*

Table 2 shows the values of MOE for the nine samples of *A.zygia* subjected to bending strength test. The mean value of MOE in bending was 6106 N/mm² which is lower than the mean values of 14092.18 N/mm² and 10462

N/mm² reported by Jimoh et al. 2017 and Mepepe (*Albizia zygia*) | ITTO, n, d) respectively. However, it is unclear in both cases if the 2 in standard or the 2 cm standards of BS 373 (1957) similar to ASTM D143 (2014) was used Recast for clarity. However, the values reported in this study are in line with the 2 cm standard of BS373 (1957) which is similar to ASTM D143. Nevertheless, the calculated mean stiffness value is within the range specified in BS 5268 part 2 (6000 N/mm² to 9500 N/mm²) for D 30 strength class.

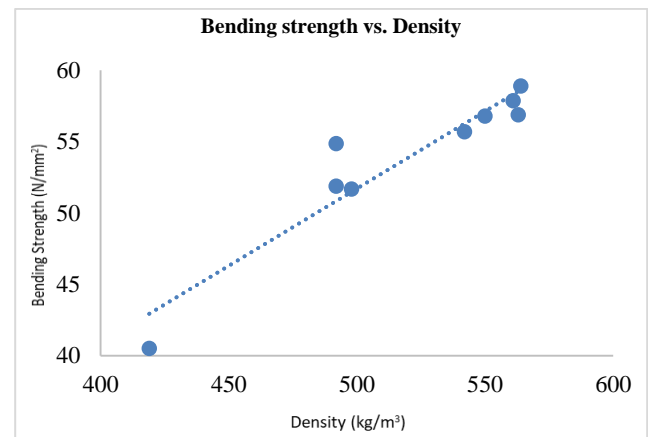


Figure 8. Graph of MOR against density at 12% moisture content

Table 2: Results of Modulus of elasticity in bending

Specimen	P _{max} (N)	f _b (N/mm ²)	Deflection (mm)	MOE (N/mm ²)
1	831	40.49	4.23	5400
2	1064	51.87	4.95	5900
3	1060	51.68	5.06	5750
4	1125	54.86	5.15	6000
5	1142	55.68	4.98	6300
6	1165	56.78	5.16	6200
7	1187	57.87	5.26	6200
8	1167	56.87	4.93	6500
9	1208	58.89	4.95	6700
Mean	1105.44	53.89	4.96	6106

Tensile strength of sawn *A.zygia*

Table 3 shows the tensile strength results at a mean moisture content of 12.10% check this value. The tensile strength of wood contributes to the engineering property of elements such as beams. Similarly, it ensures that wood structural elements subjected to large load variations can undergo gradual failure that give warning signs and allow for possible repair interventions.

Table 3. Tensile strength results.

Specimen	Failure load (N)	Tensile strength (N/mm ²)	Density (kg/m ³)	Moisture content (%)
1	1887	36.28	440	12.2
2	1886.1	36.27	433	11.7
3	1578.2	30.35	378	12.1
4	1747.2	33.6	428	12.1
5	1639	31.51	456	12.4
Mean	1747.5	33.61	427	12.1

Compressive strength of sawn *A.zygia*

Table 4 shows the compressive strength for *A.zygia* wood specimens at a mean moisture content of 12%. The mean value of the compressive strength is 42.70 N/mm² at mean moisture content of 12%. This is similar to the findings of Rahmon and Jimoh (2020), who recorded a mean compressive strength value of 36.84 N/mm².

Table 4. Compressive strength parallel to grain

Specimen	Failure load (N)	Compr. strength (N/mm ²)	Density (kg/m ³)	Moisture content (%)
1	18172.00	45.43	642.00	12.5
2	19596.00	48.99	600.00	10.8
3	18444.00	46.11	529.00	11.7
4	14470.00	36.18	454.00	12.2
5	14724.00	36.81	475.00	13.2
Mean	17081.20	42.70	540.00	12.08

Lap shear strength

Figure 9 shows the shear strength of glue laminated specimens at a mean moisture content of 7.17%. There were notable differences between the shear strength of the control beams and the glue laminated specimens (Figure 9). The glued laminated lapped joints had a mean shear strength of 2.32N/mm² while the control beams had a mean shear strength of 1.64N/mm². This shows that the glue laminated specimens had greater shear strength than the control specimens. Figure 9 shows the shear strength of control specimens (sawn wood) at a mean moisture content of 7.68%. However, it was observed that the values obtained in this study were evidently lower than those reported by Olaniran et al. (2021) who used similar specimens downscaled from the recommendations of EN 302:2013. The specimens in this current study were however further downscaled as a result of the limitation in the maximum thickness the jaws of the universal testing machine can accommodate. This clearly led to a reduction in the shear capacity of the wood specimen and the shear

area of the glue line. Consequently, size effects played a crucial role in the shear capacity of the lapped joints as attested to by Sahin and Akpınar (2021).

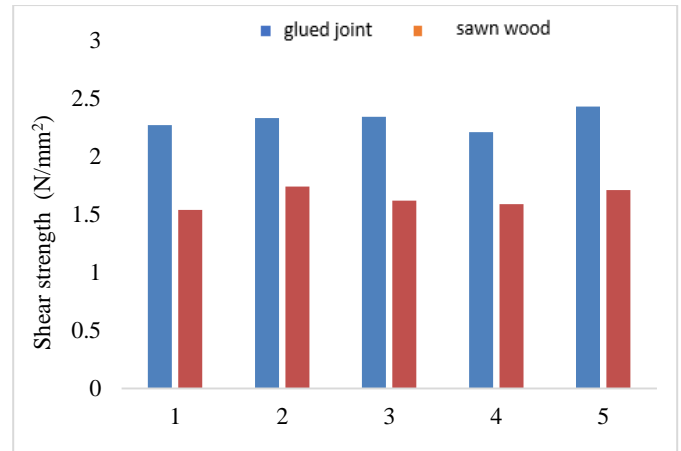


Figure 9. Lap shear strength of glued joints vs control specimen

Accelerated aging test

After three cycles of boiling and freezing the glue laminated specimens for a total of 12 hours, they had the following shear strength recorded in Table 5. The values of the strength are seen to reduce as a result of repeated cycles of boiling and freezing which affected the glued joints coupled with the increase in the moisture content of the samples as a result of prolonged soaking in water. Thus, upon subjecting the samples to AAT, 45 % of the strength in the dry use state was lost. This aligns with the findings of Raftery et al. 2024 who reported general strength reduction in the shear strength of IC-PUR bonded wood specimens subjected to vacuum-pressure soak.

Table 5. Results of AAT on bonded lap joints

Specimen	Failure load (N)	Shear strength (N/mm ²)
1	375	1.25
2	384	1.28
3	369	1.23
4	393	1.31
5	390	1.30
Mean	384	1.28

Failure mode of joints

Specimens of the lapped joints even though stronger than the control specimen failed along the glue lines after the accelerated ageing test due to the effect of repeated cycle of heating and freezing, wetting and drying as shown in Figure 10a. This demonstrates that wood joints bonded

with PUR adhesive under severe moisture and temperature exposure conditions will eventually suffer in-service delamination. Wood failure is the desired failure mode in laminated joints which was prominent in the specimens in the dry use condition as shown in Figure 10b.



Figure 10a. glued joint between tensile loading jaw



Figure 10b. wood failure in glued joints

CONCLUSION

Albizia zygia shows desirable characteristics for construction, with a density of 519.1 kg/m³ and strong dimensional stability, as shown by the minimal shrinkage values (1.17%) and swelling (6.52%). Its mechanical properties, including bending strength (53.89 N/mm²), tensile strength (33.61 N/mm²), and compressive strength (42.70 N/mm²), categories the wood species in strength class D30, which is suitable for structural applications. Furthermore, its excellent bonding properties makes it suitable for glued laminated timber (glulam) production, showing higher shear strength (2.32 N/mm²) compared to solid wood (1.64 N/mm²). However, after assessment under accelerated aging conditions, the glulam joints exhibited a significant strength reduction (45%), making it unsuitable for external use. This limits the application of PUR bonded *A. zygia* joints to internal service class 2 application, though its potential for environmentally friendly engineered wood products remains promising.

DECLARATIONS

Corresponding Author

Correspondence and requests for materials should be addressed to O.O. Ekundayo; E-mail: ooeekundayo@futa.edu.ng; ORCID: 0000-0003-1816-2393

Data availability

The datasets used and/or analysed during the current study available from the corresponding author on reasonable request.

Acknowledgements

The authors would like to acknowledge the members of staff of Department of Building Technology workshop, Forestry Wood Technology workshop and Department of Agricultural Engineering material testing laboratory of the Federal University of Technology Akure for creating a conducive environment to conduct this research.

Authors' contribution

First Author designed and supervised the experiments, analysed the data obtained while the third author performed the experiments and wrote the manuscript. Second Author revised the manuscript. Both the first and second authors read and approved the final manuscript.

Competing interests

The authors declare no competing interests in this research and publication.

REFERENCES

- Adebayo J. O., (2020). Internodal and Eco-Spatial Variability of Selected Physical and Mechanical Properties Of Glulam Bambusa Vulgaris Schrad. Exj. C. Wendi in Nigeria.
- Adegoke, A. J., Adewole, A. N., & Adelugba, A. E. (2011). Thermo-physical and mechanical properties of five wood species grown in Abeokuta, Ogun State, Nigeria.
- Albizia zygia (PROTA). (2017). Plant Use English, Retrieved 17:56, May 15, 2023 from [https://uses.plantnet-project.org/e/index.php?title=Albizia_zygia_\(PROTA\)&oldid=325921](https://uses.plantnet-project.org/e/index.php?title=Albizia_zygia_(PROTA)&oldid=325921)
- ASTM D143-21 (2021): Standard Test Methods for Small Clear Specimens of Timber, ASTM International, West Conshohocken, PA, 2009, www.astm.org
- Bing Images. (n.d.). Location map of the Federal University of Technology, Akure (FUTA) showing the study area. Retrieved June 23, 2024.
- British Standard BS 373:1957. Methods of Testing Small Clear Specimens of Timber. British standard institution.
- Ekundayo, O. O., Arum, C., & Owoyemi J. M. (2021). Forest Product Industry and Engineered Wood Products: The Nigerian Experience: Journal of Applied Sciences and Environmental Management, 25(1). <https://doi.org/10.4314/jasem.v25i1.14>
- Ekundayo, O. O., Arum, C., & Owoyemi, J. M. (2022). Bending strength evaluation of glulam beams made from selected Nigerian wood species. International Journal of Engineering, 35(11), 2120-2129. <https://doi.org/10.5829/IJE.2022.35.11B.07>
- EN302-1:2013 (2013) Adhesives for load-bearing timber structures-test methods-part 1: determination of longitudinal tensile shear strength. European Committee for Standardization, Berlin.
- Fréjaville, T., Fady, B., Kremer, A., Ducouso, A., & Benito Garzón, M. (2019). Inferring phenotypic plasticity and population responses to climate across tree species ranges using forest inventory data. Global Ecology and Biogeography, 28(9), 1259-1271. <https://doi.org/10.1111/geb.12930>
- Jimoh A.A., Rahmon R.O., Babatunde, O.Y. & Tazou, O.L. (2017). Characterization and classification of Ayunre (albiziazygia) timber specie grown in Kwara state Nigeria in accordance to BS 5268 and NCP 2: Epistemics in science, engineering and technology, 7(1), 549-557.
- Lehringer, C., & Gabriel, J. (2014). Review of recent research activities on one-component PUR-adhesives for engineered wood products. Materials and joints in timber structures: recent developments of technology, 405-420. https://doi.org/10.1007/978-94-007-7811-5_37
- Martinez, T., (2015). Sustainable Building: Why Wood Is Our Most Valuable Resource. usgbc-li.org.
- Mepepe (*Albizia zygia*) | ITTO. (n.d.). ITTO. <http://www.tropicaltimber.info/specie/mepepe-albizia-zygia/>
- Munalula, F., Seifert, T., & Meincken, M. (2016). the expected effects of climate change on tree growth and wood quality in Southern Africa. Springer Science Reviews, 4, 99-111. <https://doi.org/10.1007/s40362-017-0042-9>
- Nadir, Y. and Nagarajan, P., "The behavior of horizontally glued laminated beams using rubber wood", Construction and Building Materials, Vol. 55, (2014), 398-405. <https://doi.org/10.1016/j.conbuildmat.2014.01.032>
- Ogunwusi, A.A. (2012). Wood Properties of albizia zygia and anogeisussleiocarpus: Medium category wood species found in timber markets in Nigeria: Journal of Biology, Agriculture, and Healthcare, 2(11), 123.
- Olaniran, S.O., Clerc, G., Cabane, E. et al. Quasi-static and fatigue performance of bonded acetylated rubberwood (*Hevea brasiliensis*, Müll. Arg.). Eur. J. Wood Prod. 79, 49-58 (2021). <https://doi.org/10.1007/s00107-020-01610-0>
- Pande, P. K. (2008). Wood density variations in Meranti timbers of Shorea species of Malay Peninsula. Journal of the Timber Development Association of India, 54(1/4), 10-19.
- Raftery, G. M., Karami, Z., Pizzi, A., & Nicholson, C. L. (2024). Durability assessment of one-component polyurethane adhesives for bonding of preservative treated wood subject to artificial ageing. International Journal of Adhesion and Adhesives, 129, 103594. <https://doi.org/10.1016/j.ijadhadh.2023.103594>
- Rahmon, R. O., & Jimoh, A. A. (2020). Strength Characterization and Grading of less-used Nigerian grown Timber Species for Structural Applications. Malaysia Journal of Civil Engineering, 3. <https://doi.org/10.11113/mjce.v32n1.609>
- Ramage, H., Burridge, H., Busse-Wicher, M., Fereday, G., & Reynolds, T., (2017). Renewable and Sustainable Energy Reviews: The Wood from the trees: The Use of timber in construction, 68(1), 333-359. <https://doi.org/10.1016/j.rser.2016.09.107>
- Rosati, F., & Faria, L. (2019). Addressing the SDGs in Sustainability Reports: The Relationship with Institutional Factors: Journal of Cleaner Production, 215, 1312-1326. <https://doi.org/10.1016/j.jclepro.2018.12.107>
- Sadiku, N. A. (2018). Weight, porosity and dimensional movement classification of some Nigerian timbers. Journal of Research in Forestry, Wildlife and Environment, 10(1), 1-10.
- Sahin, R., & Akpınar, S. (2021). The effects of adherend thickness on the fatigue strength of adhesively bonded single-lap joints. International Journal of Adhesion and Adhesives, 107, 102845. <https://doi.org/10.1016/j.ijadhadh.2021.102845>
- Shirmohammadi, Y., Pizzi, A., Raftery, G. M., & Hashemi, A. (2023). One-component polyurethane adhesives in timber engineering applications: A review. International Journal of Adhesion and Adhesives, 103358. <https://doi.org/10.1016/j.ijadhadh.2023.103358>
- Wang, B., Yefei, S., & Wang, Z. (2018). Agglomeration Effect of CO2 Emissions reduction effect of technology: A spatial econometric perspective based on China's province-level

data:Journal of Cleaner Production, 204, 96-106.

<https://doi.org/10.1016/j.jclepro.2018.08.243>

Publisher's note: [Scienceline Publication](#) Ltd. remains neutral with regard to jurisdictional claims in published maps and institutional affiliations.



Open Access: This article is licensed under a Creative Commons Attribution 4.0 International License, which permits use, sharing, adaptation, distribution and reproduction in any medium or format, as long as you give appropriate credit to the original author(s) and the source, provide a link to the Creative Commons licence, and indicate if changes were made. The images or other third party material in this article are included in the article's Creative Commons licence, unless indicated otherwise in a credit line to the material. If material is not included in the article's Creative Commons licence and your intended use is not permitted by statutory regulation or exceeds the permitted use, you will need to obtain permission directly from the copyright holder. To view a copy of this licence, visit <https://creativecommons.org/licenses/by/4.0/>.

© The Author(s) 2024

The Integration of Geographic Information Systems and Building Information Modelling to Sustainably Manage Development Sites in Gaborone, Botswana

Kealeboga Moreri¹  , Mooketsi Segobye¹ , Lopang Maphale¹  and Bernard Onneng¹ 

¹University of Botswana, 4775 Notwane Rd, Gaborone, Botswana

✉Corresponding author's Email: morerik@ub.ac.bw

ABSTRACT

For many years, site development professionals and urban planners have worked in silos, yet they share a similar objective of providing a better built and natural environment. Moreover, there seems to be a stereotype in terms of focus areas; with urban planners more on the macroscale while their site development counterparts are more on the micro end. The two professional groups speak in different languages and use different instruments. For example, urban planners have introduced Geographic Information Systems (GIS) while site development professionals like architects, engineers, contractors, and facility managers advocate for Building Information Modelling (BIM). The increasing complexity of site development, their related environmental, geographical, and surrounding infrastructure is highly desired to support informed decision-making. Advancements in computer science and data technologies can make this integration easier. However, the understanding of GIS and BIM integration is still in its infancy, as innovative applications of their fusion is yet to be explored comprehensively. Therefore, this study investigates how GIS and BIM can be integrated to derive big data to support site development in Gaborone, Botswana. It will further propose a conceptual framework for integrating BIM and GIS for better site development and sustainable urban management in Gaborone.

Keywords: Building Information Modelling, Geographic Information Systems, Sustainable Urban Management, Sustainable Construction Projects, BIM-GIS Integration, Conceptual Framework

INTRODUCTION

For many years, urban planners and site development professionals have worked in silos, yet they have the same objectives of delivering better built infrastructures and natural environments. Despite having similar objectives, they speak different languages and use different instruments. For example, urban planners usually focus on macroscale projects such as city-wide information. In contrast, their site development counterparts are more on the micro end such as specific building information of a particular project. Therefore, this causes interoperability issues when these professionals share this information to other stakeholders involved, leading to information mismatch, improper documentation of developmental stages, and unnecessary confusions.

Proper documentation is necessary for building management as there are several professionals involved in a construction project. Throughout a building project, different forms and formats of information are gathered, exchanged, and recorded for efficiency and effectiveness.

Moreover, [Chen et al. \(2015\)](#) stress that proper information management is important for decision-making as it ensures that accurate information is always available on time and in the right format to the appropriate person. For example, a building project requires 3D models, material properties and quantities, map, geographic information, ground levels etc., which can be provided by technologies like Geographic information Systems (GIS) and Building Information Modelling (BIM). The GIS can be used to process and store spatial and non-spatial data of the construction project. While BIM can be used to represent and manage information for designing, constructing and operating buildings.

The lifecycle of a building project comprises of initial plans, land acquisition, inception, finance, design, construction, operation, maintenance and finally demolition or revitalization. All these stages require data that GIS and BIM can adequately process and store. However, [Lu and Tam \(2013\)](#) argue that current decision-making throughout the site development life cycle is based on missing, incorrect and even outdated information. Very

RESEARCH ARTICLE
 PII: S225204302400012-14
 Received: June 25, 2024
 Revised: September 02, 2024
 Accepted: September 05, 2024

often development sites have missing information of one stage to another of a life cycle hence creating a disconnect and 'information islands' which can negatively impact the progress of the project (Lu and Tam, 2013).

A BIM-enabled site facilitates an environment where professionals like architects can develop conceptual, schematic, and detailed designs directly in BIM software such as ArchiCAD and Autodesk Revit. The design would then be passed to engineers for engineering designs such as mechanical, electrical, carpentry, and plumbing services. During the construction and operation stage, various information will be generated which should be synchronized properly and timely in the BIM. A suggestion by Karan (2014) is that BIM information should further include the geometry of the areas of interest, their semantic and topological information. For building projects, geometric information entails the three-dimensional form of a building such as size, shape and volume; while semantic information provides descriptions of the properties components; and topological information documents of the relationship between building components, such as sunlight emission for greenhouses, connectivity of rooms, their thermal requirements and evacuation measures, and building performance analysis means.

A successful integration of GIS with BIM can lead to a cyber-physical system which is a concept that combines the physical and computational elements to facilitate smarter decisions of various industries including construction (Song et al., 2017; Wan Abdul Basir et al., 2018; Wu and Zhang, 2016). BIM aims to form a shared, single and interoperable platform where site development stakeholders such as contractors, engineers, facilities managers and clients can communicate and share information and experiences. GIS on another note is a system of capturing, storing, manipulating, analyzing and disseminating geospatial data. It has many applications related to planning, engineering, transport and logistics, management, insurance, telecommunications and business. The versatility of GIS and its 'geoinformation' connotation facilitates a basic index variable for all other information such as cartographic information, urban environment infrastructure characteristics, geo-statistics, geotechnical conditions, rock morphology and the earth topography. Moreover, GIS techniques continue to provide avenues for scientific enquiries on sustainability, governance and development.

The objective of this study is to provide insights in the form of a conceptual framework on the key components that construction professionals can focus on to sustainably

build and manage construction projects by integrating BIM and GIS technologies for efficiency and effectiveness. Sustainable Development Goal 11 which emphasizes the need to make cities and human settlements inclusive, safe, resilient and sustainable will be the main anchor and guiding principle of this study.

This study is structured as follows. Section 2 provides a review of literature regarding previous works that investigated possibilities of integrating BIM and GIS for various activities. In Section 3, a methodology for integrating BIM and GIS for sustainable construction is presented. A conceptual framework for integrating BIM and GIS for sustainable construction is then proposed in Section 4 which highlights key strategic areas of BIM and GIS integration to address challenges of Sustainable Development Goal 11 (SDG 11). Section 5 then discusses and concludes the main findings of this study and outlines further research directions.

LITERATURE REVIEW

A sizeable number of research has investigated the integration of GIS with BIM to address issues of big data in construction projects in their local communities. For example, Han et al. (2020) discussed an application prospect of GIS-BIM integration technology in construction projects particularly in site scheduling, material management, and safety management of construction personnel. Their study revealed that the application of the two technologies in construction management can save construction cost, improve project safety, and facilitate a culture of collaboration of different disciplines and aid data sharing between stakeholders.

An environmental information modelling framework was developed by Gao et al. (2020) to bridge a gap between GIS and BIM systems. The need to integrate BIM with GIS technology emanates from the notion that the former barely supports processes of construction supply chain because of its limited geospatial ability (Gao et al., 2020). The construction industry is dependent on the efficient and effective delivery of materials and equipment, environmental protection, and proper management of waste products over long distances. Therefore, GIS provides avenues to use geospatial information for transportation planning, construction and monitoring to improve efficiency in construction projects.

For high-rise buildings GIS and BIM have been integrated to address a challenge of the towering vertical construction method as it lacks comprehensive risk mitigation strategies (Elsheikh et al., 2021). The

combination of the two technologies can ensure that all project phases are well planned for. In addition, they can help establish how materials are delivered to the site in a cost-effective manner, outlining all pertinent safety measures for all stages of development. Moreover, GIS and BIM technologies can assist project managers anticipate problems before they occur and outline plausible mitigation measures in a timely manner (Thiis and Hjelseth, 2008).

A study by Hadi Hor et al. (2018) investigated possibilities of linking network technology with GIS and BIM. An intelligent Web model for urban mobile utility was presented with the goal of benefiting professionals on a wide range of methods and modalities of displaying and analyzing construction data on the internet. An integrated graph database platform was developed by Hadi Hor et al. (2018) which enabled professionals to interact with a comprehensive graph data model, perform detailed construction data mining spatial analysis in it for improved efficiency and decision-making.

BIM and GIS integration depend on big data analytics to make informed decisions (Sani and Abdul, 2018). This refers to the practice of basing decisions on the analysis of data rather than purely on intuition. Big data is popular because it has benefits, including the power of prediction, and improved decision-making. Nonetheless, Lu et al. (2018) argue that the euphoria of big data analytics for BIM and GIS integration is yet to be seen in managing developmental sites. Even though a review of literature mostly paints the BIM – GIS integration on a positive note, there are some challenges of the two technologies that need to be highlighted.

Challenges of integrating BIM with GIS

Technology

Integrating GIS with BIM for construction projects can be highly beneficial, but it also comes with several challenges which include: a) data interoperability issues, b) complexity of models, c) differing levels of detail, d) cost and resources, e) organizational silos, f) legal and privacy concerns, and g) change management. The subsections that follow will briefly describe these challenges for a better understanding of their route causes.

Data Interoperability

Data interoperability is concerned with the creation of a seamless data exchange between two or more communication platforms. However, GIS and BIM often use different data formats and standards. Therefore, interoperability issues may arise, making it difficult to

transfer spatial and non-spatial data between the two technologies (Janečka, 2019) (Figure. 1).

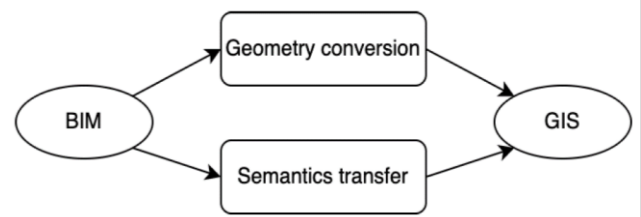


Figure 1. Data interoperability issues of integrating BIM with GIS

Complexity of models

For large scale construction projects, BIM models can be complex, which can be a challenge when integrated with GIS data. Moreover, the need to manage and update these complex models while integrating them with GIS can require extensive computational resources and expertise (Wan Abdul Basir et al., 2018).

Differing levels of detail

It is common knowledge that GIS typically deals with large scale geospatial data. In contrast, BIM focuses on detailed building information. A desire to integrate these two datasets can be challenging as a result of differences in scale and level of detail (Zhu and Wu, 2022). Moreover, it can be a challenge to harmonize these datasets to ensure consistency and accuracy throughout the project lifecycle.

Cost and resources

The integration of BIM with GIS requires investments in technology and human resources (Sheina et al., 2022). Resources need to be allocated to acquire the necessary tools, software, to develop interoperability standards and train personnel to utilize the integrated system effectively (Han et al., 2020). This can be a stumbling block to smaller companies or projects with limited budgets.

Organisational silos

Usually, organisations are managed by different departments, which subsequently leads to organisational silos and lack of collaboration (Cilliers and Greyvenstein, 2012). It is essential to overcome these challenges for a successful integration of BIM and GIS.

Legal and privacy concerns

GIS data can comprise of sensitive information such as land ownership, infrastructure details and environmental data. Therefore, integrating this data with BIM can raise some legal and privacy concerns regarding data ownership, exchange and security (Liu et al., 2017). It is crucial to ensure compliance to regulations and to

protect sensitive information when integrating BIM with GIS.

Change management

For organisations to implement an integrated BIM and GIS solution, changes in existing workflows, processes and organisational culture are required (Celeste et al., 2022). It should be noted that any resistance to change from any stakeholder involved, or lack of buy-in from decision makers, and inadequate training or appropriate personnel can hinder the successful adoption and implementation of the integrated system.

To address the outlined challenges requires coordinated efforts from all stakeholders involved, particularly industry professionals, policy makers, the private sector and academia. In addition, it is necessary to design a methodology that comprehensively addresses most of the challenges identified while considering sustainability issues, particularly those of SDG 11.

MATERIALS AND METHODS: INTEGRATING BIM AND GIS FOR SUSTAINABLE CONSTRUCTION

As stated earlier, the methodology of this study is guided by the Sustainable Development Goal 11 (SDG 11) initiative which is concerned with making cities and human settlements inclusive, safe, resilient and sustainable (Bernegger et al., 2022; Moghadam et al., 2016; T. Wang et al., 2019). The synopsis of SDG 11 stresses that cities are hubs for ideas, commerce, culture, science, productivity, social, human and economic development. Additionally, it highlights that urban planning, water, sanitation, waste management, disaster risk reduction, access to information, education, and capacity building are all relevant issues to sustainable urban development.

This study argues that the integrating of BIM and GIS technologies can address most challenges identified in SDG 11, particularly the following targets: a) Target 11.3 – enhancing inclusive and sustainable urbanization and capacity for participatory, integrated and sustainable human settlement planning and management in all countries, b) Target 11.5 – significantly reducing the number of deaths and the number of people affected by natural disasters, including water related disasters, with a focus on protecting the poor and people in vulnerable situations, c) Target 11.7 – provision of universal access to safe, inclusive and accessible, green and public spaces, d) Target 11c – supporting least developed countries, through financial and technical assistance, in building sustainable and resilient buildings utilizing local materials.

The following sub-sections discuss key application areas where BIM and GIS Integration can address the SDG 11 Targets outlined.

BIM-GIS for enhancing inclusive and sustainable urbanization

BIM plays a vital role in GIS integration (Wang et al., 2019). It can assist many professionals to work simultaneously on a project reducing chances of miscommunication and errors while it handles its documentation seamlessly. It is a single source of truth for the project information, making sure that everyone is on the same page. Three Dimensional (3D) models developed by designers in BIM can be augmented with data for asset management, which can later be extracted by GIS (Carrasco et al., 2022). This seamless data integration provides a platform for contractors to visualize and validate data of the current project, as well as bring models from different projects into a federated GIS scene which gives clients the capability to appreciate the project in a 3D environment. It further gives them the opportunity to view the design and provide insights and design guidance as the project moves from a schematic design to a conceptual design.

With BIM and GIS one can create realistic 3D models that help stakeholders visualize the final product before the actual physical implementation. This not only helps the clients understand the project better, but also assists designers to identify and resolve potential issues before they become costly problems.

BIM-GIS integration facilitates for large volumes of data to be extracted for the digital twin technology (Shi et al., 2023). Such data can then be utilized for an effective asset management throughout the lifecycle of an infrastructure project. They can provide better services for clients and improved workflows which makes the construction of a project more efficient.

Nowadays, construction companies are exploring avenues to provide digital infrastructure solutions to their clients. This entails leveraging technology and innovation in the infrastructure design community to reshape the way in which large and most complex infrastructure projects are delivered. Solutions envisaged with such technologies include cloud-based and Web-based solutions which make it possible for contractors to seamlessly access, analyse and store large volumes of data to efficiently manage maintenance schedules, track asset performance and plan for future upgrades or renovations.

BIM-GIS for a universal access to safe, inclusive and accessible green and public spaces

It is crucial for design build project successes to have a firm grasp on the larger contextual environment vehicle in which it exists (Gann and Salter, 2000). BIM and GIS integration can help improve the way companies design, build, and maintain assets with consideration for the real-world activities around them. It is essential for developing robust and sustainable solutions to problems like population growth, water scarcity and climate change. For example, BIM technology can be used to improve the management of green buildings where their various functions such as energy use, carbon emissions and ventilation analysis are used to support the sustainable development of buildings (Lu et al., 2017). According to Wang et al. (2019) the emergence of GIS-based simulation models can solve environmental and planning problems in a more accurate way for low carbon cities to test the impacts of urban layouts and building types. For example, they can be used to test the energy performance, carbon emissions, solar potential for urban design projects for sustainable urban development.

BIM-GIS for reducing the number of deaths and people affected by natural disasters,

BIM-GIS technologies can be used to identify, map, and assess locations likely to be affected by flooding through flood analysis computations and predictions. It gives users the opportunity to simulate flood occurrences directly in a 3D contextual model as well as animating those events. The determination of early flood risk assessments, urban floodplains and coastal areas can be aided by the execution of practical flood simulations along river lines and coastal areas (Dhiman et al., 2019). Through the utilization of BIM technology, a determination of the design of buildings, materials to be used and their overall structural reinforcements in such areas can be established. Additionally, GIS technology can be utilized to establish the extent to which flood water levels can affect buildings within a particular distance from the river and adequate mitigation measures outlined (Moreri et al., 2008).

Applications of BIM-GIS in energy management to support least developed countries, through financial and technical assistance

For building projects, sustainability includes energy and cost efficiency considerations. Projects that utilize both BIM-GIS technologies can benefit from energy conservation management and efficiency schemes at both building and city levels (Wang et al., 2019). For example,

GIS can facilitate the development and computation of energy-saving methods for buildings, such as the assessment and quantification of energy efficiency, mapping energy consumption and improving the targeting of regional energy supplies. Technological advancements such as smart city developments and the Internet of Things (IoT) have provided an environment where contractors can integrate BIM and GIS to develop spatially seamless digital infrastructure for urban environmental analysis (Liu et al., 2017) and climatic adaptation of buildings (Thiis and Hjelseth, 2008). The increasing affordability of sensor networks and computation power makes it possible to collect large volumes of real-time data for informed decision making in construction projects.

The IoT is concerned with enabling communication between physical and virtual devices to collect, analyse, exchange and disseminate construction information in real-time (Isikdag, 2015). It involves the utilization of sensors and area field communication technologies such as Global Positioning Systems (GPS) devices, smart mobile phones, and Radio Frequency Identification (RFID) readers to communicate with each other to create either a smart building or city. For example, a door in a smart building would connect with a fire alarm for a responsive and timely emergency evacuation. For a smart city, a bus would communicate with a bus stop in terms of estimated times of arrival at a particular bus stop. It is necessary for BIM and GIS technologies to be integrated into facilities management and smart city initiatives such that benefits associated with emergency response, urban surveillance, urban monitoring to smart buildings may be achieved from this fusion (Lu et al., 2018).

RESULTS: CONCEPTUAL RAMEWORK FOR INTEGRATING BIM AND GIS FOR SUSTAINABLE CONSTRUCTION

The conceptual framework of this study is a result of key targets identified in the methodology section which comprehensively discussed how the integration of BIM-GIS technologies can adequately address challenges of Sustainable Development Goal 11 (Figure 2). The framework for SDG 11 outlines a thorough approach to transform cities and human settlements into inclusive, robust, safe and sustainable environments. It emphasizes integrated planning, resilience building, inclusive governance and partnerships as critical components to achieve sustainable urban development worldwide.

It is anticipated that the proposed conceptual framework will facilitate an environment for better site development and sustainable urban management of construction projects in Gaborone, particularly addressing issues of SDG 11 targets.

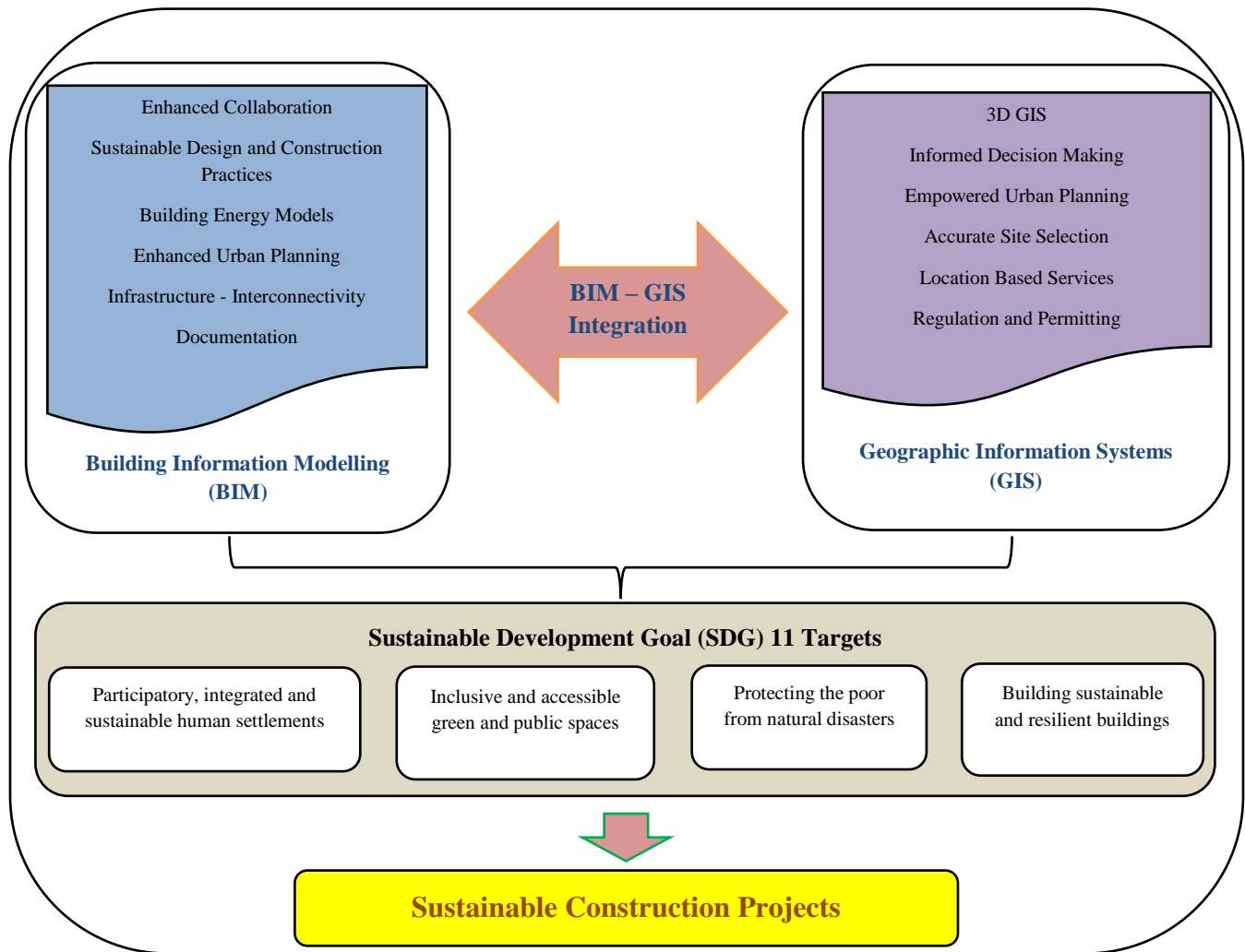


Figure 2. The conceptual framework for BIM-GIS Integration for sustainable construction projects

BIM FRAMEWORK COMPONENTS

Enhanced collaboration

BIM facilitates collaboration among project teams which improves information dissemination and sharing. Nonetheless, Wang et al. (2022) argues that challenges like unwillingness to collaborate, lack of standards and regulations inhibit effective collaboration processes in BIM enabled projects. Despite these challenges, BIM provides better communication and collaboration among various project members and key stakeholders for improved project quality and increased profits (Svalestuen et al., 2017).

Sustainable design and construction practices

Sustainable design and construction practices with BIM entail enhancing the quality of information provided

in making critical design decisions regarding the environmental impact of buildings. BIM can assist in the following areas of sustainable design: selection of building orientation to reduce costs; reduction of waste and carbon footprints; effective water harvesting avenues; and reduction of material needs and increasing the use of recycled materials (Dowsett and Harty, 2013).

Building energy models

BIM offers an extensible medium for parametric information storage of Building Energy Models (BEM) (Elnabawi, 2020). For example, it facilitates the development of energy simulation processes to be integrated with sustainable and low energy building designs which include thermal zones, weather files and occupancy operating schedules.

Enhanced urban planning

Enhanced urban planning is concerned with the development of smart cities. As such, BIM can help constructors build energy-efficient buildings in a cost effective manner while seamlessly sharing and exchanging information to all stakeholders involved (Goyal et al., 2020).

Infrastructure interconnectivity

It is crucial to establish a real-time information source on a construction site. According to Hewage and Ruwanpura (2006) workers need opportunities to view 3D and 4D (with 3D timeline) drawings, technical information, safety information, weather updates for proper management of materials on site. A BIM information booth can give constructors onsite access to updated drawings, a greater degree on the utilization of resources and other important information related to the project.

Documentation

Considering BIM as a documentation option facilitates an environment where builders can specify and input any type of information into the model at any time of the project for sufficient consumption and use by other professionals in the project. However, Wan Abdul Basir et al. (2018) argue that it can be used negatively as a tool for disseminating false information. For example, software packages have been designed to provide default values which users have to modify to input actual values of a particular project of interest. If such information is not provided, default values would be deemed inaccurate for that project.

GIS FRAMEWORK COMPONENTS

3D GIS

Three Dimensional (3D) models in GIS allow planners to visualize construction activities, identify potential sources of hazards and better plan for them prior to the actual implementation on the ground (Ebrahim et al., 2016). Unlike the traditional 2D drawings, 3D models consider locational and spatial aspects of a project which are critical in developing executable construction plans which consider consequences of surroundings on a construction plan.

Informed decision making

With GIS, workers are able to access and process information quickly which allows them to improve

planning and informed decision making to promote better organizational integration and knowledge management.

Empowered urban planning

GIS can help urban planners to simulate and evaluate environmental impacts of their projects for a better understanding of the urban environment. As a result of the continuous increase in the world's population, GIS can further empower urban planners to design innovative solutions, construct energy efficient and cost-effective structures for local communities.

Accurate site selection

Traditional means of site selection in construction projects is usually done manually based on experience. However, the complexity of current construction projects and consideration of social, environmental and economic factors for sustainability, renders traditional means insufficient. Therefore, GIS techniques are critical in construction projects as they can produce interactive multi-layered maps that allow queries to be performed to obtain optimal solutions that meet set criteria (Bansal, 2012).

Location based services

Locating construction assets such as equipment and workforce during construction is important for improving productivity and safety. Therefore, GIS can facilitate a two-way communication channel between workers and supervisors by tracking them in a 3D environment for forensic and performance analysis purposes (Shirowzhan et al., 2017).

Regulation and permitting

GIS can be used to produce cadastral maps overlaid with zoning maps to obtain insights and propose policies for land regulation and permitting. To recognize potential problematic areas, current and tentative zoning maps can be compared through different spatial criteria and thresholds for a detailed site investigation to eventually achieve a new zoning map (Lin, 2000).

DISCUSSIONS

The low accessibility of information regarding construction projects in Botswana are the main causes of inefficient actions regarding their timely execution and completion. For existing building projects, the lack of 'as-built' documentation (building components, installations, materials used, etc.), the complex task of determining the

current status of materials used, and detailed record of previous maintenance work, makes it difficult for professionals to properly plan, schedule and make improvements therein such buildings. Moreover, construction sites can also be a source of noise and dirt which creates traffic congestions that impede mobility and cause noise pollution.


Therefore, it is important for construction activities to be conducted timely using comprehensive data from BIM-GIS integration technologies. This requires reliable and accurate data on the building site as a basis for effectiveness and efficiency in planning and building. These can be achieved by an adequate integration of BIM and GIS through the conceptual framework proposed in this study.

CONCLUSION

Big data formed from GIS and BIM is the core to the success or failure of a development project. Thus BIM-GIS integration aims to create a future with an infrastructure that is more resilient and sustainable to make responsible use of the resources of our country and to cultivate conditions that are conducive for the growth of our cities and populations. This study through the utilization of the proposed framework, argues that the utilizing of BIM and GIS technologies can facilitate enhanced workflows and help project managers make quality driven decisions for sustainable construction projects. Since BIM is a digital representation of a building in the life cycle phases from design, construction, operation and finally maintenance, it is crucial that all stages are well documented and easily accessible by all stakeholders through a GIS platform. Future work will entail the implementation and evaluation of the effectiveness of the proposed framework in a case study area in Gaborone, Botswana.

DECLARATIONS

Corresponding Author

Correspondence and requests for materials should be addressed to Dr. Kealeboga Moreri; Email: morerik@ub.ac.bw;  ORCID: 0000-0002-3692-1915.

Data availability

The datasets used and/or analyzed during the current study available from the corresponding author on reasonable request.

Acknowledgements

The authors would like to acknowledge the University of Botswana for creating a conducive environment to conduct this research.

Authors' contribution

First Author performed the experiments and wrote the manuscript. Second Author analyzed the data obtained. Third Author designed the experimental process and revised the manuscript. Fourth Author assisted with the initial data collection and community engagement processes. All authors read and approved the final manuscript.

Competing interests

The authors declare no competing interests in this research and publication.

REFERENCES

- Bansal, V. (2012). Application areas of GIS in construction projects and future research directions. *International Journal of Construction Management*, 12(4), 17-36. <https://doi.org/10.1080/15623599.2012.10773198>
- Bernegger, H., Laube, P., Ochsner, P., Meslec, M., Rahn, H., Junghardt, J., & Ashworth, S. (2022). A new method combining BIM and GIS data to optimise the sustainability of new construction projects in Switzerland. *IOP Conference Series: Earth and Environmental Science*. <https://doi.org/10.1088/1755-1315/1122/1/012052>
- Carrasco, C., Lombillo, I., Sánchez-Espeso, J., & Balbás, F. (2022). Quantitative and qualitative analysis on the integration of geographic information systems and building information modeling for the generation and management of 3d models. *Buildings*, 12(10), 1672. <https://doi.org/10.3390/buildings12101672>
- Celeste, G., Lazoi, M., Mangia, M., & Mangialardi, G. (2022). Innovating the Construction Life Cycle through BIM/GIS Integration: A Review. 14(2), 766. <https://www.mdpi.com/2071-1050/14/2/766>
- Chen, K., Lu, W., Peng, Y., Rowlinson, S., & Huang, G. Q. (2015). Bridging BIM and building: From a literature review to an integrated conceptual framework. *International Journal of Project Management*, 33(6), 1405-1416. <https://doi.org/https://doi.org/10.1016/j.ijproman.2015.03.006>
- Cilliers, F., & Greyvenstein, H. (2012). The impact of silo mentality on team identity: An organisational case study. *SA Journal of Industrial Psychology*, 38(2), 1-9. <https://doi.org/10.4102/sajip.v38i2.993>
- Dhiman, R., VishnuRadhan, R., Eldho, T., & Inamdar, A. (2019). Flood risk and adaptation in Indian coastal cities: recent scenarios. *Applied Water Science*, 9(1), 5. <https://doi.org/10.1007/s13201-018-0881-9>
- Dowsett, R., & Harty, C. (2013). Evaluating the benefits of BIM for sustainable design—a review. 29th Annual ARCOM conference. <https://arcom.ac.uk/-docs/archive/2013-ARCOM-Full-Proceedings-Vol-1.pdf#page=29>
- Ebrahim, M., Mosly, I., & Abed-Elhafez, I. (2016). Building construction information system using GIS. *Arabian Journal for Science Engineering*, 41(10), 3827-3840. <https://doi.org/10.1007/s13369-015-2006-1>

- Elnabawi, M. (2020). Building information modeling-based building energy modeling: investigation of interoperability and simulation results. *Frontiers in Built Environment*, 6, 1-19. <https://doi.org/10.3389/fbuil.2020.573971>
- Elsheikh, A., Alzamili, H., Al-Zayadi, S., & Alboo-Hassan, A. (2021). Integration of GIS and BIM in Urban Planning-A Review. *IOP Conference Series: Materials Science and Engineering*. <https://doi.org/10.1088/1757-899X/1090/1/012128>
- Gann, D., & Salter, A. (2000). Innovation in project-based, service-enhanced firms: the construction of complex products and systems. *Research policy*, 29(7-8), 955-972. [https://doi.org/10.1016/S0048-7333\(00\)00114-1](https://doi.org/10.1016/S0048-7333(00)00114-1)
- Gao, Z., Ezekwem, K., & Aslam, M. (2020). An Integration of BIM and GIS for Integrated Project Delivery. *Construction Research Congress 2020*. <https://doi.org/10.1061/9780784482889.053>
- Goyal, L., Chauhan, R., Kumar, R., & Rai, H. (2020). Use of BIM in development of smart cities: a review. *IOP Conference Series: Materials Science and Engineering*. <https://doi.org/10.1088/1757-899X/955/1/012010>
- Hadi Hor, A., Gunho1, S., Claudio, P., Jadidi, M., & Afnan, A. (2018). A semantic graph database for BIM-GIS integrated information model for an intelligent urban mobility web application. *ISPRS Annals of the Photogrammetry, Remote Sensing and Spatial Information Sciences*, 4(4). <https://doi.org/10.5194/isprs-annals-IV-4-89-2018>
- Han, Z., Wang, Z., Gao, C., Wang, M., & Li, S. (2020). Application of GIS and BIM integration technology in construction management. *IOP Conference Series: Earth and Environmental Science*. <https://doi.org/10.1088/1755-1315/526/1/012161>
- Hewage, K., & Ruwanpura, J. (2006). Carpentry workers issues and efficiencies related to construction productivity in commercial construction projects in Alberta. *Canadian Journal of Civil Engineering*, 33(8), 1075-1089. <https://doi.org/10.1139/106-050>
- Isikdag, U. (2015). BIM and IoT: A synopsis from GIS perspective. *The International Archives of the Photogrammetry, Remote Sensing Spatial Information Sciences*, 40, 33-38. <https://doi.org/10.5194/isprsarchives-XL-2-W4-33-2015>
- Janečka, K. (2019). Standardization supporting future smart cities—a case of BIM/GIS and 3D cadastre. *GeoScape*, 13(2), 106-113. <https://doi.org/10.2478/geosc-2019-0010>
- Karan, E. (2014). Extending Building Information Modeling (BIM) Interoperability to Geo-Spatial Domain Using Semantic Web Technology. *Georgia Institute of Technology*. <https://core.ac.uk/download/pdf/77094757.pdf>
- Lin, F. (2000). GIS-based information flow in a land-use zoning review process. *Landscape urban planning*, 52(1), 21-32. [https://doi.org/10.1016/S0169-2046\(00\)00110-9](https://doi.org/10.1016/S0169-2046(00)00110-9)
- Liu, X., Wang, X., Wright, G., Cheng, J., Li, X., & Liu, R. (2017). A state-of-the-art review on the integration of Building Information Modeling (BIM) and Geographic Information System (GIS). *ISPRS International Journal of Geo-Information*, 6(2), 53. <https://doi.org/10.3390/ijgi6020053>
- Lu, W., & Tam, V. (2013). Construction waste management policies and their effectiveness in Hong Kong: A longitudinal review. *Renewable sustainable energy reviews*, 23, 214-223. <https://doi.org/10.1016/j.rser.2013.03.007>
- Lu, W., Peng, Y., Xue, F., Chen, K., Niu, Y., & Chen, X. (2018). The Fusion of GIS and Building Information Modeling for Big Data Analytics in Managing Development Sites. In B. Huang (Ed.), *Comprehensive Geographic Information Systems* (pp. 345-359). Elsevier. <https://doi.org/https://doi.org/10.1016/B978-0-12-409548-9.09677-9>
- Lu, Y., Wu, Z., Chang, R., & Li, Y. (2017). Building Information Modeling (BIM) for green buildings: A critical review and future directions. *Automation in construction*, 83, 134-148. <https://doi.org/https://doi.org/10.1016/j.autcon.2017.08.024>
- Moghadam, S., Lombardi, P., Mutani, G., Osello, A., & Ugliotti, F. (2016). BIM-GIS modelling for sustainable urban development. Towards post-carbon cities, SBE16 Turin, Italy, 18-19. <https://www.researchgate.net/profile/Sara-Torabi/publication/303407348.pdf>
- Moreri, K., Mioc, D., Anton, F., Nickerson, B., McGillivray, E., Morton, A., . . . Tang, P. (2008). Web based geographic information systems for a flood emergency evacuation. 3rd International ISCRAM China workshop, Harbin. https://dl.wqtxts1xzle7.cloudfront.net/49630250/Web_based_Geographic_Information_Systems20161015-6471-ygvwf1-libre.pdf
- Sani, M., & Abdul, R. (2018). GIS and BIM integration at data level: A review. *The International Archives of the Photogrammetry, Remote Sensing Spatial Information Sciences*, 42, 299-306. <https://doi.org/10.5194/isprs-archives-XLII-4-W9-299-2018>
- Sheina, S., Chubarova, K., Dementeev, D., & Kalitkin, A. (2022). Integration of BIM and GIS technologies for sustainable development of the construction industry. In *International School on Neural Networks, Initiated by IIASS and EMFCSC* (pp. 1303-1311). Springer. https://doi.org/10.1007/978-3-031-11058-0_132
- Shi, J., Pan, Z., Jiang, L., & Zhai, X. (2023). An ontology-based methodology to establish city information model of digital twin city by merging BIM, GIS and IoT. *Advanced Engineering Informatics*, 57, 102114. <https://doi.org/10.1016/j.aei.2023.102114>
- Shirowzhan, S., Sepasgozar, S., Zaini, I., & Wang, C. (2017). An integrated GIS and Wi-Fi based Locating system for improving construction labor communications. *ISARC. Proceedings of the International Symposium on Automation and Robotics in Construction*. <https://doi.org/10.22260/ISARC2017/0145>
- Song, Y., Wang, X., Tan, Y., Wu, P., Sutrisna, M., Cheng, J., & Hampson, K. (2017). Trends and opportunities of BIM-GIS integration in the architecture, engineering and construction industry: A review from a spatio-temporal statistical perspective. *ISPRS International Journal of Geo-Information*, 6(12), 397. <https://doi.org/10.3390/ijgi6120397>
- Svaestuen, F., Knotten, V., Lædre, O., Drevland, F., & Lohne, J. (2017). Using building information model (BIM) devices to improve information flow and collaboration on construction sites. *Journal of Information Technology in Construction*, 10-16. <https://ntnuopen.ntnu.no/ntnu-xmlui/handle/11250/2502827>

- Thiis, T., & Hjelseth, E. (2008). Use of BIM and GIS to enable climatic adaptations of buildings. In *Ework and Ebusiness in Architecture, Engineering and Construction* (pp. 409-417). London. <https://doi.org/10.1201/9780203883327.ch46>
- Wan Abdul Basir, W., Majid, Z., Ujang, U., Chong, A., & Sciences, S. I. (2018). Integration of GIS and BIM techniques in construction project management—A review. *The International Archives of the Photogrammetry, Remote Sensing*, 42, 307-316. <https://doi.org/10.5194/isprs-archives-XLII-4-W9-307-2018>
- Wang, K., Zhang, C., Guo, F., & Guo, S. (2022). Toward an efficient construction process: what drives BIM professionals to collaborate in BIM-enabled projects. *Journal of Management in Engineering*, 38(4), 04022033. [https://doi.org/10.1061/\(ASCE\)ME.1943-5479.0001056](https://doi.org/10.1061/(ASCE)ME.1943-5479.0001056)
- Wang, Pan, Y., & Luo, X. (2019). Integration of BIM and GIS in sustainable built environment: A review and bibliometric analysis. *Automation in construction*, 103, 41-52. <https://doi.org/10.1016/j.autcon.2019.03.005>
- Wang, T., Pan, Y., & Luo, X. (2019). Integration of BIM and GIS in sustainable built environment: A review and bibliometric analysis. *Automation in construction*, 103, 41-52. <https://doi.org/10.1016/j.autcon.2019.03.005>
- Wu, B., & Zhang, S. (2016). Integration of GIS and BIM for indoor geovisual analytics. *The International Archives of the Photogrammetry, Remote Sensing Spatial Information Sciences*, 41, 455-458. <https://doi.org/10.5194/isprs-archives-XLI-B2-455-2016>
- Zhu, J., & Wu, P. (2022). BIM/GIS data integration from the perspective of information flow. *Automation in construction*, 136, 104-166. <https://doi.org/https://doi.org/10.1016/j.autcon.2022.104166>

Publisher's note: [Scienceline Publication](#) Ltd. remains neutral with regard to jurisdictional claims in published maps and institutional affiliations.



Open Access: This article is licensed under a Creative Commons Attribution 4.0 International License, which permits use, sharing, adaptation, distribution and reproduction in any medium or format, as long as you give appropriate credit to the original author(s) and the source, provide a link to the Creative Commons licence, and indicate if changes were made. The images or other third party material in this article are included in the article's Creative Commons licence, unless indicated otherwise in a credit line to the material. If material is not included in the article's Creative Commons licence and your intended use is not permitted by statutory regulation or exceeds the permitted use, you will need to obtain permission directly from the copyright holder. To view a copy of this licence, visit <https://creativecommons.org/licenses/by/4.0/>.

© The Author(s) 2024

Comparative Analysis of Statistical Models for Predicting the Properties of Agricultural Waste-Enhanced Sandcrete Blocks

Samson O. Odeyemi¹, Michael O. Adisa, Kabir O. Kenku, Samad A. Yusuf, Mutalib A. Amuda, and Stephen Okikiola Oladejo

Department of Civil & Environmental Engineering, Kwara State University, Malete, Nigeria

[✉]Corresponding author's Email: samson.odeyemi@kwasu.edu.ng

ABSTRACT

Sandcrete blocks represent an indispensable building material, primarily composed of sand, water, and cement as a binding agent. Given the significant cost associated with cement, there is a need to produce low-cement blocks that are economically viable and cost-effective. This challenge has prompted the exploration of alternative materials to reduce cement content, simultaneously addressing environmental pollution and health risks associated with agricultural waste in rural areas. Notable examples of such alternative materials include various agricultural waste components. The primary objective of this research is to establish statistical models for predicting the compressive strength of blocks reinforced with rice husk, guinea corn husk, maize straw, and a combination of sorghum husk and straw. The research findings indicate that the density of fibre-reinforced blocks decreased as the quantity of fibre increased. Furthermore, the compressive strength of the sandcrete blocks decreased as the fibre content increased. However, compressive strengths of 2.41 N/mm², 1.90, 2.40 N/mm², and 3.01 N/mm² were achieved for rice husk, guinea corn husk, maize-straw, and a combination of sorghum husk and straw-reinforced sandcrete blocks, respectively. Only sandcrete blocks with sorghum husk and straw met the Nigerian Industrial Standard specifications (NIS 87:2000). A water-binder ratio of 0.4 was determined as optimal for all the blocks under investigation. Four models with precision values higher than 4.0 were generated to predict the compressive strengths of the blocks. This research represents a valuable contribution to developing environmentally friendly building materials for the construction industry.

Keywords: Agricultural waste; Sandcrete blocks; Statistical models; Straw.

INTRODUCTION

Sandcrete blocks have been used in all types of masonry constructions in Nigeria, and other parts of the world. Over 90% of physical infrastructures in Nigeria are made with sandcrete blocks (Erakpoweri and Onah, 2022a). The usual requirement for a good sandcrete is its satisfactory compressive strength, however, research has shown that the compressive strength of sandcrete produced commercially in several parts of Nigeria, is below the recommended standard as stipulated in the Nigerian Industry Standard (NIS 87:2000, 2000). According to Anosike and Oyebade (2012) and Ajao et al. (2018), sandcrete manufacturers in Nigeria do not adhere to the guidelines for sandcrete production as stipulated by the Standard, and this could be traced to poor implementation and monitoring on the part of the Standard Organization of Nigeria (SON) to ensure adherence to the code

(Erakpoweri and Onah, 2022a). Sandcrete blocks are made of natural sand, water, and a binder. The costliest component in the production of sandcrete blocks is cement, which is the binder (Awolusi et al., 2021). Utilizing alternative stabilizers made from less expensive local materials will greatly enhance the production of sandcrete blocks with the desired properties at a low cost. In addition, it will significantly reduce construction costs and production costs (Alejo, 2020).

Rice husk (RH) has distinct physical and chemical characteristics, such as a high ash and silica content, making it useful for industrial processing. Numerous studies have demonstrated the use of RH as fuel for a variety of purposes (Kaviyarasu et al., 2016; Shen et al., 2014). Oyetola et al. (2006) and Khan et al. (2021) studied the possibility of using Rice Husk Ash (RHA) in the production of sandcrete blocks and reported that the water/cement ratio increases with rice husk ash contents

RESEARCH ARTICLE
 PII: S225204302400013-14
 Received: June 25, 2024
 Revised: September 02, 2024
 Accepted: September 05, 2024

and that up to 40% RHA could be added as a partial replacement for cement without any significant change in compressive strength at 60 days and 28 days respectively.

Maize straw fibre is a natural and renewable agricultural by-product derived from the stalks of maize (corn) plants. It is a versatile and eco-friendly material that has gained attention in various industries, including construction, packaging, and textile (Rahman et al., 2023; Saba et al., 2015). Various studies have been conducted using maize straw fibre in engineering; Odeyemi et al. (2022) conducted a study on maize straw-reinforced sandcrete blocks and found that incorporating 5% maize straw resulted in the highest compressive strength after 28 days. This strength was found to meet the recommendations of the Nigerian Industrial Standard. Odeyemi et al. (2017) investigated the effect of straw reinforcement on clay bricks. Their study revealed that adding straw to clay bricks at a water-clay mixing ratio of 0.15 increased the compressive strength of the bricks by 148%.

Guinea corn husks are byproducts remaining after the extraction of guinea corn seeds. These husks typically end up as non-biodegradable waste in landfills, contributing to environmental pollution (Adediran et al., 2019). Odeyemi et al. (2020) conducted a study to assess how guinea corn ash influenced the mechanical attributes of lateritic concrete when used as a substitute for Ordinary Portland Cement (OPC). The most effective blend was determined to be 20% Guinea Corn Husk Ash (GCHA) combined with 80% OPC, which yielded an elevated compressive strength of 18.78 N/mm².

Sorghum, comprising 25 species of flowering plants, is a robust grass that can reach heights of up to 4.6 meters (Xiong et al., 2019). Information obtained from Statista (2023) indicates that Nigeria ranks as the world's second-largest sorghum producer, generating an annual production of 6.7 million metric tons (Oladehinde Oladipo, 2023). Tijani's (2020) research delves into the utilization of Sorghum Husk Ash (SHA) as a viable substitute for cement in the production of sandcrete blocks. The inclusion of SHA is found to enhance compressive strength while maintaining an acceptable level of block density and water absorption.

Though researchers have studied the use of straw and ashes in sandcrete blocks, there are no results on the optimization of these straws in the blocks nor are there models that can predict the strength of the blocks containing the straws. To bridge this gap, this research developed statistical predictive models for the compressive strength of agricultural waste-enhanced sandcrete blocks.

MATERIALS AND METHODS

This section enumerates the materials used and the methods adopted in getting the results for this research.

Materials

Portland Limestone Cement (PLC) of Dangote cement brand with grade 42.5R which complied with BS 8500-1 (2023) was used. The Sharp sand, which conformed to the specifications in BS EN12620 (2013) was locally sourced from Malete, Kwara state, Nigeria. The potable water used was free from impurities. Rice husk, Sorghum husk, Guinea corn husk, maize and sorghum straws were sourced locally from Oja Oba, Ilorin, Kwara state, Nigeria. The straws were broken into small sizes of about 10 centimetres.

Mix proportion

The experiment was designed using the Design Expert software package (Version 13) to optimize the agro waste (ranging from 5% to 10%) and the water-cement ratio (from 0.4 and 0.6) through a Response Surface Methodology (RSM) within a Central Composite Design (CCD). The agro-waste materials were incorporated into the sandcrete mix of ratio 1:6 (cement-to-sand ratio). Before conducting the laboratory experiments, combinations were systematically designed as required by CCD. In the first part of the study, two independent variables were considered: the specific agro-waste materials (Guinea corn husk, rice husk, and maize straw fibre) and the water-cement ratio. This led to 13 experimental runs aimed at measuring compressive strength. In another part of the study, a similar procedure was followed for a combination of sorghum husk and straw with a fixed water-cement ratio. This part produced 14 experimental runs to assess the compressive strength, water absorption, and density of the sandcrete block. Figure 1 shows a typical designed experiment interface in the Design Expert software package.

A manual method of mixing was adopted in producing the blocks of 225 mm × 225 mm × 450 mm size. Afterwards, the blocks were cured for 28 days by full immersion in water before testing for their strengths.

Property determination

The density of each block was calculated by finding the fraction of the volume of the blocks to its weight following BS EN 772- 13 (2000) as shown in (Eq. 1).

$$\text{Density} = \frac{\text{Weight of the block (kg)}}{\text{Volume of block (m}^3\text{)}} \quad (1)$$

The strengths of the blocks were determined using a STYE-2000 Analogue type compression testing machine with serial number 131010 (Figure 2) supplied by Okhard Machine Tools, Lagos, Nigeria at the Kwara State Ministry of Works' Works and Transport laboratory, Ilorin, Nigeria.

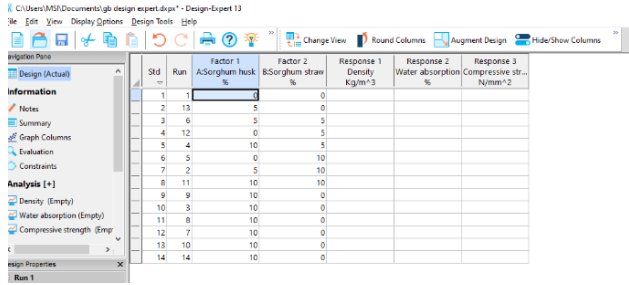


Figure 1. Design interface for Sorghum husk and sorghum straw.



Figure 2. Compressive strength test

The compressive strength was determined using (Eq. 2).

$$\text{Compressive strength} = \frac{\text{Maximum load (kN)} \times 1000}{\text{Cross-sectional Area (mm}^2\text{)}} \quad (2)$$

The water absorption capacity for the blocks was determined at the concrete laboratory of the Department of Civil Engineering, Kwara State University, Malete, following the specifications in BS EN 772-21 (2011) and calculated using (Eq. 3).

$$\text{Water absorption (\%)} = \frac{M_w - M_d}{M_d} \times 100 \quad (3)$$

Model formulation

The statistical models were constructed using the Design Expert software package utilizing the multiple linear regression technique. As illustrated in (Eq. 4), the models depict a relationship involving Y, X₁, and X₂:

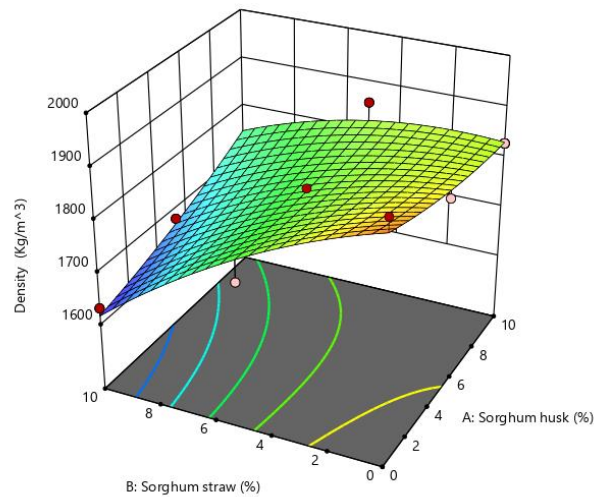
$$Y = a + bX_1 + cX_2 + \epsilon \quad (4)$$

Y represents the dependent variable, X₁ and X₂ represent the independent variables, ε represents the error term, while a, b, and c are the coefficients within the regression equations (Erakpoweri & Onah, 2022b).

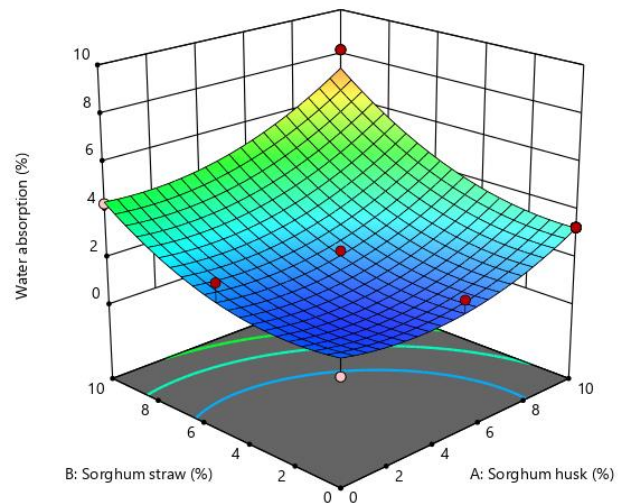
RESULTS AND DISCUSSIONS

Density result

Graphs 1 and 2 show the 3D relationship between the sorghum husks and straws with density and water absorption respectively. The graphs reveal that increasing the volume of both husk and straw in the blocks led to a reduction in the density and an increase in the water absorption capacities of the blocks. These results conform with the submission of Odeyemi et al. (2021).



Graph 1. Relationship of sorghum husks and straws with density

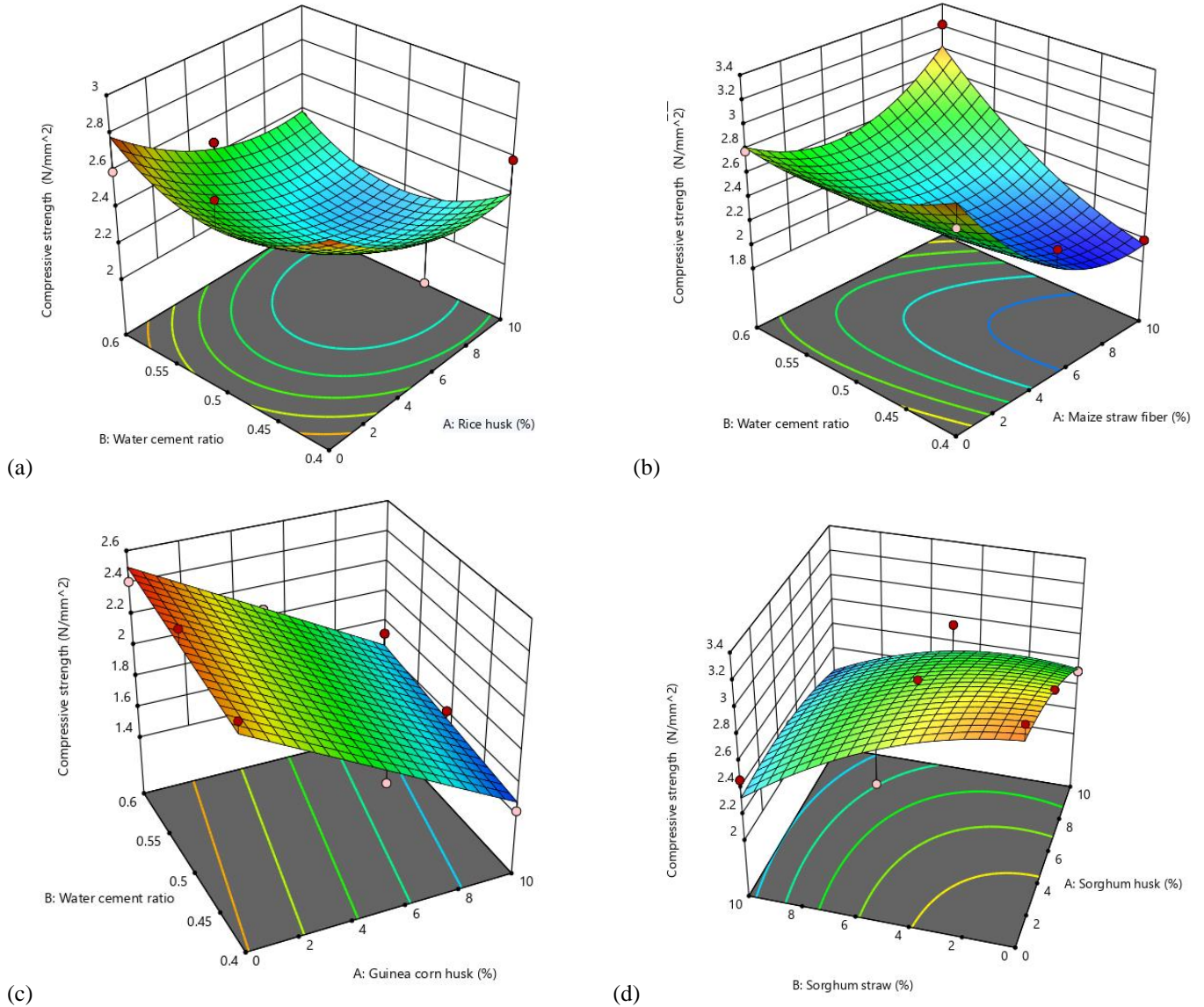


Graph 2. Relationship of sorghum husks and straws with water absorption

Compressive strength results

Graphs 3 (a-d) depict the relationship between water-cement ratio, volume of agro waste and compressive strength for rice husk, maize straw fibre, guinea corn husk, sorghum husk and straw respectively. The addition of the straws in the blocks adversely affected the strength of the

blocks. This could be due to the straws taking up some of the spaces that the sandcrete mortar could have occupied. The increase in the water-cement ratio equally led to a decline in the strength of the blocks. This is consistent with results from the literature (Neville, 2011; Odeyemi, 2021).



Graph 3. Relationship between water-cement ratio, agro waste and compressive strength (a) rice husk (b) maize straw fibre (c) guinea corn husk (d) sorghum husk and straw

Table 1. Optimized values of agro-waste incorporation in sandcrete blocks

Agro-waste	Quantity (%)	Water-cement Ratio	Density	Water absorption	Compressive Strength	Desirability (%)
Rice Husk	10	0.4	-	-	2.41	100
Guinea corn husk	4.70	0.4	-	-	1.90	59
Maize straw	10	0.4	-	-	2.40	78
Sorghum Husk	4	0.4	1841	1.75	3.01	81
Sorghum straw	6					

Optimization

From the 28th-day results for the blocks containing the various straws, an optimization process was conducted on the sandcrete blocks. The goal was to maximize the rice husks/straw content and compressive strength while minimizing the water-cement ratio. The optimized combination, strength obtained and the desirability value are presented in (Table 1). The optimized chart for the combined sorghum husk and straw sandcrete is shown in Figure 3. Only sandcrete blocks with sorghum husk and straw met the Nigerian Industrial Standard (NIS 87:2004, 2004) specifications for non-load bearing walls. However, the reported strengths are higher than the ones produced by the eight block industries reported by Odeyemi et al. (2018).

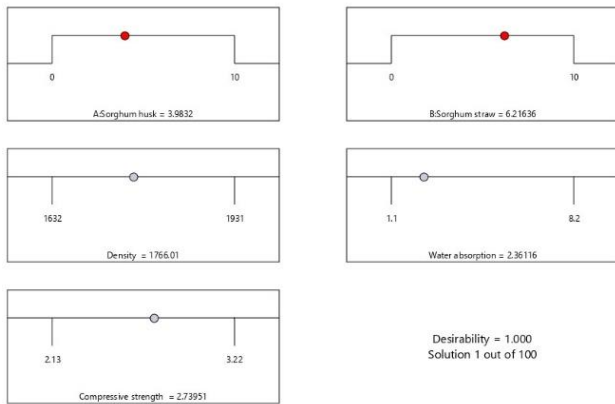


Figure 3. Optimization of sorghum husk and straw

Model equations

Equations 5-8 relate the compressive strength to the various agro-wastes and water-cement ratios.

$$C = 8.2478 - 0.0946R - 22.75W - 0.005RW + 0.0058R^2 + 22.75W^2 \tag{5}$$

$$C = 3.10 - 0.023H - 0.015S + 0.0046HS - 0.0034 H^2 - 0.0062S^2 \tag{6}$$

$$C = 7.54 - 0.52M - 17.6W + 0.675MW + 0.0138M^2 + 16.25W^2 \tag{7}$$

$$C = 0.6477 - 0.1728G + 7.1846W + 0.15GW + 0.0012G^2 - 7.0W^2 \tag{8}$$

Where C = Compressive strength, R, H, M and G = Percentage of rice, sorghum, maize and guinea corn husks respectively, S = Percentage of sorghum straw and W = Water-cement ratio.

Model validation

All the models yielded a precision value higher than 4.0 (Table 2), indicating a satisfactory signal-to-noise

ratio. This suggests that the models are dependable for guiding design exploration, thus validating the models.

Table 2. Fit statistics of all the models

Statistical parameter	Rice husk	Sorghum husk and straw	Guinea corn husk	Maize straw fibre
Adeq Precision	5.76	10.9761	33.3233	5.75

CONCLUSIONS

The following conclusions are made from this research:

1. The addition of rice, sorghum, guinea corn maize husks and sorghum straw lowers the compressive strength of sandcrete blocks.
2. Optimized strengths of 2.41 N/mm², 1.90 N/mm², 2.40 N/mm², 3.01 N/mm², were obtained for sandcrete blocks containing rice husk, guinea corn husk, maize straw and sorghum husk combined with sorghum straw respectively.
3. The strengths of sandcrete blocks containing rice, guinea corn, maize straw husks, and sorghum husks combined with sorghum straw were predicted using statistical models.

DECLARATIONS

Corresponding author

Correspondence and requests for materials should be addressed to Samson O. Odeyemi; Email: samson.odeyemi@kwasu.edu.ng ; ORCID: 0000-0001-5217-3403

Data availability

The datasets used and/or analyzed during the current study are available from the corresponding author upon reasonable request.

Acknowledgments

The authors would like to acknowledge the Tertiary Education Trust Fund (TETFund) for sponsoring the presentation of these findings at the International Conference on Civil Engineering for Sustainability and Resilience in the 21st Century and Beyond (ICCESR 2024) at the University of Botswana and the Kwara State University, Malete, Nigeria, for creating a conducive environment to conduct this research.

Authors' contribution

The first author developed the concept for the research and designed the experimental process. The second author assisted in the design of the experimental

process and writing the manuscript. The third, fourth, fifth and sixth authors carried out the bench work and wrote the draft manuscript. Both the first and second authors read and approved the final manuscript.

Competing interests

The authors declare no competing interests in this research and publication.

REFERENCES

- Adediran, A. A., Olawale, O., Ojediran, J., Aladegboye, S., Atoyebi, O. D., Akinlabi, E. T., and Adeniyi Olayanju, T. M. (2019). Properties of agro-based hybrid particleboards. *Procedia Manufacturing*, 35. <https://doi.org/10.1016/j.promfg.2019.05.064>
- Ajao, A. M., Ogunbayo, B. F., Ogundipe, K. E., Bamigboye, G. O., Ogunde, A. O., and Tunji-Olayeni, P. F. (2018). Assessment of Sandcrete Blocks Manufacturers' Compliance to Minimum Standard Requirements by Standard Organisation of Nigeria in Southwest, Nigeria. In *International Journal of Applied Engineering Research* (Vol. 13, Issue 6). https://www.researchgate.net/publication/323906468_Assessment_of_Sandcrete_Blocks_Manufacturers'_Compliance_to_Minimum_Standard_Requirements_by_Standard_Organisation_of_Nigeria_in_Southwest_Nigeria
- Alejo, A. O. (2020). Comparison of strength of sandcrete blocks produce with fine aggregate from different sources. *Nigerian Journal of Technology*, 39(2). <https://doi.org/10.4314/njt.v39i2.2>
- Anosike, M. N., & Oyebade, A. A. (2012). Sandcrete Blocks and Quality Management in Nigeria Building Industry. *Journal of Engineering, Project, and Production Management*, 2(1), 37–46. https://www.researchgate.net/publication/267782315_Sandcrete_Blocks_and_Quality_Management_in_Nigeria_Building_Industry
- Awolusi, T. F., Oguntayo, D. O., Babalola, O. E., Oke, O. L., and Akinkulore, O. O. (2021). Investigation of micronized laterite sandcrete block compressive strength. *Case Studies in Construction Materials*, 14. <https://doi.org/10.1016/j.cscm.2021.e00530>
- British Standards Institution (BSI). (2013). BS EN 12620:2013 Aggregates for concrete. *British Standards*. <https://knowledge.bsigroup.com/products/aggregates-for-concrete-1?version=standard>
- BS 8500-1:2023. (2023). *Concrete. Complementary British Standard to BS EN 206 - Method of specifying and guidance for the specifier*. <https://knowledge.bsigroup.com/products/concrete-complementary-british-standard-to-bs-en-206-method-of-specifying-and-guidance-for-the-specifier-1?version=tracked>
- BS EN 772-13:2000. (2000). *Methods of test for masonry units - Determination of net and gross dry density of masonry units (except for natural stone)*. <https://knowledge.bsigroup.com/products/methods-of-test-for-masonry-units-determination-of-net-and-gross-dry-density-of-masonry-units-except-for-natural-stone?version=standard>
- BS EN 772-21:2011. (2011). *Methods of test for masonry units. Determination of water absorption of clay and calcium silicate masonry units by cold water absorption*. <https://standardsdevelopment.bsigroup.com/projects/2010-00062#/section>
- Erakpoweri, D. O., and Onah, N. H. (2022a). Application of statistical model for predicting the compressive strength of sandcretes made with different fine aggregates available in Nsukka. *Nigerian Journal of Technology*, 41(1), 1–7. <https://doi.org/10.4314/njt.v41i1.1>
- Erakpoweri, D. O., and Onah, N. H. (2022b). Application of statistical model for predicting the compressive strength of sandcretes made with different fine aggregates available in Nsukka. *Nigerian Journal of Technology*, 41(1), 1–7. <https://doi.org/10.4314/njt.v41i1.1>
- Kaviyarasu, K., Manikandan, E., Kennedy, J., Jayachandran, M., and Maaza, M. (2016). Rice husks as a sustainable source of high quality nanostructured silica for high performance Li-ion battery requital by sol-gel method - a review. *Advanced Materials Letters*, 7(9). <https://doi.org/10.5185/amlett.2016.6192>
- Khan, W., Fahim, M., Zaman, S., Khan, S. W., Badrashi, Y. I., and Khan, F. (2021). Use of Rice Husk Ash as Partial Replacement of Cement in Sandcrete Blocks. *Advances in Science and Technology Research Journal*, 15(2). <https://doi.org/10.12913/22998624/133470>
- Neville, A. M. (2011). *Properties of Concrete* (5th ed.). Pearson Education Ltd. https://books.google.com.ng/books/about/Properties_of_Concrete.html?id=mmygngEACAAJ&redir_esc=y
- NIS 87:2000. (2000). *Standard for Sandcrete Blocks*. Nigerian Industrial Standard, Standard Organisation of Nigeria, Lagos, Nigeria.
- NIS 87:2004. (2004). *Standard for Sandcrete Blocks in Nigeria*. Nigerian Industrial Standard, Standard Organisation of Nigeria, Lagos, Nigeria.
- Odeyemi, S. O. (2021). Mechanical Properties of Granite-Gravel Porous Concrete. *International Journal of Engineering Research in Africa*, 57, 115–123. <https://doi.org/https://doi.org/10.4028/www.scientific.net/JEIRA.57.115>
- Odeyemi, S. O., Abdulwahab, R., Giwa, Z. T., Anifowose, M. A., Odeyemi, O. T., and Ezenweani, C. F. (2021). Effect of Combining Maize Straw and Palm Oil Fuel Ashes in Concrete as Partial Cement Replacement in Compression. *Trends in Sciences*, 18(19), 29. <https://doi.org/10.48048/tis.2021.29>
- Odeyemi, S. O., Akinpelu, M. A., Atoyebi, O. D., and Orire, K. J. (2018). Quality Assessment of Sandcrete Blocks Produced in Adeta, Kwara State, Nigeria. *Nigerian Journal of Technology (NIJOTECH)*, 37(1), 53–59. <https://doi.org/http://dx.doi.org/10.4314/njt.v37i1.7>
- Odeyemi, S. O., Akinpelu, M. A., Atoyebi, O. D., and Yahaya, R. T. (2017). Determination of Load Carrying Capacity of Clay Bricks Reinforced With Straw. *International Journal of Sustainable Construction Engineering & Technology*, 8(2). <https://publisher.uthm.edu.my/ojs/index.php/IJSCET/article/view/1727>

- Odeyemi, S. O., Anifowose, M. A., Bello, S. A., Giwa, Z. T., and Wilson, U. N. (2022). Strength Properties and Microstructure of Sandcrete Blocks Incorporated with Maize Straws. *Advanced Engineering Forum*, 46, 71–78. <https://doi.org/10.4028/P-KGOEZO>
- Odeyemi, S. O., Atoyebi, O. D., and Ayo, E. K. (2020). Effect of Guinea Corn Husk Ash on the Mechanical Properties of Lateritic Concrete. *IOP Conference Series: Earth and Environmental Science*, 445(1). <https://doi.org/10.1088/1755-1315/445/1/012034>
- Oladehinde Oladipo. (2023, June 16). *Nigeria's multi-billion dollar sorghum market attracts global brewers - Businessday NG*. Business Day. <https://businessday.ng/business-economy/article/nigerias-multi-billion-dollar-sorghum-market-attracts-global-brewers/>
- Oyetola, E. B., and Abdullahi, M. (2006). The use of rice husk ash in low - cost sandcrete block production. *Journal of Practices and Technologies*, 8(8). https://www.researchgate.net/publication/26449116_The_Use_of_Rice_Husk_Ash_in_Low_-_Cost_Sandcrete_Block_Production
- Rahman, M. A., Haque, S., Manokar, M. A., Kamaludeen, B.K. (2023). A review of environmental friendly green composites: production methods, current progresses, and challenges. *Springer*, 30(7), 16905–16929. <https://doi.org/10.1007/s11356-022-24879-5>
- Saba, N., Paridah, M. T., Jawaid, M., Abdan, K., and Ibrahim, N. A. (2015). Potential utilization of kenaf biomass in different applications. *Agricultural Biomass Based Potential Materials*, 1–34. https://doi.org/10.1007/978-3-319-13847-3_1
- Shen, Y., Zhao, P., and Shao, Q. (2014). Porous silica and carbon derived materials from rice husk pyrolysis char. In *Microporous and Mesoporous Materials* (Vol. 188). <https://doi.org/10.1016/j.micromeso.2014.01.005>
- Statistica. (2023). *Nigeria: production of sorghum 2010-2022 / Statista*. <https://www.statista.com/statistics/1134511/production-of-sorghum-in-nigeria/>
- Tijani, M. A., Ajagbe, W. C., Ganiyu, A. A., Aremu, A. S., and Ojewole, Y. N. (2020). Strength and Absorption of Sorghum Husk Ash Sandcrete Blocks. *Premier Journal of Engineering and Applied Science*, 1(1), 1–7. <https://pjeas.com/download.php?id=31>
- Xiong, Y., Zhang, P., Warner, R. D., and Fang, Z. (2019). Sorghum Grain: From Genotype, Nutrition, and Phenolic Profile to Its Health Benefits and Food Applications. In *Comprehensive Reviews in Food Science and Food Safety* (Vol. 18, Issue 6). <https://doi.org/10.1111/1541-4337.12506>

Publisher's note: [Scienceline Publication](#) Ltd. remains neutral with regard to jurisdictional claims in published maps and institutional affiliations.



Open Access: This article is licensed under a Creative Commons Attribution 4.0 International License, which permits use, sharing, adaptation, distribution and reproduction in any medium or format, as long as you give appropriate credit to the original author(s) and the source, provide a link to the Creative Commons licence, and indicate if changes were made. The images or other third party material in this article are included in the article's Creative Commons licence, unless indicated otherwise in a credit line to the material. If material is not included in the article's Creative Commons licence and your intended use is not permitted by statutory regulation or exceeds the permitted use, you will need to obtain permission directly from the copyright holder. To view a copy of this licence, visit <https://creativecommons.org/licenses/by/4.0/>.

Mapping Buildings from Semi-Informal Settlements Using Non-Parametric Classifiers: A Case of Old Naledi

Wame Mpoeleng , Mooketsi Segobye ✉ , Yashon Ouma , Kealeboga Moreri , Bagadzi M. Manisa ,
Boipuso Nkwae , Lopang Maphale  and Nyaladzani Nkhwanana 

University of Botswana, Gaborone, Botswana

✉ Corresponding author's Email: segobyem@ub.ac.bw

ABSTRACT

Building footprints are essential for planning and designing new infrastructure like water reticulation, electricity transmission, sewer, and road networks. They are also necessary for delivery, census, and disaster management. It is therefore important to have up-to-date maps and GIS databases for service provision. However, mapping building of footprints in semi-informal settlements is problematic because of the spatial heterogeneity of settlements. This study evaluates three non-parametric machine learning algorithms for extracting building footprints from WorldView-2 (WV2) satellite imagery in a semi-informal settlement. WV2 satellite imagery data was fused with gray-level co-occurrence matrices (GLCM) to enhance building extraction. The algorithms used include the Gaussian Mixture Model (GMM), Random Forest (RF), and Support Vector Machine (SVM). The results indicate that GLCM does not improve the detection of buildings when using the GMM algorithm, but it increases building detection with RF and SVM. The GMM algorithm achieved the highest average accuracy of 92% for building detection. However, SVM and RF have an overall accuracy of 79% and 70% respectively. Though RF did not perform very well in identifying individual buildings, its overall accuracy was high. The outcome indicates that machine learning algorithms can adequately map building footprints from high-resolution satellite imagery.

Keywords: Building detection, WorldView-2, machine learning, Gray-Level Co-Occurrence Matrix (GLCM)

INTRODUCTION

Rapid urban development in developing countries has led to the emergence of informal settlements (Hofmann et al.; Mboga et al. 2017; Matarira et al. 2022). UN-Habitat (2015) defines informal settlements as residential areas where (i) there is no security of tenure; (ii) basic services are not available, and (iii) housing is not compliant with current housing and planning regulations. Shortage of basic engineering services, such as water, sewerage and solid waste removal can lead to undesirable living conditions. These services are crucial for attaining the global SDGs, local policies (i.e. Vision 2036), disaster management, and management of humanitarian crises. However, it is difficult to provide basic services because of a shortage of spatial data in informal settlements. Spatial information is required to improve understanding of settlement morphology, population distribution and emerging settlement patterns, which are necessary for decision-making and planning (Mboga et al., 2017). It is therefore critical to have up-to-date maps and GIS

databases for better service provision and to identify and quantify services and infrastructure. Conventional, ground surveys and photogrammetry, mapping techniques have been used to gather spatial information. However, they (ground surveys and photogrammetry) are expensive, resource-intensive and time-consuming resulting in data unavailability and information gaps (Mudau and Mhangara, 2021). Consequently, there is a need for methods that can generate reliable and consistent data on the spatial distribution of built-up areas and building structures.

Earth Observation (EO) provides an alternative to conventional mapping. EO allows for the collection of continuous spatial data in satellite images. Technological advances in EO have led to the availability of high-resolution images, which can be leveraged in mapping complex areas like informal settlements. High-resolution imagery has been used in several studies for the extraction of human settlements (Hofmann et al.; Mboga et al., 2017; Shafizadeh-Moghadam et al., 2021), land use and land cover (LULC) (Tassi and Vizzari, 2020; Vizzari, 2022),

RESEARCH ARTICLE
 PII: S225204302400014-14
 Received: June 25, 2024
 Revised: September 02, 2024
 Accepted: September 05, 2024

and building detection (Zhao et al., 2018; Khatriker and Kumar, 2018). In the building detection studies, Zhao et al. (2018) used convolutional neural networks while (Khatriker and Kumar, 2018) used image segmentation. Accordingly, various methods are used in building footprint extraction, the basic layer in a spatial database.

Feature extraction from remote sensing imagery data can be done through visual image interpretation, traditional pixel-based classification, Object-based image analysis (OBIA) and machine learning techniques (Mudau and Mhangara 2021). Informal settlements are characterised by small buildings, less vegetation, and irregular patterns, hence visual interpretation is labour-intensive and time-consuming. OBIA yields better classification results, however, it requires high computational power and proprietary imaging software (Vizzari, 2022). Machine learning algorithms have also been found to produce good results and are easily available. According to Sheykhmousa et al. (2020), Random Forest (RF), Support Vector Machines (SVM), and deep learning algorithms are the most used classification methods. Deep learning techniques can retrieve complex patterns and informative features from satellite images. However, they are highly dependent on the amount of data. RF and SVM, on the other hand, have been found to learn tasks from a small amount of data, but with competitive results to deep learning (Mboga et al., 2017). GLCM indices are normally used to improve machine learning classification. For example, Burnett et al. (2019) mapped the extent of coconut using a combination of WorldView-2 (WV2) imagery and GLCM textures. While Pantoja et al. (2023) conducted LULC classification using GLCM and Landsat 8 imagery.

This study proposes to use machine-learning classifiers, GMM, RF, and SVM, to map building footprints in Old Naledi, an informal settlement in Gaborone, Botswana, using WV2 satellite imagery. To achieve this the study will (i) investigate the significance of GLCM texture features in detecting building footprints from WV2 images and (ii) explore the performance of machine-learning classifiers in extracting building footprints.

MATERIALS AND METHODS

Study area

Old Naledi, known as “Zola”, was chosen as the study area. It is located at the southern tip of Botswana’s capital, Gaborone (Figure 1). “Zola” covers a total area of around 159 hectares. The population is 18,050 as of the

2022 census (Statistics Botswana 2022). The origin of Old Naledi can be traced to the construction of Gaborone industrial areas in 1964 (Van Nostrand 1982). The area lacks proper street arrangements and public sanitation facilities. It is comprised of low-income housing which emerged as a semi-informal settlement and is an area with high crime rates in Gaborone. For planning and upgrading the area, the up to date topographical and building footprint is required.

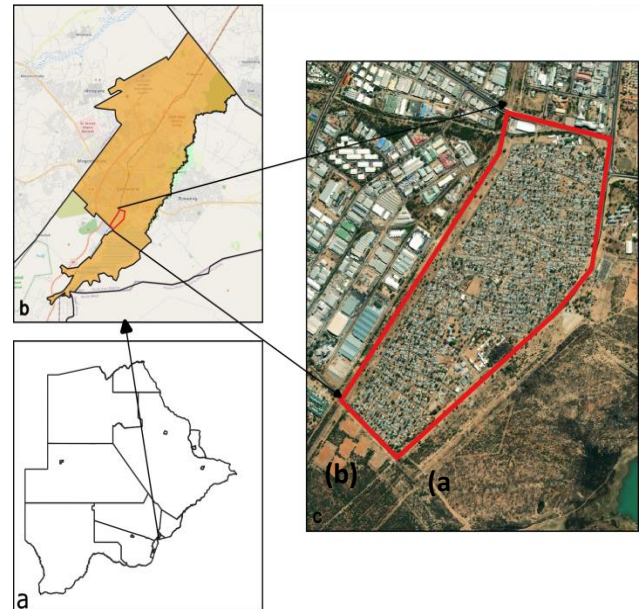


Figure 1. Study area showing (a) Botswana, (b) Gaborone and (c) Old Naledi

Methodology

Figure 2 shows the process used in extracting buildings from high-resolution satellite images. The workflow includes image composition, textural analysis, machine learning (ML) image classification, and accuracy assessment. The first step is to acquire high-resolution images from WV2 and pre-process the image to a multispectral image (MSI). To improve the resolution of the MSI image, pan-sharpening is applied using the panchromatic band of WV2 imagery.

The second stage involves calculating texture metrics using the GLCM technique. The GLCM indices are integrated with the pan-sharpened image input into ML algorithms (GMM, RF, and SVM) to classify the image pixels into buildings, bare soils, trees, roads, and grass. Finally, an accuracy assessment is conducted using the classification metrics outlined in the Accuracy Assessment Section.

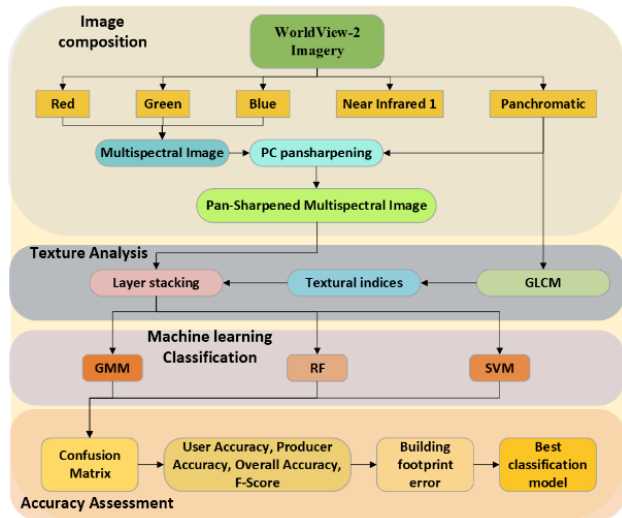


Figure 2. Flowchart of informal settlement classification using machine learning

Table 1. World View-2 spectral bands

Spectral band	Wavelength (nm)	Resolution (m)
Coastal Blue	400 - 450	1.84
Blue	450 - 510	1.84
Green	510 - 580	1.84
Yellow	585 - 625	1.84
Red	630 - 690	1.84
Red Edge	705 - 745	1.84
Near Infrared 1	770 - 895	1.84
Near Infrared 2	860 -1040	1.84
Panchromatic	450 - 800	0.46

Image composition

WorldView-2 (WV2) satellite imagery was used as the primary data source. WV2 is a DigitalGlobe satellite sensor launched in 2009 (Belfiore and Parente 2016). The sensor provides eight spectral bands and a high-resolution panchromatic band (see Table 1). This study utilized the red, green, blue, Near Infrared 1 (NIR1), and

panchromatic (PAN) bands of WV2 imagery. A multispectral image (MSI) is created by combining four low-resolution multispectral bands (Red, Green, Blue and Near Infrared 1 (RGBNIR)) through layer stacking (Figure 3(a)). By combining datasets with different signatures, layer stacking can improve the analysis and interpretation of the data and allow the visualisation of complex data.

The RGBNIR MSI image created above is a colour image with a spatial resolution of 1.84 m, and at this resolution, some objects will not be visible. On the other hand, the WV2 Panchromatic band is a monochrome (black and white) image with a spatial resolution of 0.46 m. Thus, the PAN image lacks a realistic true view of the world. The two images can be fused to produce an enhanced image with a high spatial and spectral resolution through a process called pan-sharpening (Li et al. 2017). Pan-sharpening reveals more information than the individual input image, as the image will be rich in spectral content and have high resolution (Fig. 3b).

Gray-level co-occurrence matrix (GLCM) textural features

Textural features are important for classifying data with low inter-class variability (Burnett et al. 2019) as they improve classification and avoid fuzziness (Matarira et al. 2022). The GLCM algorithm is widely used in extracting textural data from remote sensing data (Khatriker and Kumar 2018; Shafizadeh-Moghadam et al. 2021; Matarira et al. 2022). GLCM is used in the computation of spatial dependence of grey levels in an image, it creates a matrix describing the frequency of the appearance of individual pairs of values in a specific image fragment. GLCM textures can be extracted from a single multispectral band, a composite of multispectral bands, or a panchromatic band. The WV2 PAN band was used, because of its high spatial resolution. Seven textural features were extracted from the WV2 PAN, including mean, contrast, variance, second moment, entropy, homogeneity, and dissimilarity. The description of the textures is presented in Table 2.



Figure 3. WorldView-2 satellite images (a) RGBNIR image and (b) pan-sharpened image

Table 2. GLCM features calculated from PAN band and their descriptions

	GLCM Texture	Texture Group	GLCM Texture Description
1	Mean	Statistical	Measures the mean of the gray level sum distribution of the image
2	Contrast	Contrast	Measures the contrast based on the local grey level variation
3	Variance	Statistical	Measures the dispersion of the grey level distribution to emphasize the visual edges of land-cover patches
4	Second Moment	Orderliness	Measures the uniformity or energy of the grey level distribution of the image.
5	Entropy	Orderliness	Measures the degree of the disorder among pixels in the image
6	Homogeneity	Contrast	Measures the smoothness (homogeneity) of the image

Image classification using machine learning

As mentioned, three non-parametric algorithms are applied for the pixel-based image classification, and these are GMM, RF, and SVM. Input data to the machine learning algorithms is the MSI image alone and the seven (7) GLCM textural indices layer-stacked consecutively on the MSI. Therefore, eight (8) input data sets are utilized (Table 3), resulting in 24 classifications.

Table 3. layer-stacked data inputs to ML classification algorithms

Input	Image
1	MSI
2	1 + Mean
3	2 + Variance
4	3 + Contrast
5	4 + Second Moment
6	5 + Homogeneity
7	6 + Entropy
8	7 + Dissimilarity

Gaussian mixture model (GMM)

The GMM model is an unsupervised clustering method that groups subpopulations of a population based on the Gaussian distribution (Wan et al. 2019). The model is composed of multivariate Gaussian components. GMM is then used to distribute data points to the Gaussian components. Equation 1 below represents the GMM model.

$$P(x) = \sum_{i=1}^k \pi_i \mathcal{N}(x|\mu_i, \Sigma_i) \quad \#(1)$$

were $P(x)$ is the probability of pixel x , K is the number of components in the mixture, π_i is the weight of the i^{th} component, $\mathcal{N}(x|\mu_i, \Sigma_i)$ is the Gaussian distribution, μ_i is the mean vector and Σ_i is the covariance matrix. The matrix weight must satisfy the condition $\sum_{i=1}^K \pi_i = 1$ (Menezes and Poojary 2020).

Random forest (RF)

RF is a non-linear, tree-based, supervised machine-learning algorithm that was proposed by Breiman (2001) in 2001. It is an ensemble learning (multiple classifier systems) technique capable of performing both classification and regression analysis (Rahaman et al. 2019). Sub-samples or decision trees are selected through bootstrapping to ensure diversity in the decision trees. The decision trees are then trained through bootstrap aggregation (bagging) to build a model, which guarantees independence among the trees. The models from each decision tree are combined to arrive at the final model. Observations that are not used in a bootstrap sample, which are called “out-of-bag” (OOB), are used for error calculation and variable importance (Cutler et al. 2012).

Support vector machine (SVM)

SVM is a supervised machine learning algorithm for finding the optimal hyperplane that separates a dataset into predefined classes by using training data (Sheykhmousa et al. 2020). In SVM, the goal is to increase the margin of training data closest to the hyperplane from each class (Foody and Mathur 2004). The margin is the distance of training samples closest to the optimal boundary, the samples known as support vectors. The advantages of the SVM are that it is well suited to small complex data and high dimensional spaces.

Accuracy assessment

Classification accuracy assessment was computed from the confusion matrix, which is commonly used in evaluating classified maps (Barsi et al. 2018; Tassi and Vizzari 2020; Vizzari 2022). The matrix shows the number of true positives (TP) for a correct prediction, true negatives (TN) for a correct rejection, false positives (FP) for an incorrect prediction, and false negatives (FN) for a true rejection. The matrix allows for quantitative analysis of the classification using metrics in equations 2 - 5.

$$UA = \frac{TP}{TP + FP} \quad \#(2)$$

$$PA = \frac{TP}{TP + FN} \quad \#(3)$$

$$F - Score = 2 \frac{UA \times PA}{UA + PA} \quad \#(4)$$

$$OA = \frac{TP + TN}{TP + FP + TN + FN} \quad \#(5)$$

where PA is the producer’s accuracy, UA is the user accuracy meaning the, OA is the overall accuracy. PA gives the ratio of the true detected pixels against the building pixels and is related to omission error ($1 - PA$). UA is the ratio of detected pixels against all detected pixels and is concerned with the commission error ($1 - UA$). The F-score is a more sensitive and specific measure of the reliability of a classifier as it combines PA and UA .

RESULTS AND DISCUSSION

Significance of GLCM textures

Figure 4 shows an extract from the classification for each input and classification model. The figure shows more detail for input 1 (MSI) and less for inputs 2 – 8, which were layer-stacked with GLCM textures, in the GMM classification. This could indicate that GLCM textures cause GMM to overfit or underfit the data. For the RF algorithm, all images are similar showing that GLCM textures have less influence on building extraction. The SVM classification shows more detail when GLCM textures are layer-stacked on the RGBNIR image. Thus, GLCM textures improve SVM classification.

Table 4 shows the quantitative classification analysis for each input data and classification model. Table 4 confirms the results in Figure 4 results, from which it is evident that GLCM texture reduces the predicting power of GMM. When textures are introduced, the sensitivity of prediction is reduced as shown by the low PA values. The variation of PA and UA values is small for the RF classification, hence GLCM textures have less impact on RF building detection. SVM classification shows fewer false hits for input 3 (MSI + MEAN + CONTRAST) with a PA value of 99.28%. Contrast, entropy and dissimilarity reduce the predicting power of SVM.

The F-score and OA (Table 4 and Figure 5) show that the input with the best precision, sensitivity, and accuracy was input 1 for GMM and input 3 for SVM. Therefore, inputs 1 and 3 are selected as the representatives of the GMM and SVM models respectively.

For RF the inputs with the highest values differ, input 7 has the highest F-score value whereas input 6 has the

highest OA value (Table 4 and Figure 5). As OA is the accuracy of a classifier for all classes, input 6 is selected as the representative for the RF model. According to Figure 6, RF is more consistent in identifying the different classes and is more appropriate for the classification in this area.



Table 4. Classification results of the different models

Input	GMM			RF			SVM		
	PA (%)	UA (%)	F-score (%)	PA (%)	UA (%)	F-score (%)	PA (%)	VA (%)	F-score (%)
1	99.3	99.47	99.38	99.51	99.51	99.51	99.12	98.48	98.80
2	97.77	99.35	98.55	99.04	99.61	99.32	98.64	99.53	99.08
3	97.51	99.00	98.25	99.26	99.76	99.51	99.28	99.36	99.32
4	97.18	98.74	97.95	99.57	99.82	99.69	98.08	99.55	98.81
5	94.23	89.51	91.81	99.49	99.90	99.69	99.20	98.97	99.08
6	93.65	89.30	91.42	99.59	99.92	99.75	98.88	99.28	99.08
7	93.65	89.30	91.42	99.79	99.96	99.87	98.93	99.01	98.97
8	93.44	89.26	91.30	99.45	99.69	99.57	98.89	98.89	98.89

Figure 4. Classification results from the three models (GMM, RF, and SVM). The numbers on the left indicate the layer-stacked datasets derived from Table 3

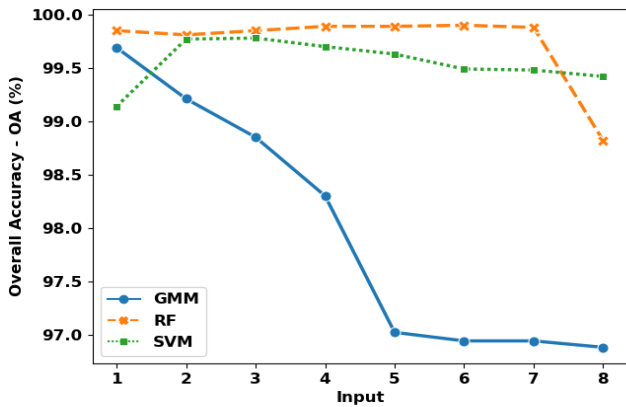


Figure 5. Overall accuracy of the classification. Input 1 is the WV2 RGBNIR image. Inputs 2 - 8 contain input 1 layer-stacked with textural features

Validation of building extraction

Three different portions were selected from the reference raster figure and compared with the best classification results from each model. The selected portions had a high ratio of buildings. For GMM the best classification used MSI as input, whereas for RF the best classification was input 6, which has MSI + Textures (Mean, Variance, Contrast, Second Moment, and homogeneity). Input 3, which had MSI + Textures (Mean,

Variance, Contrast) gave the best classification for the SVM algorithm; hence it was used here. Pixel differences were calculated between the two raster layers, reference and classified image, to find the error of building detection from each algorithm. Consequently, giving the accuracy of each model.

Figures 6–8 show the prediction errors from each algorithm and portion. A visual inspection of the images indicates that GMM gave superior results, followed by SVM and RF. RF shows misclassifications especially at the boundaries even though the input image had GLCM textural indices. In terms of building edge detection GMM and SVM gave good results. On the other hand, RF was not able to identify the building edges especially on portion 2 and 3.

Quantitative analysis indicates that GMM had fewer prediction errors with an average accuracy of 92.38% for all the portions. The highest accuracy of GMM was in portion 3 at 99.8%. RF and SVM had average accuracies of 70.53% and 79.26% respectively. Portion 1 results were the most accurate, with the lowest accuracy of 86.5% for SVM (Figure 6). Portion 2 (Figure 7), which had a high density of buildings, had the lowest accuracy for all the models at 82.90%, 64.78%, and 54.5% for GMM, SVM, and RF respectively.

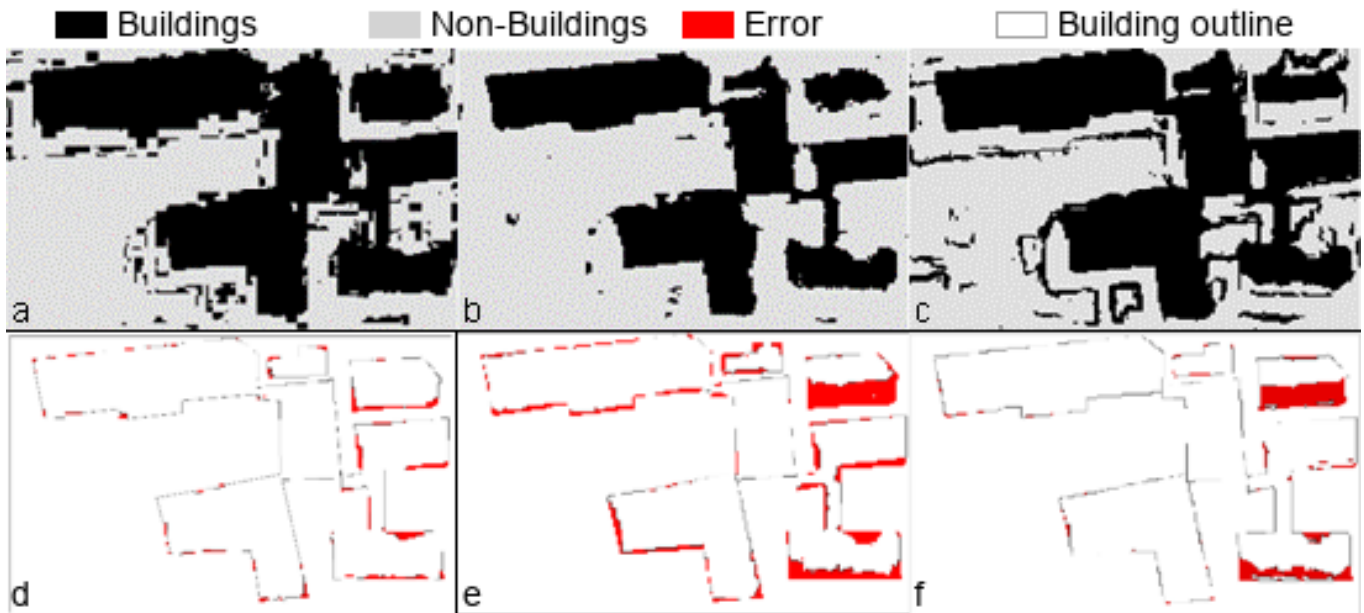


Figure 6. Classification results for image portion 1. (a), (b), and (c) are classification results for GMM, RF, and SVM respectively. Errors of the models are (d) GMM, (e) RF, and (f) SVM

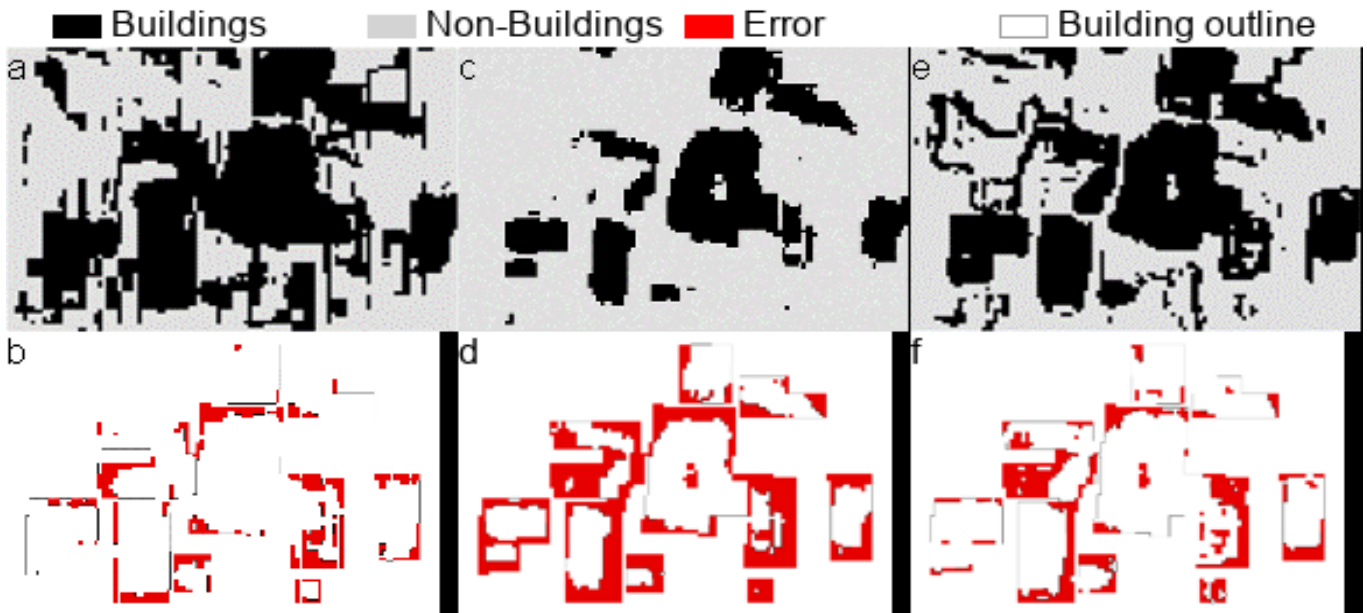


Figure 7. Classification results for image portion 2. (a), (c), and (e) are classification results for GMM, RF, and SVM respectively. Errors of the models are (b) GMM, (d) RF, and (f) SVM.

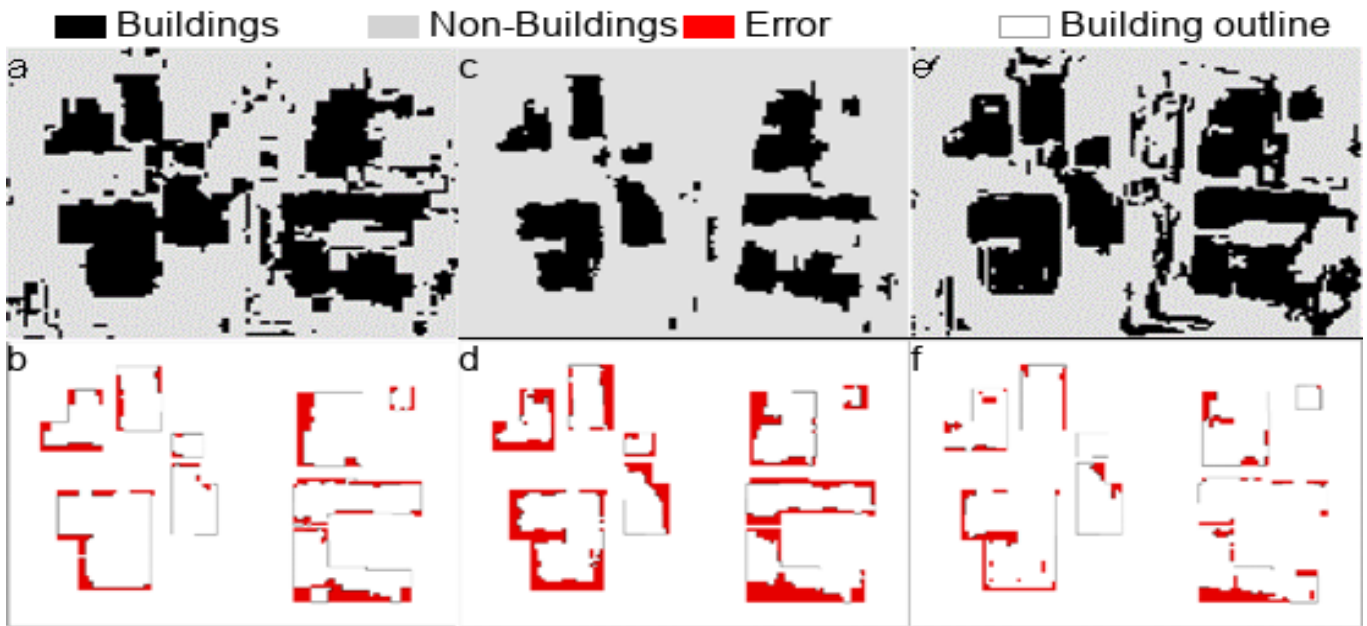


Figure 8. Classification results for portion 3. (a), (c), and (e) are classification results for GMM, RF, and SVM respectively. Errors of the models are (b) GMM, (d) RF, and (f) SVM.

CONCLUSIONS

The study has shown that integrating remote sensing and machine learning can adequately map informal settlements. The current results demonstrate that GMM performs poorly with textural indices, whereas RF and SVM need textural indices to classify features on an

image. The highest OA for RF and SVM of 99.90% and 99.78% respectively, were obtained when textural indices were fused into the WV-2 image. RF performed exceptionally well in detecting different classes in the image. However, RF did not perform well in extracting building footprints with an average accuracy of 70.5%. The model that performed well in detecting building

footprints was GMM with an accuracy of 92.4%. The outcome of settlement maps from this study was satisfactory, hence remote sensing and machine learning could be used in mapping traditional villages as they have the same spatial structure as informal settlements.

DECLARATIONS

Corresponding Author

Correspondence and requests for materials should be addressed to; E-mail: segobyem@ub.ac.bw; ORCID: <https://orcid.org/0009-0008-4028-1763>

Data availability

The datasets used and/or analysed during the current study are available from the corresponding author on reasonable request.

Acknowledgements

The authors would like to acknowledge the University of Botswana for creating a conducive environment to conducting this research.

Authors' contribution

WM performed the experiments and analysed the data obtained. MS and WM wrote the manuscript and designed the figures in consultation with YO. YO conceived and supervised the study. KM, BM, LM, BN, and NN assisted in the management of the research project. All Authors read and approve the content of the final manuscript.

Competing interests

The authors declare no competing interests in this research and publication.

REFERENCES

- Barsi Á, Kugler Zs, László I, et al (2018). Accuracy Dimensions in Remote Sensing. *The International Archives of the Photogrammetry, Remote Sensing and Spatial Information Sciences XLII-3*:61–67. DOI: <https://doi.org/10.5194/isprs-archives-XLII-3-61-2018>; [Google Scholar](#)
- Belfiore O, Parente C (2016). Comparison of Different Algorithms to Orthorectify WorldView-2 Satellite Imagery. *Algorithms* 9:67. DOI: <https://doi.org/10.3390/a9040067>; [Google Scholar](#)
- Breiman L (2001). Random Forests. *Mach Learn* 45:5–32. <https://doi.org/10.1023/A:1010933404324>
- Burnett MW, White TD, McCauley DJ, et al (2019). Quantifying coconut palm extent on Pacific islands using spectral and textural analysis of very high-resolution imagery. *Int J Remote Sens* 40:7329–7355. DOI: <https://doi.org/10.1080/01431161.2019.1594440>; [Google Scholar](#)
- Cutler A, Cutler RD, Stevens JR (2012). Random Forest. In: Zhang C, Ma Y (eds). *Ensemble Machine Learning: Methods and Applications*. Springer US, Boston, MA, pp 157–176. [Google Scholar](#)
- Foody GM, Mathur A (2004). A relative evaluation of multiclass image classification by support vector machines. *IEEE Transactions on Geoscience and Remote Sensing* 42:1335–1343. DOI: <https://doi.org/10.1109/TGRS.2004.827257>; [Google Scholar](#)
- Hofmann P, Strobl J, Blaschke T, Kux H (2008). Detecting informal settlements from QuickBird data in Rio de Janeiro using an object based approach. In: *Object-Based Image Analysis*. Springer Berlin Heidelberg, Berlin, Heidelberg, pp 531–553. [Google Scholar](#)
- Khatriker S, Kumar M (2018). Building Footprint Extraction from High Resolution Satellite Imagery Using Segmentation. *The International Archives of the Photogrammetry, Remote Sensing and Spatial Information Sciences XLII-5*:123–128. DOI: <https://doi.org/10.5194/isprs-archives-XLII-5-123-2018>; [Google Scholar](#)
- Li S, Kang X, Fang L, et al (2017). Pixel-level image fusion: A survey of the state of the art. *Information Fusion* 33:100–112. DOI: <https://doi.org/10.1016/j.inffus.2016.05.004>; [Google Scholar](#)
- Matarira D, Mutanga O, Naidu M, Vizzari M (2022). Object-Based Informal Settlement Mapping in Google Earth Engine Using the Integration of Sentinel-1, Sentinel-2, and PlanetScope Satellite Data. *Land (Basel)* 12:99. DOI: <https://doi.org/10.3390/land12010099>; [Google Scholar](#)
- Mboga N, Persello C, Bergado J, Stein A (2017). Detection of Informal Settlements from VHR Images Using Convolutional Neural Networks. *Remote Sens (Basel)* 9:1106. DOI: <https://doi.org/10.3390/rs9111106>; [Google Scholar](#)
- Menezes J, Poojary N (2020). A fusion approach to classify hyperspectral oil spill data. *Multimed Tools Appl* 79:5399–5418. <https://doi.org/10.1007/s11042-018-6709-7>; [Google Scholar](#)
- Mudau N, Mhangara P (2021) Investigation of Informal Settlement Indicators in a Densely Populated Area Using Very High Spatial Resolution Satellite Imagery. *Sustainability* 13:4735. DOI: <https://doi.org/10.3390/su13094735>; [Google Scholar](#)
- Pantoja DA, Spenassato D, Emmendorfer LR (2023) Comparison Between Classification Algorithms: Gaussian Mixture Model - GMM and Random Forest - RF, for Landsat 8 Images. *Revista de Gestão Social e Ambiental* 16:e03234. DOI: <https://doi.org/10.24857/rgsa.v16n3-015>; [Google Scholar](#)
- Rahaman MM, Thakur B, Kalra A, et al (2019) Estimating high-resolution groundwater storage from GRACE: A random forest approach. *Environments - MDPI* 6:. DOI: <https://doi.org/10.3390/environments6060063>; [Google Scholar](#)
- Shafizadeh-Moghadam H, Khazaei M, Alavipanah SK, Weng Q (2021). Google Earth Engine for large-scale land use and land cover mapping: an object-based classification approach using spectral, textural and topographical factors. *GISci*

- Remote Sens 58:914–928. DOI: <https://doi.org/10.1080/15481603.2021.1947623>; [Google Scholar](#)
- Sheykhoumousa M, Mahdianpari M, Ghanbari H, et al (2020). Support Vector Machine Versus Random Forest for Remote Sensing Image Classification: A Meta-Analysis and Systematic Review. *IEEE J Sel Top Appl Earth Obs Remote Sens* 13:6308–6325. DOI: <https://doi.org/10.1109/JSTARS.2020.3026724>; [Google Scholar](#)
- Statistics Botswana (2022). Population and Housing Census 2022 Population of Cities, Towns and Villages Version 2. <https://dataspace.princeton.edu/handle/88435/dsp01ms35tc881>; [Google Scholar](#)
- Tassi A, Vizzari M (2020). Object-Oriented LULC Classification in Google Earth Engine Combining SNIC, GLCM, and Machine Learning Algorithms. *Remote Sens (Basel)* 12:3776. DOI: <https://doi.org/10.3390/rs12223776>; [Google Scholar](#)
- UN-Habitat (2015). Habitat III issue paper 22 - informal settlements. DOI: <https://habitat3.org/wp-content/uploads/Habitat-III-Issue-Paper-22-Informal-Settlements-2.0.pdf>. Accessed 9 Jun 2024
- Van Nostrand J (1982). *Old Naledi: The Village Becomes a Town: An Outline of the Old Naledi Squatter Upgrading Project*, Gaborone, Botswana. James Iorimer & Company, Toronto
- Vizzari M (2022). PlanetScope, Sentinel-2, and Sentinel-1 Data Integration for Object-Based Land Cover Classification in Google Earth Engine. *Remote Sens (Basel)* 14:2628. DOI: <https://doi.org/10.3390/rs14112628>; [Google Scholar](#)
- Wan H, Wang H, Scotney B, Liu J (2019) A Novel Gaussian Mixture Model for Classification. In: 2019 IEEE International Conference on Systems, Man and Cybernetics (SMC). IEEE, pp 3298–3303. DOI: <https://doi.org/10.1109/SMC.2019.8914215>; [Google Scholar](#)
- Zhao K, Kang J, Jung J, Sohn G (2018). Building Extraction from Satellite Images Using Mask R-CNN with Building Boundary Regularization. In: 2018 IEEE/CVF Conference on Computer Vision and Pattern Recognition Workshops (CVPRW). IEEE, pp 242–2424. https://openaccess.thecvf.com/content_cvpr_2018_workshops/w4/html/Zhao_Building_Extraction_From_CVPR_2018_paper.html

Publisher's note: [Scienceline Publication](#) Ltd. remains neutral with regard to jurisdictional claims in published maps and institutional affiliations.



Open Access: This article is licensed under a Creative Commons Attribution 4.0 International License, which permits use, sharing, adaptation, distribution and reproduction in any medium or format, as long as you give appropriate credit to the original author(s) and the source, provide a link to the Creative Commons licence, and indicate if changes were made. The images or other third party material in this article are included in the article's Creative Commons licence, unless indicated otherwise in a credit line to the material. If material is not included in the article's Creative Commons licence and your intended use is not permitted by statutory regulation or exceeds the permitted use, you will need to obtain permission directly from the copyright holder. To view a copy of this licence, visit <https://creativecommons.org/licenses/by/4.0/>.

© The Author(s) 2024

Fluoride Concentration in Selected Water Sources of Ngamiland and Boteti Districts: Risk of Dental Fluorosis

Kelebogile B Mfundisi¹✉ , Modiredi K Marebole² , and Kelebileone Kaisara³ 

¹Okavango Research Institute, University of Botswana, Sexaxa. Shorobe road, Maun, Botswana

²University of Botswana, 4775 Notwane Rd. Gaborone, Botswana

³Okavango Research Institute, University of Botswana, Sexaxa Shorobe road, Maun, Botswana

✉ Corresponding author's Email: kelebogilemfundisi@gmail.com

ABSTRACT

Fluoride is well-known for its role in preventing dental issues and promoting strong teeth and bones. It is commonly found in water, tea, and fluoridated toothpaste. The World Health Organisation recommends fluoride concentrations between 0.5 mg/L to 1.50 mg/L in water. Excessive fluoride intake can lead to dental fluorosis which affects tooth enamel. This study aimed to investigate fluoride levels in different water sources within selected villages of Ngamiland and Central Boteti districts and assess dental fluorosis prevalence among the residents. Our objectives were to measure fluoride concentrations in various water sources, evaluate the impact of pH and salinity on fluoride levels, and determine the link between fluoride concentration and dental fluorosis prevalence. Water samples were analyzed for fluoride concentration, pH, and salinity using ion chromatograph, pH meter, and conductivity meter, respectively. Interviews were conducted in Maun, Tsau, Toteng, and Motopi regarding dental fluorosis prevalence. Results showed that groundwater in Motopi and Tsau had fluoride concentrations ranging from 2.81 – 17.05 mg/L, while Toteng tap and standpipe water had fluoride concentrations of 0.78 and 0.83 mg/L. Maun tap and standpipe water, as well as Motopi surface water, yielded fluoride concentrations ranging from 0.16 – 0.37 mg/L. Salinity and pH showed no significant relationship with fluoride concentration, with correlation coefficients of 0.09 and 0.46, respectively. In conclusion, Tsau boreholes had the highest fluoride concentration, linked to dental fluorosis in individuals aged 30 years and above. Maun tap and standpipe water, alongside Motopi tap and surface water, exhibited low fluoride concentrations, while Toteng tap, and standpipe water revealed appropriate fluoride levels. The study revealed that Salinity and pH do not influence fluoride concentration in water.

Keywords: Dental Fluorosis Risk, Groundwater Management, Surface Water Management, Ngamiland and Central Boteti Districts

INTRODUCTION

Fluoride, an anion of fluorine, is the 13th most abundant element in the earth's crust, with the chemical formula F⁻. Water is a major source of fluoride and other sources of fluoride are tea, seafood that contains bones or shells, medicinal supplements, and fluoridated toothpastes (Al Hayek et al, 2018). Fluoride is mostly recognised for its role in preventing dental caries and building strong teeth and bones. Although fluoride is important in building strong teeth and bones, an excessive or low fluoride intake can lead to health implications. The World Health Organisation (WHO) states that the appropriate level of fluoride in drinking water should be between 0.50 mg/L to 1.50 mg/L (WHO, 2006). Fluoride concentration that is greater than 1.50 mg/L is associated with dental fluorosis, and chronic exposure to fluoride levels exceeding 4.00 mg/L is associated with skeletal fluorosis (Everett, 2011).

Dental fluorosis is a dental health condition that results in decolorization of teeth from excessive exposure to fluoride during tooth development. It is characterized by

changes in the appearance of tooth enamel, ranging from subtle white streaks or spots to more severe brown discoloration and enamel pitting (Niazi and Pepper, 2023). Dental fluorosis affects children during the critical period of tooth formation, typically up to the age of eight (Everett, 2011). The severity of dental fluorosis is dose-dependent and influenced by the extent of time an individual is exposed to excessive fluoride within the critical window of development and genetic factors (Niazi and Pepper, 2023). It can manifest in varying degrees, mild cases show white streaks, lines, or small spots on enamel.

Skeletal fluorosis is a condition that affects bones in the body caused by exposure to high fluoride levels. It causes joint pain and stiffness, decreasing mobility, structural changes in the spine, and potential neurological complications (Everett, 2011). When fluoride intake is low, the protective benefits of fluoride on dental health are reduced. The main consequence of low fluoride intake is an increased risk of tooth decay; tooth enamel may be

RESEARCH ARTICLE
 PII: S225204302400015-14
 Received: June 25, 2024
 Revised: September 02, 2024
 Accepted: September 05, 2024

weaker and more susceptible to acid attacks from bacteria leading to cavities and dental problems.

Groundwater has been observed to have high levels of fluoride than surface water. This is because groundwater comes into contact with rocks and minerals that contain fluoride, leading to the dissolution of fluoride in the water. Some surface water sources are constantly replenished by groundwater which can increase the concentration of fluoride but other surface water sources get replenished by rainfall. Treated water contains a small amount of fluoride or contains an appropriate amount of fluoride, whereby the water from underground or rivers are purified.

Therefore, the aim of this study was to investigate the fluoride levels in various water sources in the selected villages of Ngamiland and Boteti districts and assess the prevalence of dental fluorosis among the residents.

MATERIALS AND METHODS

Study site

The study was conducted in the selected villages of Ngamiland District, which are Tsau, Toteng, Maun, and a village in Central Boteti District, which is Motopi as shown in the map in Figure 1.

Sampling and data collection

The water samples were collected from different water sources in the study sites. A total of twenty-two 500 ml plastic sampling bottles were used to collect water from different water sources in the study sites. Each sample had a duplicate and both were labelled then put into a cooler

box as a carrier. The coordinates of every sampling site were taken and recorded in the GPS device. The water samples were transported to Okavango Research Institute (ORI) laboratory and were kept in a refrigerator at 16°C to prevent changes in fluoride concentration. An interview was conducted at the study sites with the key informants, including Nurses from public clinics and chiefs, to inquire about the prevalence of Dental fluorosis in these locations.

Sample analysis

A pH meter was used to measure the pH level of water samples. A pH meter was first calibrated in three 50 ml bottles that contained buffers at a pH of 4.01, 7.00 and 10.01 respectively and the pH level of each sample were determined. A conductivity meter was used to determine the salinity of water samples, the conductivity meter was first calibrated in a 50 ml calibration standard containing 0.01 mol/L potassium chloride (KCl) and the salinity of each sample was determined. An Ion chromatograph was used to determine the concentration of fluoride. The manual injection method was carried out. Firstly, the ion chromatograph was blanked with 25µL of distilled water to ensure that the chromatograph system is clean and free of any residual contaminants or previous samples before injecting the samples. Then, 25µL of each water sample was injected with a syringe in an injection port and the ion chromatograph ran the analysis for 13 minutes at a flow rate of 1.2 ml/min and the column pressure at 46 psi. After 13 minutes elapsed, the fluoride concentration of the water sample was determined.

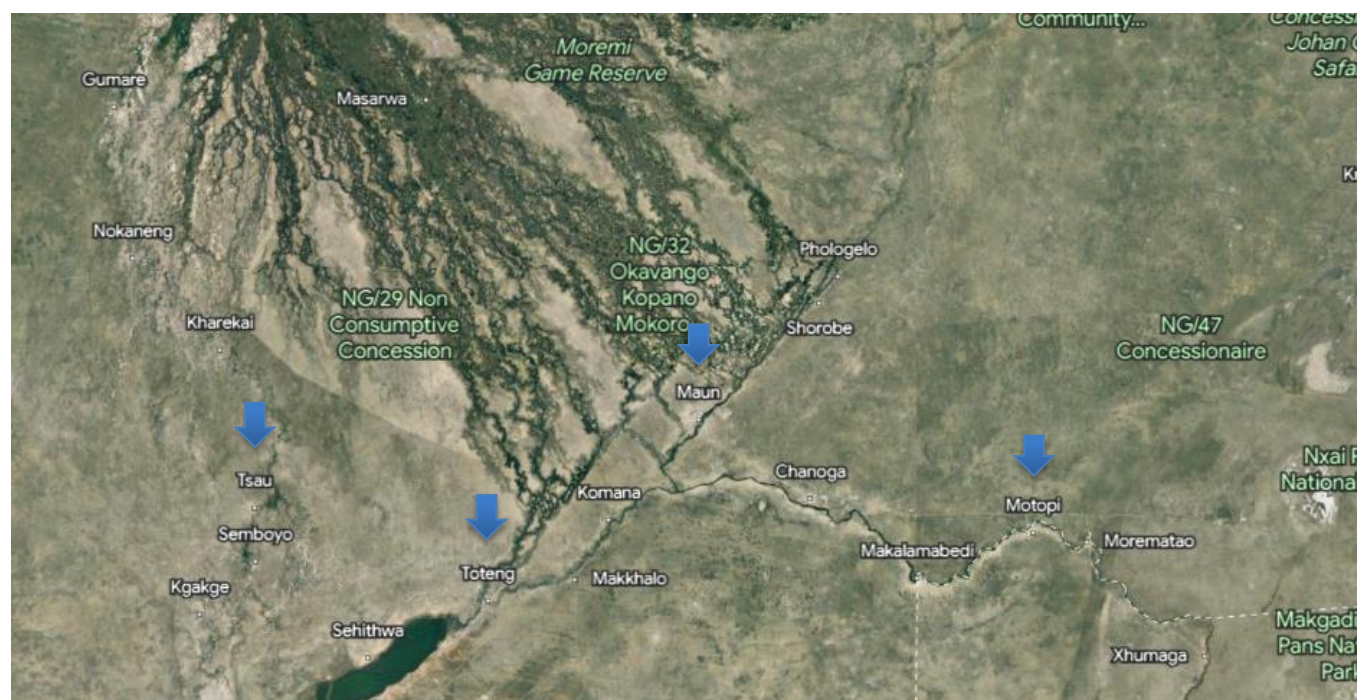


Figure 1. A map of study sites in Ngamiland and Central Boteti district (Google maps, 2023).

Water samples from the study sites were analyzed for fluoride, pH, and salinity, with the results presented in Figures 2-7. Mean (1) and standard deviation (2) were calculated to assess the variability of fluoride concentrations (Ali and Bhaskar, 2016). In this section, the fluoride concentration of tap water and surface water was analyzed and presented in a bar graph (Figure 2). The safe levels for fluoride range from 0.50 to 1.50 mg/L (WHO, 2006). Similarly, Figure 3 presents the fluoride concentration of groundwater in a bar graph, also with the same safe levels.

Figure 4 illustrates the pH levels of each sample, analyzed and presented in a bar graph with safe levels ranging from 6.5 to 9.5 (WHO, 2007). Pearson's correlation coefficient (3) was used to examine the relationship between pH and fluoride, a graph depicts the relationship in Figure 5. The saline content of each sample was presented in a bar graph in Figure 6, and the relationship between salinity and fluoride was examined using Pearson's correlation coefficient (3), a graph shows the relationship in Figure 7. The formulas for mean, standard deviation, and Pearson's correlation coefficient were applied to analyze the data:

Mean:

$$\bar{x} = \frac{\sum_{i=1}^n x_i}{n} \tag{1}$$

Standard Deviation:

$$s = \sqrt{\frac{\sum(x_i - \bar{x})^2}{n-1}} \tag{2}$$

Pearson's Correlation Coefficient:

$$r = \frac{\sum(x_i - \bar{x})(y_i - \bar{y})}{\sqrt{\sum(x_i - \bar{x})^2 \sum(y_i - \bar{y})^2}} \tag{3}$$

These calculations provided insights into the central tendency, variability, and relationships between the measured variables. In Figure 2, Toteng standpipe and tapwater fall within the fluoride safe level with fluoride concentration of 0.83 ± 0.1 mg/L and 0.78 ± 0.03 mg/L. While tapwater and standpipe in Maun, tap water and surface water in Motopi fall below the minimum fluoride safe level.

In Figure 3, the fluoride concentrations of all groundwater samples in Tsau and Motopi exceeds the maximum safe level. Tsau groundwater C has the highest fluoride concentration of 17.05 ± 0.59 mg/L, followed by Motopi ground water with 5.56 ± 0.10 mg/L, Tsau groundwater B with 5.00 ± 0.24 mg/L and Tsau groundwater A with 2.81 ± 0.49 mg/L.

The pH of all water samples depicted in bar graph in Figure 4 falls within the WHO pH safe level. Motopi groundwater has the highest pH level of 9.09 and Maun tap water B has the lowest pH level of 7.24.

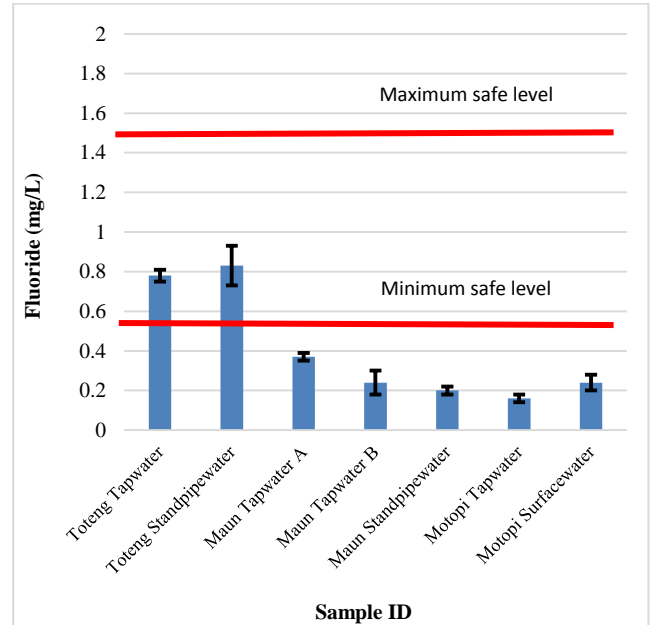


Figure 2. Fluoride concentration of tapwater in Maun, Motopi and Toteng, surface water in Motopi and standpipe water in Toteng and Maun.

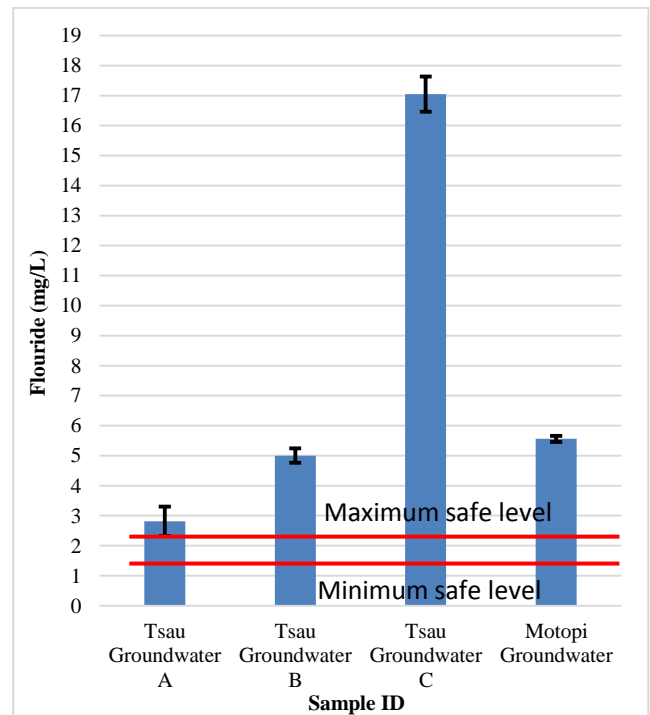


Figure 3. Fluoride concentration of groundwater in Tsau and Motopi.

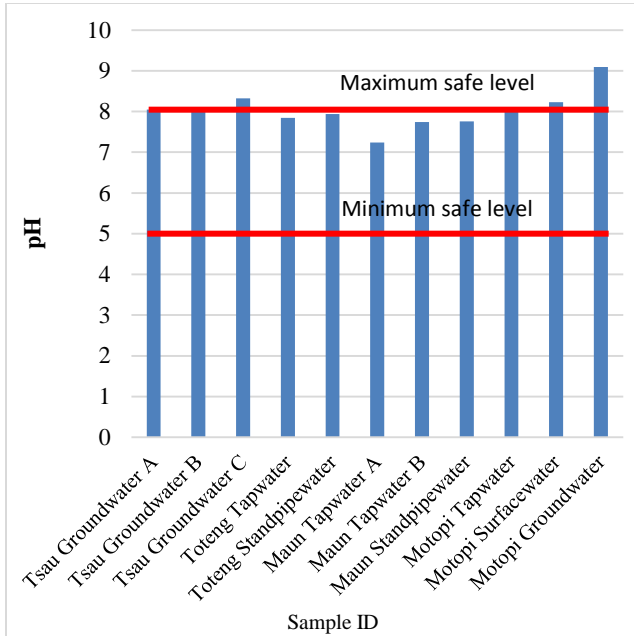


Figure 4. The pH level of different water sources in Maun, Toteng, Tsau and Motopi.

A scatter graph below shows no correlation between the pH and fluoride concentration and the correlation coefficient is 0.21. This low R^2 value indicates a weak linear relationship between fluoride concentration and pH. The equation $y=5.0867x-37.843$ represents a positive linear relationship between fluoride concentration and pH.

The saline content of Tsau groundwater A, Tsau ground water B and Motopi groundwater exceeds the safe saline limit of 1600 $\mu\text{S}/\text{cm}$ while other water samples are within the safe saline limit. Tsau groundwater A has the highest saline content of 14800 $\mu\text{S}/\text{cm}$ (Figure 6).

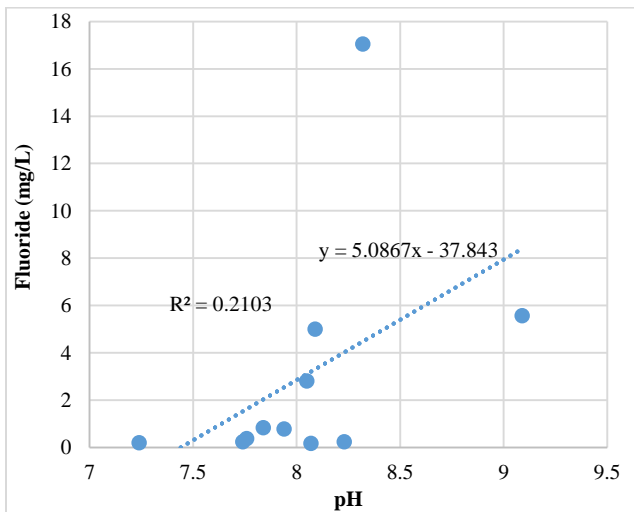


Figure 5. A relationship between the fluoride concentration and pH of various water sources.

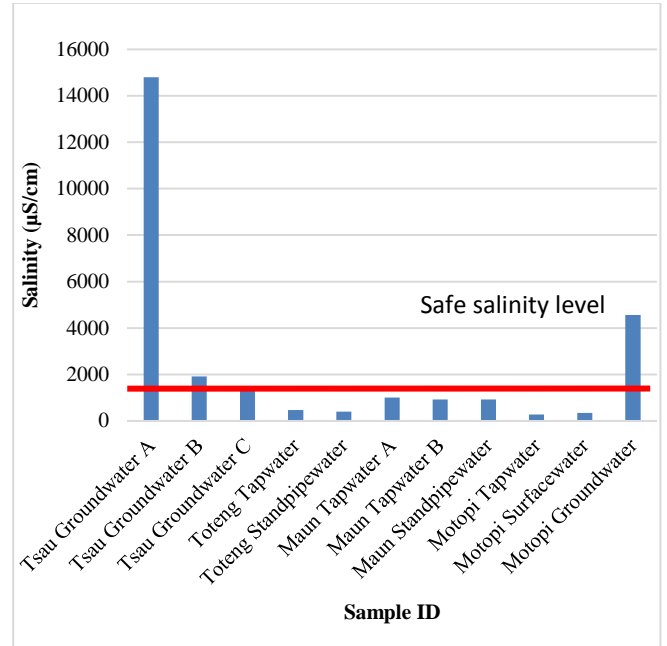


Figure 6. The saline content of different water sources in Maun, Toteng, Tsau and Motopi.

Another scatter graph shows no correlation between salinity and fluoride and the correlation coefficient is 0.003 (Figure 7). This low R^2 value suggests that there is almost no linear relationship between salinity and fluoride concentration, therefore salinity does not have an impact on fluoride concentration variation.

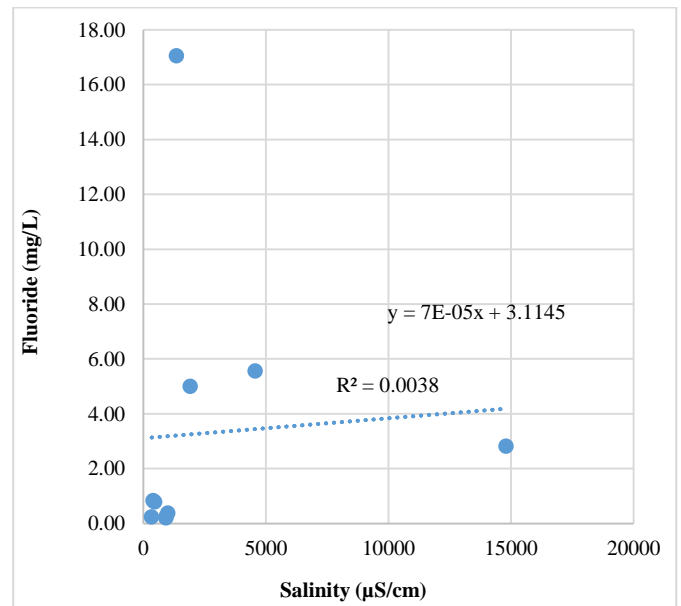


Figure 7. A relationship between salinity and fluoride concentration of various water sources.

Interview findings

- 80% of the key informants said that there is no prevalence of Dental fluorosis in Ngamiland and Central Boteti districts except in Tsau.
- 70% of the key informants said that water causes dental fluorosis.
- 71% of the key informants said that people who are 30 years and above have dental fluorosis while 29% said that people who are 29 years and below have dental fluorosis.

RESULTS AND DISCUSSION

Comparative analysis of fluoride concentrations in Maun and Motopi water sources: Tap water, Standpipe water and surface water

In Toteng, the fluoride concentrations in both tap water (0.78 ± 0.03 mg/L) and standpipe water (0.83 ± 0.1 mg/L) are within the World Health Organization (WHO) safe range of 0.50 – 1.50 mg/L, making them safe for consumption. However, in Maun and Motopi, the fluoride levels in tap water, standpipe water, and surface water are below the WHO safe level, with concentrations ranging from 0.16 ± 0.02 mg/L to 0.37 ± 0.02 mg/L. This low fluoride level can lead to weakened teeth and an increased risk of dental cavities. Differences in fluoride concentrations among various water sources in Maun and Motopi are attributed to the water coming from different boreholes (Azani-Aghdash et al., 2013).

Comparative analysis of fluoride concentrations in Tsau and Motopi ground water

The fluoride concentrations in groundwater from Tsau and Motopi are above the WHO safe level, posing a risk of dental and skeletal fluorosis. Tsau groundwater C has the highest fluoride concentration (17.05 ± 0.59 mg/L), followed by Motopi groundwater (5.56 ± 0.10 mg/L), Tsau groundwater B (5.00 ± 0.24 mg/L), and Tsau groundwater A (2.81 ± 0.49 mg/L). The high fluoride levels in Tsau and Motopi are likely due to the water coming into contact with fluoride-containing rocks and minerals. Long-term consumption of such high-fluoride water can cause dental and skeletal fluorosis, where bones become weak and bend (Brindha and Elango, 2011).

pH levels of various water sources in Maun, Toteng, Tsau and Motopi and the relationship between pH-fluoride concentration

The pH levels of water samples from Maun, Toteng, Tsau, and Motopi fall within the WHO safe range of 6.5 to

9.5, making them safe for human consumption. A scatter graph and Pearson correlation coefficient (0.21) indicate no significant correlation between pH and fluoride levels (Liu et al., 2022).

Saline content of various water sources in Maun, Toteng, Tsau and Motopi and the relationship between salinity-fluoride concentrations

In Tsau and Motopi, groundwater salinity exceeds the safe limit of 1600 μ S/cm, making it unsuitable for drinking. However, other water samples fall within the safe salinity limit. A scatter graph and Pearson correlation coefficient (0.003) show no significant correlation between salinity and fluoride levels, indicating that salinity does not affect fluoride concentration (Ahmed et al., 2019).

Perception of key informants on the prevalence and causes of Dental fluorosis among different age groups

Interviews with nurses and chiefs revealed that 80% reported no prevalence of dental fluorosis in Ngamiland and Central Boteti districts, except in Tsau. Some villages near the Makgadikgadi salt pan, like Rakops, Mokoboxane, and Mopipi, have reported cases of dental fluorosis. Key informants attribute dental fluorosis to high fluoride levels in water and note that 71% of affected individuals are aged 30 and above, while 29% are aged 5 to 19. Dental fluorosis was more prevalent between 1978 and 1984, before water treatment facilities were established.

CONCLUSION

Tsau and Motopi groundwaters have high fluoride levels, exceeding WHO limits and posing a risk of dental fluorosis, particularly among individuals aged 30 and above. In contrast, Maun and Motopi's tap/standpipe and river waters have fluoride levels below the WHO minimum, risking dental cavities, while Toteng's water is within the safe range. Understanding fluoride content in drinking water is essential for public health, as excessive fluoride can cause dental and skeletal fluorosis, while insufficient levels can lead to cavities.

DECLARATIONS

Corresponding author

Correspondence and requests for materials should be addressed to Kelebogile B Mfundisi; E-mail: kelebogilemfundisi@gmail.com

Data availability

The datasets used and/or analysed during the current study are available from the corresponding author on reasonable request.

Acknowledgements

The authors would like to acknowledge the WeMAST project for generously sponsoring this study.

Authors' contribution

The first author provided assistance and supervision for the project, and revised the manuscript. The second author conducted the experiments, analyzed the data, and authored the manuscript. The third author contributed to the laboratory work.

Competing interests

The authors declare no competing interests in this research and publication.

REFERENCES

- Ahmed A, Chakraborty R, Dibaba DT, Islam MZ, Khan KM, and Khan MA (2019). Health implications of drinking water salinity in coastal areas of Bangladesh. *International journal of Environment Research and Public Health*, 16(19): 3746. <https://doi.org/10.3390/ijerph16193746>
- Al Hayek S, Aoun A, Darwiche F, and Doumit J (2018). The fluoride debate: The pros and cons of fluoridation. *Preventive Nutrition and Food Science*, 23(4): 171–180. <https://doi.org/10.3746/pnf.2018.23.3.171>
- Ali Z, and Bhaskar SB (2016). Basic statistical tools in research and data analysis. *Indian Journal of Anaesthesia*, 60(9): 662–669. <https://doi.org/10.4103/0019-5049.190623>
- Azani-Aghdash S, Azar FP, Ghojazadeh M, Jamali Z, Mahmoudi M, and Naghavi-Behzad M (2013). Fluoride concentration of drinking waters and prevalence of fluorosis in Iran: A systematic review. *J Dent Res Dent Clin Dent Prospects*, 7(1): 1–7. doi: 10.5681/joddd.2013.001
- Brindha K, and Elango L (2011). Fluoride in groundwater: causes, implications and mitigation measures, In: Monroy SD (Ed.), *Fluoride Properties, Applications and Environmental Management*. 1: 111–136. NOVA. [google scholar: https://www.academia.edu/download/8463221/for%20website1.pdf](https://www.academia.edu/download/8463221/for%20website1.pdf)
- Everett ET (2011). Fluoride's effects on the formation of teeth and bones, and the influence of genetics. *Journal of Dental Research*, 90(5): 552–560. <https://doi.org/10.1177/0022034510384626>
- Liu H, Chen C, Li Y, Duan Z and Li Y (2022). Characteristic and correlation analysis of metro loads, In: Liu H, Chen C, Li Y, Duan Z and Li Y (Eds), *Smart Metro Station Systems* 237–267. Elsevier, <https://doi.org/10.1016/B978-0-323-90588-6.00009-3>
- Niazi FC, and Pepper T (2023). Dental fluorosis. [Updated 2023 Jun 1]. Treasure Island (FL): StatPearls Publishing <https://www.ncbi.nlm.nih.gov/books/NBK585039/> Google Scholar <https://europepmc.org/books/nbk585039>
- WHO (2006). Fluoride in Drinking-water. Edited by Bailey, K, Chilton J, Dahi E, Lennon, M, Jackson P, and Fawell J (2006), IWA Publishing, London, UK. 1–314. [ISBN: 1900222965. https://iris.who.int/bitstream/handle/10665/43514/9241563192_eng.pdf?sequence=1](https://iris.who.int/bitstream/handle/10665/43514/9241563192_eng.pdf?sequence=1)
- WHO (2007). pH in Drinking-water. Revised Background Document for Development of WHO Guidelines for Drinking-water Quality. 1–2 https://cdn.who.int/media/docs/default-source/wash-documents/wash-chemicals/ph.pdf?sfvrsn=16b10656_4

Publisher's note: [Scienceline Publication](#) Ltd. remains neutral with regard to jurisdictional claims in published maps and institutional affiliations.



Open Access: This article is licensed under a Creative Commons Attribution 4.0 International License, which permits use, sharing, adaptation, distribution and reproduction in any medium or format, as long as you give appropriate credit to the original author(s) and the source, provide a link to the Creative Commons licence, and indicate if changes were made. The images or other third party material in this article are included in the article's Creative Commons licence, unless indicated otherwise in a credit line to the material. If material is not included in the article's Creative Commons licence and your intended use is not permitted by statutory regulation or exceeds the permitted use, you will need to obtain permission directly from the copyright holder. To view a copy of this licence, visit <https://creativecommons.org/licenses/by/4.0/>.

Moment Gradient Factor Verification for Selected Monosymmetric Beams under Linear Moment Gradients

Kenny Mudenda  

Department of Civil Engineering, University of Cape Town, Private Bag X3, Rondebosch 7701, Cape Town, South Africa

Corresponding author's Email: kenny.mudenda@uct.ac.za

ABSTRACT

The reuse of doubly symmetric beams by converting them into monosymmetric section beams offers some promising outcomes and has potential for mitigating carbon footprint of structures. However, due to their complexity monosymmetric sections must be used in a configuration that allows the monosymmetry effects to act beneficially. Although the South African design standard for hot-rolled steel does not provide any guidance on the design of monosymmetric beams, the Southern African steel construction handbook provides a formula for determining the critical elastic buckling moment for monosymmetric beams. This guidance implies that the moment gradient factor used for doubly symmetric sections can be used on monosymmetric sections as well. The aim of the study was to verify the validity of this approach of extending the moment gradient factor used for doubly symmetric beams to monosymmetric beams for two specific types of monosymmetric sections. It was found that although this approach appears to be justified for monosymmetric members in single curvature bending it may produce unconservative values of the critical buckling load in double curvature bending between restraint points. The level of un-conservatism also varies for different spans of the same member. This makes it difficult to specify a single moment modification factor value for these cases. The sensitivity in terms of load reduction observed for double curvature bending case was different for the two members examined with this attributed to differences in how the shear centre moves relative to the centroid. It is recommended that the critical buckling load for monosymmetric sections be determined on a case specific basis for members in double curvature from linear moment gradients. Under single curvature bending the moment gradient factor for doubly symmetric members appears to give acceptable predictions of the critical load.

Keywords: Steel beam, Monosymmetric, Lateral-torsional buckling, Moment gradient factor

INTRODUCTION

The world is facing a climate emergency and this calls for innovative approaches as well as concerted effort in mitigating the increase in atmospheric carbon. This can be done through adoption of practices that foster reduction in anthropogenic carbon emissions or in carbon footprint in relation to construction related activities. For design engineers one way to reduce carbon footprint is to apply the practice of reuse in lieu of recycling. Recycling involves the use of energy and unless this is sourced from renewable energy it too potentially carries a significant carbon footprint. The reuse of structural members therefore provides a viable alternative for cyclic use of materials where the potentially more environmentally harmful options of disposal and introduction of new materials, or that of recycling using non-renewable energy sources are avoided. This is consistent with the options illustrated in Halliwell (2024) and discussed in part by Hayes (2024) showing the hierarchy of net zero design

that can be adopted by design engineers. 'Net zero design' is a design approach that aims to mitigate increase in atmospheric carbon emissions by reducing the carbon footprint of structures based on proactive design decisions. This concept is illustrated in Figure 1 with the 'Build less' approach being achieved through consideration of repurposing, refurbishment and reuse of structural members.

The focus of this study is the reuse option. It has been shown by Mudenda and Zingoni (2022) that monosymmetric beams of the configuration shown in Figure 2 have the potential to be used for strengthening existing doubly symmetric I-shaped sections that need to have their flexural capacity or stiffness increased for reuse purposes. These sections exhibit some peculiarities including having a coincident shear centre and centroid at a given upstand height as well as a monosymmetry constant of zero at another upstand height. These are geometrical properties typically associated with doubly symmetric sections. These monosymmetric sections, for

RESEARCH ARTICLE
 PII: S225204302400016-14
 Received: June 25, 2024
 Revised: September 02, 2024
 Accepted: September 05, 2024

the simply supported case, also have a range over which they show increase in critical elastic moment. The point of peak value is observed to be closely related to the upstand height at which the shear centre and centroid are coincident. Beyond this point the critical moments starts to decrease with increase in upstand height. The shear centre movement also follows a peculiar path in comparison to an I-shaped monosymmetric section. This is discussed later.

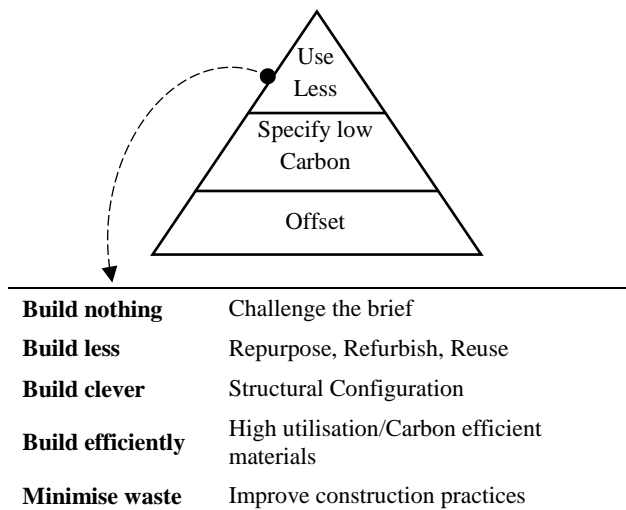


Figure 1 Hierarchy of net zero design

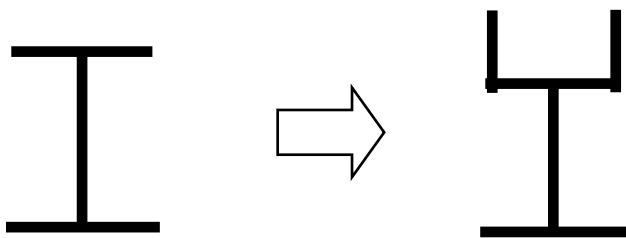


Figure 2 Doubly symmetric I-beam stiffened with flange upstands

Figure 2 shows how a doubly symmetric I-shaped steel beam is converted into a monosymmetric section by the introduction of flange upstand stiffeners. Conversion into this monosymmetric section has the potential to enhance flexural strength and stiffness of the section as discussed. This is desirable if the structure is repurposed in a manner that it needs to carry greater loads or if the member is to be used in a different structure where greater flexural strength or stiffness is needed. This can be adopted in lieu of replacing with a new I-shaped member of higher strength. Reuse in the same structure is particularly desirable as it obviates the need to incur costs of dismantling the existing member, disposing of it and potentially replacing it with a new member that also may need costly scaffolding, manpower or machinery to mount, in addition to the carbon footprint of its production.

The use of such a monosymmetric section beam as the

one considered may result in part or all of the member being subjected to a moment gradient that result in double curvature bending. For this case it is unclear whether the current guidance on the determination of the critical buckling load presented in design aids is valid. The study aims to verify such guidance provided in the South African Steel Construction Handbook (SASCH). This study is restricted to elastic critical buckling behaviour. In this preliminary study selected discrete members are investigated with a general approach to be explored in future studies on the basis of the observed outcomes.

Background

The use of monosymmetric sections for steel beams that do not have restraint to the compression flange is not so prevalent due, in part, to the complexity associated with the lateral-torsional buckling (LTB) behaviour of these sections. Lateral-torsional buckling is a stability failure that affects beams bending about their major axis and not having restraint to the compression flange. It is associated with a lateral movement of the compression flange in a direction perpendicular to the plane of loading and accompanied with twist. Early researchers such as Anderson and Trahair (1972) highlighted the ‘Wagner effect’ which arises from the shear centre and geometric centroid not being at the same location for monosymmetric beams. This effect is encapsulated in the monosymmetry constant (β_x), a geometrical property associated with monosymmetric sections. A lot of the research on monosymmetric sections has focused on I-shaped sections, tee sections and compound sections made from I-sections with a welded channel cap. In order to find the strength of the beams, in most cases the critical elastic moment must first be determined. Codes of practice typically use the critical elastic moment equation for a uniform moment loading case and then allow for other loading or bending moment profiles by making use of a moment gradient factor. The uniform moment case is typically the only case that gives a closed form mathematical solution when the boundary conditions are pin type with warping of the cross-section permitted, hence its use. The moment gradient factor proves to be a convenient way of determining the critical load for those cases that are different to the uniform moment case with simple supports. However, the determination of moment gradient factors has largely been based on doubly symmetric sections making the direct extension to monosymmetric beams questionable and needing verification. Although, the South African national standard for design of hot-rolled sections (SANS 10162-1) does not provide any guidance on design of monosymmetric sections, the Southern African Steel Construction Handbook (SASCH) provides an equation for the elastic critical buckling moment of a monosymmetric section and implies that the same moment gradient factor as that for doubly symmetric beams can be used. The equation is shown in equation (1). A simplified equation for obtaining

the monosymmetry constant has been developed by Kitipornchai and Trahair (1980). The actual equation and the simplified version for the monosymmetry constant (β_x) are shown in equations (2) and (3) respectively.

$$M_{cr,0} = \frac{\pi^2 EI_y \beta_x}{2L^2} \left[1 \pm \sqrt{1 + \frac{4}{\beta_x^2} \left(\frac{GJL^2}{\pi^2 EI_y} + \frac{C_w}{I_y} \right)} \right] \quad (1)$$

$$\beta_x = \frac{1}{I_x} \int_A y(y^2 + x^2) dA - 2y_0 \quad (2)$$

$$\beta_x = 0,9 d' \left(\frac{2I_{yc}}{I_y} - 1 \right) \left[1 - \left(\frac{I_y}{I_x} \right)^2 \right] \quad (3)$$

In these equations d' is the distance between centres of area of the two flanges, I_{yc} being the second moment of area of the compression flange about its own strong axis [about y-axis in Figure 3 (c)], x and y being plate coordinates, and y_0 the distance between shear centre and centroid. It is worth noting that when equation (3) was presented, the authors stated that it has a validity range which depends on the second moment of area ratio and this particular version was derived on the basis of an I-shaped section. The monosymmetry constant for sections considered in the current study was obtained based on equation (2) so that validity is not violated. An approach presented by Hsu et al. (2012) was adopted and used to apply the integration.

Literature study

The most prevalent early form of the moment modification factor approach is reported to be that presented by Salvadori (1955). A simple modification by who to the equation for a uniform moment case ($M_{cr,0}$) to account for other load cases was proposed as shown in equation (4). The form of the moment gradient factor also known as the Equivalent Uniform Moment Factor (EUMF) was presented as in equation (5) with M_1 and M_2 being the moment values at the ends of the unbraced length under consideration. The end moment M_1 is taken as the one with the smaller value.

$$M_{cr} = C_b M_{cr,0} \quad (4)$$

$$C_b = 1.75 + 1.05 \left(\frac{M_1}{M_2} \right) + 0.3 \left(\frac{M_1}{M_2} \right)^2 \leq 2.3 \quad (5)$$

It was indicated by Suryoatmono (2002) that this equation appears in the 1986 edition of the American Institute of Steel Construction (AISC) code. Two versions of the EUMF have been presented by Ziemian (2010) with one of them being similar to equation (5). It is clarified here that the moment ratio (M_1/M_2), denoted by ' κ ' in equation (6) is positive for double curvature and negative for single curvature. It was stated that these equations are applicable to linearly varying moments between brace points. This limitation is significant as in practice there are many cases where the bending moment will not vary linearly along the unbraced length.

$$C_b = 1.75 + 1.05\kappa + 0.3\kappa^2 \leq 2.56 \quad (6)$$

$$C_b = [0.6 - 0.4\kappa]^{-1} \leq 2.5 \quad (7)$$

It has been reported by Suryoatmono (2002) and Helwig et al. (1997) that Kirby and Nethercot (1979) presented an alternative equation for the EUMF which is applicable to both linear and nonlinear moment gradient diagrams between brace points. This equation is based on determining the maximum moment M_{max} in the unbraced span as well as moment values at quarter points (A, B and C) along the beam. This equation can be found in the 1999 versions of the AISC code in a slightly modified form as shown in equation (8).

$$C_b = \frac{12.5 M_{max}}{2.5M_{max} + 3M_A + 4M_B + 3M_C} \quad (8)$$

Many studies have been conducted to improve the accuracy of the EUMF equation, in particular to consider load height effects (when load is not placed at shear centre) as well as end conditions. So called 'quarter points' equations such as Equation (8) have been studied by Wong and Driver (2010) who proposed an improved version of this type of formula. The EUMF formula presented in the South African steel design code as well as the handbook is based on equation (6) and given as ω_2 but with the limiting value given as 2.5 instead of the 2.56 used here. It, therefore, appears that the South African design guides have not moved on from an equation meant for linearly varying bending moments to the more general 'quarter points' approach. The current study only focuses on the equations provided in the South African design guide documents.

MATERIALS AND METHODS

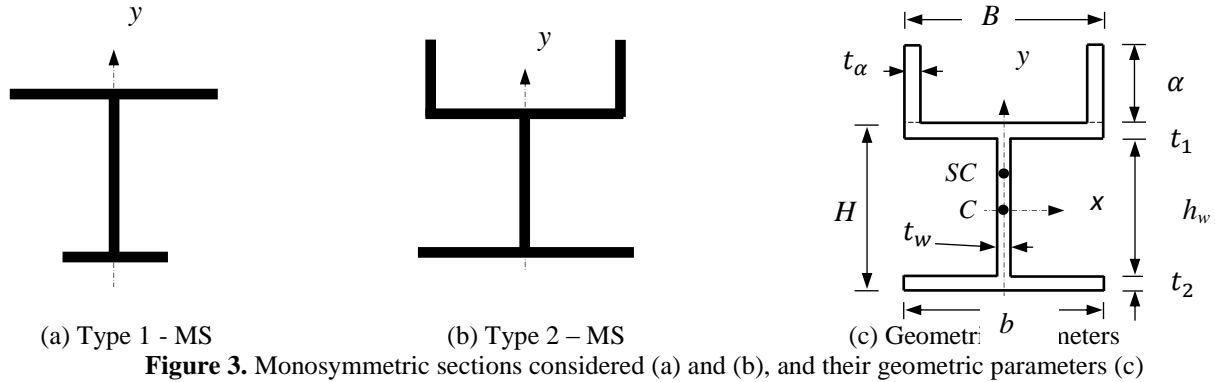
In order to determine the moment gradient factor, the critical elastic buckling moment for the uniform moment case was first obtained ($M_{cr,0}$). The bending moment was then altered to a case that differs from the uniform moment case and the critical moment determined, ($M_{cr,m}$). For example, a uniformly decreasing moment with maximum at one end and zero at the other end for the same length of the member. The ratio of the two moment values then gives the moment gradient factor as given in equation (9), with ω_2 being the moment gradient factor.

$$M_{cr,m} = \omega_2 M_{cr,0} \quad (9)$$

Two sections were considered, one being an I-shaped monosymmetric section and the other being the stiffened beam which is the subject of the study. The I-section beam is studied to provide a comparison particularly because this member has been the subject of previous studies. The two different types of monosymmetric sections are shown in Figure 3 together with the geometric parameters used. For the Type 1 section, the upstand parameters in Figure 3 (c) are set to zero. The critical elastic buckling moment was determined using equation (1) with the moment gradient factor given by equation (6) based on the code of practice (SANS 10162-1) section for design of doubly symmetric beams. The analytical results were compared to finite element analysis (details of this is missing) results. This comparison was done to verify whether using the

moment gradient factor for doubly symmetric sections for monosymmetric section behaviour predictions is a valid approach. The results are presented in tables and analysed

to determine whether the use of the code equation gives safe or unsafe results for the section cases considered.



Sections considered

The sections considered are shown in Table 1. Associated geometric properties based on Figure 3 (c) are given. An attempt was made to ensure that the members are compact so that they can attain the plastic moment, M_p . The initial slenderness parameter is given by:

$$\bar{\lambda}_{Lr} = \sqrt{\frac{M_p}{M_{cr}}} \tag{10}$$

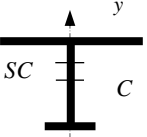
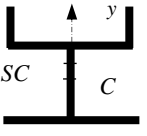
Initial slenderness parameters for the beam when subjected to the uniform moment case are selected such that the beam is slender i.e. the slenderness parameter is greater than unity (the point at which the plastic moment would match the elastic moment). In the slender beams the critical elastic moment is the critical value and therefore

the beams are always likely to suffer from a global lateral-torsional buckling failure with no local buckling provided the plate elements are not slender. The degree of monosymmetry, ρ , is also considered for the selected members. This is given by equation (11). Member lengths vary as $\bar{\lambda}_{Lr}$ varies.

$$\rho = \frac{I_{yt}}{I_{yt} + I_{yb}} \tag{11}$$

with I_{yt} the second moment of area of the top flange and I_{yb} the second moment of area of the bottom flange about the y-axis of the section. The axis is shown in Figure 3 (c) or Table 1 figures.

Table 1. Members considered for study.

Member	Description								
Type - 1 	Beam:	B / b	H	t_1	t_2	t_w	ρ		
	T1-1	150 / 75	400	10	8	5	0.91		
	T1-2	150 / 132	400	10	8	7	0.65		
	T1-3	100 / 75	250	8	5	4.5	0.79		
Type - 2 	Beam:	B / b	H	t_1	t_2	t_w	t_α	α	ρ
	T2-1	55/55	100	5.7	5.7	4.1	5.7	10	0.65
	T2-2	55/55	100	5.7	5.7	4.1	5.7	50	0.84
	T2-3	146/146	251	8.6	8.6	6	8.6	75	0.79

*All dimensions in (mm)

Finite element analysis model

The software Abaqus (which version) was used for the finite element analysis to determine linear elastic critical buckling loads. The finite element model was calibrated against benchmark problems whose closed form analytical solution was available based on uniform moment loading. The boundary conditions were applied for the simply supported case with warping of the flanges allowed to occur freely. Rotation of the section was

prevented at the end supports. These boundary conditions are shown in Figure 4 with U_i being the restrained displacement component. The longitudinal restraint U_z is applied at one end only (non-roller support end). A mesh convergence study was conducted to determine the optimum mesh size. An element size of 10 mm was found to give sufficiently accurate results and was adopted for the study.

RESULTS

Results for the two beam types for different beam slenderness and degree of monosymmetry values are presented in Tables 2 to 4. A typical buckled configuration of a monosymmetric beam is shown in Figure 5. The degree of monosymmetry was high for T1 and intermediate for T2 in the initial iteration given in Table 2. These were then interchanged for the study results

presented in Table 3. The degree of monosymmetry for T2 could not be increased too much as this could result in slender stiffeners. The results show that the moment gradient factor from the design guides produces acceptable estimates for the single curvature bending case. However, once the member is in double curvature the accuracy of the moment gradient factor start to alter. The change is, in some of the observed cases, unconservative making this particularly undesirable.

Table 2. Results for Beams T1-1 and T2-1 for three moment gradient cases (FEM vs applied SANS 10162 code equation)

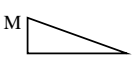
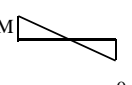
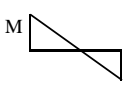
Sketch of BMD		ρ		FEM			Code		
				$\bar{\lambda}_{LT} = 1.22$	$\bar{\lambda}_{LT} = 1.61$	$\bar{\lambda}_{LT} = 2.00$	$\bar{\lambda}_{LT} = 1.22$	$\bar{\lambda}_{LT} = 1.61$	$\bar{\lambda}_{LT} = 2.00$
	T1-1	0.91	M_{cr} (kNm)	228.3	133.6	87.3	230.8	132.5	85.9
			ω_2	1.75	1.80	1.81	1.75		
	T2-1	0.65	M_{cr} (kNm)	17.8	10.1	6.5	18.2	10.5	6.8
			ω_2	1.82	1.80	1.80	1.75		
	T1-1	0.91	M_{cr} (kNm)	178.7	123.2	90.6	310	177.9	115.4
			ω_2	1.37	1.66	1.88	2.35		
	T2-1	0.65	M_{cr} (kNm)	24.4	13.7	8.7	24.4	14.1	9.2
			ω_2	2.49	2.45	2.42	2.35		
	T1-1	0.91	M_{cr} (kNm)	74.8	52.5	40.3	329.8	189.3	122.8
			ω_2	0.60	0.70	0.80	2.50		
	T2-1	0.65	M_{cr} (kNm)	22.9	13.6	8.9	26.0	15.0	9.8
			ω_2	2.34	2.43	2.47	2.50		

Table 3. Results for Beams T1-2 and T2-2 for two moment gradient cases (FEM vs applied SANS 10162 code equation)

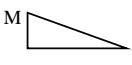
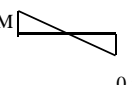
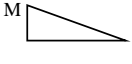
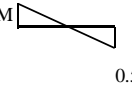
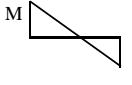
Sketch of BMD		ρ		FEM			Code		
				$\bar{\lambda}_{LT} = 1.22$	$\bar{\lambda}_{LT} = 1.61$	$\bar{\lambda}_{LT} = 2.00$	$\bar{\lambda}_{LT} = 1.22$	$\bar{\lambda}_{LT} = 1.61$	$\bar{\lambda}_{LT} = 2.00$
	T1-2	0.65	M_{cr} (kNm)	319.5	185.4	120.2	312.4	179.4	116.2
			ω_2	1.80	1.83	1.83	1.75		
	T2-2	0.84	M_{cr} (kNm)	32.3	18.0	11.4	31.2	17.8	11.6
			ω_2	1.78	1.80	1.78	1.75		
	T1-2	0.65	M_{cr} (kNm)	403.5	246.7	162.9	419.5	240.9	156.0
			ω_2	2.28	2.43	2.48	2.35		
	T2-2	0.84	M_{cr} (kNm)	42.3	24.1	15.1	41.8	24.0	15.5
			ω_2	2.35	2.41	2.36	2.35		

Table 4. Results for Beams T1-3 and T2-3 for three moment gradient cases (FEM vs applied SANS 10162 code equation)

Sketch of BMD		ρ		FEM			Code		
				$\bar{\lambda}_{LT} = 1.22$	$\bar{\lambda}_{LT} = 1.61$	$\bar{\lambda}_{LT} = 2.00$	$\bar{\lambda}_{LT} = 1.22$	$\bar{\lambda}_{LT} = 1.61$	$\bar{\lambda}_{LT} = 2.00$
	T1-3	0.79	M_{cr} (kNm)	83.4	48.0	31.1	86.8	47.1	30.4
			ω_2	1.80	1.83	1.83	1.75		
	T2-3	0.79	M_{cr} (kNm)	250.9	144.9	92.7	240.8	138.3	89.6
			ω_2	1.80	1.82	1.82	1.75		
	T1-3	0.79	M_{cr} (kNm)	98.4	60.7	40.7	116.6	63.2	40.9
			ω_2	2.13	2.31	2.39	2.35		
	T2-3	0.79	M_{cr} (kNm)	320.6	193.9	126.0	323.4	185.6	120.3
			ω_2	2.30	2.44	2.48	2.35		
	T1-3	0.79	M_{cr} (kNm)	55.4	36.2	25.9	124.0	67.3	43.5
			ω_2	1.20	1.38	1.52	2.50		
	T2-3	0.79	M_{cr} (kNm)	237.3	154.1	107.5	344.0	197.5	128.0
			ω_2	1.70	1.94	2.11	2.50		

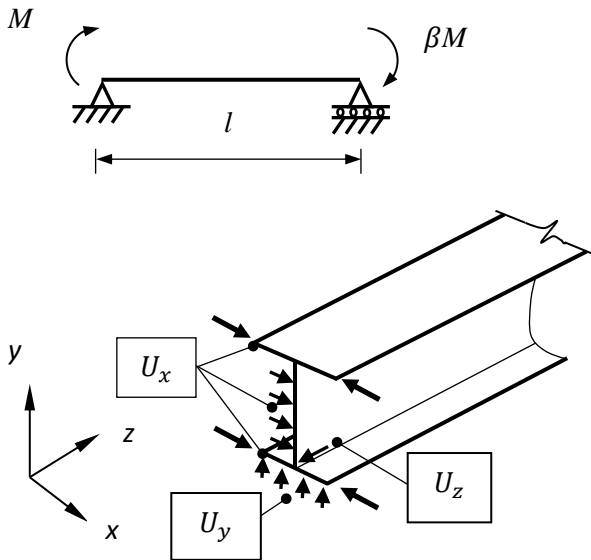


Figure 4. Boundary conditions in the finite element model

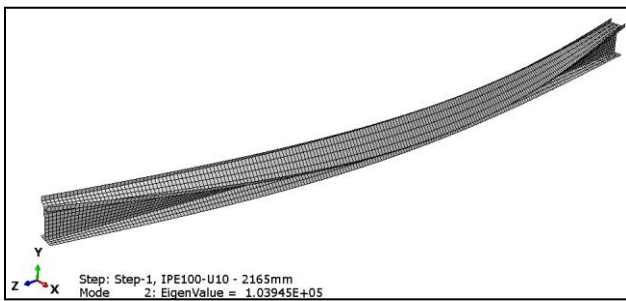


Figure 5. Buckling mode for a monosymmetric beam (Beam Type – 2)

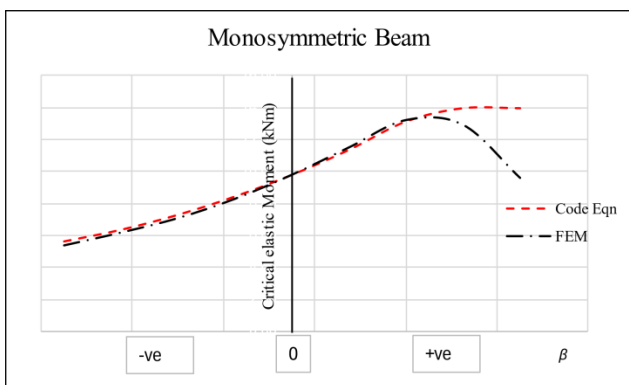


Figure 6. Critical elastic moment trend for code equation and finite element method (FEM) output

In the undesirable cases, the moment gradient factor from design guide equations produces critical moments that are greater than those predicted by the finite element models. Also, the moment gradient factor appears to change as the length of the member changes. This makes it

particularly challenging to develop a single moment gradient factor. This is a challenge that has been noted by Knobloch et al. (2020) who are involved in developing the next generation of the Eurocodes. It is noted that the Type 2 section has a lower sensitivity than the Type 1 section for the cases where the loss in accuracy of the moment gradient factor was observed. However, it is seen that for results in Tables 2 and 4, in general once the member is in double curvature there is evident loss of accuracy in moment gradient factor predicted by the equation that is provided in the code SANS 10162-1 for doubly symmetric sections. This is illustrated in Figure 6.

These results indicate that the implied guidance in the Steel design handbook can produce unconservative results for some monosymmetric sections subjected to linear moment gradients between points of restraint that cause double curvature bending. It is important that when monosymmetric sections are used in cases involving double curvature bending between points of restraints, the critical elastic moment and subsequently member strength are determined for each particular case. A generalised moment gradient factor based on doubly symmetric sections should not be used. The ‘Wagner effect’ associated with monosymmetric sections can have an effect on monosymmetric sections when they are subjected to double curvature bending. This is due to the change in transverse torques arising from longitudinal stresses when the compression and tension flanges swap along the unrestrained length.

The difference in behaviour between the Type 2 and Type 1 sections in some of the observed cases might be due to the relative position of the shear centre in relation to the centroid. For the Type 1 section the shear centre position will always be above the centroid for the degree of monosymmetry above 0.5. For the Type 2 section it has been shown by Mudenda and Zingoni (2018) that the shear centre initially moves above the centroid but at a certain upstand height it reaches a peak height and then starts to move back down even meeting the centroid again. This gives a monosymmetric section that has a coincident shear centre and centroid at a given upstand height. The shear centre then moves below the centroid as the upstand height increases. This shear centre movement can counteract the adverse effects of the negative bending part of the double curvature and hence may reduce the sensitivity of this particular cross section. A more extensive parametric study still needs to be carried out to confirm these initial observations.

CONCLUSION

The current study has shown that using the moment gradient factor developed for doubly symmetric sections on monosymmetric sections subject to lateral-torsional buckling, and subjected to double curvature from linear moment gradient between points of restraint can produce unconservative predictions. For both beam types considered the design code equation for moment gradient factor produced similar outcomes as those from finite element analysis models for the single curvature case. For the case of double curvature there was generally a noticeable deviation from code equation predictions for some cases. It appears that in certain cases such as results from Table 4, beam type 1 showed more sensitivity in deviating from code predictions than the type 2 beam. Factors leading to this behaviour still need to be investigated further. It is, however, clear that there are some cases for which the code equation would produce unconservative predictions. It is recommended that for monosymmetric sections experiencing double curvature due to linear moment gradients between points of restraint the critical buckling loads must be determined for each particular case. The use of moment gradient factors that were developed for doubly symmetric beams must be avoided for these cases.

Selected symbols

G - Shear modulus

M_{cr} - Critical elastic buckling moment

M_p - Plastic moment

β - End Moment ratio

C_b, ω_2 - Equivalent uniform moment factor/ Moment gradient factor

I_x, I_y - Major and minor axis second moment of area

E - Elastic modulus

DECLARATIONS

Corresponding author

Correspondence and requests for materials should be addressed to; E-mail: kenny.mudenda@uct.ac.za; ORCID: 0000-0003-4152-3206.

Data availability

The datasets used and/or analysed during the current study available from the corresponding author on reasonable request.

Acknowledgements

The author would like to acknowledge the Structural Engineering and Mechanics (SEM) Research Group at the

University of Cape Town for access to finite element analysis software.

Competing interests

The author declares no competing interests in this research and publication.

REFERENCES

- Anderson, J. M., & Trahair, N. S. (1972). Stability of monosymmetric beams and cantilevers. *Journal of the Structural Division*, 98(ST1), 269-286. <https://doi.org/10.1061/JSDEAG.0003114>
- Halliwell, E. (2024). Putting the net-zero hierarchy into practice. *The Structural Engineer*. Volume 102 (1), p10-11. <https://doi.org/10.56330/WSKW8501>
- Hayes, C. (2024). Putting the net-zero hierarchy into practice. *The Structural Engineer*. Volume 102 (2), p18-19. <https://doi.org/10.56330/MGEK3688>
- Helwig, T., Frank, K., & Yura, J. (1997). Lateral-torsional buckling of singly symmetric I-beams. *Journal of Structural Engineering*, 123(9), 1172-1179. [https://doi.org/10.1061/\(ASCE\)0733-9445\(1997\)123:9\(1172\)](https://doi.org/10.1061/(ASCE)0733-9445(1997)123:9(1172))
- Hsu, W., Lue, D., & Chen, Y. (2012). Deasing aid for moment strength of built-up crane runway girders. *International Journal of Steel Structures*, 12, 403-417. <https://doi.org/10.1007/s13296-012-3009-3>
- Kirby, P. A., & Nethercot, D. A. (1979). *Design for Structural Stability*. Granada Publishing.
- Kitipornchai, S., & Trahair, N. S. (1980). Buckling properties of monosymmetric I-beams. *Journal of the Structural Division-ASCE*, 106(5), 941-957. <https://doi.org/10.1061/JSDEAG.0005441>
- Knobloch, M., Bureau, A., Kuhlmann, U., da Silva, L. S., Snijder, H., Taras, A., Bours, A., -L, & Jorg, F. (2020). Structural member stability verification in the new Part 1-1 of the second generation of Eurocode 3. *Steel Construction*, 13(3), 208-222. <https://doi.org/10.1002/stco.202000027>
- Mudenda, K., & Zingoni, A. (2018). Lateral-torsional buckling behavior of hot-rolled steel beams with flange upstands. *Journal of Constructional Steel Research*, 144, 53-64. <https://doi.org/10.1016/j.jcsr.2018.01.001>
- Mudenda, K., & Zingoni, A. (2022). Steel beam upstands as a strengthening approach for hot-rolled I-shaped sections. SEMC 2022, Cape Town, South Africa. <https://doi.org/10.1201/9781003348443-158>
- SABS. (2011). The structural use of stee. Part 1: Limit-states design of hot-rolled steelwork. In *SANS 10162-1 : 2011*. 1 Dr Lategan Road, Groenkloof, Pretoria: South African Bureau of Standards.
- SAISC. (2016). *Southern Arican Steel Construction Handbook* (Eighth ed.). The Southern African Institute of Steel Construction.

Salvadori, M. G. (1955). Lateral Buckling of I-Beams. *Transactions of the American Society of Civil Engineers*, 120(1), 1165-1177.

<https://doi.org/10.1061/TACEAT.0007228>

Suryoatmono, B., & Ho, D. (2002). The moment-gradient factor in lateral-torsional buckling on wide flange steel sections. *Journal of Constructional Steel Research*, 58, 1247 - 1264.

[https://doi.org/10.1016/S0143-974X\(01\)00061-X](https://doi.org/10.1016/S0143-974X(01)00061-X)

Wong, Edgar; Driver, Robert G. (2010). Critical Evaluation of Equivalent Moment Factor Procedures for Laterally Unsupported Beams. *Engineering Journal*. American Institute of Steel Construction. Vol. 47, pp. 1-20.

<https://doi.org/10.62913/engj.v47i1.975>

Ziemian, R. D. (2010). *Guide to stability design criteria for metal structures*. John Wiley & Sons. Inc.

<https://doi.org/10.1002/9780470549087>

Publisher's note: [Scienceline Publication](#) Ltd. remains neutral with regard to jurisdictional claims in published maps and institutional affiliations.



Open Access: This article is licensed under a Creative Commons Attribution 4.0 International License, which permits use, sharing, adaptation, distribution and reproduction in any medium or format, as long as you give appropriate credit to the original author(s) and the source, provide a link to the Creative Commons licence, and indicate if changes were made. The images or other third party material in this article are included in the article's Creative Commons licence, unless indicated otherwise in a credit line to the material. If material is not included in the article's Creative Commons licence and your intended use is not permitted by statutory regulation or exceeds the permitted use, you will need to obtain permission directly from the copyright holder. To view a copy of this licence, visit <https://creativecommons.org/licenses/by/4.0/>.

© The Author(s) 2024

Experiences Encountered while Using Construction Contracts during Project Delivery in Botswana

Ssegawa Joseph Kaggwa  , Ntshwene Keneilwe , Kamaruddeen Ahmed Mohammed 

Department of Civil Engineering, Faculty of Engineering, University of Botswana, Gaborone, Private Bag: UB0061, Botswana

[✉]Corresponding author's Email: ssegawaj@ub.ac.bw

ABSTRACT

Various forms of contracts guide the construction project delivery processes across the world. To make procurement more accessible and faster, various institutions have developed what is known as standard forms of contracts (SFoC). These institutions believe that SFoCs could be used in an adopted or adapted mode to reduce the burden of writing contracts every time a project is procured. This article discusses the results of a study that investigated the effectiveness of identified SFoCs and the experiences encountered by key stakeholders in using the contracts during construction project delivery. Study participants were drawn from contractor, consulting and client organisations and completed a questionnaire with both closed and open-ended questions. 11 attributes synthesised from literature were used to measure the effectiveness of a contract. Three major SFoCs were identified as being used in Botswana: the Joint Contract Tribunal (JCT), the New Engineering Contract (NEC) and International Federation of Consulting Engineers (FIDIC). The FIDIC has a long history of use, but in recent years, the NEC entered the arena. Due to the low usage of the JCT, the discussion centred on the NEC and FIDIC contracts. Some insights were drawn from the study. Respondents did not find a big difference in the effectiveness of the two contracts (WME for NEC =3.3 and FIDIC =3.1). However, there were a few attributes for which the NEC seemed to be a better contract. These were a) simple and non-legalistic language with self-contained clauses and b) a communicative and proactive risk management regime, which respondents identified with a propensity to reduce or avoid disputes. The study had the limitations of having used a small (38) sample of respondents and the fact that NEC has not been used in the country for the length of time as the FIDIC contract.

Keywords: Construction contract, Standard forms of contract, Contract Administration, Construction industry, Botswana

INTRODUCTION

Ever since the pronouncement of the Code of Hammurabi (Urch, 1929), there has been a concerted effort to tame the vagaries of the construction work. Various contracts have been developed to stipulate the scope of construction work, identify events that might affect it, and allocate duties, responsibilities, and rights among the parties during the construction process. This is more so given the uncertainty surrounding project delivery, where risks are the norm rather than the exception. Global construction work affiliated institutions have developed various documents for decades to guide the project contract management process. There are now several pre-written or standard forms of contracts (SFoC) around the world which may be adapted or adopted by the contracting parties. SFoCs contain terms and conditions that may be

used for projects within a certain category (e.g. design and build) but give employers a chance to modify the conditions of the contract to suit the project (Murdoch and Hughes, 2007). Some authors (e.g. Gacia, 2005) have noted each has its focus, strengths and weaknesses and hence may be suitable for adaptation, depending on the peculiarities of the project and its environment. Since the formation of a contract involves acceptance of an offer, an intention to have a legally binding agreement, performance and payment, each SFoC has a way of dealing with various aspects of construction, which include, for example, (i) separation and speed of design and construction, (ii) extent of client's involvement, (iii) cost certainty, (iv) capacity for variations, (v) allocation of risk, (vi) clarity of various remedies, (vii) dealing with disputes, and (viii) project complexity (Bralić, 2019). The aim of the differentiation is to provide an appropriate

RESEARCH ARTICLE
 PII: S225204302400017-14
 Received: June 25, 2024
 Revised: September 02, 2024
 Accepted: September 05, 2024

contract form that caters for various procurement methods (e.g. traditional, design & build, turn-key, etc.), types of clients (e.g. global multilateral development banks), and nature of project work (e.g. design, construction, consulting, dredging, etc.). Essentially, each SFoC provides guidance based on the chosen procurement method and the anticipated risk events to manage them amicably and, where possible, to reduce their effect on the project outcome. Essentially, contracts attempt to reduce misunderstandings and disputes, which may be unpleasant and problematic, eventually creating a dysfunctional environment between the contractor and employer and resulting in undesirable project cost and time overruns.

Given that background, the aim of this article is to present the findings of a study that attempted to answer the following question: What are the effectiveness and the experiences encountered by key stakeholders in the construction industry in Botswana while using construction contracts during project delivery? The article is divided into five sections, including this introduction. The second section briefly reviews the literature relating to three common SFoCs, highlighting their nature and focus in relation to guiding the contract administration processes. The third section describes the research approach used in the study, while the fourth section presents results, discusses the findings that arise and ends with a conclusion.

Literature review

There are several construction contracts used across the world. Some are developed internally by organisations, while others are adopted or adapted as a standard form of contract (SFoC). Due the brevity required in this article, the discussion will centre on three commonly used SFoCs, namely the JCT Contract by Joint Contract Tribunal of the UK, the New Engineering Contract (NEC) by the Institution of Civil Engineers (ICE) of the UK and FIDIC contract by Fédération Internationale des Ingénieurs Conseils' (or the International Federation of Consulting Engineers) based in Switzerland. The choice is also reinforced by findings of a study in Botswana, which indicated these are the most prevalent construction contracts in Botswana, where the study was conducted (Ntshwene, Ssegawa and Rwelamila, 2022). The historical origins, nature and characteristics of each SFoC are highlighted next.

JCT Contracts

In 1931 the Joint Contracts Tribunal (JCT) was formed by the Royal Institute of British Architects (RIBA)

as the first JCT standard form of building contract (JCT, 2021). However, it was not until 1977 that it was referred to as JCT. Since its inception, JCT has produced a range of contract families, which has grown over time, adapting to changes in industry practice, new procurement methods, and changes in legislation (JCT, 2021). Its use now accounts for 70% of the projects in the UK (Ladner, 2023). Furthermore, due to the colonial legacy, JCT has been used in many commonwealth countries. Historically, the JCT has been more favourable to the employer, though recent editions (e.g. 1998, 2005, 2011, 2016) have aimed to balance duties, rights and risks by incorporating specific mechanisms to address issues of variations and delays (Chappell, 2017). The latest version of 2016 includes a 13-suite of contracts to cater to various clients, procurement methods, pricing methods, types, sizes, and complexity of projects. To help users select an appropriate contract for their project, JCT published a helpful guide called "Deciding on the appropriate JCT Contract 2016" (JCT, 2017). A summary of key components of a typical JCT Contract is indicated in Table 1.

Table 1. Typical sections of a JCT Contract

Component and aspects addressed
a) <i>Articles of Agreement:</i> e.g. party details; context, nature and scope of the of works, specification and pricing documentation;
b) <i>Contract Particulars:</i> e.g. completion date, date of possession, defects rectification period, liquidated/delay damages details).
c) <i>Terms and conditions:</i> definitions and interpretations; execution of works to completion and defects rectification requirements; control of the works; payment issues, SHE requirements; change control, indemnification, termination, and disputes.
d) <i>Schedules:</i> "add-ons" to a construction contract (e.g. insurance options, forms of bonds, etc.)

NEC Contracts

ICE developed the New Engineering Contract (NEC) in 1993 in the UK. Its notable early adopters were major British corporations (e.g., British Airports Authority, National Power, Scottish Hydroelectric) and a South African public electricity utility, Eskom (NEC, n.d.). The latest suite of contracts, NEC4 of 2016, consists of 10 contracts spanning supply, work, and service projects. Table 2 indicates a typical arrangement of the sections of an NEC contract.

Table 2. Typical sections of a NEC Contract

Component and aspects addressed
a) General provisions
b) Responsibilities -contractor, subcontractor & supplier's main responsibilities
c) Time progress management
d) Quality testing and defects
e) Payment
f) Compensation events,
g) Title -use of equipment plant and materials
h) Liabilities & insurance, risks, liability, insurance and indemnities
i) Termination & dispute resolution.

NEC is gaining international usage because, in its latest version, the NEC4 of 2016, it is being lauded for user-friendliness arising from its features, which include the following: First, it is viewed as being highly adaptable to suit the unique requirements of various procurement strategies, contract types and industry practices (Forward, 2002). Second, NEC4 contracts use clear and straightforward language, minimising ambiguity and potential disputes. They provide a common understanding of project parties' roles, responsibilities, obligations, and duties. This improves communication and reduces the propensity for disputes. Third, the NEC4 contract provides a mechanism for the early involvement of all parties, encouraging cooperation and open communication throughout the project lifecycle. This collaborative atmosphere sets up a proactive problem-solving mindset, leading to more efficient decision-making and improved project outcomes. Fourth, a comprehensive, proactive risk management mechanism allows for a fair allocation of risks among the parties by providing guidance on identifying, assessing, and mitigating risks, ensuring a balanced allocation of responsibilities. Lastly, an emphasis on performance management, with clear mechanisms for monitoring and control, focusing on accountability, quality delivery, and continuous improvement throughout the project duration. The contracts include provisions for performance measurement, regular reporting, and incentivisation based on achieving project objectives.

FIDIC contracts

FIDIC, which stands for International Federation of Consulting Engineers, published its first contract, titled: The Form of Contract for Works of Civil Engineering Construction, in 1957 (FIDIC, 2023). Over the years,

FIDIC has become famous for producing standard contracts for the construction and engineering industry. FIDIC's broad outreach and the support it enjoys have made its forms the mainly used contract in international construction (Seifert, 2005).

Just like the rest of SFoC houses, FIDIC has added new forms of contract, replaced previous versions with new ones and updated essential terms and clauses to keep in touch with the industry's changes and dynamics (Udom, 2014). The contracts are now famously known as the "Rainbow" edition due to the various colours of the contract suites (e.g. red, green, yellow, silver, pink, etc.) meant for various procurement methods, types of clients and projects. A typical layout of the FIDIC contract is illustrated in Table 3.

Apart from being touted as the universal contract, FIDIC contracts are viewed as having detailed procedural guidelines for managing a project with comprehensive provisions for managing unforeseen circumstances and claims. Furthermore, in recent years, the FIDIC has emphasised an amicable settlement of disputes so as not to jeopardise the progress and cost of a project. As a first step, the process usually provides for disputes to be submitted for adjudication before an Engineer or a Dispute Board. If one (or both) of the parties is dissatisfied, a period is allowed for amicable settlement. If the parties are not able to settle the dispute during the 'amicable settlement' period, the final stage is to proceed to arbitration. This way, FIDIC offers a balanced risk distribution with precise mechanisms for addressing unforeseen and exceptional circumstances that lead to delays and cost overruns. Furthermore, FIDIC contracts are adaptable to various legal systems for cross-border projects and are endorsed by global financial institutions.

Table 3. Typical sections of a FIDIC Contract

Component and aspects addressed
a) <i>General Conditions</i> : definitions and other contractual requirements and data
b) <i>Parties</i> : Roles, rights and obligations of the parties to the contract
c) <i>Project Management</i> : Project resources and project work (e.g. programme, progress, quality, changes, testing, claims suspension, termination and closure)
d) <i>Financial Issues</i> : Project finance and payments
e) <i>Risk Management</i> : Risk allocation and mitigation
f) <i>Disputes & Arbitration</i>

MATERIALS AND METHODS

In answering the research question posited earlier (i.e. what is the effectiveness and the experiences encountered by key stakeholders in the construction industry in Botswana while using construction contracts during project delivery?), a questionnaire with closed and open-ended questions was used. In Botswana, several entities manage public construction projects in the various sub-sectors, such as roads, aerodromes, power, rail, water, and buildings, and they use construction contracts for these projects. Key personnel were identified and selected from the project management entities spanning the above sectors to complete a questionnaire. The study participants were selected based on three aspects: working in the construction industry (as contractors, clients or consultants) for five years and above and a willingness to participate in the research.

Apart from requesting the demographic profile of respondents, the questionnaire sought to ascertain various aspects of the contracts they have used or they are using, e.g. type, version, form, formal training received, etc. Secondly, the questionnaire required respondents to rate the effectiveness of the contract in managing the 11 key attributes identified from literature based on the scale 5 (Excellent; 4: Very Good; 3: Good 2: Poor; 1: Very Poor). From this, weighted mean effectiveness (WME) was computed for each attribute and for each contract based on Equation 1:

$$WME = \frac{5 \cdot n_5 + 4 \cdot n_4 + 3 \cdot n_3 + 2 \cdot n_2 + 1 \cdot n_1}{5 + 4 + 3 + 2 + 1} \quad \text{Equation 1}$$

where $n_1 \dots n_5$ are the number of rating responses for the attribute. Furthermore, an open-ended question was attached to each close-ended question to solicit respondents' responses as to why they rated the 11 attributes, high (4 & 5) or low (1 & 2), for each SFoC. The responses served as a means of providing their experiences of using such a contract.

RESULTS AND DISCUSSION

This section presents the study's results and discusses the findings relating to the experiences encountered by key stakeholders while using construction contracts during project delivery in Botswana. The section, however, begins with a description of the respondents' demographic profile.

Demographic profile of respondents

Table 4 summarises the profile of 38 respondents who participated in the study. The respondents were given codes for confidentiality, namely R1 to R38. Table 4a indicates that as a standard feature of the construction industry, the majority (66%) of the respondents were male, in middle and lower management positions (95%) in their

organisations, as shown in Table 4b. The respondents were a mixed bag: working contractors, consultants and client organisations, with the latter forming the majority (58%) of respondents. Tables 4d and 4e indicate a mix of built environment professions, with engineers forming the majority (29%) of the respondents. Furthermore, all respondents had graduate degrees, and the majority (74%) were registered members of professional bodies. Lastly, Table 4g indicates that the majority (71%) of respondents had an industry experience of 10 years and above.

Table 4 (a-g). Demographic profile of the respondents.

<i>a) Gender</i>	<i>No.</i>	<i>Ratio</i>
Female	13	34%
Male	25	66%
Total	38	100%
<hr/>		
<i>b) Managerial Level</i>	<i>No.</i>	<i>Ratio</i>
Top	2	5%
Middle	23	61%
Lower	13	34%
Total	38	100%
<hr/>		
<i>c) Work sector</i>	<i>No.</i>	<i>Ratio</i>
Public (Govt. Depart., Local authority & Parastatal)	22	58%
Private client	6	16%
Contractor	5	13%
Consultant	5	13%
Total	38	100%
<hr/>		
<i>d) Profession</i>	<i>No.</i>	<i>Ratio</i>
Engineer	11	29%
Architect	9	24%
Quantity Surveyor	10	26%
Procurement officer	3	8%
Legal officer	4	11%
Other	1	3%
Total	38	100%
<hr/>		
<i>e) Educational Level</i>	<i>No.</i>	<i>Ratio</i>
Dip/Higher/Dip.	0	0%
Bachelor	25	66%
Post Graduate	13	34%
Total	38	100%
<hr/>		
<i>f) Professional Membership</i>	<i>No.</i>	<i>Ratio</i>
Yes	28	74%
No	10	26%
Total	38	100%
<hr/>		
<i>g) Experience in Years</i>	<i>No.</i>	<i>Ratio</i>
under 10	11	29%
10-19	13	34%
20-29	11	29%
30 and above	3	8%
Total	38	100%

Table 5 (a-g). Nature of Contracts used

<i>a) Contract Used</i>	<i>No.</i>	<i>Ratio</i>
Internally developed	0	0%
SoFC	38	100%
Both	<u>0</u>	<u>0%</u>
Total	38	100%
<hr/>		
<i>b) SFoC Type</i>	<i>No.</i>	<i>Ratio</i>
JCT	6	12%
FIDIC	31	62%
NEC	13	26%
Other	<u>0</u>	<u>0%</u>
Total	50	100%
<hr/>		
<i>c) Modification of SFoC</i>	<i>No.</i>	<i>Ratio</i>
Modified	38	100%
Original form	<u>0</u>	<u>0%</u>
Total	38	100%
<hr/>		
<i>d) Procurement used</i>	<i>No.</i>	<i>Ratio</i>
Traditional	38	63%
Design & Build	11	18%
Turn key (EPC)	5	8%
Others	<u>6</u>	<u>10%</u>
Total	27	100%
<hr/>		
<i>e) Nature of Contract Pricing</i>	<i>No.</i>	<i>Ratio</i>
Lump sum	10	14%
Time and materials	13	18%
Cost-plus	6	8%
Unit price	38	52%
Guaranteed max. price	<u>6</u>	<u>8%</u>
Total	<u>73</u>	<u>100%</u>
<hr/>		
<i>f) SFoC Formal training</i>	<i>No.</i>	<i>Ratio</i>
JCT	2	4%
NEC	13	28%
FIDIC	31	67%
Other	<u>0</u>	<u>0%</u>
Total	<u>46</u>	<u>100%</u>
<hr/>		
<i>g) Training providers</i>	<i>No.</i>	<i>Ratio</i>
None	0	0%
Local private institution	16	31%
Local public institution	13	25%
International individual	13	25%
International institution	10	19%
Author of the SFoC	<u>0</u>	<u>0%</u>
Total	25	100%

Nature of contracts used

Table 5 summarises the nature of contracts that the respondents have used or are using in their organisations. As Table 5a indicates, all (38) respondents who

participated in the study stated that they do not use any internally developed contract but use a Standard Form of Contract (SoFC), of which the FIDIC (65%) is the most prevalent (Table 5b) followed by the NEC (23%) and JCT (19%). All (100%) respondents noted that (Table 5c) these contracts have been modified to fit the local context. It should be noted that some indicated that they use more than one contract, especially those in local authorities who use a modified JCT contract for small projects (of less than BWP 500,000) as well as the FIDIC Contract for higher valued projects (and this is why in some cases the total responses are more than the total number of respondents of 38). In addition, those dealing with road projects also indicated using a FIDIC contract for Multilateral Development Banks (MDBs) for their 'World Bank-funded projects.

Furthermore, Table 5 d,e shows that the most common procurement route (63%) is traditional procurement, while the most commonly used suite of contracts (38%) is the one with re-measurable quantities with unit pricing, irrespective of the SFoC used. Lastly, respondents further indicated that they have received specific training on the SFoCs from various outlets, by both local and international providers, as shown in Table 5 f,g.

Experience of using SFoC

Table 6 summarises the Weighted Mean Effectiveness (WME), which reflects respondents' rating of the 11 attributes that depict an effective construction contract. As noted earlier, some respondents had used only one SFoC while others used or are still using two. Of the three main SFoC, the NEC received the highest overall average rating (WME=3.3), followed by the FIDIC (WME=3.1), while JCT received the lowest (WME=2.9), as shown at the bottom of Table 6. One Respondent (R2) noted, "First of all, it is an old modified JCT contract. However, most of the small local contractors know it well. So, we use it for low-value jobs, especially maintenance. It is easy to understand and follow but cannot guide highly valued and complex projects as it lacks most modern contracting mechanisms. The version is also client-centric, viewing 'the client as the boss' This response focused on results for the NEC and FIDIC contracts about the 11 attributes. Notably, thirteen (13) respondents who appraised the NEC have used the FIDIC contract before, and their comments were insightful. The rest of the sub-sections discuss the effectiveness and experiences of the respondents for the FIDIC and NEC contracts structured around the 11 attributes.

Table 6. Assessment of the contract attributes identified

<i>Contract attribute</i>	<i>JCT (N=6)</i>	<i>FIDIC (N=31)</i>	<i>NEC(N=13)</i>
1. Language used	3.1	2.9	3.8
2. Navigation of clauses	3.0	2.3	4.0
3. Contract layout	3.2	3.9	2.7
4. Adaptability to project context	2.9	3.5	3.6
5. Time scales for claim notices	2.7	3.1	3.2
6. Role of contracts manager	4.0	3.1	2.4
7. Management of changes	3.2	3.0	3.4
8. Management of performance	3.1	2.3	3.9
9. Allocation and management of risk	2.1	3.1	3.2
10. Force majeure or prevention events	2.2	2.7	2.8
11. Management of disputes	<u>2.2</u>	<u>3.6</u>	<u>3.6</u>
Average	2.9	3.1	3.3

1) Language used and navigation of clauses

Table 6 (rows 1 & 2) shows that in terms of simplicity of language, NEC (3.8) was rated a better contract than FIDIC (2.9). Respondents complained that despite the reduction in the use of legalist language found in the FIDIC version 2017 as compared to 1999, there were vestiges of the earlier version, as one respondent (R14) noted “long sentences and sometimes ambiguous or unclear language and non-objective terms or concepts and often this leads us to situations where the Employer and Contractor arrive at different interpretations leading to misunderstandings. The FIDIC contract should be reduced to simple English to allow construction technical personnel to understand the obligations of a party or what is required instead of requiring lawyers to interpret sometimes technical aspects which they also struggle to understand”.

Table 6 also shows that the NEC (4.0) clauses were considered easier to follow than FIDIC (2.3). Respondents (R2 and R4) further noted, "clauses and sub-clauses should be self-contained instead of the requirement to cross-reference a myriad to a get remedy...." On the other hand, those who have used the NEC contract positively touted its use of plain language simplicity and self-containment of the clauses.

2) Contract layout

In terms of the layout, respondents felt that FIDIC (3.5) had a slightly better layout than NEC (3.3) in the

sense that it followed a project management approach. As one respondent put it, “The clauses follow the progress of the project from defining the role and obligation of the parties, work needs and progress to closure or termination, but of course, there are hanging clauses like risk, indemnity, and disputes.”

3) Adaptability to project context

As to adaptability to project and local conditions, there was no significant difference between FIDIC (3.5) and NEC (3.6) as one respondent noted, “FIDIC has several suites of contracts which favours a particular procurement method and we able to modify it to allow for a change of currency, language and legal regime in which the project is delivered. With NEC, we are also able to do the same.” The adaptability of both contracts can be viewed from their broader appeal in the international arena. As Seifert (2005) noted, FIDIC is the world's most widely used international form of construction contract. However, though NEC is a relatively new contract, it has become a popular suite of contracts for public-sector works, services and supplies in the United Kingdom and Hong Kong and beyond; for example, it is taking root in Australia, New Zealand, Ireland, Netherlands, South Africa and UAE (Gerrard, 2005).

4) Time scales for claim notices

Tolson and Glover (2008) observe that under the FIDIC contract if a Contractor fails to give notice of a claim within 28 days, the Time for Completion is not extended, loses the entitlement to additional payment, and the Employer is discharged from all liability in connection with the claim. Under the NEC contract, if the Contractor does not notify of a compensation event within eight weeks (40 days) of becoming aware of the event, he is not entitled to a change in the prices, the completion date or a key date, unless the project manager should have notified the event to the Contractor but did not. Therefore, both FIDIC and NEC provide firm time scales for notices that may require time and/or monetary compensation, and if the contractor fails to give notice, the claim will fail.

Respondents indicated a slight advantage of the NEC contract (3.2) as compared to the FIDIC contract (3.1). One respondent (R10) who presented himself as a contractor noted, “The NEC contract is more practical as it gives a longer period (40 as opposed to 28 days). However, what I decry most is that both contracts do not impose the same obligation to the Employer of giving notices within a time limit.”

5) Role of the contracts manager

In FIDIC, the contracts manager is called the Engineer (even if it is an architect), while in NEC, it is called a Project Manager. In both contracts, they are employed by the Employer and play a dual role: overseeing the project work and adjudicating. However, they are expected to be impartial when deciding or determining matters related to, for example, claims or misunderstandings.

One respondent (R22) noted that "... the dual role of the contracts manager can only be effective if there is a high degree of professionalism and ethical conduct...once these are not upheld there can be accusations of employer bias or contractor collusion... a situation we often encounter"

6) Management of changes

Under NEC, variations are merely a category of compensation events (CE) assessed by the Project Manager in the same way as claims. If a variation is envisaged, the Project Manager calls for a quotation from the Contractor, which should indicate the effects of a CE on both time and cost, as these flow automatically once the CE is approved (McKenzie, 2016). The pricing decision is based on CE's effect on a defined cost plus fee. Existing rates do not bind the Project Manager during valuation. Therefore, it is highly unlikely that the Contractor will unfairly benefit or suffer a loss if existing rates are too high or too low. Therefore, if the quotation is accepted, formal instruction to undertake the work follows.

FIDIC, on the other hand, considers claims and variations as separate issues; therefore, the latter is measured and valued in the ordinary course of work. Since FIDIC is a re-measurement contract that assumes the project scope, works, drawings, etc., are well defined prior to letting the tender documents (which often is not true), it limits variations to 10% of the quantity. However, unlike in the NEC regime, entitlement to both time and cost does not automatically flow from a variation instruction - rather, each must be proved separately and is subject to time bar notices (McKenzie, 2016). Valuation of a variation is at the same or by considering rates and prices in the contract. It is noted that existing rates or rates for similar work apply. If neither of the two is available or other criteria are met, new rates are permitted at the so-called reasonable cost plus a reasonable profit.

Respondents rated NEC (3.4) a better contract in managing changes than FIDIC (3.0), and this was buttressed by respondent (R27), who observed by noting "the NEC approach is a good risk management and collaborative approach which may foster less disputes

because the quantum of work is first established and pre-priced before it is carried out. However, for the FIDIC contract, since the actual cost incurred and time expended is determined retrospectively, the Engineer has a wide discretion which tends to open up a myriad of disagreements, some of which lead to protracted disputes."

7) Management of performance

FIDIC and NEC require a contractor to provide a programme which will be used to measure time performance. The programme facilitates measuring project progress and determining damages for late completion by the contractor (delay compensation for the Contractor). The contracts define the required outcome or performance based on the Employer's quality requirements (relating to materials and artistry). They further provide for searching for defects and state the Contractor's responsibility for correcting defects and the consequence of the Contractor's failure to correct any defects. Furthermore, NEC goes further in its optional incentive schedule, X20, which may be attached to the main contract, to allow the client to state Key Performance Indicators (KPIs) and targets for various aspects of the project's performance, for example, time, quality, cost, disputes, SHE issues and sub-contractor management. The KPIs and targets are meant to incentivise the Contractor with a bonus payment for performing to the targets or above.

Respondents using the NEC contract noted that they had not explored the X20 clause, which allows for inserting incentivising KPIs. Hence, they depend on the traditional project performance measurement of cost, time, and quality.

8) Allocation and management of risk

According to Simon, Hillson and Newland (1997), risk is an event or set of circumstances that, should they occur, will have an effect on the achievement of the project's objective. Effective risk allocation and management procedures are key to any construction contract, for which Abrahamson (1984) proposed a set of five principles for allocating risk. Risk shall be allocated to a party: a) if the risk is of loss due to their willful misconduct or lack of reasonable efficiency or care; b) if they can cover the risk by insurance and allow for the premium in settling the charges, and it is most convenient and practicable for the risk to be dealt with in this way; c) if the preponderant economic benefit of running the risk accrues to the party; d) if it is in the interests of efficiency to place in the risk on the party and e) if, when the risk eventuates, the loss happens to all on the party in the first

instance, and there is no reason under any of the above headings to transfer the loss to another, or it is impracticable to do so. While it is not possible to eliminate all risks, it is now an acceptable and basic principle that a particular risk event should be allocated to the party who can best manage it and bear the risk consequences (Kozek and Hebbard, 1998).

Regarding risk allocation and management, respondents did not differentiate much between FIDIC (3.1) and NEC (3.2) regarding risk allocation. As one respondent (R19), “as a starting point in defining the duties, obligations, liabilities and rights of the Employer and Contractor, both FIDIC and NEC attempt to allocate risks fairly and reasonably” However, another respondent went further to note that “in my opinion I find NEC a slightly better contract in the sense that the requirement to include early warning signals, risk registers and to hold risk reduction meetings are an effective communication tool between the parties which minimises disputes in that way NEC is not reactive but provides a dynamic and proactive risk management regime.” This position was buttressed by another respondent (R35) who observed that “FIDIC seems to be saying I have the medicine (clauses) if things go wrong whereas NEC seems to be saying let us not wait for something to go wrong, let us try to mitigate or prevent it before it happens..” Some authors (e.g. Besaiso et al., 2018) have noted that a reactive approach produces more disputes than a proactive approach, as parties will use the contract when things go wrong or disputes surface in an attempt to find a clause that will support their contractual position or justify a claim or to allocate blame.

9) Force majeure or prevention events

An event that occurs to exempt a party from performance on the contract is referred to as force majeure in FIDIC and a prevention event for NEC. Each contract has tests which must be satisfied for an event to be classified as such. For FIDIC, a force majeure event is one which: a) is beyond a Party’s control; b) such Party could not reasonably have provided against before entering into the Contract; c) having arisen, such Party could not reasonably have avoided or overcome, and d) is not substantially attributable to the other Party. On the other hand, NEC defines prevention events as those which: a) stop the Contractor from completing the works or by the dates shown on the Accepted Programme, b) neither Party could prevent; c) an experienced Contractor would have judged that the contract dates have such a small chance of occurring that it would have been unreasonable for him to

have allowed for it; and d) is not one of the other compensation events stated in the contract. There was a small difference (2.7 for FIDIC and 2.8 for NEC) in rating the effectiveness of handling these events for the two contracts

10) Management of disputes

Cost, delay, and uncertainty of the outcome have made the construction industry move away from litigation and the growing use of alternative dispute resolution (ADR) methods, one of which is arbitration. However, arbitration has suffered a similar fate as litigation, as it was found costly, time-consuming, and the outcome unpredictable. The answer lay in adjudication. Adjudication decides matters as the project carries on, promoting project progress and cash flow. However, the adjudicator’s decision is subject to review by an arbitrator if one of the parties is sufficiently unhappy with the outcome of the adjudication (MDA, 2022). In response to the challenges of arbitration, the latest versions of FIDIC (2017) and NEC (4) have both called for a dispute adjudication board (DAB). Perhaps due to this similarity, respondents rated dispute resolution effectiveness of both contracts the same (3.6). However, one respondent (R7) highlighted experiences of using an ad-hoc and standing dispute adjudication board (DAB). She noted, “We used an ad-hoc DAB; it was cheap, and if we did not decide on one set of DAB, we could appoint another set of members. However, often, DAB members required more time to acclimatise with what had gone on at the project in order to adjudicate” She further continued “, We now have a standing DAB who meet with the Parties and conduct regular site visits so they become familiar with the project nitty-gritty. However, they seem expensive. They charge a monthly retainer fee and require the provision of, or reimbursement of, daily travel fees and accommodation costs. Furthermore, when a dispute arises they charge a daily rate to adjudicate the dispute”

CONCLUSION

The study set out to investigate the effectiveness and experiences of key stakeholders in using various contracts for construction project delivery. Three major SFoCs were identified as being used in Botswana: the NEC, FIDIC, and JCT. The local authorities mainly used a modified and old version of JCT. Due to the low usage of the JCT, the discussion centred on the NEC and FIDIC contracts. The FIDIC has a long history of use in the country, but the NEC has entered the arena in recent years. A few

concluding aspects are noted. First, respondents did not find a big overall difference in the effectiveness of the contracts as measured using the 11 identified attributes (WME for NEC =3.3 and FIDIC =3.1). However, from their experience, there were a few attributes where the NEC contract seemed to be a better contract, and these were: a) the use of simple and non-legalistic language with self-contained clauses and b) a communicative and proactive risk management regime, which they thought may result in reducing or avoiding disputes. Despite these accolades, this article ends by noting that there are pros and cons to the use each contract, and which one works best largely depends on the parties involved, the context of the project and the contracting environment. In addition, this study has the limitation of having used a small (38) sample of respondents and the fact that NEC has not been used in the country for the length of time as FIDIC.

DECLARATIONS

Corresponding author

Correspondence and requests for materials should be addressed to Ssegawa J. K.; E-mail: ssegawaj@ub.ac.bw; ORCID: 0000-0001-5272-3479

Data availability

The datasets used and/or analysed during the current study are available from the corresponding author on reasonable request.

Acknowledgements

The authors would like to acknowledge the study participants for responding to the questionnaire.

Authors' contribution

All authors participated in the study and write-up of the manuscript.

Competing interests

The authors declare no competing interests in this research and publication.

REFERENCES

- Abrahamson, M. W. (1984) Risk management. *International Construction Law Review*, 1(3), 241–64. <http://alliancecontractingelectroniclawjournal.com/wp-content/uploads/2017/04/Abrahamson-M.-1984-%E2%80%98Risk-Management%E2%80%99.pdf>
- Besaiso, H., Fenn, P., Emsley, M. and Wright, D. (2018). A comparison of the suitability of FIDIC and NEC conditions of contract in Palestine, *Engineering, Construction and Architectural Management*, 25 (2): 241-256. <http://dx.doi.org/10.1108/ECAM-10-2016-0235>
- Bralić, E. (2019). Experience in the use of FIDIC contracts on rail infrastructure project, *Građevinar*, 71 (11): 987-993. DOI: <http://casopis-gradjevinar.hr/assets/Uploads/JCE-71-2019-11-3-2710-EN.pdf>
- Chappell, J. (2017). *Understanding JCT Standard Building Contracts*, Routledge, Oxon, U. <https://www.taylorfrancis.com/books/mono/10.4324/9780203121313/understanding-jct-standard-building-contracts-david-chappell-david-chappell>
- Causeway (2023). NEC contracts explained: a guide on NEC4 and other types of NEC contracts. <https://www.causeway.com/blog/nec-contracts-explained-the-ultimate-guide>.
- Erwin J. Urch, E. J. (1929). *The Law Code of Hammurabi*, American Bar Association Journal, 15 (7): 437-441. https://heinonline.org/hol/cgi-bin/get_pdf.cgi?handle=hein.journals/abaj15§ion=135
- FIDIC (2023). *Engineering the Future: 110 years of FIDIC*, International Federation of Consulting Engineers (FIDIC), <https://fidic.org/history>
- Garcia, S. (2005). How Standards Enable Adoption of Project Management Practice. *IEEE Software*, 22(5): 22-29. <https://doi.org/10.1109/MS.2005.122>
- Forward, F. (2002). *The NEC compared and contrasted*. Thomas Telford, London. <https://www.scribd.com/document/496781565/The-NEC-Compared-and-Contrasted>
- Gerrard, R. (2005) *Relational Contracts - NEC in Perspective*, *Lean Construction Journal*, 2 (1):80-86JCT (2017). https://lean-construction-gcs.storage.googleapis.com/wp-content/uploads/2022/09/08152923/Relational_Contracts_-_NEC_in_Perspective.pdf
- JCT contract (2016) *Deciding on the appropriate, Joint Contract 2016*, Tribunal, Thomson Reuters, London, UK <https://www.jctltd.co.uk/docs/Deciding-on-the-appropriate-JCT-contract-2016.pdf>
- JCT (2021). *Setting the standard for construction contracts*, The Joint Contracts Tribunal (JCT) <https://corporate.jctltd.co.uk/about-us/our-history/#:~:text=In%201931%20the%20Joint%20Contracts,version%20was%20published%20in%20193>
- Ladner, J. (2023). *Standard form contracts: JCT*, *Out-law Guide*, Pinsent Masons: <https://www.pinsentmasons.com/out-law/guides/standard-form-contracts-jct>
- Kozek, J. and Heberd, C. (1998), “Contracts: share the risk”, *Journal of Construction Engineering and Management*, 111(2):356–361.
- Mante, J. (2018). Dispute resolution under the FIDIC and NEC Conditions: paradox of philosophies and procedures? *International construction law review*, 35(2): 182-223. <https://rgu-repository.worktribe.com/OutputFile/293338>
- McKenzie, B. (2016) *Variations in Construction Contracts: NEC3 and FIDIC Compared*, Lexology, <https://www.lexology.com/library/detail.aspx?g=0d5f996c-9ea3-4d82-af52-1b5cffa26f01>

- MDA (2022), Implementation of dispute boards on construction contracts, MDA, <https://www.mdalaw.co.za/articles/implementation-of-dispute-boards-on-construction-contracts/>
- Murdoch, J., & Hughes, W. (2007). Construction contracts: law and management, Routledge, London, UK. <https://www.taylorfrancis.com/books/mono/10.4324/9780203184981/construction-contracts-john-murdoch-hughes>
- Ntshwene, K., Ssegawa, J. K. and Rwelamila, P.D. (2022). Key performance indicators (KPIs) for measuring PMOs services in selected organisations in Botswana, *Procedia Computer Science*, 196: 964-972. <https://www.sciencedirect.com/science/article/pii/S1877050921023218>
- NEC (n.d.) Evolving to be the world's favourite procurement suite, NEC~HistoryWhitepaper_Spreads_v5.inddl, <https://www.neccontract.com/getmedia/26f7ce0e-bd69-4e01-b248-86646ba1014c/The-History-of-NEC-Whitepaper.pdf>.
- Seifert, B. (2005). International Construction Dispute Adjudication under the International Federation of Consulting Engineers Conditions of Contract and the dispute Adjudication Board. *Journal of Construction Engineering and Management*, 131(2):149-157. [https://doi.org/10.1061/\(ASCE\)1052-3928\(2005\)131:2\(149\)](https://doi.org/10.1061/(ASCE)1052-3928(2005)131:2(149))
- Simon, P. Hillson, D. & Newland, K. (1997). PRAM: Project Risk Analysis and Management Guide. Association for Project Management, Norwich, UK. https://ne.fapam.edu.br/prime-explore/publication/pdfs/project_risk_analysis_and_management_guide.pdf
- Tolson, S. and Glover, J (2008). Time bars in construction contracts and global claims, Fenwick Elliott. [https://www.fenwickelliott.com/sites/default/files/Tim e%20bars%20in%20constructions%20contracts%20and%20 global%20claims.pdf](https://www.fenwickelliott.com/sites/default/files/Tim%20e%20bars%20in%20constructions%20contracts%20and%20global%20claims.pdf)
- Udom, K. (2014). A brief introduction to FIDIC contracts, NBS. <https://www.thenbs.com/knowledge/a-brief-introduction-to-fidic-contracts>

Publisher's note: [Scienceline Publication](#) Ltd. remains neutral with regard to jurisdictional claims in published maps and institutional affiliations.



Open Access: This article is licensed under a Creative Commons Attribution 4.0 International License, which permits use, sharing, adaptation, distribution and reproduction in any medium or format, as long as you give appropriate credit to the original author(s) and the source, provide a link to the Creative Commons licence, and indicate if changes were made. The images or other third-party material in this article are included in the article's Creative Commons licence unless indicated otherwise in a credit line to the material. If material is not included in the article's Creative Commons licence and your intended use is not permitted by statutory regulation or exceeds the permitted use, you will need to obtain permission directly from the copyright holder. To view a copy of this licence, visit <https://creativecommons.org/licenses/by/4.0/>.

Fixed-Bed Adsorption Dynamics of Total Organic Carbon from Gamodubu Landfill Leachate Using Biochar Derived From Gaborone Wastewater Treatment Plant Sewage Sludge

Lamong Duke Tshenyego¹  , Phillimon T Odirile¹  and Gilbert. K. Gaboutloeloe² 

¹Department of Civil Engineering, University of Botswana, Private Bag UB0061, Gaborone, Botswana

²Department of Agricultural Engineering and Land Planning, Botswana College of Agriculture, Private Bag 0027, Gaborone, Botswana

[✉]Corresponding author's Email: tshenyegol@ub.ac.bw

ABSTRACT

In developing countries like Botswana, addressing leachate treatment presents considerable difficulties, especially regarding the management of sewage sludge (SS). This research evaluated the capacity of activated biochar, derived from sewage sludge, to adsorb Total Organic Carbon (TOC). Biochar was produced under conditions with limited oxygen, by placing approximately 50 grams of dried sewage sludge in sealed porcelain crucibles and heating them at a rate of 10°C per minute to 400°C for four hours. The resulting biochar (WWSBC400) was then stored in plastic bags in a dry environment. The pyrolysis yield was calculated as the ratio of the weight of the produced biochar to the initial weight of the dry sewage sludge. The study identified the maximum adsorption capacities (qm) for TOC in landfill leachate solutions, highlighting surface precipitation as a key adsorption mechanism for WWSBC400. Additionally, the removal of carbon ions using biochar produced from sludge at Gaborone's wastewater treatment facility was investigated. Continuous adsorption columns were utilized to demonstrate TOC solution adsorption, with performance evaluated in a fixed-bed column through model simulation. The Thomas model was used to compare experimental kinetic data, with the experimental data generally aligning well with the Thomas model, achieving a correlation coefficient (R^2) of 0.9114 for the first round of activated biochar removal. The adsorption capacity of the biochar was recorded at 389.265 mg/g after 14.5 hours of column adsorption, with regeneration studies showing varying adsorption capacities of 742.82 mg/g, 875.47 mg/g, 682.13 mg/g, and 735.21 mg/g for successive rounds. Surface precipitation was found to be a vital process for carbon adsorption onto WWSBC400. In conclusion, using sewage sludge biochar for co-contaminated soil shows potential for heavy metal immobilization, presenting a viable option for environmental rehabilitation.

Keywords: Biochar Adsorption kinetic models; Fixed-bed column, Total Organic Carbon, sewage sludge, environmental remediation.

INTRODUCTION

The relentless march of technology has transformed every aspect of our lives, becoming an indispensable part of our existence. However, this rapid advancement comes with significant consequences, notably the looming spectres of climate change and heavy metal pollution. Climate change has already inflicted profound damage upon our planet, while heavy metal pollution pervades every corner of our ecosystem (Mladenov et al., 2005). Once heavy metals infiltrate the environment, they persist across different spheres, wreaking havoc on wildlife, vegetation, and the environment at large. Urgent action is imperative to mitigate the impacts of climate change and curb heavy metal pollution before irreparable harm is done. The

choices we make today to safeguard the environment and secure a sustainable future will determine the legacy we leave for generations to come. Recent research conducted by Lehmann et al. (2011), Zhang et al. (2019), and Wang et al. (2022) has highlighted biochar as an effective solution for addressing climate change and heavy metal contamination. Biochar is a carbon-rich material produced through the thermochemical conversion of biomass under oxygen-restricted conditions. Its physical and chemical characteristics are influenced by factors such as pyrolysis temperature and the type of feedstock used, as noted by Binti et al. (2007). Biochar has shown significant potential in reducing the bioavailability and leachability of heavy metals in soils, thereby mitigating contamination as shown

RESEARCH ARTICLE
 PII: S225204302400018-14
 Received: June 25, 2024
 Revised: September 02, 2024
 Accepted: September 05, 2024

in Figure 1,. Additionally, it can improve soil quality and reduce the uptake of heavy metals by crops. The production of biochar provides a sustainable approach to managing biomass waste, as it can be generated from various biomass sources. Advances in this field have also demonstrated biochar's role in combating climate change, producing biofuels, and enhancing soil productivity. In this study, biochar was utilized to analyze the adsorption dynamics of Total Organic Carbon (TOC) from Gamodubu landfill leachate.

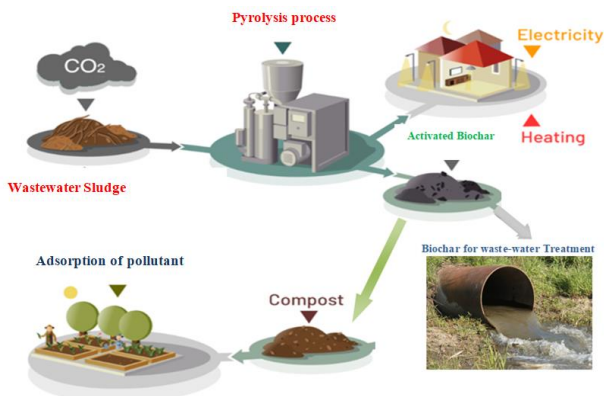


Figure 1. Conversion of Wastewater Sludge to Biochar for electricity, leachates' and soil treatment

According to Voivontas et al., (2001) metals present in industrial effluents pose risks to both human health and the environment. Biochar on the other hand which is, an economical alternative, shows promise in soil improvement such as metal adsorbent, agricultural soil improving by increasing organic content of the soil and improving water retention, thus enhancing plant resilience against harsh weather conditions. As industrial leachate treatment poses challenges, biochar can efficiently absorb hazardous elements like lead and cadmium, thus reducing their concentrations in leachate before discharge (Mladenov et al., 2005). Addition of biochar to soil amendments can also improve nutrients uptake in fields, leading to increased crop yields and promoting sustainable farming practices shown in Figure 1.

Liu et al. (2014) further highlight biochar's potential in remediating leachate and improving soil health, thereby reducing water shortage in agriculture. As the demand for sustainable farming methods rises, biochar emerges as a versatile and effective tool in addressing environmental concerns of point-source and nonpoint-source pollution. Its diverse applications, from soil enhancement to leachate treatment, contribute to building a more sustainable future for our planet.

The study examines the use of sludge-derived biochar as a sustainable solution for waste management and resource recovery in Gaborone. The study examined the effects of activated and regenerated biochar quality, and its suitability for removal of metals from leachate. By understanding how different pyrolyzed biochar affect adsorption of metals from leachate, this study will optimize the process to produce biochar with the desired properties for use in adsorption for in agricultural irrigation.

The primary goal of this study is to examine the viability of biochar as a sustainable method for long-term environmental remediation. The research objectives are to evaluate the effectiveness of biochar made from wastewater sludge in adsorbing organic carbon, to analyze the physiochemical properties and operational characteristics of the biochar, to assess the efficiency of biochar derived from wastewater sewage sludge in removing organic pollutants like Total Organic Carbon (TOC) from landfill leachate, and to determine the long-term adsorption capacity of biochar to confirm its suitability for sustainable leachate treatment and environmental remediation (Lehmann et al., 2011).

MATERIALS AND METHODS

Sampling and Sample Preparation

Sludge samples were collected from the primary settling tank and sludge drying beds at the Gaborone Wastewater Treatment Plant (GWTP) using plastic buckets with a capacity of five liters. These samples were representative of the sewage sludge generated at the plant. In the laboratory, the sludge samples underwent a series of preparation steps before analysis. This included drying, ash content analysis, and solid substance content assessment, following established standard methods such as those outlined in the Association of Official Agricultural Chemists (AOAC) 1995 procedure.

Drying of Wastewater Sludge Samples

Drying reduces the moisture content of wastewater sludge, before pyrolysis process. This minimizes energy requirement, making the process more efficient and cost-effective. Drying improved biochar quality and leads to higher yields and better properties while reducing greenhouse gas emissions and ash content. Drying experiments were conducted using a laboratory model oven dryer (Uniscope SM 9053 A laboratory oven, Surgifriend Medicals, England). Approximately 30 g to 70 g of sludge samples were loaded onto a metal tray and

dried at specified temperatures (60°C for initial experiments, and 80°C for subsequent trials). The drying process was monitored at regular intervals, with weights recorded until final moisture content of a dry weight basis (db) was achieved.

Moisture content was calculated using Equation 1, where MC represents the moisture content, W_0 is the initial sludge weight, and W_F is the final moisture content of the sludge. The moisture content (MC) was calculated from Equation 1 as shown:

$$MC = \frac{W_0 - W_F}{W_0} \quad (1)$$

The dimensionless moisture ratio (MR) during drying was calculated using Equation 2, where M represents the average moisture content at time t, M_0 is the initial moisture content, and M_E is the equilibrium moisture content on a dry basis.

$$MR = \frac{M - M_E}{M_0 - M_E} \quad (2)$$

where: MR is the dimensionless moisture ratio, M, the average moisture content at time t, M_0 the initial moisture content, and M_E , the equilibrium moisture content on dry basis.

During layer drying of wastewater sludge, the equilibrium moisture content was not determined and since this is usually not high in most of materials (Waewsak et al., 2006) the equilibrium moisture content was assumed to be zero. Thus, the moisture ratio (MR) was simplified according to Equation 3 (Kingsly et al., 2007) and Equation 2 becomes:

$$MR = \frac{M}{M_0} \quad (3)$$

The recorded moisture ratios for each sample were then used to plot the drying curves. The drying rates of the sample for each treatment were calculated based on the weight of water removed per unit time per kilogram of dry sludge, expressed in units of $\text{kg.kg}^{-1} \text{h}^{-1}$ (Sankat et al., 1996; Kingsly et al., 2007; Babalis et al., 2006).

Dry wastewater sludge optimal conditions for pyrolysis

Conducting of series of experiments varying the temperature, heating rate and feedstock ratios to determine the optimal conditions for pyrolysis was carried out using blast furnace to simulate and control the pyrolysis process. Biochar production occurred under oxygen-limited conditions, with approximately 50 g of dry sewage sludge

placed in porcelain crucibles and sealed to prevent air ingress. Heating at a rate of 10°C per minute to 400°C for four hours yielded biochar (WWSBC400), stored separately in plastic bags in a dry environment. The pyrolysis yield was calculated as the ratio of generated biochar weight to initial dry sewage sludge weight.

$$\text{Biochar yeild (\%)} = \frac{\text{char weight}}{\text{Dry waste water Sludges}} * 100 \quad (4)$$

Characterization of WWS Biochar by Physical and Chemical Properties

Laboratory tests were conducted to assess the chemical composition and physical properties of the produced biochar. The pH, porosity, and nutrient content of the biochar were measured to determine its suitability for leachate treatment applications. The Use of standard methods and equipment, such as pH meters, surface area analyzers, and nutrient analysis kits, to obtain accurate data.

Concentration and accessibility of nutrients

The biochar's total nutritional concentration is the sum of all of its nutrients. The portion of the total nutrients that plants can absorb is known as the bio-available nutrient concentration. Nutrient extraction studies using Diethylenetriamine-pentaacetic acid (DTPA) extraction were used to estimate the heavy metal in the samples.

Determination of Heavy Metals

Acid digestion was utilized to identify heavy metals. Each sample was soaked in 10 ml of 65% HNO_3 for 2 hours. About 0.3 g of each sample was used. Following filtration, the supernatant were collected for examination. The total heavy metal content in the pyrolyzed WWS biochar generated were assessed using inductively coupled plasma-mass spectrometry (7500 cx ICP-MS connected to an ASX-500 auto sampler, Agilent Kolosionis et al., (2021). Elemental analysis experiments were carried out with Thermo-Flash 2000 CHN-S elemental analyzer using the ASTM-D5373-16 method (ASTM-D5373 2018) (Kolosionis et al. 2021a) at the environmental science laboratory.

Adsorptive Properties of Activated, Regenerated WWS Biochar

According to Saadi and Fazaeli (2013), adsorption and removal of contaminants from leachate was conducted with the use of batch or continuous flow experiments using real leachate samples containing contaminants. Pyrolyzed biochar samples was monitored to remove of

heavy metals, organic pollutants, and nutrients over time. The concentration of contaminants before and after adsorption using appropriate analytical techniques, such as atomic absorption spectrophotometry was measured (Turro et al., 2011).

Adsorption Tests

The adsorption test used Botswana Gamodubu Landfill Leachate (GLL) as the initial solution. The color was measured in a continuous adsorption mode from the effluent collector. Activated WWS Biochar was added to the column, and a peristaltic pump was used to deliver concentrated solution through the column at specific flow rate as shown in Figure 2 (Kolosionis et al., 2021b).

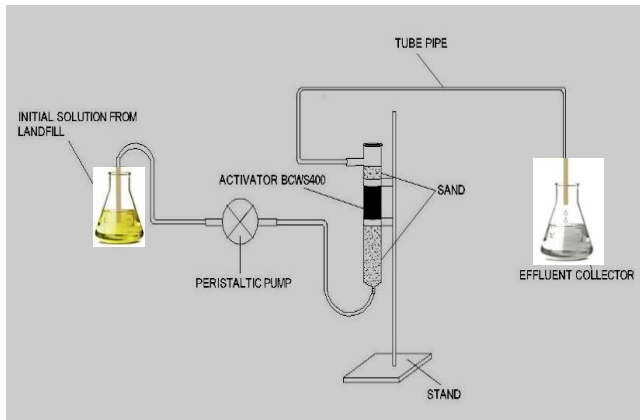


Figure 2. Column Adsorption experimental setup for adsorption of pollutants from leachate effluent

Fixed bed adsorption data analysis

To construct, optimize, and manage an adsorption column for water treatment, understanding the influence of operational parameters on breakthrough curves (BTC) and the maximum capacity of the fixed bed is essential. BTC modeling and simulation utilized linearized equations from models such as the Thomas, Yoon-Nelson, and Adams-Bohart, as adopted from Brion-Roby et al. (2018). These models are actively researched for large-scale removal of heavy metal effluents, with practical studies determining breakthrough curves and saturation points of the adsorption process.

$$\ln \left[\frac{C_t}{C_0 - C_t} \right] = (Kt) - KT \quad (5)$$

For Yoon Nelson Equation 5 where; C_0 is Influent concentration, C_t is Outlet Concentration at time t (mg/L), K is Rate constant and T is time required for 50% adsorbate breakthrough and

$$\ln \left[\frac{C_t}{C_0} \right] = (K_{AB} C_0 t) - K_{AB} N_0 \left(\frac{Z}{U_0} \right) \quad (6)$$

For Adams Bohart Equation 6 where C_0 is Influent concentration, C_t is Outlet Concentration at time t (mg/L), K_{AB} is Kinetic constant, Z is Bed depth of the fixed bed column, U_0 is Superficial velocity (cm/min and N_0 is Saturation Concentration.

$$\ln \left[\frac{C_t}{C_0} \right] - 1 = K_{th} \left(\frac{q_0 m - C_0 t}{Q} \right) \quad (7)$$

For Thomas model Equation 7 where: C_0 is Influent concentration, C_t is Outlet Concentration at time t (mg/L) K_{th} is Thomas rate constant, q_0 is equilibrium adsorption uptake (g), Q is The flow rate (ml/min, t is v/Q (v)ml (v) the effluent volume and , N_0 is Saturation Concentration. The Tomas model was used in this article.

Regeneration studies

Column adsorption was carried out using washed biochar, using the same flow rate of 1.12 m/s and the same adsorption test setup as in Figure 2, the results were compared in order to determine the efficacy of the column for repeated usage after adsorption (Patel, 2019). An evaluation of the reusability of the biochar by performing multiple adsorption-desorption cycles was made .This finding is important for practical applications where the biochar column may need to be regenerated and reused multiple times. This finding is promising for industries looking to implement sustainable and cost-effective treatment methods for leachate or wastewater purification. Further research is needed to optimize the regeneration process and maximize the longevity of the biochar column for continuous use in various applications (Chen et al., 2016). The following equations (Khadhri et al., 2019) were used to calculate the total mass of the TOC retained in the column q_{tot} (mg), the maximum column adsorption capacity q_c (mg/g); the total mass of TOC pumped into the column m_{tot} (mg) and the removal percentage R : The equations used to calculate these parameters are as follows:

$$q_{tot} = (C_0 - C_t) \times V \quad (8)$$

$$q_c = q_{tot}/m \quad (9)$$

$$m_{tot} = C_0 \times V \quad (10)$$

$$R = \frac{m_{tot} - q_{tot}}{m_{tot}} \times 100 \quad (11)$$

where C_0 is the initial concentration of the carbon adsorbate, C_t is the concentration at time t , V is the volume of the column, m is the mass of the adsorbent, and R is the removal percentage. These Equations 8-11 provide a quantitative analysis of the organic and inorganic carbon adsorption process in the column (Binti et al., 2007).

RESULTS AND DISCUSSION

Sludge drying results

The drying times for WWTP sewage sludge exhibit significant variation across different sample regions, particularly as the drying beds descend. This variation can result in drying periods of up to nine hours. The drying process is notably influenced by both the moisture content and the moisture ratio loss pivotal factors that impact the efficiency of the drying process as shown in Figure 3. Notably, sludge from Layer 1 of the drying bed demands additional energy for drying, making it the most energy-intensive layer, followed by layers two and three. In contrast, drying wastewater sludge (WWS) from the GWWTP primary settling tank proves to need highest energy and time-consuming.

The drying rate presented by Figure 4, observed at a constant temperature of 80°C, displays a linear trend, signifying consistent moisture loss over time. To visually represent this trend, a moisture ratio curve was constructed for each sample, offering a clear indication of the moisture loss progression.

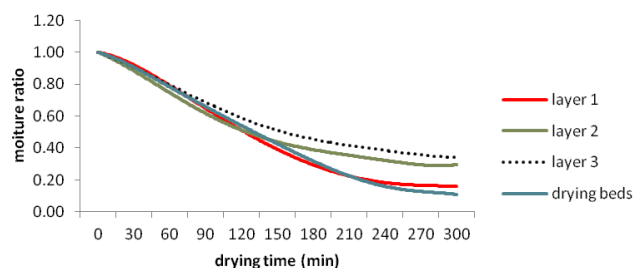


Figure 3. Comparison of sludge moisture ratios drying temperature of 80 °C

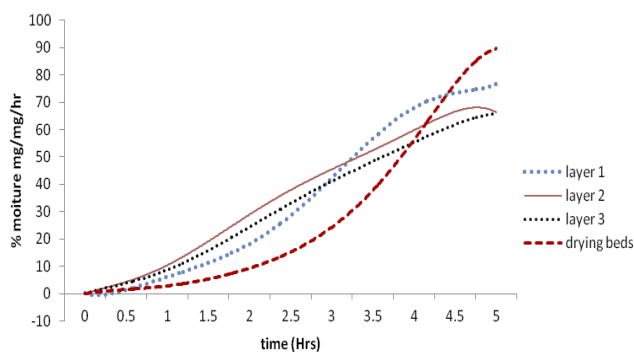


Figure 4. Comparison of Sewage Drying Rates at temperature of 80 °C

Layer 1, from Figure 3 is characterized by a higher initial moisture ratio, exhibits more pronounced variation between the start and end of the drying experiment, while

Layer 3, owing to its higher solid content, demonstrates comparatively less variation. An intriguing observation emerges when comparing the drying behavior of Layer 1 samples with that of sludge from the GWWTP primary settling tank, suggesting similarities in their drying characteristics. This is the fact that they both have highest initial moisture content. Drying WWS at elevated temperatures expedites the process, as evidenced by a corresponding increase in the moisture ratio versus time curve. Despite the higher energy requirement associated with higher temperatures, this method demonstrates the potential for rapid sludge drying.

The study further explores the impact of drying rate on temperature changes and the speed at which samples dry at different temperatures. While the majority of moisture is lost per hour in the drying beds as shown in Figure 4, layers two and three exhibit less comparable moisture loss rates. However, the overall drying process exhibits a gradual decrease in speed, with a notable shift observed from three and a half hours to five hours for achieving 90% moisture elimination.

Wastewater Sludge Pyrolysis under Optimal Conditions

The study utilized desiccators to preserve dried Wastewater Sludge (WWS) samples prior to pyrolysis experiments. WWS was finely crushed to 0.5 mm particle sizes, dried at 105°C for 24 hours, and stored in airtight plastic containers. Pyrolysis, following the method described by Yuan and Xu (2012) was employed to produce WWS Biochar. Approximately 50 g of dried wastewater sludge was placed in porcelain crucibles, sealed to exclude air, and subjected to heating in a furnace for four hours. Following cooling, the samples were crushed and weighed to determine the combined weight of ashes and biochar. The resultant chars were designated as Wastewater Sludge Biochar 400 (WWSBC400) and stored in individual plastic bags within a dry environment. Acid-washed biochars are recognized for their thermal stability, facilitating steady combustion.

Table 1. Mass Reduction and ash produced after pyrolysis

Measures of Central Tendency.	Sample Mass (g)	Mass reduction (%)	Mass of ash (g)	final mass (g)
Total	353.83	372.77	6.11	347.72
Average	27.22	28.67	0.47	49.67
Standard Deviation	5.23	0.91	0.09	85.93
Standard Error	2.27	2.39	0.04	4.14

Thirteen experiments on sludge pyrolysis revealed an average mass reduction of 28.67% as shown by Table 1. The consistency observed across data sets suggests a reliable and consistent reduction in mass, underscoring the viability of pyrolysis as an effective sludge treatment method. The substantial average reduction in final mass (71.33%) highlights the efficacy of pyrolysis in organic material elimination and sludge volume reduction. The low standard deviation and standard error values further affirm the precision and reliability of the results obtained, consolidating pyrolysis as a promising treatment avenue.

The char yield percentage was determined as per Equation 12. The high char yield percentage indicates that sewage sludge has the potential to yield a significant amount of biochar through pyrolysis. This elevated char output underscores the efficient adsorption capabilities of biochar derived from sewage sludge, encompassing both organic and inorganic carbon molecules.

$$\text{Char yeild (\%)} = \frac{\text{char weight}}{\text{Dry Micro Sieved Sludges}} * 100 \quad (12)$$

$$\text{Char yeild (\%)} = \frac{347.72}{353.83} * 100 = 98.27\%$$

WSBC400 Char Activation and Water Washing Techniques

The study involved washing samples by adding 40 g of BCWSS400 to a conical flask containing 100 ml of washing water solutions. The mixture was shaken at 200 rpm for 24 hours, separated by filtration, washed and dried at 105°C for 24 hours to remove moisture. The supernatants were then filtered with PTFE 0.45 µm syringe filters, acidified, and stored for column adsorption. Chars produced at moderate temperatures (400°C) were not resistant to these washing techniques, indicating unstable forms. The efficient decrease in yield after washing suggests that ash components in the char did not remain intact and could not compromise the fuel's heating value as mentioned by Kolosionis et al., (2021b).

Char Yield Percentage after Washing about 96.1%. The resulting WWSBC400 was then impregnated with a 2 grams per grams of (NaOH) sodium hydroxide solution, then put in porcelain crucibles and heated for two hours at 800 °C at a heating rate of 5 °C per minute in a furnace. The samples were then cooled then washed through distilled water and filtered with PTFE 0.45 µm syringe filters resulted in Activated Biochar (WWSABC400), which was rinsed in 0.1 moles per litre (mol/L) hydrochloric acid and then washed with water distilled in a Soxhlet extractor until neutralization to pH range between six and eight (6- 8). WWSABC400 was then dried for 24

hours at 105°C. Lastly the WWSABC400 was Crushed and sieved, and kept in desiccator ready for adsorption column test (Khadhri et al., 2019).

Characterization WWS Biochar by Physical and Chemical Properties

Proximate Analysis

Table 2 presents the findings of the proximate analysis for solid wastewater sludge, pyrolyzed wastewater sludge, and activated wastewater sludge. For WWSBC400, and WWSABC400, Table 2 solid sample had an ash content that was 56.80 weight percent greater than that of the activated wastewater sludge and 55.43 percentage weight higher than that of the pyrolyzed samples.

The pyrolyzed samples exhibited lower fixed carbon concentrations than activated sewage sludge, indicating improved biochar adsorption. The pyrolysis process eliminated volatile organic molecules, rendering biochar more stable and eco-friendly. The volatile content of sewage sludge significantly decreased during pyrolysis and activation, suggesting biochar may preserve both types of carbon. The higher fixed carbon content suggests better carbon adsorption capabilities compared to the original sewage sludge with very low fixed carbon.

Table 2. Proximate results for Solid, Pyrolysed and Activated Sludge

Proximate analysis parameter	Solid Sample	pyrolysed Sample WWSBC400	activated Sample WWSABC400
Volatile	75.09	15.07	12.65
Ashe	86.54	31.11	29.74
fixed Carbon	-61.63	53.82	57.61

Determination of Heavy Metals

To identify heavy metals, an acid digestion process was used. Approximately 0.5 grams of each sample were subjected to digestion in Aqua Regia, a mixture consisting of 2 ml of 65% hydrochloric acid (HCl) and 6 ml of nitric acid (HNO₃). The samples were processed in a microwave digester at 100°C for 120 minutes, as described by Kolosionis et al. (2021).

The extract was filtered and diluted with deionizer water before analyzing the heavy metal content of raw sludge SMMSS, WWSBC400, WWSABC400, and regenerated biochar. Inorganic elements were concentrated in MSBC400, which was produced during pyrolysis. The average adsorption capacities of various metals were

evaluated for SMSS, PS, AS, and RS. SMSS biochar exhibited high adsorption capacities for Fe, Cu, and Al, suggesting its potential for removing these metals from leachate as shown in Figure 5. However, further research is necessary to understand the adsorption mechanisms and optimize biochar utilization for carbon adsorption (Agrafioti et al., 2013; Zhou et al., 2017).

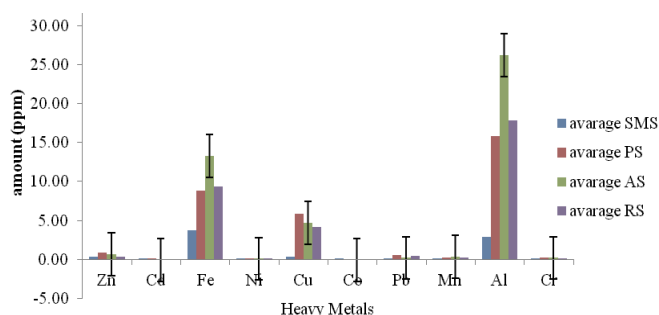


Figure 5. Elementary results of raw sludge SMSS, pyrolyzed sludge PS, activated sludge AS, and Regenerated Sludge RS.

The higher heating values (HHVs)

The results as presented in Figure 6 showed that biochar derived from sewage sludge had a high potential for both organic inorganic carbon adsorption and energy generation. The HHVs of the samples were found to be within the range of 20.834 magajoule per kilograms (MJ/kg) to 24.834 MJ/kg, indicating significant energy content. This suggests that biochar produced from micro sieved sewage sludge can be a valuable resource for carbon sequestration and energy production.

The study investigated the Heating Values (HHVs) of sewage sludge samples and found biochar to be a promising renewable energy source due to its substantial energy content. The combined average HHV was calculated to be 24.834 MJ/kg, with a standard deviation of 0.655.

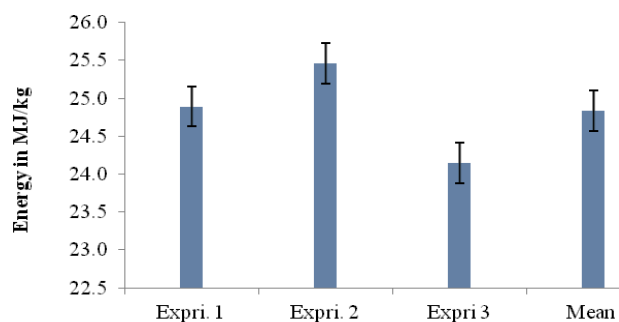


Figure 6. Experiment for Bob calorimeter WWS Biochar Calorific Value

Variations in HHV levels across different experiments may be attributed to differences in feedstock or manufacturing processes. However, despite these fluctuations, the average HHV remains within a useful range for carbon adsorption applications, highlighting the potential of biochar for carbon sequestration (Kolosionis et al., 2021b). For the calculation of the Fuel Ratio (FR), the following Equation 12 was utilized:

$$HHV_{af}(\%) = \frac{HHV}{(100 - ash\%)} \times 100 \tag{12}$$

$$HHV_{af}(\%) = \frac{24.834}{(100 - 6.11\%)} \times 100 = 26.45$$

For the calculation of the fuel ratio (FR), the following Equation 13 were used:

$$FR\ for = \frac{Fixed\ carbon}{Volatile\ matter} \tag{13}$$

$$FR\ for = \frac{57.61}{12.65} = 4.5541$$

Biochar derived from sludge, characterized by a higher proportion of fixed carbon compared to volatile matter, demonstrates potential for energy production. With a Fuel Ratio (FR) value of 4.55, indicating its high energy content, it qualifies as a suitable fuel source for energy production as supported by Voivontas et al. (2001).

Adsorptive Properties of Activated, Regenerated WWS Biochar

The study employed the linear Thomas adsorption model to simulate the adsorption process of Total Organic Carbon (TOC from landfill influent using Wastewater Sludge Biochar (WWSABC400) as the adsorbent medium. Results indicated a notably high adsorption capacity, underscoring the effectiveness of WWSABC400 in contaminant removal. This robust adsorption capacity, coupled with its potential for energy generation, positions biochar sludge as a promising contender for sustainable solutions across various environmental remediation endeavours (Graves et al., 2022). Figures 7 and 8 depict the adsorption of TOC from Gamodubu landfill leachate experiment data after multiple rounds of biochar regeneration.

The application of the Thomas kinetic model to the activated wastewater sludge biochar resulted in a linear plot of $\ln(C_0/(C_t - 1))$ versus time for TOC as presented in Figure 7. The slope of -0.9089 for TOC corresponds to the multiplied influent concentration $(-K \cdot C_0)$ of the Thomas model constant, with an intercept of 6.5107 corresponding to Equation 7 ($Kq_0 \cdot m/Q$). The linear Tomas model exhibited a high degree of conformity with the experimental data, achieving an R^2 value of 0.9114 for the first round of activated biochar removal.

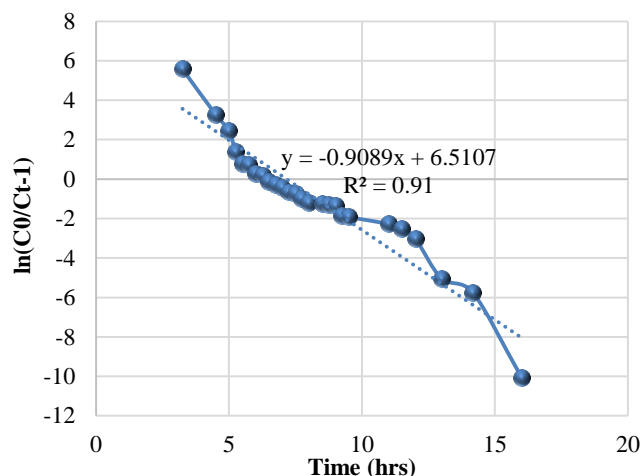


Figure 7. First round Activated biochar Adsorption (WWSABC400) of TOC for Gamodubu landfill leachate experiment data fitted to Tomas linear model

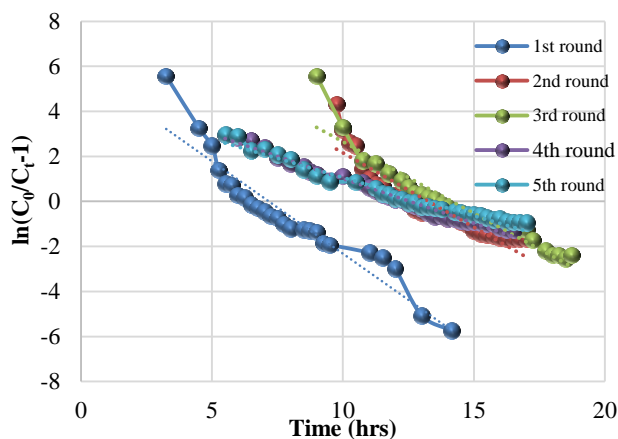


Figure 8. Comparison between Regenerated biochar (2nd round to 5th round) and Activated biochar for Adsorption of TOC for Gamodubu landfill leachate experiments all fitted to Tomas linear model.

The study utilized the linear Thomas adsorption model to assess the adsorption of Total Organic Carbon (TOC) from Gamodubu landfill leachate using activated WWS biochar WWSABC400. The biochar exhibited an adsorption capacity of 389.265 mg/g after 14.5 hours of column adsorption for the first round. Successive rounds of regeneration yielded varying adsorption capacities, with values of 742.82 mg/g, 875.47 mg/g, 682.13 mg/g, and 735.21 mg/g observed after the first, second, third, and fourth regenerations, respectively. The results depicted in Figures 7 and 8 suggest that, activated and regenerated WWS biochar exhibits substantial adsorption capacity for TOC, with promising potential for sustainable environmental remediation applications.

CONCLUSION

In conclusion, this study demonstrated the potential of biochar derived from sewage sludge at the Gaborone Wastewater Treatment Plant (GWTP) for the adsorption of Total Organic Carbon (TOC) from Gamodubu landfill leachate. The research found that biochar produced under controlled pyrolysis conditions (WWSBC400) exhibited significant adsorption capacities, making it a viable option for environmental remediation. The biochar showed a remarkable TOC removal rate of 94.89% after 17 hours of column adsorption, highlighting its effectiveness in contaminant removal. The use of sewage sludge biochar offers an innovative approach to recycling waste materials, contributing to a circular economy and reducing waste disposal costs. Beyond leachate treatment, biochar improves soil fertility and water quality, promoting sustainable agricultural practices. The high energy content of biochar (24.834 MJ/kg) suggests its potential as a renewable energy source, further enhancing its utility in sustainable development.

DECLARATIONS

Corresponding Author

Correspondence and requests for materials should be addressed to Lamong Duke Tshenyego; E-mail: Tshenyegol@ub.ac.bw; ORCID: 0000-0002-6545-0980.

Data availability

The datasets used and/or analysed during the current study available from the corresponding author on reasonable request.

Acknowledgements

The authors would like to thank and acknowledge the Office of Research and Development (ORD) at University of Botswana for the graduate and ethical consideration to provideresearch funding opportunity.. Department of Civil Engineering for creating a conducive environment to conduct this research.

Authors' contribution

First Author performed the experiments, analysed the data obtained and wrote the manuscript. Second Author designed the experimental process and revised the manuscript. Both authors read and approved the final manuscript.

Competing interests

The authors declare no competing interests in this research and publication.

REFERENCES

- Agrafioti, E., Bouras, G., Kalderis, D., & Diamadopoulos, E. (2013). Biochar production by sewage sludge pyrolysis. *Journal of Analytical and Applied Pyrolysis*, 101(iii), 72–78. <https://doi.org/10.1016/j.jaap.2013.02.010>
- Babalís, S. J., Papanicolaou, E., Kyriakis, N., & Belessiotis, V. G. (2006). Evaluation of thin-layer drying models for describing drying kinetics of figs (*Ficus carica*). *Journal of Food Engineering*, 75(2), 205–214. <https://doi.org/10.1016/j.jfoodeng.2005.04.008>
- Binti, A. I. N., Thesis, J., & June, S. (2007). *THE PRODUCTION AND CHARACTERIZATION OF ACTIVATED CARBON USING LOCAL AGRICULTURAL. Jun* <https://core.ac.uk/download/pdf/11933114.pdf>.
- Brion-Roby, R., Gagnon, J., Deschênes, J. S., & Chabot, B. (2018). Investigation of fixed bed adsorption column operation parameters using a chitosan material for treatment of arsenate contaminated water. *Journal of Environmental Chemical Engineering*, 6(1), 505–511. <https://doi.org/10.1016/j.jece.2017.12.032>
- Chen, D., Guo, H., Li, R., Li, L., Pan, G., Chang, A., & Joseph, S. (2016). Low uptake affinity cultivars with biochar to tackle Cd-tainted rice — A field study over four rice seasons in Hunan, China. *Science of the Total Environment*, 541(October), 1489–1498. <https://doi.org/10.1016/j.scitotenv.2015.10.052>
- Graves, C., Kolar, P., Shah, S., Grimes, J., & Sharara, M. (2022). Can Biochar Improve the Sustainability of Animal Production? *Applied Sciences (Switzerland)*, 12(10), 1–23. <https://doi.org/10.3390/app12105042>
- Khadhri, N., El Khames Saad, M., Ben Mosbah, M., & Moussaoui, Y. (2019). Batch and continuous column adsorption of indigo carmine onto activated carbon derived from date palm petiole. *Journal of Environmental Chemical Engineering*, 7(1). <https://doi.org/10.1016/j.jece.2018.11.020>
- Kingsly, R. P., Goyal, R. K., Manikantan, M. R., & Ilyas, S. M. (2007). Effects of pretreatments and drying air temperature on drying behaviour of peach slice. *International Journal of Food Science and Technology*, 42(1), 65–69. <https://doi.org/10.1111/j.1365-2621.2006.01210.x>
- Kolosionis, A., Kastanaki, E., Veksha, A., Wang, H., He, C., Lisak, G., & Giannis, A. (2021a). The Effects of Washing Techniques on Thermal Combustion Properties of Sewage Sludge Chars. *International Journal of Environmental Research*, 15(2), 285–297. <https://doi.org/10.1007/s41742-021-00312-6>
- Kolosionis, A., Kastanaki, E., Veksha, A., Wang, H., He, C., Lisak, G., & Giannis, A. (2021b). The Effects of Washing Techniques on Thermal Combustion Properties of Sewage Sludge Chars. *International Journal of Environmental Research*, 15(2), 285–297. <https://doi.org/10.1007/s41742-021-00312-6>
- Liu, T., Liu, B., & Zhang, W. (2014). Nutrients and heavy metals in biochar produced by sewage sludge pyrolysis: Its application in soil amendment. *Polish Journal of Environmental Studies*, 23(1), 271–275. <https://www.researchgate.net/profile/Arvind-Singh->
- Mladenov, N., Strzepek, K., & Serumola, O. M. (2005). Water quality assessment and modeling of an effluent-dominated stream, the Notwane River, Botswana. *Environmental Monitoring and Assessment*, 109(1–3), 97–121. <https://doi.org/10.1007/s10661-005-5842-8>
- Patel, H. (2019). Fixed-bed column adsorption study: a comprehensive review. *Applied Water Science*, 9(3), 1–17. <https://doi.org/10.1007/s13201-019-0927-7>
- Saadi, Z., Saadi, R., & Fazaali, R. (2013). Fixed-bed adsorption dynamics of Pb (II) adsorption from aqueous solution using nanostructured γ -alumina. *Journal of Nanostructure in Chemistry*, 3(1), 2–9. <https://doi.org/10.1186/2193-8865-3-48>
- Sankat, C. K., Castaigne, F., & Maharaj, R. (1996). The air drying behaviour of fresh and osmotically dehydrated banana slices. *International Journal of Food Science and Technology*, 31(2), 123–135. <https://doi.org/10.1111/j.1365-2621.1996.332-35.x>
- Turro, E., Giannis, A., Cossu, R., Gidararakos, E., Mantzavinos, D., & Katsaounis, A. (2011). Electrochemical oxidation of stabilized landfill leachate on DSA electrodes. *Journal of Hazardous Materials*, 190(1–3), 460–465. <https://doi.org/10.1016/j.jhazmat.2011.03.085>
- Voivontas, D., Assimacopoulos, D., & Koukios, E. G. (2001). *Assessment of biomass potential for power production : a GIS based method*. 20, 101–112. <https://environ.chemeng.ntua.gr/gr/uploads/doc/Papers/Rene wable%20Energy/2001>.
- Waewsak, J., Chindaruksa, S., & Punlek, C. (2006). A mathematical modeling study of hot air drying for some agricultural products. *Thammasat International Journal of Science and Technology*, 11(1), 14–20.
- Yuan, J. H., & Xu, R. K. (2012). Effects of biochars generated from crop residues on chemical properties of acid soils from tropical and subtropical China. *Soil Research*, 50(7), 570–578. <https://doi.org/10.1071/SR12118>
- Zhou, D., Liu, D., Gao, F., Li, M., & Luo, X. (2017). Effects of biochar-derived sewage sludge on heavy metal adsorption and immobilization in soils. *International Journal of Environmental Research and Public Health*, 14(7). <https://doi.org/10.3390/ijerph14070681>

Publisher's note: [Scienceline Publication](#) Ltd. remains neutral with regard to jurisdictional claims in published maps and institutional affiliations.



Open Access: This article is licensed under a Creative Commons Attribution 4.0 International License, which permits use, sharing, adaptation, distribution and reproduction in any medium or format, as long as you give appropriate credit to the original author(s) and the source, provide a link to the Creative Commons licence, and indicate if changes were made. The images or other third party material in this article are included in the article's Creative Commons licence, unless indicated otherwise in a credit line to the material. If material is not included in the article's Creative Commons licence and your intended use is not permitted by statutory regulation or exceeds the permitted use, you will need to obtain permission directly from the copyright holder. To view a copy of this licence, visit <https://creativecommons.org/licenses/by/4.0/>.

© The Author(s) 2024

Designing Ergonomic Safety Boots for Sustainable Construction in Botswana: A Case Study of Worker Foot Health

Kebonyetsala Botshabelo¹ , Oanthata Jester Sealetsa¹ ✉, Keiphe Setlhatlhanyo¹ , Richie Moalosi¹ ,
Yaone Rapitsenyane¹ , and Patrick Dichabeng¹ 

Department of Industrial Design and Technology, Faculty of Engineering and Technology, University of Botswana, Office 128, Block 248, Corner of Notwane and Mobuto Road, Gaborone, Botswana

✉ Corresponding author's Email: sealetsa@ub.ac.bw

ABSTRACT

The most essential asset in every construction work is the workers. In this regard, sustainability in construction must include and be centred on this vital resource. However, research indicates that civil engineers and construction workers often advocate for sustainability in infrastructural developments. This critical asset in construction often needs more consideration when people are engaged in construction work despite the many ergonomics challenges widely reported in the industry. This leads to workers in this industry being grossly afflicted by injuries such as musculoskeletal disorders, particularly of the foot. In addition, changes in global temperatures, attributed to global warming, situate civil engineers and construction workers, as they often work in open and challenging terrains, at risk of heat-related illnesses such as heat hyperpyrexia and heat exhaustion, which may also aggravate these musculoskeletal disorders conditions. However, it is pretty disturbing to notice that such illnesses are less investigated, particularly musculoskeletal disorders of the feet, which may be exasperated by the dire heat conditions noticeable in Botswana. This is because there is often a need for more knowledge and understanding of the risks associated with musculoskeletal disorders (MSDs). Furthermore, expertise in ergonomics is limited to assisting in the design of work as well as its conditions. This bequeaths both civil engineers and construction workers to operate under very challenging conditions despite pursuance of sustainability. Therefore, this case study investigated the prevalence of musculoskeletal disorders of the feet in the construction industry in Botswana with the purpose of designing a safety boot that matches the anthropometric measurements of the construction workers' feet. The research culminates in the design of a safety boot that is based on the workers' anthropometric measurements to prevent the occurrence of MSDs. The results of the study indicate that workers in this industry suffer from toe bunions, cons, toe deformities, smelly feet, etc. The study additionally indicates foot size differences across Botswana's tribes. These differences may have severe implications for the use of safety boots and the development of ergonomics illnesses, mainly since the current safety boots used are imported from elsewhere with no modification to address the anthropometric foot measurements of Botswana. It is anticipated that the research will provide the necessary awareness that can help civil engineers explore sustainability not only from the context of infrastructural development (objects) but also from the perspective of workers (humans). This underscores the need for further research and action in this critical area.

Keywords: Construction Worker Ergonomics, Musculoskeletal Disorders, Safety Boot Design, Anthropometric Measurements, Heat-related Illnesses, Sustainable Construction Practices

INTRODUCTION

Ergonomics, the science of designing and arranging workplaces, products, and systems to fit the people who use them, plays a crucial role in enhancing productivity, safety, and comfort. In the context of the construction industry, ergonomics is particularly significant due to the physically demanding nature of the work, which often involves manual labour, heavy lifting, and prolonged periods of standing or walking. In Botswana, the construction industry is a crucial driver of economic growth, contributing significantly to infrastructure

development. However, the sector faces challenges related to worker safety and health, particularly concerning the use of safety boots that may need to meet ergonomic standards. This study focuses on the ergonomic challenges associated with safety boots and their impact on construction workers in Botswana. The motivation for this study arises from the increasing recognition of the importance of worker safety and well-being in achieving sustainable infrastructural development. Despite advancements in construction technologies and practices, the industry continues to grapple with high rates of work-related injuries and musculoskeletal disorders. In

RESEARCH ARTICLE
 PII: S225204302400019-14
 Received: June 25, 2024
 Revised: September 02, 2024
 Accepted: September 05, 2024

Botswana, construction workers often need help with safety boots that are uncomfortable, poorly fitting, and inadequate in protecting against hazards. Addressing these ergonomic issues is crucial not only for improving worker health and safety but also for enhancing productivity and job satisfaction. By examining the specific challenges related to safety boots, this study aims to contribute to the broader goal of sustainable infrastructural development in Botswana. The primary objectives of this study were to:

- Investigate the ergonomic challenges faced by construction industry workers in Botswana, with a specific focus on safety boots.
- Assess the impact of these challenges on worker health, safety, and productivity.
- Identify the factors contributing to ergonomic issues in the design and provision of safety boots.
- Provide recommendations for improving the ergonomic design and availability of safety boots to enhance worker safety and well-being.

The paper is structured as follows: (i) a literature review of existing research on ergonomics in construction, focusing on the role of safety footwear, common ergonomic issues, and their impacts on worker health and safety; (ii) a description of the research methods used to gather data on the ergonomic challenges faced by construction workers in Botswana, including surveys, interviews, and observational studies; (iii) presentation the results of the study, discussing the specific ergonomic challenges related to safety boots, their causes, and their effects on worker safety and productivity; and (iv) summarises the key findings of the study, emphasising the importance of ergonomic safety boots for sustainable infrastructural development and the steps needed to improve worker safety and well-being in Botswana.

Literature review

According to the US Bureau of Labour Statistics (2018), the Construction Industry ranks fourth among the most dangerous industries in the United States of America after Transport, Installation Maintenance and Repair and Agriculture. The industry is reported to have an incident rate of 127.3 per 10,000 full-time employees. This is based on a variety of roles associated with construction work, which ranges, for example, from building to heavy and civil engineer constructors. It is reported further that workers in this industry use dangerous equipment and tools, are exposed to hazardous material and are sometimes required to work on elevated vicinities in confined spaces. However, in the midst of all this

seemingly dangerous landscape is the use of the safety boots. The use of safety boots is intended to keep construction workers safe from potential foot injuries.

Despite the critical role safety boots play in the construction industry, research on the effects of safety boots on users appears to be scanty, particularly in countries such as Botswana, which are still struggling to establish their position on the issue of sustainability for both workers and infrastructural developments. Nevertheless, where there has been evidence of research, such work dwells on the protection offered by the safety boots from interferences or hazards from the external environment. Minimal regard is given to what goes on within the safety boot itself when worn. [Oschsmann et al. \(2016\)](#) concur with this view. For example, in their study to look at the influence of different safety boots on gait and plantar pressure in the automotive industry, [Oschmann et al. \(2016\)](#) opined that the overall function of safety boots is chiefly based on the avoidance of injury in case of an industrial accident. The authors proceed further to assert that safety boots must also be seen as a long-term preventative instrument for maintaining the health of employees, particularly in preventing Musculoskeletal Disorders, as they can affect users' gait parameters.

Additionally, research shows a variety of injuries that may be caused by Occupational footwear. For example, [Barigga et al. \(2024\)](#), [Dobson et al. \(2017\)](#), [Orr et al. \(2022\)](#), and [Dumbhare et al. \(2022\)](#) reviewed the literature on the injuries caused by occupational footwear. They found that inappropriate footwear can cause injuries to the foot and other related bone structures with calluses, nail injuries (ingrown) and plantar fasciitis or bursitis. On the other hand, [Dobson et al. \(2017\)](#) conducted a systematic review of the literature on occupational footwear. They concluded that work safety boots design affects the way the worker walks (gait), observing that safety boots are often designed for occupational safety at the expense of comfort. The issue of gait as a problem is also captured by [Orr et al. \(2022\)](#). In their study, they also found occupational footwear to impact gait, angular velocity, joint ranges of motion, posture and balance, heart rate, temperature, muscle activity and selected occupational tasks. Furthermore, [Dumbhare et al. \(2022\)](#) conducted a study to determine the prevalence of foot problems associated with wearing safety footwear in factory employees wearing footwear for prolonged periods. In this study, the researchers found that 62.5% of workers suffered from plantar fasciitis while 30% had dead skin (corns), 12.5% reported having blisters/swelling on the foot and bunion (bulge) on the joint at the base of the big

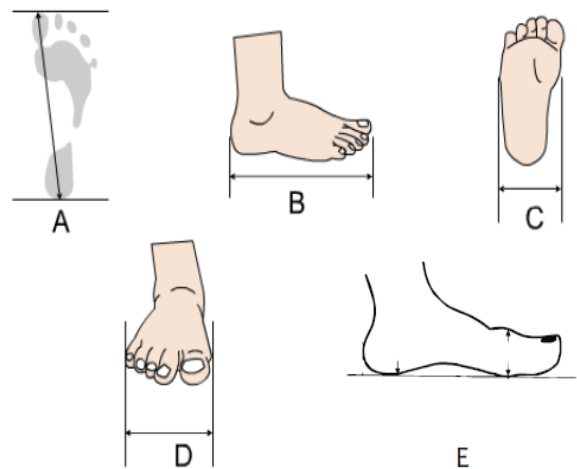
toe. The study showed a significant prevalence of foot problems caused by wearing safety footwear.

Of relevance to this study is the sustainability goal of incorporating ethical human considerations in construction, the achievement of which is notably dependent on the application of ergonomics. According to the joint document by International Ergonomics Association (IEA) and the International Labour Organisation (2019), Ergonomics is the branch of science dedicated to studying how people interact with other components of a system. In order to maximise both total system performance and human well-being, this profession also applies theory, principles, data, and methodologies to design. The understanding of ergonomics is expected to facilitate the design of products, tasks and environments that fulfil the user’s physical and cognitive requirements (Nadadur et al., 2012). Furthermore, ergonomics advances the goal of and recognition of human variability and, as such, could play a significant role in helping construction and civil engineers design products, tasks and environments that cater for this human variability, thus promoting sustainability in the industry. It is crucial to understand that the field of ergonomics is replete with techniques that can be used to address this sustainability goal. One such technique is to apply anthropometric (human body measurements) data of the local users in the design of safety boots for the construction industry in Botswana.

The authors argue that the construction industry in Botswana promotes the use of ill-designed safety boots that do not conform to the anthropometric measurements of local workers. This is premised on the fact that there is no local anthropometrics data bank to tap from, which can be used to influence the design of ergonomic safety boots for construction men and women workers in Botswana. Most of the available safety boots originate from outside Botswana (China, Australia, South Africa and the USA). In minimal situations where manufacturing is done locally, foot measurements and standards used to create safety boots are based on something other than the anthropometric data of locals but on users from safety boot’s point of origin. Safety footwear is mandatory in the construction industry, and workers are usually engaged in an eight-hour day shift (Barriga et al., 2024). That means, as long as such vital data is not available, workers in the industry will continue to suffer from musculoskeletal disorders of the feet, making it difficult for the local construction industry to achieve sustainability when the very asset central to infrastructural development is not healthy.

MATERIALS AND METHODS

One way of achieving sustainability in this regard is to design safety boots based on the anthropometric measurements of construction workers in Botswana. When designing a product to interact with the human body, designers consider the size and shape of people. However, human sizes and shapes differ considerably across nations. Such variance is also evident in Botswana. In a demonstration of this variance, a pilot study was conducted that involved collecting anthropometric data from workers in construction companies in the main villages in Botswana. About 100 construction workers, comprising 82 males and 18 females aged 33-54, were randomly sampled and recruited from different districts of the country for involvement in the study. In addition, observations and interviews were also held, and relevant data was collected. Anthropometric data from five different dimensions of areas of the foot were obtained. The dimensions covered the foot length, ball of foot length, outside ball of foot length, foot breadth diagonal, heel breadth, navicular height, instep height and heel to malleolus. These dimensions are represented as A, B, C, D, and E in Figure 1.



POINT	MEASUREMENT
A	Long cross foot length
B	Foot length
C	MTP Width
D	Toes Width
E	MTPJ Height

Figure 1. Foot areas measured

After that, the data was processed with statistical software (SPSS) to determine the means, standard deviation,

minimum and maximum values, as well as the 5th, 50th and 95th percentiles for each foot segment. The Pheasant & Haslegrave (2018) Protocols were used to collect data. In this regard, three measurements for each foot area measured were obtained, and later, an average was calculated to represent a specific foot area measurement. This was purely done to reduce the margin of error in data recording. From the data collected, about eight communities emerged in the study. These communities are captured in the research as TA, TB, TC, TD, TE, TF, TG, TH, TI and TJ. They are shown in Tables 1, 2, 3 and 4.

The data was later analysed to determine the 95thile, and 5% being the two extremes (largest and smallest) of the user population relevant to the design of the safety boots for each of the foot areas measured. It was here necessary to use percentiles rather than averages as using averages may have severely disadvantaged users with more than average dimensions (i.e. half the users). These percentiles were then used to calculate the correct dimensions of the boot. For purposes of Intellectual Property (IP) the dimensions are not included in the paper. Furthermore, for ethical considerations, the authors used letters as references to tribes that emerged from the study. These are TA, TB, TC, TD, TE, TF, TG, TH, TI, and TJ. Table 1 shows differences in foot size for males, while Table 2 shows differences in female foot size.

Table 1. Largest male foot anthropometrics among community

Tribe	Measurement in (cm)				
	A	B	C	D	E
1 TA	31.0	11.3	6.9	6.1	9.1
2 TB	28.6	11.0	7.2	6.6	9.2
3 TC	26.8	10.9	7.4	6.3	8.4
4 TD	31.4	10.8	7.1	6.4	8.5
5 TE	31.0	11.3	6.9	6.1	9.1
6 TF	30.9	10.8	7.0	6.4	8.6
7 TG	30.1	10.5	6.9	6.3	8.0
8 TH	30.8	11.2	7.0	6.7	8.8
9 TI	30.2	10.9	6.9	6.4	7.9
10 TJ	29.6	11.1	6.5	6.2	8.8
Average	30.0	11.0	7.0	6.4	8.6
SD	1.41	0.25	0.23	0.20	0.45

Table 2. Smallest male foot anthropometrics among community

Tribe	Measurement in (cm)				
	A	B	C	D	E
1 TA	25.8	9.6	6.4	6.1	7.5
2 TB	27.0	9.9	6.7	6.2	8.1
3 TC	25.9	9.8	6.5	6.3	7.9
4 TD	29.5	10.0	6.9	6.5	7.4
5 TE	28.2	10.9	7.0	6.2	8.8
6 TF	24.8	9.3	6.0	5.6	7.4
7 TG	27.4	10.1	6.9	6.5	8.1
8 TH	30.2	10.4	7.2	6.7	8.8
9 TI	26.9	9.8	6.6	6.3	7.8
10 TJ	28.8	10.4	6.9	6.2	8.5
Average	27.5	10.0	6.7	6.3	8.0
SD	1.73	0.46	0.35	0.3	0.53

Table 3. Largest female foot anthropometrics among community

Tribe	Measurement in (cm)				
	A	B	C	D	E
1 TF	23.7	8.4	5.8	4.7	5.7
2 TG	24.1	8.7	6.4	5.3	6.1
3 TD	21.6	9.3	6.1	4.8	6.5
4 TB	21.4	9.0	6.0	5.2	6.1
5 TA	20.5	8.4	5.9	5.0	5.8
Average	22.3	8.8	6.0	5.0	6.0
SD	1.56	0.39	0.23	0.25	0.31

Table 4. Smallest female foot anthropometrics among community

Tribe	Measurement in (cm)				
	A	B	C	D	E
1 TF	17.9	9.2	6.2	5.2	6.7
2 TG	20.8	7.9	5.9	4.7	5.9
3 TD	20.4	8.0	5.8	5.0	5.7
4 TB	21.4	9.0	6.0	5.2	6.1
5 TA	19.6	8.7	6.4	5.4	6.6
Average	20.0	8.6	6.1	5.1	6.2
SD	1.35	0.59	0.24	0.26	0.44

RESULTS AND DISCUSSION

Foot-related injuries

Construction workers in Botswana often suffer from various foot-related injuries and illnesses. One common issue observed is the development of corns or calluses, which may develop from repeated friction and pressure on the skin, often caused by ill-fitting boots. There was evidence of workers wearing boots with loose soles and torn or softened heels (Figure 2). These compromised safety boots may not protect workers from dangerous materials on the ground, such as sharp objects and nails. The deterioration of these boots also increases the risk of slips, trips, and falls, further compromising workplace safety.

Symptoms of calluses were found on the underside of workers' feet, along with skin discoloration and damage. These symptoms not only cause discomfort but can also alter a worker's gait, potentially leading to musculoskeletal issues if left unaddressed.

Figure 3 illustrates damaged boot soles. In some instances, the soles seemed to peel off from the safety shoes. Such boots no longer offer adequate protection from injuries that can be caused by nails or other sharp objects on the ground. This level of damage also compromises the boot's ability to provide proper support and cushioning, which could contribute to fatigue and long-term foot health issues.



Figure 2. Worn-out boot in use.



Figure 3. Worn-out safety boot sole.

Feet dimension and design

The results of the study revealed differences in feet anthropometrics measurements across male workers and female workers. For example, the average cross-foot length for males is 30 cm (Table 1), while the average cross-foot length for females is 22 cm (Table 3). This accounts for a difference of 8 cm between males' and females' feet. The longest male cross-foot length measured a whopping 31.4 cm, while the longest female cross-foot length measured 24.1 cm. These differences were also apparent across the different communities in Botswana. For example, Community D (TD) accounted for the largest male cross-foot length, while Community G (TG) accounted for the longest female cross-foot length, and Community B (TB) accounted for the smallest cross-foot length (Tables 1, 2 and 3). As can be observed, one's foot could be shorter in one dimension, while its other areas could be larger. For example, while Community D (TD) have the largest cross-foot length of 31.4 cm, they have a 10.8-foot length and 8.6 MTPJ less than TA and TB,

respectively, as shown in Table 1. These differences can create severe challenges for designers, hence the use of percentile values and not average dimensions for the design. Furthermore, it was clear from the study that in this company, construction workers had foot-related injuries such as cons/calluses and bunions. Notably, 80% of the boots were worn out and had only been used for a period of three months. Some of the safety boots had their steel-caps exposed and their soles torn out. The same safety boots allowed water to penetrate the feet when worn and in contact with water. Furthermore, soil and mud accessed the inside of the safety boots, and the safety boots were found to be extremely heavy. In addition, workers generally wore worn-out safety boots, as shown in Figures 2 and 3. This is not surprising as some of the safety boots are used as regular shoes even beyond the legal eight-hour per day period of work. Equipped with this data, the researchers applied the University of Botswana New Product Development (UBNPD) process to design the safety boot (Figure 4). Inspired by the work of (Kotler and Keller, 2006), this approach also considers the socio-cultural context, sustainability considerations throughout the development process of a product and competencies needed in the model. It reflects on the design landscape to enhance sustainability (Rapitsenyane and Sserunjogi, 2023). The process in Figure 4 offers a structured approach through a five-phased design process (inquire, define, design, validate and deliver) in which sustainability is taken up at each phase (Moalosi and Rapitsenyane, 2023).

In this regard, sustainability is attained by applying anthropometric data to innovate an ergonomic safety boot, as depicted in Figures 4 and 5. The prototype has a pending design utility model to be granted by the Companies Intellectual Property Authority. Figure 6 depicts the prototype of an ergonomic safety boot designed using anthropometric data obtained from local construction workers.

Limitations of the study

The first limitation encountered centred on culture. Traditionally, in Botswana, it is taboo to require people to provide their foot measurements. This practice is associated with witchcraft referred to in the local language as ‘go tsa lonao’ and interpreted to mean having information about one foot for witchcraft purposes. The researchers came across a lot of resistance as construction workers were initially reluctant to provide relevant data. The presence of foot injuries and disease symptoms did not help the situation either, as more workers had such health problems. For them to provide data, construction workers were required to reveal their injuries and wounds by removing their safety boots for data collection. Finally, as this was a design exercise meant to come up with an innovation, intellectual property issues were also a limitation, as some information and data would have to be held back before proper protection documents could be finalised.

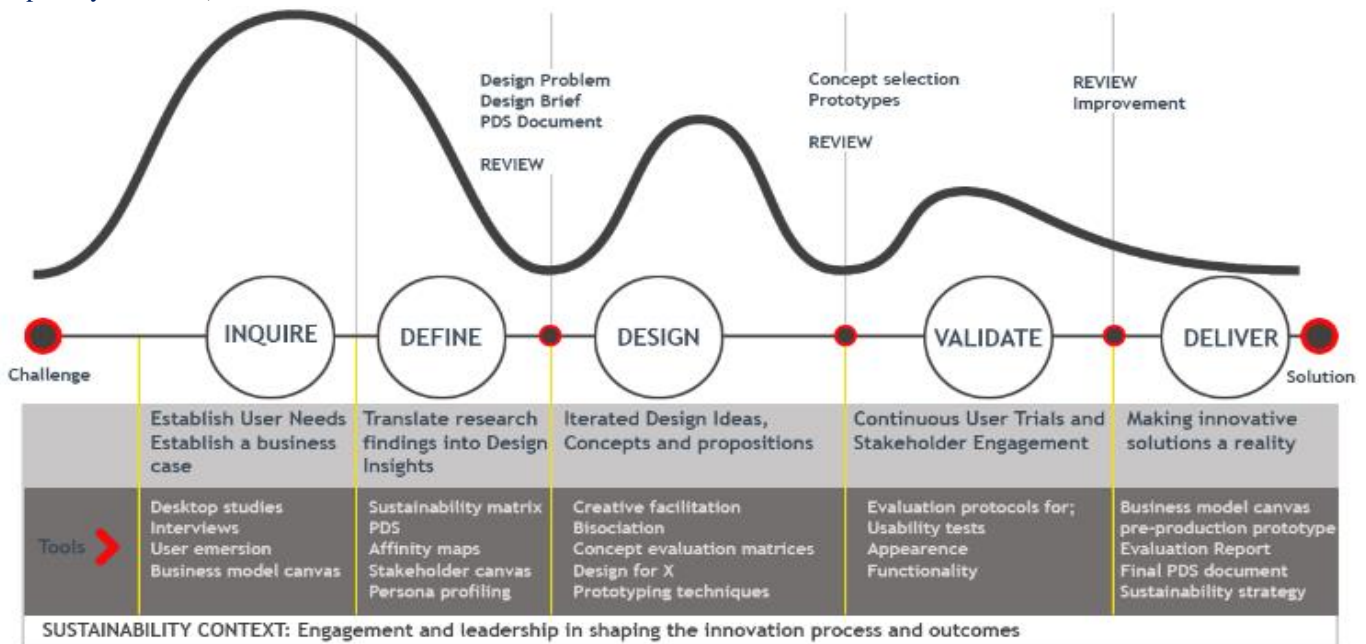


Figure 4. The University of Botswana New Product Development process (Moalosi and Rapitsenyane, 2023).



Figure 5. The designed safety boot



Figure 6. Ergonomic Safety Boot prototype for construction workers in Botswana.

CONCLUSION AND RECOMMENDATION

This study has highlighted the critical role of ergonomics in promoting sustainable infrastructural developments in Botswana, with a specific focus on the ergonomic challenges faced by construction industry workers due to safety boots. By investigating the ergonomic issues related to safety boots, we have underscored the significant impact these challenges have on worker health, safety, and productivity. The findings reveal that poorly designed safety boots contribute to discomfort, injuries, and reduced efficiency among construction workers, which, in turn, affects overall project outcomes and sustainability goals.

The objectives of this study were to explore the specific ergonomic challenges associated with safety boots, assess their impact on workers, identify contributing factors, and provide recommendations for improvement. Through detailed analysis of the data obtained from construction workers, the objectives were to provide valuable insights into the ergonomic shortcomings of current safety footwear and offer practical solutions for enhancing their design and availability. Ergonomics supports sustainability in many ways, as it can enhance health by reducing the risks of injuries and illness in the workplace. When designing a product to interact with the human body, designers consider the size and shape of people. However, human sizes and shapes differ considerably across nations. Such variance is also evident in Botswana. The safety boot designed based on anthropometric data demonstrates how such data can be used to protect people in the construction industry, and this is how sustainability in this context can be achieved.

Addressing the ergonomic needs of construction workers, particularly in the context of safety boots, will significantly improve worker well-being, reduce injury rates, and boost productivity. This, in turn, supports the broader goal of sustainable infrastructural development in Botswana, ensuring that construction projects are not only economically viable but also socially responsible and environmentally sound. Implementing the recommendations from this study can lead to better-designed safety boots that cater to the ergonomic needs of workers, thereby fostering a safer, healthier, and more productive construction industry.

To address the ergonomic challenges highlighted in this study, it is recommended to collaborate with footwear manufacturers to develop safety boots tailored to the specific anthropometric measurements of Botswana's construction workforce. Utilising local data will ensure a better fit, enhance comfort, and reduce foot-related injuries. Implementing training programs focused on the importance of proper footwear, foot health, and ergonomics can empower workers to make informed choices and promote a culture of safety. Additionally, adopting culturally sensitive data collection methods—such as indirect measurements or anonymised data gathering—can overcome barriers and facilitate the

acquisition of accurate information necessary for designing ergonomic safety equipment.

DECLARATIONS

Corresponding author

Correspondence and requests for materials should be addressed to Oanthata Jester Sealetsa; E-mail: sealetsa@ub.ac.bw; ORCID: <https://orcid.org/0000-0003-2023-355X>

Data availability

The datasets used and/or analysed during the current study available from the corresponding author on reasonable request.

Author's contribution

All authors contributed equally to this work.

Consent to publish

Not applicable.

Competing interests

The authors declare no competing interests in this research and publication.

REFERENCES

- Dobson, J. A., Riddiford-Harland, D. L., Bell, A. F., & Steele, J. R. (2017). Effect of work boot type on work footwear habits, lower limb pain, and perceptions of work boot fit and comfort in underground coal miners. *Applied Ergonomics*, 60, 146–153. <https://doi.org/10.1016/j.apergo.2016.11.008>
- Dumbhare, S. A., Nagarwala, R. M., Shyam, A. K., & Sancheti, P. K. (2022). Prevalence of foot problems associated with wearing safety footwear in factory employees. *International Journal of Community Medicine and Public Health*, 9(8), 3135. <https://doi.org/10.18203/2394-6040.ijcmph20222013>
- Kotler, P., Keller, K. L., Ang, S. H., Tan, C. T., & Leong, S. M. (2018). *Marketing management: an Asian perspective*. Pearson.
- Moalosi, R., & Rapitsenyane, Y. (Eds.). (2023). *African Industrial Design Practice: Perspectives on Ubuntu Philosophy*. Taylor & Francis. <https://doi.org/10.4324/9781003270249>
- Nadadur, G., & Parkinson, M. B. (2013). The role of anthropometry in designing for sustainability. *Ergonomics*, 56(3), 422–439. <https://doi.org/10.1080/00140139.2012.718801>
- Ochsmann, E., Noll, U., Ellegast, R., Hermanns, I., & Kraus, T. (2016). Influence of different safety shoes on gait and plantar pressure: A standardised examination of workers in the automotive industry. *Journal of Occupational Health*, 58(5), 404–412. <https://doi.org/10.1539/joh.15-0193-OA>
- Orr, R., Maupin, D., Palmer, R., Canetti, E. F., Simas, V., & Schram, B. (2022). The impact of footwear on occupational task performance and musculoskeletal injury risk: A scoping review to inform tactical footwear. *International Journal of Environmental Research and Public Health*, 19(17), 10703. <https://doi.org/10.3390/ijerph191710703>
- Pereira-Barriga, M. C., Borrero-Hernández, J. M., García-Iglesias, J. J., López-López, D., Ruiz-Frutos, C., Allande-Cussó, R., & Gómez-Salgado, J. (2024). A review of the injuries caused by occupational footwear. *Occupational Medicine*, 74(3), 218–224. <https://doi.org/10.1093/occmed/kqae003>
- Pheasant, S., & Haslegrave, C. M. (2018). *Bodyspace: Anthropometry, ergonomics and the design of work*. CRC Press. <https://doi.org/10.1201/9781315375212>
- Rapitsenyane, Y., & Sserunjogi, P. (2023). New product development contextual approach. In Moalosi, R., & Rapitsenyane, Y. (Eds.), *African Industrial Design Practice: Perspectives on Ubuntu Philosophy* (pp. 179–200). Taylor & Francis. <https://doi.org/10.4324/9781003270249>
- The International Ergonomic Association (IEA) and The International Labour Organisation (ILO). (2019). Principles and guidelines for HF/E design and management of work systems joint document.
- U.S. Bureau of Labor Statistics. (2018). *Occupational outlook handbook*. U.S. Department of Labor. <https://www.bls.gov/ooh/>

Publisher's note: [Scienceline Publication](#) Ltd. remains neutral with regard to jurisdictional claims in published maps and institutional affiliations.



Open Access: This article is licensed under a Creative Commons Attribution 4.0 International License, which permits use, sharing, adaptation, distribution and reproduction in any medium or format, as long as you give appropriate credit to the original author(s) and the source, provide a link to the Creative Commons licence, and indicate if changes were made. The images or other third party material in this article are included in the article's Creative Commons licence, unless indicated otherwise in a credit line to the material. If material is not included in the article's Creative Commons licence and your intended use is not permitted by statutory regulation or exceeds the permitted use, you will need to obtain permission directly from the copyright holder. To view a copy of this licence, visit <https://creativecommons.org/licenses/by/4.0/>.

© The Author(s) 2024

Effects of Resampled DEM on Watershed Characteristics and Prediction of Sediment Load in Oyun Watershed, Kwara, Nigeria

Adeniyi. G. Adeogun¹ , Abdulrasheed. W. Mansur² , and Abdurasaq. A. Mohammed³ 

¹Department of Civil Engineering, Kwara State University, Malete, Kwara State, 241104, Nigeria

²Department of Civil Engineering, Kwara State Polytechnic, Ilorin, Kwara State, 241102, Nigeria

³National Centre for Hydropower Research and Development, University of Ilorin, Ilorin, 240003, Nigeria

[✉]Corresponding author's Email: adeniyi.adeogun@kwasu.edu.ng

ABSTRACT

Understanding the terrain and its impact on watershed characteristics, streamflow, and sediment loading is crucial for effective water resource management. This study investigates the influence of resampled Digital Elevation Models (DEM) on the prediction of watershed characteristics, streamflow, and sediment loading upstream of Oyun River Watershed, Nigeria. Various DEM resolutions, ranging from 30-meter to 90-meter, were analysed to assess their effects on hydrological predictions. To delineate the watershed, a DEM of 90-meter resolution was sourced from the space Shuttle Radar Topography Mission (SRTM), and the ASTER global DEM data sources. The 90-meter resolution was resampled to four different resolutions which are 75-meter, 60-meter, 45-meter, and 30-meter resolutions. The watershed and streamline were delineated, and the hydrologic simulation was performed using Soil and Water Assessment Tool (SWAT). The research findings revealed that changes in DEM resolution had a negligible impact on streamflow predictions within the Oyun River Watershed. However, a noticeable impact was observed in the prediction of sediment concentration. The 90-meter resolution DEM yielded the lowest predicted sediment concentration, measuring 2.28 mg/l, while the 30-meter resampled DEM produced the highest value at 5.21mg/l. Similarly, the sediment yield (SYLD t/ha) exhibited considerable variation across the different DEM resolutions, with the 90-meter DEM demonstrating the lowest value of approximately 528.90 t/ha, and the 30-meter DEM registering the highest at 2145.57 t/ha. Overall, this research highlights the necessity of careful DEM selection in hydrological modelling to ensure a comprehensive understanding of watershed dynamics, particularly in regions where sediment transport and water quality are of paramount concern.

Keywords: DEM, Hydrological Modelling, Nigeria, Sediment Loads, Watershed

INTRODUCTION

Accurate prediction of streamflow, sediment concentration and yield in a river catchment is essential for sustainable management of water resources at the watershed level. To achieve this, hydrological modelling is necessary, and the application of Geographical Information Systems (GIS) combined with Digital Elevation Model (DEM) has significantly improved this process. Digital Elevation Models (DEMs) play a pivotal role in understanding and modelling terrain characteristics, which have far-reaching implications for various fields, including hydrology, geology, environmental science, and engineering. DEMs are digital representations of the Earth's surface, capturing elevation data at discrete points in a grid format. They are instrumental in depicting topographic features, such as mountains, valleys, and river basins, which are essential for a range of applications.

However, one common challenge associated with the use of DEMs in hydrological modelling is their spatial resolution, which refers to the size of each grid cell and, consequently, the level of detail they can capture. In many cases, DEMs are derived from remote sensing data sources, such as satellite imagery or airborne LiDAR (Light Detection and Ranging), and the chosen spatial resolution may not fully capture local topographic variations or fine-scale features. To address this limitation, researchers often employ resampling techniques. Resampling involves altering the spatial resolution of a DEM by aggregating or disaggregating data points. By doing so, researchers can enhance the level of detail in specific regions or reduce computational demands for large-scale analyses. The selection of an appropriate resampling technique is a critical decision in DEM processing, as it directly impacts the accuracy and reliability of subsequent analyses. Digital Elevation

RESEARCH ARTICLE
 PII: S225204302400020-14
 Received: June 25, 2024
 Revised: September 02, 2024
 Accepted: September 05, 2024

Models (DEMs) are essential tools for studying land surface processes and modelling the flow of water and sediment in river catchments (Viglione et al., 2013). DEMs provide a digital representation of the elevation of the land surface, typically at a spatial resolution ranging from several meters to several kilometres (Dávila-Hernández et al., 2022; Badamasi et al., 2022). DEMs can be used for a wide range of applications, including terrain analysis, land use planning, environmental monitoring, and hydrological modelling (Tang et al., 2009). The development of DEMs has revolutionized hydrological modelling by providing a detailed and accurate description of the topography of river catchments (Wu et al., 2013).

Based on the foregoing, it is common to resample DEMs to a coarser resolution to reduce computational requirements (Dixon and Earls, 2009; Choi et al., 2015; Muthusamy et al., 2021). Resampling involves averaging or aggregating elevation values over larger grid cells, which can result in a loss of fine-scale terrain details (Badamasi et al., 2022). However, high-resolution DEMs can also pose computational challenges due to their large file size and processing requirements. Therefore, it is essential to carefully consider the effects of DEM resolution on the accuracy of predictions and to use appropriate methods to account for errors introduced by resampling.

This research investigated the effects of various resolutions by resampling of an existing DEM. The study's specific goal was to use DEM, GIS, and SWAT to model the drainage pattern and predict the flow and sediment loadings on river catchment in Nigeria. Some challenges and opportunities of using SWAT to predict basin water characteristics within a river catchment could be identified through the application of SWAT for hydrological modelling and prediction of flow and sediment loadings.

MATERIALS AND METHODS

Description of the Study Area

The study area is Oyun River Basin, which has a terrain elevation of 259 meters above sea level and can be found between latitudes 90. 501 and 80. 241 North and Longitudes 40. 381 and 40. 031 East. The river Oyun, which starts near Ila Orangun in Osun State of Nigeria at an elevation of 465.003 m above the sea level, flows for about 80 kilometres to the northeast and converges with river Asa in Kwara State. The area of Oyun in Kwara State is located southeast of Ilorin and is known for its open and undulating terrain, rocky outcrops, and varying slopes in the northwestern portion. It is a region of Nigeria's grass

plains that is mostly used for farming with only a small section of forest reserve. River Oyun is a major water source for Offa town and its neighboring areas, and it also supplies raw water for the University of Ilorin, Ilorin water supply scheme. Figure 1 shows a map of the Oyun River basin, which includes a network of rivers and catchment areas.

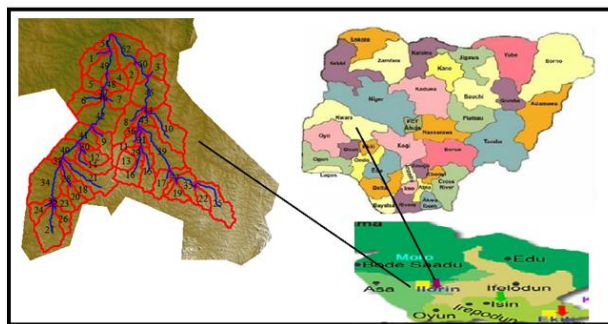


Figure 1. Map of Nigeria showing the location map of the study area.

Model Selection and Description

The model used in this study is the soil and water Assessment Tool, SWAT (Neitsch et al., 2005). The selection of SWAT for this study was based on many reasons. For instance, SWAT is an existing software that is available for free on SWAT website. Also, based on past studies, it has been confirmed as an efficient tool in the modelling of hydrological processes (Adeogun et al., 22; Adeogun et al., 2015; Adeogun et.al, 2014; Betrie et al, 2011). The SWAT model originated from the collaborative efforts of the U.S. Department of Agriculture – Agriculture Research Service (USDA-ARS) and operates on a continuous time basis as a conceptual model. Its integral components encompass weather patterns, hydrological processes, erosion and sedimentation dynamics, plant growth mechanisms, among others. Within the agricultural realm, it accounts for variables like fertilizers, crops, tillage methods, grazing, and even the incorporation of point source loads (Neitsch et al., 2009).

Model Input Data

The basic spatial input datasets used by the model include the Digital Elevation Model (DEM), Land use/cover data, soil data and weather data. Digital elevation model used in this study is of resolution 90 m x 90 m and was obtained from online database developed by United State Department of Agriculture (CGIAR, 2012). The DEM (Figures 2 to 6) provides the basis for watershed delineation into sub-basins. The Land use map (Figure 7)

used for the modelling was downloaded from the Global Land Cover Characterization (GLCC) database and has a spatial resolution of 1Km and 24 classes of landuse representation (GLCC, 2012). The digital soil data for the study was extracted from harmonized digital soil map of the world (Harmonized World Soil Database (HWSD) produced by Food and Agriculture Organization of the United Nations, Rome (Nachtergaele et al., 2009). Meteorological data necessary to run the SWAT model was obtained from Nigerian Meteorological Agency (NIMET) station based in Ilorin, Kwara State. The data collected includes daily precipitation, maximum and minimum temperature, solar radiation, relative humidity, and wind speed. The weather variables for driving the hydrological balance within the watershed were for a period of 19 hydrological years i.e. (January 1, 2001, to December 31, 2019).

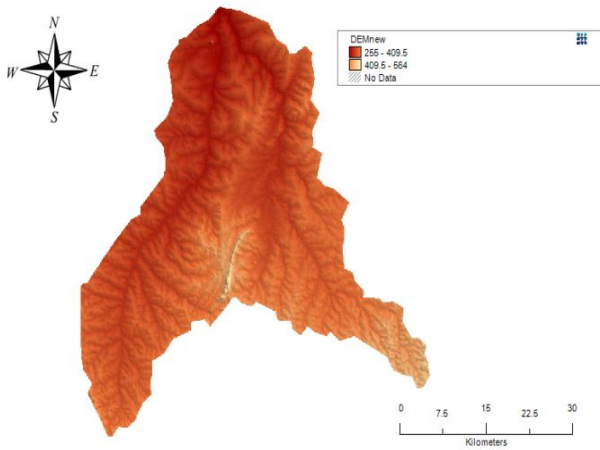


Figure 2. DEM of 90 m resolution of the study area.

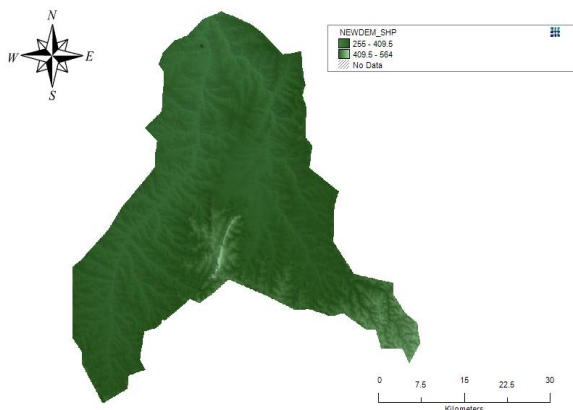


Figure 3. DEM of 75 m resolution of the study area.

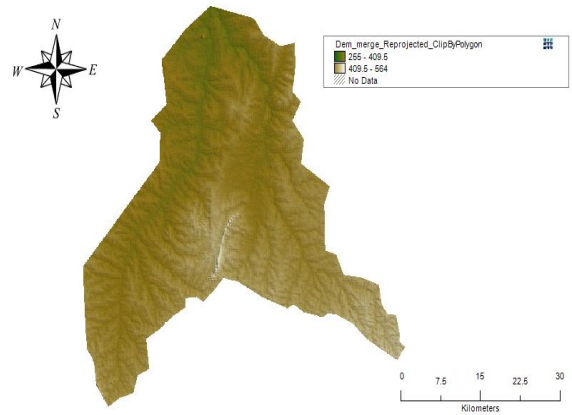


Figure 4. DEM of 60 m resolution of the study area.

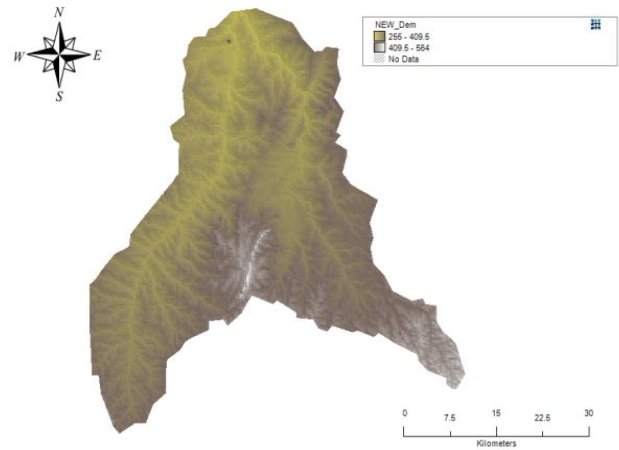


Figure 5. DEM of 45m resolution of the study area.

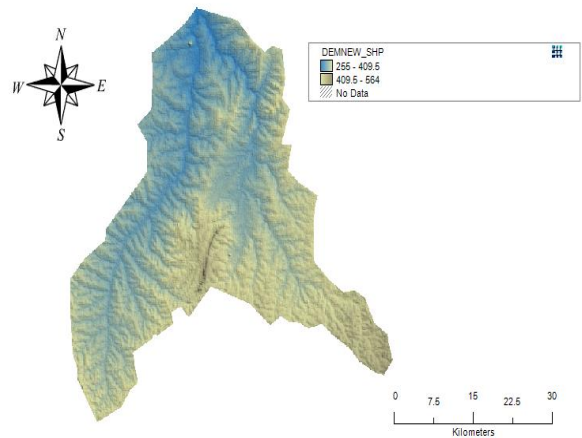


Figure 6. DEM of 30 m resolution of the study area.

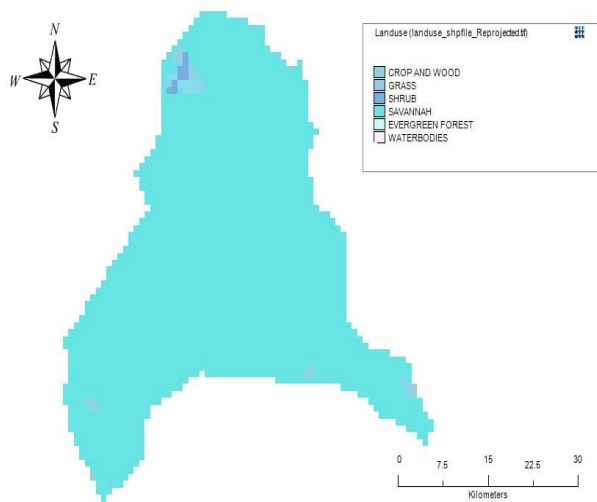


Figure 7. Landuse map of the study area.

Watershed delineation into sub-basins and Hydrologic Response Units (HRUs)

The delineation of the watershed was achieved using resampled DEM of the study area. A total of 55 sub-basins were created in the watershed and was subdivided into 59 hydrologic response unit (HRUs) for all the resampled DEM and the watershed was delineated automatically. The HRU is the smallest spatial unit needed for running the hydrological model. Figure 8 shows the delineated subbasins of the study area for all the resampled DEM.

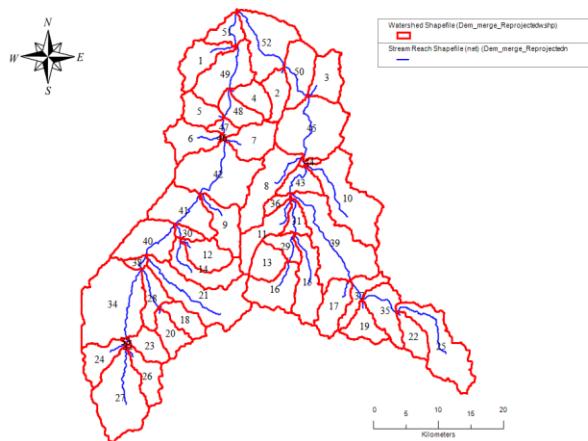


Figure 8. Watershed Delineation and Hydrological Response Unit (HRU)

SWAT Setup and Run

SWAT was executed using the Soil Conservation Service (SCS) Runoff Curve Number method for estimating surface runoff from precipitation. The SCS curve number method is a rainfall-runoff model that was designed for computing excess rainfall (direct runoff).

This method assumes an initial abstraction before ponding that is related to curve number. The daily weather was prepared and imported into the model. The resampled DEM of resolution 90 m, 75 m, 60 m, /45m, 30m were used in turn in conjunction with other spatial and temporal data for the prediction of flow and the sediment loadings. The simulation period is from 01 January 2001 to Dec 31, 2019. All the necessary files needed to run SWAT were written, and the appropriate selection of weather sources done before running the SWAT executables.

RESULTS AND DISCUSSION

Effect of DEM Resolution on Watershed Characteristics

The analysis of the effect of DEM resolution on watershed characteristics revealed a clear relationship between DEM resolution and watershed area (check Table 1 for details). As the DEM resolution becomes finer (smaller), the calculated watershed area generally decreases. For instance, the 30-meter DEM resolution results in the smallest watershed area, while the 90-meter resolution yields the largest. This trend suggests that higher resolutions capture finer details of the terrain, resulting in the identification of smaller, more defined watersheds. In essence, higher resolution DEMs provide a more accurate representation of the landscape's intricacies, allowing for the delineation of smaller drainage areas. The study also examined the number of sub-basins across different DEM resolutions. Interestingly, the number of sub-basins remains relatively consistent across the various resolutions, with only minor variations. This finding indicates that the delineation of sub-basins is less sensitive to changes in DEM resolution compared to watershed area. While higher resolutions offer greater detail in terrain representation, they do not significantly impact the overall number of sub-basins. This suggests that sub-basin delineation may be less influenced by the level of detail in the elevation data.

The analysis of cumulative stream length provides insights into how DEM resolution affects the representation of stream networks within watersheds. It is observed that as DEM resolution becomes finer, the cumulative stream length generally increases. This phenomenon can be attributed to the improved accuracy in depicting the elevation data at higher resolutions. Finer resolutions allow for a more precise identification of stream channels and, consequently, lead to longer cumulative stream lengths. Therefore, researchers aiming to analyse stream networks in detail should opt for higher-

resolution DEMs to ensure accurate results. The assessment of average slope values across different DEM resolutions indicates a notable trend. Lower DEM resolutions tend to produce slightly higher average slope values, which signify steeper terrain representation. Conversely, higher DEM resolutions result in slightly lower average slopes, indicating a smoother representation of the terrain. This trend highlights the importance of considering DEM resolution when assessing the steepness of a landscape. Coarser resolutions may exaggerate slope values, while finer resolutions provide a more realistic depiction of the terrain's gradient.

Effect of Resampled DEM on the prediction of Stream Flow

At the outset, the lowest predicted average annual stream flow value observed was 2229.91m³/s. This value was obtained using a lower resolution of 90 m by 90 m for the hydrological modelling process. However, when the DEM resolution was adjusted to a finer level of 75m, the maximum predicted stream flow value increased to 2345.14 m³/s. This suggests that refining the resolution of the DEM can lead to higher predicted stream flow values. Further experimentation with resolutions of 45 m and 30m resulted in a relatively stable range of predicted stream flow values. At a resolution of 45m, the stream flow values remained consistently between 2341.29 m³/s and

2344.19 m³/s, while at 30 m resolution, a similar stability was observed. This stability in the predicted values implies that reducing the DEM resolution beyond 60 m might not significantly impact the stream flow predictions.

Similarly, for average monthly predicted flow, the lowest predicted value of 185.83 m³/s was obtained using a coarser DEM resolution of 90m by 90m. However, upon refining the DEM resolution to 75m, this value increased to its peak at 195.43 m³/s. It was noticed that there was a remarkable consistency within the range of 195.11 m³/s to 195.10 m³/s. This consistency emerged at even finer resolutions, specifically 45 m and 30 m respectively. The steadfastness in values across these resolutions implies that modifications to the DEM resolution below the 60 m threshold bear minimal impact on the projected stream flow values pertaining to the river. The study's findings align with prior research conducted by Ghaffari (2011) and Arega et al. (2015), both of which concluded that DEMs resolutions have a notable influence on predicted runoff, sediment yield, and stream flow values. This emphasizes the importance of considering DEM resolution's impact on hydrological processes, underlining the need for optimizing DEM resolution to ensure accurate measurement and prediction of stream flow. Table 2 provides more details information about predicted flow and sediment by each of resampled DEM.

Table 1. DEM resolutions and watershed characteristics in the study area

DEM	Sub-basins	Cum. Stream length (m)	Average slope
90 m	55	287,136	0.17
75 m	53	288,276	0.16
60 m	53	289,765	0.16
45 m	53	291,283	0.17
30 m	53	292,110	0.17

Table 2. Details information on predicted flow and sediment by each of resampled DEM

S/N	DEM(m)	Av. Annual Flow(m ³ /s)	Monthly sedcon(mg/l)	Sed.Yld(t/ha)
1	90 x 90	2229.9	19075.0	528.9
2	75 x 75	2345.1	41986.9	1926.1
3	60 x 60	2338.0	40537.3	1965.1
4	45 x 45	2341.3	42181.2	2080.0
5	30 x 30	2341.2	43437.2	2145.6

Effect on the Prediction of Sediment Concentration and Sediment Yield

The results highlighted the significance of DEM resolution on sediment concentration measurements. Among the various resampled DEM resolutions, it was the 30m resolution that stood out, recording the highest predicted sediment concentration value of 521,246.94

mg/l. This finding underscored the substantial influence of DEM resolution on sediment concentration measurements. Further analysis unveiled a direct correlation between predicted sediment concentration and DEM resolution. This correlation was consistent throughout the resolution range, with the 90 m resolution revealing the lowest sediment concentration of 228,899.70 mg/l, as indicated in

Table 2. The sediment yield values varied significantly between different DEM resolutions. For instance, the 90 m resolution DEM yielded the lowest sediment yield value of approximately 528.90 t/ha, while the 30m resampled DEM demonstrated the highest value of 2145.57 t/ha. This discovery held crucial implications, suggesting that the precision of sediment yield estimates is greatly influenced by the DEM resolution chosen.

Table 2 provides a comprehensive glimpse into the monthly predictions across various resampled DEM resolutions, unveiling crucial insights into the interplay between DEM resolution and key hydrological metrics. Predicted flow values serve as a vital indicator of water movement, representing the volume of water traversing a specific river point over a given time frame. In parallel, sediment concentration values quantify the quantity of suspended sediment particles within the water column, measured in milligrams per liter (mg/l).

Additionally, sediment yield values encapsulate the mass of sediment transported across a unit area, expressed in tons per hectare (t/ha). Upon analysis, a consistent trend was observed with the finer DEM resolutions yield marginally higher predicted flow values and sediment concentration levels. This trend follows logically, as finer resolutions capture complex terrain details more comprehensively, thereby enabling more accurate simulations of flow dynamics and sediment transport processes. The parallel increase in sediment yield values with finer DEM resolutions signifies that the heightened detail enables the modeling of sediment transport with greater precision. As the resolution becomes finer, the model can account for smaller variations in terrain, enhancing its ability to estimate sediment transport across the landscape.

CONCLUSIONS

Based on the outcome of this study, the following can be concluded:

- i. The SWAT model's analysis revealed significant variations in streamflow, with Subbasin 51 having the highest streamflow and Subbasin 23 the lowest. This emphasizes the need for tailored management strategies considering local factors and watershed characteristics to effectively address water resource challenges.
- ii. As the Digital Elevation Model (DEM) resolution became finer, shifting from 90m x 90m to 30m x 30m, there was a consistent increase in predicted sediment concentration, indicating that finer resolutions provide a more detailed representation of terrain and hydrological features, leading to higher sediment concentration predictions.
- iii. Moreover, there was a consistent trend of increasing values in both sediment yield and concentration as the DEM resolution decreased, implying that finer resolutions better capture localized terrain variations and hydrological features, resulting in elevated sediment predictions.

In conclusion, this study provided significant contributions to the understanding of sediment-related dynamics in relation to DEM resolution. The intricate relationship between sediment concentration, sediment yield, and DEM resolution has far-reaching implications for water resource management, erosion control, and environmental planning.

DECLARATIONS

Corresponding Author

Correspondence and requests for materials should be addressed to Adeniyi. G. Adeogun; E-mail: adeniyi.adeogun@kwasu.edu.ng; ORCID: <https://orcid.org/0000-0003-2109-0327>

Data availability

The datasets used and/or analysed during the current study available from the corresponding author on reasonable request.

Acknowledgements

The authors would like to acknowledge the management of the Kwara State University, Malete, Nigeria for creating a conducive environment to conduct this research.

Authors' contribution

A.G. Adeogun: Conceptualization, methodology, writing original manuscript, review and editing.

A.W. Mansur: data collection, Model analysis.

A.A. Mohammed: Review, editing and validation of model.

Competing interests

The authors declare no competing interests in this research and publication.

REFERENCES

- Adeogun AG, Ganiyu HO, Adetoro AE and Idowu BS (2022) Effects of Watershed Delineation on the Prediction of Water Quality Parameters in Gaa Akanbi Area, Ilorin. LAUTECH Journal of Civil and Environmental Studies, 8(1): 92-104. DOI: <https://doi.org/10.36108/laujoces/2202.80.0101>
- Adeogun AG, Sule, BF, Salami, AW, and Daramola, MO (2014). Validation of SWAT Model for Prediction of Water Yield and Water Balance: Case Study of Upstream Catchment of Jebba Dam in Nigeria. International Journal of Civil and Environmental Engineering, 8(2): 264-270. <https://zenodo.org/record/1090581/files/9997357.pdf>
- Adeogun A, Sule B, Salami A, and Okeola O, (2014). GIS-based Hydrological Modelling using SWAT: Case Study of Upstream Watershed of Jebba Reservoir in Nigeria. Nigerian Journal of Technology, 33(3): 351-358. DOI: DOI: <https://doi.org/10.4314/njt.v33i3.13>

- Betrie GD, Mohammed YA, Griensven V and Srinivasan R, (2011) Sediment Management Modelling in the Blue Nile Basin using SWAT. Hydrology and Earth System Sciences, 15: 807-818. <https://doi.org/10.5194/hess-15-807-201>
- Arega S Y (2023) Impact of DEM Resolution, Sources and Resampling Techniques on Performance of SWAT Model in Upper Blue Nile Catchment, Chapter 12, INTECH OPEN,1-17.DOI: <http://dx.doi.org/10.5772/intechopen.109526>
- Badamasi H (2022). A Review of GIS-Based Hydrological Models for Sustainable Groundwater Management. Current Directions in Water Scarcity Research, 7: 183-200. <https://doi.org/10.1016/B978-0-323-91910-4.00012-1>
- CGIAR (2022). SRTM 90m Digital Elevation Data, available at <http://srtm.csi.cgiar.org/>, accessed on 23rdDecember 2022.
- Dávila-Hernández S, González-Trinidad J, Júnez-Ferreira HE, Bautista-Capetillo CF, Ávila MH, Escareño CJ, Ortiz-Letechipia J, Rovelo RCO and López-Baltazar EA (2022) Effects of the Digital Elevation Model and Hydrological Processing Algorithms on the Geomorphological Parameterization. Water, 14, 1-25. <https://doi.org/10.3390/w14152363>
- Dixon B, and Earls J (2009). Resample or Not?! Effects of Resolution of DEMs in Watershed Modeling, Hydrological Sciences, 23(12): 1714 - 1724, <https://doi.org/10.1002/hyp.7306>
- Ghaffari G, (2011). The Impact of DEM Resolution on Runoff and Sediment Modelling Result Research Journal of Environmental Science, 5(8): 691-702. <https://doi.org/10.3923/rjes.2011.691.702>
- GLCC (2022). Global Land Cover Characterization, available at <http://edc2.usgs.gov/glcc/glcc.php>, Cited on 13/10/2022
- Muthusamy M, Casado MR, Butler D, and Leinster, P (2021) Understanding the Effects of Digital Elevation Model Resolution in Urban Fluvial Flood Modelling, Journal of Hydrology, Volume 596: 126088, (ISSN: 00221694), <https://doi.org/10.1016/j.jhydrol.2021.126088>.
- Nachtergaele F, Velthuisen HV and Verelst L (2009), Harmonized World Soil Database (HWSD). Food and Agriculture Organization of the United Nations, Rome <https://doi.org/10.4060/cc3823en>
- Neitsch SL, Arnold JG, Kiniry JR and Williams JR (2011) SWAT: Soil and Water Assessment Tool Theoretical Documentation Version 2009. USDA, ARS, Temple. <https://swat.tamu.edu/media/99192/swat2009-theory.pdf>
- Neitsch SL, Arnold JG, Kiniry JR and Williams JR (2005). SWAT Theoretical Documentation Version 2005. Grassland, Soil and Water Research Laboratory, Agricultural Research Service, Temple, Texas. <https://swat.tamu.edu/media/1292/SWAT2005theory.pdf>
- Tang Q, Gao H, Lu H and Lettenmaier DP (2009). Remote Sensing: Hydrology, Progress in Physical Geography 33(4): 490-509. <https://doi.org/10.1177/0309133309346650>
- Viglione A, Parajka J, Rogger M, Salinas JL, Laaha G, Sivapalan M and Blöschl G (2013). Comparative Assessment of Predictions in Ungauged Basins – Part 1: Runoff-Hydrograph Studies. Hydrology and Earth System Sciences, 17(5): 1783-1795. <https://doi.org/10.5194/hess-17-1783-2013>
- Wu Q, Liu J, Liang E, Li, X and Zhang X (2013). Advances in Digital Elevation Model Research: A Review. Journal of Geographical Sciences, 23(6): 1007-1020. <https://doi.org/10.1007/s11442-013-1044-4>

Publisher's note: [Scienceline Publication](#) Ltd. remains neutral with regard to jurisdictional claims in published maps and institutional affiliations.



Open Access: This article is licensed under a Creative Commons Attribution 4.0 International License, which permits use, sharing, adaptation, distribution and reproduction in any medium or format, as long as you give appropriate credit to the original author(s) and the source, provide a link to the Creative Commons licence, and indicate if changes were made. The images or other third party material in this article are included in the article's Creative Commons licence, unless indicated otherwise in a credit line to the material. If material is not included in the article's Creative Commons licence and your intended use is not permitted by statutory regulation or exceeds the permitted use, you will need to obtain permission directly from the copyright holder. To view a copy of this licence, visit <https://creativecommons.org/licenses/by/4.0/>.

Stakeholders Influence on Construction Project Success

Hope Kasuka Mwakamui¹  , and Keneilwe Ntshwene² 

¹Department of Construction Engineering, Gaborone University College of Law and Professional Studies, P.O BOX 201095 Gaborone, Botswana

²Department of Civil Engineering, University of Botswana, Private Bag UB 0022 Gaborone, Botswana

✉Corresponding author's Email: hope.mwakamui@guc.ac.bw

ABSTRACT

For the past decade Botswana's construction industry has been embroiled in a lot of controversies based on construction project constraints. These are characterized by construction project delays, budget overruns as well as scope creep and some of these construction projects have been deemed unsuccessful by different stakeholders. To find a mitigating factor for these problems, construction project constraints must be investigated beyond just the triple constraints to provide a solution for the Botswana construction industry. Therefore, the overall purpose of this study was to investigate how construction project constraints and stakeholders influence the outcome of a project. The study adopted a qualitative approach through face-to-face interviews with selected stakeholders such as construction professionals, clients and other beneficiaries in the Gaborone and greater Gaborone areas. Thematic analysis was used to analyze data. The findings of the study established that the success of a construction project is subjective and is based on who is being asked, the construction professionals, the client and other beneficiaries had different perspectives on success of a project. The study revealed that initial constraints in a construction project tend to be carried along to the final stages of a construction project. However new few construction project constraints also emerge at the final stages of a construction project. The study found that stakeholders such as the client and other beneficiaries have a significant impact on construction projects due to their influence both positive and negative depending on the level of engagement.

Keywords: Factors of project success, Project constraints, Stakeholders, Triple constraints

INTRODUCTION

A construction project is a temporary endeavor in which multi disciplines in the built environment collaborate for a common goal within a defined start and finish time by factoring in the triple constraints (Sunke, 2009). Historically project success has been linked to the iron triangle of time, cost, and quality (Barnes, 1988). A case can be put that balancing only the triple constraints may at times prove to be futile, its critical for project managers to balance beyond the iron triangle. Therefore, there is need to analyze the impact and negotiate other sides of the construction project constraints to deliver a service or product (Prakash, 2021). Many topical issues which have implications for the construction industry have so far only been discussed, but few to a significant extent in the context of industrialized countries regarding construction project constrains (Ofori, 2000). The main objective of construction projects is to complete the construction on time and within budget without sacrificing quality (Sweis, 2013). For most construction industries including that of Botswana, the attributes of cost, time and quality are often elusive. While the industry has been commended in improving and upgrading construction and civil

engineering infrastructure, some reports indicate otherwise (Sentongo, 2005). Therefore, the objective of the study was to investigate the influence of stakeholders on construction project success. The rest of the paper is structured as follows: presentation of the background followed by methods, results and lastly conclusions.

Background

This section discusses the project constraints, triple constraints, other project constraints and shift to project success, project stakeholders and how this affect project success.

• Project constraints

A constraint is an aspect that limits system performance in each environment (Mayer et al., 1995). Most studies when they discuss project constraints in construction project management, focus mostly on the triple constraints of time, cost, and quality. However, construction projects have become more complex and as such have become multiple constraints based (Mishra and Mallik, 2017). Therefore, the section will seek to highlight on the iron triangle and discuss other project constraints that affect construction projects.

RESEARCH ARTICLE
 PII: S225204302400021-14
 Received: June 25, 2024
 Revised: September 02, 2024
 Accepted: September 05, 2024

- **The triple constraints**

The theory of the triple constraint states that: the triple constraint, is a triangle of time, cost and performance that bounds the universe within which every project must be accomplished (Dobson, 2004). The triple constraints were originally conceived as a framework to enable project managers to evaluate and balance the competing demands of cost, time, and quality as illustrated in Figure 1 (Atkinson, 1999). Subsequently the triple constraints became the de facto method that defines and measures project success with the general perception amongst project managers, that a successful project is based on these three criteria alone (Shenhar and Dvir, 2007).



Figure 1. Iron triangle. Source: Atkinson (1999).

- **Other project constraints**

A construction work environment infuses a multi-party participation; therefore, needs and constraints in a multi discipline situation bring complications in the construction sector (Lau & Kong, 2004). Amusan et al., (2021) states that the modern-day construction industry projects are high risk and have given way to more constraints beyond the iron triangle and as such these constraints threaten the successful delivery of construction projects. Mishra and Mallik (2017) and several other scholars identified construction project constraints into the following categories: economic constraints legal constraints environmental constraints technical constraints social constraints and political constraints.

- **Project success**

Successful project can be defined as having achieved the project objectives: within time within cost and at the desired performance/technology level while utilizing the assigned resources effectively and efficiently and are accepted by the customer (Kerzner, 2018). However, project success is not to be simply meeting the pre-defined triple constraint set as adjusted during the project. Project success is also in the eye of the beholder, that is, those individuals, enterprises, agencies, institutions, who are the stakeholders (Cleland and Ireland 2002). While we would like to say that we have a clear set of goals by using the

triple constraint, we see that this varies based on the perspective of the stakeholder (Cuellar, 2010).

- **Project success factors**

Construction project success factors tend to be a bit more specific. Rockart (1979) stated that success factors of construction projects can be identified in the following ways: a controlled number of ways in which success is guarantee; aspects of the business side of the construction project that must be monitored aggressively by management and critical areas where good performance is a requirement to achieve construction project success.

While most publications have looked at factors of success from a much more general viewpoint, few with a point of focus. Chen and Chen (2007) streamlined the focus of factors of project success in the construction industry in terms of stakeholder partnerships. The emphasis lies in the ability for forged partnership to be effective and bear fruits in terms of progress. Chen and Chen (2007) stated that early partnerships ensure the smooth running of a construction project, because as known construction projects are multi-disciplined with experts from different knowledge areas of specialization. Other scholars such as Lewis (1995) mentioned that by partnering with say, material suppliers early into a construction project this in turn will give the contractor an expedited advantage in terms of supply of materials. These sentiments were also expressed by Mohr and Spekman (1994) who reiterated that by engaging government, law makers and other regulatory bodies this reduces the chances of disputes arising in a construction project. Therefore, project success factors can be summarized to include the following: project procurement, project management, project participants, physical environment, time, cost, and quality criteria, safety criteria, client satisfaction criteria, employee satisfaction criteria, learning and development criteria, profitability criteria, internal- process related, labour related, material and equipment related., construction site related, collaborative team cultures, consistent objectives and resource sharing.

- **Project stakeholders**

Project participants entail different key players or stakeholders who share a commonality of being vested in a construction project (Didenko and Konovets, 2009). There are several participants in construction project and an important one is certainly the government. The government is responsible for provision of different types of permits, enforcement of laws and regulations that have a significant impact on the success of a construction project (Le et al., 2020). Clients who form part of the project participants allow a construction project to run

their financing (Elawi et al., 2016). But in totality all project parties must clearly understand their roles at the pre-construction phase to have any chance of success (Le et al., 2020). Therefore, any construction project runs the risk if being unsuccessful when stakeholders do not fulfil their roles.

MATERIALS AND METHODS

This study investigated how the influence of stakeholders affects construction project success. A qualitative approach was used for this study. A qualitative approach of the study provided in depth look at how construction project constraints and stakeholders affect the outcome of a construction project. A qualitative approach tends to explore and discover issues about a particular issue of study (Tsang, 2013). The researcher engaged the Ministry of Infrastructure and Housing Development and Department of Roads under the Ministry of Transport and Infrastructure Botswana to identify an inventory list of all completed government funded construction projects from 2016 to 2020 based on availability of records and personnel engaged in those projects. Under those projects, construction professionals under government ministries, departments, and contractors as well as other parties such as law enforcement and religious groups who were involved or affected in the selected projects were interviewed. Contractors had to be registered with Public Procurement and Asset Disposal Board (PPADB) with Grade D or E. Therefore, convenience sampling was adopted. Etikan (2016) stated that convenience sampling is applicable to both qualitative and quantitative studies. To ensure confidentiality of participants, all identifying information was replaced with codes as indicated in Table 1.

Interviews (one-on-one interviews) were used. One on one interviews are most effective for participants who are articulate, well versed and can share ideas comfortably without hesitation (Plano Clark and Creswell, 2015). The study adopted thematic analysis with an inductive approach. This is quite a flexible method that can be used in a wide range of learning and teaching spheres (Clarke and Braun, 2013).

Table 1.

Participant group	Code	No	Ratio
Construction professionals	C1-C7	7	(1:2.57)
Project beneficiaries	B1-B2	2	(1:9)
Clients	S1-S2	2	(1:9)
Contractors	T1-T7	7	(1:2.57)

RESULTS AND DISCUSSION

Stakeholders influence on construction projects.

All construction projects have people, organizations, or entities with a vested interest whether directly or indirectly. For stakeholders engaged, there was a positive impact in terms of project progress because they were able to provide sound advice where applicable but for those less engaged the project was negatively affected in terms of constraints such as time. The results are presented under the following categories which were generated through thematic analysis: Advice to the contractor, influence with regular meetings late update on project progress safety and legal matters with client and undefined roles.

Advice to contractor

The construction professionals that were interviewed stated that one of the key aspects that influence the success of a construction project was the ability to take advice from stakeholders. To take all their considerations, assess and selectively decide which would be more beneficial to achieve the project goals. The quote from project beneficiaries below highlights this.

“Because they engaged us, and we would also give advice where we can. I remember that there were some areas where there were corners, there were also some temporary roads that went near residential homes, where we advised for speed humps to be constructed to limit vehicle movement” (B1, 2021).

The quote suggests that the advice of other stakeholders can affect construction project success as they ultimately will utilize the infrastructure or facility and if their advice is not adhered to, there’s danger of the facility not being utilized effectively. Positive feedback from stakeholders also proved to be effective on the side of the contractor as well who stated.

“We engage with the chiefs, we engage with the Council, and we engage with service providers like BPC and Bofinet, stakeholders who are for the project and those who are against the project,” (T1, 2021).

Influence using regular meetings

Other stakeholders play a pivotal role in the delivery of the any public funded construction project, as they may provide a key insight into what could be implemented. The commitment and attitude of stakeholders (beneficiaries) can be defined as the perception stakeholders have regarding the project, be it supportive or non-supportive. B1 said:

“We are a stakeholder, so obviously these projects fall under the Ministry of Transport (Department of Roads). But obviously when the project starts, the planning phase we are normally engaged. They say we are going to build a road, and they normally ask for our input, what we think”. (B1, 2021)

Much of the participants, particularly other stakeholders expressed that they wish the contractors would engage them early in the project to provide their input save for project beneficiaries. One of the key stakeholders of the road project, a main liner church felt both the client and contractor had not done enough to engage them early in the project.

“They only contacted us once for a meeting at state owned offices to inform us they need our land”, (B2, 2021).

Other stakeholders bemoaned with similar sentiments; This was reiterated by C2:

“We were only made aware of the teaching hospital officially through a meeting once there was an intention to open in it, this was in 2017”, (C2, 2021)

The stakeholders appear to be divided in their opinion as far as, how much leeway they were given to have an influence in public funded construction projects. As a factor of construction project success influence of stakeholders is a crucial element for a positive outcome.

Late update on project progress

Through the narratives over the interviews, it was obvious that one of the constraints identified was the communication breakdown between construction professionals from government and those from the contractor. Some of the parties had indicated that there was always a delayed or late update on the project progress. The T2 stated:

“So, we were having some problems with some of the information missing. Unless if it’s a design and build, so we were not designing, so we want information to come quickly so that we can make orders.” (T2, 2021)

The quote suggests that communication between all parties involved is quite essential to not only ensure productivity on site but to keep everyone up to date with the on goings of a construction project. It is a key factor for construction project success. Similar sentiments were shared by construction professionals under independent contractors who highlighted instances which could be considered as a constraint, that the communication and relay of information was poor which led to delay of some construction works. The supported this statement by explaining:

“So, we were having some problems with some information missing, some of the drawings were lacking information and then when you want information you hear the guy (client’s architect) has gone to Maun”. (C2, 2021)

Safety and legal matters with client

Within every construction project both public funded or private funded, it is relevant for safety to be the key factors that affect the success of a project. Safety is an issue that is a performance indicator of project success. Interviewed stakeholders and construction professionals under contractors had indicated the sensitivity of safety as a measurable component of progress.

“Our influence is traffic flow and road safety. When we get there, we look at the safety, how safe it is and what are the effects of works on motor vehicle drivers. To minimize the risk of car crashes, and to determine whether road signs are okay, are they visible at night”, (B2, 2021).

Safety issues in the public funded project concern both the public in general and the site human resources. The T2 supported this statement by explaining:

“Every morning at the airport when you come in, you don’t have guns and those “things”,” (T2, 2021)

Undefined roles

During the interviews conducted some construction professionals expressed a lack of defined roles regarding some public projects which was a source of conflict and dispute. Clients tend to interfere and overexert their authority in some instances. The C2 stated:

“The client came and then saw a door for somebody who was a neighbour, I think it is military hanger, so when the client saw that door, he stated that he prefers it, so we advised him to go and tell the architect “ (C2, 2021).

The aspect of the client overexerting their authority is based on a lack of understanding of contractually defined roles on a construction project. The influence of the client as well as client representatives bears a significant factor on the construction project performance. Stakeholder influence had positively and negatively affected the construction projects outcome. Some beneficiaries of infrastructure believed that the contractor and the client did sufficient efforts to engage them by holding meetings and providing a platform for offering advice where appropriate. However, other beneficiaries had a different point of view. The influence of the other stakeholders seemed to have a mixed effect on the outcome of the construction project.

The study revealed that stakeholders have a significant impact on the construction project outcome due

to their influence. For stakeholders engaged, there was a positive impact in terms of project progress because they were able to provide sound advice where applicable but for those less engaged the project was negatively affected in terms of time. While on the other hand others argued that they were relegated to just by standers, yet they had a vested interest in the construction project. Their influence was significant on the construction project, which is what Artur (2016) argued by stating that managers are encouraged to involved supportive stakeholders and monitor the marginal ones to ensure a successful construction project.

CONCLUSION AND RECOMMENDATIONS

The study posits that stakeholders have a considerable amount of influence on a construction project's outcome which could be deemed positive or negative. Firstly, other stakeholders such as project beneficiaries have indicated that they made several positive contributions to construction projects by providing sound advice and some form of commentary on matters involving safety of the public throughout the project duration. For road construction projects certain beneficiaries provided invaluable advice on provision of visible safety road signs and traffic diversion. This allowed for production on site to uninterrupted which gave the construction project a positive outlook.

The study further revealed that construction professionals under the contractor were dissatisfied with the interference that the client would have directly on the construction project. This was indicated by construction professionals, that the roles in a construction project must be clearly defined. This undue influence of the client led to sour relations between the contractor and client. While contractors through construction professionals may claim that a construction project was successful by their accord, the client was left dissatisfied on occasions where they could not influence the on-going of works on site. Lastly the study did reveal that while certain beneficiaries outlook was positive others indicated dissatisfaction as they were not allowed to have significant influence in the construction project, entities who owned properties around the projects, where land appropriation issues came up. These beneficiaries were of the belief that their influence could have had a positive outcome on the construction project.

DECLARATIONS

Corresponding author

Correspondence and requests for materials should be addressed to: hope.mwakamui@guc.ac.bw or ntshwenek@ub.ac.bw and ORCIDiDs for all authors: <https://orcid.org/0009-0005-5209-4736>; <https://orcid.org/0000-0002-7726-6996>

Data availability

The datasets used and/or analyzed during the current study can be made available from the corresponding authors on reasonable request.

Author's contribution

All authors contributed equally to this work.

Acknowledgements

The authors thank several members of the Botswana public service, those in several ministries, law enforcement as well as several private contractors for the consent in the data collection of this study

Consent to publish

Not applicable.

Competing interests

The authors declare no competing interests in this research and publication.

REFERENCES

- Amusan, L., Aigbavboa, C., Olubiyi, T., & Babatunde, O. (2021). Informatics approach to innovative site management practices for improving construction works. *International Review of Civil Engineering*, 12, 108-122. DOI: <https://doi.org/10.15866/irece.v12i2.20260>
- Atkinson, R. (1999). Project management: Cost, time and quality, two best guesses and a phenomenon, it's time to accept other success criteria. *International Journal of Project Management*, 17(6), 337-342. [https://doi.org/10.1016/S0263-7863\(98\)00069-6](https://doi.org/10.1016/S0263-7863(98)00069-6).
- Chen, W. T., & Chen, T.-T. (2007). Critical success factors for partnering in Taiwan. *International Journal of Project Management*, 25, 475-484. DOI: <https://doi.org/10.1016/j.ijproman.2006.12.003>
- Cheng, Y.M. (2014). An Exploration into Cost-Influencing Factors on Construction Projects. *International Journal of Project Management*, 32, 850-860. DOI: <https://doi.org/10.1016/j.ijproman.2013.10.003>
- Clarke, V., & Braun, V. (2013). Teaching thematic analysis: Overcoming challenges and developing strategies for effective learning. *The Psychologist*, 26(2), 120-123. [Google Scholar](https://scholar.google.com)
- Cleland, D., & Ireland, L. (2002). *Project management: Strategic design and implementation* (4th ed.). McGraw-Hill. Google Scholar: <https://scholar.google.com>

- Cuellar, M. (2010). Assessing project success: Moving beyond the triple constraint. Proceedings of the 5th International Research Workshop on Information Technology Project Management (IRWITPM), 18–28. <http://www.michaelcuellar.net/resume/publications/CuellarIRWITPM2010.pdf>
- Didenko, I., & Konovets, I. (2009). Success Factors in Construction Projects: A Study of Housing Projects in Ukraine. (Dissertation, Handelshögskolan vid Umeå universitet). Retrieved from <https://urn.kb.se/resolve?urn=urn:nbn:se:umu:diva-1975>
- Dobson, M. S. (2004). The Triple Constraints in Project Management. Berrett-Koehler Publishers. Retrieved from <https://books.google.co.bw/books?id=uBIFDwAAQBAJ>
- Elawi, G., Algahtany, M., & Kashiwagi, D. (2016). Owners' Perspective of Factors Contributing to Project Delay: Case Studies of Road and Bridge Projects in Saudi Arabia. *Procedia Engineering*, 145, 1402–1409. DOI: <https://doi.org/10.1016/j.proeng.2016.04.176>
- Etikan, I. (2016). Comparison of Convenience Sampling and Purposive Sampling. *American Journal of Theoretical and Applied Statistics*, 5, 1. DOI: <https://doi.org/10.11648/j.ajtas.20160501.11>
- Kerzner, H. (2018). Value-Driven Project Management. In *Project Management Best Practices*. DOI: <https://doi.org/10.1002/9781119470717.ch16>
- Larson, E. W., & Gray, C. F. (2011). *Project Management: The Managerial Process*. McGraw-Hill Irwin. <https://books.google.co.bw/books?id=IWEonQAACAAJ>
- Lau, E., & Kong, J. J. (2006). Identification of constraints in construction projects to improve performance. In *Proceedings of the Joint Conference on Construction, Culture, Innovation and Management*, Dubai, November (pp. 26-29). [Google Scholar](https://doi.org/10.1016/j.jjproman.2008.03.003)
- Le, N., Chong, W., & Kashiwagi, D. (2020). Success Factors for Project Risk Management in Construction Projects: A Vietnam Case Study. *Journal for the Advancement of Performance Information and Value*, 12, 63. DOI: <https://doi.org/10.37265/japiv.v12i2.126>
- Lewis, J. P. (1995). Fundamentals of project management. American Management Association. [Google Scholar](https://doi.org/10.1016/j.jjproman.2008.03.003)
- Luu, V. T., Kim, S.-Y., Tuan, N. Van, & Ogunlana, S. O. (2009). Quantifying schedule risk in construction projects using Bayesian belief networks. *International Journal of Project Management*, 27(1), 39–50. DOI: <https://doi.org/10.1016/j.jjproman.2008.03.003>
- Mayer, R. J., Davis, J. H., & Schoorman, F. D. (1995). The role of trust in construction projects. *Journal of Construction Engineering and Management*, 121(3), 241-248. DOI: [https://doi.org/10.1061/\(ASCE\)0733-9364\(1995\)121:3\(241\)](https://doi.org/10.1061/(ASCE)0733-9364(1995)121:3(241))
- Mishra, A. K., & Mallik, K. (2017). Factors and impact of risk management practice on success of construction projects of housing developers, Kathmandu, Nepal. *International Journal of Scientific and Basic Applied Research*, 36, 206-232. [Google Scholar](https://doi.org/10.1061/(ASCE)0733-9364(1995)121:3(241))
- Mohr, J., & Spekman, R. (1994). Characteristics of partnership success: Partnership attributes, communication behavior, and conflict resolution techniques. *Strategic Management Journal*, 15(2), 135-152. DOI: <https://doi.org/10.1002/smj.4250150205>
- Ofori, G. (2000). Challenges of construction industries in developing countries: Lessons from various countries. In *2nd international conference on construction in developing countries: challenges facing the construction industry in developing countries*, Gaborone. 5(24), 15-17. [Google Scholar](https://doi.org/10.1002/smj.4250150205)
- Plano Clark, V. L., & Creswell, J. W. (2015). Understanding Research: A Consumer's Guide, (2nd Edition). In *Journal of Emergency Nursing* (Vol. 30, Issue 6). [Google Scholar](https://doi.org/10.1002/smj.4250150205)
- Prakash, A. (2021). Major barriers for sustainable development in Indian construction industry. *Emerg. Res. Innovations Civil. Eng.(ERICE)*. [Google Scholar](https://doi.org/10.1002/smj.4250150205)
- Rockart, J. (1979). Chief executives define their own data needs. *Harvard Business Review*, 52(2), 81-93. [Google Scholar](https://doi.org/10.1002/smj.4250150205)
- Sentongo, J.L. (2005). Causes of poor performance and sometimes outright failure among citizen contractors in Botswana. MBA diss. University of DeMontfort. [Google Scholar](https://doi.org/10.1002/smj.4250150205)
- Shenhar, A.J., & Dvir, D. (2007). Project Management Research: The Challenge and Opportunity. *Project Management Journal*, 38(2), 93-99. <https://doi.org/10.1177/875697280703800210>
- Sunke, N. (2009). Planning of construction projects: A managerial approach. Saarbrücken, Germany: VDM Verlag. <https://dspace.ub.uni-siegen.de/handle/ubsi/393>
- Sweis, G. (2013). Factors Affecting Time Overruns in Public Construction Projects: The Case of Jordan. *International Journal of Business and Management*, 8, 120. DOI: <https://doi.org/10.5539/ijbm.v8n23p120>
- Tsang, E. (2013). Generalizing from research findings: The merits of case studies. *International Journal of Management Reviews*, 16(4), 369-383. DOI: <https://doi.org/10.1111/ijmr.12024>




Publisher's note: [Scienceline Publication](https://www.scienceopen.com) Ltd. remains neutral with regard to jurisdictional claims in published maps and institutional affiliations.



Open Access: This article is licensed under a Creative Commons Attribution 4.0 International License, which permits use, sharing, adaptation, distribution and reproduction in any medium or format, as long as you give appropriate credit to the original author(s) and the source, provide a link to the Creative Commons licence, and indicate if changes were made. The images or other third party material in this article are included in the article's Creative Commons licence, unless indicated otherwise in a credit line to the material. If material is not included in the article's Creative Commons licence and your intended use is not permitted by statutory regulation or exceeds the permitted use, you will need to obtain permission directly from the copyright holder. To view a copy of this licence, visit <https://creativecommons.org/licenses/by/4.0/>.

© The Author(s) 2024

Integrating Prophet Forecasting with Gaussian Mixture Model-Hidden Markov Model (GMM-HMM) for Early Warning System in Dam Deformation Monitoring

Thalosang Tshireletso^{1,2}  , and Pilate Moyo² 

¹Department of Civil Engineering, University of Botswana, Gaborone, Botswana

²Department of Civil Engineering, University of Cape Town, Cape Town, South Africa

[✉]Corresponding author's Email: tshireletsot@ub.ac.bw

ABSTRACT

Ensuring dam safety requires a monitoring system that can predict deformations and detect anomalies in real-time. This study combines the forecasting capabilities of the Prophet model with the real-time anomaly detection of a Gaussian Mixture Model-Hidden Markov Model (GMM-HMM) framework. The Prophet model analyses historical deformation data to forecast future deformations, enabling early issue identification. The GMM-HMM framework continuously monitors incoming data to detect deviations from predictions. Results shows that the GMM-HMM, with 10 components and a Mahalanobis distance threshold of 0.1, achieved a precision of 0.602, recall of 1.0, and F-1 score of 0.751, ensuring high sensitivity and accurate anomaly detection. The GMM-HMM was then used to detect anomalies on Prophet forecasted radial deformations. Anomalies were detected on upper limit and lower limit deformations. This combined approach enhances dam safety by integrating predictive and real-time monitoring capabilities, offering a comprehensive early warning system for dam infrastructure.

Keywords: Gaussian Mixture Model, Hidden Markov Model, Prophet Model, Dam Deformation Forecasting

INTRODUCTION

Dam deformation monitoring is a critical aspect of ensuring the structural integrity and safety of dams. These large-scale structures are key components in managing water resources, controlling floods, and generating hydroelectric power (Rong et al., 2024). Over the past decades, a plethora of techniques and methodologies have been developed and refined to monitor dam deformations and detect any potential risks of failure (Fraleay and Raftery, 2002). However, given the rapidly evolving environmental conditions and the inevitable aging of infrastructure, the urgent need for more advanced, consistent, and reliable early warning systems has become increasingly evident (Šakić et al., 2022).

Without a doubt, early warning systems play a pivotal, arguably indispensable role in mitigating the risks associated with dam failures. They achieve this by providing timely alerts to any potential deformations or structural instabilities, essentially acting as the first line of defence (Pang et al., 2023). With the data from these

systems, authorities are enabled to take proactive measures, such as initiating evacuation procedures or implementing reinforcement measures, which are crucial in preventing catastrophic consequences and preserving life and property (Bahrami et al., 2021).

In the broader field of infrastructure monitoring, Gaussian Mixture Model-Hidden Markov Model (GMM-HMM) has found applications in detecting anomalies in time series data from a diverse range of sources. These include, but are not limited to, structural health monitoring sensors, traffic flow sensors, and environmental sensors. For example, in the context of bridge health monitoring, GMM-HMM has been effectively used to identify abnormal vibrations or structural changes that are indicative of potential defects or damage (Coraça et al., 2022). Similarly, in the realm of railway infrastructure monitoring, GMM-HMM has been employed to detect anomalies in track conditions, such as rail irregularities or track geometry deviations, which could pose serious safety hazards.

RESEARCH ARTICLE
 PII: S225204302400022-14
 Received: June 25, 2024
 Revised: September 02, 2024
 Accepted: September 05, 2024

Despite its demonstrated efficacy in these and other domains of infrastructure monitoring, GMM-HMM has not yet been directly applied to dam deformation anomaly detection. While dams represent critical and high-value infrastructure assets requiring robust and reliable monitoring systems, the application of GMM-HMM specifically to dam deformation data remains an unexplored frontier. Nonetheless, the principles and methodologies of GMM-HMM are conceptually well-suited to the challenges of dam deformation monitoring, where the detection of subtle anomalies in time-varying deformation patterns is crucial for ensuring dam safety.

By leveraging the capabilities of GMM-HMM in modelling temporal dynamics and detecting anomalies, there is a significant potential opportunity to enhance existing dam deformation monitoring systems. Moreover, the development of more effective early warning systems for dam safety could be realized. The integration of GMM-HMM with other predictive modelling techniques, like Prophet Forecasting, could further enhance the accuracy and reliability of anomaly detection in dam deformation data.

The motivation behind integrating Prophet Forecasting with GMM-HMM stems from the complementary strengths of these two approaches in time series analysis and pattern recognition, respectively (Hassani et al., 2019). Prophet Forecasting, a system developed by Facebook, has gained prominence for its ability to handle time series data with irregularities, such as seasonality, holidays, and outliers. On the other hand, GMM-HMM is well-suited for modelling complex temporal patterns and detecting anomalies (Benoit et al., 2013).

By integrating Prophet Forecasting with GMM-HMM, we aim to harness the predictive capabilities of Prophet to forecast dam deformation trends accurately. Subsequently, the GMM-HMM component will leverage these forecasts to detect deviations from expected patterns and issue early warnings in real-time. This hybrid approach offers a synergistic solution that combines the robustness of statistical forecasting with the flexibility of probabilistic modelling, thereby enhancing the reliability and effectiveness of dam deformation monitoring systems.

Our research aims to pioneer the development of a groundbreaking framework that seamlessly integrates Prophet Forecasting with Gaussian Mixture Model Hidden Markov Model (GMM-HMM) to bolster early warning systems tailored specifically for dam deformation monitoring. This innovative integration harnesses the predictive capabilities of Prophet Forecasting, renowned

for its adeptness in handling irregular time series data, to forecast dam deformation trends with heightened accuracy. Leveraging the robustness of GMM-HMM, which excels in discerning complex temporal patterns and anomalies, our framework promises a synergistic solution for detecting deviations from expected deformation patterns in real-time.

MATERIALS AND METHODS

The study was based on Roode Elsberg dam, located in Western Cape, South Africa. The monitoring system included measurement of environmental and operational conditions, water temperatures, measured by thermometers embedded on the dam wall; water level; deformations; and accelerations. The monitoring was carried out by Concrete Materials and Structural Integrity Research Unit (CoMSIRU)/UCT and the Department of Water and Sanitation.

Roode elsberg dam

Roode Elsberg dam is in the Western Cape province, South Africa, about 130 km northeast of Cape Town near the town of de Doorns, at coordinates (33.4361°S, 19.5680°E), Figure 1. Construction of the dam was completed in 1969, and its main purpose is irrigation of vineyards in the surrounding farms and limited domestic use via a 7-km tunnel. The dam is a double curvature concrete arch dam with a centrally located spillway and gross capacity of 8.21 million m³. The height to the lowest foundation point is 72 m, and the length of the crest is 274 m, consisting of two galleries, one following the foundation level and one top instrumentation gallery located about 20 m above the foundation level.



Figure 1. Roode Elsberg dam

Roode Elsberg dam-monitoring system

To understand the behaviour of Roode Elsberg, two monitoring systems were installed on the dam. These included a continuously monitored GPS system at four

survey beacons in 2010 and a dynamic monitoring system at the dam crest in 2013. In addition, environmental and operational conditions were measured, i.e., water level measured using staff gauges and water temperatures; a weather station; and a suite of thermometers located at different water levels: 26.23 m, 46.62 m, and 47.30 m. Figure 2 shows the layout of the Roode Elsberg GPS monitoring systems, where blue indicates control stations P01 and P02 while red indicates rover stations P203 and P206 on the left and right flanks, respectively.

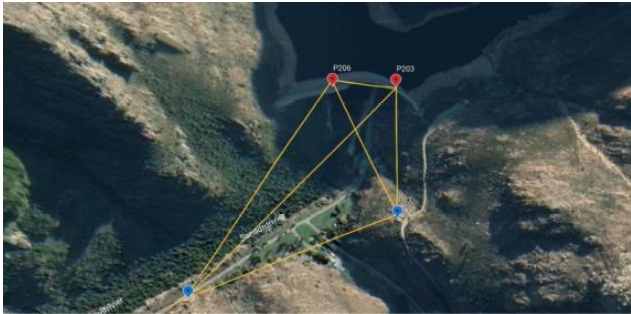


Figure 2. Roode Elsberg GPS monitoring system

Measurement of environmental and operational factors

Results from ambient vibration surveys, carried out on the dam, indicated that there was a need to install a continuous dynamic monitoring system to capture any changes in the behaviour of the dam. This system consists of three forced balanced accelerometers installed on the dam crest and a data acquisition system in the upper gallery of the dam (Figure 3).



Figure 3. Dynamic monitoring system

Measurement of environmental and operational factors

The environmental and operational factors include ambient temperature (AT), water temperature, and water level. Ambient temperature is measured by the weather station installed on the dam crest, and water levels are measured by staff gauges. There are also thermometers that are embedded into the dam wall at different levels to measure water temperatures; Figure 4 below shows the

position of water temperatures on the dam wall. There are 6 thermometers on each side of the wall; avg1-R indicates that thermometer 1 is on the right flank and avg1-L indicates that thermometer 1 is on the left flank. Avg1-R and avg2-R are on the same level, avg3-R and avg4-R are on the same level, and avg5-R and avg6-R are on the same level, as indicated by Figure 4. This applies to thermometers on the left flank.

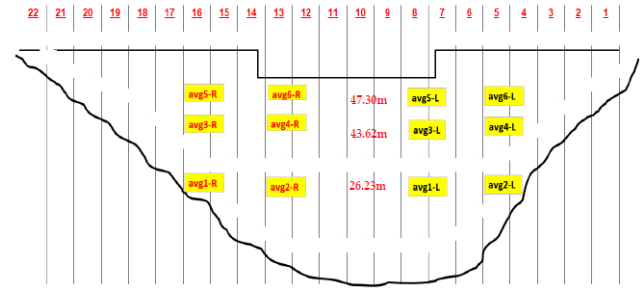


Figure 4. Wall thermometers measuring water temperature

Prophet forecasting model

Prophet is a powerful and comprehensive forecasting model that has been designed specifically to manoeuvre time series data with non-regular patterns such as seasonal variations and holidays (Taylor and Letham, 2018). Unlike other forecasting models, Prophet employs an additive model that deconstructs the time series data into its basic components, which include trend, seasonality, and holiday factors. This methodical separation of components allows for precise prediction capabilities, even when the data set contains outliers or incomplete data.

To capture non-linear trends that develop over time, the model employs a piecewise linear or logistic growth curve. This is particularly useful in situations where the data does not follow a consistent linear pattern. Furthermore, Prophet incorporates Fourier series to model recurring patterns, adding another layer of accuracy to the forecast. In an innovative move, Prophet integrates uncertainty estimation directly into the forecasting process. It achieves this by incorporating Bayesian inference methods, an approach that is grounded in the principles of Bayesian statistics. This allows for a more comprehensive evaluation of prediction uncertainty, which can be crucial in strategic decision making.

The additive model that is the cornerstone of Prophet's forecasting capabilities can be represented as follows:

$$y(t) = g(t) + s(t) + h(t) + \epsilon_t \tag{1}$$

where $g(t)$ represents the trend component, $s(t)$ represents the seasonal component, $h(t)$ represents the holiday component and ε_t is the error term. $y(t)$ represents the value of the time series at time t . Here, t stands for the specific time at which the observation is made.

Prophet is a robust forecasting model developed by Facebook that decomposes time series data into trend, seasonality, and holiday effects. This decomposition enables the model to capture and interpret the underlying patterns in the data.

Trend component

Prophet models the trend component using a piecewise linear or logistic growth model. For piecewise linear growth, the trend is given by:

$$g(t) = k + \sum_{i=1}^n a_i(t - t_i)1_{\{t \geq t_i\}} \tag{2}$$

where $T(t)$ is the trend at time t , k is the initial growth rate, a_i are the rate changes at changepoints t_i , and $1_{\{t \geq t_i\}}$ is an indicator function that is 1 if $t \geq t_i$ and 0 otherwise (Taylor & Letham, 2018). For logistic growth, the trend component is modelled as:

$$g(t) = \frac{c}{1 + \exp(-k(t-m))} \tag{3}$$

where C is the carrying capacity, k is the growth rate, and m is the midpoint of the growth (Taylor and Letham, 2018).

Seasonality component

Seasonality in Prophet is modelled using Fourier series:

$$s(t) = \sum_{k=1}^N \left(a_k \cos\left(\frac{2\pi kt}{P}\right) + b_k \sin\left(\frac{2\pi kt}{P}\right) \right) \tag{4}$$

where $S(t)$ is the seasonal component at time t , P is the period (e.g., 365.25 for yearly seasonality), and a_k, b_k are the coefficients of the Fourier series (Taylor and Letham, 2018).

Holiday effects

Prophet incorporates holiday effects by adding an additional component:

$$h(t) = \sum_{i=1}^m \lambda_i 1_{\{t \in H_i\}} \tag{5}$$

where $h(t)$ represents the holiday effect, λ_i are the holiday effects coefficients, and H_i are the holiday intervals (Taylor and Letham, 2018).

Gaussian mixture model hidden Markov model (GMM-HMM)

GMM-HMM combines the advantages of Gaussian Mixture Models (GMM) and Hidden Markov Models (HMM) to model intricate temporal patterns and identifies anomalies in time series data (Bicego et al., 2019). The GMM component uses a mixture of Gaussian distributions to model the probability distribution of observations at each time step, allowing for a flexible representation of data with multiple underlying patterns. On the other hand, the HMM component captures the temporal dependencies between observations by defining a set of hidden states and transition probabilities between these states. By jointly learning the parameters of the GMM and HMM using Expectation-Maximization (EM) algorithms, GMM-HMM can effectively spot abnormal patterns and anomalies in the time series.

The joint probability distribution of the observations and hidden states in GMM-HMM can be represented as:

$$p(X, Z | \theta) = p(z_1 | \pi) \prod_{t=2}^T p(z_t | z_{t-1}, A) \prod_{t=1}^T p(x_t | z_t, \mu, \Sigma) \tag{6}$$

where:

- $X = \{x_1, x_2, \dots, x_T\}$ are the observed data points,
- $Z = \{z_1, z_2, \dots, z_T\}$ are the hidden states,
- θ represents the model parameters,
- π is the initial state probability vector,
- A is the state transition probability matrix,
- μ and Σ are the mean and covariance matrices of the Gaussian components.

Integration of models for early warning system

The dam’s radial deformations (RD206) situated on the right flank, are the target variable while ambient temperature, water level and six variables that represents the water temperatures on the right flank (avg1-R, avg2-R, avg3-R, avg4-R, avg5-R and avg6-R) are the features.

Therefore, let $W(t)$ represent the vector of all features (including RD206) at time t . The Prophet model generates forecasts for all features at time $t+1$ based on historical data to time t , represented as:

$$\widehat{W}(t + 1) = Prophet_Forecast(W(1:t)) \tag{7}$$

where, $\hat{W}(t+1)$ represents the forecasted values of all features at time $t+1$. Given the forecasted values $\hat{W}(t+1)$ for all features at time $t+1$, including RD206, the data is input into the GMM-HMM model for anomaly detection.

Let $Z(t+1)$ represents the hidden states corresponding to the forecasted values $\hat{W}(t+1)$ at time $t+1$. The likelihood of observing forecasted data $\hat{W}(t+1)$ given a learnt GMM-HMM parameters θ can be computed using the forward algorithm:

$$p(\hat{W}(t+1)|\theta) = \sum_z p(\hat{W}(t+1), Z|\theta) \quad (8)$$

θ (Theta) refers to the set of parameters in the machine learning model, specifically in the GMM-HMM framework. These parameters are essential because they determine how the model fits the data. In this context, θ includes:

GMM Parameters: In the Gaussian Mixture Model, θ consists of the weights, means, and covariances of the Gaussian components that describe the distribution of data. These parameters help in modelling the probability distribution of the observed data.

- **Weights (π):** Represent the proportion of each Gaussian component in the mixture.
- **Means (μ):** The centre of each Gaussian component, indicating where the data points are likely to cluster.
- **Covariances (Σ):** Capture the spread and orientation of each Gaussian component, reflecting how much variability there is in different directions.

HMM Parameters: In the Hidden Markov Model, θ also includes parameters that describe the hidden state dynamics:

- **Transition probabilities (A):** The probability of moving from one hidden state to another.
- **Emission probabilities (B):** The probability of observing a particular set of data given the current hidden state.

Anomaly detection is then computed on the probability of observing the forecasted data given the learnt GMM-HMM parameters.

Mahalanobis distance

The Mahalanobis distance was introduced into the GMM-HMM to detect anomalies. The Mahalanobis distance can be used to identify outliers or anomalies by comparing the distance of each data point to the distribution of normal data points. Data points with Mahalanobis distances exceeding a certain threshold are considered anomalies, as they deviate significantly from the expected distribution (Mahalanobis, 1936). The

Mahalanobis distance measures how many standard deviations away a point is from the mean of the distribution along each dimension, considering the correlation between dimensions:

$$D(x, \mu, \Sigma) = \sqrt{(x - \mu)^T \Sigma^{-1} (x - \mu)} \quad (9)$$

where x is the vector of observed values (data point) for which we want to compute the Mahalanobis distance, μ is the mean vector of the distribution of the dataset, it represents the average values of each feature. Σ is the covariance matrix of the distribution of the dataset. It represents the variances and covariances between each pair of features.

RESULTS AND DISCUSSION

Model tuning

The process of tuning the Gaussian Mixture Model - Hidden Markov Model (GMM-HMM) to achieve its optimal performance was primarily done by adjusting the number of components and the Mahalanobis distance threshold. It was observed that the number of components had a considerable influence on the precision of the model but had minimal impact on its recall and F1-score, figure 4. The highest level of precision was achieved when the number of components was set to 5 and 10. On the other hand, adjusting the Mahalanobis distance threshold seemed to have a more profound impact on all the evaluation metrics, figure 5. A higher recall and F1 score were observed at a threshold of 0.1. Following this, the number of components was further adjusted using the values 5 and 10 for more fine-tuning. The best performance was observed when the number of components was set to 10, table 1.

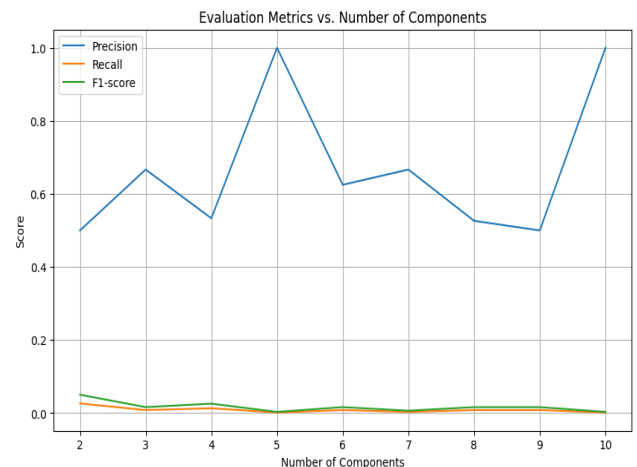


Figure 5. Evaluation Metrics against number of components

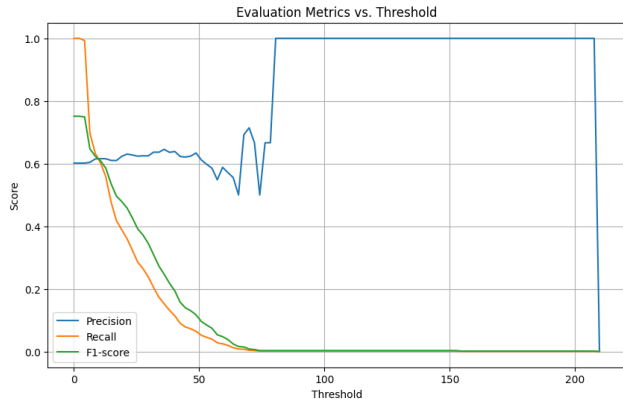


Figure 6. Evaluation metrics against threshold.

Table 1. Best performance.

Evaluation Matrices	Best value
Threshold	0.1
Precision	0.602
Recall	1.0
F-1 Score	0.751

The evaluation matrices in table 1 provided insightful information about the anomaly detection model's performance. Notably, a 0.1 threshold, demonstrating a balanced trade-off between precision and recall. The precision, approximately 0.602, shows that a significant portion of the flagged anomalies were indeed real, highlighting the model's aptitude for identifying true positives. Meanwhile, a recall score of 1.0 indicates the model's exceptional ability to detect all actual anomalies, reducing the chance of missing critical events. The F-1 score of 0.751 confirms the model's overall effectiveness, achieving a balance between precision and recall. This equilibrium is vital in practical applications, where missing anomalies or false alarms can have significant consequences. These optimal outcomes emphasize the model's efficacy in accurately identifying anomalies while maintaining high sensitivity. This boosts confidence in its use for important tasks, such as dam safety management.

Anomaly detection for forecasted radial deformations

The Prophet Model was utilized to generate forecasts under three distinct scenarios, each representing a different possible outcome. These scenarios were the forecasted lower boundary, the forecasted average, and the forecasted higher boundary. Upon careful examination of these predictions, anomalies were identified in only the forecasted upper scenario and the forecasted lower

scenario. These anomalies are represented by black circles within the data visualization. The detected anomalies were discovered to fall within a specific range of radial displacements, specifically, between -0.01 and 0.01, figure 6. This range corresponds to the period when the dam is moving in the downstream direction, figure 7. It's important to note that this downstream movement is a result of the dam filling up. Interestingly, instances of anomalies have only been detected when the water levels within the dam dropped to low levels.

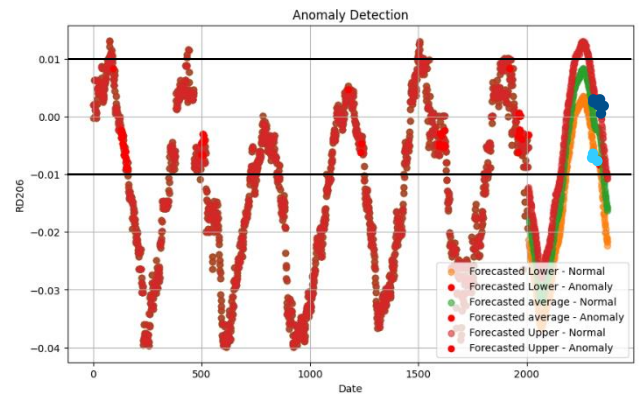


Figure 7. Forecasted anomalies.

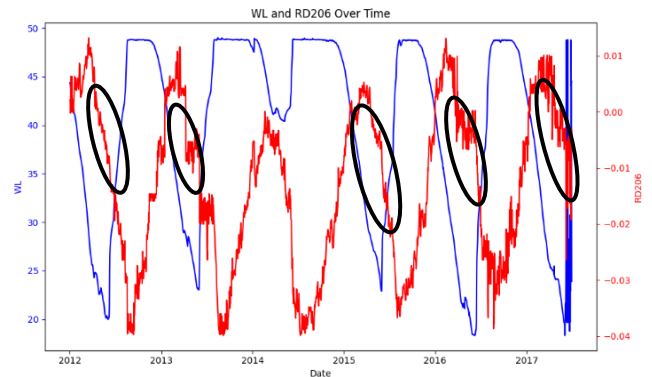


Figure 8. Regions where most anomalies occur.

CONCLUSIONS

The research has made significant strides in the field of dam deformation monitoring by leveraging the Gaussian Mixture Model-Hidden Markov Model (GMM-HMM) framework in tandem with Prophet Forecasting. By integrating the predictive capabilities of Prophet Forecasting, which is renowned for its accuracy in predicting trends, with the anomaly detection strengths of the GMM-HMM, we provided an innovative, robust, and effective solution for real-time detection of deviations from expected deformation patterns. This synergistic

approach holds considerable promise for augmenting the accuracy and reliability of dam deformation monitoring systems, thereby significantly mitigating risks associated with dam failure and ensuring the safety of these critical infrastructures. The results of the evaluation demonstrated promising performance of the integrated framework in anomaly detection for dam deformation data. The precision score of approximately 0.602 indicated a significant proportion of correctly identified anomalies, thereby highlighting the model's effectiveness in distinguishing between normal and anomalous deformation patterns. Furthermore, the recall score of 1.0 reflected the model's exceptional sensitivity and capacity to capture all actual anomalies without missing any true positive instances. In addition to these, the F1-score, which is a harmonic mean of precision and recall, stood at 0.751, affirming the balanced performance of the model in accurately identifying deviations from expected deformation patterns without favouring either recall or precision disproportionately. These evaluation metrics collectively underscore the effectiveness of the integrated GMM-HMM and Prophet Forecasting framework in enhancing early warning systems for dam safety and demonstrate its potential for broader applications in infrastructure monitoring.

DECLARATIONS

Corresponding author

Correspondence and requests for materials should be addressed to Thalasang Tshireletso; E-mail: tshireletsot@ub.ac.bw; ORCID: 0000-0002-5112-8077

Data availability

The datasets used and/or analysed during the current study available from the corresponding author on reasonable request.

Acknowledgements

We would like to acknowledge the Department of Water and Sanitation, South Africa for allowing us to use their dam, Roode Elsberg. This research was funded by Water Research Commission, South Africa under project name Climate change impacts on the safety of dams in South Africa. Project number K5-2749

Authors' contribution

First Author designed the experimental process, performed the experiments, analysed the data obtained and

wrote the manuscript. Second Author revised the manuscript. Both authors read and approved the final manuscript

Competing interests

The authors declare no conflict of interest.

REFERENCES

- Benoit, L., Briole, P., Martin, O., & Thom, C. (2013). Real-time deformation monitoring by a wireless network of low-cost GPS. *Journal of Applied Geodesy*, 7(3), 161-172. <https://doi.org/10.1515/jag-2013-0023>
- Bicego, M., Lovato, P., Rota, B., & Farinelli, A. (2019). Gaussian mixture models for time series clustering: a review. *Pattern Recognition*, 87, 298-314. <https://doi.org/10.1016/j.patcog.2018.10.020>
- Šakić Trogrlić, R., van den Homberg, M., Budimir, M., McQuistan, C., Sneddon, A., & Golding, B. (2022). Early warning systems and their role in disaster risk reduction. In *Towards the "Perfect" Weather Warning: Bridging Disciplinary Gaps through Partnership and Communication* (pp. 11-46). Springer. <https://doi.org/10.1007/978-3-030-98989-7>
- Pang, Z., Jin, Q., Fan, P., Jiang, W., Lv, J., Zhang, P., Cui, X., Zhao, C., & Zhang, Z. (2023). Deformation Monitoring and Analysis of Reservoir Dams Based on SBAS-InSAR Technology—Banqiao Reservoir. *Remote Sensing*, 15(12), 3062. <https://doi.org/10.3390/rs15123062>
- Fraley, C., & Raftery, A. E. (2002). Model-based clustering, discriminant analysis, and density estimation. *Journal of the American Statistical Association*, 97(458), 611-631. <https://doi.org/10.1198/016214502760047131>
- Coraça, E. M., Ferreira, J. V., & Nóbrega, E. G. O. (2022). An unsupervised structural health monitoring framework based on Variational Autoencoders and Hidden Markov Models. *Reliability Engineering & System Safety*, 227, 109025. <https://doi.org/10.1016/j.res.2022.109025>
- Mahalanobis, P. C. (1936). On the generalised distance in statistics. *Proceedings of the National Institute of Sciences of India*, 12(1), 49-55. [Google Scholar](https://scholar.google.com/)
- Rong, Z., Pang, R., Xu, B., & Zhou, Y. (2024). Dam safety monitoring data anomaly recognition using multiple-point model with local outlier factor. *Automation in Construction*, 151, 105290. <https://doi.org/10.1016/j.autcon.2024.105290>
- Hassani, H., Rua, A., Sirimal Silva, E., & Thomakos, D. (2019). Monthly forecasting of GDP with mixed-frequency multivariate singular spectrum analysis. *International Journal of Forecasting*, 35(3), 821-830. <https://doi.org/10.1016/j.ijforecast.2019.03.021>
- Taylor, S. J., & Letham, B. (2018). Forecasting at scale. *The American Statistician*, 72(1), 37-45. <https://doi.org/10.1080/00031305.2017.1380080>
- Bahrami, O., Wang, W., & Lynch, J.P. (2021). Hidden Markov models for sequential damage detection of bridges. In *Bridge Maintenance, Safety, Management, Life-Cycle*

Sustainability and Innovations (1st ed., pp. 7). CRC Press.
eBook ISBN: 9780429279119.
<https://www.taylorfrancis.com/chapters/edit/10.1201/9780>

[429279119-209/hidden-markov-models-sequential-damage-detection-bridges-bahrami-wang-lynch](https://doi.org/10.1201/9780429279119-hidden-markov-models-sequential-damage-detection-bridges-bahrami-wang-lynch)

Publisher's note: [Scienceline Publication](#) Ltd. remains neutral with regard to jurisdictional claims in published maps and institutional affiliations.



Open Access: This article is licensed under a Creative Commons Attribution 4.0 International License, which permits use, sharing, adaptation, distribution and reproduction in any medium or format, as long as you give appropriate credit to the original author(s) and the source, provide a link to the Creative Commons licence, and indicate if changes were made. The images or other third party material in this article are included in the article's Creative Commons licence, unless indicated otherwise in a credit line to the material. If material is not included in the article's Creative Commons licence and your intended use is not permitted by statutory regulation or exceeds the permitted use, you will need to obtain permission directly from the copyright holder. To view a copy of this licence, visit <https://creativecommons.org/licenses/by/4.0/>.

© The Author(s) 2024

Navigating Climate Change: A Review of Policies in Botswana, Africa, and Beyond

Mmoloki Makoba¹ , Tshenolo Laron Chaba² , and Question Jaden Ramontsho³ 

¹Civil engineering, University of Botswana, Private Bag UB 0022, Gaborone, Botswana

²Mineral Resource Department, School of Earth Sciences and Engineering, Botswana International University of Science and Technology, Private Bag 16, Palapye, Botswana

³Department of Social Sciences & Humanities - Economics and History, University of Michigan, 303 E Kearsley Street:245 University Pavilion, Flint, USA

^{*}Corresponding author's Email: makobam@ub.ac.bw

ABSTRACT

This paper is an insightful perspective analysis of Botswana climate change policies in an effort to establish their effectiveness in relation to regional and international initiatives. For a critical review of both mitigation and adaptation efforts by different countries, the effectiveness is analysed, including their strengths and inadequacies noted, and recommendations made towards enhancing policy coherence and effectiveness. It examines the steps Botswana and other countries have taken to cut greenhouse gas emissions, improve energy efficiency, support the use of renewable energy sources, and implement sustainable land management practices. The paper also delves into Botswana's efforts to build climate resilience, such as creating a National Adaptation Plan and incorporating climate considerations across various sectors.

Keywords: Climate change policies, Policy review, International agreements, Sustainable development, Botswana

INTRODUCTION

Botswana, a landlocked country located in the southern part of Africa, faces significant challenges because of climate change, predominantly rising temperatures, which has a negative effect on the environment, economy, and people of this country (World Bank, 2010). Recognizing the need to solve this matter, Botswana has implemented various policies and strategies to mitigate effects of climate change and enhance resilience in sectors like agriculture (Boyd, 2023). These initiatives are very crucial to Botswana as well as in Africa and at global scales. Encompassing the climate policies of Botswana at regional and global frameworks is vitally important in fostering teamwork and strengthening the global response to climate change.

Botswana's strategies and programmes implemented to combat climate change stretch outside regional considerations to reverberate with inclusion in global climate agendas (Koboto et al., 2012). Participating in international platforms such as the United Nations Framework Convention on Climate Change (UNFCCC), with nations around the world, is one approach which this country is active in shaping and forging negotiations and action for climate. The involvement of Botswana can only highlight its dedication to the global urgency of combating climate change, which will need coordinated actions and collective accountability on a worldwide scale.

Understanding Botswana's climate change plans and their alignment with regional and international frameworks is needed for comprehending the country's contributions to climate action. Exploring the experiences of Botswana, their challenges and success towards climate change policy implementation might give important lessons to other African countries as well as the global community. Scrutinizing the relationship between Botswana's policies and other nations' can help foster cooperation which will fortify the response of the world's community towards climate change at both regional and global levels. Botswana's climate policies reflect its commitment to addressing the effects of climate change within Africa and on an international scale (Koboto et al., 2012). By emphasizing both mitigation and adaptation tactics, Botswana aims to support resilient and sustainable regional development in order to achieve the world's climate objectives.

METHODOLOGY

This study uses a qualitative methodology, utilizing an extensive and comprehensive analysis of climate change policy including a look at their origins, effects, and policies, adaptation techniques, and mitigation plans. A desktop investigation was carried out to compile relevant information about climate policy in Botswana, Africa, and

REVIEW
 PII: S225204302400023-14
 Received: June 25, 2024
 Revised: September 02, 2024
 Accepted: September 05, 2024

other relevant sources worldwide. The goal of this research was to give a thorough grasp of climate policy globally, awareness that the impacts of climate change cut beyond national borders and influence every region of the earth.

CLIMATE CHANGE POLICIES

Overview of Botswana's Climate

Climate exerts a critical influence on human well-being and socio-economic activities, profoundly affecting health, agriculture, and overall livelihoods (UNDP, 2018; Mugari et al., 2020). Botswana's climate vulnerability is relatively correlated to its extreme water scarcity (Crawford, 2016) with five key sectors that stand out as particularly susceptible: water resources, public health, agricultural yields, grassland ecosystems, and forestry. Botswana's climate is semi-arid (Batisani and Yarnal, 2010; Kenabatho et al., 2012; Crawford, 2016; Botswana, 2019; World Bank Group, 2021; Omari Motsumi et al., 2023) which is defined by high temperatures and low unreliable rainfall. There are distinct dry and wet seasons throughout the nation, with variations throughout several districts. The scorching months of May through October are known as the dry season. The daytime highs routinely rise above 30°C and, in some places, even reach above 40°C accompanied by low levels of humidity. Conversely, the rainy season, prevailing from the month of November until April, offers relief with cooler temperatures and occasional rainfall, typically ranging from 250 mm to 650 mm (BES, 2019), the national average annual rainfall stands at 450 mm.

Climate Change Policies: Botswana

Studies carried out by different government agencies and experts in the field (Abucar and Molutsi, 1993; JNS, 1994; Dube and Sekhwela, 2007; The World Bank, 2010; Hambira and Saarinen, 2015; Juana et al., 2016; UNDP, 2017; Spear et al., 2018; Madebwe, 2019; Mugari, Masundire and Bolaane, 2020; Batisani et al., 2021) underscores Botswana's elevated susceptibility to changes in the climate. This susceptibility encompasses significant economic factors and is expected to increase in the absence of efficient adaptation and mitigation strategies. In spite of this, Climate change is not now a top national priority for the government. This absence of prioritization has led to, lack of utilization of climate change policy, legislation, and strategy to solve the effects. Still, the possibility of future climate change and the related environmental risks are recognised in the Plan for National

Development 10 (Government, 2022). A few industries from the highly affected sectors; gender, agriculture, water, health and energy, have adopted strategies for climate adaptation and mitigating measures, such as government backing for solar energy systems in the energy industry (Fabre and Magombo, 2009; Crawford, 2016; Botswana, 2019; World Bank Group, 2021). Climate policy is essential for guiding response efforts to reduce or mitigate the consequences of changing climate (Ayers, Huq and Westminster, 2008; UNESCO, 2023). A lot of industrialized nations are currently developing broad programmes to combat climate change (Crawford, 2016; OECD, 2018; World Bank Group, 2021; Bhattacharya, Kharas and McArthur, 2023).

Nevertheless, as per Hambura and Saarinen (2015), they have not yet made them sector specific. In contrast, as one of the developing nations, Botswana has outperformed other nations. The nation of Botswana acknowledged the necessity of addressing climate change and has made a number of efforts to create and put climate policy into action. In order to increase resilience to climate change, climate policy is required by encouraging low-emission climate practices and incorporating climate change concerns into different industries. The nation's commitment to addressing the challenges caused by climate change does not begin today. International protocols or environmental as table 1 indicates Botswana as a signatory at world level while Table 2 indicates the local policies adopted over the years.

In light of the information in Table 3, inferences on the suitability of the climate policies were successful or not. The forestry and land-use change major negative value emissions (Net Carbon Sink: -42,941 Gg CO₂ eq) show that the land-use policies of Botswana are taking up more carbon than they are releasing. This implies effective laws or procedures for helping to sequester carbon in forest conservation, afforestation, or replanting projects and mitigating climate change. Additionally, the data show that the nation is still generating GHS from the sectors of trash, agriculture, and energy. This is due to the nation's heavy reliance on fossil fuels energy and lack of basic understanding of waste management and sustainable agriculture managerial techniques. The GHG emissions are increasing with time also because of an increase in the future energy demand (UNDP, 2021). It is clear that in order to combat this, the government has put in place policies (Table 2) that encourage the use of renewable energy, energy-saving techniques, and lowering dependence on fuels high in carbon and adoption of sustainable farming methods, waste measures for recycling

and management. Although substantial, the 7,434.223 Gg CO₂ eq total emissions are only largely and partially countered by the significant negative value of emissions from forestry and changes in land use, producing a -35,506.777 Gg CO₂ eq in total. This indicates that, all things considered, Botswana is serving as a carbon sink which is a good result in the framework of international efforts to tackle climate change prolonged efforts to improve mitigation strategies and climate change legislation across a range of industries can help increase Botswana's resistance to climate change and its part in the global climate movement.

In 2014, Botswana initiated a thorough climate change policy drafted by a team led by Dr. Oduetse Koboto, a consultant from the United Nations Development Programme (UNDP), cooperated with members from UNDP and the Ministry of Environment, Wildlife, and Tourism (MEWT) (UNDP, 2017). The policy prioritises adaptation amongst different sectors, including agriculture, water, human health, biodiversity, ecosystems, forest management, reducing risks, mitigation, sustainable energy, transport emissions, and waste management. It advocates for integrated strategies such as Climate SMART Agriculture, sustainable water management, studies on climate change's health impacts, biodiversity conservation, forest rehabilitation, risk mitigation plans, mandatory mitigation plans, introduction of carbon budgets and markets, investment in green technologies, reforms in transportation, and integrated waste management practices. These measures aim to enhance Botswana's resilience on climate change, mitigate greenhouse gas emissions, and enhance sustainable development across multiple sectors.

Climate Change Policies: Africa

Africa, which is the continent most vulnerable to climate change, has called urgently for actions to support the effort to arrest this major global challenge, despite the

continent's lesser contribution (UNEP, 2023). The major share of CO₂ emissions in the energy field comes from the combustion of fossil fuels either for power generation or to fuel vehicles and machines (EIA, 2023). Another notable source is the carbon-intensive cement industry which represents a consistent case of source composition; several nations are grappling with such problems in the face of specific policies. In South Africa, for example, the carbon tax policy provides for industrial emissions, including those emanating from cement production; the policy envisions the uptake of cleaner technologies and practices (South African Revenue Service, 2023).

Botswana's Frameworks pertaining to climate have as a result undergone change while adhering strictly to this regional promise to strengthen climate resilience, support sustainable development, and safeguard ecosystems, people, and wildlife in Botswana. This will be done in an effort to make sure it can meaningfully participate in the group effort to mitigate the negative effects of climate change and that these are codified in robust climate policies that are subject to compliance with those established within the Sustainable Development Goals and Agenda 2063 of the African Union.

Climate Change Policies: Global Context

Countries have established international policies to guide their efforts in mitigating climate change, building capacity, and promoting sustainability. Cement production is a significant focus in these policies due to its high CO₂ emissions. For instance, the European Union's Emissions Trading System (ETS) includes cement manufacturers, incentivizing reductions in emissions through market mechanisms (European Commission, 2024). Similarly, China has introduced stringent emission standards and promotes the use of alternative materials in cement production to reduce its carbon footprint.

Table 1. Showing the Environmental conventions where Botswana was once a signatory. Adapted from (The World Bank, 2010)

Convention	Ratification date
The Vienna Convention for the protection of preservation of the Ozone layer	04/12/1991
The Protocol on Montreal on the Substances that deplete the Ozone layer	4/12/1991
The London Amendment to the Montreal Protocol	13/5/1997
The Copenhagen Modification to the Montreal Protocol	13/5/1997
The United Nations Framework Convention on Climate Change (UNFCCC)	27/4/1994
Kyoto Agreement	7/8/ 2003

Table 2. Botswana Climate Policies with years of adoption (World Bank Group, 2021).

Policy/ Adoption year	Policy explanation
National Climate Change Policy (energy policy draft) 2014	Outlines measures for both adaptation and mitigation adaptation, focusing on sectors like energy, agriculture, water, health, and risk mitigation.
National Adaptation Plan (NAP) Framework Policy 2020	Identifies priority areas for action, including sustainable water use, agriculture, health, and disaster risk reduction
Climate-Smart Agriculture (CSA) Initiatives 2020	Initiatives that integrate climate adaptation and mitigation measures into agricultural practices and policies.
Climate Change Strategy and Action Plan 2018	Strategies to enhance resilience and reduce vulnerability to climate-related hazards such as floods, droughts, and storms.
Botswana Climate Change Response Policy (BCCRP) 2016	Strategies to enhance resilience and reduce vulnerability to climate-related hazards such as floods, droughts, and storms.

Table 3. Showing the Greenhouse gas (GHG) inventory of Botswana for 2000 (MEWT, 2009).

Industry	Emissions Gg CO ₂ eq	Sink Gg CO ₂ eq
Energy	5 537.9	-
Agriculture	1 785	-
Waste	111.3	-
Land-use change and forestry	-	- 42 941
Total emissions	7 434.2	-
Net Total (after subtracting sink)	- 35 506.8	-

Table 4. African Climate Change Policies with years they were adopted. (CAADP 2013, SADC 2003, AREI 2015, African Union Framework on Climate Change 2014, ARC 2012)

Policy	Year it was adopted	Signatory countries
Comprehensive Africa Agriculture Development Program (CAADP) - African Union	Adopted at the African Union Assembly in 2013.	All 55 African Union member states
Southern African Development Community (SADC) Regional Agricultural Policy	Adopted in 2003	All 16 SADC member states
African Union's Africa Renewable Energy Initiative (AREI)	Launched at the United Nations Climate Change Conference (COP21) in Paris in 2015, with the endorsement of African heads of state and governments.	50 countries
African Union's Continental Framework on Climate Change	Adopted in 2014	All 55 AU member states
African Risk Capacity (ARC)	Established in 2012 and has since provided climate risk insurance to several African countries.	34 African States
African Union's African Adaptation Initiative (AAI)	Adopted at COP21 in Paris in 2015	54 African states
SADC Climate Change Strategy and Action Plan	Adopted by the Southern African Development Community (SADC) in 2015	All SADC member states
ECOWAS Climate Change Policy	Adopted by ECOWAS Authority of Heads of State and Government in 2013	15 ECOWAS member States
ECOWAS Renewable Energy Policy	Adopted by the ECOWAS Authority of Heads of State and Government in 2013	15 ECOWAS member states

Table 5: Key Global Climate Change Policies and Years Adopted (UNFCCC Annual Report, 2022). The table below outlines 5 critical global policies that form the foundation climate change policies, including their years of adoption and the number of signatory countries out of a total of 197.

Policy	Year of adoption	No of signed countries/parties
Kyoto Protocol	1997	192
Paris Agreement	2015	196
Montreal Protocol	1987	197
Copenhagen Accord	2009	140
Glasgow Climate Pact	2021	197

ANALYSIS OF CLIMATE CHANGE POLICIES

Botswana

Botswana's current solar energy policies aim to adapt and mitigate climate change impacts. The policies focus on various sectors including energy, agriculture, water resources, health, and disaster risk reduction. Botswana has committed to reducing its reliance on coal-generated energy, which currently accounts for 80% of its overall demand. The country plans to reach 25% of total energy consumption from renewable sources by 2030. Additionally, Botswana is exploring opportunities in the gas industry to provide clean thermal energy solutions. The launch of Solar PV IPP Projects (235 MW), particularly the Mmadinare and Jwaneng solar plants, is a significant step towards achieving these goals and these projects are projected to produce 100 MW of energy each by 2025. Botswana has also made strides in agriculture through the Climate-Smart Agriculture (CSA) Initiatives policy. Particularly to improve genetic features of the livestock breeds such as the Musi breed which took genetic upgrades of 7 varieties to make it tolerate drought conditions. Another success was to use genes of crops with the mentioned traits: drought resistance; tolerance to extreme temperatures; early maturity to produce a local Kalahari early Pearl, Kanye Standard and 65D hybrid seeds (African Development Bank, 2023).

In its latest move to tackle climate change, Botswana has made a framework for the National Adaptation plan which will help in building the nation's adaptive capacity and resilience and facilitate the integration of climate change adaptation into relevant policies. It addresses the medium and long-term adaptation needs. It also stipulates the approaches and guiding principles to be used. It further provides direction in the coordination, implementation and resource mobilization of the NAP process. I urge all relevant sectors and actors to use this Framework as a guide in pursuing climate change adaptation planning.

Africa

Africa has developed climate change-specific policies tailored to its member states, aiming to mitigate the continent's vulnerability to climate change impacts, transition to cleaner energy alternatives, and modernize agricultural practices for enhanced productivity. One such initiative is the African Renewable Energy Initiative (AREI), which was embraced by numerous countries in 2015. AREI seeks to promote renewable energy adoption throughout Africa to improve energy accessibility,

security, and climate change mitigation efforts. Kenya stands out as a commendable example in implementing AREI. The country has substantially expanded its renewable energy capacity, with geothermal and wind sources contributing to over 70 percent of its electricity generation. This shift has not only reduced reliance on fossil fuels but also improved energy access and facilitated greenhouse gas emissions reduction. Kenya aims to achieve 100 percent renewable power by 2030 and to foster green industries by 2040, as per the International Renewable Energy Agency (IRENA).

With renewables constituting nearly 90 percent of energy generated and consumed in 2021, Kenya emerges as a frontrunner in Africa's clean energy transition, according to the International Energy Agency (IEA). Additionally, Kenya has made significant strides in attaining universal electricity access, doubling access from 32 percent in 2013 to 75 percent in 2022, thereby transitioning away from biofuels for energy use. Kenya also has the Climate Change Act, enacted in 2016 to provide a regulatory framework for enhanced response to climate change, including mitigation efforts in industrial sectors (Wambua, 2019). The act emphasizes the importance of adopting sustainable practices and technologies in heavy industries like cement manufacturing. South Africa is another country making efforts to reduce emissions. Implemented in 2019, South Africa's Carbon Tax Act imposes a tax on greenhouse gas emissions from various sectors, including cement. This policy aims to encourage industries to adopt cleaner technologies and reduce their carbon footprint. The tax rate started at R120 (approximately \$8) per ton of CO₂-eq, with allowances and exemptions to help industries transition (Loewald, 2024).

Another significant regional initiative is the Comprehensive Africa Agriculture Development Programme (CAADP), which aims to achieve an annual agricultural growth rate of at least 6 percent and allocate a minimum of 10 percent of national budgets to agriculture among participating countries.

Global scale

The cement industry and fossil fuels are one of the largest contributors to global carbon dioxide emissions, with the cement industry accounting for approximately 7-8% of total emissions (Andrew, 2018). The production process is highly energy-intensive and relies heavily on fossil fuels, which releases a significant amount of CO₂. The demand for cement is growing due to rapid

urbanization and infrastructure development, exacerbating the environmental impact.

Countries have established international policies to guide their efforts in reducing emissions and mitigating climate change, building capacity, and promoting sustainability. The European Union Emissions Trading System (EU ETS) is a cornerstone of the EU's policy to combat climate change (European Commission, 2024). It is the world's first major carbon market and remains the largest one. The system caps the total level of greenhouse gas emissions from installations covered by the system and reduces the cap over time. Cement producers must hold allowances for their emissions, incentivizing the reduction of CO₂ output through efficiency improvements and technological innovation. Another prominent policy is the Global Economic Policy for Renewable Energy Promotion, which has been embraced by numerous nations, shaping their domestic frameworks accordingly. For instance, Germany's *Energiewende* (Energy Transition) Policy, initiated in 2010, aimed to significantly increase renewable energy generation, with a target for renewables to constitute over 40% of electricity production by 2020. Remarkably, Germany not only achieved this goal but also reduced greenhouse gas emissions by over 35% compared to 1990 levels, as reported by the World Economic Forum Energy Transition 2023 report. The policy has stimulated investments in renewable energy infrastructure, fostering job creation and economic growth.

Denmark, having adopted renewable energy policies since the 1970s, ratified the Global Economic Policy for Renewable Energy Promotion, leveraging initiatives such as feed-in tariffs and wind power promotion. Consequently, Denmark has emerged as a global leader in wind energy, with wind power playing a substantial role in its electricity generation. The country remains committed to research and development to further advance renewable energy technologies. In the United States, the adoption of the Global Economic Policy for Renewable Energy Promotion led to the establishment of Renewable Portfolio Standards (RPS) policies, mandating a specific percentage of electricity generation from renewable sources. Many states have made significant strides in increasing renewable energy capacity since implementing RPS policies, with renewables contributing nearly 20% of total electricity generation in the US as of 2020, according to the U.S. Energy Information Administration (EIA). However, challenges persist in achieving more ambitious renewable energy objectives, including policy uncertainties and infrastructure constraints.

Furthermore, the Paris Agreement has been embraced globally, serving as a foundation for countries to develop their policy frameworks, including agriculture-related measures in their Nationally Determined Contributions (NDCs) to mitigate greenhouse gas emissions and bolster resilience to climate change in the agricultural sector. Brazil, for instance, has committed to reducing greenhouse gas emissions by 37% by 2025 and over 53.1% of emissions from deforestation by 2030 under the Paris Agreement, implementing policies to combat deforestation in the Amazon rainforest and promote sustainable land use practices.

Similarly, China has set ambitious targets within its Paris Agreement commitments, aiming for CO₂ emissions to peak before 2030 and achieving carbon neutrality by 2060. The country has implemented various measures in the agricultural sector to address emissions, including improving soil health, increasing the use of organic fertilizers, and reducing methane emissions from rice cultivation and livestock farming. China has also expanded its low-carbon initiatives, with numerous pilot cities, industrial parks, and communities dedicated to reducing carbon emissions. Additionally, advancements in farming practices, such as selecting heat, drought, and low-light-resistant crop varieties, coupled with expanded irrigation areas, demonstrate China's commitment to mitigating climate change impacts in agriculture.

CONCLUSION

Analysing national, regional, and international climate change policies demonstrates that nations are realising more and more how important it is to combat climate change through policy interventions. For instance, Botswana has made impressive strides towards switching to renewable energy sources, namely solar energy. Implementing climate-smart agricultural activities to increase resilience and sustainability. The creation of the National Adaptation Plan framework represents a proactive approach to developing adaptive capability and incorporating climate change adaptation into relevant policies. Similarly, in Africa, measures such as the African Renewable Energy Initiative and the Comprehensive Africa Agriculture Development Programme highlight the continent's commitment to transitioning to cleaner energy sources and boosting sustainable agriculture. Globally, initiatives such as the Global Economic Policy for Renewable Energy Promotion and the Paris Agreement highlight countries' combined efforts to reduce greenhouse gas emissions and strengthen resilience to climate change.

However, problems remain, including the need for improved policy implementation, resource mobilisation, and international cooperation to meet ambitious climate targets.

To effectively address the climate issue, governments must prioritise taking action on climate change, make investments in infrastructure for renewable energy, encourage sustainable behaviour, and form international coalitions. To capitalise on past successes and accelerate climate action, local authorities should prioritise putting climate change legislation into effect and maintaining strong regional and international cooperation. The following suggestions are recommended in order to help strengthen climate change legislation to achieve climate goals:

To enhance the implementation of existing climate policies, authorities should put first their successful execution plans, checking that they align with national development priorities and allocate adequate resources for this purpose. Including knowledge-sharing and capacity-building seminars and activities in the plan is also of great importance in improving technical competency and increase climate change awareness among local residents, policymakers, and stakeholders.

Strengthen International Cooperation: Countries should strengthen their regional and international frameworks for collaboration and knowledge-sharing in order to optimize on best practices, generate capital, and transfer technology for climate action. Governments should accelerate the transition to renewable energy sources through policy incentives, investment frameworks, and regulatory reforms in order to reduce reliance on fossil fuels and reduce greenhouse gas emissions. **Promote Sustainable Agriculture:** Agricultural policy should prioritise sustainable practices, soil conservation, agroforestry, and climate-smart technology to improve resilience, food security, and rural livelihoods while reducing agricultural emissions.

Invest in Climate Resilience: To ensure resilience to the effects of climate change, governments should prioritise investments in climate resilience infrastructure, early warning systems, risk mitigation strategies, and community-based adaptation projects.

DECLARATIONS

Corresponding Author

Correspondence and requests for materials should be addressed to Mmoloki Makoba, PhD; E-mail: makobam@ub.ac.bw; ORCID: 0009-0000-3021-2109

Data availability

The datasets used and/or analyzed during the current study available from the corresponding author on reasonable request.

Acknowledgements

The authors express their appreciation and special thanks to Ms. Boitumelo Marumo, a member of the Botswana Climate Change Network, for her valuable contribution in sharing her expertise on Botswana's climate change and relevant literature essential for this paper.

Authors' contribution

Dr. Mmoloki Makoba, Ms. Tshenolo Larona Chaba, and Mr. Question Jaden Ramontsho collaborated in gathering and examining literature for this paper. Furthermore, Dr Mmoloki Makoba undertook the task of composing the abstract, introduction and contributed valuable feedback and revisions during the writing stages. Tshenolo L Chaba authored the sections on Overview of Botswana's climate, Climate Policies in Botswana, conclusion, recommendation, and analyzed Botswana's policies. Meanwhile, Question J Ramontsho composed the sections on Africa and Global policies and conducted the evaluation of African and Global Policies.

Competing interests

The authors declare no competing interests in this research and publication.

REFERENCES

- Abucar, M. H., Molutsi, P. (1993). Environmental policy in Botswana: A critique. *Africa Today*, 40(1): 61–73. Available at: <https://www.jstor.org/stable/4186888>
- Andrew, R. M. (2018). Global CO₂ emissions from cement production. *Earth System Science Data*, 10(1): 195–217. DOI: <https://doi.org/10.5194/essd-10-195-2018>
- Ayers, J. M., Huq, S., Westminster, L. (2008). Supporting adaptation to climate change: What role for official development assistance? *Development Studies Association Annual Conference 2008: Development's Invisible Hands: Development Futures in a Changing Climate*, 27(6): 675–692. DOI: <https://doi.org/10.1111/j.1467-7679.2009.00465.x>
- Batisani, N., et al. (2021). Retooling smallholder farming systems for climate change resilience across Botswana arid zones. *African Handbook of Climate Change Adaptation*, 339–362. DOI: https://doi.org/10.1007/978-3-030-45106-6_168
- Batisani, N., Yarnal, B. (2010). Rainfall variability and trends in semi-arid Botswana: Implications for climate change

- adaptation policy. *Applied Geography*, 30(4): 483–489. DOI: <https://doi.org/10.1016/j.apgeog.2009.10.007>
- Bhattacharya, A., Kharas, H., McArthur, J. W. (2023). Developing countries are key to climate action. Brookings Institution, United States of America. Available at: <https://coilink.org/20.500.12592/q9qzc8>
- Botswana Environment Statistics (2019). Botswana Environment Statistics-Climate Digest. Statistics Botswana, Gaborone, Botswana. March: 1–21.
- Boyd, D. R. (2023). Statement at the conclusion of country visit to Botswana: United Nations Special Rapporteur on Human Rights and the Environment.
- Crawford, A. (2016). Review of current and planned adaptation action in Botswana. Available at: <https://www.iisd.org/system/files/publications/idl-55863-botswana.pdf>
- Dube, O. P., Sekhwela, M. B. M. (2007). Community coping strategies in semiarid Limpopo Basin part of Botswana: Enhancing adaptation capacity to climate change. DOI: <https://doi.org/10.13140/RG.2.1.5138.3449>
- Economic Commission for Africa (2011). Fossil fuels in Africa in the context of a carbon constrained future. United Nations Economic Commission for Africa African Climate Policy Centre. Available at: <http://www.uneca.org/acpc/>
- European Commission (2024). ETS2: Buildings, road transport and additional sectors. Available at: https://climate.ec.europa.eu/eu-action/eu-emissions-trading-system-eu-ets/ets2-buildings-road-transport-and-additional-sectors_en
- Fabre, J., Magombo, G. (2009). National Energy Policy Strategy Implementation Plan. USAID/Southern Africa, Gaborone, Botswana. Available at: https://pdf.usaid.gov/pdf_docs/pnadu851.pdf
- Government of Botswana (2019). Botswana’s first biennial update report to the United Nations Framework Convention on Climate Change. October 2019. Available at: <https://unfccc.int/documents/201214>
- Government of Botswana (2022). Botswana adaptation initiatives. Republic of Botswana. Available at: <https://napexpo.org/2022/wp-content/uploads/2022/08/Botswana-adaptation-initiatives.pdf>
- Hambira, W. L., Saarinen, J. (2015). Policymakers’ perceptions of the tourism–climate change nexus: Policy needs and constraints in Botswana. *Development Southern Africa*, 32(3): 350–362. DOI: <https://doi.org/10.1080/0376835X.2015.1010716>
- Jns, M. (1994). The Botswana government’s environmental policies and the need to institutionalize lifelong environmental education. Available at: <https://files.eric.ed.gov/fulltext/ED384525.pdf>
- Juana, J., et al. (2016). Climate change perceptions and adaptations for livestock farmers in Botswana. *International Journal of Economic Issues*, 9(1): 1–21. Available at: <https://www.researchgate.net/publication/307931501>
- Kenabatho, P. K., Parida, B. P., Moalafhi, D. B. (2012). The value of large-scale climate variables in climate change assessment: The case of Botswana’s rainfall. *Physics and Chemistry of the Earth*, 50–52: 64–71. DOI: <https://doi.org/10.1016/j.pce.2012.08.006>
- Koboto, O., et al. (2012). Botswana climate change response policy. Available at: [https://info.undp.org/docs/pdc/Documents/BWA/DRAFT%20CLIMATE%20CHANGE%20RESPONSE%20POLICY%20%20version%20%20\(2\).doc](https://info.undp.org/docs/pdc/Documents/BWA/DRAFT%20CLIMATE%20CHANGE%20RESPONSE%20POLICY%20%20version%20%20(2).doc)
- Loewald, C. (2024). Carbon taxation in South Africa and the risks of carbon border adjustment mechanisms. South African Reserve Bank, April 25. Available at: <http://www.resbank.co.za>
- Madebwe, T. (2019). Enhancing Botswana’s environmental performance by 2023. *Law, Environment and Development Journal*, 15(1): 62–70. DOI: <https://doi.org/10.25501/SOAS.00033082>
- Motsumi, K. O., Ziervogel, G., New, M. (2023). Drought governance: A cross-level governance analysis in Botswana. *Climate Risk Management*, 42: 100557. DOI: <https://doi.org/10.1016/j.crm.2023.100557>
- Mugari, E., Masundire, H., Bolaane, M. (2020). Adapting to climate change in semi-arid rural areas: A case of the Limpopo basin part of Botswana. *Sustainability*, 12(20): 8292. DOI: <https://doi.org/10.3390/su12208292>
- OECD/The World Bank/UN Environment (2018). Financing climate futures: Rethinking infrastructure. OECD Publishing. DOI: <https://doi.org/10.1787/9789264308114-en>
- Spear, D., et al. (2018). Vulnerability and adaptation to climate change in the semi-arid regions of Southern Africa. Available at: <http://www.uct.ac.za/>
- South African Revenue Service (SARS) (2022). Carbon tax. Available at: <https://www.sars.gov.za/customs-and-excise/excise/environmental-levy-products/carbon-tax/>
- U.S. Energy Information Administration (EIA) (2023). Where greenhouse gases come from. Available at: <https://www.eia.gov/energyexplained/energy-and-the-environment/where-greenhouse-gases-come-from.php>
- UNDP (2017). Botswana climate change response policy draft version 2. Available at: https://www.undp.org/sites/g/files/zskgke326/files/2022-06/CPD_BWA_-_%20Final%20Approved%20EXB.pdf
- UNDP (2018). Final strategy: A national climate change strategy for Botswana. Available at: <https://drmime.sadc.int/>
- UNDP (2021). The Botswana climate change policy. Ministry of Environment, Natural Resources Conservation and Tourism. Available at: <https://faolex.fao.org/docs/pdf/bot229878.pdf>
- UNEP (2021). Responding to climate change: Regional initiatives. Available at: <https://www.unep.org/regions/africa/regional-initiatives/responding-climate-change>
- UNESCO (2023). Updated policy document on climate action for World Heritage. Available at: <https://whc.unesco.org/archive/2023/whc23-24ga-INF8-en.pdf>
- Wambua, C. (2019). The Kenya Climate Change Act 2016: Emerging lessons from a pioneer law. *Carbon & Climate Law Review*, 13(4): 257–269. Available at: <https://www.jstor.org/stable/26895682>

World Bank (2010). Botswana climate variability and change: Understanding the risks draft policy note. Available at: <https://www.car.org.bw/wp-content/uploads/2016/06/Botswana-Climate-Change-Policy-Note.pdf>

World Bank (2010). Botswana: Enhancing environmental sustainability in the implementation of the NDP10 draft

policy note. Available at: <https://www.car.org.bw/wp-content/uploads/2016/06/Botswana-Environment-Policy-Note-October2010-final.pdf>

World Bank Group (2021). Climate risk country profile: Botswana. Available at: <https://www.worldbank.org/>

Publisher's note: [Scienceline Publication](#) Ltd. remains neutral with regard to jurisdictional claims in published maps and institutional affiliations.



Open Access: This article is licensed under a Creative Commons Attribution 4.0 International License, which permits use, sharing, adaptation, distribution and reproduction in any medium or format, as long as you give appropriate credit to the original author(s) and the source, provide a link to the Creative Commons licence, and indicate if changes were made. The images or other third party material in this article are included in the article's Creative Commons licence, unless indicated otherwise in a credit line to the material. If material is not included in the article's Creative Commons licence and your intended use is not permitted by statutory regulation or exceeds the permitted use, you will need to obtain permission directly from the copyright holder. To view a copy of this licence, visit <https://creativecommons.org/licenses/by/4.0/>.

© The Author(s) 2024

Flexible Vegetation Behavior under Varying Areal Densities and Effects on Flow Structures: Numerical Observations

Afis O. Busari¹  and Kelvin A. John² 

¹Department of Civil and Mining Engineering, University of Namibia, JEDS Campus, Ongwediva 15006, Namibia

²Department of Civil Engineering, University of Abuja, Federal Capital Territory, Abuja 00234, Nigeria

✉ Corresponding author's Email: abusari@unam.na

ABSTRACT

This study carried out extensive numerical studies on a refined “One dimensional (1-D) Reynolds Averaging Navier-Stokes (RANS) Model” for vegetated open channel flow. In the 1-D RANS model, the Spalart Allmaras closure model was used to model the turbulence caused by eddies within the vegetation zone and the interface between the top of the vegetation and the clear water zone. In this work, numerical simulations using 1-D RANS model are carried out using dataset obtained from the laboratory under different hydraulic conditions of varying areal vegetation densities. Three classes of highly flexible vegetation densities were simulated: low, medium and highly dense vegetation. The model predictions in terms of mean vertical stream-wise velocity profile and Reynolds Shear Stresses were compared with the laboratory flume experimental results. The 1-D RANS model performances were satisfactory for low and medium densities. However, discrepancies were seen in the model prediction for highly dense vegetation. Hence, the hydraulic roughness parameters in the numerical model has been modified for model re-calibration to capture the position of zero-displacement of velocities. Using the modified parameters, the velocity profiles and the Reynolds Shear Stresses were predicted with very low uncertainty.

Keywords: Zero-displacement parameter, 1-D RANS model, Reynolds shear stresses, areal density, flexible vegetation

INTRODUCTION

The importance of vegetation as a component of aquatic ecosystems cannot be over-emphasized. It has ecological benefits in improving water quality and reducing soil erosion by altering the flow magnitude (Truong and Uijttewaal, 2019; Abdullahi and Busari, 2021). Numerical simulation is an effective approach to show the flow structure in a vegetated channel when the right turbulent modeling is combined with continuity and momentum equations (Li and Busari, 2019; Manko and Busari, 2020).

In-banks vegetation or emergent and submerged floodplain vegetation in rivers and streams have significantly affects the lateral and vertical velocity distributions of flow especially on the turbulence statistics (Chiaradia et al., 2019).

Accurate quantification of the bulk effects of flow-vegetation interaction is a significant challenge in the field of eco-hydraulics as well as of great importance in the design of flood protection or stream restoration schemes (Errico et al., 2019). It has been established that both density and distribution of submerged aquatic weeds had a

significant impact on the efficiency and equitability of water distribution (Di Stefano et al., 2022). Thus, increasing the density or distribution of vegetation in a channel, reduces the flow and attenuate the downstream flow and consequently the upstream will be subjected to flooding.

In spite of the above, vegetation has the ability to increase bank stability, reduce erosion and turbidity, provide habitat for aquatic and terrestrial wildlife, attenuate downstream floods, present aesthetic properties and filter pollutants (Ferro and Porto, 2018).

Sequel to the above ecological functions, efforts are now being made at the global level for restoration and rehabilitation of the waterways, flood plain management and restoration of river ecosystems. To understand the impact of vegetation roughness on inducing frictional resistance to flow, more research is needed and to achieve this, both experimental study and numerical simulation are performed considering the effect of vegetal density, plants' flexibility, and channel slope on flow structures by incorporating a zero-displacement parameter to capture the scale of turbulence vis-à-vis the position of zero velocity

RESEARCH ARTICLE
 PII: S225204302400024-14
 Received: June 25, 2024
 Revised: September 02, 2024
 Accepted: September 05, 2024

near the bed. To this note, the paper presents a 1-D RANS model that includes all essential hydraulic parameters to enhance the accurate prediction of the flow structures in a shallow vegetated watercourse. More so, the study provides an extensive dataset for the validation and subsequent recalibration of the index variables of zero-displacement parameters.

MODEL THEORETICAL BACKGROUND

One dimensional model

In this study a refined 1-D version of the model developed by (Busari and Li, 2006) has been used, in the model, vegetated flows are assumed unidirectional for shallow flow depth. Multi-dimensional models require more laborious and time-consuming for the generation of a large number of synthetic data.

Several experimental cases were simulated using the model. The dataset is obtained from the laboratory experiments which contain nine variables for blade-type vegetation: flow depth (h), Energy slope (S) stem width (B), vegetation height (k_v), vegetal thickness (t), flow rate (Q) flexural rigidity (EI) and number of strips or stems per unit Area (N) and drag coefficient (C_d).

Governing equations

Continuity equations and horizontal momentum equation, represented by (Eqn. 1) and (Eqn. 2) respectively.

$$\frac{\partial u_i}{\partial x_i} = 0 \quad i = 1 \quad (1)$$

$$\frac{\partial u_i}{\partial t} + u_j \frac{\partial u_i}{\partial x_j} = \frac{\partial}{\partial x_j} \left[v_m \left(\frac{\partial u_i}{\partial x_j} + \frac{\partial u_j}{\partial x_i} \right) + \frac{\tau_{ij}}{\rho} \right] - \frac{1}{\rho} \frac{\partial p}{\partial x_i} - \frac{1}{\rho} F_i + g_i \quad i=1, j=3 \quad (2)$$

where x_i ($= x_1$) = coordinate in horizontal direction (m); u_i ($= u_1$) = time-averaged velocity in horizontal direction (m/s); $u_j = 0$; t = time (s); ρ = fluid density (kg/m^3); v_m = molecular viscosity (m^2s^{-1}); $\tau_{ij} = -\rho u'_i u'_j$ = Reynolds stresses (N/m^2); p = pressure (N/m^2) is assumed to be a constant; $F_i = F_x$ (N/m^3) is the resistance force components per unit volume induced by vegetation in x directions; g_i is the x -component of the gravitational acceleration and is set to gS_0 , where S_0 = channel bottom slope.

The Reynolds stresses are represented by the eddy viscosity model (Eqn. 3):

$$\frac{\tau_{ij}}{\rho} = -\overline{u'_i u'_j} = -2\nu_t \left(\frac{\partial u_i}{\partial x_j} + \frac{\partial u_j}{\partial x_i} \right) - \frac{2}{3} \delta_{ij} k \quad i=1, j=3 \quad (3)$$

where $k = 1/2 \overline{u'_i u'_i}$ = turbulent kinetic energy (m^2s^{-2}) which can be absorbed into the pressure gradient term and ν_t = eddy viscosity (m^2s^{-1}).

Turbulence closure model

The eddy viscosity ν_t is specified by the Spalart-Allmaras (S-A) turbulence model which involves the solution of a new eddy viscosity variable, v . The version of the model used is for near-wall region and moderate Reynolds number (Spalart and Allmaras, 1994). The S-A model is intrinsically a transport equation for the eddy viscosity developed under the well-known Boussinesq hypothesis and it is as follows (Eqn. 4):

$$\frac{\partial v}{\partial t} + u_j \frac{\partial v}{\partial x_j} = C_{b1} \tilde{S}_v v + \frac{1}{\rho} \left\{ \frac{\partial}{\partial x_j} \left[(v + v_m) \left(\frac{\partial v}{\partial x_j} \right) \right] + C_{b2} \left(\frac{\partial v}{\partial x_j} \frac{\partial v}{\partial x_j} \right) \right\} - C_{w1} f_w \left(\frac{v}{d} \right)^2 \quad (4)$$

The eddy viscosity and its magnitude including the constants of the model are well defined in (Spalart and Allmaras, 1994).

The vegetation induced drag force

On the influence of vegetation, the resistance force due to vegetation is defined by the quadratic friction law. The drag force is resulted from wake formation downstream of the stem. The average force per unit volume within the vegetation domain is obtained by (Eqn.5)

$$F_i = N f_i = \frac{1}{2} \rho C_d N B u_i \sqrt{u_i u_j} = \frac{1}{2} \rho f_{rk} u_i \sqrt{u_j u_{j=i}} \quad (5)$$

where N = vegetation density (defined as the number of stems per unit area, $1/m^2$) and $f_{rk} = C_d N B$.

Flexibility accountability using (Large deflection theory of analysis)

A large deflection analysis based on the Euler-Bernoulli law for bending of a slender transducer has been used to determine the large deflection of the plant stem. The analysis modeled each vegetation stem as a vertical in-extensible non-prismatic slender transducer of length, l . The water flows produce variable distributed loads $q_x(s)$ on the transducer along the x -direction. According to Euler-Bernoulli's law, the local bending moment is proportional to the local curvature.

$$M(s) = EI(s) \frac{\frac{d^2 \delta}{ds^2}}{1 - \left(\frac{d\delta}{ds} \right)^2} \quad (6)$$

where, M is the bending moment (Nm), s is the local ordinate along the transducer, E is the modulus of elasticity (N/m^2), I is the Second moment of area (m^4) and, δ is the deflection in x -direction (m).

The equilibrium of forces and momentum gives

$$\frac{d^2 M}{ds^2} + \frac{dM}{ds} \frac{\frac{d\delta d^2 \delta}{ds ds^2}}{\left[1 - \left(\frac{d\delta}{ds} \right)^2 \right]} = -q_x(s) \sqrt{1 - \left(\frac{d\delta}{ds} \right)^2} \quad (7)$$

Combining of (Eqns. 6 and 7) yielded a fourth order nonlinear (Eqn. 8) in the deflection δ

$$\frac{d^2}{ds^2} \left[EI(s) \frac{d^2 \delta}{ds^2} \right] + \frac{d}{ds} \left[EI(s) \frac{d^2 \delta}{ds^2} \right] \frac{d \delta a^2 \delta}{ds ds^2} \left[\frac{d \delta}{ds} \right] = -q_x(s) \sqrt{1 - \left(\frac{d \delta}{ds} \right)^2} \quad (8)$$

The vegetation stem is taken as inextensible as the total length remains constant. By dividing the stem into n equal part of constant length Δs , the z -ordinate of the i^{th} node is obtained by (Eqn.9)

$$z_i = \sum_{j=1}^{i=n} \sqrt{\Delta s^2 - (\delta_i - \delta_{i-1})^2} \quad (9)$$

Numerical methods and boundary conditions

The deflected height of the stem is then equal to z_n . The (Eqn. 9) is then solved using a quasi-linearized central finite difference scheme. To minimize computational effort, the solution can be expressed in non-dimensional form relating the deflected height of vegetation to the applied force, hence, it is approximated by a polynomial.

At the free surface, zero pressure and zero gradients of velocity component are specified:

$$p = 0 \quad \text{and} \quad \frac{\partial u_i}{\partial \sigma} = 0 \quad (10)$$

At the bottom, the logarithmic law wall function is given by (Eqn.11)

$$u = u_w \left[\frac{1}{\kappa} \ln \left(\frac{u_w z}{\nu_m} \right) + B \right], \quad v = \kappa z u_w \quad (11)$$

where u_w = wall shear velocity (m/s); z = distance from the wall (m); and $B = 8.5$. By knowing the velocity at the point next to the wall with distance, z the wall shear stress can be computed iteratively.

The above equations were coded script using C++ language. The bulk drag coefficient is estimated as (Eqn.12):

$$\frac{C_d \lambda k_v}{2B^2 h^3} \frac{Q^2}{(1 - \phi \frac{k_v}{h})^3} - gS = - \left(g - \frac{Q^2}{B^2 h^3} \right) \frac{\Delta h}{\Delta x} \quad (12)$$

The solid volume fraction of the vegetation zone is defined by $\phi = NBt = \lambda t$ (-). The frontal area of vegetation per unit volume (areal density) is then given by $\lambda = NB$ (m^{-1}). The Δx , is a small longitudinal distance and Δh is the resulted change in the hydraulic head (water level difference) due to the change. These parameters are captured in the model (Figure 1).

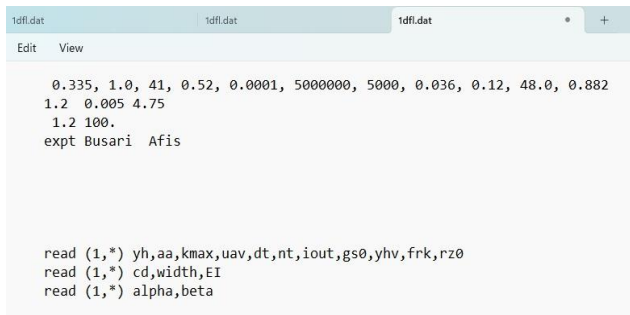


Figure 1. Modelled hydraulic conditions/Input data file

RESULTS AND DISCUSSION

Recently, Azorji and Busari, (2021) and Abdullahi and Busari, (2021) carried out extensive laboratory flume experiments and field investigations on flexible vegetation growth in waterways with varying areal densities. Hence, the need for this study to further validate the 1-D RANS model towards its application to highly dense flexible vegetation under laboratory control experiments and field studies. A screenshot of the simulation time step and stage is shown in Figure 2).

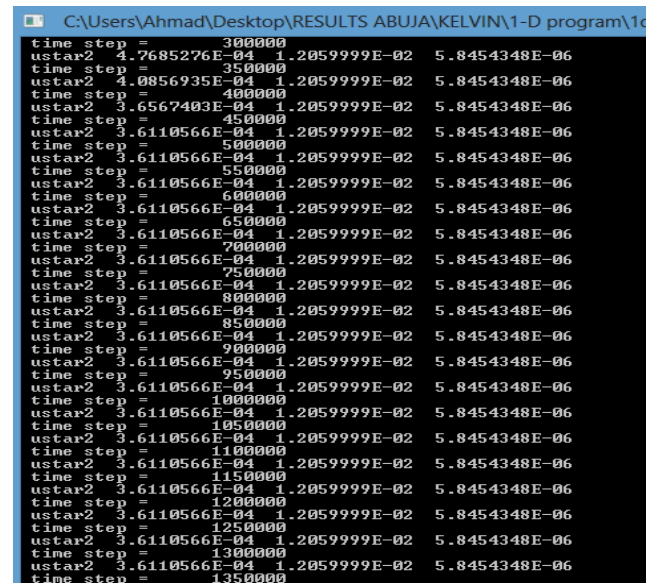


Figure 2. Simulation stage and Time step

General experimental hydraulic conditions

In the studies, Azorji and Busari, (2021) and Abdullahi and Busari, (2021) categorized areal vegetal density into three (3) categories: (i) less dense; (ii) dense vegetation and (iii) high density vegetation. The hydraulic parameters are shown in (Table 1). The details of the flume experiment conducted can be found in (Azorji and Busari, 2021; Abdullahi and Busari, 2021). The maximum discharge throughout the experiment was 50 cm³/hr.

Table 1. Hydraulic conditions

Author	Hydraulic parameters		Density class
	Vegetation parameter	Flow parameter	
Azorji and Busari, (2021)	$B = 0.0076 m$; $10 \leq N \leq 540 m^{-2}$; $0.3 \leq C_d \leq 0.7$; $k_v = 0.12 m$	$h = 0.35 m$; $10^{-2} \leq gS \leq 0.04$	Low
Abdullahi and Busari, (2021)	$B = 0.0022 m$; $600 \leq N \leq 3200 m^{-2}$; $0.6 \leq C_d \leq 1.2$; $k_v = 0.34 m$	$h = 0.62 m$; $gS = 10^{-2}$	Medium
Abdullahi and Busari, (2021)	$B = 0.0022 m$; $4250 \leq N \leq 8000 m^{-2}$; $0.8 \leq C_d \leq 1.0$; $k_v = 0.34 m$	$h = 0.62 m$; $gS = 10^{-2}$	High

Modeling of low vegetal density

Vertical mean stream-wise velocity profile

The result in Figure 3 clearly indicates the influence of vegetation density on the velocity profile in a vegetated canopy. On both axes, the variables are normalized. The shear velocity ($u^* = \sqrt{gS(h - k_v)}$) on the horizontal axis to yield scaling parameters.

The entire shape of low density vegetation (e.g. $10 \leq N \leq 90 m^{-2}$) from the depth of zero-displacement within the vegetation zone through the clear water zone follows an exponential law. The trend changes as the density increases. For $90 \leq N \leq 210 m^{-2}$, a point of inflexion is observed slightly at the interface between the deflected vegetation height (see the green dotted line) and clear water zone. Hence, the shape of the velocity profile above the vegetation zone begins to change from exponential to logarithmic law, whereas the nature of the velocity profile within the vegetation zone remains exponential. Beyond, $N=210$, the profile is defined as S-shape. It can be observed that the RANS model predicted all the shape and profile transformations as observed in the laboratory experiment.

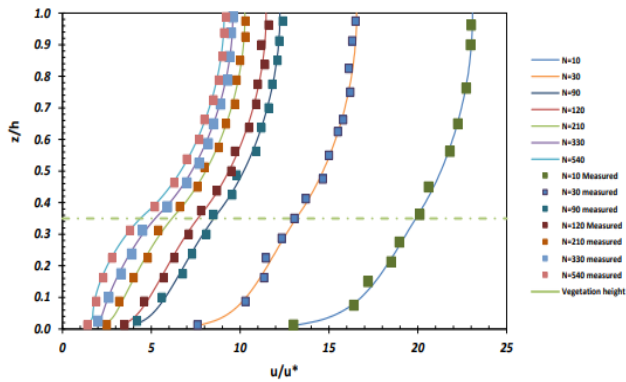


Figure 3. Mean vertical stream-wise velocity profile for flexible, less dense areal vegetation

Reynolds shear stresses in a low density vegetated channel flow

The Figure 4 shows the predictive power of the 1-D RANS model to replicate the measured Reynolds shear stresses ($-uw/$). The values of the max shear stresses at the interface between the top of the vegetation and the clear water zone are highly correlated with the laboratory observed values for the varying areal densities. The results show the instability of the shear stresses just above channel bed due induced vegetation drag by the flow hydraulic resistance from the vegetation.

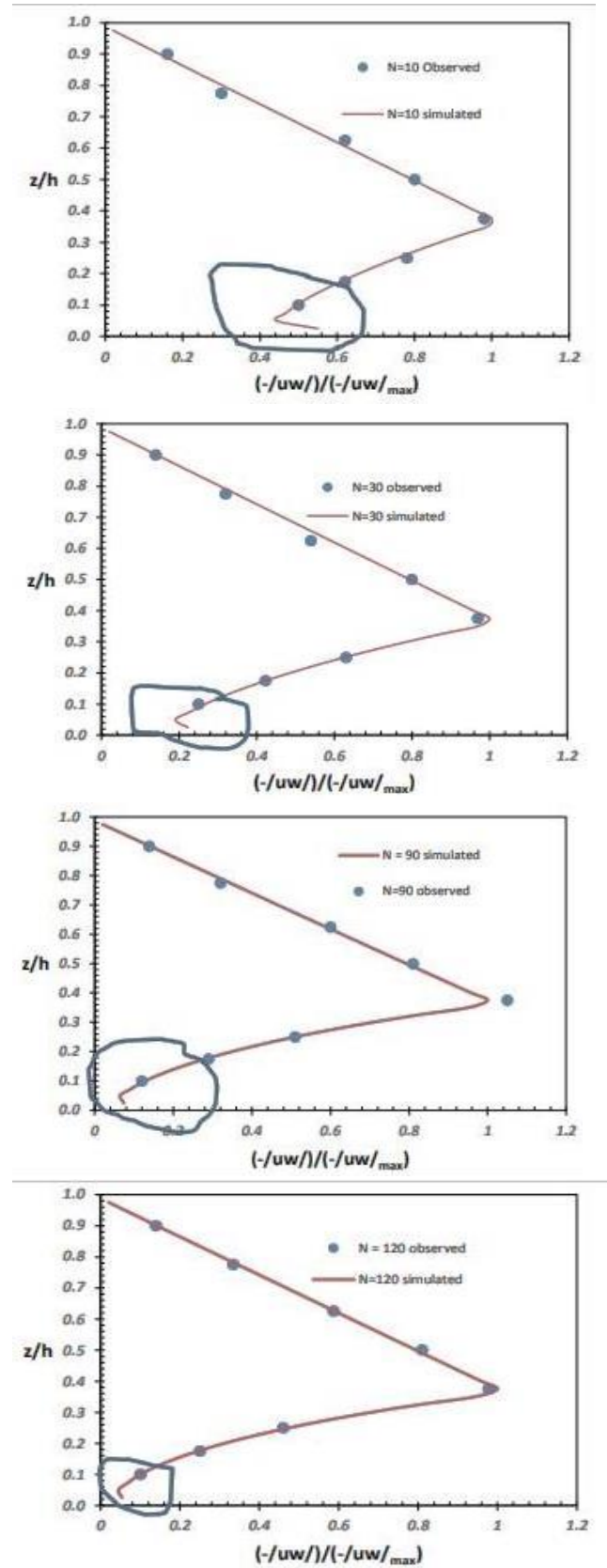


Figure 4. Measured and modelled longitudinal Reynolds shear stresses (low vegetal density).

Modeling of medium vegetal density

Vertical mean stream-wise velocity profile

Figure 5 shows that the experimentally predicted S-shaped vertical mean stream-wise velocity profile was perfectly replicated by the RANS model. The replication is very good from the measured point above the channel bed up to the water surface. It apparent that the points of inflexion are entirely below the deflected heights (the horizontal dotted line) of the vegetation. The location of point of the inflexion rises towards the vegetation height with increasing vegetal density due to the reduction in the vortex shedding at the interface between the vegetation zone and the clear water zone.

Reynolds shear stresses in a medium dense vegetated channel flow

In Figure 6, a good correlation exists between the experimental and modelled results. The prediction was perfect up to the position of the least shear stresses. The scale of the vortex produced became minimal as the

vegetation resistance balanced the gravitational flow forces.

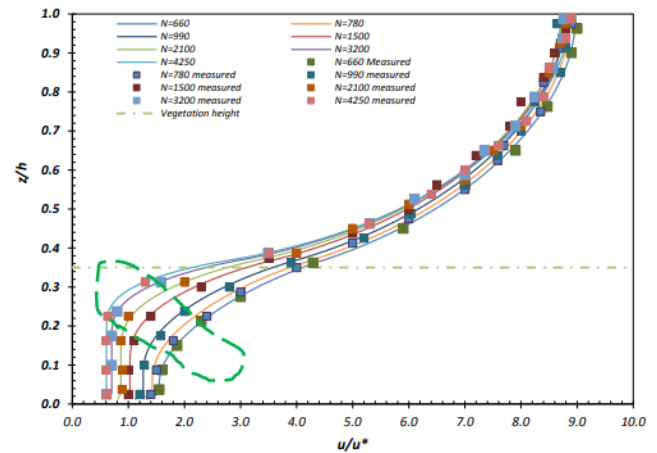


Figure 5. Mean vertical stream-wise velocity profile for flexible, medium dense areal vegetation

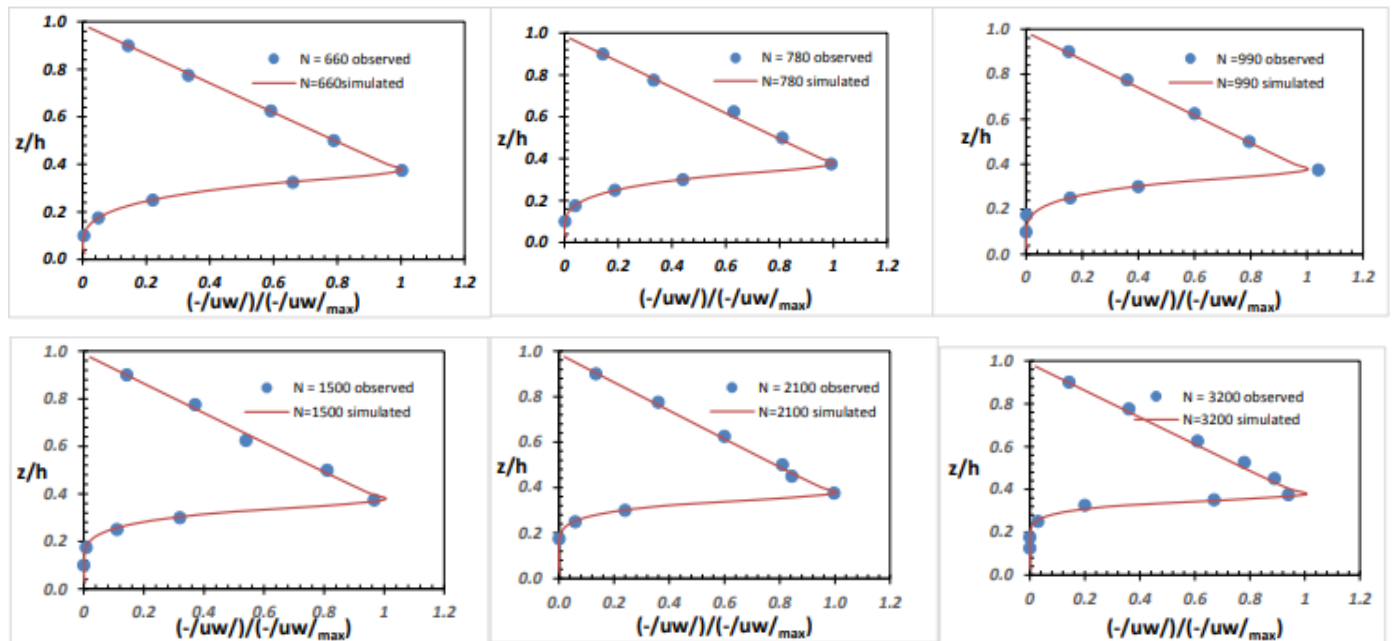


Figure 6. Measured and simulated Reynolds Shear Stresses (medium density vegetation)

Modeling of highly dense vegetal cover

Vertical mean stream-wise velocity profile

Figure 7 shows the model prediction of velocity profile against the experimental results. The RANS model under-predicted the velocities with the vegetation zone for the range vegetal densities and the reduced turbulent scale becomes difficult to replicate. Its predictive capability decreases for $N = 7000$ and 8000 due to over-estimation

of the mean velocity close to the water surface. This variation could be attributed to the secondary current produced at the interface between the boundary wall and flowing water. To account for this deficiency in the model prediction, the roughness parameters in the zero-displacement equation used in the model need to be recalibrated.

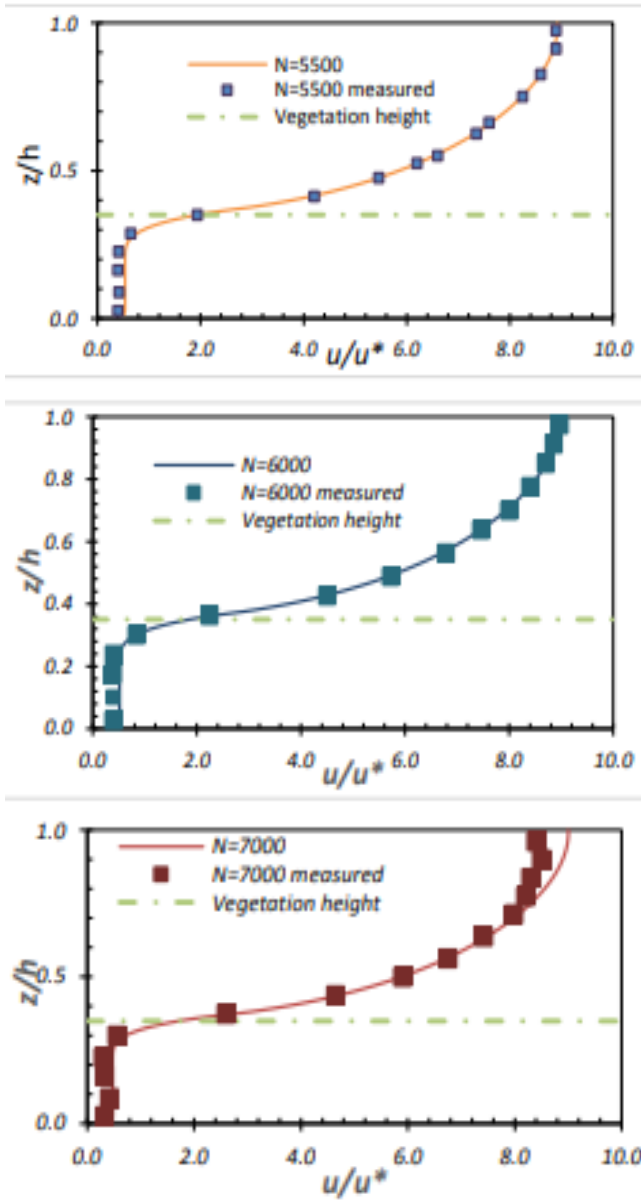


Figure 7. Mean vertical stream-wise velocity profile for very dense flexible vegetation

Reynolds shear stresses in a highly dense vegetated channel flow

In Figure 8, a good correlation exists between the experimental and modelled results. However, discrepancies arise due to low correlations of results especially in the vegetation zone arising from high-value prediction of Reynolds shear stresses. The scale of the vortex produced became minimal as the vegetation resistance balanced the gravitational flow forces.

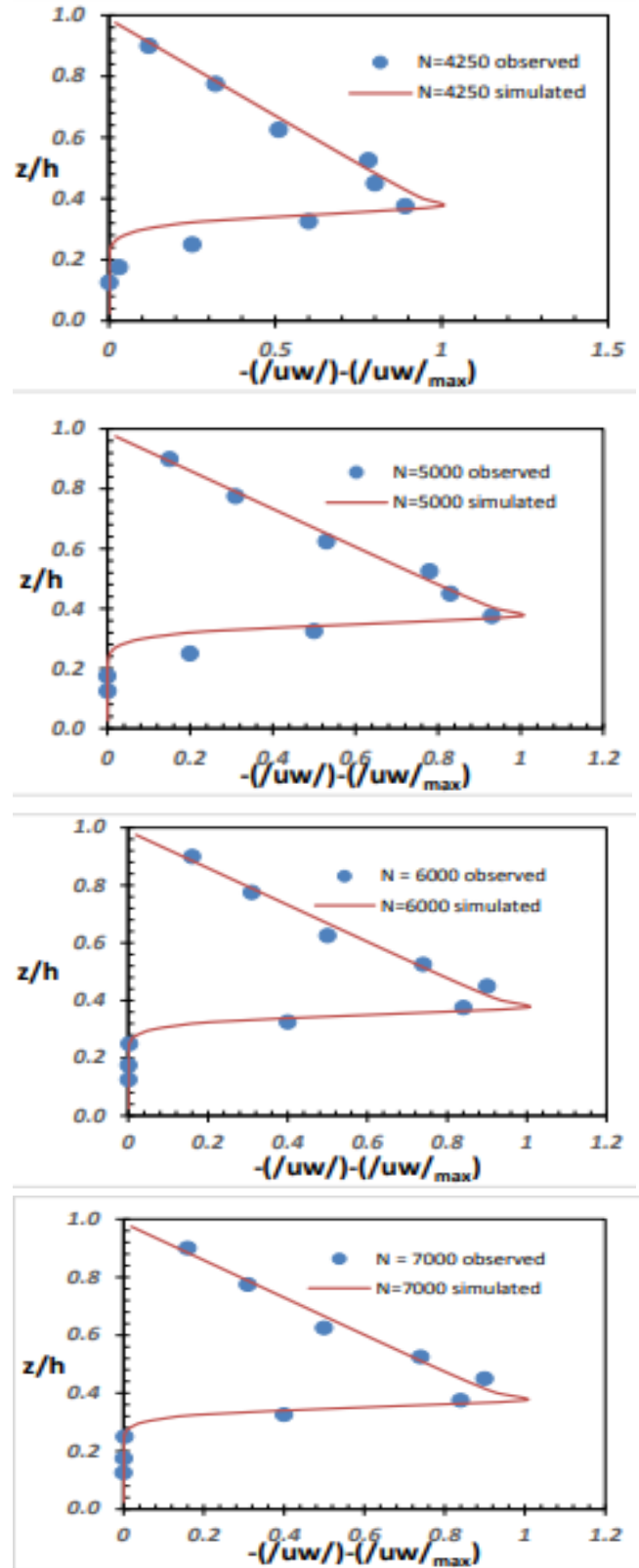


Figure 8. Measured and simulated Reynolds Shear Stresses (high density vegetation)

Re-calibration of hydraulic roughness parameters

In the case of wall-bounded shear flow, the turbulence length scale L is proportional to the distance from the point of interest to the channel bed. In the presence of varying vegetation sizes, the turbulence length scale is reduced to allow turbulence eddies above the vegetation zone to reach the channel bed. A zero-plane displacement parameter, Z_o is introduced to simulate the reduction in the turbulence length scale. The L value of a point at level Z is obtained by (Eqn. 13)

$$\begin{cases} L = Z - Z_o, & Z > k_d > Z_o \\ L = Z (k_d - Z_o)/k_d, & Z < k_d \end{cases} \quad (13)$$

where k_d is the deflected height of vegetation (m).

This study adopted the empirical equation of Z_o developed by (Busari and Li, 2016) which is given by (Eqn. 13):

$$\frac{Z_o}{k_d} = \frac{f_v^\beta}{f_v^\beta + \alpha\beta} \quad (14)$$

These roughness parameter indices are given as $\alpha = 0.7$ and $\beta = 0.5$. For very high density as presented in this work, there is need to recalibrate these indices to fit the reduction in turbulent length scale required for highly dense vegetation. The parameters were varied within a suitable range until the modeled velocity profile matched the experimentally observed profile. Based on this, the best results is obtained for $\alpha = 0.56$ and $\beta = 0.64$.

Modified vertical mean stream-wise velocity profile using the calibrated α and β

The velocity profiles are reproduced using the modified values of α and β in the (Eqn.14) to obtain a new Z_o value which is then fed into the numerical input file. The newly obtained mean vertical stream-wise velocities are shown in Figure 9.

Relationship between Maximum Reynolds Shear Stress and Vegetal Densities

In Figure 10, the fitting of the relationship between the maximum Reynolds Shear Stresses and the vegetation density shows a non-linearity properties of power law for low vegetal covers.

In Figure 11, the fitting of the relationship between the maximum Reynolds Shear Stresses and the vegetation density shows perfect linearity properties for medium vegetal covers.

In Figure 12, the fitting of the relationship between the maximum Reynolds Shear Stresses and the vegetation density shows perfect linearity properties for highly dense vegetation as observed in Figure 8. This implies that the deflection of vegetation at high densities is lowered as the vegetal density increases, due to increase in the hydraulic resistance to the flow. Hence, more water will be diverted above the vegetation zone.

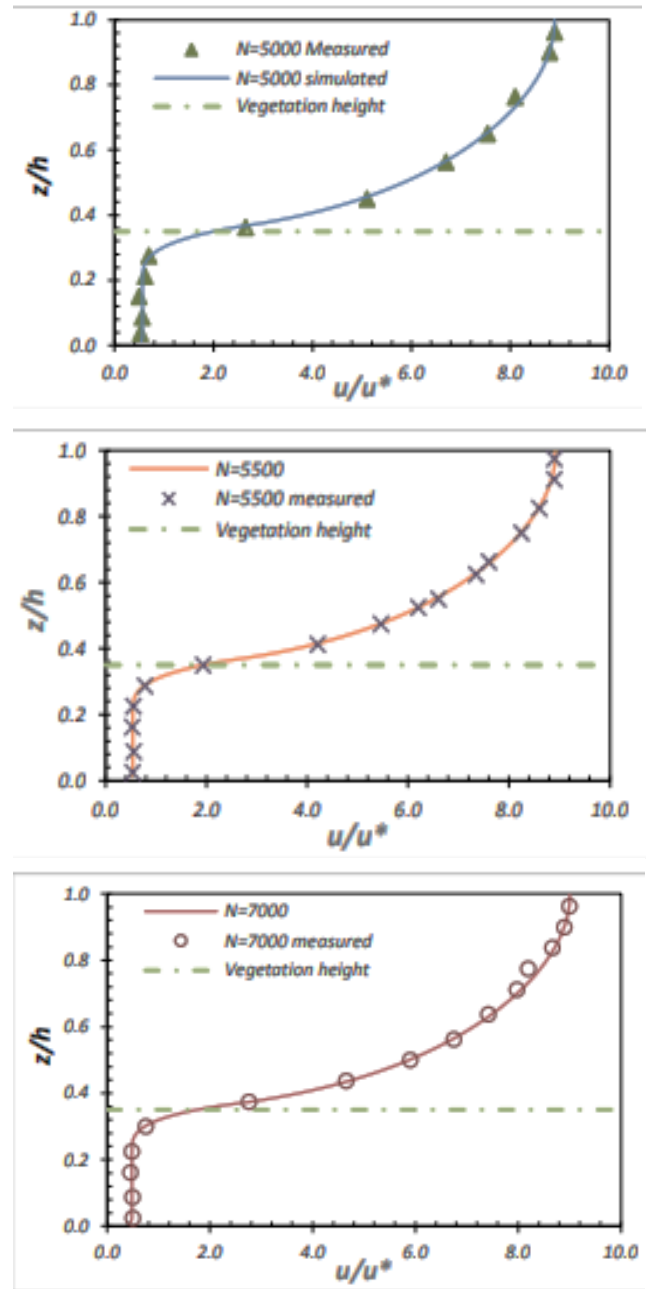


Figure 9. Mean vertical stream-wise vel. profile for dense flexible vegetation ($\alpha = 0.56$ and $\beta = 0.64$)

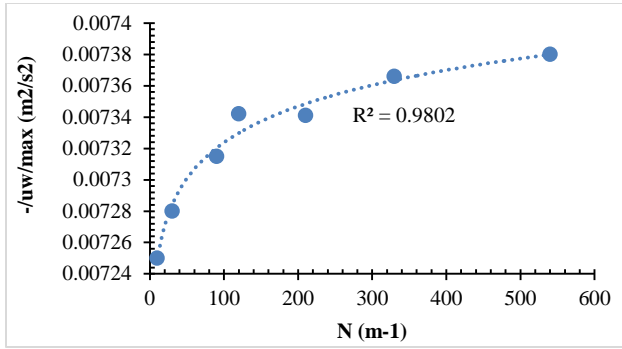


Figure 10. Maximum Reynolds Shear Stresses and vegetation density (Class I)

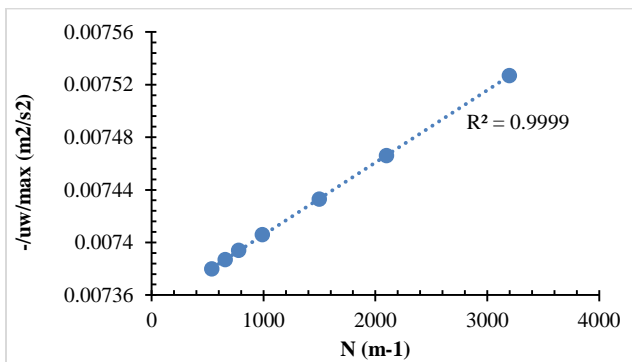


Figure 11. Maximum Reynolds Shear Stresses and vegetation density (Class II)

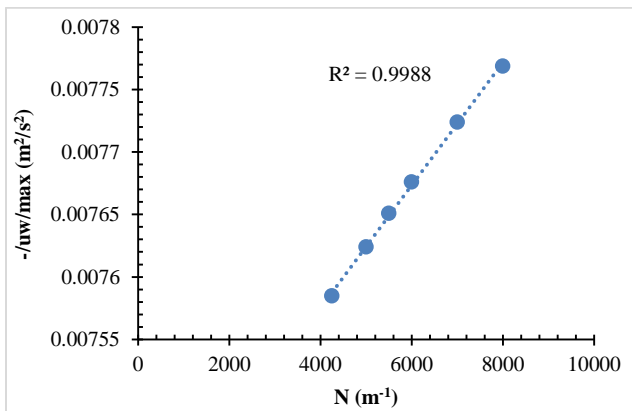


Figure 12. Maximum Reynolds Shear Stresses and vegetation density (Class III)

CONCLUSIONS

The present study deepens the understanding of vegetated channel modeling by taking into consideration the influence of zero-plane displacement parameter and the effect of varying vegetation density on the vertical mean stream-wise velocity profile of submerged flexible vegetation through the numerical simulation of laboratory flume experiments of vegetative open channel flow. The

study verifies the dependency of the shapes of the vertical mean stream-wise velocity profile on the vegetal areal densities; in addition, the model replicate the vertical mean stream-wise velocity profile and Reynolds shear stress profile for varying vegetal areal densities. However, discrepancy was found in the prediction for very high density. Based on the recalibration of hydraulic roughness parameters, the 1-D RANS model replicate the vertical mean stream-wise velocity profile and Reynolds Shear Stresses accurately.

DECLARATIONS

Corresponding author

Correspondence and requests for materials should be addressed to Busari Afis; E-mail: abusari@unam.na; ORCID: 0000-0002-5737-8384

Data availability

The datasets used and/or analyzed during the current study available from the corresponding author on reasonable request.

Author’s contribution

J. Kelvin participated in the design of study and ran the simulation; A.O. Busari is responsible for the conceptualization, methodology, analysis and overall discussion of modelled results and finally the review and editing of manuscript.

Acknowledgements

The author thanks the University of Namibia for funding the dissemination of output of this research.

Competing interests

The authors declare no competing interests in this research and publication.

REFERENCES

Abdullahi N, Busari AO (2021). Modeling of Open Channel Flow: A review. *Iconic Research and Engineering Journals*. Volume 4, Issue 9. 18-33. [View article \(google.com\)](#)

Abdullahi N, Busari, A. O (2021). Experimental study on the effect of River Bank vegetation in open channel flow. *Proceedings of the 6th Hybrid conference of Nigerian Institution of Mechanical Engineers, Minna, Nigeria* page 59-68. [Google Scholar](#)

- Azorji C, Busari, AO (2021). The effect of vegetation density on flow characteristics in submerged vegetation. Proceedings of the 6th Hybrid conference of Nigerian Institution of Engineers, Minna, Nigeria. 98-106. [Google Scholar](#)
- Busari AO, Li CW (2016). Bulk drag in a regular array of emergent vegetation stems under gradually varied flow. *Journal of Hydro-environmental Research*, volume 12, 59–69. <https://doi.org/10.1016/J.JHER.2016.02.003>
- Chiaradia EA., Gandolfi C, Bischetti GB (2019). Flow resistance of partially flexible vegetation: A full-scale study with natural plants. *Journal of Agricultural Engineering*, 50, 55–65. <https://doi.org/10.4081/jae.2019.885>
- Di Stefano C, Nicosia A, Palmeri V, Pampalone V, Ferro V (2022). Rill flow velocity and resistance law: A review. *Earth-Science Reviews*, 231. <https://doi.org/10.1016/j.earscirev.2022.104092>
- Errico A, Lama GFC, Francalanci S, Chirico GB, Solari L, Preti, F (2019). Flow dynamics and turbulence patterns in a drainage channel colonized by common reed under different scenarios of vegetation management. *Ecological Engineering*, 133, 39–52. <https://doi.org/10.1016/j.ecoleng.2019.04.016>
- Ferro V, Porto P (2018). Applying hypothesis of self-similarity for flow resistance law in Calabrian gravel bed rivers (Fiumare). *Journal of Hydraulic Engineering*, 144, 1–11. [https://doi.org/10.1061/\(ASCE\)HY.19437900.0001385](https://doi.org/10.1061/(ASCE)HY.19437900.0001385)
- Li CW, Busari AO (2019). Hybrid modeling of flows over submerged prismatic vegetation with different areal densities. *Journal Engineering Applications of Computational Fluid Mechanics* 13(1), 493-505. <https://doi.org/10.1080/19942060.2019.1610501>
- Manko A, Busari AO (2020). Estimation of vegetative hydraulic resistance in an open channel flow. Presented at the 18th International Conference of Nigerian Institution of Civil Engineers (NICE), Abuja, Nigeria. [View article \(google.com\)](#)
- Spalart PR, Allmaras SR (1994). A one-equation turbulence model for aerodynamic flows. *La Recherche Aeronautique*, volume 1, number 1, pp 5-21. <https://doi.org/10.2514/6.1992-439>
- Sulaimon M, Busari AO (2019). Hydraulic modeling of nature-based approach to submerged flexible Vegetation lining. International Conference of Engineering and Environmental Sciences (ICEES), Osun State University, Nigeria (Nov. 5-7, 2019). [View article \(google.com\)](#)
- Truong SH, Uijtewaal WSJ (2019). Transverse momentum exchange induced by large coherent structures in a vegetated compound channel. *Journal of Water Resources Research*, 55. <https://doi.org/10.1029/2018WR023273>

Publisher's note: [Scienceline Publication](#) Ltd. remains neutral with regard to jurisdictional claims in published maps and institutional affiliations.



Open Access: This article is licensed under a Creative Commons Attribution 4.0 International License, which permits use, sharing, adaptation, distribution and reproduction in any medium or format, as long as you give appropriate credit to the original author(s) and the source, provide a link to the Creative Commons licence, and indicate if changes were made. The images or other third party material in this article are included in the article's Creative Commons licence, unless indicated otherwise in a credit line to the material. If material is not included in the article's Creative Commons licence and your intended use is not permitted by statutory regulation or exceeds the permitted use, you will need to obtain permission directly from the copyright holder. To view a copy of this licence, visit <https://creativecommons.org/licenses/by/4.0/>.

Performance-Based Evaluation of Steel Fibre Reinforced Normal- and High-Strength Concretes Using Statistical Analysis of Experimental Database

Adekunle P. Adewuyi[✉] , and Odette Animbom 

Department of Civil Engineering, University of Botswana, Gaborone, Botswana

[✉]Corresponding author's Email: AdewuyiA@ub.ac.bw

ABSTRACT

The widespread acceptance of concrete can be attributed to its unique characteristics, despite inherent drawbacks such as brittleness and weak tensile strength. The study was aimed at evaluating the optimal content and characterization of steel fibres required to impede crack propagation and enhance overall strength of concrete. The influence of critical factors like fibre content, length, diameter, and volume fraction on the performance of steel fibre reinforced concretes (SFRC) through statistical analysis of 209 experimental data. The influence of these factors on the compressive, flexural, and tensile strengths of concrete was analyzed as a function of the mean and coefficient of variation of the normalized strength values. The study found that steel fibres in concrete produced success rates of 67.9% (7.1% average strength improvement = ASI) in compressive strength, 78.5% (38.2% ASI) in flexural strength and 84.2% (23.8% ASI) in tensile strength. The study further separately examined the impact of steel fibres on both normal strength concretes (NSC) and high strength concretes (HSC). The findings indicated an overall success rate of 60% (6.97% ASI), 69.9% (38.36% ASI), and 75.6% (23.59% ASI) for compressive, flexural, and split tensile strength, respectively, in NSC. However, higher degree of strength enhancement of 74.0% (7.16% ASI), 84.8% (39.21% ASI), and 86.6% (23.51% ASI) were recorded for compressive, flexural, and split tensile strength, respectively in HSC. The research underscores the effectiveness of incorporating steel fibres as a reinforcement strategy in enhancing various strength aspects of concrete.

Keywords: Fibre reinforced concrete, steel fibres, compressive strength, tensile strength, flexural strength, normalized strength, average strength improvement.

INTRODUCTION

Concrete is practically the most widely used construction material, which contributes immensely to global economic growth and infrastructural development (Adewuyi et al., 2015). However, concrete has low flexural and tensile strength and lacks the ability to resist cracks (Kim et al., 2019; Sidiq et al., 2019). The incorporation of fibers into concrete matrices, to produce fiber reinforced concrete (FRC) has been found to enhance the tensile and flexural strength of concrete. Steel fibre reinforced concrete (SFRC) is a composite material comprising of cement, fine and coarse aggregates, and discrete discontinuous steel fibres (Zhang et al., 2014; Balagopal et al., 2022). Numerous studies have reported the influences of incorporating steel fibres on the mechanical properties of concrete, but the research findings differ across different studies. Consequently, this study embarks on a comprehensive performance-based analysis of SFRCs through the application of statistical analysis to an

extensive experimental database. The aim of the study was to systematically evaluate the influence of key parameters namely the type of steel fibre, the percentage fiber content or volume fraction, the fibre geometry (i.e. the length, diameter or the aspect ratio of fibre) on the mechanical and durability properties of SFRC from normal and high strength concrete. This sheds light on the intricate interactions between the constituents and their impact on overall performance.

MATERIALS AND METHODS

Data extraction from experimental studies

The database of 209 experimental investigations conducted on steel FRC of a large variety of concrete mixes, covered various ranges of compressive strength of the mixes, volume fraction of the fibres, fibre aspect ratio, fibre tensile strength and modulus of elasticity. The criteria considered for selection of suitable experimental data from relevant literature included the impact factor,

RESEARCH ARTICLE
 PII: S225204302400025-14
 Received: June 25, 2024
 Revised: September 02, 2024
 Accepted: September 05, 2024

publication year, and citation count. Data documented only in specialized research publications in high quality journals of impact factors of 0.554 – 7.675, of citations ranging from zero (for the most recently published articles) to 1103 within the publication years 2010 to 2023. Table 1 shows the properties of concrete, steel fibres and fibre content in the SFRC experimental programme.

Control specimens accounted for 17.2% of the total sample size. Figure 1 shows the graphical distribution of the SFRC in terms of the fibre geometry was hooked – 82%, straight – 9%, corrugated – 3%, crimped – 2%, closed – 2% and round ended steel fibres – 1%. It also evident from Figure 1(b) that the corrugated steel fibre had the highest strength enhancement of 82.6% (for flexure) and 68.1% (for tension), followed by straight, hooked, crimped, closed and the least enhanced fibre was the round steel fibres. While no steel fibre compromised the compressive strength threshold, the maximum enhancement was 14% (for round steel fibre), followed by hooked (9.03%), corrugated (8%), straight (6.9%), crimped (5.1%) and the least was closed steel fibre (2.7%). Moreover, in terms of the success rate or otherwise as shown in Figure 1(c), all the FRC samples concrete scrimped and closed steel fibers recorded 100% success rates in compression, flexure and tension. Straight and corrugated SFRCs recorded 100% success rates in flexure and tension, while there were 15% and 16.7% failure rates for samples in compression. Hooked FRCs samples all passed the tensile strength threshold, but 17.8% and 4.27% of the samples fell short in compression and flexure. Finally, all the round steel FRCs passed compressive strength assessment, but only one-half of the samples passed the flexural strength limit.

Fibres were classified as normal strength (≤ 50 MPa) and high strength (> 50 MPa) according to Eurocode 2. Data collection criteria included impact factor, publication year, and citation count. The experimental database comprises 90 samples normal strength concrete (43% of entire experimental data), while high strength concrete (119 samples) accounted for the remaining 57%.

Table 1. Properties of the steel fibres

Properties	Values
Concrete compressive strength (MPa)	18-195
Volume fraction (%)	0.05-5
Fibre length (mm)	13-130
Fibre diameter (mm)	0.2-1.6
Tensile strength of fibres (MPa)	250-2660
Elastic modulus of fibres (GPa)	200-210

Evaluation of strength enhancement based on normalization of test data

The data was normalized with respect to the control to account for different concrete grades in the experimental dataset. This created a benchmark for analysis, where values below one meant decreased strength, values at one showed no improvement, and values above one indicated increased strength.

The normalized strength ratio (NSR) is expressed as the ratio of strength of fibre reinforced concrete to the strength of plain concrete without fibre.

$$(1) \quad NSR = \frac{\text{Strength of fibre reinforced concrete}}{\text{Strength of equivalent grade of plain content}}$$

The normalized strength ratio (NSR) is expressed in terms of the compressive, tensile and flexural strengths designated as NCS, NTS and NFS.

$$(2) \quad \text{Normalized compressive strength, } NCS = \frac{f'_{ck}}{f'_{ck0}}$$

$$(3) \quad \text{Normalized tensile strength, } NTS = \frac{f'_{ct}}{f'_{ct0}}$$

$$(4) \quad \text{Normalized flexural strength, } NFS = \frac{f'_{cf}}{f'_{cf0}}$$

where f'_{ck0} , f'_{ct0} and f'_{cf0} are compressive, tensile and flexural strength of plain concrete (with no fibres) respectively. Likewise, f'_{ck} , f'_{ct} and f'_{cf} are compressive, tensile and flexural strength of fibre reinforced concrete respectively.

Degree of success and failure

The efficiency of FRC is measured as the extent to which the normalization exceeds a threshold of 1. Hence the success rate (SR) and the failure rate (FR) is calculated as given by equations (5) and (6). A sample is said to be successful when $NSR \geq 1$, while a failed sample has $NSR < 1$. The optimal constituent parameters are then determined by accessing the degree of success based on the frequency of the parameters that produced the best strength efficiency of FRC.

The success rate is determined as the percentage ratio of the successful samples to the entire population size of investigated samples, while failure rate was calculated as the percentage ratio of failed samples to the entire population size. The calculation of success and failure involved applying the formulae.

$$(5) \quad \text{Success rate (SR)} = \frac{\text{Number of successful samples}}{\text{Total population size}} \times 100\%$$

$$(6) \quad \text{Failure rate (FR)} = \frac{\text{Number of failed samples}}{\text{Total population size}} \times 100\%$$

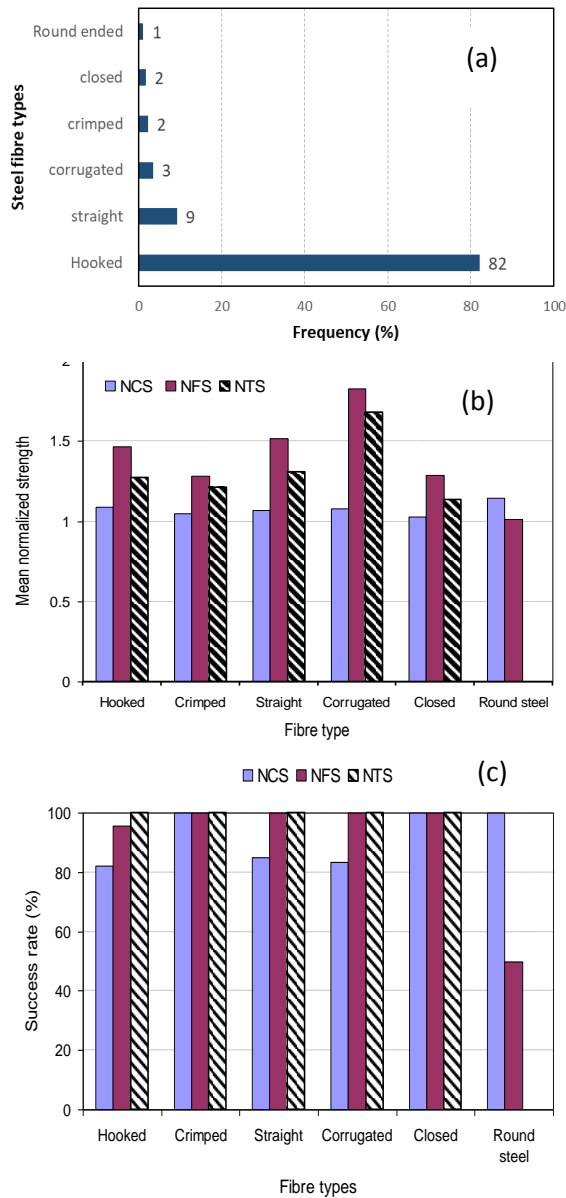


Figure 1. Distribution, mean normalized strengths and efficiency of different steel fibres in SFRC experimental scheme

RESULTS AND DISCUSSION

Statistical description of data distribution

Table 2 shows the statistical parameters in terms of the mean, standard deviation, coefficient of variance, skewness and kurtosis values for the normalized compressive, tensile and flexural strength for steel fibre reinforced concretes. It is evident from the findings that introduction of fibres in plain concrete enhanced the flexural and tensile properties by 38.2% and 23.8%

respectively, while the compressive strength was only improved by a single digit 7.1%. The coefficient of variation of the data were within the 30% reliability bracket.

Table 2. Statistical parameters of the normalized strengths of hardened steel FRC

Statistical parameter	Mean	Standard deviation	CoV (%)
Compressive strength	1.071	0.117	11
Flexural strength	1.382	0.399	28.8
Tensile strength	1.238	0.237	19.2

Effect of fibre volume fraction on concrete properties

Figure 2 presents the performance of SFRC in terms of the normalized strength values and the success/failure rate of different volume fractions of embedded steel. The performance of the SFRC in terms of the volume fraction is presented for compression, flexure and tension in the subsequent sections, while Figure 2(d) shows that fibre volume content range 1.0 to 1.5% produced the optimal performance and by extension the highest success rate.

Compressive strength

Some literature indicates that adding steel fibre to concrete can enhance compressive strength by 4-19% (Ali et al., 2022; Zhang et al., 2020). However, studies also suggest that steel fiber under 1.0% may not significantly impact compressive strength (Rizzuti & Bencardino, 2014; Soulioti et al., 2011). Figure 2 presents the influence of the volume fraction of different geometric properties and shapes of steel fibres on the normalized strengths of FRC. Figure 2(a) illustrates the impact of steel fibre volume fraction on concrete’s compressive strength. Optimal strength enhancement was achieved at 1.5% volume fraction. Nonetheless, within the 0.5-2% range, the data consistently provided useful insights, particularly highlighting 1.5% as yielding the highest average increase of 15.68%. Additionally, it demonstrated a success rate of 86.96% alongside a 13.04% failure rate.

Flexural strength

The flexural strengths of SFRC are reported to be significantly higher, ranging from 3% to 81% greater than those of the reference mixture (Ali et al., 2022; Zhang et al., 2020). This is due to the bridging effect of the fibers, which inhibits fracture propagation and enhances flexural performance through stress redistribution (Jun et al., 2023). Figure 2(b) quantifies the influence of volume fraction of steel fibers on the flexural strength of FRC. The most significant improvement was observed at 1.5%

volume fraction. However, data points were well-distributed across 0.5%, 1%, and 2% volume fractions. Notably, 1.5% (98.87% average increase) and 2% (61.12% average increase) fiber volumes exhibited the most substantial enhancements. It was found that while both 1.5% and 2% showed a 100% success rate, the average strength enhancement was higher at 1.5%.

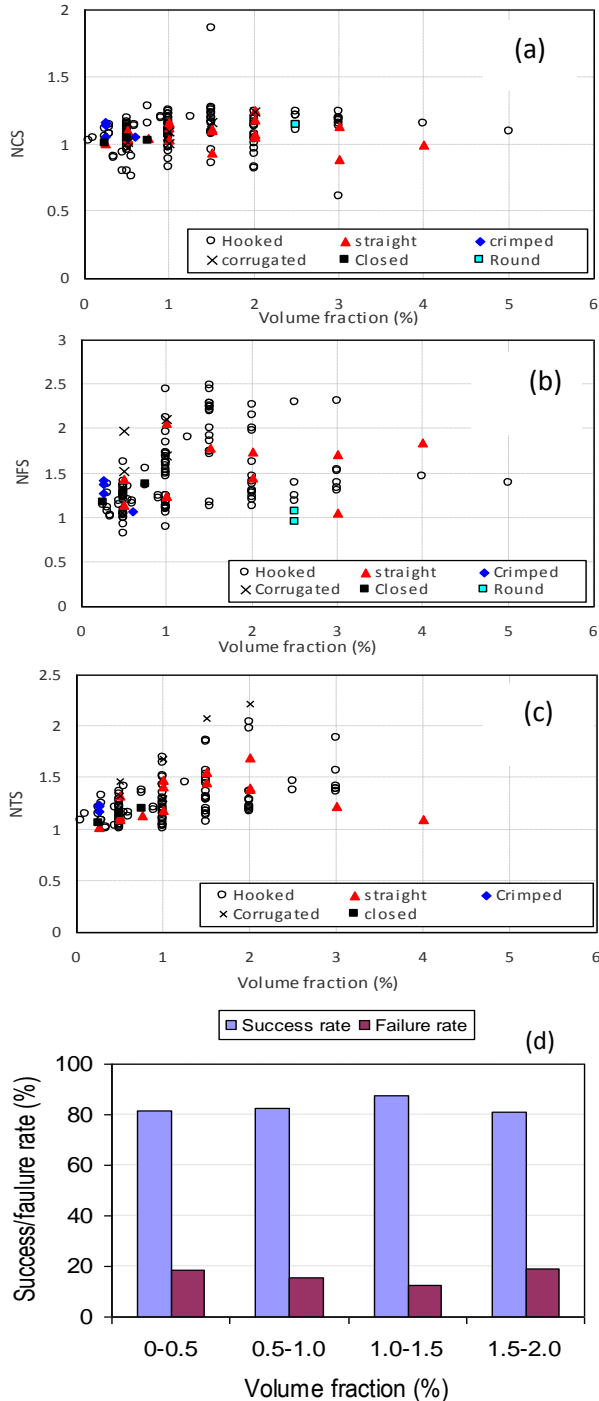


Figure 2. Normalized compressive, flexural and tensile strength of SFRCs with respect to the volume fraction

Split tensile strength

According to various studies, the inclusion of steel fibers in concrete has been shown to notably enhance the split tensile strength of the material surpassing the reference mixture by approximately 11–54% (Ali et al., 2022; Zhang et al., 2020). Figure 2(c) illustrates the impact of steel fiber volume fraction on concrete's tensile strength. The highest enhancement was observed at a 2% fiber content, resulting in a 47.16% increase and a 100% success rate. However, data points were well-distributed across 0.5%, 1%, and 1.5% volume fractions, resulting in respective increases of 17.63%, 28.41%, and 41.77% in NTS. These findings highlight a positive correlation between NTS and fiber volume, with the optimum volume identified as 2%.

Effect of fibre length on concrete properties

Compressive strength capacity of FRC

Figure 3 shows the effects of fibre length on the strength of concrete in compression, tension and flexure. As shown in Figure 3(a), most of the data points were within the volume fractions of 0-0.5%, 0.5-1.0%, 1.0-1.5% and 1.5-2.0%. The subsequent analysis focused solely on these specific volume fractions. Table 3 summarizes the success rates and failure rates in enhancing compressive strength. The highest success rate is achieved at the volume fraction range of 1.0 to 1.5%. The optimal fibre lengths within this range, contributing to an enhanced compressive strength, was found to be between 30-60 mm resulting in a 19.36% increase in compressive strength.

Table 3. Summary of success and failure rates for compressive strength of SFRC.

Volume fraction	Success rate (%)	Failure rate (%)
0-0.5	81.48	18.52
0.5-1.0	82.35	15.68
1.0-1.5	87.5	12.5
1.5-2.0	80.95	19.05

Tensile performance of FRC at different fibre lengths

Figure 3(b) illustrates the impact of steel fibre length on the split tensile strength of concrete. By observation, most data points were within the volume fractions of 0 to 0.5%, 0.5 to 1.0%, and 1.0 to 1.5%. The analysis focused solely on these specific volume fractions. Table 4 summarises the success and failure rates in enhancing the split tensile strength. There is a 0% failure rate for all fibre volume fraction ranges. The average increase in the tensile strength is 15.93, 26.83%, 41.96%, and Considering the

increase, the range from 1.0 to 1.5% offers the best enhancement. The optimal fibre lengths within this range, contributing to an enhanced split tensile strength, were found to be in the range of 30-60 mm.

Table 4. Summary of success and failure rates for split tensile strength of SFRC.

Volume fraction	Success rate (%)	Failure rate (%)
0-0.5	100	0
0.5-1.0	100	0
1.0-1.5	100	0
0-0.5	100	0

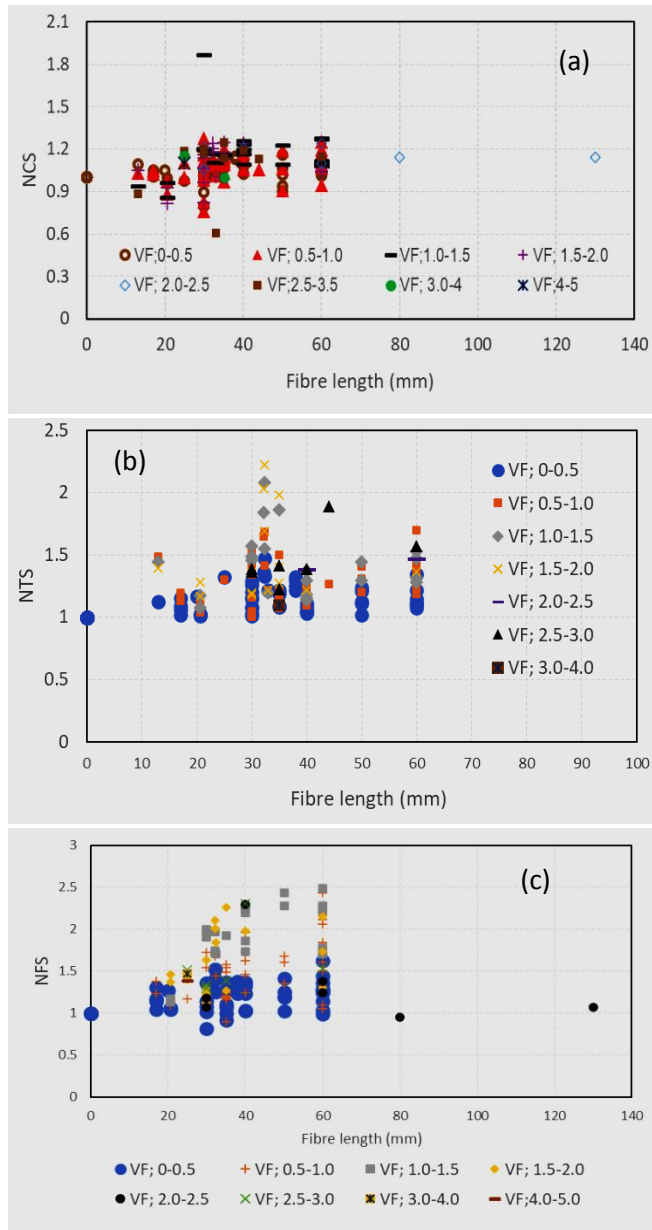


Figure 3. Normalized compressive, flexural and tensile strength of SFRC with respect to fibre length.

Flexural assessment of FRC at varying fibre lengths

The effects of steel fiber lengths on concrete flexural strength are illustrated in Figure 3(c). Most data points clustered within volume fractions of 0 to 0.5%, 0.5 to 1.0%, and 1.0 to 1.5% brackets. The analysis concentrated specifically on these volume fractions is summarised in Table 5. Noting that the 1-1.5% range yielded the highest average increase in flexural strength of 96.58%. Considering this, and keeping the volume fraction at the optimum 1.5%, the most impactful lengths within this range were 30 mm, 40 mm, 50 mm, and 60 mm, resulting in respective increases of 95.5%, 105.7%, 136.0%, and 111.9%. The findings indicated a positive correlation between length and flexural strength, with 50 mm identified as the optimal length.

Table 5. Summary of success and failure rates for flexural strength of SFRC.

Volume fraction	Success rate (%)	Failure rate (%)
0-0.5	91.11	8.89
0.5-1.0	97.67	2.33
1.0-1.5	100	0

Effect of fibre diameter on concrete properties

Influence of fibre size on compressive strength

Figure 4(a) depicts the influence of fibre diameter on the mechanical properties SFRCs. The preceding analysis has shown that 1.0-1.5% volume fraction is the most beneficial and effective volume fraction for SFRCs.

Within this range, maintaining a volume fraction of 1.5%, key fiber diameters were around 0.5 mm, 0.62 mm, 0.75 mm, and 1.03 mm, resulting in average NCS of 1.1941, 1.1782, 1.1648, and 0.9059. These values correspond to strength enhancement of 19.41%, 17.82%, 16.48%, and a reduction of 9.41% in NCS, respectively for the four classes of fibre diameters. The findings revealed that the compressive strengths decrease as the size of the fibre increase, where 0.5 mm was the optimal diameter.

Influence of fibre diameter on tensile strength of SFRC

The effect of steel fiber diameter on the split tensile strength of SFRC is illustrated in Figure 4(b). Having concluded from preliminary assessment of volume fraction and its effect on the mechanical properties of SFRC, 1-1.5% volume fraction was found as the optimal fibre content in FRC. Building the investigation on the optimal volume fraction of 1.5% for different fibre sizes 0.55 mm, 0.75 mm, 1.03 mm, and 1.05 mm, the average split tensile strength corresponds to an enhancement of 53.4%, 36.4%, 22.8%, and 21.9%, respectively. The results indicate that the average tensile strength of SFRCs decrease as the fibre length increased. diameter increases. The optimum fibre diameter to achieve the most enhanced split tensile strength was 0.55 mm.

Influence of fibre diameter on flexural strength of SFRCs

Figure 4(c) presents the influence of fibre diameter on the flexural strength of concrete. For the established optimal fibre volume of 1.0-1.5%, the normalized flexural strength corresponding to the key diameters 0.5 mm, 0.62 mm, 0.75 mm, and 1.03 mm were 0.95, 1.21, 1.20 and 1.05 respectively. The results demonstrate a positive parabolic correlation such that the flexural strength increases with fibre diameter and attained the maximum NFS of 1.225 (or 22.5% strength enhancement) at optimum fibre size of 0.65 mm.

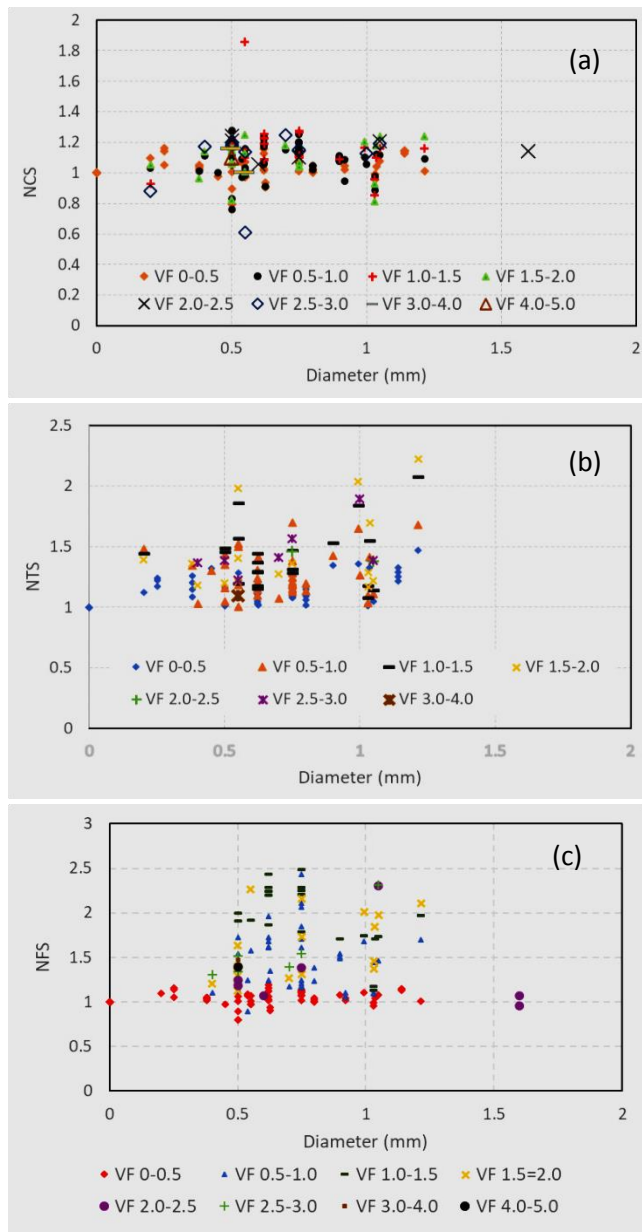


Figure 4. Normalized compressive, flexural and tensile strength of SFRC with respect to fibre diameter.

Performance of SFRC Based on normal and high strength concrete

Many experimental investigations have been conducted on fibre reinforced concretes based on different grades of concrete. These concrete grades can be categorized into the normal strength concrete (NSC) with characteristic compressive cylinder strength of concrete not exceeding 50 N/mm², while the high strength concrete (HSC) have compressive cylinder strength greater than 50 N/mm². It has been established in the preceding sections that though the introduction of fibres improve the tensile and flexural capacities of SFRC, it occasionally does so at the expense of the compressive strength. The following sub-sections describe the influence of that grade of concrete on the overall performance of steel FRC.

Influence of concrete grade on the compressive strength of SFRCs

The scattered plots of the normalized compressive strength (NCS) of steel FRC of varying volume fractions for the normal- strength concrete (NSC) and high-strength concrete (HSC) are shown in Figure 5(a) and Figure 5(b) respectively. The NSC produced an average increase of 4.41% in the compressive strength, while only 14.19% of the samples fell below the control threshold. On the other hand, the HSC exhibited an average 9.11% enhancement in compressive where 12.6% fell below the control compressive strength. It is therefore evident that FRC performed slightly better in concrete of high grade compared to the normal strength concrete.

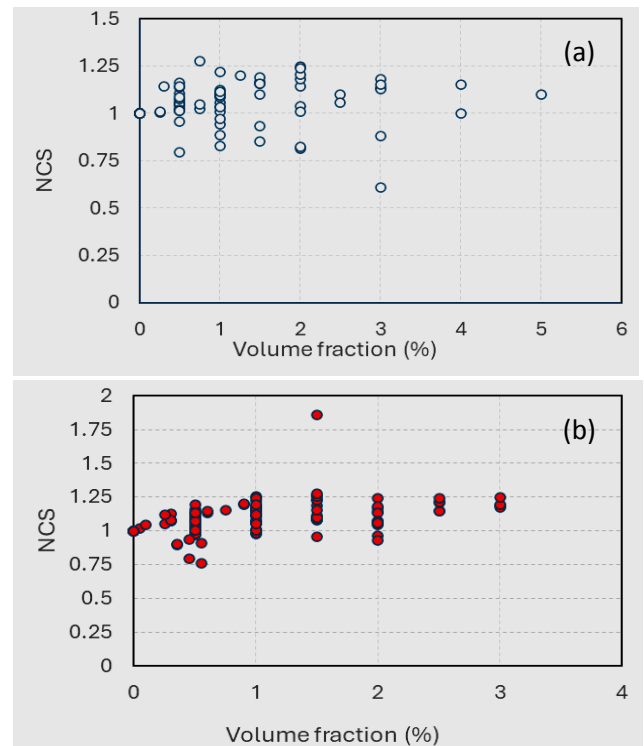


Figure 5. Normalized compressive strength for SFRC produced from (a) normal strength concrete and (b) high strength concrete.

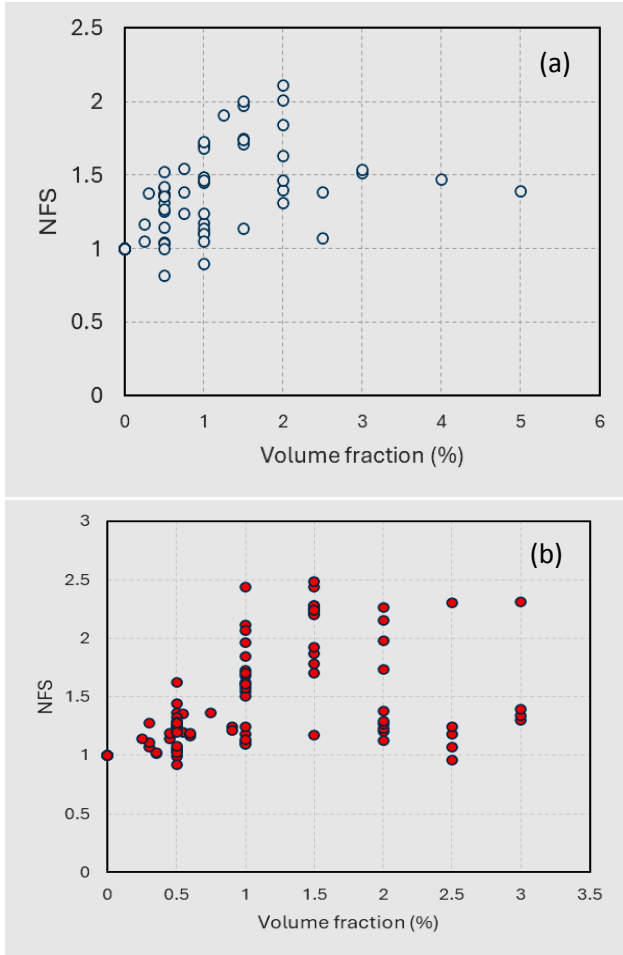


Figure 6. Normalized flexural strength for SFRC produced from (a) normal strength concrete and (b) high strength concrete.

Influence of concrete grade on the flexural strength of SFRCs

Figure 6(a) and Figure 6(b) present the comparison and contrast between the normalized flexural strength of the NSC and HSC in terms of the volume fractions. NSC exhibited an average of 13.87% improvement in the normalized flexural strength with only 5.88% failure (i.e. below the flexural strength of the corresponding control concrete). The HSC, on the other hand, produced a 43.93% increase with only 3.03% of the tested samples below the control threshold values. This has further shown that HSC had 26.4% improvement in strength and additional 21.4% samples crossing the flexural strength threshold over the NSC for similar volume fractions.

Influence of concrete grade on the split tensile strength of SFRCs

Steel fibre reinforced NSC provided 18.80% increase in the tensile strength where not less than 75.38% of the tested samples crossed the tensile strength threshold for control concretes. Conversely, steel fibres in HSC

performed slightly better with 21.22% improvement in tensile strength with 86.6% of the samples crossing the tensile strength threshold. These results show that HSC had 2.03% improvement in strength and additional 14.9% samples crossing the tensile strength threshold over the corresponding NSC for similar volume fractions. Based on the increase in the average NTS and the success rate, it can be concluded that HSC offers a better enhancement of split tensile strength compared to NSC. Figure 7(a) and Figure 7 (b) present the comparison and contrast between the normalized split tensile strength of the NSC and HSC in terms of the volume fractions.

Figure 8 presents the summary of the performance of SFRC produced from both normal- and high-strength concretes as a measure of the success ratings and strength enhancement in terms of the compressive, flexural and tensile strength. It is noteworthy that this improvement does not match the cost of producing the high strength concrete.

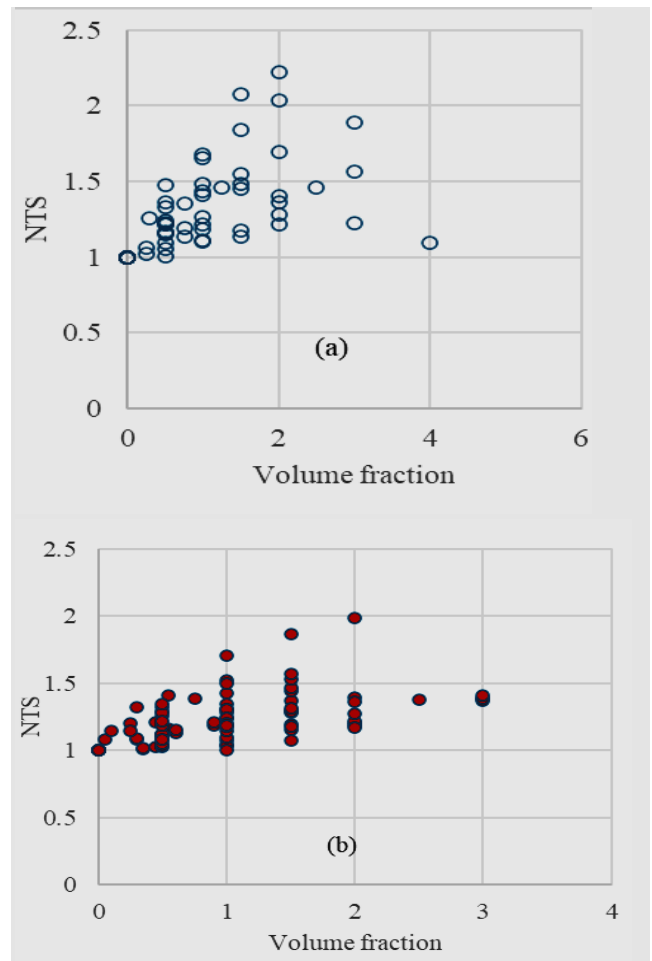


Figure 7. Normalized split tensile strength for SFRC produced from (a) normal strength concrete and (b) high strength concrete.

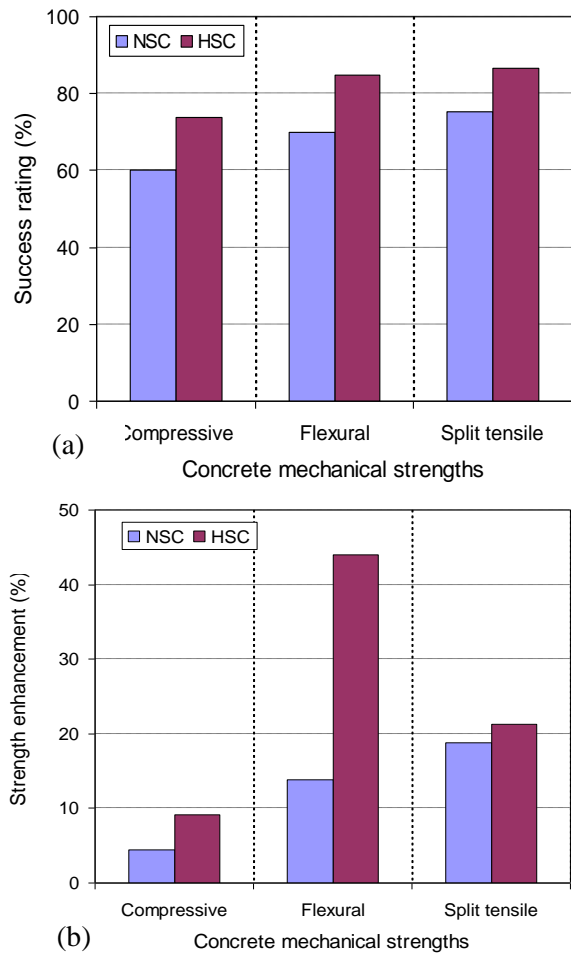


Figure 8. Performance of SFRC produced from NSC and HSC in terms of (a) success ratings and (b) strength enhancement.

CONCLUSION

The influence of critical factors like fibre content, length, diameter, and volume fraction on the performance of steel fibre reinforced concretes (SFRC) for both the normal- and high-strength concrete is presented in this paper. Statistical analysis was made from 209 experimental database of SFRC, 82% of which were produced from hooked steel fibres. The following conclusion can be drawn from the study.

The incorporation of steel fibres into concrete led to an increase in all three strengths. The optimal volume fraction was 1.5% for compressive and flexural capacity, and 2.0% for tensile strength.

The length of the steel fibre has a direct influence on the performance of steel FRC. The optimum length was

between 30 to 60 mm for compressive and tensile strengths, while the flexural strength was maximum at an optimum length of 50 mm.

The diameter of the fibre had been found to affect the mechanical properties of SFRC. The optimum diameter of fibre were 0.5 mm, 0.55 mm and 0.62 mm for compressive, tensile and flexural strength, respectively.

High-strength concrete had better influence on the performance of steel FRC than the normal-strength concrete in terms of the success ratings and the mechanical strengths. However, the strength and performance enhancement do not significantly match the cost of production of HSC-based FRC.

DECLARATIONS

Corresponding Author

Correspondence and requests for materials should be addressed to AdewuyiA@ub.ac.bw; ORCID: 0000-0001-8190-7357. The ORCID for Odette Animbom: 0009-0009-1530-8714.

Data availability

The datasets used and/or analyzed during the current study available from the corresponding author on reasonable request.

Acknowledgements

The authors would like to acknowledge the technical staff of the Structural Engineering Laboratory of the Department of Civil Engineering for their support and for creating a conducive environment to conduct this research.

Authors' contribution

A.P. Adewuyi developed the research idea, identified the research gaps in the body of knowledge and concrete technology in practice, designed data extraction processes, contributed to data analysis, interpreted the results and revised the manuscript. O. Animbom presented the proposal, analyzed data, interpreted the results and wrote the manuscript under the supervision and guidance of A.P. Adewuyi. Both authors read and approved the final manuscript.

Competing interests

The authors declare no competing interests in this research and publication.

REFERENCES

- Adewuyi, A. P., Otukoya, A. A., Olaniyi, O. A. & Olafusi, O. S. (2015). Comparative studies of steel, bamboo and rattan as reinforcing bars in concrete: tensile and flexural characteristics. *Open Journal of Civil Engineering*, 5(2), 228-238. <https://doi.org/10.4236/ojce.2015.52023>





- Ali, A. M., Falah, M. W., Hafedh, A. A., Al-Khafaji, Z. S., & Radhi, S. (2022). Evaluation the influence of steel-fiber on the concrete characteristics. *Periodicals of Engineering and Natural Sciences*, 10(3), Article 3. <https://doi.org/10.21533/pen.v10i3.3111>
- Balagopal, V., Panicker, A. S., Arathy, M. S., Sandeep, S., & Pillai, S. K. (2022). Influence of fibers on the mechanical properties of cementitious composites—A review. *Materials Today: Proceedings*, 65, 1846–1850. <https://doi.org/10.1016/j.matpr.2022.05.023>
- Jun, H., Seo, D. J., Lim, D. Y., Park, J. G., & Heo, G. (2023, March 9). Effect of Carbon and Steel Fibers on the Strength Properties and Electrical Conductivity of Fiber-Reinforced Cement Mortar. *Applied Sciences*. <https://doi.org/10.3390/app13063522>
- Kim, S., Kim, D.J., Kim, S.-W., Park, C. (2019). Tensile behavior characteristics of high-performance slurry-infiltrated fiber-reinforced cementitious composite with respect to fiber volume fraction. *Materials*, 12(20), 3335. <https://doi.org/10.3390/ma12203335>
- Rizzuti, L., & Bencardino, F. (2014). Effects of fibre volume fraction on the compressive and flexural experimental behaviour of SFRC. *Contemporary Engineering Sciences*, 7, 379–390. <https://doi.org/10.12988/ces.2014.4218>
- Sidiq, A., Gravina, R., & Giustozzi, F. (2019). Is concrete healing really efficient? A review. *Construction and Building Materials*, 205, 257–273. <https://doi.org/10.1016/j.conbuildmat.2019.02.002>
- Zhang, L., Zhao, J., Fan, C., & Wang, Z. (2020). Effect of Surface Shape and Content of Steel Fiber on Mechanical Properties of Concrete. *Advances in Civil Engineering*, 2020, 1–11. <https://doi.org/10.1155/2020/8834507>
- Zhang, X. X., Abd Elazim, A. M., Ruiz, G., & Yu, R. C. (2014). Fracture behaviour of steel fibre-reinforced concrete at a wide range of loading rates. *International Journal of Impact Engineering*, 71, 89–96. <https://doi.org/10.1016/j.ijimpeng.2014.04.009>

Publisher’s note: [Scienceline Publication](#) Ltd. remains neutral with regard to jurisdictional claims in published maps and institutional affiliations.



Open Access: This article is licensed under a Creative Commons Attribution 4.0 International License, which permits use, sharing, adaptation, distribution and reproduction in any medium or format, as long as you give appropriate credit to the original author(s) and the source, provide a link to the Creative Commons licence, and indicate if changes were made. The images or other third party material in this article are included in the article’s Creative Commons licence, unless indicated otherwise in a credit line to the material. If material is not included in the article’s Creative Commons licence and your intended use is not permitted by statutory regulation or exceeds the permitted use, you will need to obtain permission directly from the copyright holder. To view a copy of this licence, visit <https://creativecommons.org/licenses/by/4.0/>.

Empirical Scrutiny of Geopolymer Concrete Containing Locally Produced Superplasticizer under Varied Temperatures

Lucia Omolayo Agashua¹✉ , Chinwuba Arum^{1,2} , Bamitale Dorcas Oluyemi-Ayibiowu¹  and Catherine Mayowa Ikumapayi¹ 

¹Civil and Environmental Engineering Department, Federal University of Technology Akure, 340252, Nigeria

²Civil and Mining Engineering Department, JEDS Campus, University of Namibia, Namibia

✉Corresponding author's Email: agashualight@gmail.com

ABSTRACT

Cement manufacturing companies contribute greatly to carbon-dioxide emission during production, hence there is need for novel eco-friendly or biodegradable cementitious material, which has the same strength and also durable. Geopolymers which are eco-friendly waste materials, which can also reduce construction cost, are therefore considered for this purpose. The geopolymer stabilizing materials, fly ash (FA), kaolin clays powder (KCP), rice husk ash (RHA), and alkaline activator (procured sodium silicate, waste-created sodium silicate and sodium hydroxide) were added at 0, 2.5, 5, 7.5, and 10%, to the naturally created superplasticizer geopolymer concrete (GPC), so as to solve the problem of workability and efflorescence associated with fly ash based GPC. FTIR results shows major absorbance band at the region between 950 and 3250 cm^{-1} . It means that addition of the naturally made superplasticizer to the geopolymer concrete lowered the viscosity and increased the flow behavior of concrete. The geopolymer concrete consists of super plasticizer (1.5%) and optimum of various binders i.e. 5% FA + 7.5% KC + 10% RHA + aggregate + water. At temperature above 70°C both compressive strength and weight decreases, for naturally made and purchased sodium silicate. The optimal geopolymer product showed substantial strength and durability enhancements at 70°C temperatures, with strength and durability values decline above 70°C, indicating material deterioration. A positive correlation between hot-state temperature, strength and durability properties was also established. The R^2 of the Feret on the test set reaches 0.967, indicating its excellent predictive performance.

Keywords: Rice Husk, Fourier Transform Infrared Spectroscopy, Waste-created sodium silicate, Superplasticizer; Eco-friendly

INTRODUCTION

Material for both structural and non-structural concrete applications around the globe It is also known as alkali-activated cement, inorganic polymer concrete, and geocement (Agashua et al., 2023; Abdelli et al., 2017; Adeshokan and Arum, 2023). GPC is dual face materials that combine strong alkaline solutions as activator as well as aluminosilicate materials as binders (Agashua et al., 2023; Obebe et al., 2023). Highly oxidize to corrosion and fire substances, shrinks below convectional concrete, has excellent durability, high compressive, tensile and flexural strengths. There are abundant raw materials which exist for the creation of geopolymers from industrial as well as natural minerals trashes. Besides, its synthesis process guzzles much less energy, particularly those created from industrial rubishes (Omotayo and Arum, 2022; Agashua and Ogiye, 2018; Pelisser et al., 2021). The aluminosilicates can be sourced from numerous pozzolanic materials which possess ample quantities of

silica together with alumina which are mostly rubishes from industrial or agrarian debris for instances ground granulated blast furnace slag (GGBFS), bagasse ash (BA), fly ash (FA), rice husk ash (RHA), palm oil fuel ash (POFA) Kaolin clay and that are used to lessen contaminant impact from natural resources consumption (Abdelli et al., 2017; Phoo-ngernkham et al., 2017; Samantasinghar and Singh, 2020; Rui et al., 2024). This agronomic and industrial debris are utilized individually or blended to serve as the aluminosilicate source in creating geopolymers for sustainable construction (Samantasinghar and Singh, 2020). While, alkaline activators are the second decisive constituent of GPC needed to reacts and polymerizing the aluminosilicates silica together with alumina contents presents in the aluminosilicate (Arum et al., 2022; Babatola and Arum, 2020; Chouhan et al., 2018). These are strong alkaline solutions like K_2SiO_3 , (potassium silicate), NaOH (sodium hydroxide), as well as Na_2SiO_3 (sodium silicate), or combination of these

RESEARCH ARTICLE
 PII: S225204302400026-14
 Received: June 25, 2024
 Revised: September 02, 2024
 Accepted: September 05, 2024

hydroxides and silicates for reacting aluminium (Al) as well as silicon (Si) atoms. More, the geopolymerization procedure depends solely on the reactivity together with concentration of alkaline activator with a lesser quantity of water to binder ratio (Adeshokan and Arum, 2023; Cong and Cheng, 2021; Dewi et al., 2018; Faluyi et al., 2021; Hassan et al. 2019). However, curing temperature of geopolymer concrete results in high early strength but causes a porous geopolymer mix, which reduces the strength at later age (Jindal and Sharma, 2020). This reduction in strength at greater temperatures is owing to early and swift evaporation of water, which not only disturbs the geopolymerization process, but also increases porosity (Shill et al., 2020). Thus, this research evaluated the behaviour of geopolymer concrete created via class-F fly ash, kaolin clay, and rice husk ash as binder and NaOH and Na₂SiO₃ as alkaline activator.

Materials and process of geopolymer concrete

Materials utilized in this experiment were river sand, sodium hydroxide, kaolin clay, crushed granite, factory-created sodium silicate, Portland cement, naturally made sodium silicate as well as super plasticizer, and drinkable water. Further, the GP concrete was thoroughly mixed and Four sets of fly ash based geopolymer concrete was produced which are control concrete, Partially replaced GPC using factory-produced sodium silicate, Partially replaced GPC using laboratory-produced sodium silicate and GPC using laboratory-produced sodium silicate with laboratory-created superplasticizer (LCS) (Table 1). Then workability and strength test were carried out on the four categories of samplings created. Chemical analysis on selected binders (kaolin clay, fly ash and rice husk ash), alkaline activators (sodium silicate and sodium hydroxide) and geopolymer concrete were carried out in the laboratory of Chemical and Material as illustrated in Figures 1 and 2.

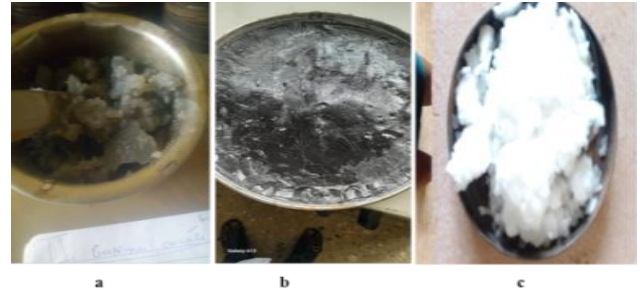


Figure 1. I (a and b) Water curing of geopolymer concrete, c) Air drying of geopolymer concrete and II) Alkaline activator (NaOH and Na₂SiO₃), b) laboratory-produced Na₂SiO₃, and c) NaOH.



Figure 2. I= a) Geopolymer concrete using each binders and super plasticizer separately; b) Demolding of different geopolymer using each binders and super plasticizer after 48 hours casting, and c) geopolymer made using optimum values obtained from each binders. II= a) Cement; b) laboratory-created super plasticizer (from rice husk) and c) Fly ash, rice husk ash as well as kaolin clay.



Physical, strength and durability tests were done in the Nigerian Building and Road Research Institute (NBRRI) Jabi Abuja and Federal Ministry of Works (FMW), concrete and pavement unit Sheda Abuja. The GP concretes were cast and removed from the moulds after 24 hours, and cured in water between 7 to 56 days. The design of geopolymer concrete in this research is presented in Figure 3.

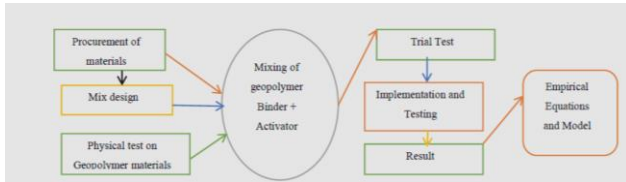


Figure 3. Design process of geopolymer concrete.

RESULTS AND DISCUSSION

Outcome of Fourier transform infrared spectroscopy (FTIR) scrutiny

FTIR characterization result for binders ashes is as displayed in Tables 2(a-c). This illustrate that the fly ash has highest key absorbance band at the region between 467.9 and 3695.8 cm^{-1} . Then, followed by RHA with extreme band of 2084 cm^{-1} and lower band of 798 cm^{-1} and the lowest was Kaolin clay with greatest value of 3690 cm^{-1} and lowest value of 749 cm^{-1} . Also fly ash notable transmittance between 7.1 and 49.9% was the extreme. The results of FTIR reveal that these binders possess different functional groups namely; alkenes, amides, alkenes, alkynes, acyl chloride and alky halides. An Amine is a type of compound that is derived from ammonia (NH_3), that is amines are derivatives of ammonia. The lower aliphatic amines with a fishy smell are gaseous in nature. Alkynes are traditionally identified as acetylenes, although the term acetylene also denotes C_2H_2 , which is an hydrocarbons with single and double carbon-carbon bonds. Fly-ash possesses majorly; Aluminumoxide (Al_2O_3) at 23.6% as well as Silicon dioxide (SiO_2) at 52.2% and lesser quantity of Iron (III) oxide (Fe_2O_3) at 7.39%. While, kaolin clay key constituents were 52% of Silicon dioxide (SiO_2) and 35% of Aluminumoxide (Al_2O_3) together with 2% Potassium oxide (K_2O) which is insignificant quantity. Likewise, RHA shows significant amount of Silicon dioxide (SiO_2) at 93.3% and Potassium oxide (K_2O) at 3.40% with insignificant quantity of P_2O_5 at 2.1%.

1) FTIR Scrutiny for Laboratory-produced Superplasticizer

Fourier transform infrared spectroscopy (FTIR) characterization was employed to investigate the presence of different inorganic and organic bonds in the novel LP superplasticizer and the spectrum obtained is shown in Figure 4. Figure 4 illustrates the major absorbance band at the region between 500 and 3000 cm^{-1} . The significant peaks which were observed at 617, 707 and 778 cm^{-1} were attributed to O-Si-O and Si-O-Si bending vibrations

of in situ-synthesized inorganic silicate. Although the intensities of their bands were low compared to those of other bands, their presence confirmed the in situ formation of sodium silicate by the action of sodium hydroxide on inorganic silica from rice husk. On the other hand, one intensified band situated at 1428 cm^{-1} was a band characteristic of O-C-O stretching vibrations of sodium carbonate, which was believed to originate due to the action of sodium (Na) with atmospheric carbonate. Its high intensity was an indication of the highly reactive nature of sodium to form compounds such as sodium carbonate. The other small diffused bands at 918–1003 and 1251 cm^{-1} corresponded to Si-O stretching in silicate glasses and weak C-O stretching in native cellulose, respectively.

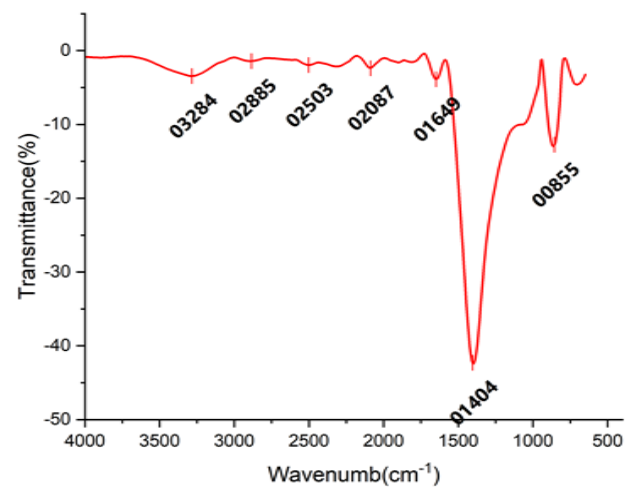


Figure 4. Different vibrational modes in FTIR region obtained for LP superplasticizer.

Some characteristic weak peaks in the LP superplasticizer spectrum at the frequency region of 1650 cm^{-1} were attributed to quadrant ring stretching in lignin and carbonyl stretching including C=O stretching originating from organic fractions present in the LP superplasticizer, whereas small bands at 2309 and 2900 cm^{-1} were associated with $\text{dCH}_2 + \text{dOCH} + \text{dCCH}$ and $-\text{CH}$ stretching vibrations from fructose and native cellulose. These results again confirmed the XRD results and indicated the formation of inorganic and organic compounds in the LP superplasticizer. Results of FTIR analysis demonstrated that the addition of the LP superplasticizer to the geopolymer concrete lowered the viscosity and increased the flow behavior of concrete, as an effect of the presence of organic fractions in the LP superplasticizer imparted by alkaline digestion of rice husk (Tatal et al., 2020; Silva et al., 2020).

2) XRD Scrutiny for laboratory-produced Superplasticizer

The XRD spectrum of the LP superplasticizer is shown in Figure 5, which indicates the presence of a number of peaks with varying intensities.

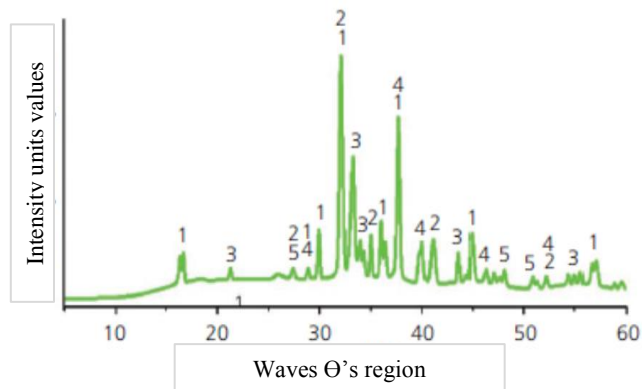


Figure 5. XRD spectrum of novel LP superplasticizer. 1: sodium hydroxide; 2: sodium silicate; 3: native cellulose; 4: b-D-fructose; 5: phenol.

The spectrum shows a broad non-symmetrical hump between 5.2 and 18° 1q, indicating the presence of non-crystalline phases and the vitreous nature of the LP superplasticizer. In fact, the vitreous nature actively participated in the geopolymerization reaction and resulted in good mechanical strength of the geopolymeric concrete. The two major inorganic phases reported in the novel LP superplasticizer were sodium silicate (Na_4SiO_4) and sodium hydroxide. Three minor organic phases originated due to the action of alkali on rice husk, and these were native cellulose ($\text{C}_6\text{H}_{12}\text{O}_6$)_x, b-D-fructose ($\text{C}_6\text{H}_{12}\text{O}_6$) and phenol ($\text{C}_6\text{H}_6\text{O}$). The action of sodium hydroxide on the inorganic silica present on the outer surface of rice husk resulted in the in situ synthesis of sodium silicate, which provided an intense amorphous nature to the developed LP superplasticizer. It is to be noted that sodium silicate acts as a seeding agent for geopolymerization reactions and, in the present study, it was synthesized in situ by the continuous alkaline digestion of rice husk and thus promoted the degree of geopolymerization reactions during the addition of the LP superplasticizer to the concrete mixture. The plasticizing effects were contributed by organic phases in the LP superplasticizer – namely, native cellulose, fructose and phenol. XRD peaks provided strong signals of crystalline cellulose in the LP superplasticizer sample, whereas the amorphous part of the cellulose structure is represented by a broad and less clear diffraction pattern. The evolution of native cellulose in the LP superplasticizer directly indicated the action of

alkali on rice husk during high-temperature alkaline digestion. Due to the complexity of the structures of hemicelluloses and lignin, it is difficult to envisage the complete transformations and rearrangements during alkaline digestion of rice husk, but XRD peaks of the resulting inorganic and organic fractions clearly indicated the action of sodium hydroxide on the rice husk inorganic silica and organic cellulose, hemicellulose and lignin to produce hydrolysis products such as b-D-fructose and phenol in the LP superplasticizer. Furthermore, it is to be pointed out that the commercially available water-reducing organic plasticizers for cement concrete systems perform the function of dispersants into the mixture, where they provide electric repulsion of positive and negative charges and hence the charged cement grains tend to separate from each other to acquire good flowability.

3) Scanning electron Microscopy (SEM) of geopolymer materials

SEM was carried out to study the morphology and microstructure of the selected samples (Obebe et al., 2023; Jindal and Sharma, 2020; Muhammad et al., 2019; Palcis, 2023; Shill et al., 2020; Silva et al., 2020). Thus, a comparison between the microstructure of various binders and alkaline activator were conducted and presented in Figures 6 (a-c). Sodium silicate was noticed at $300 \times 894 \mu\text{m}$, $500 \times 536 \mu\text{m}$ and $3000 \times 268 \mu\text{m}$ and the pulverized RHA was crusted with a platinum coating before performing the experiment, so as to enhance the visibility problem encountered during smooth charge conductivity exact topographic examination. SEM result for RHA also confirmed the result of chemical configuration of RHA by XRF, where at spectrum⁻¹, larger quantity of silicon, lesser amount of alumina and oxygen were perceived ascertaining the presence of a large quantity of silica which is in line with result of Phoongerkham, (2017) and Chouhan et al., (2018). Figure 6a for various scanning level displays that most of fly ash particles will form strong bond with the aggregate, and an additional dense gel will also formed if activated. Voids ratio and extended micro cracks will be remarkably decreased because of the dense gel that filled the voids and micro cracks if the binders used in producing geopolymer concrete. The kaolin structure has number of sheets per layer of about 10-50 pieces, size of 1-10 μm and huge quantity of quartz mineral which is the dirtiness of kaolin mineral. Laboratory-produced silicate will cause more homogeneous, compact, and finer microstructure (Figures 6b & c), this is similar to the observation by Dewi et al., 2018, after usage.

Table 1. Mix design values for FA-based geopolymer concrete

Mix ID	Molarity	Aggregate (kg/m ³)		Binders (Kg)				SS/SH Ratio	Density (kg/m ³)	Water (liter/m ³)	Age (days)	Slump (mm)
		Fine	Coarse	Cement	Fly	RHA	KC					
A ₁	-	360	720	720	-	-	-	2239	184.2	28	110	
A ₂	12	1080	2160	320	180	120	100	2252	184.7	28	112	
A ₃	12	1080	2160	-	360	180	180	2257	184.2	28	112	
A ₄	12	1080	2160	-	360	180	180	2260	187.4	28	114	

A₁ is control concrete; A₂ is partially replaced geopolymer concrete (GPC); A₃ is GPC using factory-produced sodium silicate and A₄ is GPC using laboratory-produced sodium silicate. SS is sodium silicate; SH is sodium hydroxide; RHA is rice husk ash and KC is kaolin clay.

Table 2a. FTIR values for fly ash

Band (cm ⁻¹)	Transmittance (%)	Functional group
791.8	27.7	Alkenes = CR'R'' s = C-H bend
1635.2	90.9	Alkenes Vw-m C=C Stretch
3695-8	27.4	Amides R-C (O) – NH ₂ , w-m N-H Symmetric and asym stretch
3450-3	49.9	Amides R-C (O) – NH ₂ , w-m N-H Symmetric and asym stretch
1041-3	7.1	Alkyl halides, R-F Vs C-F Stretch
912-6	32.4	Alkenes RCH = CH ₂ , m+ s = C-H bend
467.9	12.2	Alkyl halides R-I, C-I stretch
3623-4	13.4	Amides R-C (O)- NH-R , N-H stretch

FTIR is Fourier transform infrared spectroscopy

Table 2b. FTIR values for kaolin clay

Band (cm ⁻¹)	Transmittance (%)	Functional group
1982.9	101	Alkynes R-C = C-4, medium C=C stretch
3690.1	75.4	Amines – R- NH ₂ , N-H symmetric and asym. Stretch, weak
3623	72.5	Amines – R- NH ₂ , N-H symmetric and asym. Stretch, weak
1114.5	75.2	Akyl halides R-F, very strongs, C- F stretch
790.2	70.1	Alkenes strong, RCH = R'R C-H band.
749.2	68.2	Alkyl halides R-CL, strong, C-CL stretch.
909.5	30.1	Alkenes, m+s = C-H bend, RCH = CH ₂
998.9	25.0	Alkenes, m+s = C-H bend, RCH = CH ₂

FTIR is Fourier transform infrared spectroscopy and RHA is rice husk ash

Table 2c. FTIR values for RHA

Band (cm ⁻¹)	Transmittance (%)	Functional group
2083.6	98.2	Alkynes R-C = C-H, medium, C= stretch
1982.9	98.0	Alkynes R-C = C-H, medium, C= stretch
1848.8	97.9	Acyl chlorides Ar – C(O) – Cl, C- 0 stretch
797.7	89.7	Alkyl halides intensity, strong, C-CL stretch
1058.6	62.4	Alkyl halides intensity, very strong, C-CF stretch

FTIR is Fourier transform infrared spectroscopy

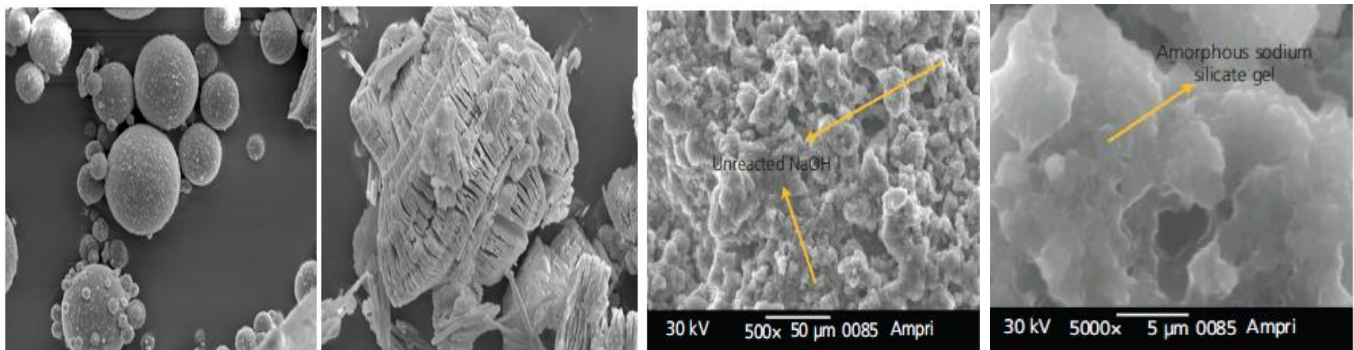


Figure 6. a) Morphology of fly ash; b) morphology of kaolin observed; c & d) SEM imageries of laboratory-created superplasticizer at four varied displaying the presence of extremely unstructured sodium silicate gel together with unoxidize sodium hydroxide.

The outcomes of the SEM and FTIR scrutinizes also support the SEM scrutiny.

4) SEM analysis on hardened concrete

SEM was carried out on hardened concrete cured by immersion in 5% sodium sulphate + 5% magnesium sulphate, 5% sodium chloride, 5% sodium sulphate, 3% sulphuric acid and water at 90 days. Comparison between the morphology and microstructure of various immersion were presented in Figures 5-7. Atomic concentrations of geopolymer concrete immersed in water and sodium sulphate solution shows 61.39% and 39.99% respectively for water and sodium sulphate immersion respectively for silicon content, while weight concentration for silicon content also confirm water at 56.31% as highest values, followed by sodium chloride value of 35.27% and least values for both atomic and weight concentration was sulphuric acid immersion with 32.93 and 28.24% respectively (Figures 7 & 8).

Aluminium content followed trend of sodium chloride (22.13% and 18.78%) as the extreme level, and sodium sulphate at 21.96% and 18.57% for both atomic and weight concentration measurement. The lowest immersion level was water (16.37%) and sulphuric acid (13.98%) for atomic and weight concentration respectively. Both atomic and weight concentration measurement for calcium content reveals highest values of 23.52% and 28.78% for sodium chloride immersion and 22.67% and 27.98% (sodium + magnesium sulphate) immersion, whereas water immersion has the least values 10.96% and 14.35%. But iron content highest values noticed from atomic measurement analysis was sulphuric acid (8.15%) and sodium + magnesium sulphate (6.32%), also weight concentration followed the same pattern of 10.86% (sodium + magnesium sulphate) as the greatest value but next as sodium chloride at 8.66%, while both concentration scrutiny displayed lowest value of 10.96% and 14.35% respectively for sulphuric acid immersion. SEM analysis on binders was used to ascertain if the selected binders are pozzolans or not; while on alkaline activators is to differentiate the impact of alkaline elements on various compositions of the alkali-activated flyash GPC. SEM on binders materials revealed that each binder have Silicon dioxide (SiO_2), Aluminumoxide (Al_2O_3), and iron (III) oxide calcium as vital materials and lesser amount of K_2O , Fe_2O_3 , TiO_2 , MgO and SO_3 , which ascertain that the three binders are pozzolans. Whereas, SEM on hardened concrete was employed so as to know microstructure and durability characteristics of geopolymers concrete after immersion inside 5 different chemicals and water. Similarly, SEM on hardened concrete at 90 days shows that various chemicals used has little or no effect on pozzolanic contents and other materials in the fly ash-based geopolymer, but greatly affected by water immersion. Furthermore, the outcome of durability impact on the hardened concrete shows that various chemicals

used has little or no effect pozzolanic contents and other materials in the fly ash-based geopolymer, but greatly affected by water immersion i.e water immersion decreases the geopolymer contents. Similarly, these outcomes also confirm tremendous improvement observed in the values of flexural , compressive and split tensile strength of geopolymer concrete immersed in 4 different chemicals, while water was the least. These verdicts are in agreement with the result of silicon, alumina, calcium and iron as resolute by [Adbelli et al., \(2017\)](#); [Omotayo and Arum, \(2023\)](#); [Samantasinghar and Singh, \(2020\)](#); [Rui et al., \(2024\)](#) and [Arum et al., \(2022\)](#).

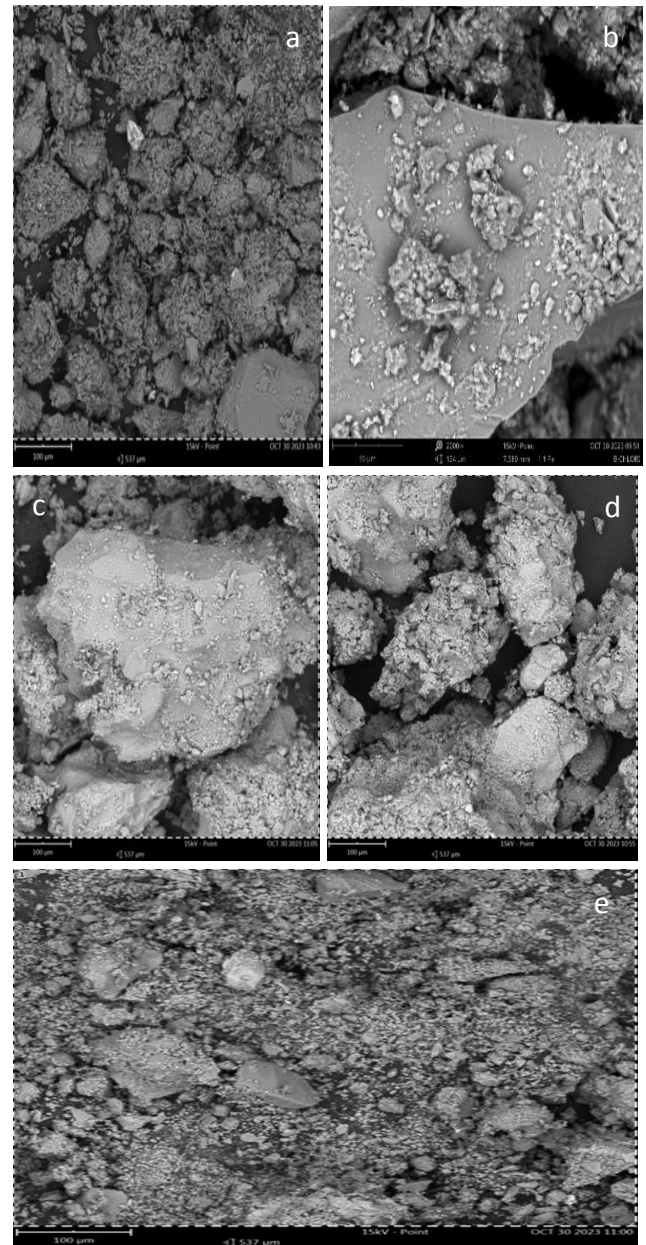


Figure 7. Outcome of GPC cured in (a) acid, (b) chloride and (c) water, (d) sulphate, and (e) magnesium immersion at 90 days.

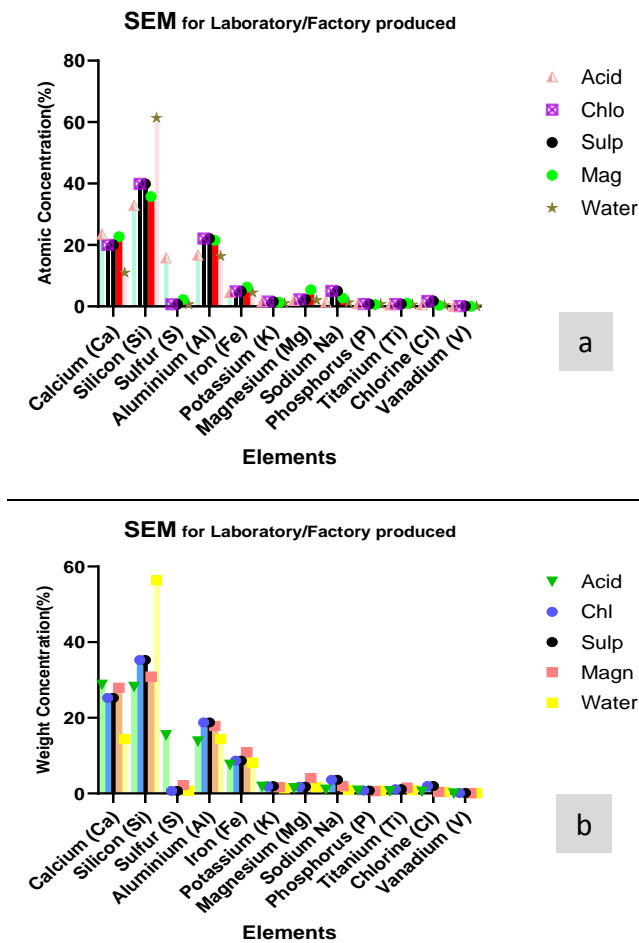


Figure 8. Outcome of SEM: a) Atomic concentration, and b) Weight concentration at 90 days.

5) Outcome of partially replacement compressive experiment

The compressive strength results for the various partially replaced geopolymer concrete are shown in Figures 9 and 10. The result shows that activation of cement based geopolymer reduces the compressive strength with increase in the percentage of cement with binders. However at 56 days, 7.5% partial replacement met the target strength of 1:1:5:3 mix ratio. Similarly, the compressive strength of the cement based geopolymer activated with 5% sodium silicate to reduce as the percentage of the binder increases. It is also observed that with the increase in the sodium silicate procured (i.e from 2.5% to 5% Na₂SiO₃), there was a gross increase in the compressive strength which led to the optimum percentage replacement to move from 7.5% to 12.5%. This indicate that the more the percentage addition of sodium silicate, the better the compressive strength for all the percentage replacement. The decrement in the compressive strength of the partially replaced fly ash-RHA geopolymer concrete owing to an imbalance of the Al/Si quotient, as binders contains slight quantity of alumina (Arum et al. 2022). On

the other hand, there could be an issue of dissolution of the silica extant in binders owing to lesser sodium hydroxide molar concentration as well as low temperature conditions of roughly 22–23 °C which would have stalled the polycondensation deeds of amorphous aluminosilicate GP products (Agashua et al., 2023; Phoo-ngernkham et al., 2017; Samantasinghar and Singh, 2020; Jindal and Sharma, 2020).

6) Outcome of total replacement compressive experiment

The result of the compressive strength at different days for the total replacement geopolymer concrete made from naturally made and procured sodium silicate are shown in Figures 11 and 12. Figures 10 and 11 shows that the naturally made sodium silicate increases the compressive strength as the temperature increases, with the optimum temperature of 70°C. The average compressive strength obtained at 70°C for the naturally made sodium silicate is 37.43N/mm², which is 273.21% percentage increment when compared with the control with the compressive strength of 13.7N/mm². Furthermore, the result of the procured sodium silicate shows an increment in the compressive strength of the geopolymer concrete as the temperature increases, even throughout the temperature variation from 25°C to 80°C. The average compressive strength obtained at 80°C for the procured sodium silicate is 31.03N/mm², which is 226.5% percentage increment when compared with the control with the compressive strength of 13.7N/mm². This is an indication that both the natural and the procured sodium silicate enhance the compressive strength of geopolymer concrete even more than double the control values. The behavior of the sodium silicate either procured or naturally made can probably be traced to the present aluminosilicates in the binders, which they help to polymerized. Similar result has also be reported in the literature that, addition of silicate source as an activator blended with hydroxide source will promote the condensation process of GPC (Adeshokan and Arum, 2023; Muhammad et al., 2019; Silva et al., 2020). The geopolymer concrete consists of super plasticizer (1.5%) and optimum of various binders i.e 5% FA + 7.5% KC + 10% RHA + aggregate + water at 7 and 14 days crushing for naturally made sodium silicate. The result shows that the naturally made sodium silicate increases the compressive strength as the curing temperature increases, with the optimum temperature still at 70°C. The average compressive strength obtained for 7 days at 70°C for the naturally made sodium silicate is 37.43N/mm², which gave 248.54% percentage increment when compared with the 14 days compressive strength of 93.03N/mm². The result indicates that the compressive strength of geopolymer concrete is a function of the curing days as well as curing temperature. The development of compressive strength at the various days was affected by the addition of the superplasticizer. However, the usage of superplasticizer

on the concrete strength must be limited to 1.5 because literature proves it that the optimum amount of

superplasticizer is 1.5 (Omotayo and Arum, 2022; Muhammad et al., 2020; Palcis, 2023; Dewi et al., 2018).

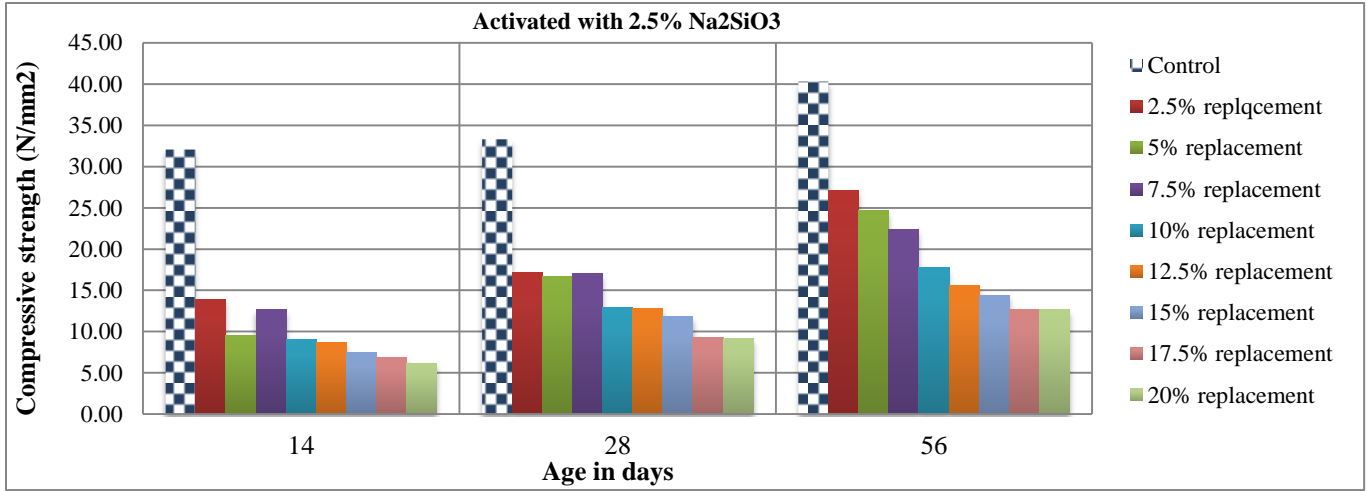


Figure 9. Compressive strength of partially replaced cement geopolymer concrete at different aging periods with 2.5% Na₂SiO₃.

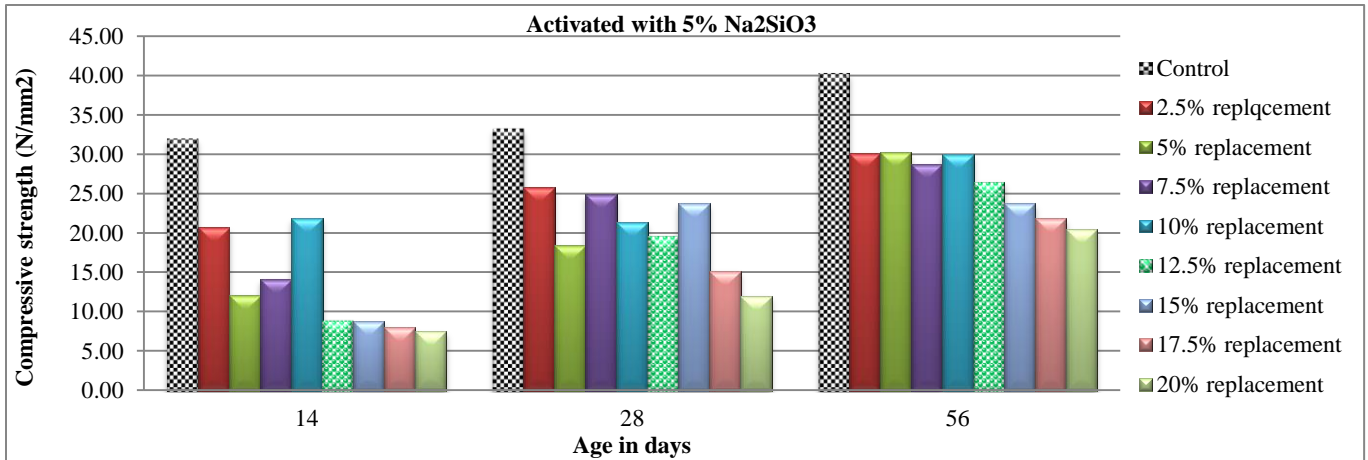


Figure 10. Compressive strength of partially replaced cement geopolymer concrete at different aging periods with 5% Na₂SiO₃.

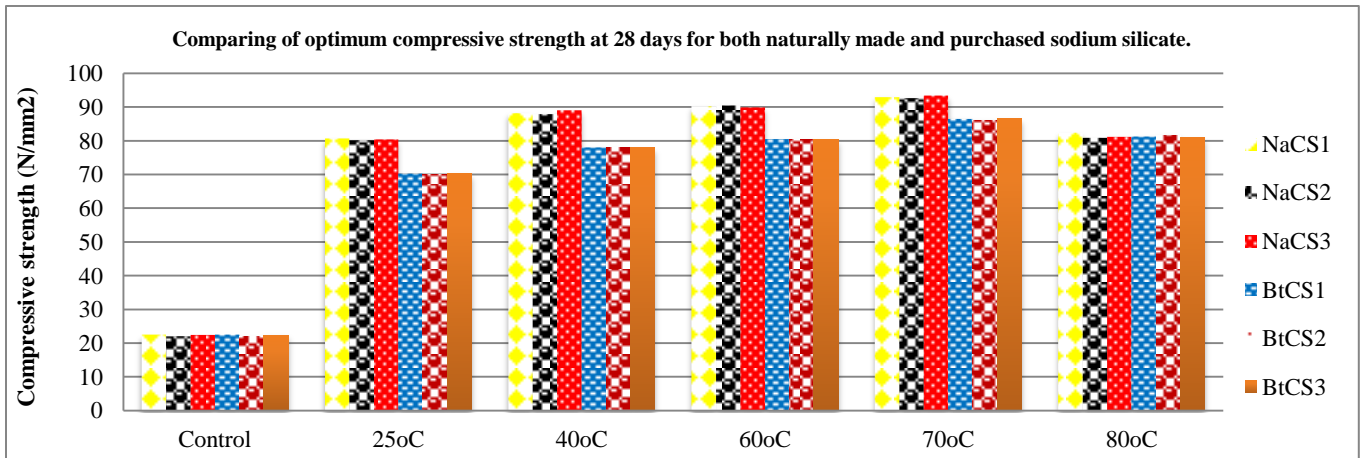


Figure 11. Optimum of Compressive strength at 28 days for various hot temperature. (Na: Naturally made sodium silicate; Bt: Purchased sodium silicate; CS: compressive strength).

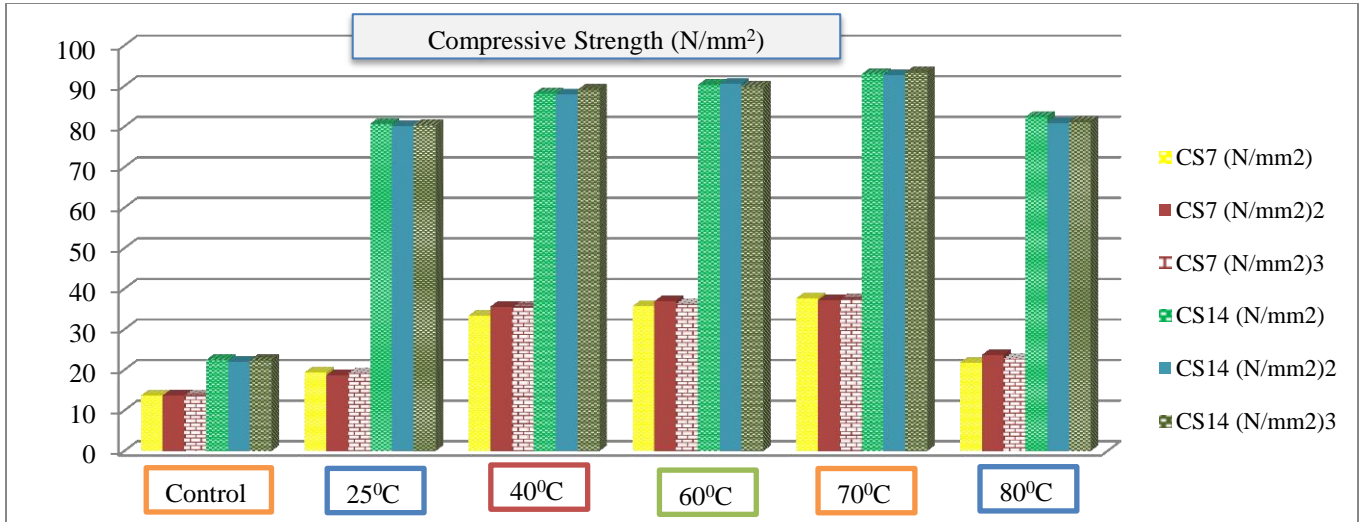


Figure 12. Compressive strength analysis outcome of varying temperature for 7 and 14 days (CS7: compressive strength at 7 days; CS14: compressive strength at 14 days)

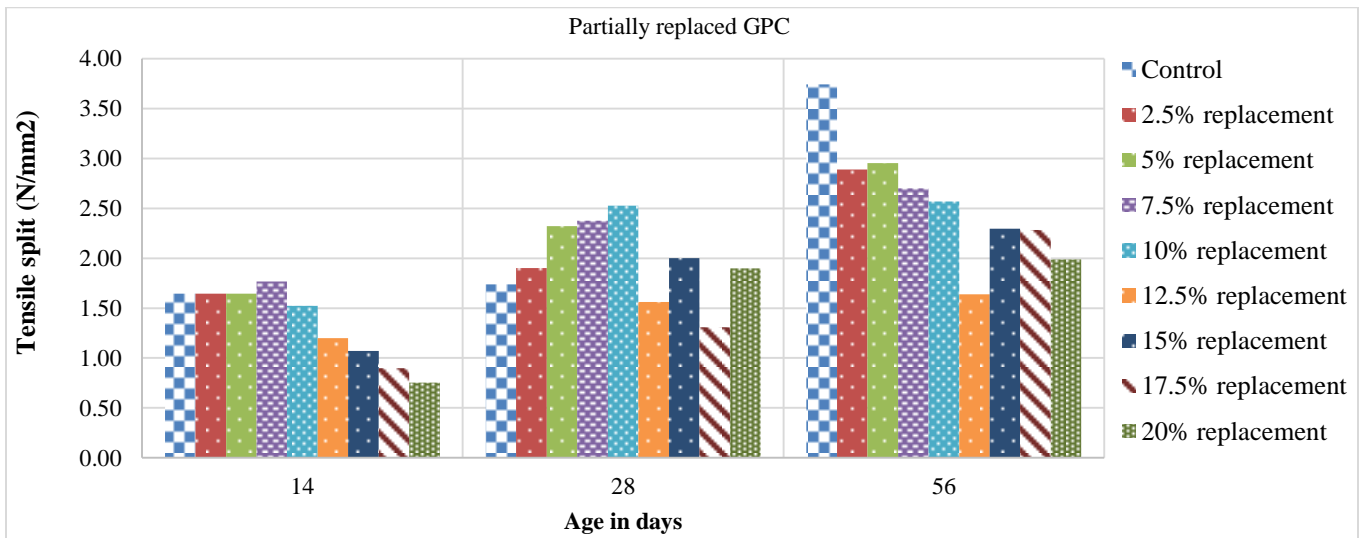


Figure 13. Split tensile strength test for activated fly ash based geopolymer.

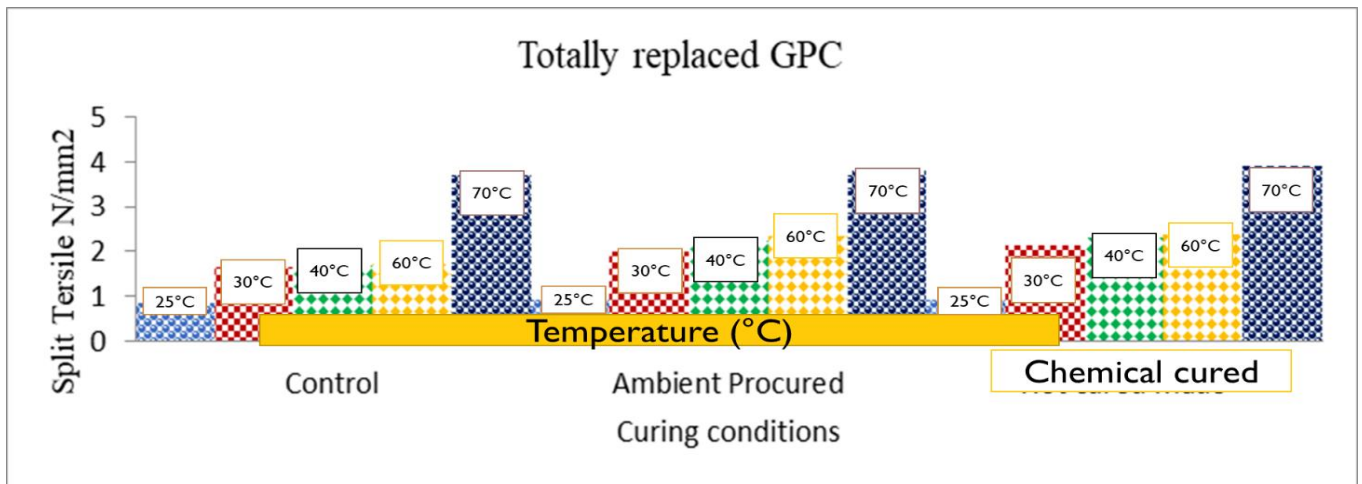


Figure 14. Split tensile strength test for activated fly ash based geopolymer. GPC = geopolymer concrete.

7) Outcome of split tensile strength analysis

The result of split tensile strength for the various partially and totally replaced geopolymer concrete are shown in Figures 13 and 14. Figure 13 demonstrated reduction in split tensile strength values as percentage replacement is increasing. While, as days increases totally replaced GP concrete increases as shown in Figure 14. Also, the outcome of totally replaced under differ different curing conditions displays that there is substantial increment on geopolymer concrete from naturally made sodium silicate with 1.1% percentage increment compared with control value of 0.87N/mm² at 7 days. Hence, using combine binders such as, kaolin clay and RHA to activate fly ash geopolymer substantially enhanced the totally replaced geopolymer concrete splitting tensile strength compared with partially replaced. Similar to compressive strength values, naturally made sodium silicate achieved higher splitting tensile strength values at different days of various hot-curing. It was ascertain from the experimental data that the indirect tensile values are at extreme compared to OPC for the mixes containing exact or beyond 30% replacement of cement with FA- KC - RHA. It was apparent that fly ash -RHA blended GPC specimens required at least of 13 h oven curing at 70⁰C temperatures (Bellium et al., 2019; Sing, 2018). Also, with the extra little quantities of Kaolin clay to FA-RHA based GPC, the oven curing can be avoided, and the desired strength, though below oven curing can be attained at ambient curing circumstances. It is evident that the increases of RHA content in the mixes the strength values were also increasing (Adeshokan and Arum, 2023; Obebe et al., 2023; Omotayo and Arum, 2022; Agashua and Ogbiye, 2018; Pelisser et al., 2021; Palcis, 2023). The highest splitting tensile strength was recorded when using GPC with 7.5% kaolin clay and 10% RHA with 5% fly ash content. Palcis (2023) had the same conclusion for Fly-ash based GPC.

8) Porosity and sorptivity for optimum laboratory/factory produced with superplasticizer

The outcome of porosity and sorptivity test for optimum laboratory/factory produced with superplasticizer is presented in Figures 15 and 16. Figure 15 reveals 5.2% and 4.7% at 70⁰C as the highest and 2.6% and 2.0% at 25⁰C as the lowest porosity values for laboratory and factory -produced sodium silicate GPC respectively. Whereas control highest value at 70⁰C was 2.8% and least value of 1.34% at 25⁰C. As temperature increases, porosity values both laboratory and factory-produced sodium silicate GPC enhanced, but reduce after 70⁰C.

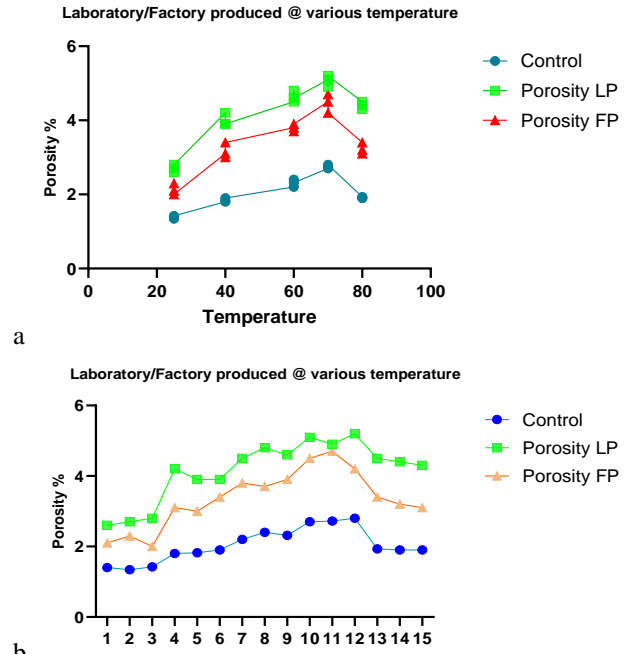


Figure 15. a) Varying temperature vs absorption, b).Absorption vs control of laboratory/factory-created sodium silicate.

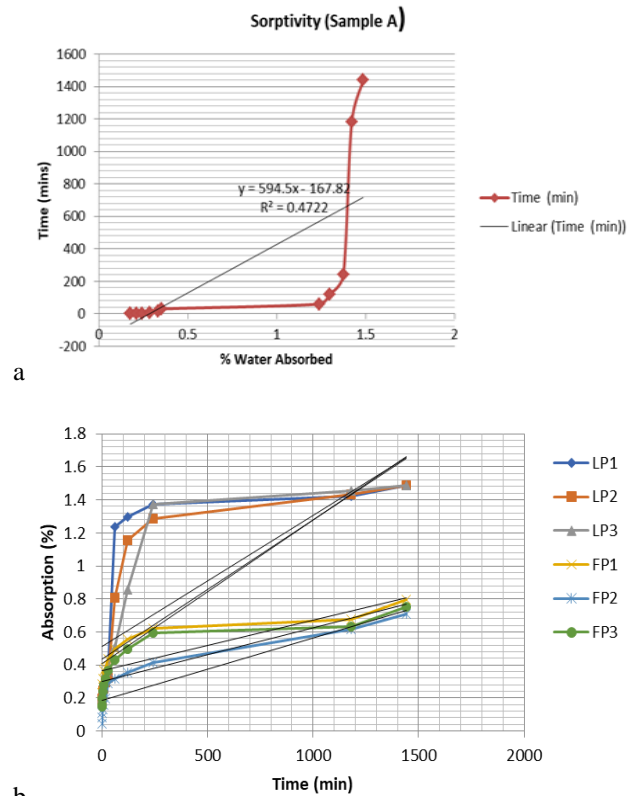


Figure 16. a) Sorptivity outcome of varying temperature and b) Outcome of varying temperature for optimum absorption level.

Sorptivity test (Figures 16) at initial time of 0.5min has the least water absorption values of 0.169019% and 0.044513%, and highest water absorption values of 1.487628% and 0.798575% at 1440mins for laboratory and factory-produced sodium silicate GPC respectively. As the time enhanced, absorption values also increases for both concrete. These results is in agreement with the totally replaced strength analysis result, which shows that as temperature enhances, GPC concrete strength amplifies. Pelisser et al., (2021), Cong and Cheng, (2021), and Dewi et al., (2018) had the same supposition for Fly-ash based GPC.

9) FA-based geopolymer concrete model formular

Two (Feret and Abram) models were utilized for the mixture proportion of concrete method and the outcome are display in Figures 17 and 18. P values, determination coefficient R², correlation coefficient R and the standard error are estimated so as to ascertain the accuracy of the Feret and regression model. Besides, there is need to known whether the variables are correlated and they are abridged in Table 3.

Regression analysis was done on the modified models to find the empirical constant of the best fit equation with a extreme R² values and lowest loss function. Data pre-processing or normalization was carried out also, because the dataset has input values with varied scales. Thus, this approach accurately ascertains the minimum as well as maximum noticeable values, since redundant predictors can alter models precision and lead to unreliable predictions. Besides, the relation expressed formular from modified model used are represented in (Eqn 1 – 2). Eqn (1) was generalized from number of specimens (A, B, C, D and E) i.e independent variable, which are correlated to the Y (dependent variable). Thus, the correlation (Table 4) can be ascertain as diverse sets of experimental data points (dependent variables - Y1 to Y15) and (independent variable: A (A₁ to A₁₅), B (B₁ to B₁₅), C (C₁ to C₁₅), D (D₁ to D₁₅) and E (E₁ and E₁₅). Whereas, constant K (K₁, K₂, K₃, K₄ and K₅) are proportionality coefficients between diverse Y and A - E values.

The resulting 28 days strength prediction model for flyash-based GPC mixes are summarized by the Eqn (2)

$$Y = [K1 (A)^{N1}]x [K2 (B)^{N2}]x [K3 (C)^{N3}] x$$

$$[K4 (D)^{N4}]x [K5 (E)^{N5}] \tag{1}$$

$$28 \text{ days} = -125.73 + 0.709 (7 \text{ days}) + 0.0324b + 0.056d \tag{2}$$

Where; d is density and b is binders (such as cement, flyash, rice husk ash and kaolin clay), Y is dependent variables, A to E is independent variables.

These models predicts compressive strength of conventional concrete from the concentration of cement in cement paste, which also include maximum paste thickness around aggregate particles and the effect of age of conventional concrete. Experimental results indicated that there is a strong relationship between the compressive strength of geopolymer concrete and the geopolymer binder concentration.

A) FA-based geopolymer concrete prediction process

As recommended by previous researcher such as Chouhan et al., (2018), Palcis, (2023) and Silva et al., (2020), the predictive performance of the Feret and Abram model is measured using the Mean Absolute Error (MAE), Mean Absolute Percentage Error (MAPE), Root Mean Squared Error (RMSE), Forecast Bias (B), and coefficient of determination (R²) metrics. The coefficient of determination (R²), which is calculated using Equations (3 and 4), and others through (Equations 5-7), are popular metric for evaluating models.

$$R^2 = 1 - [\sum_{i=1}^n (y_i - t_i)^2 \div \sum_{i=1}^n (t_i - \bar{t})^2] \tag{3}$$

$$R^2 = 1 - \{ \sum_{i=1}^n (Predicted_i - Actual_i)^2 - \sum_{i=1}^n (Actual_i - \bar{Actual})^2 \} \tag{4}$$

Where, *Predicted i* signifies the anticipated strength of *ith* sample, *Actuali* symbolizes the actual strength of *ith* sample and *Actual* exemplifies the mean of all samplings' actual strength.

n is the number of specimens, *ti* signifies observed outcomes, *yi* means projected outcomes, *t̄* is the sampling mean (i.e., $t = \sum_{i=1}^n t/n$).

$$MAPE = \frac{1}{N} \sum_{i=1}^n \{ |(Actual_i - Predicted_i) \div Actual_i| \} \times 100\% \tag{5}$$

$$RMSE = \sqrt{\frac{1}{N} \sum_{i=1}^n (Actual_i - Prediction_i)^2} \tag{6}$$

Table 3. FA-based GPC statistical analysis output

	Regression Statistics	Parameters		Coefficient		P-Value
Multiple R	0.99	Intercept		b_0	-125.7	0.00031
R^2	0.97	7 days CS	X_1	b_1	0.71	0.00011
Adjusted R^2	0.96	Binders	X_2	b_2	0.032	0.0133
Standard Error	1.58	Density	X_3	b_3	0.056	0.00021
Observations	94					
ANOVA		df		SS	SH	F
Regression		3		3437.704	1145.65	455.65
Residual		23		55.251	2.513	
Total		26		3492.951		

Style of silica, Alumina together with ratio of Al/si and Ca/(Si + Al)

Combination	SiO ₂	Al ₂ O ₃ mol	Al/Si	Ca/(Si + Al)
A+B+C (1)	0.87	0.24	0.28	0.20
B+C+D (2)	0.83	0.23	0.28	0.35
C+D+E (3)	0.78	0.23	0.29	0.32
D+E+F (\$)	0.74	0.22	0.30	0.40

Highpoints of the regression equations of the various experimental specimens.

Classification of Mol samples	Linear regression equation
Al/Si, Correction Coefficient = 0.97 (12M, 7 days)	$y = 19.18 + 11.11x$
Al/Si, Corr. Coef = 0.98 (12M, 28 days)	$y = 15.10 + 7.57x$

Statistical parameters and errors encounter during forecasting of the required Empirical model

Models	MAE	RMSE	R^2	Bias
Feret	2.392 ± 0.21	3.459 ± 0.35	0.959 ± 0.01	0.648 ± 0.47
Abram	2.343 ± 0.26	3.854 ± 0.50	0.957 ± 0.01	0.139 ± 0.18

SS is sodium silicate; SH is sodium hydroxide and Mol is molarity, MAE is mean absolute error and RMSE is the root mean square error.

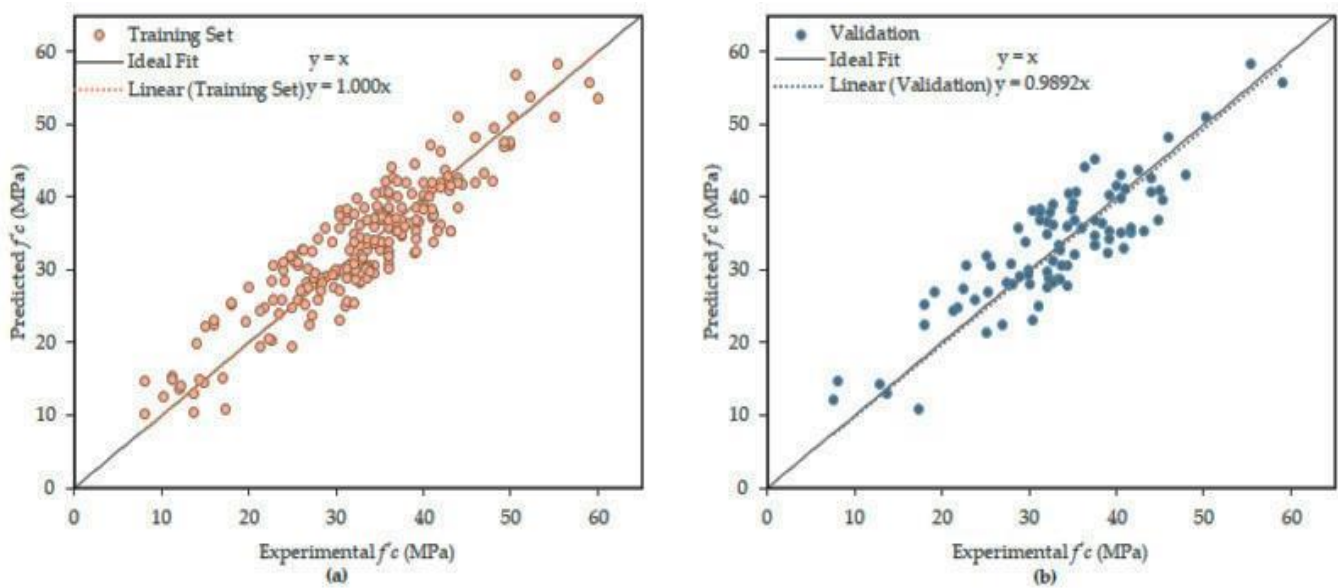


Figure 17. Experimental and forecasted values for compressive strength scrutiny: a) training and b) validation set values at various curing temperature.

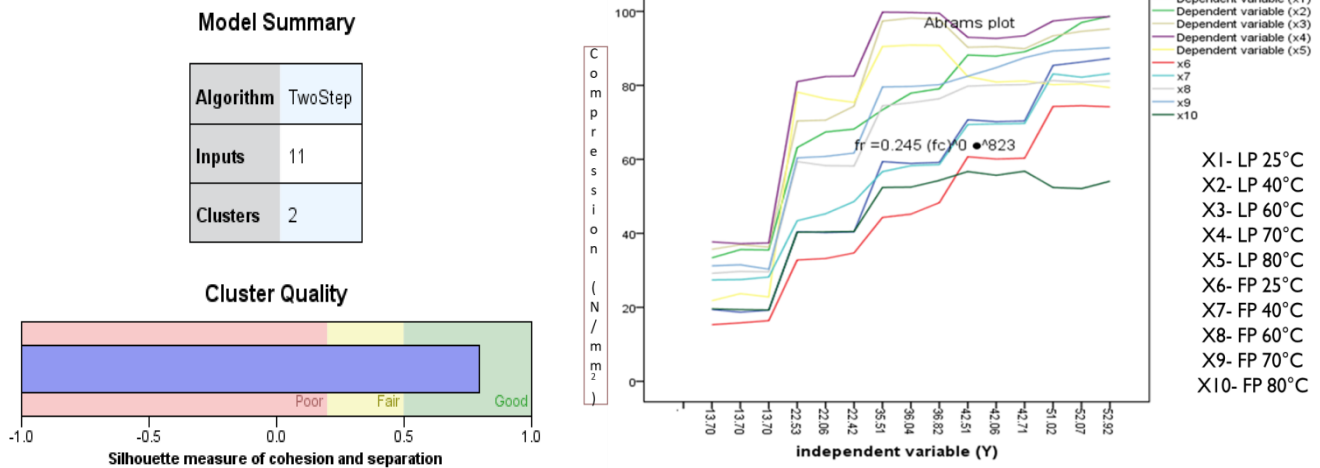


Figure 18. a) Model prediction cluster quality; b) independence vs dependence variable at various curing temperature. LP=Laboratory produce); FP=Factory produced.

Table 4. Dependent and independent variables (laboratory- produced GPC)

Sample ID	Various days	Control	25°C	40°C	60°C	70°C	80°C
		Y (dependent)	A (Independent)	B (Independent)	C (Independent)	D (Independent)	E (Independent)
A	ST7a	Y ₁ (0.87)	A ₁ (0.92)	B ₁ (0.93)	C ₁ (0.94)	D ₁ (0.96)	E ₁ (0.94)
A	ST7b	Y ₂ (0.86)	A ₂ (0.91)	B ₂ (0.94)	C ₂ (0.94)	D ₂ (0.97)	E ₂ (0.92)
A	ST7c	Y ₃ (0.86)	A ₃ (0.93)	B ₃ (0.93)	C ₃ (0.95)	D ₃ (0.96)	E ₃ (0.93)
B	ST14a	Y ₄ (1.65)	A ₄ (2.02)	B ₄ (2.04)	C ₄ (2.07)	D ₄ (2.15)	E ₄ (2.09)
B	ST14b	Y ₅ (1.65)	A ₅ (2.02)	B ₅ (2.05)	C ₅ (2.09)	D ₅ (2.14)	E ₅ (2.08)
B	ST14c	Y ₆ (1.66)	A ₆ (2.03)	B ₆ (2.04)	C ₆ (2.08)	D ₆ (2.16)	E ₆ (2.07)
C	ST21a	Y ₇ (1.69)	A ₇ (2.23)	B ₇ (2.25)	C ₇ (2.28)	D ₇ (2.32)	E ₇ (2.12)
C	ST21b	Y ₈ (1.68)	A ₈ (2.24)	B ₈ (2.26)	C ₈ (2.29)	D ₈ (2.31)	E ₈ (2.20)
C	ST21c	Y ₉ (1.69)	A ₉ (2.22)	B ₉ (2.25)	C ₉ (2.27)	D ₉ (2.33)	E ₉ (2.19)
D	ST28a	Y ₁₀ (1.73)	A ₁₀ (2.35)	B ₁₀ (2.37)	C ₁₀ (2.39)	D ₁₀ (2.40)	E ₁₀ (2.21)
D	ST28b	Y ₁₁ (1.72)	A ₁₁ (2.36)	B ₁₁ (2.38)	C ₁₁ (2.4)	D ₁₁ (2.43)	E ₁₁ (2.19)
D	ST28c	Y ₁₂ (1.73)	A ₁₂ (2.34)	B ₁₂ (2.38)	C ₁₂ (2.42)	D ₁₂ (2.44)	E ₁₂ (2.18)
E	ST56a	Y ₁₃ (3.33)	A ₁₃ (3.31)	B ₁₃ (3.34)	C ₁₃ (3.41)	D ₁₃ (3.91)	E ₁₃ (3.02)
E	ST56b	Y ₁₄ (3.34)	A ₁₄ (3.30)	B ₁₄ (3.36)	C ₁₄ (3.42)	D ₁₄ (3.90)	E ₁₄ (3.04)
E	ST56c	Y ₁₅ (3.36)	A ₁₅ (3.29)	B ₁₅ (3.35)	C ₁₅ (3.43)	D ₁₅ (3.92)	E ₁₅ (3.03)

$$MAE = \frac{1}{N} \sum_{i=1}^N |Actual_i - Predicted_i| \quad (7)$$

The value of R^2 is not up to 1 with 1 signifying model perfect fit. The horizontal axis is the observed strength and the vertical axis symbolizes the strength anticipated by the Feret model. In all, the data points that were clustered near the diagonal line for both test as well as training sets, demonstrating that the model provides precise values of the compressive strength (Figure 17a). Further, series of machine learning predictive models were then employed to predict the compressive strength of geopolymer

concrete with laboratory-produced sodium silicate and hydroxide alkaline as activator (Figure 17b). These regression predictive techniques were divided into three main categories which are trees, Gaussian and Support Vector Machine techniques together with linear regression using the regression learner application in Matlab version 2022. Their performance were also rated using the Root Mean Square Error (RMSE), Mean Square Error (MSE), Mean Absolute Error (MAE) and R-square error indices, the lower the result of these performance indices. Figure 17c shows that the difference between the true and

predicted was minimal for all except one of the plot which shows good predictive returns. Likewise, more of the errors are close to the zero residual line, showing positive returns in error minimization and good predictive performances. It is perceived that the anticipated formulation gives close results to the experimental data and the usage of alkali solution ratios in the creation of geopolymer concrete enhances the calculated values statistically.

B) Performance, void ratio, extended micro cracks and reliability impact of FA-based geopolymer concrete

The performance of flyash-RHA based GPC can be improve through addition of moderate amount of kaolin clay and 1.5% laboratory produced superplasticizer, so as to solve problem of hot curing and workability issues associated with it. For this type of flyash-RHA geopolymer concrete (FRGPC), the workability enhanced from the production to the concrete placement time and minimal slump loss ensued over 2 hours (in contrast with ordinary Portland cement (OPC) concrete. Besides, with strain gauge embedded techniques there is little initial in situ expansion and tensile stain growth till 14 day. But at 90 days OPC concrete cracked but FRGPC concrete remain uncracked. This behavior can be as a result of higher tensile strain capability of FRGPC than OPC concrete created through higher creep and lesser elastic modulus. Reliability of the expected performance of flyash-RHA GPC is evaluated through various methodologies based on Ferret, linear regression and specialized reliability software package. Reliability methodologies that were considered comprised full coupling with an Feret and Abram modified equations and surface response centered approaches together with first order reliability techniques or importance sampling approach.

C) Geopolymerization, thermal conductivity and stability of FA-based geopolymer concrete

Flyash-RHA based GPC have unveiled significant resistance to higher temperatures with addition of moderate amount of kaolin during production, as verified in the laboratory against cracking, durability and strength degradation. At optimum curing temperature of 60°C for metakaolin based geopolymers shows the best mechanical and physical properties. This is an indication that below or above 60°C curing temperature greatly affect metakaolin based geopolymers adversely. While, FRGPC activated with pure kaolin trend is as curing days increases both factory-produced and laboratory-produced geopolymer

concrete increases, with the optimum temperature at 70°C. Also, Thermal conductivity (k-value) which is a material's property that ascertains its heat conduction ability reveals that FA-RHA based GPC was below that of control (OPC) concrete. So as to simulate heat transfer via the GPC, the thermal diffusivity was computed, via 500 × 500 mm OPC as control and flyash-RHA GPC (partial and pure GPC). The outcome shown an extremely small thermal conductivities of 100% laboratory-created sodium silicate fly ashes- RHA geopolymer (LCSSFRGP) concrete, ranging from 0.048 to 0.087 W/mK, advocate for a possible usage of LCSSFRGP for thermal insulation, for instance fireproofing materials. Besides, witnessed results proved that the thermal conductivity of LCSSFRGP concrete almost linearly reduced as cement content increased whereas the discrepancy of thermal conductivity of LCSSFRGP concrete caused by ambient temperature was relatively low. Furthermore, the thermal conductivity of LCSSFRGP concrete was lesser than that of factory-created geopolymer concrete.

Flyash-RHA GPC can considerably enhance the thermal stability of geopolymers, i.e with optimum of various binders of 5% FA + 7.5% KC + 10% RHA + 1.5% superplasticizer aggregate + water, the better thermal stability were between 700°C to 900°C.

CONCLUSION

This research discusses experimental studies of locally made super-plasticizer geopolymer concrete. SEM and FTIR reveal clearly that all the binders selected have calcium, alumina and silica as vital materials and others in lesser quantities. Strength test for partially replaced cement GPC at different curing days up to 56 days, signifies that up to 10% replacement of other binders the compressive strength increases. While optimum for naturally made super plasticizer were 1.5% and various binders as 5% FA + 7.5% KC + 10% RHA + aggregate + water for both naturally made and readymade sodium silicate. The result also shows that as hot temperature increases both compressive strength increases, while the weight of GPC was decreases till 70°C. There is reduction in split tensile strength values as percentage replacement is increasing, but for totally replaced GP as days increases split tensile strength values increases. This indicate that the more the percentage addition of sodium silicate, the better the strength for total percentage replacement. Likewise, durability impact on the hardened concrete shows that various chemicals used except water has little or no effect on pozzolanic contents and other materials in

the fly ash-based geopolymer, It can be concluded that geopolymer concrete made from rice husk ash, fly ash and kaolin clay with combination of alkaline activator from both natural and factory-produced sodium silicate are good material for high performance concrete. Finally, linear regression, Feret and Abrams modeling shows that the difference between the true and predicted was minimal, which indicate good predictive returns.

DECLARATIONS

Corresponding Author

Correspondence and requests for materials should be addressed to Lucia Omolayo Agashua; agashualight@gmail.com; ORCID: 0000-0002-5262-5710.

Data availability

The datasets used and/or analysed during the current study available from the corresponding author on reasonable request.

Acknowledgements

The authors would like to acknowledge the Nigerian Building and Road Research Institute (NBRI) Jabi Abuja, Federal Ministry of Works, concrete and pavement unit Sheda Abuja laboratories and Chemical and Material Engineering laboratory, Umaru Musa Yaradua University Dutsin Ma, Kastina. for creating a conducive environment to conduct this research.

Authors' contribution

Agashua LO performed the experiments, Agashua LO, Arum C and Ikumapayi CM analysed the data obtained and wrote the manuscript. Arum C and Oluyemi-Ayibowu designed the experimental process and revised the manuscript. All the authors read and approved the final manuscript.

Competing interests

The authors declare no competing interests in this research and publication.

REFERENCES

- Abdelli K, Tahlaïti M and Oudjit MN. (2017). Influence of the origin of metakaolin on pozzolanic reactivity of mortars Energy Procedia.139(2), 230-235. Available at: <https://doi.org/10.1016/j.egypro.2017.11.201>
- Adeshokan M and Arum C. (2023). Comparison between the Compressive Strength of Binary and Ternary Alkaline activated Pozzolanic Concrete. J. Appl. Sci. Environ. Manage., 27 (1), 747-752. Available at: <https://dx.doi.org/10.4314/jasem.v27i4.15>
- Agashua LO, Ogiye AS, Amu OO, Oluyemi-Ayibowu BD, Igibah CE and Onakunle O. (2023). Grapher Analysis and the Impact of Sodium Silicate Activator on Strength of Kaolin-rice husk ash stabilized laterite. Materials Today Proceedings, 74 (2), 377-388. Available at: <https://doi.org/10.1016/j.matpr.2022.09.171>
- Agashua LO and Ogiye AS. (2018). Influence of Cement, Bitumen and Lime on Some Lateritic Soil Samples as Pavement Material. ICESW IOP Publishing. IOP Conf. Series: Materials Science and Engineering 413 (1), 1-13. Available at: <https://doi.org/10.1088/1757-899X/413/1/012012>
- Arum C, Akande SP and Alabi SA. (2022). Strength Evaluation of Pozzolanic Concrete Containing Calcined Ceramic Waste And Glass Waste Powder. Journal of Engineering and Engineering Technology 16(1), 113-119. Available at: <https://doi.org/10.51459/futajeet.2022.16.1.420>
- Babatola O and Arum C. (2020). Determination of the Compressive Strength of Concrete from Binary Cement and Ternary Aggregates. Open Journal of Civil Engineering 10(4), 385 - 402. Available at: <https://doi.org/10.4236/ojce.2020.104029>
- Bellum RR, Nerella R, Madduru SRC and Indukuri CSR. (2019). Mix design and mechanical properties of fly ash and GGBFS-synthesized alkali-activated concrete (AAC). *Infrastructures*, 4(2): 20-29. Available at: <https://doi.org/10.3390/infrastructures4020020>
- Chouhan R.K, Mudgal M, Bisarya A and Srivastava A.K. (2018). Rice-husk-based superplasticizer to increase performance of fly ash based geopolymer concrete. *Emerging Materials Research*, 7(3), 1-32. Available at: <https://doi.org/10.1680/jemmr.18.00035>
- Cong P and Cheng Y. (2021). Advances in geopolymer materials: A comprehensive review. *Journal of Traffic and Transportation Engineering (English Edition)*, 8(2), 1-12. Available at: <https://doi.org/10.1016/j.jtte.2021.03.004>
- Dewi R, Agusnar H, Alfian Z and Tamrin T. (2018). Characterization of technical kaolin using XRF, SEM, XRD, FTIR and its potentials as industrial raw materials. *Journal of Physics Conference Series*, 1116(4), 11-23. Available at: <https://doi.org/10.1088/1742-6596/1116/4/042010>
- Faluyi F, Arum C, Ikumapayi CM and Alabi SA. (2021). Review of the Compressive Strength Predictor Variables of Geopolymer Concrete. *FUOYE Journal of Engineering and Technology*, 7(3), 1-11. Available at: <https://doi.org/10.46792/fuoyejet.v7i3.884>
- Hassan A, Arif M and Shariq M. (2019). Effect of curing condition on the mechanical properties of fly ash-based geopolymer concrete. *SN Appl Sci.*, 1(2), 1694 – 1707. Available at: <https://doi.org/10.1007/s42452-019-1774-8>
- Jindal BB and Sharma R. (2020). The effect of nano materials on properties of geopolymers derived from industrial byproducts: a state-of-the-art review. *Construction and Building Materials*, 252(1), 119-128. AVAILABLE AT: <https://doi.org/10.1016/j.conbuildmat.2020.119028>

- Obebe MD, Ikumapayi CM and Alaneme KK. (2023). Structural performance evaluation of concrete mixes containing recycled concrete aggregate and calcined termite mound for low-cost housing. *Alexandria Engineering Journal* 72(2), 237–346. Available at: <https://dx.doi.org/10.1016/j.aej.2023.03.095>
- Omotayo OO and Arum C. (2022). Challenges and Prospects of Widespread Adoption of Pozzolans for Building Construction: A Statistical Assessment. *International Journal of Engineering*. 35(10):1929-1940. Available at: <https://doi.org/10.5829/ije.2022.35.10a.12>
- Muhammad NS, Hadi I and Shelley P. (2019). Optimum mix design of geopolymer pastes and concretes cured in ambient condition based on compressive strength, setting time and workability. *Journal of Building Engineering*, 23(2), 301-313. Available at: <https://doi.org/10.1016/j.jobe.2019.02.006>
- Palcis RP. (2023). The Effect of Water Quality on Concrete Strength and Permeability: A Review of the Use of Chlorinated Water vs. Top Water in Concrete Mix Design. 2(1), 1-10. Available at: <https://doi.org/10.13140/RG.2.2.29845.81126/1>
- Pelisser F, Bernardin A.M and Michel M.D. (2021). Compressive strength, modulus of elasticity and hardness of geopolymeric cement synthesized from non-calcined natural kaolin. *Journal of Cleaner Production*. 280 (1), 124-136. Available at: <https://doi.org/10.1016/j.jclepro.2020.124293>
- Phoo-ngernkham T, Hanjitsuwan S, Damrongwiriyanupap N and Chindaprasirt P. (2017). Effect of sodium hydroxide and sodium silicate solutions on strengths of alkali activated high calcium fly ash containing Portland cement. *KSCE J.Civ. Eng.*, 21(6), 2202–2210. Available at: <https://doi.org/10.1007/s12205-016-0327-6>
- Rui L, Jizhao L, Huigang X, Da Y, Wenwei Y. (2024). Chloride ion diffusion performance of concrete and its influence on scour resistance. *Structures*, 60 (1), 105789. Available at: <https://doi.org/10.1016/j.istruc.2023.105789>
- Samantasinghar S and Singh S. (2020). Effects of curing environment on strength and microstructure of alkali-activated flyash-slag binder. *Construction and Building Materials*. 235(2), 117481. Available at: <https://doi.org/10.1016/j.conbuildmat.2019.117481>
- Shill SK, Al-Deen S and Ashraf M. (2020). Resistance of fly ash based geopolymer mortar to both chemicals and high thermal cycles simultaneously. *Construction and Building Materials* 239(2), 117886. Available at: <https://doi.org/10.1016/j.conbuildmat.2019.117886>
- Silva G, Kim S and Aguilar R. (2020) Natural fibers as reinforcement additives for geopolymer a review of potential eco-friendly applications to the construction industry. *Sustainable Materials and Technologies* 23(1), 42-56. Available at: <https://doi.org/10.1016/j.susmat.2019.e00132>
- Tatal, A, Partschefeld, S., Schneider, J., and Osburg, A. (2020). Effects of Bio-Based Plasticizers, Made From Starch, on the Properties of Fresh and Hardened Metakaolin-Geopolymer Mortar. *Geopolymer*, 68(1), 413–427. Available at: <https://doi.org/10.1007/s42860-020-00084-8>

Publisher's note: [Scienceline Publication](#) Ltd. remains neutral with regard to jurisdictional claims in published maps and institutional affiliations.



Open Access: This article is licensed under a Creative Commons Attribution 4.0 International License, which permits use, sharing, adaptation, distribution and reproduction in any medium or format, as long as you give appropriate credit to the original author(s) and the source, provide a link to the Creative Commons licence, and indicate if changes were made. The images or other third party material in this article are included in the article's Creative Commons licence, unless indicated otherwise in a credit line to the material. If material is not included in the article's Creative Commons licence and your intended use is not permitted by statutory regulation or exceeds the permitted use, you will need to obtain permission directly from the copyright holder. To view a copy of this licence, visit <https://creativecommons.org/licenses/by/4.0/>.

An Analysis of Water Demand of the Rural Population within the Iishana System, Namibia

Junias Eino¹  , Valentine Yato Katte¹ , Afis Olumide Busari¹ , Evanilton Edgar Serrão Pires⁴ , Petrina Johannes¹ , Monique Fahrenberg² , Christian Reinhardt-Imjela² , Robert Jüpner³  and Achim Schulte² 

¹Department of Civil and Mining Engineering, University of Namibia, Ongwediva, Namibia

²Freie Universität Berlin, Institute of Geographical Science, Applied Physical Geography – Environmental Hydrology, Germany

³Technische Universität Kaiserslautern-Landau, Germany

⁴Departamento de Engenharia, Instituto Superior Politécnico Tundavala, Angola

✉ Corresponding author's Email: juniaseino@gmail.com

ABSTRACT

The Namibian people, particularly, those living within the Iishana system, which is a subset of the Cuvelai Basin, often encounter recurrent floods and droughts. After each rainy season, the Iishana system dries up gradually, hence, water for both agriculture and potable purposes becomes crucial. With the anticipated new water infrastructural development and rehabilitation of existing ones, it will be necessary to ascertain the water demand of the rural population, for the quantification of the supply potential to improve water availability. This study adopts historical water consumption per capita recommended within the Iishana system to determine the rural population demand. Considering a thirty years' population projection, the water demand of the Iishana system is properly estimated. Moreover, the historical hydrological dataset daily data for the period 2012–2021 was used for the analysis. The current demand is estimated at 2,479 cubic meters per day. The projections of water demand for the rural population for 2033, 2043, and 2053 are 0.9, 0.5, and 0.1 Mm³/year, respectively. More so, the surface water resource potential of the system is estimated at an average of 300 mm/year. The region loses more water through evaporation than it receives in the wet season. Around 2500 mm of water evaporates from the surface annually, giving a water deficit of 2200 mm/year. The region's flat, shallow landscape, high evaporation rate, and the inadequacy of infrastructure have made the area vulnerable in terms of water security for both agricultural and potable purposes, resulting in droughts after the rainy season. With these findings, it is recommended to build water infrastructures within the region to improve the well-being and livelihood of rural communities.

Keywords: Water demand, Water supply, Rural population, Per capita demand, Iishana system, Namibia

INTRODUCTION

Water is a finite and vulnerable resource, vital to sustain life, development, and the environment, and should be recognized as an economic good, according to the Dublin principles (Mays, 2011). Water has evolved into a highly intricate commodity as it has been subjected to the principle of supply and demand. While planning a water supply scheme, water demand is assessed, to know the quantity of water required for an area (Basak, 2003).

The challenges associated with a water supply and its management have become a vital concern. Due to increased population growth, complimented by climate change, the water demand has increased, putting more pressure on the limited available water resources. Water shortage, access to clean water, and sanitation have meant

that water planners must balance finite water resources among domestic, agricultural, and ecosystem uses (United Nations-Water, 2018). To attain this, the full integration of water supplies, water quality, and environmental considerations must be necessitated (World Bank, 2022).

The estimation of water demand is very complex and intense. (MAWF, 2014) stated the various mathematical models that are, however, utilized for predicting future water demand. These include extrapolating historical trends, using simulation modelling, or correlating demand with socio-economic factors. These methods differ in complexity based on the number of criteria considered and how extensively water users are broken down by sectors, geographical location, season, or other variables (MAWF, 2014).

RESEARCH ARTICLE
 PII: S225204302400027-14
 Received: June 25, 2024
 Revised: September 02, 2024
 Accepted: September 05, 2024

decades. This average is then added to the present population and the population of successive decades to obtain the projected population. The population predicted by this method is the lowest among all forecasting methods. The forecasted population (P_n) after 'n' decades from the last known census can be calculated using the following (Eq. 1):

$$P_n = P_0 + n\bar{x} \quad (1)$$

Where: P_0 is the population at the last known census, \bar{x} is the arithmetic mean of population increase in the known decades, and n is the number of decades between the last census and the future.

Geometrical increase method

In this method, it is assumed that the percentage increase in population remains constant. The percentage increase is calculated from available census records. Subsequently, the population of future decades is estimated using this percentage increase. This method yields the highest predicted population of all. The forecasted population (P_n) after 'n' decades is given by (Eq.2):

$$P_n = P_0 \left(1 + \frac{r}{100}\right)^n \quad (2)$$

Where: P_0 is the population at the last known census, r is the probable rate of population increase per year (%)

Incremental increase method

In this method, the average population increase is calculated using the arithmetic increase method. Then, the average incremental increase is calculated. Finally, both averages are combined to project the population in future decades. The population predicted by this method falls between the predictions of the arithmetic increase method and the geometrical increase method. The population after "n" decades from the last known census is given by (Eq.3):

$$P_n = P_0 + l_a + nl_c \quad (3)$$

Where: P_0 is the population at the last known census, l_a is the average Arithmetical increase, l_c is the average Incremental increase.

Decreasing rate of growth method

The growth of life is limited. At times, growth starts off fast and then slows down. To calculate this, the average decrease in percentage increase is determined and subtracted from the percentage increase of each following decade. This average is then used to predict the population of the following decades (Eq. 4).

$$P_n = P_0 + \left(\frac{r-r_1}{100}\right) \times P_0 \quad (4)$$

Where: P_0 is the population at the last known census, r is the population increase for the last census (%), r_1 is the decrease in the percentage increase in population.

Procedures for calculating water demand

Water demand for domestic use

Water demand for domestic is the water consumed in residential houses for drinking, cooking, bathing, sanitation, and gardening, and depends mainly on living conditions (Mays, 2011). Using the adopted historical water consumption per capita of 40l/c/d for the Iishana system (MAWF, 2014), the domestic water demand is determined, successfully. The theoretical demand for water was calculated by multiplying the projected rural population by the individual domestic consumption.

Water demand for livestock

Livestock demand is water required for livestock drinking and depends on the age, stock size, and climatic conditions (Mays, 2011). On average, Large Stock Unit (LSU), including cattle, donkeys, or horses, consume about 45 liters/stock unit/day (MAWF, 2014). The livestock demand was computed by multiplying the livestock figure with the appropriate water consumption. Livestock numbers for the study area are calculated based on the carrying capacity of the rural areas at 10 ha/LSU (MAWF, 2014).

Water provision procedures

Water provision was determined based on the historical hydrological dataset daily data for the period 2012-2021, obtained from (SASSCAL WeatherNet). The study considered the Okalongo, Mahenene, Omafo, and Ogongo weather stations within the Iishana system, as depicted in Figure 3.

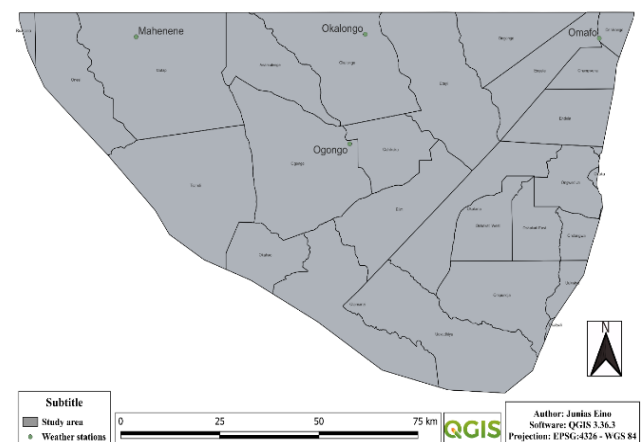


Figure 3. Weather stations within the Iishana system

RESULTS AND DISCUSSION

Population forecasting and justification of the adopted method

The probable future population is estimated using different methods highlighted in section 2.2. Theoretical results obtained from each of these methods are then compared with the actual population in 2023. Figure 4 shows the comparison of the actual and estimated population by various approaches for the Iishana system. The Arithmetic Increase Method (A.I.M) gives higher results than the actual one. The Geometric Increase Method (G.I.M) and the Incremental Increase Method (I.I.M) gave almost the same results, and the results are higher than the actual one. The Decreasing Rate of growth Method (D.R.M) exceeded the actual population slightly. This method gave satisfactory results compared to the other three methods. Hence, the Decreasing Rate of growth Method is used to estimate the probable future population.

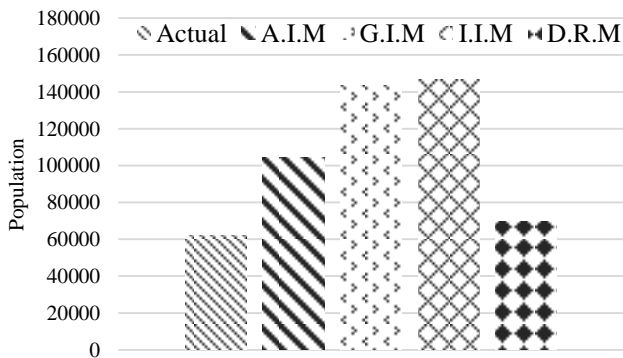


Figure 4. Comparison of actual and estimated population for the Iishana system

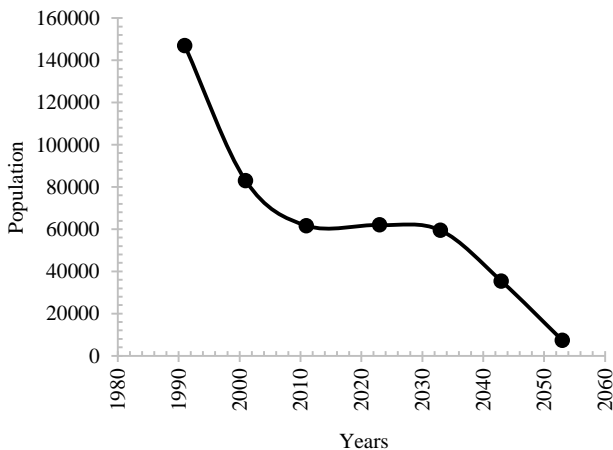


Figure 5. Estimation of the probable future population for the Iishana system.

Figure 4 shows the estimation of the probable future population for the Iishana system using the Decreasing Rate of growth Method. A declining population has been predicted furtherance to previous trend based on census data. A significant declining population difference of 84,970 has been observed between 1991 and 2023 (Table 1).

Current rural water demand estimation

The estimated water demand for the present year 2023/24 was calculated based on the current domestic population and livestock numbers, using adopted water consumption norms. The resulting estimate of the current rural water demand is shown in Table 3.

The total current rural water demand was calculated at 6,761 m³/d, with the domestic demand at 2,479 m³/d and the livestock demand at 4,282 m³/d, being 37% and 63% of the total, respectively (Figure 6).

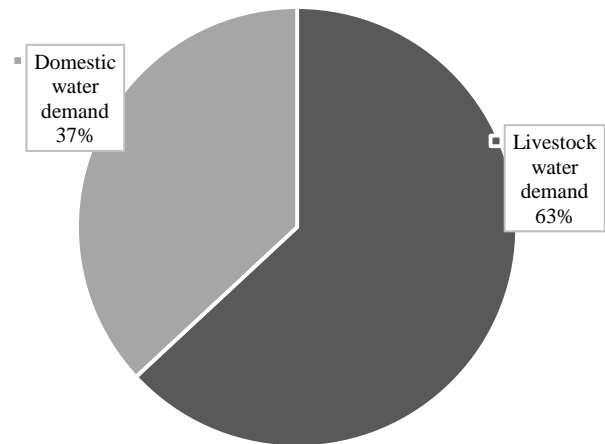


Figure 6. The water demand for various purposes within the Iishana system

Projected future rural water demand of the Iishana system

The anticipated future demand for water in the rural areas were estimated based on the projected future rural population. However, livestock numbers are not considered because they depend on the grazing capacity of the rangeland, which is not expected to improve over time. Figure 7 displays the estimated water demand for the rural population for the Iishana system. The water demand projections for 2033, 2043, and 2053 are 0.9, 0.5, and 0.1 Mm³/year, respectively. The decrease in water demand is a result of a population decline (Figure 5), as people move from rural to urban migration for better economic and social opportunities (Census, 2011). The urban population

increased by 75%, while the rural population decreased by 58% over a thirty-two (32) year period, from 1991 to 2023 (Table 2). The well-being and livelihood of rural communities are greatly affected by several challenges such as poor maintenance of water infrastructure, long distances to communal taps, inability to pay for municipal water supply, limited capacity to carry water, and specific times allocated for collecting water (Arendt *et al.*, 2021; Niipare, 2020; Shooya, 2017).

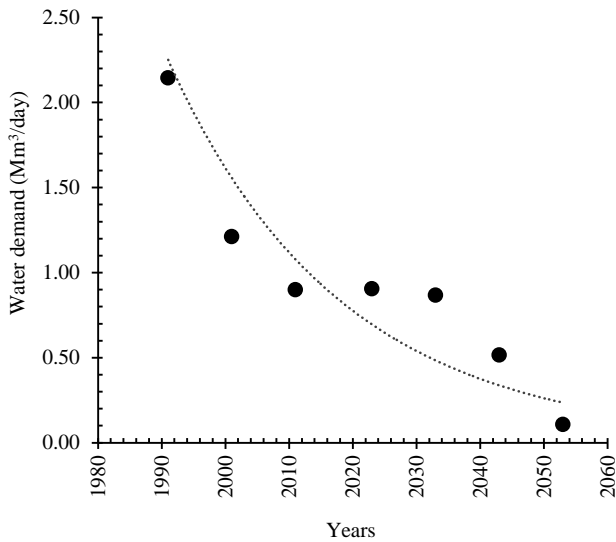


Figure 7. Estimated water demand for the rural population for the Iishana system.

Water provision

To estimate the supply potential for the Iishana system, the daily weather data were obtained from four key stations: Okalongo, Mahenene, Omafo, and Ogongo. However, it is found that both Omafo and Okalongo stations have limited data records from 2019 to 2021, with several missing data records. The Mahenene station has hydrological data from 2012 to 2019 but also with missing data records. On the other hand, the Ogongo station has satisfactory daily data records, making it the most reliable station out of the three. With hydrological data sets covering 2012 to 2021, the data from the Ogongo station is used to estimate precipitation, temperature, and evaporation rates for the Iishana system. The evaporation rate (E_r) is calculated using the energy balance method (Han, 2010) as follows (4):

$$E_r = \frac{1}{l_v \rho_w} (R_n - H_s - G) \tag{4}$$

Where: E_r is evaporation rate (m/s), H_s is sensible heat flux (in W/m^2 , to change liquid water temperature), G is the ground heat flux (in W/m^2 , to change underlying soil temperature), R_n is the net radiation flux (W/m^2), ρ_w is water specific density (kg/m^3), l_v is the latent heat of vapourization (J/kg), calculated using (5).

$$l_v = 2.5 \times 10^6 - 2370T \tag{5}$$

Where T is temperature in $^{\circ}C$.

Precipitation

The Figure 8 depicts the total yearly precipitation for the Iishana system, recorded at Ogongo station. The results display that the annual average precipitation in the Iishana system is about 300mm. The lowest recorded precipitation was below average in 2018 (marking the beginning of 2019 drought), while the highest precipitation of 600mm was recorded in 2020. The rainwater received flows down to the Etosha pan by gravity, resulting in a shortage of water within the region (Dragnich *et al.*, 2007).

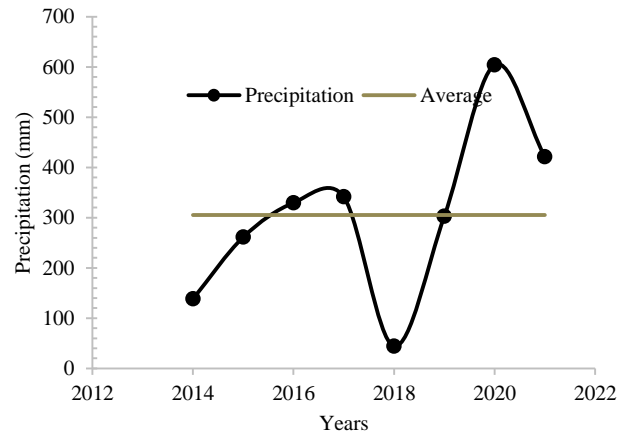


Figure 8. Total yearly precipitation for the Iishana system (2014-2021), recorded at Ogongo station.

Temperature

Figure 9 and Figure 10 show the temperature pattern for the Iishana system, recorded at Ogongo station. It is visible that the temperature series followed a positive trend in both figures. The water that remains in the Iishana (stream) and surface water bodies evaporates because of a high temperature. The computed annual evaporation rate is 2500 millimeters (using (4) and (5)). With an average of 300mm of rainfall annually (Figure 8), the amount of water evaporating is eight (8) times more than the amount of rainfall (Figure 11).

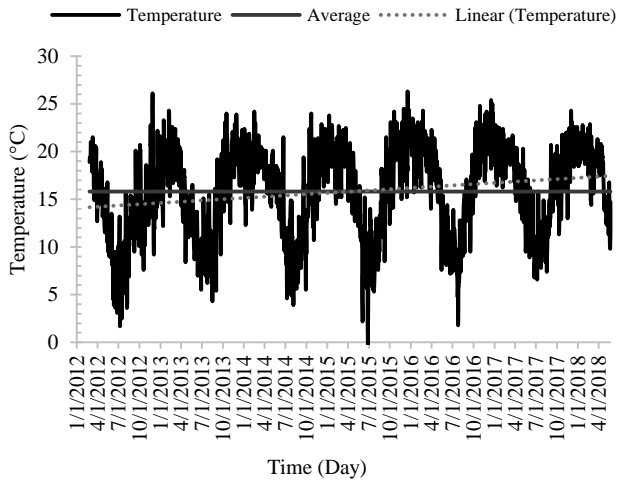


Figure 9. Daily temperature for the Iishana system (2012-2018), recorded at Ogongo station.

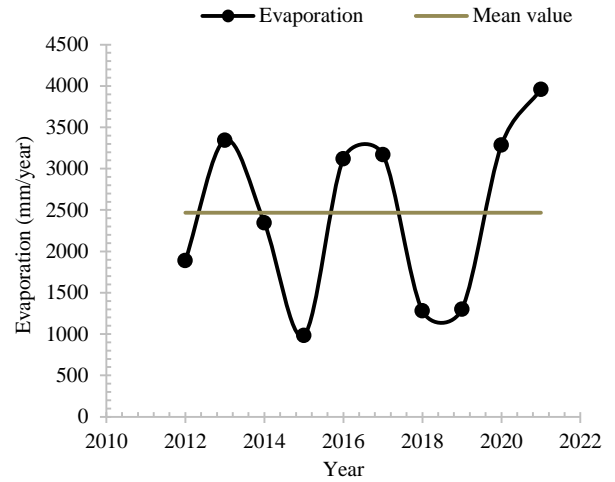


Figure 11. Evaporation within the Iishana system

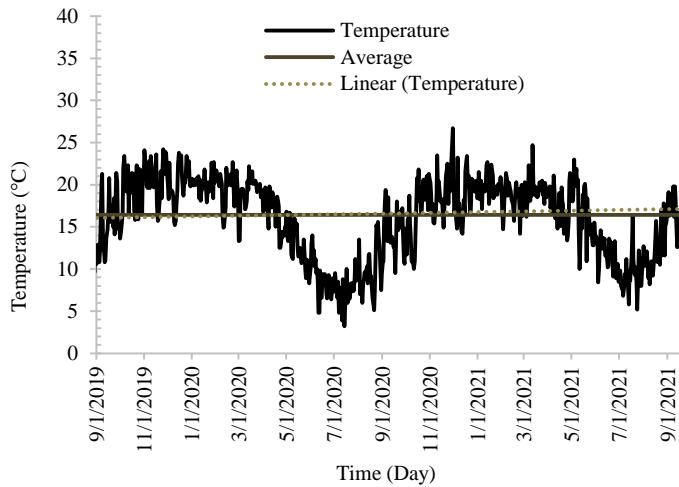


Figure 10. Daily temperature for the Iishana system (2019-2021), recorded at Ogongo station.

Table 2. The population within the Iishana system from 1991 to 2023 (Census, 1991, 2011, 2023)

Year	Region	Area km ²	Population Density per km ² Person/ km ²	Population Per region [No]	Population [Total No]	Urban Population [Total]	Rural Population [Total]
[1]	[2]	[3]	[4]	[5]	[6]*	[7]	[8]
2023	Ohangwena	1,136	32	36,352	174,733	112,764	61,969
	Oshana	2,411	27	65,097			
	Omusati	6,107	12	73,284			
2011	Ohangwena	1,136	23	26,128	129,311	67,664	61,647
	Oshana	2,411	20	48,220			
	Omusati	6,107	9	54,963			
2001	Ohangwena	1,136	21	23,856	124,628	41,637	82,991
	Oshana	2,411	19	45,809			
	Omusati	6,107	9	54,963			
1991	Ohangwena	1,136	18	20,448	174,739	27,800	146,939
	Oshana	2,411	26	62,686			
	Omusati	6,107	15	91,605			

*Total population numbers for the 3 regions in the respective year.

Table 3. Estimated current (2023/24) water demand of the Iishana system

Domestic			Livestock				Total Rural Water Demand
Rural Population	Water Consumption Per capita	Demand	Area	Livestock Numbers*	Water Consumption per stock	Demand	
[Total]	[m ³ /capita/d]	[m ³ /d]	[ha]	[Total]	[m ³ /capita/d]	[m ³ /d]	[m ³ /d]
61,969	0.04	2,479	951,587	95,156	0.045	4,282	6,761

*Equivalent large stock units

CONCLUSION AND RECOMMENDATION

This study analyzed the water demand of the rural population within the Namibian Iishana system. The current water demand of the rural population is estimated at 2,479 m³/d, with projections of 0.9, 0.5, and 0.1 Mm³/year for 2033, 2043, and 2053 respectively. The region's flat, shallow landscape, high evaporation rate, and lack of proper infrastructure have made the area vulnerable in terms of water security for both agricultural and potable purposes, resulting in droughts after the rainy season.

With these findings, it is recommended to build water infrastructures within the region to improve the well-being and livelihood of rural communities. One engineering practice involves increasing the storage capacity of the natural basins in the study area by removing the accumulated sediment to retain sufficient water to increase water availability. Additionally, increasing the depth of the pans may help reduce the rate of evaporation. Furthermore, planting of trees within the basin will enhance ecological restoration, reduce flooding and enhance rural livelihoods' ability to withstand the impacts of climate change.

DECLARATIONS

Corresponding author

Correspondence and requests for materials should be addressed to Mr. Eino Junias; E-mail: juniaseino@gmail.com; ORCID: <https://orcid.org/0009-0004-7169-1117>

Data availability

The datasets used and/or analysed during the current study available from the corresponding author on reasonable request.

Acknowledgements

The authors would like to acknowledge the University of Namibia for creating a conducive environment to conduct this research. More so, the author

would like to extend thanks for the financial support of this study, provided by Bundesministerium für Bildung und Forschung (BMBF) through the Southern African Science Service Centre for Climate Change and Adaptive Land Management (SASSCAL).

Authors' contribution

First Author analysed the data obtained and wrote the manuscript. Second and third Author supervised and revised the manuscript.

Competing interests

The authors declare no competing interests in this research and publication.

REFERENCES

- Arendt, R., Beck, L., Faulstich, L., Johannes, P., Lengright, J., Martinis, S., & Ullmann, T. (2021). Natural pans as an important surface water resource in the cuvelai basin—metrics for storage volume calculations and identification of potential augmentation sites. *Water (Switzerland)*, 13(2). DOI: <https://doi.org/10.3390/w13020177>
- Basak, N. N. (2003). *Environmental Engineering*. 1st Edition, Tata McGraw-Hill. New Delhi. Available at: <https://dokumen.pub/environmental-engineering-1ed-0070494630-9780070494633.html>
- Census. (1991). *Population and Housing Census*. Available at: https://cms.my.na/assets/documents/1991_Population_and_Housing_Census_Basic_Analysis_with_Highlights.pdf
- Census. (2011). *Namibia 2011 Population and Housing Census Main Report*. Available at: https://nsa.nsa.org.na/new_publications/namibia-population-and-housing-census-main-report-2011/
- Census. (2023). *2023 Population & Housing Census Preliminary Report 2023 Population & Housing Census*. Available at: <https://nsa.org.na/>
- Dragnich, P. A., Dungca, A. C., Pendelton, N. L., & Tracy, A. R. (2007). The Cuvelai-Etoshia Basin Management Approach: Assessing Water Resource Management in the Iishana Sub-Basin. Available at: <http://theeis.com/elibrary/search/6505>
- Drees, L., Luetkemeier, R., Liehr, S., & Stein, L. (2017). Blended drought index: Integrated drought hazard assessment in the Cuvelai-Basin. *Climate*, 5(51). DOI: <https://doi.org/10.3390/cli5030051>

- Han, D. (2010). *Concise Hydrology*. Ventus Publishing Aps. Available at: <http://bookboon.com/uk/student/civil/concise-hydrology>
- MAWF. (2014). A pre-feasibility study into: The augmentation of water supply to the central area of Namibia and the Cuvelai. Available at: <http://the-eis.com/elibrary/index.php/search/9203>
- Mays, L. W. (2011). *Water Resources Engineering* (2nd ed.). John Wiley & Sons, Inc. Hoboken. 201:748-6011
- Mendelsohn, J., & Weber, B. (2011). The Cuvelai Basin its water and people in Angola. Available at: <https://www.raison.com.na/>
- Niipare, E. (2020). Assessment of floodwater harvesting infrastructures in the Namibian Cuvelai-Etosha basin. Available at: <https://repository.unam.edu.na/items/afea18ea-5b85-469c-aa19-309908467113>
- Rangaiah, J., Mallikarjuna, V., & Udaya Bhaskar, P. (2021). Water Demand Analysis for Selected Rural Regions in Visakhapatnam District. IOP Conference Series: Earth and Environmental Science, 796(1). DOI: <https://doi.org/10.1088/1755-1315/796/1/012045>
- SASSCAL WeatherNet. SASSCAL WeatherNet. Available at: <https://sasscalweather.net/>
- Shifidi, V. T. (2016). Impact of flooding on rural livelihoods of the Cuvelai Basin in Northern Namibia. *Journal of Geography and Regional Planning*, 9(6), 104–121. DOI: <https://doi.org/10.5897/jgrp2015.0536>
- Shooya, O. N. (2017). Barriers and enablers to water access and community wellbeing in the Onesi constituency of Namibia: The case of Okalonga B and Onandjandja villages. Available at: <http://hdl.handle.net/11427/27527>
- United Nations-Water. (2018). *World Water Development Report 2018*. Available at: <https://www.unwater.org/publications/world-water-development-report-2018>
- World Bank. (2022, October 5). *Water Resources Management Overview*. Available at: <https://www.worldbank.org/en/topic/waterresourcesmanagement#2>

Publisher's note: [Scienceline Publication](#) Ltd. remains neutral with regard to jurisdictional claims in published maps and institutional affiliations.



Open Access: This article is licensed under a Creative Commons Attribution 4.0 International License, which permits use, sharing, adaptation, distribution and reproduction in any medium or format, as long as you give appropriate credit to the original author(s) and the source, provide a link to the Creative Commons licence, and indicate if changes were made. The images or other third party material in this article are included in the article's Creative Commons licence, unless indicated otherwise in a credit line to the material. If material is not included in the article's Creative Commons licence and your intended use is not permitted by statutory regulation or exceeds the permitted use, you will need to obtain permission directly from the copyright holder. To view a copy of this licence, visit <https://creativecommons.org/licenses/by/4.0/>.

Meeting the Sustainability Emergency in Built Environment Curricula through Tripartite Pedagogy Quasi-Experimentation

Nonso Izuchukwu Ewurum , Njideka Maryclara Aguome , Keone Kelobonye , and Fidelis Ifeanyi Emoh 

Department of Architecture & Planning, University of Botswana, Gaborone, Botswana

✉ Corresponding author's Email: aguomen@ub.ac.bw

ABSTRACT

This study evaluates the effectiveness of a tripartite pedagogy framework integrating specialized tracks, optional minors, and experiential learning to enhance sustainability education in built environment curricula. Employing a mixed-methods quasi-experimental design, the research assessed 239 industrial training students in Enugu, Nigeria. Results from the t-test demonstrate significant improvements in sustainability knowledge post-intervention and high interest in optional sustainability courses. Repeated measures of ANOVA revealed substantial enhancements in students' ability to apply sustainability concepts over time. Qualitative data highlighted practical challenges in experiential learning, including resource constraints. The findings provide empirical support for the tripartite approach, extending previous research by quantifying impacts on practical skills development. This study contributes to the limited body of evidence on integrated sustainability education interventions in the Global South, demonstrating significant improvements in students' sustainability knowledge and application skills through a tripartite pedagogy framework. The findings highlight the potential of specialized tracks, optional minors, and experiential learning to bridge the gap between academic preparation and industry needs. It is recommended that educational institutions prioritize these integrative approaches and address resource constraints to enhance the effectiveness and scalability of sustainability education in built environment curricula.

Keywords: Building Research Establishment Environmental Assessment Methodology, Built environment curricula, Experiential learning, Optional minors, Specialized tracks, Sustainability competencies

INTRODUCTION

The built environment sector significantly impacts global environmental quality, resource consumption, and public health. Correspondingly, recent data from the [United Nations Environment Programme \(2022\)](#) highlights a worrying increase in building energy demand, rising by over 4% since 2020, driven by rapid urbanization. This escalating ecological footprint underscores the urgent need for a paradigm shift in built environment practices towards sustainability ([Agboola et al., 2024](#)). Sustainability in the built environment involves economically viable, environmentally responsible, and socially equitable approaches to design, construction, and operation. This includes green building, low-impact development, renewable energy integration, and transit-oriented development ([Durdyev et al., 2018](#)). While critics argue that sustainable practices are costly, proponents emphasize that the long-term benefits outweigh initial investments ([Ewurum et al., 2020](#)).

Thus, the urgency to mitigate environmental degradation, health impacts, and resource depletion, while

enhancing resilience, underscores the need for skilled professionals in sustainability. However, current educational programs inadequately prepare built environment professionals ([Ohueri, 2022](#)). For instance, a systematic review of 89 global university programs shows limited and uncoordinated integration of sustainability concepts, leaving graduates underprepared for key practices like retrofitting structures, performing energy audits, and engaging stakeholders ([Rajabifard et al., 2023](#)).

This disconnect between academic preparation and industry needs hampers the transition to sustainable practices. Compounding the situation, rapid technological advancements and evolving societal expectations further pressure educational institutions to update curricula systematically to include sustainability as a core competency ([Taneja et al., 2022](#)). In this respect, promising interventions comprise specialization tracks, optional minors in sustainability-related fields, and experiential learning opportunities ([Angelaki et al., 2024](#); [Hou et al., 2023](#); [Ribeiro et al., 2021](#)). [Ewurum et al. \(2024\)](#) argue that the effectiveness of these interventions is impeded by their focus on siloed rather than integrated

RESEARCH ARTICLE
 PII: S225204302400028-14
 Received: June 25, 2024
 Revised: September 02, 2024
 Accepted: September 05, 2024

reforms. This view further corroborates a 2021 report by the World Health Organization citing that this fragmented approach limits the mainstreaming of sustainability concepts, suggesting the need for multiple complementary approaches within an overarching framework (WHO, 2021).

Accordingly, we present a tripartite pedagogy framework that integrates specialization tracks, optional minors, and experiential learning to create a robust framework for sustainability education. Wright (2021) underscores the critical deficiency of empirical studies concerning the application and assessment of this framework, especially within the Global South, while highlighting the pivotal role of faculty readiness in its effective integration. In light of the foregoing, research on tripartite pedagogy experimentation is essential to address the sustainability emergency in built environment curricula. The findings may inform evidence-based curricular reforms, bridge the gap between academia and industry, as well as develop a workforce capable of managing a resource-efficient built environment with minimized environmental impact.

Accordingly, the study aims to evaluate the effectiveness of integrating optional minors, specialized courses, and experiential learning opportunities into built environment curricula to enhance sustainability education and preparedness among students. The objectives of the study are to assess the short-term impact of a 2-week specialized crash course on students' sustainability knowledge, ascertain student interest levels for post-specialization track optional courses in the built environment, and examine the practical impact of a 1-month experiential learning program on students' ability to apply sustainability concepts in real-world scenarios.

Review of related literature

The integration of specialization tracks in green building and sustainable development within built environment education is supported by foundational educational theories. The concept of "deep learning" emphasizes intensive engagement with specific knowledge domains, allowing students to develop robust and transferable skills (Liu et al., 2024). Specialization tracks enable students to focus on elective courses in sustainability, fostering a comprehensive understanding of sustainable construction project management (Kovačević, 2022). "Situated learning" theory suggests that learning is most effective in authentic, contextualized settings (Donaldson et al., 2020). Specialization tracks provide opportunities to apply sustainability concepts in real-world

projects, bridging the gap between theory and practice. Additionally, the "constructivist" approach highlights the active construction of knowledge through collaborative and problem-based activities, enabling students to engage with sustainability challenges and develop problem-solving skills (Mityr, 2021).

Studies emphasize the practical considerations for implementing specialization tracks in green building and sustainable development, such as ensuring faculty expertise and access to specialized facilities (Asfaw et al., 2022). Optional minors in sustainability-related fields are supported by educational theories like "elective" learning, allowing students to tailor their experiences to their interests and career goals. "Interdisciplinary" and "transdisciplinary" education, as noted by Scharoun et al. (2023), are essential for integrating these minors, promoting knowledge synthesis from diverse disciplines to address complex sustainability challenges. Implementing these minors also requires resources for specialized coursework, credit allocation, course sequencing, and evaluating impacts on student outcomes (Strumbos et al., 2018).

Elbaghdadi (2023) explains that "experiential learning theory" emphasizes knowledge construction through hands-on, contextualized learning. In sustainability-focused built environment curricula, this can be achieved through real-world projects, field trips, and internships. However, many firms do not fully adopt sustainability principles, highlighting the need for graduates with sustainable construction management skills to provide authentic learning settings. This approach aligns with "situated learning theory," which advocates for learning in real-world contexts. Implementing experiential learning requires industry partnerships (Olawumi & Chan, 2020), access to facilities and resources (Chagnon-Lessard et al., 2021), and integration into the broader curriculum (Fini et al., 2018).

Despite limited studies on specialization tracks in built environment sustainability education, literature shows promising results. Ribeiro et al. (2021) found that green building and sustainable development tracks enhance students' awareness, knowledge, and inclination towards sustainable practices, while Angelaki et al. (2024) noted increased engagement and curriculum relevance. Robust evidence supports experiential learning, showing that hands-on experiences, like design projects and internships, significantly improve knowledge, engagement, problem-solving skills, and application of sustainable practices (Hou et al., 2023; Ordaz et al., 2021). Evidence on optional minors is limited but promising,

enhancing student awareness, knowledge, and professional development satisfaction (Griesinger, 2023; Holison, 2023). However, the majority of existing research on these interventions predominantly focuses on programs in the Global North, with limited evidence regarding their application and impacts, as a tripartite, in the Global South.

MATERIALS AND METHODS

This study employed a mixed-methods quasi-experimental design to evaluate the effectiveness of a tripartite pedagogy framework for enhancing sustainability education in built environment curricula. A quasi-experimental design was chosen due to its suitability for educational research where randomization is not feasible, and its ability to establish causal relationships in real-world settings.

The study was conducted at the Institute of Management & Technology (IMT), Enugu, Nigeria, focusing on 58 Industrial Training students of Real Estate and 181 of Civil Engineering departments. This institution was selected due to its prominence in built environment education in the region and its willingness to implement curricular innovations. For the experiential learning component, partnerships were established with three firms in Enugu: Ezealigo Associates, Ezech Ezech & Co., and Onwudingo Construction Limited. These firms were chosen based on their engagement in sustainable construction practices and willingness to participate in the study. A randomly selected sample of 6 students were each sent to Ezealigo and Eze Ezech, while 29 students were sent to the various construction sites of Onwudingo Limited.

The Building Research Establishment Environmental Assessment Method (BREEAM) was utilized as the sustainability intervention framework for this study, due to its comprehensive approach to sustainability assessment, international recognition, and adaptability to various contexts. A multi-method approach to data collection was employed to address the study's objectives. For objective 1 (impact of specialized crash course), pre- and post-intervention knowledge tests were administered to measure changes in students' sustainability knowledge. Reflective journals were maintained by students throughout the course to capture qualitative insights into their learning experiences. Paired sample t-tests were conducted to compare pre- and post-intervention knowledge test scores, allowing for the assessment of significant changes in student knowledge (Kim, 2015).

Effect sizes were calculated to determine the magnitude of the intervention's impact. Qualitative data from reflective journals were analyzed using content analysis to identify key learning outcomes and experiences (Krippendorff, 2018).

For objective 2 (student interest levels), a Likert-scale questionnaire was administered to assess student interest in optional sustainability courses after undergoing specialized tracks. Descriptive statistics were used to analyze the Likert-scale data, including measures of central tendency and dispersion. This process also involved semi-structured interviews with a subset of students to gain deeper insights into their motivations and perceptions. For objective 3 (impact of experiential learning), a practical assessment was conducted before and after the experiential learning program to evaluate students' ability to apply sustainability concepts. Observational data was collected by researchers during the experiential learning activities, in addition to semi-structured interviews with industry partners to gather their perspectives on student performance and program effectiveness.

Paired sample t-tests were used to analyze the pre- and post-intervention practical assessment scores. However, given the complexity of real-world application, a repeated measures ANOVA was also conducted to account for potential time-dependent effects and individual differences in learning trajectories (Maxwell & Delaney, 2004). Qualitative data from observations and interviews were analyzed using grounded theory techniques to develop a theoretical understanding of how experiential learning impacts sustainability competencies (Charmaz, 2014). All statistical analyses were performed using SPSS version 27.0, with a significance level set at $p < 0.05$. Qualitative data analysis was facilitated by NVivo 12 software to ensure systematic coding and theme identification.

DISCUSSIONS

As per objective 1, the paired sample t-test results indicate a significant increase in sustainability knowledge post-intervention ($t(238) = 8.56, p < 0.01$). The large t-value and small p-value suggest strong evidence against the null hypothesis, and the Cohen's d value indicates a medium effect size. Examination of reflective journals revealed enhanced understanding and appreciation of sustainability concepts. Descriptive statistics in Figure 1 shows high student interest in optional sustainability courses after the specialized tracks intervention.

Results in Figure 1 indicate a higher-than-average interest level of built environment students concerning registering for optional minors on sustainability principles. Interviews indicated that students valued the relevance of these courses to their career aspirations and were mostly fascinated by the fresh impetus they offered. For objective 3, the repeated measures ANOVA results demonstrate significant improvements in students' ability to apply sustainability concepts over time [$f(2,236) = 15.43, p < 0.01$], while the partial eta squared (η^2) suggests a moderate effect size, implying that the intervention had a substantial practical impact on students' abilities. Figure 2 confirms the veracity of this result by providing descriptive statistics for each time point, showing a clear upward trend in mean scores and a decrease in standard deviation, suggesting both improvement and convergence in students' abilities over time.

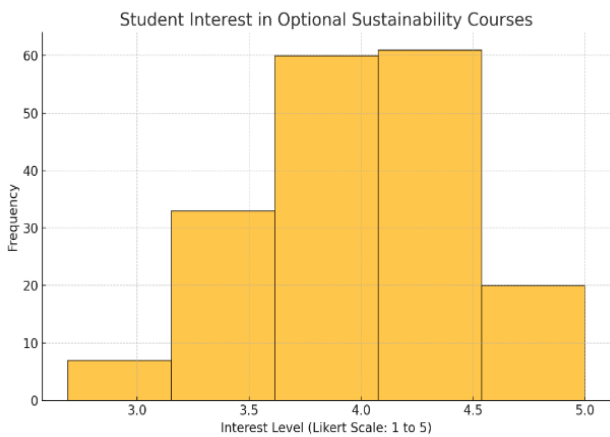


Figure 1: Interest levels in sustainability optional minors (Source: Field Survey, 2024).

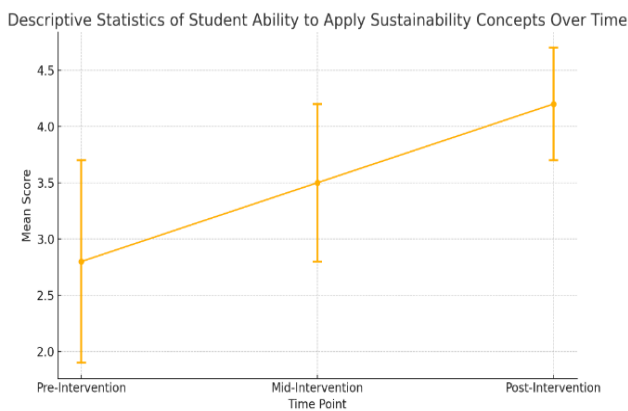


Figure 2: Effectiveness of experiential learning intervention (Source: Field Survey, 2024).

The graph (Figure 2) shows a clear upward trend in mean scores across the three time points, where pre-intervention had a mean score of around 2.8, mid-intervention had a mean score of around 3.4, and post-intervention with a mean score of around 4.2. This steady increase suggests a consistent improvement in students' abilities to apply sustainability concepts as they progress through the intervention. While the repeated measures ANOVA results confirm that these improvements are statistically significant, qualitative data highlighted practical challenges and learning outcomes, such as real-world constraints related to time, resource availability, and the limited access to sustainable materials and technologies posed significant hurdles.

The study's findings provide compelling evidence for the effectiveness of a tripartite pedagogy framework in enhancing sustainability education within built environment curricula. The significant increase in students' sustainability knowledge post-intervention ($t(238) = 8.56, p < 0.01$) aligns with previous research by Ribeiro et al. (2021) and Angelaki et al. (2024), confirming the value of specialized tracks in enhancing deeper understanding of sustainability concepts. The high interest levels in optional sustainability courses post-intervention (Figure 1) corroborate the findings of Griesinger (2023) and Holison (2023), suggesting that exposure to specialized tracks can indeed stimulate student engagement with sustainability-related fields. This outcome underscores the potential of optional minors as a complementary strategy within the tripartite framework. The repeated measures ANOVA results ($F(2, 236) = 15.43, p < 0.01$) demonstrating significant improvements in students' ability to apply sustainability concepts over time are particularly noteworthy. This finding extends the work of Hou et al. (2023) and Ordaz et al. (2021) by quantifying the impact of experiential learning on practical skills development. The moderate effect size (partial η^2) indicates a substantial practical impact, reinforcing the value of hands-on experiences in sustainability education. However, the qualitative data highlighting practical challenges such as time constraints, limited resources, and restricted access to sustainable materials reveal important limitations of the experiential learning component. These findings echo the concerns raised by Chagnon-Lessard et al. (2021) regarding the need for appropriate facilities and resources in implementing experiential learning opportunities.

Practical Insights

The study provides empirical support for the integration of specialized tracks, optional minors, and

experiential learning opportunities in built environment curricula. So, it is recommended that educational stakeholders should consider adopting this tripartite approach to enhance sustainability education by prioritizing faculty development programs to ensure instructors possess the necessary expertise to effectively deliver specialized courses and guide experiential learning activities. The identified practical challenges in experiential learning highlight the need for institutions to allocate adequate resources, including sustainable materials and technologies, to support effective implementation of hands-on learning experiences. Conversely, its success underscores the importance of developing strong partnerships between educational institutions and industry stakeholders engaged in sustainable practices.

Policy Insights

Policymakers and accreditation bodies should consider revising standards for built environment programs and incentivize industry participation in sustainability education initiatives to explicitly include sustainability competencies and experiential learning requirements. Government and educational funding bodies should prioritize resources for institutions implementing comprehensive sustainability education programs, particularly those incorporating experiential learning components. Professional bodies should consider developing sustainability certifications for built environment graduates, recognizing the specialized knowledge and skills acquired through programs implementing the tripartite pedagogy framework.

CONCLUSION

This study demonstrates that the tripartite pedagogy framework, integrating specialized tracks, optional minors, and experiential learning, significantly enhanced sustainability education in built environment curricula. The findings reveal notable improvements in students' sustainability knowledge, interest in optional sustainability courses, and practical application of sustainability concepts over time. These results accentuate the framework's efficacy in preparing students for sustainable practices, addressing the critical skills gap in the built environment sector.

Recommendations

Educational institutions should adopt the tripartite pedagogy framework to reform the built environment

curricula, with emphasis on faculty development, industry collaboration, and adequate resource allocation for experiential learning. Policymakers and accreditation bodies are encouraged to incorporate sustainability competencies and experiential learning as core standards to ensure graduates are equipped for sustainable practices in the built environment.

DECLARATIONS

Corresponding author

Correspondence and requests for materials should be addressed to Njideka Maryclara Aguome; E-mail: aguomen@ub.ac.bw, ORCID: 0000-0002-6668-9731

Data availability

The datasets used and/or analysed during the current study available from the corresponding author on reasonable request.

Acknowledgments

The authors would like to acknowledge Ezech Ezech and Company, Ezealigo Associates, Onwudinjo Construction Ltd., and the Institute of Management and Technology, Enugu for creating a conducive environment to conduct this research.

Authors' contribution

NIE: conceptualization (supporting), formal analysis (lead), investigation, methodology (lead), resources (lead), writing, analysis of the data obtained, and original draft (lead). NMA: conceptualization (lead), formal analysis (supporting), writing (review and editing), methodology (equal), validation (lead), supervision (lead). KK: Conceptualisation (supporting), formal analysis (supporting), investigation (supporting), methodology (supporting), validation (supporting), writing (review and editing: supporting). FIE: Investigation (supporting), methodology (supporting), supervision (lead), validation (lead), writing (review and editing: supporting).

Competing interests

The authors declare no competing interests in this research and publication.

REFERENCES

Agboola, O. P., Alotaibi, B. S., Dodo, Y. A., Abuhussain, M. A., & Abuhussain, M. (2024). Built environment transformation in Nigeria: the effects of a regenerative framework. *Journal*

- of Asian Architecture and Building Engineering, 23(2), 789-812. <https://doi.org/10.1080/13467581.2023.2238045>
- Angelaki, M. E., Bersimis, F., Karvounidis, T., & Douligeris, C. (2024). Towards more sustainable higher education institutions: Implementing the sustainable development goals and embedding sustainability into the information and computer technology curricula. *Education and Information Technologies*, 29(4), 5079-5113. <https://doi.org/10.1007/s10639-023-12025-8>
- Asfaw, A., Blais, A., Brown, K. R., Candelaria, J., Cantwell, C., Carr, L. D., ... & Singh, C. (2022). Building a quantum engineering undergraduate program. *IEEE Transactions on Education*, 65(2), 220-242. <https://brream.com>. <https://doi.org/10.1109/TE.2022.3144943>
- Chagnon-Lessard, N., Gosselin, L., Barnabé, S., Bello-Ochende, T., Fendt, S., Goers, S., ... & Zhang, P. (2021). Smart campuses: extensive review of the last decade of research and current challenges. *IEEE Access*, 9, 124200-124234. <https://doi.org/10.1109/ACCESS.2021.3109516>
- Donaldson, T., Fore, G. A., Filippelli, G. M., & Hess, J. L. (2020). A systematic review of the literature on situated learning in the geosciences: Beyond the classroom. *International Journal of Science Education*, 42(5), 722-743. <https://doi.org/10.1080/09500693.2020.1727060>
- Durdyev, S., Zavadskas, E. K., Thurnell, D., Banaitis, A., & Ihtiyar, A. (2018). Sustainable construction industry in Cambodia: Awareness, drivers and barriers. *Sustainability*, 10(2), 392. <https://doi.org/10.3390/su10020392>
- Elbaghdadi, Z. (2023). Instructional design and development tools for online adult education: a literature review.
- Ewurum, N.I., Onyebueke, V.U. & Nnamani, C.O. (2020). Capacity need for sustainable housing delivery: Reflections on Nigeria. Faculty of Environmental Studies UNEC International Conference on Theoretical and Analytical Frameworks for Sustainable Development in Africa
- Fini, E. H., Awadallah, F., Parast, M. M., & Abu-Lebdeh, T. (2018). The impact of project-based learning on improving student learning outcomes of sustainability concepts in transportation engineering courses. *European Journal of Engineering Education*, 43(3), 473-488. <https://doi.org/10.1080/03043797.2017.1393045>
- Griesinger, T. M. (2023). An Exploration of Students' Interests in Pursuing Careers in Environmental Sustainability.
- Holison, J. E. (2023). Assessing the Knowledge on Sustainability and Barriers to Daily Sustainable Practices Among Faculty and Students in Higher Education: the Case of Eastern Illinois University.
- Hou, H., Lai, J. H., & Wu, H. (2023). Project-based learning and pedagogies for virtual reality-aided green building education: case study on a university course. *International Journal of Sustainability in Higher Education*, 24(6), 1308-1327. <https://doi.org/10.1108/IJSHE-06-2022-0197>
- Kovačević, M. (2022). The effect of a general versus narrow undergraduate curriculum on graduate specialization: The case of a Dutch liberal arts college. *The Curriculum Journal*, 33(4), 618-635. <https://doi.org/10.1002/curj.158>
- Liu, Y., Li, S., & Cui, D. (2024). Analysis of translation teaching skills in colleges and universities based on deep learning. *Computers in Human Behavior*, 108212. <https://doi.org/10.1016/j.chb.2024.108212>
- Mitry, M. M. (2021). Translating constructivism into pedagogy from philosophy to practice: Active project-based learning. *The International Journal of Humanities Education*, 19(1), 39. <https://doi.org/10.18848/2327-0063/CGP/v19i01/39-51>
- Ohueri, C. C. (2022). The integrated BIM-MyCREST process model for reengineering the green building design practices. A thesis submitted in fulfillment of the requirements for the award of the degree of Doctor of Philosophy Civil Engineering (Construction Management). Faculty of Engineering, Computing, and Science. Swinburne University of Technology.
- Olawumi, T. O., & Chan, D. W. (2020). Key drivers for smart and sustainable practices in the built environment. *Engineering, Construction, and Architectural Management*, 27(6), 1257-1281. <https://doi.org/10.1108/ECAM-06-2019-0305>
- Ordaz, K., Tan, K., Skett, S., & Herremans, I. M. (2021). Developing leadership qualities in environmental sustainability through university co-curricular activities. *International Journal of Sustainability in Higher Education*, 22(7), 1609-1629. <https://doi.org/10.1108/IJSHE-10-2020-0421>
- Rajabifard, A., Kahalimoghadam, M., Lumantarna, E., Herath, N., Hui, F. K. P., & Assarkhaniki, Z. (2021). Applying SDGs as a systematic approach for incorporating sustainability in higher education. *International Journal of Sustainability in Higher Education*, 22(6), 1266-1284. <https://doi.org/10.1108/IJSHE-10-2020-0418>
- Ribeiro, J. M. P., Hoeckesfeld, L., Dal Magro, C. B., Favretto, J., Barichello, R., Lenzi, F. C., ... & De Andrade, J. B. S. O. (2021). Green Campus Initiatives as sustainable development dissemination at higher education institutions: Students' perceptions. *Journal of Cleaner Production*, 312, 127671. <https://doi.org/10.1016/j.jclepro.2021.127671>
- Scharoun, L., Meth, D., Crowther, P., Brough, D., Burton, L. O., & Teixeira, M. F. L. A. (Eds.). (2023). *Contemporary Design Education in Australia: Creating Transdisciplinary Futures*. Intellect Books.
- Strumbos, D., Linderman, D., & Hicks, C. C. (2018). Postsecondary pathways out of poverty: City University of New York Accelerated Study in Associate Programs and the case for national policy. *RSF: The Russell Sage Foundation Journal of the Social Sciences*, 4(3), 100-117. <https://doi.org/10.7758/rsf.2018.4.3.06>
- Taneja, S., Jaggi, P., Jewandah, S., & Ozen, E. (2022). Role of Social Inclusion in Sustainable Urban Developments: An Analyse by PRISMA. *Journal homepage: http://iieta.org/journals/ij dne*, 17(6), 937-942. <https://doi.org/10.18280/ij dne.170615>
- United Nations Environment Programme (2022). 2022 global status for buildings and construction. <https://www.unep.org/resources/publication/2022-global-status-report-buildings-and-construction>
- Wright, S. (2021). *The Importance of Rigor and Engagement on Student Achievement and Mastery: An Evaluation Study* (Doctoral dissertation, University of Southern California).

Publisher's note: [Scienceline Publication](#) Ltd. remains neutral with regard to jurisdictional claims in published maps and institutional affiliations.



Open Access: This article is licensed under a Creative Commons Attribution 4.0 International License, which permits use, sharing, adaptation, distribution and reproduction in any medium or format, as long as you give appropriate credit to the original author(s) and the source, provide a link to the Creative Commons licence, and indicate if changes were made. The images or other third party material in this article are included in the article's Creative Commons licence, unless indicated otherwise in a credit line to the material. If material is not included in the article's Creative Commons licence and your intended use is not permitted by statutory regulation or exceeds the permitted use, you will need to obtain permission directly from the copyright holder. To view a copy of this licence, visit <https://creativecommons.org/licenses/by/4.0/>.

© The Author(s) 2024

Enhancing Water Level Prediction through a Hybrid Feature Selection Approach

Thalosang Tshireletso^{1,4}✉ , Yashon Ouma¹ , Ditiro Moalafhi³ , and George Anderson² 

¹Department of Civil Engineering, University of Botswana, Gaborone, Botswana

²Department of Computer Sciences, University of Botswana, Gaborone, Botswana

³Department of Wildlife and Aquatic Resources, Botswana University of Agriculture and Natural Resources, Sebele, Botswana

⁴Department of Civil Engineering, University of Cape Town, Cape Town, South Africa

✉ Corresponding author's Email: tshireletsot@ub.ac.bw

ABSTRACT

Accurate prediction of water levels (WL) is essential for various applications, from flood management to environmental monitoring. In this study, an enhanced approach to feature selection tailored for water level prediction models is presented. Our method integrates Mutual Information and Recursive Feature Elimination with Cross-Validation (RFECV), augmented by the Non-Dominated Sorting Genetic Algorithm II (NSGA-II), to systematically evaluate and refine subsets of features. Mutual Information facilitates the identification of relevant feature dependencies, while RFECV iteratively eliminates less informative features to optimize predictive accuracy. The inclusion of NSGA-II further enhances the selection process by considering multiple conflicting objectives simultaneously, such as maximizing R^2 score and minimizing the number of selected features, RMSE, and MAE. Through extensive experimentation and validation on real-world datasets, we demonstrate the effectiveness of our hybrid feature selection approach in capturing intricate relationships within the data, leading to significantly improved predictive performance in water level prediction models.

Keywords: Mutual Information, Recursive Feature Elimination with Cross validation, Non-Dominated Sorting Genetic Algorithm II

INTRODUCTION

In the era of big data and complex datasets, the task of accurately predicting outcomes or trends from data has become increasingly vital across various domains (Li et al., 2019; Saeys et al., 2007). Regression modelling stands as a cornerstone in numerous fields, from finance to healthcare, where understanding and forecasting numerical outcomes are paramount (Guyon and Elisseeff, 2003). However, amidst the abundance of available features, selecting the most relevant ones that contribute significantly to the predictive power of a model becomes crucial. This necessity forms the crux of our study, as we delve into the realm of feature selection and its implications on regression modelling accuracy.

The significance of feature selection reverberates throughout the landscape of machine learning, impacting not only the performance of models but also their interpretability and computational efficiency (Li et al., 2019; Dash and Liu, 1997). By distilling datasets to their most informative attributes, feature selection mitigates the

curse of dimensionality, alleviating issues such as overfitting and enhancing model generalization. Moreover, in domains where resource constraints or interpretability are paramount, selecting a parsimonious set of features aids in building more comprehensible and deployable models.

The objective of this paper is to explore the efficacy of feature selection techniques in enhancing the performance of regression models. To achieve this objective, we adopt a two-fold approach: firstly, we investigate traditional feature selection methods such as Mutual Information and Recursive Feature Elimination with Cross-Validation (RFECV), evaluating their impact on model accuracy and feature subset size. Subsequently, we employ multi-objective optimization techniques, leveraging the Non-dominated Sorting Genetic Algorithm II (NSGA-II), to identify Pareto-optimal solutions that balance model accuracy and feature subset complexity (Deb, et al., 2002; Kohavi and John, 1997).

Through this endeavour, we aim to provide insights into the trade-offs inherent in feature selection and

RESEARCH ARTICLE
 PII: S225204302400029-14
 Received: June 25, 2024
 Revised: September 02, 2024
 Accepted: September 05, 2024

empower practitioners with knowledge to make informed decisions when building regression models. By elucidating the interplay between feature selection methods and model performance, this study contributes to advancing the understanding of best practices in regression modelling, thereby facilitating more robust and interpretable predictive analytics solutions.

Background and related work

The field of feature selection and regression modelling is a vast and intricate domain, and numerous studies have been carried out, scrutinizing various techniques and their effectiveness across a wide array of domains. Prominent among these are the comparative studies carried out by Kohavi and John (1997). They evaluated the performance of wrapper methods, particularly recursive feature elimination (RFE), with a keen focus on enhancing the accuracy of regression models. Their findings were enlightening, showing significant improvements in R-squared values and a decrease in mean squared error when RFE was applied in contrast to the baseline models.

In the same vein, Dash and Liu in 1997 embarked on a deep exploration of the application of filter methods, particularly mutual information-based feature selection. They showcased how these techniques bring about notable enhancements in predictive accuracy and model interpretability across a myriad of regression tasks. Their work served as a seminal contribution to the field, and it has been widely referenced in subsequent studies.

In recent times, hybrid approaches have gained considerable traction with the aim of synergizing the strengths of different feature selection techniques. An exemplary work in this regard is that of Hsu et al. in 2011. They proposed a ground breaking framework that seamlessly integrates filter and wrapper methods. The performance of their hybrid approach was superior in terms of both accuracy and computational efficiency. It achieved state-of-the-art results on benchmark datasets, surpassing the performance of individual feature selection methods.

In addition to these academic advancements, domain-specific applications have also showcased the practical utility of feature selection. An excellent example of this is in the finance sector, where researchers have utilized feature selection to identify key predictors for stock price forecasting models. This has led to more accurate predictions and has informed investment decisions (Yang, et al., 2019), contributing significantly to the field of financial forecasting.

Healthcare is another sector where feature selection techniques have played a pivotal role. They have been instrumental in identifying biomarkers and clinical predictors for disease diagnosis and prognosis (Saeys et al., 2007). By selecting relevant features from high-dimensional medical datasets, researchers have achieved remarkable accuracies in predicting patient outcomes and guiding personalized treatment strategies.

Furthermore, in environmental science, feature selection has been applied to remote sensing data for land cover classification and ecological modelling (Heman et al., 2013). These applications underscore the versatility and efficacy of feature selection in addressing real-world challenges across various domains.

Through empirical validation and rigorous evaluation, these studies have not only advanced our understanding of feature selection techniques but also provided practical insights into their application and impact on regression model performance. By leveraging the collective knowledge generated from these works, our study aims to contribute further to the evolving landscape of feature selection and regression modelling, ultimately enhancing predictive accuracy and interpretability in data-driven decision-making processes.

MATERIALS AND METHODS

Experimental Setup

The MI-RFECV-NSGA-II feature selection method to the test using various predictor variables and a target variable. To ensure we had a clean dataset, we handled missing values and encoded categorical variables. We split the dataset into training and testing sets, using the 80-20 standard for training and testing respectively, and kept a consistent random seed for reproducibility.

A combination of Mutual Information (MI), Recursive Feature Elimination with Cross-Validation (RFECV), and the Non-Dominated Sorting Genetic Algorithm II (NSGA-II) for feature selection. MI and RFECV helped us identify a subset of relevant features. The NSGA-II algorithm was then used to optimize the feature subset by maximizing the coefficient of determination (R^2) and minimizing the selected features. Afterwards, Random Forest (RF) regression model was trained using the features identified by the NSGA-II algorithm.

The RF model was trained and tested using different performance metrics, such as R^2 score, Mean Absolute Error (MAE), and Root Mean Squared Error (RMSE), which were used to judge its accuracy and generalization

capabilities. Finally, we compared how our RF model, trained with features selected by NSGA-II, stood up against RF models trained with other feature selection techniques like MI and RFECV. This comparison gave us a better understanding of how effective the MI-RFECV-NSGA-II feature selection method is in pinpointing informative features for regression tasks.

Mutual information (MI)

Mutual information measures the dependency between two variables, in this case, each feature and the target variable 'WL' (water level). The mutual information between a feature X_i and the target variable Y is calculated as:

$$I(X_i; Y) = \sum_{x_i \in X_i} \sum_{y \in Y} p(x_i, y) \log \left(\frac{p(x_i, y)}{p(x_i)p(y)} \right) \quad (1)$$

Where:

- $p(x_i, y)$ is the joint probability mass function of X_i and Y
- $p(x_i)$ and $p(y)$ are the marginal probability mass functions of X_i and Y respectively.

Features with higher mutual information scores are considered more informative.

Recursive feature elimination with cross-validation (RFECV)

The RFECV recursively removes less informative features and selects the subset that optimizes model performance, typically measured using cross-validation. The process involves training the model with the current set of features and evaluating its performance. Features with the lowest importance, often determined by their coefficients in the model, are pruned iteratively until the desired number of features is reached. The selection process can be represented as:

$$\arg \min_{features} (MSE_{CV}) \quad (2)$$

Where:

- MSE_{CV} is the mean squared error evaluated through cross-validation.

Multi-objective optimization with NSGA-II

NSGA-II aims to optimize four conflicting objectives simultaneously: maximizing R^2 (coefficient of determination), minimizing the number of selected features, minimizing RMSE, and minimizing MAE. Let's denote these objectives as f_1 , f_2 , f_3 , and f_4 respectively.

The output of NSGA-II consists of a set of Pareto-optimal solutions, denoted as Pareto, representing trade-offs between R^2 , the number of selected features, RMSE,

and MAE. Each solution in Pareto represents a unique combination of these objectives, providing insights into the optimal feature subsets that balance predictive accuracy, model simplicity, and error metrics.

RESULTS AND DISCUSSION

The initial Random Forest (RF) model performed well, but improved after applying feature selection techniques, table 1. The RF model with Mutual Information Recursive Feature Elimination with Cross-Validation (MI-RFECV) showed increased R^2 and decreased RMSE, despite a slight increase in MAE. Further enhancement was achieved with the addition of the NSGA-II optimization algorithm, leading to significant performance improvements. This underlines the effectiveness of feature selection, especially MI-RFECV-NSGA-II, in improving RF model accuracy and reducing errors.

Table 1 - Results for RF without feature selection, RF with MI-RFECV and RF with RFECV-NSGA-II

Model	R^2	RMSE	MAE
RF without Feature selection	0.735	9.680	5.314
RF with MI-RFECV	0.804	8.311	6.769
RF with MI-RFEV-NSGA-II	0.896	4.485	2.598

Table 2 - Comparison of the study with recent studies

Method	R^2	RMSE	MAE
RF with MI-RFECV-NSGA	0.896	4.485	2.598
Chamlal et al (2023)	0.870	-	-
Sandru & David (2019)	-	8.930	6.250
El Touati et al (2023)	-	5.270	4.910
Hsu et al (2011)	0.860	7.540	-
Al-Aghbari et al (2022)	-	5.680	-
Sun et al (2021)	-	4.810	3.230

The study results highlight the effectiveness of feature selection techniques in improving the predictive accuracy of regression models, especially for environmental data analysis. A significant improvement in model performance when using Mutual Information Recursive Feature Elimination with Cross-Validation (MI-RFECV) was seen. This improvement was further amplified when integrating the Non-Dominated Sorting Genetic Algorithm II (NSGA-II) in the feature selection process.

Recent studies, Table 2, align with the findings of this research, emphasizing the role of advanced feature

selection and optimization in achieving higher predictive accuracy.

Chamlal et al. (2023) proposed a two-step feature selection procedure for handling high-dimensional data, focusing on balancing computational efficiency and prediction performance. While their method demonstrates substantial improvement in model accuracy, it does not address the simultaneous optimization of conflicting objectives, such as minimizing RMSE and MAE, which our MI-RFECV-NSGA-II approach successfully achieves.

Şandru and David (2019) introduced a unified feature selection and hyperparameter optimization framework based on Bayesian methods. Although their approach streamlines regression modelling, the lack of integration with multi-objective optimization frameworks limits its ability to balance prediction performance against feature subset complexity, as achieved in our study. In comparison, MI-RFECV-NSGA-II provides a comprehensive solution, enhancing generalization and predictive performance.

El Touati et al. (2023) presented an adaptive feature selection method that dynamically refines feature subsets in machine learning models. While effective in improving computational efficiency and accuracy, their approach lacks the ability to optimize multiple objectives simultaneously. By contrast, our method explicitly incorporates multi-objective optimization through NSGA-II, achieving an R^2 of 0.896 while significantly reducing RMSE and MAE.

In the context of environmental and hydrological modelling, Al-Aghbari et al. (2022) demonstrated a hybrid multi-objective optimization approach for water flooding applications. Their work highlights the potential of multi-objective algorithms in environmental systems but focuses more on physical processes than feature selection.

Similarly, Sun et al. (2021) explored adaptive surrogate modelling for hybrid optimization, showcasing the advantages of multi-objective optimization in constrained scenarios. These studies reinforce the importance of incorporating multi-objective frameworks, which our MI-RFECV-NSGA-II method leverages for improved regression performance.

Overall, this study demonstrates that the integration of feature selection techniques like MI-RFECV with advanced multi-objective optimization algorithms such as NSGA-II significantly outperforms traditional and recent hybrid methods. This is evident in the remarkable improvement in R^2 , RMSE, and MAE metrics, highlighting the robustness and applicability of the

proposed approach for complex predictive modelling tasks.

CONCLUSION

The study was conducted on feature selection in regression modelling, with a special focus on environmental data analysis. After careful experimentation and evaluation, the following conclusions were reached about the effectiveness of feature selection techniques and their influence on model performance.

It's clear that feature selection is key to improving the predictive accuracy of regression models. Traditional methods like Mutual Information and Recursive Feature Elimination with Cross-Validation (MI-RFECV) are quite good at identifying relevant features and boosting performance metrics such as the R^2 score, RMSE, and MAE. However, when the Non-Dominated Sorting Genetic Algorithm II (NSGA-II) was incorporated into the feature selection process, the MI-RFECV-NSGA-II approach led to significant improvements in predictive accuracy. It delivered higher R^2 scores, and reduced error rates compared to the standard methods.

Comparing the results archived to results from previous studies, it's evident that MI-RFECV-NSGA-II outperforms traditional feature selection methods. While earlier methods have shown positive results in improving model accuracy, this study takes it a step further. Leveraging the optimization capabilities of NSGA-II to identify more optimal feature subsets. The resulting enhancement in model performance metrics suggests that MI-RFECV-NSGA-II provides a more structured and efficient approach to feature selection, especially in high-dimensional datasets and complex regression tasks.

DECLARATIONS

Corresponding author

Correspondence and requests for materials should be addressed to Thalasang Tshireletso; E-mail: tshireletsot@ub.ac.bw; ORCID: 0000-0002-5112-8077

Data availability

The datasets used and/or analysed during the current study available from the corresponding author on reasonable request.

Acknowledgements

This research project was funded by both the USAID Partnerships for Enhanced Engagement in Research

(PEER) under the PEER program cooperative agreement number: AID-OAA-A-11- 00012 and the University of Botswana, Office of Research and Development (ORD).

Authors' contribution

Conceptualization and Methodology; Thalasang Tshireletso; Supervision; Yashon Ouma, Ditiro Moalafhi and Geroge Anderson. Funding Acquisition; Yashon Ouma. All authors have read and agreed to the published version of the manuscript.

Competing interests

The authors declare no conflict of interest.

REFERENCES

- Ahmed, I., Abu, M., & El-Henawy, I. (2017). A Feature Selection Algorithm based on Mutual Information using Local Non-uniformity Correction Estimator. *International Journal of Advanced Computer Science and Applications*, 8(6). DOI: [10.14569/IJACSA.2017.080656](https://doi.org/10.14569/IJACSA.2017.080656)
- Al-Aghbari, M., Gujarathi, A., Al-Wadhahi, M., & Chakraborti, N. (2022). Hybrid Multi-objective Optimization Approach in Water Flooding. *Journal of Energy Resources Technology*, 145(3), 032103. <https://doi.org/10.1115/1.4052623>
- Chamlal, H., Benzmane, A., & Ouaderhman, T. (2023). A Two-Step Feature Selection Procedure to Handle High-Dimensional Data in Regression Problems. *2023 International Conference on Decision Aid Sciences and Applications(DASA)*. <https://doi.org/10.1109/DASA59624.2023.10286637>
- Dash, M., & Liu, H. (1997). Feature selection for classification. *Intelligent Data Analysis*, 1(1-4), 131-156. [https://doi.org/10.1016/S1088-467X\(97\)00008-5](https://doi.org/10.1016/S1088-467X(97)00008-5)
- Deb, K., Pratap, A., Agarwal, S., & Meyarivan, T. (2002) - A fast and elitist multiobjective genetic algorithm: NSGA-II. *IEEE Transactions on Evolutionary Computation*, 6(2), 182-197. DOI: [10.1109/4235.996017](https://doi.org/10.1109/4235.996017)
- El Touati, Y., Ben Slimane, J., & Saidani, T. (2023). Adaptive Method for Feature Selection in the Machine Learning Context. *Engineering, Technology & Applied Science Research*, 13(2), 123-130. <https://doi.org/10.48084/etasr.7401>
- Guyon, I., & Elisseeff, A. (2003). An introduction to variable and feature selection. *Journal of Machine Learning Research*, 3, 1157-1182. Available at <http://jmlr.csail.mit.edu/papers/volume3/guyon03a/guyon03a.pdf>.
- Herman, G., Zhang, B., Wang, Y., & Ye, G. (2013). Mutual information-based method for selecting informative feature sets. *Pattern Recognition*, 46(12), 3315-3327. DOI: [10.1016/j.patcog.2013.04.021](https://doi.org/10.1016/j.patcog.2013.04.021)
- Kohavi, R., & John, G. H. (1997). Wrappers for feature subset selection. *Artificial Intelligence*, 97(1-2), 273-324. DOI: [10.1016/S0004-3702\(97\)00043-X](https://doi.org/10.1016/S0004-3702(97)00043-X).
- Hsu, H.-H., Hsieh, C.-W., & Lu, M.-D. (2011). Hybrid feature selection by combining filters and wrappers. *Expert Systems with Applications*, 38(7), 8144-8150. DOI: [10.1016/j.eswa.2010.12.156](https://doi.org/10.1016/j.eswa.2010.12.156).
- Saeyns, Y., Inza, I., & Larrañaga, P. (2007). A review of feature selection techniques in bioinformatics. *Bioinformatics*, 23(19), 2507-2517. DOI: [10.1093/bioinformatics/btm344](https://doi.org/10.1093/bioinformatics/btm344).
- Şandru, E.-D., & David, E. (2019). Unified Feature Selection and Hyperparameter Bayesian Optimization for Machine Learning-Based Regression. *International Symposium on Signals, Circuits and Systems (ISSCS)*. <https://doi.org/10.1109/ISSCS.2019.8801728>
- Sun, R., Duan, Q., & Mao, X. (2021). A Multi-Objective Adaptive Surrogate Modelling-Based Optimization Algorithm for Constrained Hybrid Problems. *Environmental Modelling & Software*, 144, 105272. <https://doi.org/10.1016/j.envsoft.2021.105272>

Publisher's note: [Scienceline Publication](https://www.scienceline.com) Ltd. remains neutral with regard to jurisdictional claims in published maps and institutional affiliations.




Open Access: This article is licensed under a Creative Commons Attribution 4.0 International License, which permits use, sharing, adaptation, distribution and reproduction in any medium or format, as long as you give appropriate credit to the original author(s) and the source, provide a link to the Creative Commons licence, and indicate if changes were made. The images or other third party material in this article are included in the article's Creative Commons licence, unless indicated otherwise in a credit line to the material. If material is not included in the article's Creative Commons licence and your intended use is not permitted by statutory regulation or exceeds the permitted use, you will need to obtain permission directly from the copyright holder. To view a copy of this licence, visit <https://creativecommons.org/licenses/by/4.0/>.

Investigation of Performance of Copper Slag and Ore Tailings Novel Trial Self-compacting Concrete Mixtures

Annabelle Fidler¹  and Damilola Oyewumi Oyejobi²  

¹University of Botswana, 4775 Notwane Rd, Gaborone, Botswana

²University of Botswana, 4775 Notwane Rd, Gaborone, Botswana

 Corresponding author's Email: oyejobido@ub.ac.bw

ABSTRACT

A non-conventional concrete with the properties of flow-ability, filling-ability, and passing-ability without any need for mechanical compaction but flow under self-weight is known as self-compacting concrete. This study developed trial mixtures for self-compacting concrete (SCC) using locally available waste products. The copper slag and ore tailings from Bamangwato Concessions Limited Mine in Selebi-Phikwe, Botswana were used as source of fine aggregate, and fines substitute. Eight mix proportions were developed with the quantities of cement, granite, copper slag, ore tailings and water-cement ratio as variables. The mix proportions were developed in accordance with recommendations from American Concrete Institute (ACI 237R-07) and fresh SCC properties (flow ability, passing ability, filling-ability, and segregation) were performed to assess the performance of the mixes. It was observed that the range of slump flow values were between (500 – 750 mm), V-funnel values (1.46 – 7.46 s), passing-ability of (0.76 – 1.0). The hardened properties of SCC (strength and density) were between 8.1 and 33.3 MPa, and 2093 to 2406 kg/m³ respectively. It could be concluded that SCC produced from mine wastes (copper slag and ore tailings) is found suitable for the use in unreinforced and normal concrete applications.

Keywords: Self-compacting concrete, filling-ability, flow-ability, passing-ability, slump flow, segregation and compressive strength.

INTRODUCTION

Concrete composed of conventional materials but flow without mechanical compaction rather than its own weight and without segregation is referred to self-compacting concrete (SCC) (Habibi and Ghomashi, 2018). However, understanding how to distinguish between a bonafide SCC and a conventional concrete holds significant importance. SCC has exceptional workability and boasts distinct advantages over conventional 'flowing' concrete. Studies such as Benaicha et al. (2019) has indicated that SCC has superior performance over conventional concrete which include rheological and mechanical properties. Unlike conventional concrete, SCC does not need any form of compaction. Other good quality of SCC as reported in Su et al. (2001) included high fluidity, better resistance to segregation and filling ability property. It effectively resists segregation, ensuring that its constituent materials remain uniformly distributed during transportation and placement. Furthermore, SCC keeps a stable composition throughout these processes. It should be noted that SCC comprises the same ingredients with traditional concrete which include fine and coarse aggregates, cement, mineral additive and admixture to positively alter the performance of concrete. However, the ultimate composition of the mixture and its properties in the fresh state exhibit notable differences. The

performance of SCC has largely been described to be the function of raw materials and their inherent characteristics (Ashish and Verma, 2019). In material composition, high amount of mineral fillers which include supplementary cementitious materials and finely divided powder, and admixtures such as viscosity modifying admixture, water reducing admixture and high range water reducing admixture for SCC rheological and stability control are normally added in greater proportions. Additionally, SCC is known to employ reduced quantity, and lower maximum size of coarse aggregate. The alterations made to the composition of the mixture have an impact on the properties and performance of the concrete once it has reached its hardened condition. Furthermore, Ashish and Verma (2019) explained performance and application requirements have been identified as major determining factor when developing SCC mixes.

The production of good self-compacting qualities takes precedence over the later toughened features, which receive less initial attention as a result. The mass ratio of mixture composition in one cubic metre volume of concrete is a function of cement and fines content, quantity of paste, dosage of admixture, size and volume of fine and coarse aggregates all together. The mechanical, stability and other durability properties of SCC can then be tested and verified using similar approaches for conventional concrete. Because there are so many ways in

RESEARCH ARTICLE
 PII: S225204302400030-14
 Received: June 25, 2024
 Revised: September 02, 2024
 Accepted: September 05, 2024

Flow- ability property of SCC

The procedure for this test followed ASTM C143/C143 M (2015) modified with the intention of determining free flow of the concrete when there is no obstruction. The concrete was poured into the slump cone at once without either manual or mechanical vibration. This was followed with lifting of the cone within approximately 30 seconds of filling and the concrete subsided under its own weight. The typical flow is shown in Figure 2 and the mean of the values taken from different directions is reported as the slump flow value of the SCC.



Figure 2. Slump flow of developed SCC

Filling-ability property of SCC

The SCC ability to fill the container is measured using the fabricated V-shaped funnel shown in Figure 3 similar

to the recommendations given in European guidelines EN12350-1 as per the dimensions. The equipment was set up on a firm ground with a receiving container below it. The V-shaped funnel in Figure 3 was dampened with no trace of water. With the bottom of the funnel kept shut, the funnel is filled with concrete without any agitation when filled and levelled. Subsequently, the funnel gate is opened and the interval between when the gate was opened and when we could see vertically through the funnel was taken as the flow time measured in seconds.



Figure 3. V-Funnel apparatus filled with fresh concrete.

Table 1. Mix Proportions for trial mixture

TM	Cement (kg)	Fine Aggregates (kg)	Coarse Aggregates (kg)	Water (kg)	Tailings (kg)	Slump flow (mm)	V- funnel (seconds)	Passing- ability	Segregation	28-day Strength (N/mm ²)
1	7.45	11.76	10.29	5.55	7.32	500	7.50	0.80	9	33.50
2	7.45	11.76	10.29	6.55	7.32	590	6.20	0.81	10	28.10
3	7.14	9.96	8.71	6.32	6.93	610	4.20	0.84	10	24.60
4	7.55	9.96	8.71	6.68	7.33	640	2.10	0.93	11	36.10
5	7.96	9.96	8.71	7.05	7.73	750	1.50	1.00	12	23.70
6	14.10	9.96	8.71	6.32	0	615	2.50	0.89	16	34.70
7	13.36	9.96	8.71	6.68	0.70	630	2.10	0.92	16	39.90
8	12.66	9.96	8.71	7.05	1.41	642	1.50	0.96	16	31.10

Passing- ability characteristic of SCC

The fabricated L-box shown in Figure 4 is conformable to the specification given in European standard and is used to measure passing ratio between the depth of concrete in the L-box (H2) and the concrete depth behind the gate (H1). Fresh concrete sampled in line with EN 12350- 1 was poured into the L box vertical

compartment and allowed it to stand for one minute. This is followed by the gentle opening of the gate for concrete to pass between the two smooth bars of twelve millimeters diameter with gap interval of 59 mm. At the end of the movement, vertical distances between the top of concrete and top of the horizontal portion of the L box were measured and the mean height of the concrete was

calculated. The ratio of H2/H1 gives the passing ability result of the L-box test.

Sieve segregation resistance property of SCC

A PVC cylinder was divided into three equal parts which were stacked together. Sampled concrete was poured into the stack of cylinders, ensuring they do not shift and allowed to settle for approximately 15 minutes. Once the time elapsed the cylinders were separated and placed on separate 4.75 mm sieves. After a waiting period of 120 seconds, the weight of the passed material is measured. This is followed with the calculation of segregation ratio which was taken as the fraction of the material that passed the sieve. The resistance of SCC to segregation was inspected visually and measured with sieve test.



Figure 4 - L- box apparatus with SCC

Compressive strength of SCC

ASTM C39/C39 M (2021) standard was used for the determination of compressive strength of SCC. After the cast, the cubes are allowed to undergo a day rest and later transferred to the water tank for water curing until the testing date, which was carried out on 7, 14, and 28 days.

RESULTS AND DISCUSSIONS

Slump flow values of SCC

The spread of SCC fresh concrete is measured from different directions with the values of average diameter reported in Table 1. All the mixes apart from TM1 met the

specification for slump flow class range of (550 – 650 mm) according to European guidelines. TM 5 falls into slump flow 2 (660 – 750 mm). For mixes 1 and 2 in Figure 5, the slight increase in the slump flow was because of additional water, Table 1, however, slight reduction in cement content, copper slag and coarse aggregate with light increase in water resulted in increase in slump flow with optimal slump value of 750 mm. With drastic reduction in tailings and increase in cement content (mixes 6 – 8) and at constant fine and coarse aggregates respectively, there was also increase in slump flow values. Mix numbers 2, 3, 4 and 5 yielded good slump values and this could be attributed to a well-balanced mix proportions.

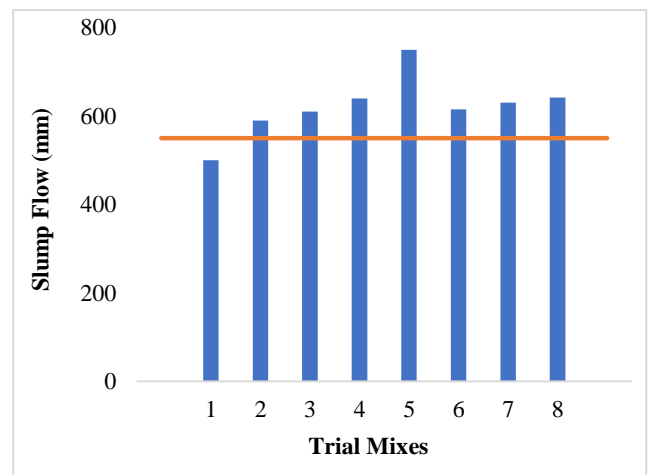


Figure 5. Slump Flows values for mixes

Filling-ability result of SCC

TM1 to TM 8 conformed to criteria of less than 10 seconds stipulated for funnel class VF 1, Table 1 and Figure 6 respectively. It was observed that flow time of concrete at constant fine and coarse aggregates was dependent on both tailings and cement. Also, it could be deduced that an increase in slump flow values is accomplished by reduction in the time taken, with the least time being 1.5 seconds for slump flow value of 750 mm.

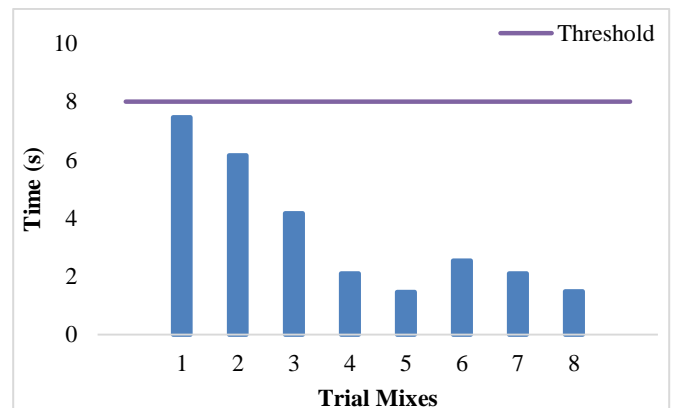


Figure 6. V-Funnel results for SCC mixes

Passing-ability values of SCC

All the mixes met the specification for the passing ability requirement for PA1 class with 2 reinforcement bars according to EN 206-1: 2013, the highest value of 1 is recorded for TM5, Table 1 and Figure 7. Previously, TM5 had been reported to have 750 mm slump flow and 1.5 seconds for flow time. The amount of powder (tailings) in the mix and good spherical shape, and well graded copper slag play significant role in this.

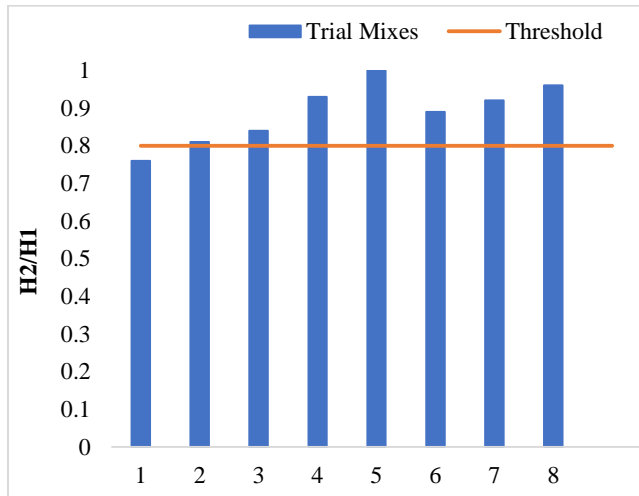


Figure 7. L-Box result for SCC

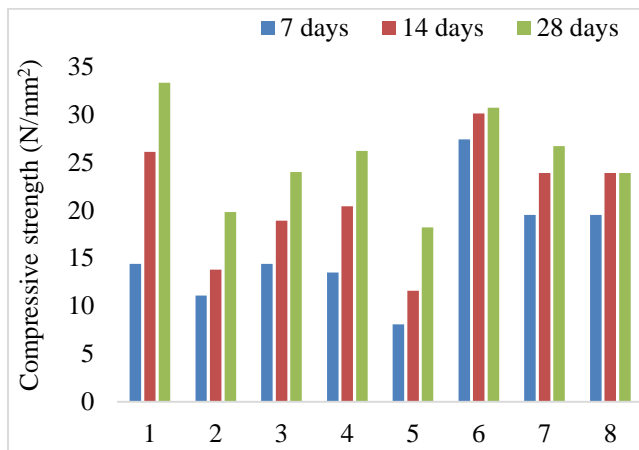


Figure 8. Compressive strength of SCC

Sieve segregation resistance values of SCC

From the physical observation, there was limited or no bleed water from the mix. When calculated in percentage, mixes 1 and 2 had the least segregation value, Table 1, the highest segregation values of 12, 13 and 14 could be because of increase in cement content. In all, all the mixes have values that are below 20 according to European specifications.

Compressive strength of SCC

The trend of strength development is illustrated in Figure 8 across the curing age. The mixes with good SCC characteristics are marked with lower compressive strengths and this could be because of moderate high water-cement ratio in the mixes, tailings in the mixes only served as filler and not as binder.

CONCLUSIONS

This study has found that copper slag could be an excellent choice for making self-compacting concrete due to its rounded particles which aid in workability when fresh and its moderate strength when hardened. Ore tailings increase the flow ability however high quantity makes the concrete prone to segregation when fresh and weakens its strength when hardened. The mixes with slump flow values between 550 and 650 mm fall in SF1 and can find their use in lightly reinforced or unreinforced concrete structures, structures with small sections and casting that involves pump injections. For other mixes above this limit (> 660 and ≤ 750 mm), they can be used for normal applications. In addition, the filling ability results indicated that SCC has inherent property to flow and fill the available space without any need for special vibration. The minimum passing achieved by all mixes indicated that the developed mixes could pass through obstructions without any blocking. From the visual inspection shows that the developed mixes were cohesive and homogeneous with limited amount of segregation. Lastly, the compressive strength reveals that the developed mixes could be used for varying project applications such as lightly reinforced or unreinforced concrete structures.

DECLARATIONS

Corresponding author

Correspondence and requests for materials should be addressed to D.O. Oyejobi; Email: oyejobido@ub.ac.bw; ORCID: [0000-0002-6482-0396](https://orcid.org/0000-0002-6482-0396)

Data availability

The datasets used and/or analysed during the current study available from the corresponding author on reasonable request.

Acknowledgements

The authors would like to acknowledge the following.

- Technicians at Roads department, Ministry of Transport and Communications, Gaborone, Botswana for creating a conducive environment to conduct this research.
- Department of Tertiary Education and Funding for sponsoring this research through student book allowance.

Authors' contribution

First Author performed the experiments, analysed the data obtained and wrote the manuscript. Second Author designed the experimental process and revised the manuscript. Both authors read and approved the final manuscript.

Competing interests

The authors declare no competing interests in this research and publication.

REFERENCES

- Ashish, Deepankar Kumar, & Verma, Surender Kumar. (2019). An overview on mixture design of self-compacting concrete. *Structural Concrete*, 20(1), 371-395. <https://doi.org/10.1002/suco.201700279>
- ACI PRC-237-07 (2019) Self-Consolidating Concrete ISBN: 9780870312441. 38800 Country Club Drive. www. Concrete. Org
- ASTM C39/C39M (2021) Standard Test Method for Compressive Strength of Cylindrical Concrete Specimens. Copyright © ASTM International, 100 Barr Harbor Drive, PO Box C700, West Conshohocken, PA 19428-2959. United States
- ASTM C143/C143M (2015) Standard Test Method for Slump of Hydraulic-Cement Concrete. ASTM International, 100 Barr Harbor Drive, PO Box C700, West Conshohocken, PA 19428-2959. United States
- Benaicha, M, Alaoui, A Hafidi, Jalbaud, O, & Burtshell, Y. (2019). Dosage effect of superplasticizer on self-compacting concrete: Correlation between rheology and strength. *Journal of Materials Research and Technology*, 8(2), 2063-2069. <https://doi.org/10.1016/j.jmrt.2019.01.015>
- BS EN 12350-1 (2019) Testing fresh concrete- Part 1: Sampling and common apparatus. 978-0-539-07272-3. BSI
- BS EN 206:2013 (2013) Concrete- Specification, performance, production and conformity published by BSI Standards Limited 2014 ISBN 978 0 580 85966 3 ICS 91.100.30 CEN-CENELEC Management Centre: Avenue Marnix 17, B-1000 Brussels.
- Gabasiane, TS, Bhero, Shepherd, & Danha, Gwiranai. (2019). Waste management and treatment of copper slag BCL, Selebi Phikwe Botswana. *Procedia Manufacturing*, 35, 494-499. <https://doi.org/10.1016/j.promfg.2019.05.071>
- Gallagher, Louise, & Peduzzi, Pascal. (2019). Sand and sustainability: Finding new solutions for environmental governance of global sand resources.
- Habibi, Alireza, & Ghomashi, Jian. (2018). Development of an optimum mix design method for self-compacting concrete based on experimental results. *Construction and Building Materials*, 168, 113-123. <https://doi.org/10.1016/j.conbuildmat.2018.02.113>
- Okamura, Hajime, & Ozawa, Kazumasa. (1994). Mix design method for self-compactable concrete. *Doboku Gakkai Ronbunshu*, 1994(496), 1-8. https://doi.org/10.2208/jscej.1994.496_1
- Onuaguluchi, Obinna, & Eren, Özgür. (2012). Recycling of copper tailings as an additive in cement mortars. *Construction and Building Materials*, 37, 723-727. <https://doi.org/10.1016/j.conbuildmat.2012.08.009>
- Oyejobi, DO, Adewuyi, AP, Yusuf, SO, Oyebanji, YO, Suleiman, I, & Hassan, IA. (2023). Performance of blended cement mortar modified with fly ash and copper slag. *Materials Today: Proceedings*, 86, 104-110. <https://doi.org/10.1016/j.matpr.2023.03.294>
- Su, Nan, Hsu, Kung-Chung, & Chai, His-Wen. (2001). A simple mix design method for self-compacting concrete. *Cement and concrete research*, 31(12), 1799-1807. [https://doi.org/10.1016/S0008-8846\(01\)00566-X](https://doi.org/10.1016/S0008-8846(01)00566-X)
- Zhao, Jiangshan, Ni, Kun, Su, Youpo, & Shi, Yunxing. (2021). An evaluation of iron ore tailings characteristics and iron ore tailings concrete properties. *Construction and Building Materials*, 286, 122968. <https://doi.org/10.1016/j.conbuildmat.2021.122968>

Publisher's note: [Scienceline Publication](#) Ltd. remains neutral with regard to jurisdictional claims in published maps and institutional affiliations.



Open Access: This article is licensed under a Creative Commons Attribution 4.0 International License, which permits use, sharing, adaptation, distribution and reproduction in any medium or format, as long as you give appropriate credit to the original author(s) and the source, provide a link to the Creative Commons licence, and indicate if changes were made. The images or other third party material in this article are included in the article's Creative Commons licence, unless indicated otherwise in a credit line to the material. If material is not included in the article's Creative Commons licence and your intended use is not permitted by statutory regulation or exceeds the permitted use, you will need to obtain permission directly from the copyright holder. To view a copy of this licence, visit <https://creativecommons.org/licenses/by/4.0/>.

Efficacy of Direct SPT-Based Pile Design Methods in Residual Soils of Southern Africa

Tshepo Masilo  and Mahongo Dithinde  

Department of Civil Engineering, University of Botswana, Gaborone, Botswana

Corresponding author's Email: dithinde@ub.ac.bw

ABSTRACT

Direct SPT-based pile design methods are very popular these days despite the fact that many of such methods are based on small databases of pile load tests. Due to the dependence of soil behaviour on geological setting and site specific conditions, it is possible that some of the methods do not produce good prediction of pile capacity. Accordingly this paper presents the evaluation of two SPT-based pile design methods in residual soils against a pile load test database from the Southern African region. The methods include the (i) Franki-SA method reported in Byrne et al. (1995) and (ii) Decourt Method (1995). The pile load tests consist of 26 cases of bored piles in residual soil with each case accompanied by SPT measurements. The SPT measurements were used to calculate the predicted capacity in accordance with the procedure for each of the two methods while the pile load tests were used to determine the measured capacity. The findings of the evaluation indicate that the Decourt method is more reliable and accurate than the SA method. The poor performance of the SA methods suggests further studies to develop specific calculation factors for base and shaft capacities in residual soils.

Keywords: SPT-based pile methods, Load Bearing Capacity, Pile Load Test, Chin extrapolation method, Terzhagi's 10% criteria, Rank Index.

INTRODUCTION

Pile foundations are commonly used to support heavy structures, where shallow foundations are not suitable. These foundations can withstand substantial tensile and lateral forces, deriving their load-bearing capacity from shaft and base resistance. The Standard Penetration Test (SPT) is a widely used and cost-effective field test for soil investigation, providing crucial data pile design. Notably, the SPT N-value is extensively utilized in designing structural foundations, especially for assessing pile bearing capacity (Meyerhof, 1976; Shioi and Fukui, 1982; Decourt, 1995; Robert, 1997).

The interaction between piles and the surrounding soil presents a complex geotechnical challenge. Understanding this interaction is essential for ensuring the safety and performance of pile foundations. However, challenges persist in accurately predicting how piles will behave in specific soil conditions, particularly in contexts like residual soils, which exhibit heterogeneous and weathered properties. This knowledge gap underscores the need for efficient design methods and verification through pile load testing (Fellenius, 2018). The purpose of this paper is to assess the efficiency SA-SPT based pile design method in residual soils in comparison with the well-established Decourt method.

The pile load test dataset was obtained from the database reported in Dithinde et al. (2011). The Franki-SA and Decourt methods are commonly used for estimating pile capacities but rely on limited databases that may not fully represent Southern Africa's unique conditions. In today's safety-focused engineering industry, it is important not only to ensure the safety of design methods but also to quantify their accuracy. This study aligns with the approach advocated by Sandgren and Cameron (2002), aiming to assess the uncertainty of SPT empirical methods by comparing predicted pile capacities with actual measurements. By shedding light on the safety and economic viability of these design methods for pile foundations in Southern Africa, this research contributes to enhancing engineering practices in the region.

MATERIALS AND METHODS

Compilation of pile load test database

The database contains essential data from full-scale pile load tests, soil profiles, and field tests, crucial for detailed load and resistance analysis. Pile load tests data was collected from various sources, mainly piling companies in South Africa, Botswana, Lesotho, Zambia, eSwatini, and Tanzania. Twenty-six cases were specifically selected for the study. The database includes three pile types:

RESEARCH ARTICLE
 PII: S225204302400031-14
 Received: June 25, 2024
 Revised: September 02, 2024
 Accepted: September 05, 2024

- i. Expanded base (Franki) piles
- ii. Auger piles
- iii. Continuous Flight Auger (CFA) piles.

Table 1 summarizes key information from the compiled cases, including pile descriptions, types, shaft and base diameters, and lengths.

Frank-SA method

The shaft and base pile capacities were computed by using the corrected N values in conjunction with factors obtained from Tables 2 and 3. There are different factors for shaft and base capacities depending on the type of pile and the soil conditions, etc.).

Table 1. Pile cases descriptions

Case No.	Pile type	Shaft dia. (mm)	Base dia.(mm)	Length (m)	SPT N-value	
					Base	Shaft
1	Auger	600	600	11.5	Ref.	80
2	Auger	600	600	6.5	Ref.	15
3	Franki	600	800	6.5	60	15
4	Auger	610	610	9	100	20
5	Auger	610	610	7	100	20
6	CFA	750	750	13	100	20
7	Auger	450	450	9	Ref.	Ref.
8	CFA	350	350	5	Ref.	20
9	CFA	500	500	6	Ref.	20
10	CFA	600	600	6	20	10
11	CFA	450	450	6	100	20
12	CFA	300	300	6	Ref.	20
13	CFA	600	600	9.6	Ref.	20
14	CFA	400	400	8.7	100	20
15	CFA	350	350	8.7	60	20
16	CFA	410	410	11	100	20
17	Auger	615	615	12	32	28
18	Auger	615	615	12	32	28
19	Auger	610	610	7	90	70
20	Auger	610	610	5	90	70
21	Auger	500	500	7.8	Ref.	17
22	Franki	450	600	15.5	40	13
23	Auger	750	750	10.2	Ref.	35
24	Auger	450	450	8	100	17
25	Auger	450	450	8	100	17
26	Auger	450	450	8	Ref.	12

Table 2. Factors for calculating ultimate shaft capacity

Test	Pile						Franki Wet Shaft	Franki Ram Shaft	Forum Wet Shaft	Forum Ram Shaft
	Auger	Auger U/S	CFA	Oscill.	Precast	Tube				
Piles in Non-cohesive Soils										
CPT q_c	5	5	5	5	8	8	8	12	5	8
SPT 'N'	2.5	2.5	2.5	2.5	4	4	4	6	2.5	4
Max (kPa)	125	80	125	125	150	150	150	200	125	150
Piles in Cohesive Soils										
CPT q_c	10	10	10	10	15	15	15	30	10	15
SPT 'N'	2.5	2.5	2.5	2.5	3.0	3.0	3.0	4.5	2.5	3.5
α	0.4	0.4	0.4	0.4	0.6	0.6	0.4	0.6	0.4	0.5
Max (kPa)	150	80	125	125	150	150	150	200	125	150

Table 3. Factors for calculating base capacity

Test	Pile						Franki	Franki	Forum	Forum
	Auger	Auger U/S	CFA	Oscill.	Precast	Tube	Wet Shaft	Ram Shaft	Wet Shaft	Ram Shaft
Piles in non-cohesive soils										
CPT q_c	0.5 q_c	0.5 q_c	0.5 q_c	0.5 q_c	1.0 q_c	1.0 q_c	1.2 q_c	1.2 q_c	1.0 q_c	1.0 q_c
SPT 'N'	300	300	300	300	400	400	500	500	400	400
Max (kPa)	8000	8000	8000	8000	20000	15000	15000	15000	15000	15000
Piles in cohesive soils										
CPT q_c	0.45 q_c	0.45 q_c	0.45 q_c	0.45 q_c	0.45 q_c	0.45 q_c	0.60 q_c	0.60 q_c	0.50 q_c	0.50 q_c
SPT 'N'	50	50	50	50	50	50	60	60	50	50
α	9	9	9	9	9	9	9 - 20	9 - 20	9 - 12	9 - 12
Max (kPa)	4500	4500	4500	4500	4500	4500	6000	6000	5000	5000

Table 4. "α" Values

Pile type	α			β		
	Clay	Sand	Residual soils	Clay	Sand	Residual soils
Driven	1	1	1	1	1	1
Bored piles (in general)	0.85	0.5	0.6	0.85	0.5	0.6
Bored piles (with mud)	0.85	0.5	0.6	0.9	0.5	0.75
CFA continuous flight auger	0.3	0.3	0.3	1	1	1
Minipiles, without pressure grouting	0.85	0.5	0.6	1.5	1.5	1.5
Pressure grouted minipiles	1	1	1	0.3	0.3	0.3

The base and shaft resistance are calculated as per Eq. 1 and Eq. 2 respectively.

$$Q_b = (N_1)_{60} F_b \leq q_{max} \quad [1]$$

$$q_s = (N_1)_{60} F_s \leq q_{max} \quad [2]$$

Where q_b is the base resistance, q_s is the shaft resistance, $(N_1)_b$ is the SPT N-value for the base, $(N_1)_s$ is the SPT N-value for the shaft, F_b is the pile base resistance factor (Table 4), F_s is the pile shaft resistance factor (Table 5) and q_{max} indicates the maximum allowable pile capacity for the pile design situation.

The ultimate pile base and shaft capacities were calculated as (Eq. 3 and Eq. 4 respectively):

$$Q_b = q_b A_b \quad [3]$$

$$Q_s = q_s A_s \quad [4]$$

Where Q_b represents base capacity, A_b is the cross-sectional area of the pile base, Q_s is: base capacity and A_s the surface area of the pile shaft.

Decourt method

The ultimate pile capacity using the Decourt Method was determined by following the method's key Eqs 5 -8 in conjunction with coefficient specific to soil types and pile types, as shown in the provided Table 4 and 5.

For the base:

$$q_b = k_b N_b \quad [5]$$

Where q_b is the base resistance, k_b is a coefficient specific to the type of soil and installation method, N_b is the corrected SPT value around the pile base.

For the shaft:

$$q_s = \alpha(2.8N_s + 10) \quad [6]$$

Where, q_s is the shaft resistance, α accounts for the type of pile being used, N_s is the corrected SPT value around the pile shaft.

The ultimate pile capacity (Q_u) was then calculated as follows: $Q_u = q_b A_b + q_s A_s$ [7]

Table 5. "k" Values

Soil type	k (kPa)
Clays	120
Clayey silts (residual soils)	200
Sandy silts (residual soils)	250
Sands	400

Determination of measured pile capacity pile

The collected pile load test data were further processed by plotting load versus settlement to produce load-deflection curves. The load-deflection curves were then used to determine the ultimate pile capacity or measured capacity (Q_m). However, majority of the test piles were working piles and therefore not tested to failure and requires extrapolation procedure to determine the

ultimate capacity e.g. (e.g. Chin, 1970 and 1971; Fleming 1992; Decourt, 1999). On account of its popularity, Chin extrapolation method was adopted for this study.

Evaluation of performance of methods studied

The performance of the methods were accessed by comparing their predicted capacity (Q_p) to the measured capacity (Q_m). The comparison was achieved through (i) model uncertainty (M) statistics and (ii) best fit (Q_{fit} and the associated coefficient of determination (R^2). The model uncertainty or model factor (M) was determined from Eq. 8.

$$M = \frac{Q_m}{Q_p} \quad [8]$$

Where: Q_m = pile capacity” interpreted from a load test, to represent the measured capacity; Q_p = pile capacity generally predicted using Franki and Decourt method.

In addition to the measure of centrality and dispersion, the mean (mM) and standard deviation (sM) of the model factor were considered as indicators of the accuracy and precision of the predication method. An accurate and precise method gives $mM = 1$ and $sM = 0$ respectively, which means that for each pile case, the predicted pile capacity equals to the measured capacity (an ideal case). However, due to uncertainties of prediction models, the results of an ideal case cannot be attained in practice. Therefore in reality, the method is better when mM is close to 1 and sM is close to 0. In general when $mM > 1$, the predicted capacity is less than the interpreted capacity, which is conservative and safe whereas when $mM < 1$, the predicted capacity is greater than the interpreted capacity, which is not conservative and unsafe.

The ‘best fit’ was based on the equation of the best fit line of predicted versus measured capacity with the corresponding coefficient of determination (R^2). On the basis of regression analysis, the general equation of the best fit line is given by Eq. 9.

$$Q_{fit} = bQ_p \quad [9]$$

Where Q_{fit} is the least squares average of the measured capacity corresponding to a given predicted capacity values; b is a regression constant denoting the slope of the line; and Q_p is the predicted capacity.

Associated with each regression equation is the coefficient of determination (R^2). This is a statistical measure of goodness of fit between the predicted and measured values. More specifically, R^2 measures the proportion of the total variance in the dependent variable explained by the independent variable. For the purposes of this paper, R^2 was taken as a measure of the degree of agreement between the measured and predicted capacity.

RESULTS AND DISCUSSION

Predicted versus measured pile capacities

Tables 6 present the results of predicted and measured pile capacities and Table 7 presents associated M-statistics for the both Franki and Decourt methods. Further analysis of Table 7 indicated that the Decourt method has a mean that suggests the predicted pile capacities are close to the measured pile capacities. In contrast, the Franki method has a mean that indicates the predicted capacities are significantly higher than the measured capacities. Additionally, the Decourt method has a lower standard deviation, indicating less scatter in the predictions. In contrast, the Franki method has a higher standard deviation, suggesting more variability in the predictions. The COVs are comparable even though the Decourt method has relatively a lower value. Overall, these results suggest that the Decourt method is more accurate and reliable for predicting pile capacity in residual soils.

Table 7. Summary statistics for the model factor

Method	N	Mean	Std. Dev.	COV
Decourt	26	1.01	0.50	0.50
Franki	26	2.38	1.41	0.59

Evaluation of performance through best fit

Figures 3 and 4 present scatter plots of Q_m Vs Q_p for Decourt and SA method respectively. The best fit parameters (i.e. b and R^2) are shown in Table 8. The Decourt method shows a better fit and stronger relationship between predicted and measured capacities, with “ b ” of 1.44 and R^2 of 0.71, indicating that 71% of the variability in measured capacity is explained by the predicted capacity. In contrast, the Franki-SA method has a lower ($b = 0.97$) and R^2 of 0.20, meaning only 20% of the variability in measured capacity is explained by the predicted capacity, indicating a weaker relationship. Based on the evaluation results, the Decourt method is again better than SA method. The relative accuracy of the Decourt method has been reported by other researchers. In this regard, based on three rank index criterion results Henrina et al 2024 found that the best and efficient direct SPT method is the one proposed by Decourt. The relatively poor performance of the SA- Method is attributed to the fact that it does not have specific factors for calculating base and shaft capacities in residual soils as is the case with the Decourt Method. Therefore further studies for determination of SPT factors in residual soils for the SA method are required.

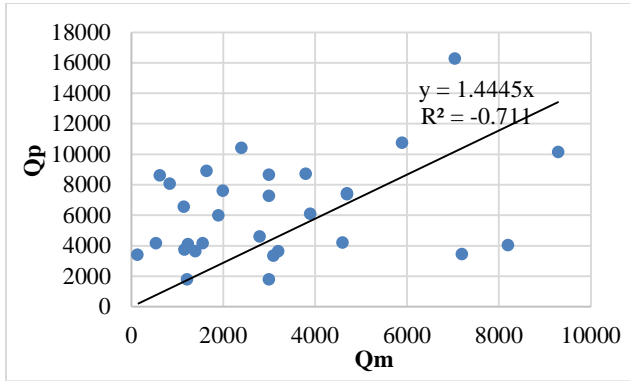


Figure 3. Scatter plot of Q_m Vs Q_p for Decourt method

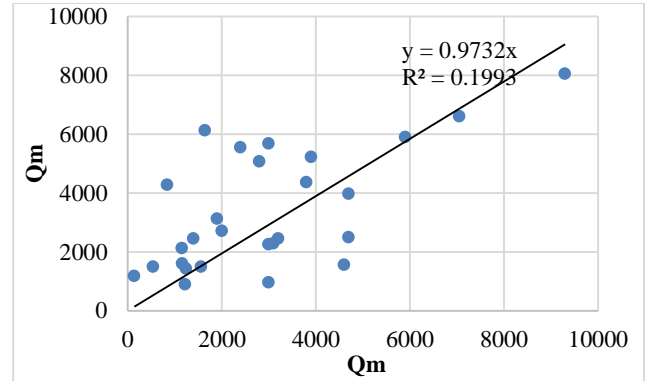


Figure 4. Scatter plot of Q_m Vs Q_p for SA SPT method

Table 8. Best Fit Parameters

Method	b	R ²
Franki	0.97	0.20
Decourt	1.445	0.71

Table 6. Predicted and Measured capacities

Case	Measured Capacity	Predicted Capacities	
		Franki	Decourt
1	4700	3989	4779
2	3000	1138	3150
3	3000	1108	3053
4	2850	1514	3431
5	1920	1331	3285
6	4700	2636	5632
7	3100	1889	2603
8	820	438	1008
9	800	914	2223
10	780	537	1323
11	1230	781	1833
12	1200	437	886
13	3200	1531	3373
14	1390	818	1609
15	875	683	1277
16	1600	1039	1882
17	3100	2099	3131
18	3100	2099	3131
19	1595	2287	3928
20	540	818	2391
21	4970	4028	8325
22	1950	2388	2872
23	3320	3208	5976
24	1600	834	1886
25	1900	1212	3397
26	2230	1078	3307

CONCLUSIONS

In conclusion, the evaluation of the Decourt and Franki methods for predicting pile capacity in residual soils in Southern Africa has revealed that the Decourt method provides better fit between the predicted and measured capacities. Furthermore, the SA method depicts high variability with $mM = 2.36$ and $sM = 1.41$ compared to the Decourt method with $mM = 1.01$ and $sM = 0.5$. Accordingly the uncertainty shown by the SA method is too high for the method to be adopted for practical design of piles in residual soil.

The poor performance of the SA method against the Data base is attributed to absence of specific base and shaft calculation factors for residual soils compared to Decourt method. Therefore further studies are required to develop specific SPT factors for design of piles in residual soils of Sothorn Africa.

DECLARATIONS

Corresponding author

Correspondence and requests for materials should be addressed to Mahongo Dithinde; E-mail: dithinde@ub.ac.bw; ORCID: <https://orcid.org/0000-0002-4541-7438>

Data availability

The datasets used and/or analysed during the current study available from the corresponding author on reasonable request.

Author's contribution

Mahongo Dithinde contributed pile load test database which he has previously used to characterize model uncertainties for theoretical pile design methods. Tshepo Maislo under the guidance of Dithinde evaluated

the SA SPT-based pile design method against the database for piles in residual soils. She further compared the performance of the SA- Method with that of the well-established Decourt Method.

Acknowledgements

Not applicable

Consent to publish

Not applicable.

Competing interests

The authors declare no competing interests in this research and publication.

REFERENCES



- Byrne, G., Everett, J. P., Schwartz, K., Friedlaender, E. A., Mackintosh, N., and Wetter, C. (1995). A Guide to Practical Geotechnical Engineering in Southern Africa, Third Edition, Franki.
- Chin, F. K. (1970). Estimation of the pile Ultimate Load of Piles Not Carried to Failure. Proceedings of the 2nd Southern Asian Conference on Soil Engineering, pp. 81-90.
- Chin, F. K. (1971). Discussions on Pile test. Journal of Soil Mechanics and Foundation Engineering, ASCE, Vol. 97, No. 6, pp. 930-932.
- Chin, F. K. (1971). Discussions on Pile test. Journal of Soil Mechanics and Foundation Engineering, ASCE, Vol. 97, No. 6, pp. 930-932. <https://doi.org/10.1061/JSFEAQ.0001623>.
- Decourt, L. (1999). Behaviour of foundations under working load conditions. Proceedings of the 11th Pan American Conference on Soil Mechanics and Geotechnical Engineering, Foz Dolguassu, Brazil, Vol. 4, pp. 453-488.
- Decourt, L., (1995). Prediction of load-settlement relationships for foundations on the basis of the SPT T, Ciclo de Conferencias Internacionales, Leonardo Zeevaert, UNAM, Mexico, 1995, pp. 85-104.
- Dithinde M, Phoon KK, De Wet M and Retief JV (2011). Characterisation of Model Uncertainty in the Static Pile Design Formula. Journal of Geotechnical and Geoenvironmental Engineering, ASCE, Vol. 137, No. 1. [https://doi.org/10.1061/\(ASCE\)GT.1943-5606.0000401](https://doi.org/10.1061/(ASCE)GT.1943-5606.0000401).
- Fellenius BH (2018) Basics of foundation design, a text book. Revised Electronic Edition, [www.Fellenius.net].
- Fleming, W. G. K. (1992). A new method for single pile settlement prediction and analysis; Geotechnique, Vol. 42, No. 3, pp. 411-425. <https://doi.org/10.1680/geot.1992.42.3.411>.
- Henrina, S., Bahsan, E., and Ilyas, T. (2024). Comparison of direct SPT method for calculating axial capacity of piles in Jakarta Area. IOP Conf. Series: Materials Science and Engineering 673 (2019) 012027. doi:10.1088/1757-899X/673/1/012027 .
- Meyerhof, G. G. (1976). Bearing capacity and settlement of pile foundations. Journal of Geotechnical Engineering, ASCE, Vol. 102, No. 3, pp. 196-228. <https://doi.org/10.1061/AJGEB6.0000243>.
- Sandgren, E., and Cameron, T. M. (2002). Robust design optimization of structures through consideration of variation, Computers & Structures, Volume 80, Issues 20–21, Pp 1605-1613. [https://doi.org/10.1016/S0045-7949\(02\)00160-8](https://doi.org/10.1016/S0045-7949(02)00160-8).
- Robert, Y. (1997). A few comments on pile design. Canadian Geotechnical Journal. Vol. 34: 560–567. <https://doi.org/10.1139/t97-024>.
- Shioi, Y., Fukui, J., 1982. Application of N-value to design of foundations in Japan. In: Proceeding of the second European symposium on penetration testing, pp. 159-116. <https://doi.org/10.1201/9780203743959-27>.

Publisher's note: [Scienceline Publication](#) Ltd. remains neutral with regard to jurisdictional claims in published maps and institutional affiliations.



Open Access: This article is licensed under a Creative Commons Attribution 4.0 International License, which permits use, sharing, adaptation, distribution and reproduction in any medium or format, as long as you give appropriate credit to the original author(s) and the source, provide a link to the Creative Commons licence, and indicate if changes were made. The images or other third party material in this article are included in the article's Creative Commons licence, unless indicated otherwise in a credit line to the material. If material is not included in the article's Creative Commons licence and your intended use is not permitted by statutory regulation or exceeds the permitted use, you will need to obtain permission directly from the copyright holder. To view a copy of this licence, visit <https://creativecommons.org/licenses/by/4.0/>.

Behaviour of Fly-Ash Geopolymer Mortar in Simulated Environments

Damilola Oyewumi Oyejobi  

Department of Civil Engineering, Faculty of Engineering, University of Botswana, Gaborone, Private Bag: UB0061, Botswana

✉ Corresponding author's Email: oyejobido@ub.ac.bw

ABSTRACT

Concrete and mortar usually found themselves in normal and harsh environments. The environment has great influence on the mechanical and durability behaviours of the concrete. In this study, fly ash was processed using circular economy concept and subsequently used as precursor for geopolymer mortar. The fly ash from Morupule power plant station has previously been characterized for its physical, chemical, and microstructural properties. Based on its suitability, the fresh and mechanical properties of the geopolymer mortar were carried out, and afterward, the durability behaviour is investigated in this study. The geopolymer mortar was formulated from the mixture of fly ash, sand and alkaline activators and cured thermally at 70°C. The behaviour of the geopolymer mortar in sulphuric acid solution, sodium sulphate solution, water absorption and fire resistance properties were simulated, and their loss in compressive strength and weight were determined. The laboratory experiment indicated that geopolymer mortars are highly resistant to sulphate attack, water absorption with moderate resistance against sulfuric acid and fire resistance. The effects of varying other parameters on the performance of concrete can be looked into in the future studies.

Keywords: Geopolymer mortar, environment, durability, mechanical, fly ash, circular economy

INTRODUCTION

The drive to have sustainable, environmentally friendly, and economical construction materials has shifted research focus to investigation of alternative construction materials for cement and aggregates. The research has led to the understanding that pozzolans are good replacement of cement in concrete and mortar production. There are some common pozzolans that have been embraced in the industry and currently being used to produce blended cement in some part of the world which include fly ash, ground granulated blast furnace slag and silica fume. These pozzolans have cementitious ability in the presence of lime. Pozzolans are known to be rich in silicon oxide and aluminum oxide and have binding qualities in the presence of alkali activators to produce geopolymer products through geopolymerisation process.

The management of waste has some drawbacks due to the limited landfill for disposal and enhancing environmental pollution. On the other hand, construction materials produced using such wastes can lower the cost of construction materials. Hence, there is an awakening to investigate ways of turning these wastes into useful products that can enhance economy, innovation, and sustainable infrastructure. Some of the wastes that are generated massively in Botswana are fly ash, bottom ash

and other mining wastes. The production of these wastes will be on the rise annually based on the energy demand and population increase, hence, more damage to the environment if different utilization strategies are not investigated. Therefore, the need to re-use and benefit the wastes (fly ash, copper slag, ore tailings, rice husk, blast furnace slag) that are pozzolanic in nature into useful resource is high.

According to Cossu and Williams (2015), there is no unified definition to the word circular economy. However, there is a cutting-edge understanding which revolves on extending the life-span of the material. MacArthur (2014) and Pratt and Lenaghan (2015) applauded the application of circular economy to reducing utilization of primary material, preserving natural resources and cutting down carbon footprint. The other socio-economic benefits of circular economy have been identified to be increase in gross domestic products, EEA (European Environment Agency) (2016), and significant savings in primary resource and energy, Schulze (2016). Shilar et al. (2022) utilized granite waste powder in the range of (10 – 30%) as a substitute to GGBS to produce geopolymer concrete with the variation of molarity from 12 to 18 M. It was reported that workability and mechanical performance of GGBS replaced with GPC performed very well up to 20%.

RESEARCH ARTICLE
 PII: S225204302400032-14
 Received: June 25, 2024
 Revised: September 02, 2024
 Accepted: September 05, 2024

Huseien et al. (2018) worked on GGBFS geopolymer mortar modified with metakaolin for repair applications. With careful manipulation of the chemistry of binder oxides of Na₂O: dry binder of 8% and ratio of SiO₂ to Na₂O of 1.16, early strength of 48 MPa was achieved at the age of 24 hours at ambient temperature. Various fresh and mechanical tests including shear bond attested that the product as potential repair applications. Zhang et al. (2021) analyzed mechanical performance of metakaolin fly ash based geopolymer mortar modified with nano-silica and polyvinyl alcohol fibres. It was deduced that addition of nano silica to 1.5 % of the total binder improved compressive strength, elastic modulus and fracture energy.

Thokchom et al. (2009) reported that geopolymer mortar in sulfur acid suffered severe attack in the loss of strength compared to its counterparts in nitric acid under the same working conditions. An article by Bakharev (2005) presented an investigation into durability of geopolymer materials manufactured using a class F fly ash (FA) and alkaline activators when exposed to 5% solutions of acetic and sulfuric acids. The results showed that some geopolymer materials made with sodium silicate and a combination of sodium hydroxide and potassium hydroxide as activators showed a notable reduction in strength. A paper by Kong et al. (2007) investigated the effect of elevated temperatures on geopolymers manufactured using metakaolin and fly ash of various mixture proportions concluded that the fly ash-based geopolymers have large numbers of small pores which facilitate the escape of moisture when heated, thus causing minimal damage to the geopolymer matrix. The strength increase in fly ash geopolymers is also partly attributed to the sintering reactions of un-reacted fly ash particles.

This current work is focused on the coal fly ash from Botswana Power Plants located in Morupule, Botswana. Botswana is a country in the southern part of Africa with an estimated population of 2,352,000 million by United Nations as at 2020, United Nations (2019). The republic is endowed with enormous and diverse solid minerals including diamond and coal among many others, Figure 1 shows the spatial distribution of the minerals across the country.

The energy company, Botswana Power Corporation, BPC was enacted in the year 1970 as a corporation responsible for generation, transmission and distribution of electric power, the functions she has been dutifully performed since inception. BPC, is a coal- based thermal plant located in Palapye town on 22.5515° S, 27.1147° E with generation installed capacity of 132 MW from Morupule A power station and 600 MW from Morupule B

power station respectively. The source of the coal for the two plants is Morupule Colliery Coal Mine (MCM) which is also located at the outskirts of Palapye. Botswana coal production, consumption, and coal ash generation are shown in Figures 2 and 3 respectively.

This study is aimed at examining the durability properties of the fly-ash based geopolymer activated with alkaline activators. The mix design is developed for the fly ash which is followed with determination of the compressive strength and resistance of the geopolymer mortar in acidic, basic, water and fire conditions.

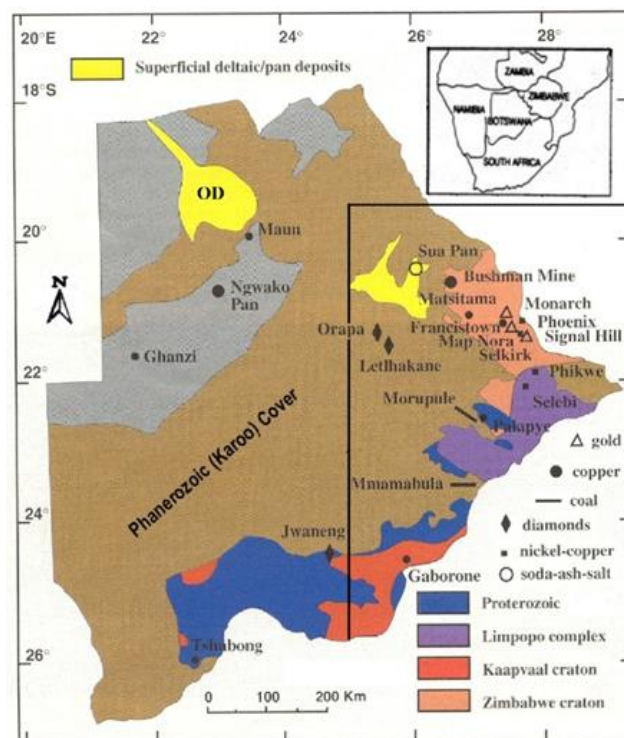


Figure 1. Geological map of Botswana showing main minerals (Ranganai et al., 2015).

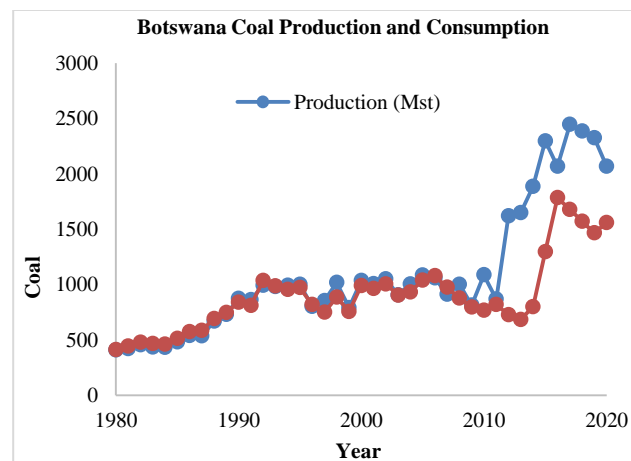


Figure 2. Botswana coal production and consumption (Mst) (EIA, 2020).

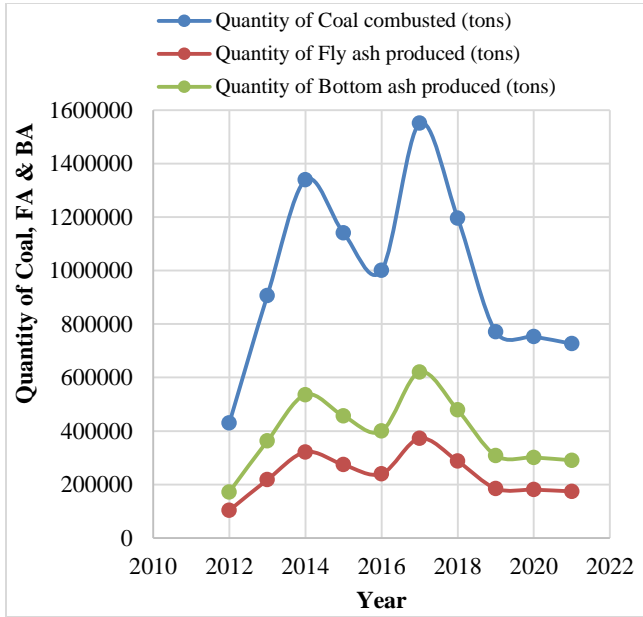


Figure 3. Quantity of Fly and bottom ashes generated between 2012 and 2021

MATERIALS AND METHODS

The fly ash used for this study was sourced from Botswana Power Plant in Morupule, Palapye located at 22.5515° S, 27.1147° E. The as-received fly ash was fine but later ground in a ball mill to obtain finer particles. The samples were further sieved with 75 μm sieve and tested for their inherent properties. The particle size distribution of the fly ash is shown in Figure 4 with $d_{10} = 3.81\mu\text{m}$, $d_{50} = 21.24\mu\text{m}$, and $d_{90} = 51.43\mu\text{m}$. The specific gravity and specific surface area are calculated as 2.52 and 0.74 m²/g respectively.

The results of the chemical and mineral compositions of the fly ash as determined by XRF and XRD are given in Table 1 and Figure 5. The scanning electron microscopy micrograph in Figure 6 shows that the fly ash is spherical in shape.

The fine aggregate used for the geopolymer mortar was sourced locally and was washed and oven dried for 24 hours. The alkaline activators for this project are Sodium hydroxide of (97 – 100 %) purity and sodium silicate with 14.7% Na₂O, 29.4% SiO₂ and 55.9% of water.

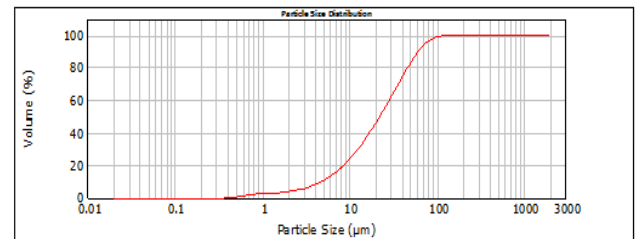


Figure 4. Particle size distribution of fly ash

Table 1. Chemical composition of the fly ash

Oxides	(%)	(%)	0.09
Fe ₂ O ₃	8.75	P ₂ O ₅	0.23
SiO ₂	41.90	MnO	0.09
Al ₂ O ₃	32.24	Cl	0.02
CaO	8.9	Cr ₂ O ₃	0.05
SO ₃	2.06	SrO	0.127
K ₂ O	0.75	ZnO	0.02
MgO	0.94	ZrO ₂	0.14
Na ₂ O	0.44	-	-

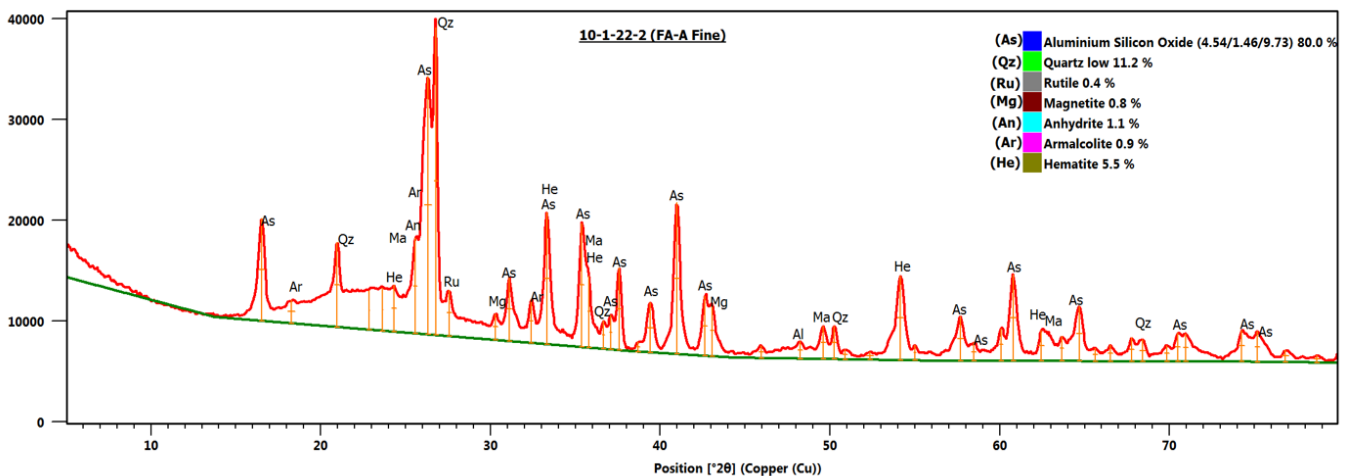


Figure 5. Mineral composition of the fly ash

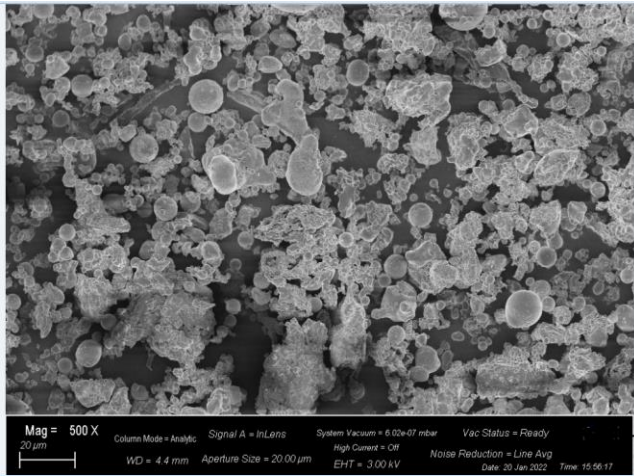


Figure 6. Scanning electron microscopy micrograph of fly ash

Compressive strength of geopolymer mortar

The geopolymer mortar mix design in Table 2 was earlier reported in Oyejobi et al. (2023), the production of geopolymer samples for the purpose of testing fresh and mechanical properties were also documented and illustrated in Figure 7. This procedure is followed by thermal curing at the temperature of 70°C for the period of 24 hours and left at ambient temperature until the testing date. The universal testing machine is 2000 kN and the settings followed the recommendation in ASTM C109-2020. At the end of 28 days, the samples were taken out for different durability tests which are outlined in the following sub-sections.

Table 2. Geopolymer mix design

Mix ID	1
Fly ash (g)	423
Sand (g)	1163
Molarity	12
Na ₂ SiO ₃	127
NaOH	85
Na ₂ SiO ₃ /NaOH	1.5
Alkaline liquid/Fly ash	0.5



Figure 7. Production of geopolymer mortar

Chemical resistance of geopolymer mortar

The procedure in ASTM C267-06 was modified and used for simulation of test conditions like acidic conditions in real life. Highly concentrated sulphuric acid (98 – 100%) at 5% weight was adopted. To keep the acidic level, the solution was monitored and changed every week for the duration of 12 weeks. At the test date, weight of the sample was taken, and the weight change was calculated as:

$$\text{Weight change} = \left[\frac{A-B}{B} \right] * 100 \dots\dots\dots 1$$

A = Weight of specimen after immersion (g) and
 B = weight of specimen before immersion (g).

The appearance of the specimens was monitored, and the compressive strength determined.

Resistance of geopolymer mortar to sulphate solution

Sodium sulphate of molar weight of 142.04 g/mol was used to make 5% sodium sulphate solution. The specimens were immersed inside the solution for a period of three months. At the end of the immersion period, length change in the prism and resistance of the specimens to the sulphate were determined. This test modified the outline in ASTM C1012-09.

Water absorption test for geopolymer mortar

Percent absorption of geopolymer specimen was determined in accordance with ASTM C642-06. The geopolymer specimens after the end of 28 days were dried in an oven at a temperature of 105 °C for a period of 25 hours. After cooling, the geopolymer specimens were fully immersed inside the cold water for a period of 48 hours. Their masses were determined after surface-dried with towel and increase in mass was less than 0.5%. The absorption after immersion in percent was determined as

$$\text{Percent absorption} = \left\{ \frac{B-A}{A} \right\} * 100 \dots\dots\dots 2$$

A = mass of oven-dried sample in air (g), B = mass of surface-dried sample in air after immersion, g.

Fire Resistance of Geopolymer Mortar

A laboratory furnace with maximum temperature of 1500°C was used to test the fire resistance of the geopolymer specimens. Specimens were subjected to temperature of 500, 700 and 1000 °C respectively at the heating rate of 5 °C per minute. This is in accordance with methodology given by RILEM 129-MHT (2020) recommendation. The temperature was maintained for a period of 2 hours, thereafter, the samples were allowed to cool down for 5 hours. The mass of the specimens before heating and after heating were noted before the compressive strength was determined.

RESULTS AND DISCUSSIONS

Compressive strength of geopolymer mortar

The compressive strength of geopolymer mortar is shown in Figure 8 with 52 MPa at 28 days. This value is equivalent to 52.5 MPa for Portland cement and the binder is suitable for construction. In addition, early gain strength is observed at day three with insignificant reduction of 4% at the 28 days. The strength gain can be attributed to good proportion of silica oxide and aluminum, high specific surface area of the fly ash which when combined with alkaline activators, they formed right geopolymer matrix.

Result of water absorption of geopolymer mortar

The response of the geopolymer mortar in terms of water absorption and reduction in compressive strength is shown in Figure 9. As the days of sample immersion in water progresses, there was a corresponding increase in water absorption which subsequently lead to reduction in the compressive strength at 28 and 56 immersion days, the percent of water absorption was almost the same with a slight drop in strength. This suggests that the pores have been fully saturated with maximum percent water absorption less than 6% and almost 2% reduction in compressive strength at 56 days.

Result of resistance of geopolymer mortar to Sulfuric acid

At 5% acidic solution, the resistance of the geopolymer mortar over 90 days immersion period is reported in Fig. 10. The weight loss under the attack of acid solution was marginally small and increased with time. This could be attributed to densified mixture which was characterized with low water absorption. In Sata et al. (2012), a weight loss between 1.4 to 3.6% depending on the precursor but this was much lower compared to range of 77.2 to 95.7% as recorded for blended cement and Ordinary Portland Cement (OPC) mortar. A lower mass loss was credited to the stability of aluminosilicate framework in (Yang et al., 1996). There was a drop in the compressive strength over the immersion period with (%). These percentage reductions were much lower when compared with ordinary Portland cement-based mortar. In Djobo et al. (2016), 60% loss in strength was reported for volcanic based geopolymer mortar. Hence the resistance could be said to be a function of precursor characteristic.

Result of resistance of geopolymer mortar to Sodium Sulphate solution

In sodium sulphate solution, there was no change in colour, and the structural integrity was maintained. The result in Figure 11 follows the same trend with

geopolymer response to sulphuric acid; however, the reduction in strength and loss of weight were much lower in sodium sulphate solution compared to Fig. 10. This shows that geopolymer mortar has higher resistance to basic attack.

Result of resistance of geopolymer mortar in elevated temperature

The geopolymer samples show visible cracks when exposed to fire resistance. In Fig. 12, the weight loss at 500 and 1000°C were higher compared to 700°C. The geopolymer product formed at 700°C could be regarded to be more stable and behaved like ceramic and at a temperature beyond 700°C, there was thermal expansion which resulted in the significant loss of compressive strength.

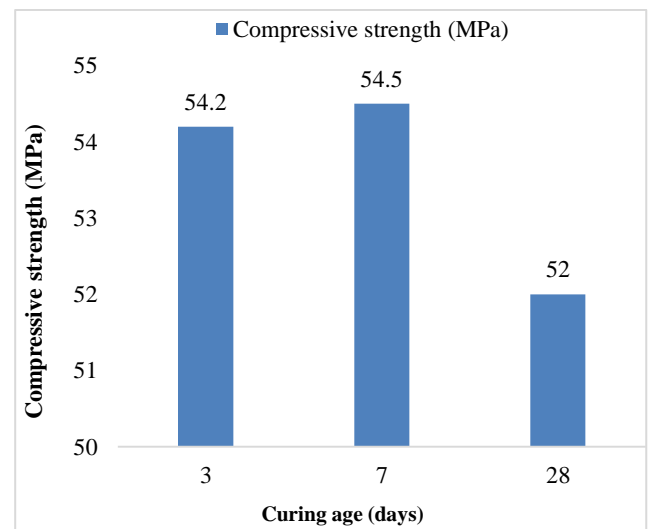


Figure 8. Compressive strength of geopolymer mortar

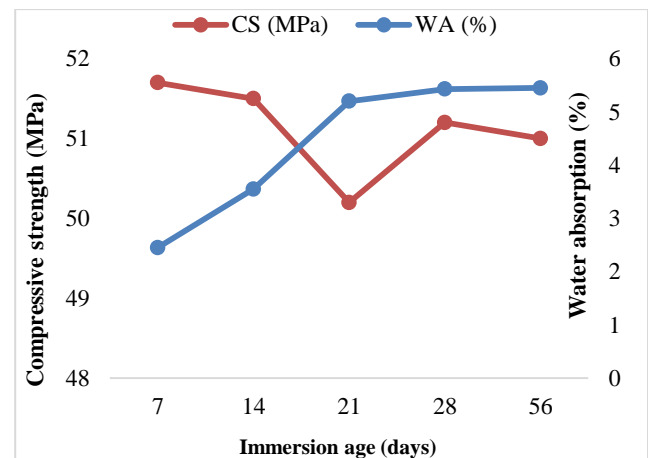


Figure 9. Effect of water absorption on the compressive strength

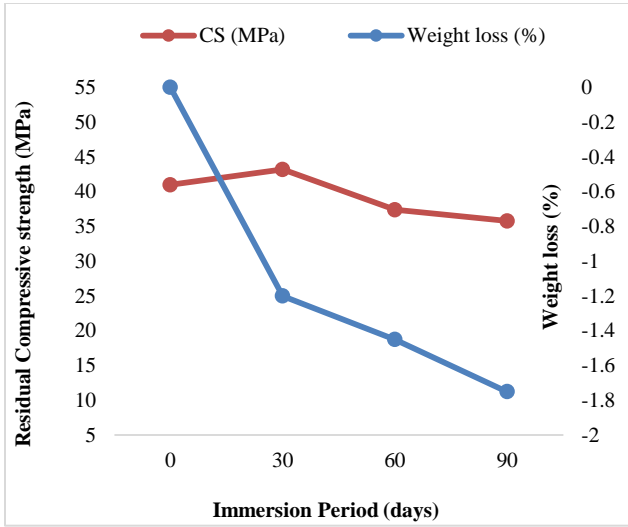


Figure 10. Resistance of geopolymer mortar to sulfuric acid

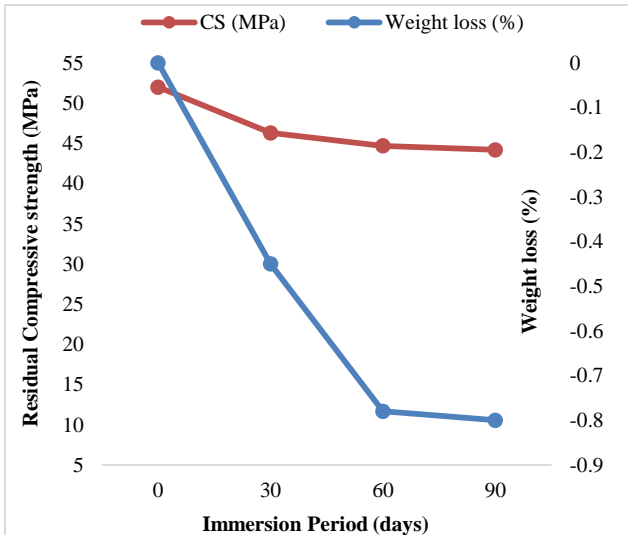


Figure 11. Resistance of geopolymer mortar to sodium sulphate solution

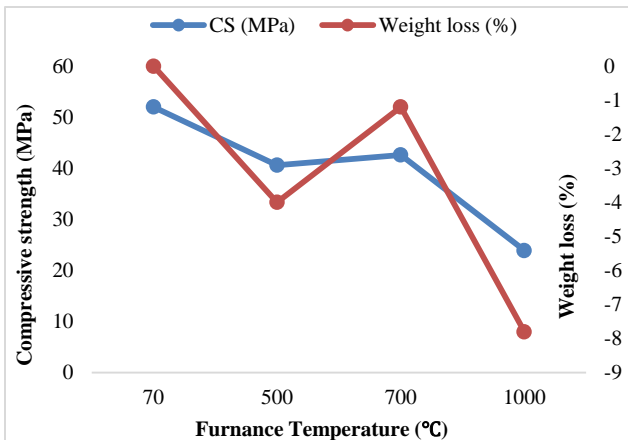


Figure 12. Resistance of geopolymer mortar in elevated temperature

CONCLUSIONS

The raw fly ash was re-engineered using circular economy concept and the performance of the fly-ash based geopolymer is reported as follows:

The fly ash from Morupule power plant is characterized and classified as Class F based on its properties.

The geopolymer binder performed excellently in terms of compressive strength with maximum compressive strength of 52 MPa.

In hierarchy of resistance in simulated service conditions, it is of order of water absorption, sulphate attack, acid attack, and elevated temperature with maximum residual strengths of 98%, 85%, 69% and 46%, respectively.

The recycling of industrial waste from Botswana Power Corporation requires lesser energy for binder production, saves environment from pollution and degradation and found suitable, sustainable and durable for the use as construction material.

DECLARATIONS

Corresponding Author

Correspondence and requests for materials should be addressed to Dr. Damilola Oyewumi Oyejobi; Email: damilolaoyejobi@gmail.com; ORCID: 0000-0002-6482-0396

Data availability

The datasets used and/or analysed during the current study are available from the corresponding author on reasonable request.

Acknowledgements

The author would like to thank University of Botswana for sponsoring the presentation of these findings at the International Conference on Civil Engineering for Sustainability and Resilience in the 21st Century and Beyond (ICCESR 2024) at the University of Botswana, Gaborone, Botswana.

Authors' contribution

The author developed the concept, carried out the experiment and wrote the manuscript.

Competing interests

The author declare no competing interests in this research and publication

REFERENCES

- ASTM C 267-06 “Standard Test Methods for Chemical Resistance of Mortars, Grouts, and Monolithic Surfacing and Polymer Concretes,” American Society for Testing and Materials (ASTM) International, West Conshohocken, 2006.
- ASTM C1012-09, “Standard Test Method for Length Change of Hydraulic-Cement Mortars Exposed to a Sulfate Solution,” American Society for Testing and Materials (ASTM) International, West Conshohocken, 2009.
- ASTM C109/C109M (2020) Standard Test Method for Compressive Strength of Hydraulic Cement Mortars (Using 2-in. or [50-mm] Cube Specimens). ASTM International, West Conshohocken, PA. <https://www.astm.org/>
- ASTM Standard C642 (2006) Standard Test Method for Density, Absorption, and Voids in Hardened Concrete. ASTM International, West Conshohocken, PA. <https://www.astm.org/>
- Bakharev, T. (2005). Resistance of geopolymer materials to acid attack. *Cement and Concrete Research*, 35(4), 658–670. <https://doi.org/10.1016/j.cemconres.2004.06.005>
- Cossu, R., & Williams, I. D. (2015). Urban mining: Concepts, terminology, challenges. *Waste Management*, 45, 1–3. <https://doi.org/10.1016/j.wasman.2015.09.040>
- Djobo, J. N. Y., Elimbi, A., Tchakouté, H. K., & Kumar, S. (2016). Mechanical properties and durability of volcanic ash based geopolymer mortars. *Construction & Building Materials*, 124, 606–614. <https://doi.org/10.1016/j.conbuildmat.2016.07.141>
- EEA (European Environment Agency). (2016). Circular economy in Europe Developing the Knowledge Base. European Environment Agency, Copenhagen, Denmark, EEA Report No. 2/2016.
- EIA (2020). "Independent statistics & Analysis." U.S. Energy Information Administration, 1000 Independence Ave., SW Washington, DC 20585, <https://www.eia.gov/international/overview/world>
- EIA. (2020). Independent statistics & Analysis. U.S. Energy Information Administration, 1000 Independence Ave., SW Washington, DC 20585. <https://www.eia.gov/international/overview/world>
- Huseien, G. F., Mirza, J., Ismail, M., Ghoshal, S. K., & Ariffin, M. A. M. (2018). Effect of metakaolin replaced granulated blast furnace slag on fresh and early strength properties of geopolymer mortar. *Ain Shams Engineering Journal*, 9(4), 1557-1566.
- Kong, D. L., Sanjayan, J. G., & Sagoe-Crentsil, K. (2007). Comparative performance of geopolymers made with metakaolin and fly ash after exposure to elevated temperatures. *Cement and Concrete Research*, 37(12), 1583–1589. <https://doi.org/10.1016/j.cemconres.2007.08.021>
- MacArthur, E. (2013). Towards the circular economy. *Journal of Industrial Ecology*, 2(1), 23-44.
- Oyejobi, D., Jameel, M., Adewuyi, A., Aina, S., Avudaiappan, S., & Maureira-Carsalade, N. (2023). Analyzing influence of mix design constituents on compressive strength, setting times, and workability of geopolymer mortar and paste. *Advances in Civil Engineering*, 2023, 1–15. <https://doi.org/10.1155/2023/5522056>
- Pratt, K., & Lenaghan, M. (2015). The Carbon Impacts of the Circular Economy Summary Report. *Zero Waste Scott*, 15, 15.
- Ranganai, R. T., Moidaki, M., & G King, J. (2015). Magnetic susceptibility of soils from eastern Botswana: A reconnaissance survey and potential applications. *Journal of Geography and Geology*, 7(4), 45-64.
- Recommendations of RILEM TC 129-MHT: Test methods for mechanical properties of concrete at high temperatures. Part 8: Steady-state creep and creep recovery for service and accident conditions
- Sata, V., Sathonsaowaphak, A., & Chindaprasit, P. (2012). Resistance of lignite bottom ash geopolymer mortar to sulfate and sulfuric acid attack. *Cement & Concrete Composites*, 34(5), 700–708. <https://doi.org/10.1016/j.cemconcomp.2012.01.010>
- Schulze, Günther. (2016). Growth within: A circular economy vision for a competitive Europe. Ellen MacArthur Foundation and the McKinsey Center for Business and Environment, 1-22.
- Shilar, Fatheali A, Ganachari, Sharanabasava V, Patil, Veerabhadragouda B, Nisar, Kottakkaran Sooppy, Abdel-Aty, Abdel-Haleem, & Yahia, IS. (2022). Evaluation of the effect of granite waste powder by varying the molarity of activator on the mechanical properties of ground granulated blast-furnace slag-based geopolymer concrete. *Polymers*, 14(2), 306.
- Thokchom, S., Ghosh, P., & Ghosh, S. (2009). Resistance of fly ash based geopolymer mortars in sulfuric acid. *ARPN J. Eng. Appl. Sci*, 4(1), 65-70.
- United Nations. (2019). World Population Prospects 2019. Department of Economic and Social Affairs, Online Edition. Rev. 1
- Yang, S., Zhongzi, X., & Mingshu, T. (1996). The process of sulfate attack on cement mortars. *Advanced Cement Based Materials*, 4(1), 1–5. [https://doi.org/10.1016/s1065-7355\(96\)90057-7](https://doi.org/10.1016/s1065-7355(96)90057-7)
- Zhang, P., Wang, K., Wang, J., Guo, J., & Ling, Y. (2021). Macroscopic and microscopic analyses on mechanical performance of metakaolin/fly ash based geopolymer mortar. *Journal of Cleaner Production*, 294, 126193. <https://doi.org/10.1016/j.jclepro.2021.126193>

Publisher’s note: [Scienceline Publication](https://www.scienceline.com) Ltd. remains neutral with regard to jurisdictional claims in published maps and institutional affiliations.



Open Access: This article is licensed under a Creative Commons Attribution 4.0 International License, which permits use, sharing, adaptation, distribution and reproduction in any medium or format, as long as you give appropriate credit to the original author(s) and the source, provide a link to the Creative Commons licence, and indicate if changes were made. The images or other third party material in this article are included in the article’s Creative Commons licence, unless indicated otherwise in a credit line to the material. If material is not included in the article’s Creative Commons licence and your intended use is not permitted by statutory regulation or exceeds the permitted use, you will need to obtain permission directly from the copyright holder. To view a copy of this licence, visit <https://creativecommons.org/licenses/by/4.0/>.

Flexural Behaviour of Concrete Beams Reinforced with Major Steel Bars under Normal and Corrosive Operational Conditions

Adekunle P. Adewuyi  and Gaolatlhe B. Eric 

Department of Civil Engineering, University of Botswana, Gaborone, Botswana

Corresponding author's Email: adewuyiA@ub.ac.bw

ABSTRACT

Quality assurance of construction materials is very fundamental for structural safety, reliability, serviceability, and durability of constructed civil infrastructure. Inflow of defective or substandard building and construction materials into the industry, particularly reinforcing steel bars, is responsible for many structurally deficient constructed facilities which often lead to failure or ultimate collapse of reinforced concrete (RC) structures. Characterization of steel rebars from two major manufacturers into Botswana construction industry, designated herein as M1 and M2, were conducted as a basis for the evaluation of the quality assurance and control of the products. The flexural behaviour of their respective RC beams, designated herein as B-M1 and B-M2, of dimension $150 \times 200 \times 3000$ mm and subject to four-point loading tests were determined under normal and artificially induced corrosion conditions to assess the influence of steel rebars M1 and M2 on the stiffness and load-carrying capacity. The average yield strengths of steel reinforcing bars were 427 N/mm^2 for M1 and 459 N/mm^2 for M2. The moduli of elasticity for M1 and M2 were 203 GPa and 205 GPa, respectively. The percentage elongation was found to be 7.93% for M1 and 7.24% for M2. The flexural strength of beams reinforced with M1 was 7% and 16.5% lower than RC beam with M2 under normal and accelerated corrosion of 5% of NaCl solution for 60 hours condition, respectively. The flexural behaviour of RC beams reinforced with B-M1 had a lower flexural strength under both normal and corrosive environmental conditions as compared to B-M2. The flexural strength of B-M1 had reduced from 48.5 N/mm^2 to 41.0 N/mm^2 , while B-M2 reduced from 52.2 N/mm^2 to 49.2 N/mm^2 . This represented loss of load-carrying capacity of 15.4% and 5.8% for B-M1 and B-M2 respectively due to exposure to corrosive environment. The findings revealed disparity in bending capacity due to the low interfacial bonding due to reduced relative rib areas. A more intensive quality control of imported steel should be ensured at the ports of entry by relevant regulatory agencies.

Keywords: Flexural capacity, Stiffness, Reinforcing bars, Relative rib area, Interfacial bonding, Accelerated corrosion, Ultimate load.

INTRODUCTION

Concrete, generally regarded as the oldest and most widely used construction material, plays a vital role in global infrastructural development and economic growth (Adewuyi et al., 2015). The preference for reinforced concrete (RC) as a construction material is influenced by its durability and fire resistance, structural versatility and formality, and the complementary properties between the reinforcing steel bars and concrete (Makul, 2020). Extensive studies have been carried out to investigate flexural behaviour of RC beams using three- or four-point loading with identical geometric dimensions and steel bar specimens (Qui et al. 2022; Adewuyi et al. 2015; Djmaluddin 2013; Li et al. 2020; Kim & Kim 2019; Ignjatovic et al. 2013). However, research gaps on this subject are yet to be filled to compare the performance of different reinforcing steel bars from different

manufacturers in tension and flexure, and under the influence of progressive corrosion, hence the need to do this study. Studies on flexural behaviour of RC elements are primarily focused on the failure modes, first cracking load, ultimate load, deflection, stiffness, ductility and crack patterns.

The process of corrosion of the reinforcements is recognized as the most predominant degradation mechanism of RC structures that leads to structural deterioration and functional failure (Verstryngge et al., 2022). Corrosion of reinforcing bars progressively and ultimately reduces capacity and the residual service life of the structure, thereby creating huge economical loss and environmental problems (Kunawisarut et al., 2024). Its enhancement of the RC section ductility is often as the expense of their long-term performance in the form of the loss of flexural strength, deformation behaviour, bond strength and different cracking modes (Peng et al., 2021).

RESEARCH ARTICLE
 PII: S225204302400033-14
 Received: June 25, 2024
 Revised: September 02, 2024
 Accepted: September 05, 2024

The products of corrosion process are a complex mixture of iron oxides, hydroxides and hydrated oxides that progress based on the local environmental condition (Adewuyi et al. 2022; Rodrigues et al., 2021). Early detection of corrosion and prompt maintenance could help reduce the life cycle cost thereby extending the service life of structures. Embedded steel rebars in concrete are often secured against corrosion during the service life of the structure by providing adequate nominal cover since concrete is both durable and resistant against corrosion and fire (Fouad et al., 2016). The progressive corrosion of RC flexural structures is illustrated by a uniform dissolution of the whole surface as shown in Figure 1a or by a local attack which is called ‘pitting’ corrosion when it is much localized as shown in Figure 1b. It may also manifest at the microscopic level as ‘inter- or trans-granular’ (Figure 1c) attack when metal grains are very locally affected.

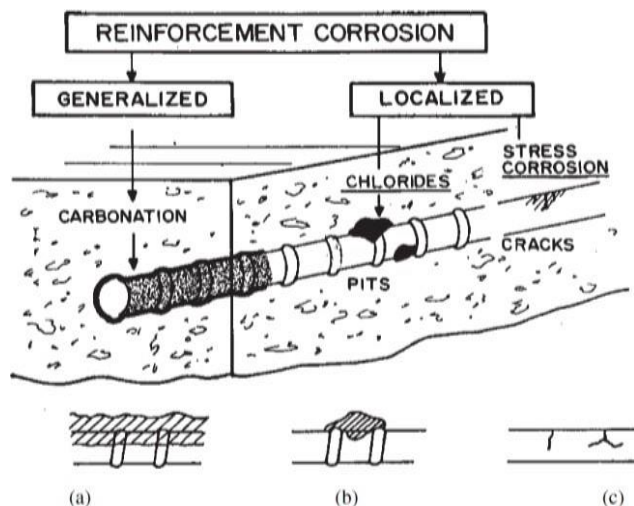


Figure 1. Categorization of corrosion of steel rebars as (a) carbonation, (b) chloride attack and (c) stress corrosion cracking.

Recent studies on corrosion of reinforcement in concrete structures were reported extensively in literature (Almusallam 2001; Bertolini et al. 2013; Hunkeler 2005; Patil et al. 2017). The effect of corrosion of reinforcement to tension stiffening results in local reduction of cross-sectional area of tension reinforcement leading to reduction of its stiffness, bond strength and therefore the change contribution of concrete in tension between cracks (Huang et al., 2020; Li et al., 2018, Wei et al., 2018).

The aftereffects of corrosion damage on the mechanical properties of the steel reinforcement are significant and adequately reported by Apostolopoulos & Papadakis (2008). Corrosion in reinforced concrete

structures first manifests in the form of deterioration of steel bars in terms of loss of tensile and bond strengths, erosion of ribs, which weakens its ability to transfer the tensile stresses from concrete to steel. The progressive deterioration also extends to the surrounding concrete and manifests in the form of spalling of concrete cover because of the expansion of the corrosion products. The composite action of the steel and concrete is ultimately weakened by the loss of the interfacial bonding initiated by the lubricant effect of the corrosion products and by cracking of the concrete cover (Adewuyi et al. 2022; Maaddawy et al., 2005).

The strength and fracture behaviour of concrete are progressively affected by crack width and pattern, connectivity, and torsion. Timely and accurate diagnosis of these parameters helps to estimate the level of damage and reliably predict the residual service life of concrete (Brandt and Jozwiak-Niedzwiedzka, 2012). The stresses in the reinforcement at the cracked section at various load stages is a measure of the incidence of uniaxial tension and flexural cracking (Soltani et al., 2013). Hence, progressive cracking and loss of steel-concrete interfacial bonding in the form of slippage of steel rebars worsen the serviceability requirements of RC beams, and even much more by corrosion of reinforcement (Li et al., 2018; Siddika et al., 2020; Ballim et al., 2003).

Most short-term experimental studies on durability assessment of RC beams were based on accelerated corrosion. Since corrosion is a time-dependent phenomenon, accelerated laboratory corrosion tests are adopted to assess the effects of corrosion on the performance of RC structures in terms of the duration of exposure as well as the severity of the environmental conditions (Altoubat et al., 2016; Ballim et al., 2003; Fernandez et al., 2016; Malumbela et al., 2009; Słowik 2018, Zhang et al., 2018). Extensive studies have been conducted to monitor the effects of corrosion on various structural performance characteristics of RC flexural members such as mass loss, load-deflection pattern, stiffness and bond strength under ultimate load testing conditions. Ballim et al. (2003) reported 40–70% increase in deflections of tested beams relative to the deflection of the corresponding control samples when up to 6% of the mass of steel bars was lost to corrosion.

Maaddawy et al. (2005) found a 22% faster crack width propagation under sustained loading conditions than in an unloaded condition. It was reported that 8.9% and 22.2% rebars mass loss produced 6.4% and 20.0% strength loss, respectively. Fernandez et al. (2016) confirmed an increase in deflection and ductility in all corroded RC

beams under sustained service loading conditions during the corrosion phase. Yoon et al. (2000) recommended that the influence of service load on the structural performance of RC beams should be considered in combination with material properties and environmental conditions.

This study was primarily aimed at comparatively assessing the influence of M1 and M2 steel rebars on the flexural behaviour of RC beams, herein designated as B-M1 and B-M2, under normal and artificially induced corrosive environments. Better understanding of the relationship between the corrosion of rebars and integrity RC structures is essential to assist owners and managers of large-scale constructed concrete infrastructure to map out plans for maintenance and repairs strategies and efficient deployment of limited financial and human resources.

MATERIALS AND METHODS

The concrete used in this study consisted of PPC BOTCHEM cement of grade 32.5R of relative density 3.0. Coarse aggregate of 19 mm maximum nominal size and crusher dust as fine aggregate were sourced from Kgale Quarry Site. The water/cement ratio of 0.55 was adopted in the concrete mix. Twelve samples of simply supported RC beams each of dimensions 150 mm × 200 mm × 3000 mm of 30 N/mm² target concrete compressive cube strength at 28th day were cast, cured and tested for the experimental study. The beams were reinforced with M1 and M2 steel reinforcements and detailed as shown in Figure 2 and subjected to a sustained service loading to investigate the flexural behaviour under normal and artificially induced accelerated corrosion conditions.

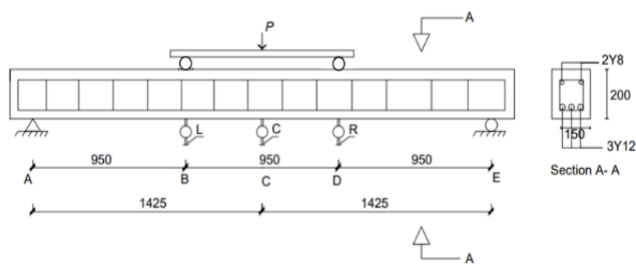


Figure 2. Four-point loading bending test setup for RC beams.

The beams were reinforced with three bars of 12 mm (3Y12) diameter high yield strength deformed (HYSD) steel bars at the tension zone, and 2 bars of 8 mm (2Y8) diameter hanger bars at the compression zone. The concrete nominal cover to longitudinal bars and shear links was 20 mm. Two-legged vertical shear stirrups of 8 mm nominal diameter size were provided at 125 mm

centres (Y8@125 mm). After casting and demoulding of concrete, all the test specimens were subjected to a 28 days of continuous curing condition at room temperature prior testing to ensure sufficient degree of hydration of the cement paste. The protruded rebar portions for the purpose of electrical connection for the accelerated corrosion procedure, were covered in 2 layers of insulating tape to prevent them from getting in contact with curing water and remain non-corroded.

Six RC beam specimens, three of which were separately reinforced with M1 and M2 steel rebars, were subjected to four-point bending test procedure under normal exposure condition. For the remaining six beams, three beam specimens were separately reinforced with M1 and M2 steel rebars. The three embedded tension rebars were separately subjected to an artificially induced accelerated corrosion process comprising a passage of constant current of 0.5 A through a DC power supply for the period of study. The lateral deflection under varying load intensity on the RC beams were measured by three dial gauges with accuracy to 0.01 mm and displacement transducers placed at the mid-span and at 950 mm from either supports and subjected to a sustained service load corresponding to 12 percent of the ultimate load for a 60-hour exposure duration and subsequently loaded progressively to failure. The beams were tested for four-point loading in a flexural testing frame. Line loads were applied equally at the third-points to either supports via the rollers from the load from the hydraulic jack centrally applied to a channel steel beam as shown in Figure 2 in accordance with ASTM C78 (2018). Crack microscope (of 0.02 mm resolution) was used to measure crack widths on the concrete surface under load increment. Crack length and width, on the other hand, were measured using crack metre as the applied load was progressively increased at a uniform load rate. The same procedure was employed under corrosive exposure condition.

A pond of size 150 × 700 × 50 mm placed at the top of the middle-third of the beam and containing 5% sodium chloride (NaCl) solution to accelerate corrosion process of the RC beams. A stainless-steel cathode was fixed on top of the beam over the length of 700 mm as shown in Figure 3. The brine, that is NaCl, solution was changed after every 3 hours to maintain the concentration of the aqueous solution. After sixty hours, dial gauges were set to zero, took off the pond and tested beam for flexural behaviour by loading beams at intervals of 0.25 tons using a hydraulic jack. Current-induced corrosion flowed from the positive terminals of the DC power supply to the tension reinforcements, and then through the saturated concrete

and sodium chloride solution to the stainless-steel plate which was connected to the negative terminals of the DC power supply. Tests were run by monitoring sustained load first for 60 hours to ensure that corrosion initiation takes place. Deflection and cracks of the RC beams were monitored under the sustained load.



Figure 3. Pond placed and sealed at the center of the beam for accelerated corrosion.

RESULTS AND DISCUSSION

Flexural behaviour of RC beams with M1 and M2 rebars in a non-corrosive environment

The load-deflection plots in Figure 4(a) shows higher deflection at midspan, where B-M1 recorded a maximum deflection of 39.8 mm at midspan and 35.4 mm at one third point at an ultimate failure load of 63.8 kN. Beam B-M2 had a higher load carrying capacity of 68.7 kN with a corresponding deflection of 34.5 mm at midspan and 34.1 mm at one third point. The higher failure load recorded in B-M2 than B-M1 could be attributed to the higher yield strength of 459 N/mm² for M2 compared to the 427 N/mm² recorded for M1. During the progressive loading-initiated cracking, B-M1 had its first cracking load at 17.2 kN, while B-M2 experienced early cracking at 9.8 kN. This was almost twice the first cracking load of B-M1. Loss of flexural rigidity of the all the beam specimens was obvious after the occurrence of the first crack, and each specimen began to exhibit a lower second order stiffness and entirely different structural behaviours. The stiffness of B-M1 at midspan changed from 1.9 to 1.4 which was a slight change as compared to stiffness of B-M2 which significantly changed from 4.9 to 3.1.

A similar trend at one third span was followed for both B-M1 and B-M2 as shown in Figure 4(b). The stiffness for B-M2 reduced by 67% after first crack hence bringing the total deflection to 34 mm which is closer to 35 mm of B-M 1. Low load rate was employed in the study because it has been established by Li et al. (2018) that a higher loading level decreases flexural stiffness of RC beams, while a lower loading rate produces a relatively higher flexural stiffness. The ductility ratio of a flexural test is often determined as the ratio of the ultimate curvature to the yield curvature of a section. In this study, however, the ductility ratios were measured as a function of the ratio of deflection at ultimate load to the corresponding value at the instance of first cracks. The ratio of the first crack to ultimate failure were 26.9% and 14.3% for B-M1 and B-M2 respectively. The ratio implies that B-M2 was more ductile since B-M1 could only resist load to about 73% and B-M2 about 86% after the first crack observation. Ridha et al. (2018) attributed the relatively lower values of ductility ratio recorded in the experimental programme to the brittleness of the tested RC beams.

The mode of ultimate failure of B-M1 was flexural tension failure with crushed concrete in the compression zone. However, beams B-M2 had diagonal shear tension failure as shown in Figure 5. For the flexural failure scenario, there was a progressive deflection which began as a set of parallel tiny vertical cracks that progressed as the beam was subjected to a gradually increasing load and terminated as crushing of the concrete within the vicinity of the point of maximum moment (Li et al., 2018). However, in the case of shear mode of failure, the first crack appeared vertically on the side surface at the midspan of beams. As the load increased at a slow, but constant rate, inclined or diagonal cracks were initiated at the shear-flexural zone near the support point, which incidentally the point of maximum shear, and gradually progressed toward the third point of load application.

The ultimate failure occurred quite suddenly as the inclined cracks widened up from left end of the support and propagated towards the point of load application by the roller at the third point of the beam. The results of shear failure could be related to point load being shifted to the left since the load was applied manually by the jack. The shear span to depth ratio was higher which supports that the reinforcement used was sufficient to resist shear (Abigaz, Liu & Yilachew, 2021). The shear failure could be related to reinforcement that was used for shear, had low rib height and no gaps which could temper with bond between concrete and reinforcement.

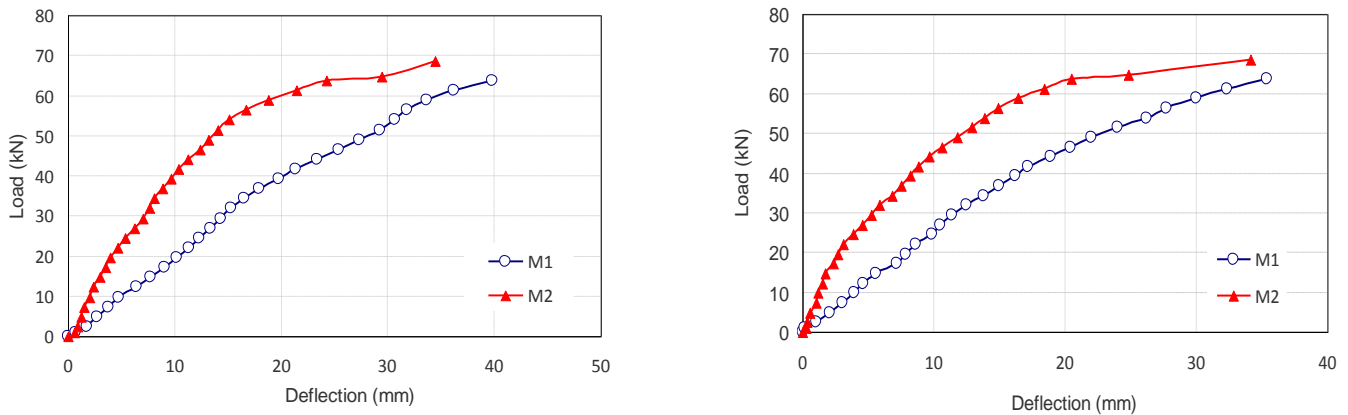


Figure 4. Load- deflection curves of RC beams embedded with M1 and M2 steel bars at (a) midspan and (b) one-third span.



Figure5. Flexural test failure patterns of controlled specimens of RC beam reinforced with (a) M1 and (b) M2 at ultimate failure

Flexural behaviour of corrosion-induced RC beams with M1 and M2 steel bars

Deflection and cracks were monitored consistently at an interval of 3 hours for 60 hours. No cracks were recorded for all beams under sustained loading. This could be because the sustained load was lower than the initial first cracking load when non corroded beams were tested. Steel reinforcing bars embedded could have not

corroded enough to cause any crack as the corrosion products are expected to expand and cause cracking of concrete beams. Deflection values were slightly low as shown in Figure6. The deformation of the RC beams under sustained loading is linearly elastic as revealed by the almost linear deflection- time graphs.

The midspan deflection under sustained loading for M1 ranged between 0.715 mm to 0.978 mm at a rate of

0.0034 mm/hr, while the corresponding deflection for M2 ranged from 0.878 mm and 1.104 mm with a slope of 0.0041 mm/hr for the entire 60 hours duration. On the other hand, the deflection measurements at one-third points of beams M1 and M2 are practically comparable ranging between 0.369 mm and 0.576 mm at a rate of 0.0037 mm/hr for the 60 hours monitoring duration. This shows that the corroding RC beams were still under elastic deformation hence slight changes in the first crack formation when the beams were then tested under third point loading until failure. In overall, the flexural failure modes of the specimens which is common and highly recommended, was characterized by the yielding of steel rebars, multiple micro cracks, and lastly crushing which agrees to results obtained by Qiu et al. (2022).

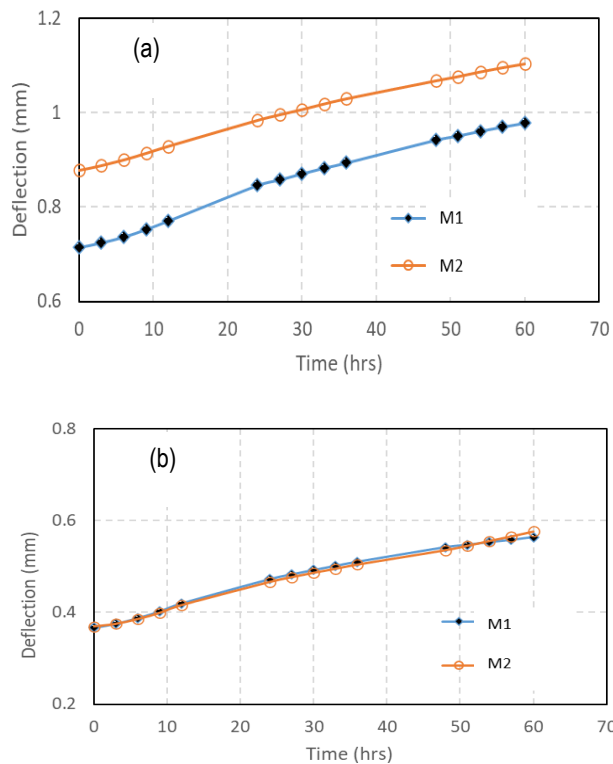


Figure 6. Deflection of the RC beams under sustained loading at (a) the midspan and (b) one third span.

After 60 hours of sustained loading, RC beams were unloaded from the sustained loading then set dial gauges to zero so as to load beams from zero until failure load. The load-deflection plots for RC beams subjected to corrosion in Figure 7 show relatively high deflection at midspan, where B-M1 had a failure load of 54.0 kN with a corresponding deflection of 47.3 mm at midspan and 41.1 mm at quarter span whereas B-M2 had the highest failure

load of 64.7 kN with a corresponding deflection of 41.8 mm at midspan and 38.5 mm at one third point. Steady load-initiated cracking in which B- M1 had its first crack noticed at 12.3 kN, while B-M2 experienced its first cracking at 14.7 kN. The rigidity of the beam test specimen decreased immediately after the first crack initiated. Afterwards, each RC beam test specimens began to have a different behaviour with a much lower flexural stiffness.

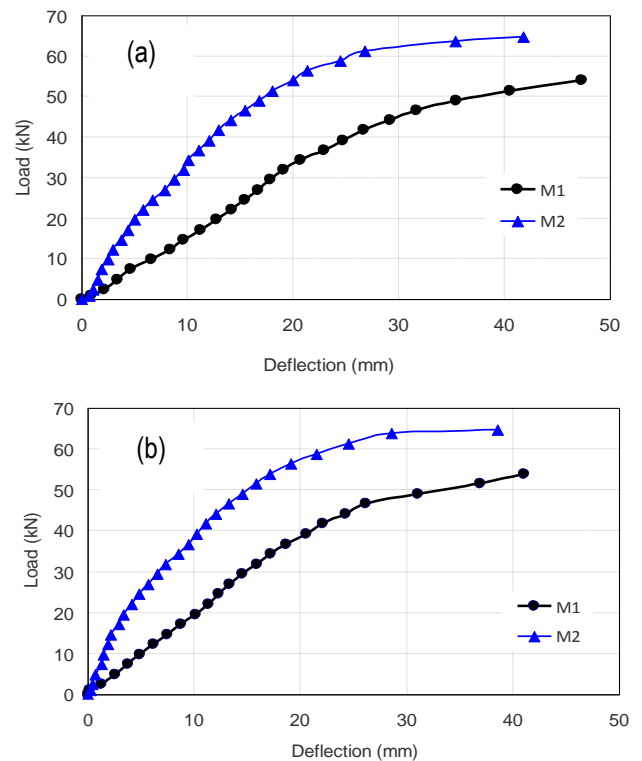


Figure 7. Load-deflection curves of corrosion induced RC beams at (a) midspan and (b) one-third span.

The stiffness before first crack of B-M1 at midspan was twice smaller than stiffness of B-M2 hence low deflection for B-M1 than B-M2. The stiffness after first crack followed the same trend at midspan. However, at one third span, the stiffness for B-M1 was constant before and after first crack. The stiffness for B-M2 reduced by 50% after first crack hence reducing deflection at one third span. The percentage of the first crack load to the ultimate failure were both relatively low. B-M1 had 26.9% residual capacity after the first crack, while rattan RC beams had exhausted 14.3% of its load-carrying capacity after the first crack.

With an increase in cracking and possible bond slippage there is increase the serviceability deflections of a reinforced concrete (RC) beam which has deteriorated

because of corrosion of reinforcement (Ballim et al., 2003). The failure mode of both B-M1 and B-M2 flexural tension failure with more cracks noticed at midspan and few at the outer span as shown in Figure 7. The most significant failure modes in this study are the shear and flexural failures. However, flexural failure mode is preferred to shear failure due to brittleness and catastrophic failure form of the shear failure, because it allows the possibility of stress redistribution. Full advantage of the potential ductility of the RC members can be achieved by selecting geometric properties of concrete sections and tensile strength of steel reinforcing bars that would guarantee flexural failure mode instead of the sudden, brittle and catastrophic shear failure, which occurs with no advance warning of distress.

Comparison of flexural behaviour RC beams embedded with M1 and M2 rebars at midspan under normal and corrosive induced environmental conditions

The results of beams before introducing corrosive environment (M1-norm and M2-norm) and during induced corrosion (M1-corr and M2-corr) were compared in Figure 8. The results showed an increase in deflection and decrease in ultimate load after beams have been exposed to corrosion. It was evident from the study that corrosion of the longitudinal steel rebars manifested in the form of mass loss and strength loss which reduced the slope and the geometric properties of the load-deformation curve of RC beams. These translated into a general reduction in ductility, flexural stiffness, and bending strength. The bending strength of B-M1 reduced from 48.49 N/mm² to 41.04 N/mm² while B-M2 reduced from 52.21 N/mm² to 49.17 N/mm².

This shows that B-M2 could resist failure in bending better than B-M1 even after beams were exposed to corrosion. This shows reduction in strength for B-M1 and B-M2 to be 15.4% and 5.8% respectively in terms of percentage of corroded failure load to normal failure load. After subjecting RC beams to accelerated corrosive condition, the percentage ratio of the first crack load to the ultimate failure load for B-M1 decreased from 86% to 65%, while B-M2 increased from 73% to 81.7%. Comparing the failure load values and deflection values, it is evident that the non-corroded steel-RC beam performed better in resisting bending than the corroded steel-RC beam, and thus demonstrating that corrosion adversely affects the flexural strength of reinforced concrete. In conclusion, a significant reduction in the load-carrying capacity and an inversely proportional increase in

corresponding deflection. This invariably severely reduced the RC structural performance at various service load levels. The most technical factor that can be attributed to this deterioration trend was simply the loss of stiffness due to reduction in steel geometric cross-section as well as yield and ultimate tensile strength. It is quite clear that deflections are strongly influenced by corrosion of steel (Fernandez et al., 2016). This is because there is an increase in deflection as RC beams get exposed to corrosive environment for all the RC beams.

CONCLUSION

The flexural behaviour of RC beams reinforced with B-M1 had a lower flexural strength for both normal beams and beams under corrosive environment as compared to B-M2. The flexural strength of B-M1 had reduced from 48.49 N/mm² to 41.04 N/mm² while B-M2 reduced from 52.21 N/mm² to 49.17 N/mm². This was proven by higher failure loads of B-M2. In addition, this links to high tensile strengths obtained in steel bar specimen of M2. The results showed a decrease in stiffness after first crack for all samples. The mode of failure experienced by 75% of the beams was flexural tension failure at ultimate failure load. The signs of this type of failure were development of cracks at the tension side of the beam which further extend to the compression side. These cracks are mostly vertical and located at the middle third of the beam. Great deflection is another sign of flexural tension failure as it was expected. One-quarter of the tested beams failed by diagonal tension shear without any warning of impending failure. The research revealed that corrosion reduces the flexural strength and increases the ductility of RC beams. M2-RC beams exhibited higher strength compared to M1-RC beams under the normal and corrosive exposure conditions. The loss of flexural capacity to similar exposure to corrosion for B-M1 and B-M2 were 15.4% and 5.8% respectively. This is partly connected to the slightly higher tensile strength and relative rib areas of M2 reinforcing bars.

DECLARATIONS

Corresponding Author

Correspondence and requests for materials should be addressed to Adekunle P. Adewuyi; Email: AdewuyiA@ub.ac.bw; ORCID: 0000-0001-8190-7357

Data availability

The datasets used and/or analysed during the current study available from the corresponding author on reasonable request.

Acknowledgements

The authors would like to acknowledge the Office of Research and Development of the University of Botswana for the internal funding for this research project R1207. The technical staff of the Structural Engineering Laboratory of the Department of Civil Engineering are also appreciated for their support and for creating a conducive environment to conduct this research.

Authors' contribution

AP Adewuyi originated the research concept, identified the research gaps in the existing literature, designed the experimental process, analysed the data, and revised the manuscript. **GB Eric** developed the proposal, conducted the laboratory experimental study, analysed the results and wrote the manuscript. Both authors read and approved the final manuscript

Competing interests

The authors declare no competing interests in this research and publication.

REFERENCES

- Adewuyi, A.P., Eric, G.B., and Kanyeto, O.J. (2022) Characterization of major reinforcing bars for concrete works in Botswana construction industry, *Current Perspectives and New Directions in Mechanics, Modelling and Design*. <https://doi.org/10.1201/9781003348443-203>
- Adewuyi, A.P., Otukoya, A.A., Olaniyi, O.A. and Olafusi, O.S. (2015). Comparative studies of steel, bamboo and rattan as reinforcing bars in concrete: tensile and flexural characteristics. *Open Journal of Civil Engineering*, 5(2), 228-238. <https://doi.org/10.4236/ojce.2015.52023>
- Almusallam, A. (2001). Effect of degree of corrosion on the properties of reinforcing steel bars. *Construction and Building Materials*, 15(8), 361-368. [https://doi.org/10.1016/S0950-0618\(01\)00009-5](https://doi.org/10.1016/S0950-0618(01)00009-5)
- Altoubat, S., Maalej, M. and Shaikh, F.U. (2016). Laboratory simulation of corrosion damage in reinforced concrete. *International Journal of Concrete Structures and Materials*, 10(3), 1-9. <https://doi.org/10.1007/s40069-016-0138-7>
- Apostolopoulos, C.A. and Papadakis, V.G. (2008). Consequences of steel corrosion on the ductility properties of reinforcement bar. *Construction and Building Materials*, 22(12), 2316-2324. <https://doi.org/10.1016/j.conbuildmat.2007.10.006>
- ASTM C78 - 09 (2010). Standard test method for flexural strength of concrete (Using simple beam with third-point loading). ASTM International, West Conshohocken.
- Ballim, Y., Reid, J.C. and Kemp, A.R. (2003). Deflection of RC beams under simultaneous load and steel corrosion. *Magazine of Concrete Research*, 55(4), 405-406. <https://doi.org/10.1680/mac.2003.55.4.405>
- Brandt, A.M. and Józwiak-Niedźwiedzka, D. (2012). Diagnosis of Concrete Quality by Structural Analysis. ASTM International. *Advances in Civil Engineering Materials*, 1(1): ACEM20120004. <https://doi.org/10.1520/ACEM20120004>
- Bertolini, L., Elsener, B., Pedferri, P. and Polder, R. (2013). *Corrosion of Steel in Concrete: Prevention, Diagnosis, and Repair*, 2nd Edition. Weinheim: Wiley-VCH. <https://doi.org/10.1002/9783527651696>
- Djamaluddin, R. (2013). Flexural behaviour of external reinforced concrete beams. *Procedia Engineering*, 54, 252 - 260. <https://doi.org/10.1016/j.proeng.2013.03.023>
- Fernandez, I., Herrador, M.F., Marí, A.R. and Bairán, J.M. (2016). Structural effects of steel reinforcement corrosion on statically indeterminate reinforced concrete members. *Materials and structures*, 49, 4959 - 4973. <https://doi.org/10.1617/s11527-016-0836-2>
- Fouad, N., Saifelddeen, M. A., Huang, H. & Wu, Z. S. (2016). Early corrosion monitoring of reinforcing steel bars by using long-gauge carbon fiber sensors. *Journal of Civil Structural Health Monitoring*, 6, 691-701. <https://doi.org/10.1007/s13349-016-0190-7>
- Huang, L., Ye, H., Jin, X., Jin, N. & Xu, Z. (2020). Corrosion-induced shear performance degradation of reinforced concrete beams. *Construction and Building Materials*, Elsevier, 248(1), p. 118668. <https://doi.org/10.1016/j.conbuildmat.2020.118668>
- Hunkeler, F. (2005). Corrosion in reinforced concrete: Processes and mechanisms. Cambridge: Woodhead Publishing Limited. <https://doi.org/10.1201/9781439823439.ch1>
- Ignjatovic, I. S., Marinkovic, S. B., Miskovic, Z. M. & Savic, A. R. (2013). Flexural behavior of reinforced recycled aggregate concrete beams under short-term loading. *Materials and Structures*, 46, 1045-1059. <https://doi.org/10.1617/s11527-012-9952-9>
- Kim, S. & Kim, S. (2019). Flexural Behavior of concrete beams with steel bar and FRP reinforcement. *Journal of Asian Architecture and Building Engineering*, 18(2), 89-97. <https://doi.org/10.1080/13467581.2019.1596814>
- Kunawisarut, A., Iwanami, M., Chijiwa, N. and Nakayama, K. (2024). Assessment of bond deterioration in corroded RC members incorporating cracking response and tension stiffening. *Structure and Infrastructure Engineering*, 20(4): 581-593. <https://doi.org/10.1080/15732479.2022.2131843>
- Li, H., Li, B., Jin, R., Li, S. and Yu, J. G. (2018). Effects of sustained loading and corrosion on the performance of reinforced concrete beams. *Construction and Building Materials*, 169, 179-187. <https://doi.org/10.1016/j.conbuildmat.2018.02.199>
- Li, Q., Guo, W., Liu, C., Kuang, Y. and Geng, H. (2020). Experimental and theoretical studies on flexural performance of stainless steel reinforced concrete beams. *Advances in Civil Engineering*, 2020(1), 4048750. <https://doi.org/10.1155/2020/4048750>
- Maaddawy, T. E., Soudki, K. and Topper, T. (2005). Analytical Model to Predict Nonlinear Flexural Behavior of Corroded RC beams. *ACI Structural Journal*, 102(4): 550-559. <https://doi.org/10.14359/14559>

- Makul, N. (2020). Advanced smart concrete - A review of current progress, benefits and challenges. *Journal of Cleaner Production*, 274(20): 122899. <https://doi.org/10.1016/j.jclepro.2020.122899>
- Malumbela, G., Moyo, P. and Alexander, M. (2009). Behaviour of RC beams corroded under sustained service loads. *Construction and Building Materials*, 23(11). 3346-3351. <https://doi.org/10.1016/j.conbuildmat.2009.06.005>
- Patil, A. N., Birajdar, B. G. and Dawari, B. M. (2017). Influence of corrosion on flexural strength of concrete. *Journal of Structural Engineering and Management*, 4, 35-42.
- Peng, L., Zhao, Y. and Zhang, H. (2021). Flexural behavior and durability properties of recycled aggregate concrete (RAC) beams subjected to long-term loading and chloride attacks. *Construction and Building Materials*, 277(29). 122277. <https://doi.org/10.1016/j.conbuildmat.2021.122277>
- Qiu, M., Hu, Y., Shao, X., Zhu, Y., Li, P. and Li, X. (2022). Experimental investigation on flexural and ductile behaviors of rebar-reinforced ultra-high-performance concrete beams. *Structural Concrete*, 23(3). 1533-1554. <https://doi.org/10.1002/suco.202100794>
- Ridha, M., Sarsam, K. and Al-Shaarbaf I. (2018). Experimental study on shear resistance of reactive powder concrete beams without stirrups. *Mechanics of Advanced Materials and Structures*, 27(12). 1006-1018. <https://doi.org/10.1080/15376494.2018.1504258>
- Rodrigues, R., Gaboreau, S., Gance, J., Ignatiadis, I. and Betelu, S. (2021). Reinforced concrete structures: A review of corrosion mechanisms and advances in electrical methods for corrosion monitoring. *Construction and Building Materials*, 269(1). 121240. <https://doi.org/10.1016/j.conbuildmat.2020.121240>
- Siddika, A., Al Mamun, A., Ferdous, W. and Alyousef, R., (2020). Performances, challenges and opportunities in strengthening reinforced concrete structures by using FRPs - A state-of-the-art review. *Engineering Failure Analysis*, 110(1): 104480. <https://doi.org/10.1016/j.engfailanal.2020.104480>
- Soltani, A., Harries, K.A. and Shahrooz, B. (2013). Crack opening behavior of concrete reinforced with high strength reinforcing steel. *International Journal of Concrete Structures and Materials*, 7(4): 253-264. <https://doi.org/10.1007/s40069-013-0054-z>
- Słowik, M. (2018). The analysis of failure in concrete and reinforced concrete beams with different reinforcement ratio. International Centre for Settlement of Investment Disputes 89, 885-895. Washington: *Archive of Applied Mechanics*. <https://doi.org/10.1007/s00419-018-1476-5>
- Verstrynghe, E., Van Steen, C., Vandecruys, E. and Wevers, M. (2022). Steel corrosion damage monitoring in reinforced concrete structures with the acoustic emission technique: A review. Steel corrosion damage monitoring in reinforced concrete structures with the acoustic emission technique: A review, 349(26). p. 128732. <https://doi.org/10.1016/j.conbuildmat.2022.128732>
- Wei, Y., Wu, Z., Huang, J. and Liang, S. (2018). Comparison of compressive, tensile, and flexural creep of early-age concretes under sealed and drying conditions. *Journal of Materials in Civil Engineering*, 30(11). p. 04018289. [https://doi.org/10.1061/\(ASCE\)MT.1943-5533.0002495](https://doi.org/10.1061/(ASCE)MT.1943-5533.0002495)
- Yoon, S., Wang, K., Weiss, J.W. and Shah, S.P. (2000). Interaction between loading, corrosion, and serviceability of reinforced concrete. *ACI Structural Journal*, 97(6), 637-644. <https://doi.org/10.14359/9977>
- Zhang, W., Zhang, H., Gu, X. and Liu, W. (2018). Structural behavior of corroded reinforced concrete beams under sustained loading. *Construction and Building Materials*, 174, 675-683. <https://doi.org/10.1016/j.conbuildmat.2018.04.145>

Publisher's note: [Scienceline Publication](#) Ltd. remains neutral with regard to jurisdictional claims in published maps and institutional affiliations.



Open Access: This article is licensed under a Creative Commons Attribution 4.0 International License, which permits use, sharing, adaptation, distribution and reproduction in any medium or format, as long as you give appropriate credit to the original author(s) and the source, provide a link to the Creative Commons licence, and indicate if changes were made. The images or other third party material in this article are included in the article's Creative Commons licence, unless indicated otherwise in a credit line to the material. If material is not included in the article's Creative Commons licence and your intended use is not permitted by statutory regulation or exceeds the permitted use, you will need to obtain permission directly from the copyright holder. To view a copy of this licence, visit <https://creativecommons.org/licenses/by/4.0/>.

The Use of Machine Learning Approach to Predict Pile Capacity in Non-Cohesive Soils

Lesego Palalane  and Mahongo Dithinde  

Department of Civil Engineering, University of Botswana, Gaborone, Botswana

✉ Corresponding author's Email: dithinde@ub.ac.bw

ABSTRACT

Existing theoretical and empirical pile design methods cannot accurately model the complex interaction between piles and soil. Consequently, there is a growing trend towards utilizing machine learning techniques to better capture the nonlinear soil-pile interaction. This paper aims to predict the capacity of bored piles in cohesionless soils using a machine learning approach. The machine learning algorithm was trained using a database of 18 bored pile cases in non-cohesive soils and validated with a separate dataset of 8 bored piles in cohesionless soil. Moreover, the performance of the machine learning method was compared with that of a traditional pile design method (i.e., SA-SPT method) in Southern Africa. The evaluation was based on the ratio of measured capacity to predicted capacity (Q_m/Q_p) statistics and the coefficient of determination (R^2). The results showed an R^2 of 0.89 for the machine learning method compared to 0.85 for the SA-SPT method, indicating the superior accuracy of the machine learning approach in predicting pile capacity.

Keywords: Machine learning, SPT-based pile methods, Load Bearing Capacity, Full-scale Load Test, Chin extrapolation method, Terzhagi's 10% criteria.

INTRODUCTION

Pile foundations are vital for supporting critical and complex structures due to their ability to accommodate varying soil conditions and withstand both vertical and lateral loads. The reliability of structures supported by piles hinges upon the performance and behavior of these foundational elements, as emphasized by Zhang et al. (2020).

Despite their importance, the interaction between soil and piles remains a highly complex and not fully understood phenomenon. Various theoretical and empirical methods, such as the Franki Africa method described by Johnson et al. (2001), have been developed to model soil-pile behavior. However, current procedures for pile design typically rely on semi-empirical approaches based on elastic theories and pile load test data.

Assessing pile capacity in non-cohesive soils, such as sand and gravel, poses significant challenges due to their granular composition and unpredictable behavior. Traditional pile design methods (e.g. Meyerhof, 1976, Decourt 1995, etc.) oversimplify the complex soil-pile interaction and generally neglect factors like soil gradation, particle shape, and compaction. Generally the soil properties are determined using the standard penetration test (SPT). However, SPT has a number of limitations as stated by Seed et al. (1985) and Skempton (1986). The main limitation is the measured SPT-N values are not well related to the pile loading process. Pile load

tests are commonly used to verify nominal resistances, but they can be costly and time-consuming. Moreover, the determination of pile capacity based on load-settlement curves lacks a single standard methodology, leading to a wide range of results and making pile design somewhat of a subjective exercise, as noted by Horvitz et al. (1981) and Shariatmadari et al. (2008).

Given these challenges, there has been a recent trend toward leveraging machine learning techniques, as noted by Yago et al. (2021), to better model the intricate and nonlinear connections between piles and surrounding soil, reflecting their increasing adoption across various engineering applications. Shoaib and Abu-Farsakh (2023) emphasized the importance of carefully selecting input variables that influence the output, particularly in predicting ultimate pile capacity (Q_p).

MATERIALS AND METHODS

Pile load test data

The main input data in this study comprised of a static pile load tests database of 26 cases from Southern Africa (South Africa, Botswana, Lesotho, Mozambique, Zambia and Swaziland and Tanzania) along with the associated geotechnical data (soil profiles, field and laboratory test

RESEARCH ARTICLE
 PII: S225204302400034-14
 Received: June 25, 2024
 Revised: September 02, 2024
 Accepted: September 05, 2024

results). The details of the test piles and associated geotechnical data are presented in Appendix 1.

Determination of measured Pile Capacity

The static pile load test field records were further processed by plotting the load versus the head deflection to produce load-deflection curves. The load-deflection curves were then used to estimate the ultimate pile capacity or measured capacity (Q_m). However, majority of the test piles are working piles tested to a maximum load varying from one and half to two times the design load which limits the movement to which the pile head is subjected and requires extrapolation procedure to determine the ultimate capacity e.g. (e.g. Chin, 1970; Fleming, 1992; Decourt, 1999). On account of its popularity, Chin extrapolation method was adopted for this study. The values of measured capacities were compared with the predicted capacities obtained from Machine learning model and direct Southern African SPT method.

Development a machine learning model

The study used a Multiple Linear Regression (MLR) model developed using the SPSS Modeler to determine the predicted capacities. The SPSS Modeler randomly subdivided the 26 pile cases into (i) 18 dataset for model training and (ii) 8 dataset for model validation. The dataset for model training was structured into two main categories: independent variables and a dependent variable.

Independent variables encompassed factors believed to influence the pile's capacity, such as the length of the pile, area of the base and shaft as shown in Appendix 2. The dependent variable is the measured pile capacity obtained from pile load tests as previously described

The stream flow in Figure 1 shows how the dataset was partitioned into model training (70%) and model validation (30%) sets. After training, the MLR model was tested using the reserved testing set to assess its effectiveness in making accurate predictions on unseen data. The trained model was then applied to predict pile capacity by utilizing the adjusted coefficients in a linear equation, and the predicted pile capacity was analyzed and compared with the measured pile capacity.

Validation of the developed model

As previously mentioned, the developed Machine Learning model was validated using a randomly selected dataset of 8 piles cases. The regression coefficients derived from the 18 pile cases model training dataset were

applied to predict the pile capacity of the eight (8) pile cases to validate the model's ability to extend its predictions to novel and unseen data.

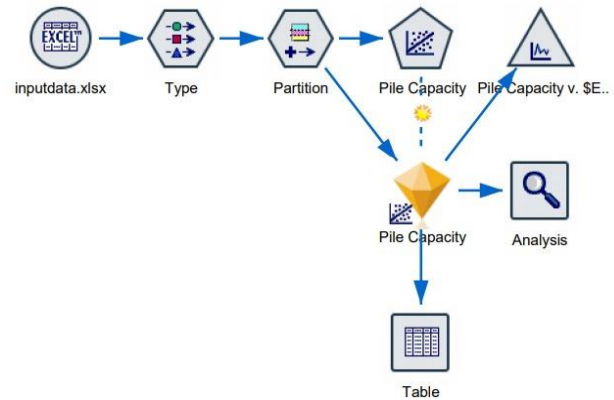


Figure 1. Stream flow diagram

Performance of the machine learning method

The performance of the MLR model was evaluated using statistical metrics, including coefficient of determination (R^2) which is a measure of fit between the measured capacity and predicted capacity from ML model. Furthermore, performance was evaluated on the basis of ML model uncertainty statistics (Mean, Standard Deviation, and Coefficient of Variation) which are a good indicator of the accuracy and precision of predicted capacities. The model uncertainty or model factor (M) was determined from Eq. 1.

$$M = \frac{Q_m}{Q_p} \tag{1}$$

Where Q_m = “capacity” interpreted from a load test, to represent the measured capacity; Q_p = capacity generally predicted using machine learning model, and M = model factor.

Comparison with the SA SPT method

For the Southern Africa SPT Method (SA-Method), the ultimate pile capacity for both shaft and base for all the 26 cases was computed using the following equations;

$$q_b = (N_1)_{60b} F_b \leq q_{max} \tag{2}$$

$$q_s = (N_1)_{60s} F_s \leq q_{max} \tag{3}$$

Furthermore, ultimate pile base and shaft capacity are determined by:

$$Q_b = q_b * A_b = q_b * \left(\frac{\pi d^2}{4}\right) \tag{4}$$

$$Q_s = q_s A_s = q_s (\pi dl) \tag{5}$$

$$Q_{ult} = Q_b + Q_s = q_b\left(\frac{\pi d^2}{4}\right) + q_s(\pi dl) \quad [6]$$

Where Q_{ult} = ultimate pile capacity; Q_b = base pile capacity; Q_s = shaft pile capacity; q_b = base bearing pressure; q_s = shaft bearing pressure.

RESULTS AND DISCUSSIONS

Machine learning results

The multiple regression equation derived from the SPSS Modeler was formulated in the form of Eq. 8, where the coefficients represent the contributions of each independent variable to the prediction of pile design capacity.

$$Q_p = -2641.984 + 30.112L + 66.468N_b + 45.619N_s + 3988.987A_b + 63.725A_s \quad [8]$$

Where Q_p : Predicted Pile Capacity, L = Length, N_b = SPTN for base, N_s = SPT-N for shaft, A_b =Area of base and A_s = Area of shaft

The measured capacities (Q_m) obtained and the predicted capacities (Q_p) from the ML model are presented in Table 1. The ensuing model factors computed as per Eq.1 are also shown in Table 1.

To gain better insight, the measured capacities were plotted against the predicted capacities as shown in Figure 2.

It can be seen from Figure 2 that the R^2 is 0.90 which indicate an excellent fit between the predicted and measured pile capacities. On the basis of the R^2 , it can be inferred that the Machine Learning method predicts pile capacity with high accuracy.

Further insight is shown by the summary statistics of the model factor which are also shown in Fig. 2. At $\mu = 0.99$ and $COV = 0.30$, the ML pile capacity prediction method is relatively very good. The superiority of Machine Learning method in predicting pile capacity compared to traditional empirical methods has been other studies (e.g. Gomes et al 2021, Shoaib and Abu-Farsakh, 2023).

For example, Gomes et al reported that all machine learning techniques investigated obtained a root mean squared error (RMSE) below 710, surpassing Meyerhof’s and Décourt-Quaresma’s semi-empirical methods, which both obtained RMSE values close to 900.

Table 1. Q_m and Q_p for ML model

Case	Q_m	Q_p	$M = Q_m/Q_p$
1	1427	1647	0.866
2	3319	3226	1.029
3	3315	3265	1.015
4	1224	992	1.234
5	887	939	0.944
6	1587	939	1.690
7	1087	774	1.405
8	1361	939	1.449
9	990	884	1.120
10	4706	4543	1.036
11	1232	1647	0.748
12	435	1307	0.333
13	1136	1143	0.994
14	653	541	1.205
15	943	1064	0.886
16	1695	1623	1.044
17	1227	1397	0.878
18	617	969	0.637

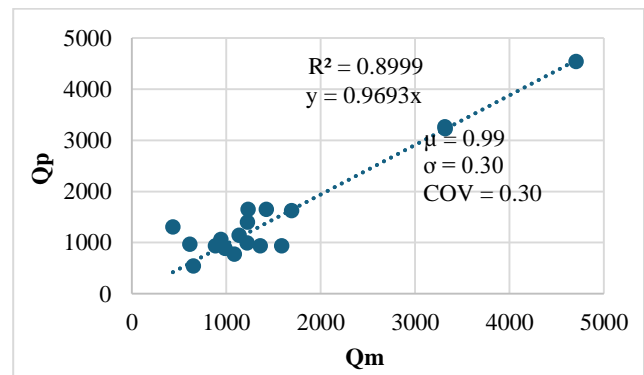


Figure 2- Scatter plot of Q_m Vs Q_p

Validation results

The measured and predicted capacities for the 8 validation cases together with the model factors are presented in Table 2. Furthermore, a plot of the measured versus predicted capacities is presented in Figure 3. Further analysis of Figure 3 shows an R^2 of 0.74 which is good enough for geotechnical work. The Model factor statistics are even better at $\mu = 1.03$ and $COV = 0.24$. This implies that the developed Machine Learning Model can be used to predict pile capacity for bored piles in non-cohesive soils outside the current database.

Table 2. Q_m and Q_p for validation cases

Case	Q_m	Q_p	$m = Q_m/Q_p$
1	1055	1514	0.70
2	1453	2110	0.69
3	1483	1217	1.22
4	1799	1458	1.23
5	2375	2247	1.06
6	3094	2878	1.08
7	4606	3618	1.27
8	3154	2988	1.06

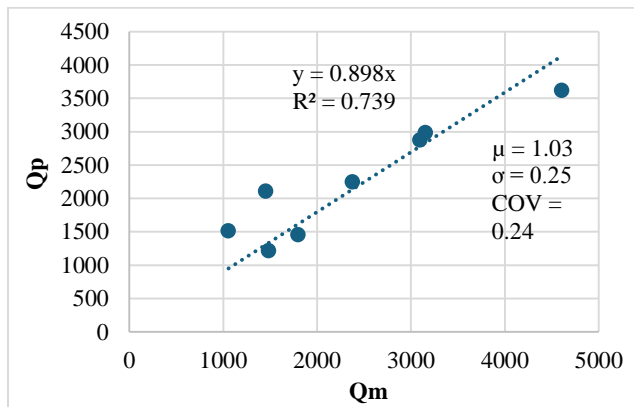


Figure 3: Scatter plot of Q_m Vs Q_p for validation data

Results for SA SPT-based method

For comparison purposes, the measured capacities, predicted capacities and model factors of the SA- SPT based method are presented in Table 3. The R^2 is 0.84 (Figure 4) which is good but lower than that yielded by the ML method. However, the Model factor statistics at $\mu = 0.87$ and $COV = 0.25$ is slightly better, especially the COV which is a measure of variability. The key point here is that the results of the ML method are comparable with that of the well-established SA- SPT based method.

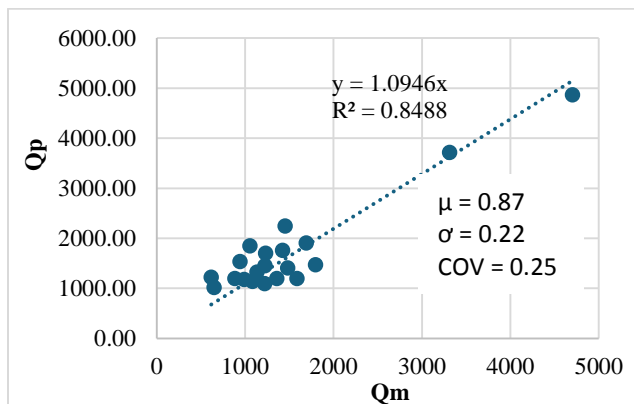


Figure 4: Scatter plot of Q_m Vs Q_p for SA SPT method

Table 3: Q_m and Q_p for SA- SPT based method

Case	Measured pile capacity	Predicted pile capacity	$M = Q_m/Q_p$
1	1427	1754.97	0.813
2	3319	4583.09	0.724
3	3315	3713.36	0.893
4	1224	1088.5	1.124
5	887	1192.31	0.744
6	1587	1192.31	1.331
7	1087	1134.12	0.958
8	1361	1192.31	1.141
9	990	1172.91	0.844
10	4706	4860.7	0.968
11	1232	1694.94	0.727
12	435	1586.46	0.274
13	1136	1321.98	0.860
14	653	1014.73	0.643
15	943	1528.82	0.617
16	1695	1898.7	0.893
17	1227	1448.27	0.847
18	617	1216.49	0.507
19	1055	1842.94	0.572
20	1453	2242.7	0.648
21	1483	1403.7	1.056
22	1799	1467.71	1.225
23	2375	4721.78	0.503
24	3094	5721.56	0.541
25	4606	9545.19	0.483
26	3154	7954.32	0.396

CONCLUSIONS

A plot of Q_m versus Q_p for the Machine Learning approach yielded a high R^2 of 0.9, which is an indication that the method is very accurate in predicting pile capacity. Model validation results produced R^2 of 0.74 and model factor statistics of $\mu = 1.03$ and $COV = 0.24$ which are very good. This implies that the developed Machine Learning Model can be used to predict pile capacity for bored piles in non-cohesive soils outside the current database. The results of the well-established SA-SPT method (R^2 of 0.84 and M- statistics of $\mu = 0.87$ and $COV = 0.25$) is comparable to that of the ML method.

For further research, it is recommended that more pile load test data be collected for both training and validating the Machine Learning Model.

DECLARATIONS

Corresponding author

Correspondence and requests for materials should be addressed to Mahongo Dithinde; E-mail:

dithinde@ub.ac.bw; ORCID: <https://orcid.org/0000-0002-4541-7438>

Data availability

The datasets used and/or analysed during the current study available from the corresponding author on reasonable request.

Author's contribution

Mahongo Dithinde has collected a lot of pile load test data across Southern Africa for various soils condition and pile types. Lesego Palalane applied Machine learning method to ultimate capacity of piles in non-cohesive soils extracted from the load test database availed by Dithinde.

Acknowledgements

The authors would like to Faculty IT Unit for assistance with SPSS modeler required for Machning Learning analysis for this study.

Consent to publish

Not applicable.

Competing interests

The authors declare no competing interests in this research and publication.

REFERENCES

- Chin, F.K. 1970. Estimation of Pile Not Carried to Failure, Proceedings 2nd Southeast Asian Conference on Soil Engineering, Singapore, 81-90.
- Decourt, L. (1999). Behaviour of foundations under working load conditions. Proceedings of the 11th Pan American Conference on Soil Mechanics and Geotechnical Engineering, Foz Dolguassu, Brazil, Vol. 4, pp. 453-488.
- Decourt, L., (1995). Prediction of load-settlement relationships for foundations on the basis of the SPT T, Ciclo de Conferencias Internacionales, Leonardo Zeevaert, UNAM, Mexico, 1995, pp. 85-104.
- Fleming, W. G. K. (1992). A new method for single pile settlement prediction and analysis; *Geotechnique*, Vol. 42, No. 3, pp. 411-425. <https://doi.org/10.1680/geot.1992.42.3.411>
- Johnson, K., Karunasena, W., Sivakugan, N., & Guazzo, A. (2001). Modeling Pile-Soil Interaction Using Contact Surfaces. In S. Valliappan & N. Khalili (Eds.), *Computational Mechanics–New Frontiers for the New Millennium* (pp. 375-380). Elsevier. ISBN 9780080439815. <https://doi.org/10.1016/B978-0-08-043981-5.50058-4>.
- Horvitz G.E., Stettler D.R. and Crowser J.C. (1981). Comparison of predicted and observed pile capacity. In Proceedings of a session sponsored by the Geotechnical Engineering Division at the ASCE National Convention (pp. 413-433).
- Meyerhof, G. G. (1976). Bearing capacity and settlement of pile foundations. *Journal of Geotechnical Engineering, ASCE*, Vol. 102, No. 3, pp. 196-228. <https://doi.org/10.1061/AJGEB6.0000243>.
- Seed B., Tokimatsu K., Harder M and Chung. (1985). Influence of SPT Procedures in Soil Liquefaction Resistance Evaluations. *Journal of Geotechnical Engineering, ASCE*. 111(12): 1425-1445. [https://doi.org/10.1061/\(ASCE\)0733-9410\(1985\)111:12\(1425\)](https://doi.org/10.1061/(ASCE)0733-9410(1985)111:12(1425))
- Shariatmadari, N., Eslami, A., & Karimpour-Fard, M. (2008). Bearing capacity of driven piles in sands from SPT–applied to 60 case histories. *Iranian Journal of Science & Technology, Transaction B, Engineering*, 32(B2), 125-140.
- Skempton A. W. 1986. Standard Penetration Test Procedures and the Effects in Sands of Overburden Pressure, Relative Density, Particle Size, Ageing and Over consolidation. *Geotechnique*. 36(3): 25-447. <https://doi.org/10.1680/geot.1986.36.3.425>.
- Shoaib, M. M., & Abu-Farsakh, M. Y. (2023). Exploring Tree-Based Machine Learning Models to Estimate the Ultimate Pile Capacity From Cone Penetration Test Data. *Transportation Research Record. Advance online publication*. <https://doi.org/10.1177/03611981231170128>.
- Yago, Gomes & Verri, Filipe & Ribeiro, Dimas. (2021). Use of machine learning techniques for predicting the bearing capacity of piles. *Soils and Rocks*. 44. 1-14. <https://doi.org/10.28927/SR.2021.074921>.
- Zhang, W., Goh, A. T. C., Zhang, R., Li, Y., & Wei, N. (2020). Chapter 19 - Back-propagation neural network modeling on the load–settlement response of single piles. In P. Samui, D. T. Bui, S. Chakraborty, & R. C. Deo (Eds.), *Handbook of Probabilistic Models* (pp. 467-487). Butterworth-Heinemann. <https://doi.org/10.1016/B978-0-12-816514-0.00019-9>.

Appendix 1: Pile load tests database

Case	Soil type		Pile type	Shaft dia. (mm)	Base dia.(mm)	SPT N-value		Length (m)
	Base	Shaft				base	Shaft	
1	Medium dense sandy gravel	Medium dense sandy gravel	Auger	430	430	30	20	8
2	Gravel	Gravel	Auger	600	750	30	20	9
3	Gravel	Gravel	Auger	750	600	30	20	11
4	Sand	Sand	CFA	360	350	29	14	7.8
5	Sand	Sand	CFA	400	400	23	13	9.5
6	Sand	Sand	CFA	400	400	23	13	9.5
7	Sand	Sand	CFA	400	400	23	13	8
8	Sand	Sand	CFA	400	400	23	13	9.5
9	Sand	Sand	CFA	400	400	23	13	9
10	Sand	Sand	Auger	520	520	38	38	16.5
11	Sand	Sand	Auger	430	430	25	17	11.5
12	Dense sand	Sand	Auger	450	450	25	15	9
13	Sand	Sand	CFA	400	400	22	17	10
14	Sand	Sand	CFA	400	400	19	16	7
15	Sand	Sand	CFA	500	500	19	16	7.8
16	Sand	Sand	CFA	500	500	22	17	10
17	Sand	Sand	CFA	400	400	25	16	11
18	Sand	Sand	CFA	400	400	24	13	9.2
19	Sand	Sand	CFA	500	500	25	14	9.5
20	Sand	Sand	CFA	500	500	26	17	11.8
21	Sand	Sand	CFA	500	500	13	14	12.3
22	Sand	Sand	CFA	500	500	13	13	14.5
23	very dense sand	Sand	Franki	520	760	17	9	12
24	Dense gravel	medium sand	Franki	520	760	17	14	15
25	dense sand	medium sand	Franki	520	760	36	32	6
26	very dense sand	medium sand	Franki	520	760	30	20	8

Appendix 2: Input data used in MLR Model

Case No.	Length	SPT N-base	SPT N-shaft	Area-base	Area-shaft	Q _m
1	8	28.5	19	0.15	10.81	1427
2	9	28.5	19	0.44	16.96	3319
3	11	28.5	20	0.28	25.92	3315
4	7.8	27.55	13.3	0.1	8.82	1224
5	9.5	21.85	12.35	0.13	11.94	887
6	9.5	21.85	12.35	0.13	11.94	1587
7	8	21.85	12.35	0.13	10.05	1087
8	9.5	21.85	12.35	0.13	11.94	1361
9	9	21.85	12.35	0.13	11.31	990
10	16.5	36.1	38	0.21	26.95	4706
11	11.5	23.75	17	0.15	15.54	1232
12	9	23.75	14.25	0.16	12.72	435
13	10	20.9	17	0.13	12.57	1136
14	7	18.05	15.2	0.13	8.8	653
15	7.8	18.05	15.2	0.2	12.25	943
16	10	20.9	17	0.2	15.71	1695
17	11	23.75	16	0.13	13.82	1227
18	9.2	22.8	12.35	0.13	11.56	617
19	9.5	23.75	11.9	0.2	14.92	1055
20	11.8	24.7	17	0.2	18.54	1453
21	12.3	12.35	14	0.2	19.32	1483
22	14.5	12.35	13	0.2	22.78	1799
23	12	16.15	9	0.45	19.6	2375
24	15	16.15	14	0.45	24.5	3094
25	6	34.2	30.4	0.45	9.8	4606
26	8	28.5	19	0.45	13.07	3154

Publisher’s note: [Scienceline Publication](#) Ltd. remains neutral with regard to jurisdictional claims in published maps and institutional affiliations.



Open Access: This article is licensed under a Creative Commons Attribution 4.0 International License, which permits use, sharing, adaptation, distribution and reproduction in any medium or format, as long as you give appropriate credit to the original author(s) and the source, provide a link to the Creative Commons licence, and indicate if changes were made. The images or other third party material in this article are included in the article’s Creative Commons licence, unless indicated otherwise in a credit line to the material. If material is not included in the article’s Creative Commons licence and your intended use is not permitted by statutory regulation or exceeds the permitted use, you will need to obtain permission directly from the copyright holder. To view a copy of this licence, visit <https://creativecommons.org/licenses/by/4.0/>.

Geotechnical Characterization of the Manyana Black Cotton Soils in Botswana

Mompoloki Ndala Marumo , Gabatsoswe Lebitsa , and Goitseone Malumbela 

Botswana International University of Science and Technology, P/Bag 16, Palapye, Botswana

✉ Corresponding author's Email: darriesmorule@gmail.com

ABSTRACT

The Manyana Village is divided into two types of soils. The center of the village is covered with sand that overlays clays from weathered dolerite whilst the eastern side is covered with exposed clays. Houses constructed on the eastern side of the village are prone to severe cracking attributed to the black cotton soils. The paper hints at shrink-swell mechanism of black cotton soils as a possible explanation for the cracking observed on the houses. Three laboratory methods of identifying and characterizing expansive soils are discussed followed by use of Dynamic Cone Penetration (DCP) in field-testing as well as use of indicator tests and particle sizing in the laboratory. The experimental results have shown a high field moisture content of (18 to 27%) in the eastern part of the village which was three times larger than moisture content at the village center. The clays had a plasticity index range of 12% to 30% with a clay content of 21% to 47% whilst the sandy areas were non-plastic with a clay content of at most 4%. The clay minerals identified from the samples tested were vermiculite, illite, kaolinite and montmorillonite. The soil samples from the village had low potential expansiveness whilst most samples on black cotton soil had a medium to high potential of expansiveness. The bearing capacity estimated from DCP data at depths of 1m throughout the village were 72 kPa to 275 kPa under dry conditions. A draft plasticity index map of Manyana village was produced based on the results of the investigation, the next step is to investigate the effectiveness of different soil stabilization methods for this area and taking in to consideration cost, durability and environmental impact.

Keywords: Black cotton soil, Cracking, Moisture content, Plasticity index, Bearing capacity.

INTRODUCTION

Manyana village occupies 6.57 km² of land of which 30% is covered with expansive soils (black cotton soil) and the other 70% is covered with silty sands. The area is relatively flat with the altitude above mean sea level varying from 1121 m on the north to 1142 m on the south (Figure 1). This flat land is surrounded by relatively low-lying hill range to the south, west and northwest.

Dolerite outcrops are exposed in the eastern part of Manyana area as in Figure 2. Fresh hand specimen of the dolerite is dark grey, medium to coarse grained with abundant plagioclase and 30% to 40% quartz content. Weathered parts of the dolerite were observed as greyish brown to light grey with dark brown to grey spots. Reddish brown weathered dolerite also does occur in the southern part of the area. There are no exposures of the dolerite in the village built up area.

Alteration of the dolerite resulted in the formation of clay deposits (Key, 1983). The alteration process of dolerite into clays is greater in the village centre where the dolerite is in contact with the Manyelanong Hill formation, resulting in thicker clayey profiles. These clays are

covered by transported sandy deposits from the nearby sandstone ridges, but clays are predominantly exposed in the eastern part of the village

Many structures at Manyana Village experience extensive cracking of walls, flooring and all their respective masonry as shown in Figure 3. These cracks propagate from the ground to the roof levels, on the floors extending from wall end to wall end. The cracks range from hairline to aperture widths of as much as 50 mm and more. Manyana Village elders have called for assistance from various Government Organs. One such organ is the Department of Geological Survey who through a report by [Ngonidzashe et al. \(2014\)](#) attributed cracking of houses in the Manyana Village to the presence of clays associated with the weathering of dolerite. This was however, not substantiated by research and as such residents continued to experience the problem of cracking. It is therefore essential that substantive research be carried out to establish the cause of cracking of houses in the Manyana Village and develop a strategy to mitigate the problem on existing structures and how best to avoid it in future developments.

RESEARCH ARTICLE
 PII: S225204302400035-14
 Received: June 25, 2024
 Revised: September 02, 2024
 Accepted: September 05, 2024

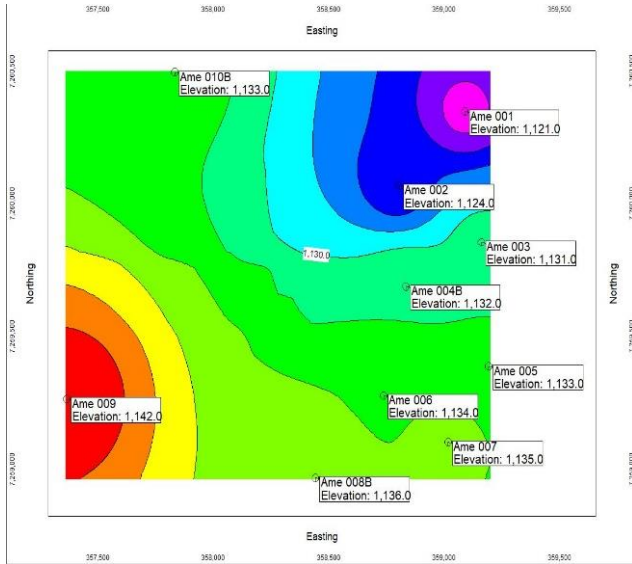


Figure 1. Altitude of the study area

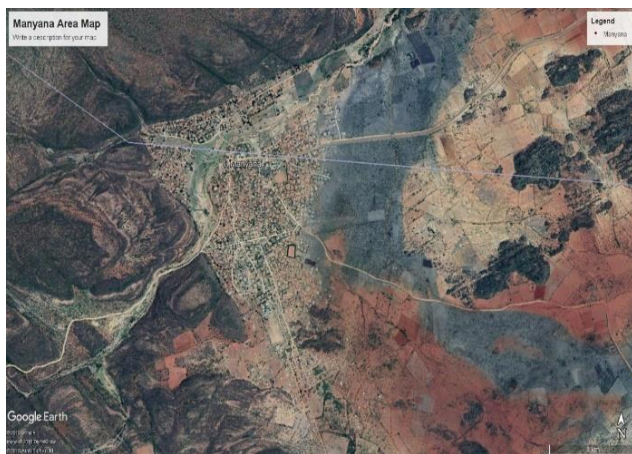


Figure 2. location of the village and outcrops around the village. Source: Google earth map

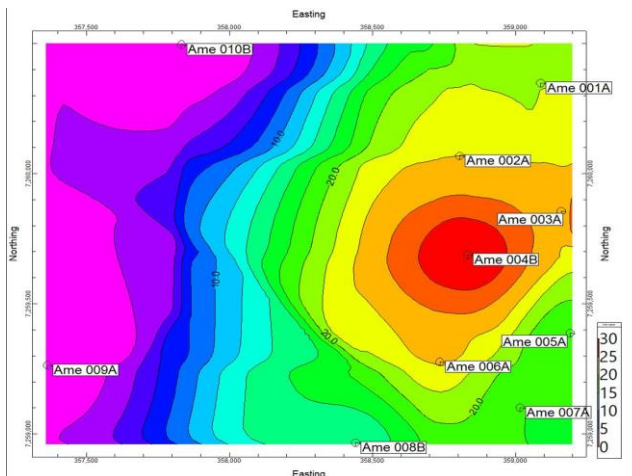


Figure 3a. Plasticity Index map from the observed results

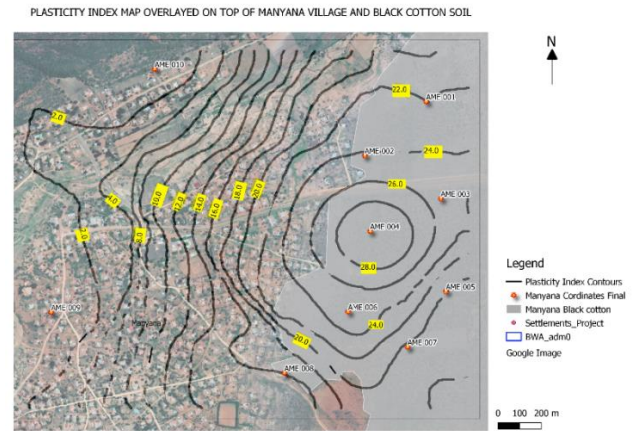


Figure 3b. Overlaying of plasticity Index map on top of Manyana village

Regarding clays in other parts of the world, Zornberg et al. (2008) characterised Eagle Ford clay for the design and remediation of roadways constructed on poor subgrade materials. Zornberg et al. (2008) found that the clays have a Plasticity index of 47% and clay content was 97%. They found that 24 hrs was necessary for 1 cm specimen of compacted clay to swell to an equilibrium height in the centrifuge permeameter.

MATERIALS AND METHODS

The study intends to establish the cause of cracking of houses in the Manyana Village and develop a strategy to mitigate the problem on existing structures and how best to avoid it in future developments. The tests were done in order to determine the characteristics of black cotton soil and to establish the geotechnical properties of black cotton soil prior construction. The first part of this work which is covered by this paper is characterization of black cotton soil in the area using field and laboratory tests as indicated in Table 1. The in-situ testing was carried out using a Dynamic Cone Penetration (DCP) apparatus whose values were used to predict the California Bearing Ratio (CBR) of the soil. During trial pitting the moisture condition, colour, consistency, structure, soil texture and origin of each layer of the soil profile (MCCSSO) as proposed by Jennings, Brink & Williams (1973) was used.

Table 1. Activities done at the field and tests done at the lab

Field Work	Laboratory Tests
In-situ testing (Using DCP)	Grain Size Analysis Hydrometer Atterberg Limits
Trial pitting and profile According to MCCSSO	Moisture Content
Use DCP to predict CBR	Specific Gravity

Selection of sampling sites

An area to be sampled was delineated into triangles and all the triangles were sampled in the centre as a representative of the delineated triangle. Figure 3a shows the sampling points. As shown in the figure, most sampling points were within the area covered with black cotton soil with two additional points within the village chosen as controls (AME 009 and AME 010). Quality assurance and quality control (QA/QC) of the results was carried out in the laboratory during analysis as where some of the tests were repeated to check the validity of the results.

Field work

Fieldwork entailed carrying out DCP tests at selected points and manually excavating test pits to depths of between 1 m and 1.5 m to obtain samples for laboratory testing. The DCP test was used to obtain a direct and rapid in-situ evaluation of the structural strength of the layers whilst the samples were to be used in the laboratory to determine pedological conditions and the possible presence of perched ground water bodies.

Thirteen disturbed samples were taken from individual horizons from the test pits for geotechnical and mineralogical determinations and when it was found that different profiles were found within the same pit, samples were separated and labelled A and B as it can be seen at Ame 004, Ame 008 and Ame 010.

The DCP test apparatus was assembled and placed at the test location with the initial penetration of the rod recorded to provide a zeroing scale. While holding the rod vertically, the weight was raised to the top of the rod 575 mm above the anvil and dropped. The penetration of the rod was measured after each drop which was later plotted to give penetration in millimeters per blow (mm/blow).

Sampling

Disturbed soil sampling was used to sample as the horizons of the pit were critical in observing change in horizons inside the pit. These samples were labelled and sent to the laboratory for testing. The field observation of moisture condition, colour, consistency, structure, soil texture and origin (MCCSSO) of each layer of the soil profile was used as proposed by Jennings, Brink and Williams (1973).

Sample preparation

Samples were prepared in accordance with AASHTO T87-86. As per the AASHTO method, the samples were air dried for a minimum of 24 hrs then soil boulders were

pulverized using rubber covered mallet. A riffle box was then used to get representative samples.

Standard laboratory tests on black cotton soil

All the tests that were carried out are summarized in Table 2.

Table 2. Activities or tests that were done

Test	Standard
Moisture Content	ASTM D 4643-08
Particle Size	ASTM D 422-63 (2007)
Hydrometer	ASTM D 422-63 (2007)
Specific Gravity	ASTM D 854-14
Atterberg Limits	ASTM D 4318

RESULTS

This section presents and discusses results from the experimental work.

Moisture content

Moisture Content was conducted as per ASTM D4643 – 08. Table 3 shows the moisture content of all sample pits from Ame 001 to Ame 010. The table shows sample pits that were sited on top of black cotton soil had high moisture content ranging from 10.6% to 27% with the lowest at Ame 008B and the highest at Ame 003 as compared to samples outside the black cotton soil region with moisture content ranging between 5.7% and 6.1% with the lowest at Ame 009 and the highest at Ame 0010A. It is likely that the samples located within the Black cotton soils contained more clay minerals than the samples located closer to the village as clay will absorb more water and take time to release it. The clay minerals by virtue of their relatively large surface area coupled with their net negative charge attract and retain more water (Knappett and Craig, 2012) hence the higher moisture content at sample pits that were sited on top of black cotton soil being three times higher than those located in sandy areas.

Dynamic Cone Penetrometer (DCP)

A total of ten DCP tests were conducted in the study area to complement information obtained from trial pits. The DCP penetration rates (mm/blow) allowed for estimation of the bearing capacity of in-situ soil horizons up to a depth of 1m. Figure 6 shows results for DCP tests

in terms of variation of penetration rates (mm/blow) with depth. The average penetration rates in most pits ranged between 24mm/blow and 17mm/ blow indicating soft to firm consistencies. This translates to the presumed allowable bearing capacities ranging between 72 kPa and 275 kPa within the first 1m of the pits. At depths of below 900 mm, almost all the samples had similar penetration rates that ranged between 16 and 18 mm/blow.

Higher values of load bearing capacity are attributed to the presence some ferricrete nodules in some soils such as at Ame 008 and dense clayey materials with some weakly developed cementation in others such as at Ame 001 Soils at Ame 010 contained loose aeolian deposits and therefore exhibited lower values of load bearing capacity of below 60 kPa and penetration values that averaged below 38 mm/blow.

Grain Size Analysis

Grain size test analysis was conducted as per ASTM D 422- 63 (2007). Figure 4 shows results of the particle size distribution of all the samples. The figure shows that at particle sizes of below 0.002, which is clay content, samples located on a region with black cotton soils had different percentages of clay content ranging from 21.4 % at Ame 008B and 46.8% at Ame 003A. At Ame 10A, Ame 10B and Ame 9 which were within the village, the samples showed clay contents of 0, 0.2 and 4.2 respectively. It needs to be noted that AME 9 and 10 which are located at the village comprise about 80% of particle sizes between silty sand and clayey silt as observed from Figure 7. However the low content of clay sized particles ($-2\mu\text{m}$ size) means a low content of clay minerals and reduced likelihood to shrink and swell with moisture variations. Therefore, where these samples were found there were no signs of cracking to houses that were close, which can be attributed to low values of clay content. The results have also been summarized in Table 5.

Atterberg limits

Atterberg Limit tests were carried out as per TMH 1 - A1 to A3 testing procedures and the results are shown in Table 5. The liquid limit ranged between 33% at Ame 005 and 59% at Ame 003A. The highest plastic limit of 33% was obtained at Ame 002 and Ame 005 whilst the highest plasticity index of 30% was obtained at Ame 004A and Ame 004B. The lowest plasticity Index were found at Ame 008B at a value of 12%. Linear shrinkage ranged between 6% at Ame 008B and 12.2% at Ame 003.

Figure 3a shows a plasticity map from the results. The figure clearly shows that the plasticity index increases

from the village towards the region with black cotton soil. The highest plasticity index is at Ame 004 with a value of 30% and is represented by red colour.

After calculating all the plasticity index of all the samples, the map for plasticity index values was overlaid on top of the Manyana Village as shown in figure 3b. From the figure, it can be observed that the black cotton covers close to 30 % of the village. Plasticity Index increases as one moves from the village towards the black cotton soil and the highest Plasticity Index was found at Ame 004, which is at the centre of the Black Cotton soil area. The two points (Ame 009 and Ame 010) that were within the village were at plasticity Index of 0 that showed the soil within the village is slightly plastic to non-plastic. At the boundary between the village and the black cotton soil area, it was observed that the plasticity index was ranging from 18% to 26%. It was also apparent that even houses close to the boundary had cracked because of the high plasticity index values.

Specific gravity (G_s)

Table 6 shows tests results for specific gravity. It ranged from 2.32 for Ame 001A to 2.66 for Ame 010B. From the results, soils with high G_s values had low clay content while those with high clay content had low G_s values. It was noted that some samples with high G_s values had some nodules of ferricrete which probably contributed to the high G_s values.

Mineralogy

The XRD test results in Table 7 show that all samples contained at least one clay mineral (Montmorillonite, Kaolinite, Illite, Vermiculite and Nacrite). The specific gravity of the minerals (Deer et. al, 1992) are also given in the table. Montmorillonite as an expansive mineral was found more on Ame 001 at a value of 23% followed by Ame 007 at a value of 6% and traces of it was found in Ame 004 up to Ame 006. Clay minerals present in the samples which are overly expansive can lead to cracking of overlying structures. When all the clay minerals were grouped together it was observed that Ame 001 had a high concentration at a value of 77% followed by Ame 002 with a value of 76%. Samples within the village were found to have clay content ranging from 0 to 3%. From the clay minerals that were identified, it is concluded that the clay mineralogy could have led to cracking on houses that are constructed on top of soils containing the expansive minerals especially given the wetting and drying cycle.

Van der Merwe's empirical method for the estimation of potential ground heave

In order to classify samples using Van Der Merwe's empirical methods, plasticity index was plotted against percentage of clay particles in Figure 9 to give a classification of heave potential curve (*Van der Merwe, 1964*). The figure shows that samples fell in areas of possible high potential heave to areas of low potential heave. Ame 004A and Ame 004B samples plotted on high

potential heave whereas Ame 008B plotted on the margin between low and medium potential heave. A further examination of the figure shows that the Van Der Merwe classification method relies on results from other tests such as the use of the results from Atterberg limits (plasticity index (PI)) and results from grain size for clay content. It follows then that any inherent weaknesses in those test results are transferred to the Van Der Merwe classification.

Table 3. Moisture content of all the samples

Sample No	Ame 001	Ame 002	Ame 003	Ame 004A	Ame 004B	Ame 005	Ame 006	Ame 007	Ame 008A	Ame 008B	Ame 009	Ame 0010A	Ame 0010B
Moisture (%)	21.8	22.8	27.0	22.7	21.2	22.5	23.6	17.8	14.1	10.6	5.7	6.1	5.8

Table 4. Particle size distribution of all the samples and USC System

Sample No	Ame 001	Ame 002	Ame 003	Ame 004A	Ame 004B	Ame 005	Ame 006	Ame 007	Ame 008A	Ame 008B	Ame 009	Ame 0010A	Ame 0010B
Gravel	0.9	0.7	0.0	2.4	2.0	0.6	0.1	0.4	0.6	0.2	0.00	0.0	0.0
Sand	37.0	45.8	37.7	33.1	33.3	27.9	21.8	28.3	33.8	51.1	82.1	98.4	98.4
Silt	28.9	21.3	15.5	29.2	29.5	27.4	37.2	32.5	35.1	27.3	13.7	16.0	14.0
Clay	32.2	33.2	46.8	35.3	35.2	44.1	40.9	38.8	30.5	21.4	4.20	0.0	0.2
USCS	CL	MH	CH	CH	CH	MH	CH	ML	CL	SC	SM	SP	SP

Table 5. Atterberg Limits results of all the samples

Sample No	Ame 001	Ame 002	Ame 003	Ame 004A	Ame 004B	Ame 005	Ame 006	Ame 007	Ame 008A	Ame 008B	Ame 009	Ame 0010A	Ame 0010B
Liquid Limit (LL)	48	57	59	58	57	51	51	46	36	33	NV	NV	NV
Plastic Limit (PL)	26	33	31	28	27	33	26	28	21	21	NP	NP	NP
Plasticity Index (PI)	22	24	28	30	30	18	25	18	15	12	NP	NP	NP
Shrinkage	8.4	10.9	12.2	10.0	8.8	8.7	6.5	8.9	7.7	6.0	NP	NP	NP

Table 6. Observed values or Specific Gravity of all the samples

Sample No	Ame 001	Ame 002	Ame 003	Ame 004A	Ame 004B	Ame 005	Ame 006	Ame 007	Ame 008A	Ame 008B	Ame 009	Ame 0010A	Ame 0010B
Specific gravity (g/cm ³)	2.32	2.37	2.34	2.45	2.34	2.43	2.40	2.41	2.62	2.54	2.62	2.52	2.66

Table 7. Mineralogy of all the samples

	Specific Gravity	Ame 001	Ame 002	Ame 003	Ame 004A	Ame 004B	Ame 005	Ame 006	Ame 007	Ame 008A	Ame 008B	Ame 009	Ame 0010A	Ame 0010B
Quartz	2.65	15	11	43	7	6	40	44	45	30	30	84	80	85
Albite	2.62	-	6	-	-	-	-	-	-	-	-	3	-	-
Actinolite	3.00	-	5	19	-	-	-	3	3	-	3	-	-	2
Kaolinite	2.65	-	32	-	-	-	-	-	-	-	-	-	1	1
Montmorillonite	2.5	23	-	1	Traces	Traces	Traces	Traces	6	3	3	-	-	-
Illite	2.75	-	32	-	-	-	-	-	-	-	-	-	2	-
Vermiculite	2.30	54	12	2	-	-	-	13	6	11	15	-	-	-
Nacrite	2.60	-	-	-	9	10	8	7	9	14	9	-	-	2
Calcite	2.72	8	2	35	4	2	-	-	-	-	-	-	3	-
Phlogopite	2.82	-	-	-	80	82	52	27	18	29	40	5	14	10
Annite	3.30	-	-	-	-	-	-	6	13	13	-	8	-	-

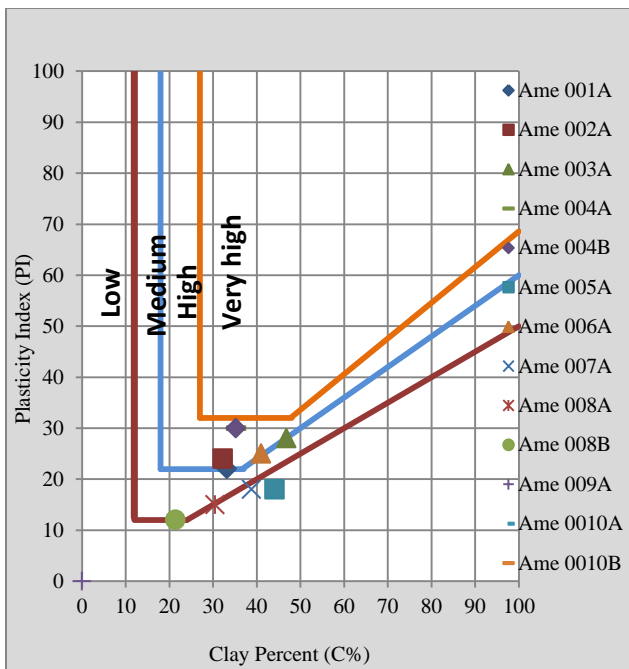


Figure 4. Van Der Merwe classification of all the samples

DISCUSSION

The results of the field work and laboratory tests carried out under this study have shown that at the centre of the Manyana village where weathered dolerite derived clays are covered with sand the soils provide a better foundation for houses. The soils at the centre of Manyana village are non-plastic with a clay content of up to 4% and they have a low potential expansiveness and a relatively high bearing capacity. The soils on the eastern side of the village on the contrary are clays with plasticity index range of 12 to 30% and clay content of 21 to 47%. The soils exhibit a medium to high potential of expansiveness, a low bearing capacity as well as a high field moisture content (18 to 27%). The bearing capacity range based on DCP correlations was 72kPa to 275kPa under dry conditions. A plasticity index map of Manyana village depicting these conditions has been compiled and it showed that Black cotton soils cover approximately 30% of the village from the eastern side of the village. One of the constraints of the study was sampling during the wet season where it was difficult to move within the study area due to the slippery nature of clay when wet.

Overall it is suggested that the village growth avoid eastern Manyana (which could be reserved for agricultural use) where the heavy clays predominate. It would also be advisable to carry out more tests to adequately delineate the area to be avoided.

DECLARATIONS

Corresponding Author

Correspondence and requests for materials should be addressed to Mompoloki Ndala Marumo; E-mail: darriesmorule@gmail.com; ORCID: 0000-0000-0000-0000

Data availability

The datasets used and/or analysed during the current study available from the corresponding author on reasonable request.

Acknowledgements

The authors would like to acknowledge the Department of Civil and Environmental Engineering at Botswana International University of Science and Technology and Botswana Geoscience Institute (BGI) for creating a conducive environment to conduct this research.

Authors' contribution

First Author performed the experiments, analysed the data obtained and wrote the manuscript. Second and Third Author designed the experimental process and revised the manuscript. Both authors read and approved the final manuscript

Competing interests

The authors declare no competing interests in this research and publication.

REFERENCES

Aderniji, F. A, (1991) "Recharge function of vertisolic vadose Zone in sub-sahelian Chad Basin". Proceeding 1st International Conference on AridZone Ideology Hydrology and water resources, Maduguri, pp, 331 – 348.

ASTM D422-63(2007), Standard Test Method for Particle-Size Analysis of Soils (Withdrawn 2016), ASTM International, West Conshohocken, PA, 2007, www.astm.org

ASTM D422-63(2007), Standard Test Method for Particle-Size Analysis of Soils (Withdrawn 2016), ASTM International, West Conshohocken, PA, 2007, www.astm.org

ASTM D4318-17, Standard Test Method for Liquid Limit, Plastic Limit, and Plasticity Index of Soils, ASTM International, West Conshohocken, PA, 2017, www.astm.org

ASTM D4643-17, Standard Test Method for Determination of Water Content of Soil and Rock by Microwave Oven Heating, ASTM International, West Conshohocken, PA, 2017, www.astm.org

ASTM D854-14, Standard Test Method for Specific Gravity of Soil Solids by Water Pycnometer, ASTM International, West Conshohocken, PA, 2014, www.astm.org

- Deer, W. A., Howie, R. A., and Zussman, J., 1992, *An Introduction to the Rock-Forming Minerals*, 2nd edition: Harlow, Essex, United Kingdom, Pearson Education
- Guidelines for Soil and Rock Logging in South Africa, 2nd Impression 2001, eds. A.B.A. Brink and R.M.H. Bruin, Proceedings, Geoterminology Workshop organised by AEG, SAICE and SAIEG, 1990.
- Jennings J. E., Brink A. B. A., Williams A. A. B. (1973) Revised guide to soil profiling for civil engineering purposes in southern Africa. *Trans. S. Afr. Inst. civ. Engrs* 15:3–12.
- Key R. M. (1983) *The Geology of the Area Around Gaborone and Lobatse, Kweneng, Kgatleng, Southern and East Districts*. Geological Survey of Botswana., District Memoir 5.
- Knappett J.A. and Craig R.F., 2012, *Craig's Soil Mechanics*, Spon Press Taylor and Francis, 8th Ed., London, U.K.
- Ngonidzashe I, T., Ratshosa N, Tlhako O, Lekula M, Nyepetsi M, (2014), "The Manyana Cracking Houses Investigations Report", Department of Geological Survey.
- Republic of Botswana, Ministry of Lands, Housing and Environment (2001) *Manyana Development Plan*. Final Development Plan (1999 – 2023).
- Sabat A. K, Pati S (2014), A Review of Literature on Stabilization of Expansive Soil Using Solid Wastes. *Electronic Journal of Geotechnical Engineering*
- Van der Merwe, D.H., (1964) The prediction of heave from the plasticity index and the percentage clay fraction of soils. *The Civil Engineer in South Africa*. June 1964, pp 103-107.
- Zornberg J.A, Kuhn, A, J, Plaisted, M, D, (2008), Characterization of the Swelling Properties of Highly Plastic Clays Using Centrifuge Technology, Texas Department of Transportation, Research and Technology Implementation Office.

Publisher's note: [Scienceline Publication](#) Ltd. remains neutral with regard to jurisdictional claims in published maps and institutional affiliations.



Open Access: This article is licensed under a Creative Commons Attribution 4.0 International License, which permits use, sharing, adaptation, distribution and reproduction in any medium or format, as long as you give appropriate credit to the original author(s) and the source, provide a link to the Creative Commons licence, and indicate if changes were made. The images or other third party material in this article are included in the article's Creative Commons licence, unless indicated otherwise in a credit line to the material. If material is not included in the article's Creative Commons licence and your intended use is not permitted by statutory regulation or exceeds the permitted use, you will need to obtain permission directly from the copyright holder. To view a copy of this licence, visit <https://creativecommons.org/licenses/by/4.0/>.

© The Author(s) 2024

Evaluation of the Compressive Strength and Sorptivity of Pozzolanic Concrete Containing Calcined Termite Mound

Catherine Mayowa Ikumapayi¹, Chinwuba Arum¹, Victor Arum¹, Michael Olamide Omoyajowo¹,
Oluwafemi Oluwademilade Omotayo¹, and Ogaga Junior Ohwofasa²

¹Department of Civil and Environmental Engineering, Federal University of Technology, Akure, Ondo State, Nigeria

²Department of Civil Engineering and Water Resources, University of Delta, Agbor, Delta State, Nigeria

✉ Corresponding author's Email: cmikumapayi@futa.edu.ng

ABSTRACT

Pozzolans have long been established as viable materials for the partial replacement of cement in concrete. However, the extent to which they can be used is still under investigation. Pozzolans do not in themselves have cementitious value but can react chemically with calcium hydroxide and moisture to produce cementitious compounds. Pozzolanic concretes have been reported to have varied properties in term of compressive strength and durability properties which need to be ascertained. This research focuses on Calcined Termite Mound (CTM) and its influence on the compressive strength and sorptivity of concrete. Several tests were carried out to ascertain the physical, chemical, and mineralogical properties of CTM and conventional concrete constituents. Some of these tests include bulk density, setting time, aggregate crushing value (ACV), aggregate impact value (AIV), slump test, X-Ray Fluorescence (XRF), X-Ray Diffraction (XRD), sorptivity, and compressive strength tests. Compressive strength tests results for concrete containing Ordinary Portland Cement (OPC) and CTM cement blends show that CTM has higher silica content compared to OPC and can be classified as Class-N pozzolans. It is also richer in calcium oxide. The study also reveals that CTM has an optimum replacement level of 5% with strength of 13.4 MPa at 28 days, which is higher than the 12.4 MPa of control concrete. Also, the result of sorptivity test for OPC-CTM blended concrete gave lower resistance to sorptivity. Regression models were developed to predict the compressive strengths of OPC-CTM concrete as a function of % replacement level and curing age.

Keywords: Calcine termite mound; Compressive strength; Pozzolanic concrete; Sorptivity.

INTRODUCTION

Concrete, an essential for construction material, poses significant environmental challenges due to material consumption and CO₂ emissions from Portland cement manufacturing. Therefore, transitioning to sustainable concrete construction practices is imperative to mitigate these impacts. This involves reducing concrete usage in buildings and replacing Portland cement with supplementary cementitious materials derived from industrial by-products, such as fly ash and slag. [Altair and Kabir \(2010\)](#) asserts the increasing use of pozzolans in the cement industry due to their environmental sustainability. Natural pozzolans help reduce carbon dioxide emissions by decreasing cement production and consumption, thereby mitigating the release of greenhouse gases into the atmosphere. [Sapal and Wegner \(2017\)](#) reveals that for a long time, the practice of combining Portland cement and pozzolanic materials for the purpose of construction has been prevalent. Albeit, in time past, an advanced knowledge of the characteristics of these materials and their impact on concrete had not been completely understood. However, studies are now being

carried out to determine the physical, chemical, and mechanical properties of these pozzolans, and how they affect the performance of concrete mixes.

Pozzolans are solid materials with little or no cementitious value, composed of aluminous, siliceous, or amorphous siliceous content. When these materials react with calcium hydroxide [Ca (OH)₂] in the presence of water, they form compounds with properties like that of cement through cement hydration reactions ([Bumanis et al., 2020](#)). This pozzolanic reaction leads to increase in some mechanical properties of concrete such as compressive, tensile, and flexural strength, modulus of elasticity and durability ([Dembovska et al., 2017](#)). Pozzolans occur naturally and industrially. Examples of natural pozzolans are zeolite and volcanic pumice. On the other hand, artificial pozzolans include agricultural and industrial byproducts such as rice husk and fly ash. No matter the form in which they occur, these materials find use in being added to cement, as they produce some added benefits to a concrete mix.

[Khan and Alhozaimy \(2011\)](#) opine that pozzolans offer economic benefits by replacing the expensive portion of Portland cement with a more affordable natural or

RESEARCH ARTICLE
 PII: S225204302400036-14
 Received: June 25, 2024
 Revised: September 02, 2024
 Accepted: September 05, 2024

artificial pozzolan. They also postulated that pozzolans increase the strength and durability of concrete mixes, enhancing their resistance to sulfate and thermal attack, as well as improving chemical durability. The performance of concrete mixes produced from the use of pozzolanic materials depends on the type of pozzolan, each possessing its unique characteristics, including fineness ratio, surface area, thermal properties, corrosion resistance, and mechanical properties like compressive strength, flexural strength, shrinkage and creep, and modulus of elasticity. These properties influence the characteristics of concrete (Al-chaar and Alkadi, 2013).

Ikumapayi *et al.*, (2023) highlighted the potential use of termite mounds as pozzolans, both in calcined and uncalcined forms, for concrete production. The results indicate that calcined termite mounds exhibit comparable compressive strengths to control mixes, suggesting their potential for concrete applications, while uncalcined termite mounds show lower strengths, making them more suitable for termite mound blocks. Similar study on the potential of uncalcined soldier-ant mound clay in improving the strength characteristics of cement concrete beam was investigated. The results showed that while SAMC reduced concrete density and increased setting times, with increase in SAMC content (Ikponmwosa *et al.*, 2019). An optimal 5% SAMC content improved structural performance compared to normal concrete. The performance of blended cement mortar mixtures containing termite mound and lime for building construction was assessed. Tests conducted on 50 x 50 x 50 mm cube specimens evaluated compressive strength, water absorption, and resistance to magnesium sulphate exposure. Results demonstrated that compressive strength increased with age but decreased with higher percentage replacements of cement with lime and termite mound. Notably, at 25% termite mound content, compressive strength increased by 66.73%, 69.23%, 84.62%, and 100% at curing ages of 7, 14, 21, and 28 days respectively, suggesting that up to 25% replacement of termite mound and lime is suitable for mortar composition (Olanrewaju *et al.*, 2019).

Guyo *et al.*, (2019) explores the potential of calcined termite hill clay powder (CTHCP) as a partial replacement for ordinary Portland cement in C-25 grade concrete production. The research involved collecting samples from the Bokuluboma vicinity, calcining them at 650°C, and assessing their chemical composition. Various properties of concrete mixes with CTHCP replacing cement were investigated, revealing that up to 11.3% replacement achieved the target compressive strength of 34MPa at 28 days. Moreover, the mix remained workable up to 25% replacement, with faster setting times compared to the control mix, suggesting CTHCP as a suitable partial cement replacement, especially at 11.3% for C-25 grade concrete production.

It is a known fact that pozzolanic materials improve the properties of concrete mixes such as durability,

compressive strength, and workability. However, the extent to which these pozzolanic materials influence the performance of concrete when they partially replaced with of Portland cement in concrete mixes has not been fully explored. Also, the effects of some pozzolanic materials like rice husk ash, sugarcane bagasse ash, fly ash, palm oil fuel ash on the properties of concrete has been studied considerably to a great extent. Meanwhile, little or no research has been done on calcined termite mound to determine its influence on the performance of concrete. This study focuses on evaluating the sorptivity and compressive strength performances of concrete mixes with calcined termite mound blends with the view of establishing its industrial acceptability. This study also provide regression models for the prediction of the compressive strength of the resulting pozzolanic concrete.

MATERIALS AND METHOD

Materials

The materials used for this study were sourced from Akure, Nigeria and tested to ensure that they meet all the necessary standards. Dangote Portland cement, grade 42.5, type 1 general-purpose cement as per the American Society for Testing and Materials Standards - ASTM C150, (2012) was obtained from a retail shop outlet within Akure metropolis, Ondo State, Nigeria. Termite mound was obtained from a farmland in the Federal University of Technology Akure and heated at a controlled temperature of 600°C to produce calcined termite mound, which was used as the pozzolanic material. The portion of the calcined termite mound (CTM) finer than sieve No 425 were used. Also, an X-ray Fluorescence (XRF) analysis, and X-ray diffraction (XRD) test were carried out to determine the chemical and the mineralogical composition of the calcined soil. The physical properties of the binder are shown in Table 1.

Table 1. Physical properties of the binders

Properties / Parameters	OPC	CTM
Specific gravity (kg/m ³)	3.02	2.53
Initial setting time (minutes)	75	-
Final setting time (minutes)	270	-
Normal consistency (%)	26	-
Moisture content (%)	-	16.35
Dry density (g/cm ³)	-	0.458

The oxide composition of calcined termite mound are presented in Table 2. Based on ASTM C618 (2019), the calcined termite mound is Class N; since the sum of SiO₂, Fe₂O₃, and Al₂O₃ is greater than 70% and the composition of SO₃, is not up to 4%. Notably silica content is significantly higher (56.176%) than any other oxide in the material.

Table 2. Chemical composition of the calcined

Composition	Concentration (%)
SiO ₂	56.176
Al ₂ O ₃	19.49
Fe ₂ O ₃	13.079
CaO	0.949
MgO	0.00
SO ₃	0.181
TiO ₂	4.517
LOI	3.86
SiO ₂ +Al ₂ O ₃ +Fe ₂ O ₃	88.742

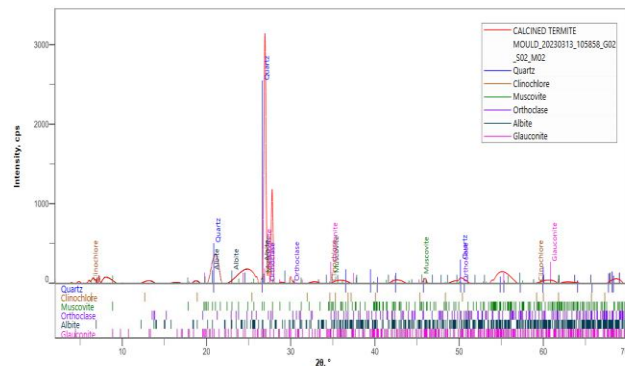


Figure 1. XRD Analysis of Calcined Termite Mound

The minerals found in the CTM sample are outlined in Figure 1. Quartz was identified as the primary crystalline phase, followed by Orthoclase. Traces of minerals such as Muscovite, Albite, Clinoclase, and Glauconite were also present in the specimen, exhibiting smaller but well-dispersed peak intensities compared to Quartz and Orthoclase. However, the highest peak intensities were detected at approximately $2\theta = 27^\circ$ and 28° for Quartz and Orthoclase, respectively.

The aggregates used in this study include fine and coarse aggregate. The coarse aggregate consists of crushed granite with maximum sizes of 12.5mm, sourced within the Akure metropolis and used in all concrete mixes. These coarse aggregates conform to the recommendations of British Standards - BS 882, (1992). The fine aggregate comprises sand with particle sizes finer than 4.75mm, sourced from a local quarry in Akure, Ondo State, Nigeria. The physical properties of both the coarse and fine aggregates used for the tests are presented in Table 3.

Potable water, sourced from a borehole in a construction site within the Federal University of Technology Akure, was used to cast and cure the concrete specimens. This water meets the requirements of concrete mixing water as per British Standards (BS EN, 1997).

Table 3. Physical properties of coarse and fine aggregates

Properties	Result
Specific gravity (kg/m ³) of sand	2.35
Aggregate crushing value (ACV) of granite	21.44%
Aggregate impact value (AIV) of granite	11.34%
Bulk density (kg/m ³) of granite	1528.7

Method

- Mix design:

A series of trial mixtures was conducted to establish the suitable mix design for the proposed concrete mixtures of grade 20 MPa. Dangote Portland cement was partially replaced with the Calcined Termite Mound (CTM), in a level of 5% to 20% at a 5% step size increment. A total of 45 concrete cube test specimens were produced to evaluate the compressive strength and 45 cylindrical test specimens for sorptivity evaluation. These concrete cube test specimens were produced using a mix ratio 1:2:4, and a constant water-binder ratio of 0.55.

- Preparation, casting and curing of pozzolanic concrete:

The cement, CTM, fine and coarse aggregates were measured by weight and then manually mixed. The mixing was done very well to achieve a thorough mix. Slump and compacting tests were used for the workability assessment (British Standards - BS 1881-103, 1993). For each test day and replacement level, a total of 3 concrete cubes with side dimension of 150mm x 150mm x 150mm were cast for the compressive strength test; while 3 cylindrical concrete samples with 100mm diameter and 50mm thickness were cast for the sorptivity test. The cast samples were left for 24 hours before being demolded from its form and placed in a water tank. The concrete samples were cured (by immersion in water) for 7, 28, and 56days. For each curing age, 15 test specimens for compressive strength and 15 test specimens for sorptivity test were evaluated.

- Test on hardened concrete:

Compressive strength of the concrete samples were determined with the use of universal compressive machine with a load capacity of 1000kN, and load rate of 0.5MPa/s. The test procedure was in accordance with the standard (ASTM C 39, 2001). At each test day, three test specimens from each mixes were tested and the average of these readings was taken as the compressive strength of that mix.

The sorptivity test was carried out as per the requirements of American Society for Testing and Materials Standards - ASTM C1585, (2013). This test allows for one directional flow of water through the unsealed end of the concrete. The setup for sorptivity test is shown in Figure 2. Before this test was carried out, the weight and diameters of all the test specimens were measured. A plastic tray of water to a depth of 3mm was

held to the ground and the unsealed surface of the specimens was placed over steel supports inside the tray.

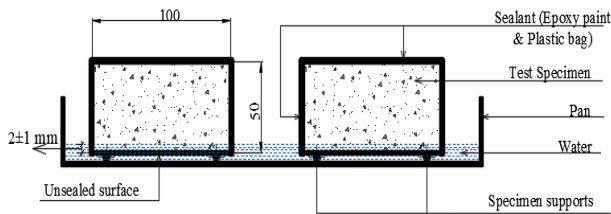


Figure 2. Setup for water absorption test (Ohwofasa et al., 2023).

The initial mass and the masses of the samples after it was partially placed in water to a depth of 3mm at time intervals of 1, 2, 4, 8, 10, 20, 30, 110, and 120 mins, was recorded. During the test, water was re-filled into the tray to maintain a water depth of 3mm. The water absorption rate (i) is calculated using the Equation 1.

$$i = \frac{m_b - m_a}{a \times d} \text{ mm} \quad 1$$

Where:

$m_b - m_a$ is the change in specimen mass in grams, at the time t ,

a is the exposed area of the specimen, mm^2 ; d = density of the water, g/mm^3

The sorptivity coefficient, S is the slope of the best fit line of a graph of water absorption rate, i against the square root of time, t in secs.

RESULTS AND DISCUSSIONS

Fresh concrete properties

The slump and compacting factor test results are shown in Table 4. The results show that the slump values and compaction factor of the cement mix decreased with an increase in the percentage replacement level of CTM. Hence, the slump value and compaction factor are highest at control (0%) and lowest at 20% replacement levels. The decrease in the slump and compacting factor values with increasing proportions of CTM is an indication of low workability of the mix (Fapohunda and Daramola, 2019).

Table 4. Effect of CTM on workability properties of concrete

Mix Designation	Slump	Compaction Factor	Workability	Type
B1 (0%)	50	0.88	Stiff Plastic	TRUE
B1-2 (5%)	45	0.82	Stiff Plastic	TRUE
B1-3 (10%)	42	0.80	Stiff Plastic	TRUE
B1-4 (15%)	40	0.78	Stiff Plastic	TRUE
B1-5 (20%)	35	0.76	Stiff Plastic	TRUE

The results of the workability from the slump test satisfied the specified range of 35mm to 50mm. Likewise the results from compacting factor test which ranges between 0.76 and 0.88 fell within the specified range of 0.7 to 0.99. The outcomes of the two tests show the workability to be satisfactory.

Hardened concrete properties

Compressive strength:

The compressive strengths of the OPC-CTM concrete mixes at days 7, 28, and 56 of curing are depicted in Figure 3. A progressive decrease in compressive strength was observed with increasing CTM replacement. The compressive strength ranged from 8.2 to 13.4 MPa at day 28 and 8.8 to 13.9 MPa at day 56. While the compressive strength of all test samples increased with curing duration, the rate of strength development slowed after day 28. Notably, the 5% CTM replacement (designated as B1-2) exhibited the optimum compressive strength at all curing ages, with values of 10.6 MPa, 13.4 MPa, and 13.9 MPa for days 7, 28, and 56, respectively. At day 28, mix B1-2 surpassed the compressive strength of the control mix by 8%. This improvement suggests a pozzolanic reaction between CTM and the calcium hydroxide (Portlandite) released during cement hydration.

The decrease in compressive strength with higher CTM replacement levels can be attributed to the overconsumption or dilution of Portlandite, hindering the formation of additional hydration products and consequently impacting overall concrete strength. The trends in the strength development of the CTM concretes are similar to those reported in the literature (Elinwa, 2006; Olaniyi and Umoh, 2014).

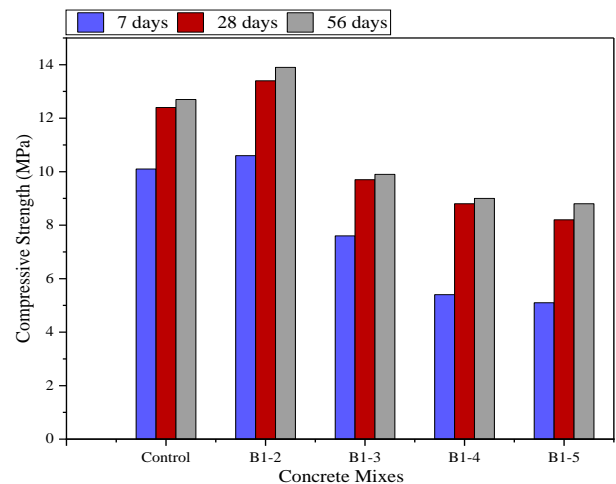


Figure 3. Compressive strength development.

Sorptivity:

The rate of water absorption of the concrete mixes at day 28 is illustrated in Figure 4. A regression analysis was employed to fit a line to the data, plotting the amount of absorption (in millimeters) against the square root of time

(in seconds). The slope of this line provides the sorptivity of the concrete mixes.

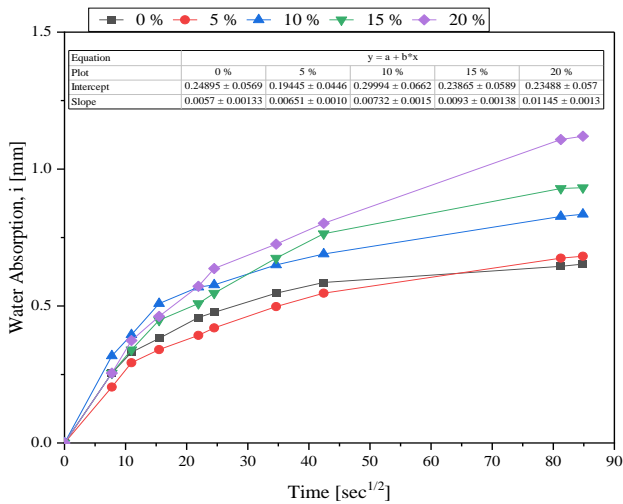


Figure 4. The rate of water absorption of the concrete mixes at day 28.

The sorptivity for all test specimens at day 28 is illustrated in Figure 5. The sorptivity coefficient generally exhibited an upward trend with an increase in CTM replacement. The control mix demonstrated the lowest sorptivity value (0.0057 mm/sec^{1/2}), whereas the 20% CTM replacement level exhibited the highest sorptivity value (0.0115 mm/sec^{1/2}). The percentage increase of the CTM mixes with respect to the control was 14.2%, 28.4%, 63.2%, and 100% for the mixes designated with 5%, 10%, 15%, and 20% replacement, respectively. The addition of calcined termite mound to the cement resulted in an increase in the resulting concrete’s sorptivity. This outcome can be attributed to the porosity and absorbent properties of calcined clay to water. Previous studies have shown that the incorporation of calcined brick powder as a supplement for cement up to 40% led to an increase in both porosity and sorptivity (Mohan *et al.*, 2020).

- Mineralogical characterization and scanning electron microscopy:

The mineralogical composition of the calcined termite mound (CTM) concrete samples for days 28 and 56 is presented in Figures 6 and 7, respectively. It is noteworthy that the initial crystalline phases underwent considerable changes during the hydration of the CTM concrete. At days 28 and 56, Calcite, Portlandite, Quartz, and Lime were found to be widely distributed in the spectrum. However, minerals such as Muscovite, Orthoclase and Osumilite exhibited smaller constructive peak intensities compared to other minerals, possibly attributed to differences in atomic arrangement or packing patterns. Minerals such as Calcite, Portlandite, Quartz, and Lime displayed more noticeable peaks in the crystalline phase. The highest peak intensity was observed at approximately

2θ = 30° for Calcite, while other minerals with noticeable peaks fell within the range of 2θ = 18 - 50°.

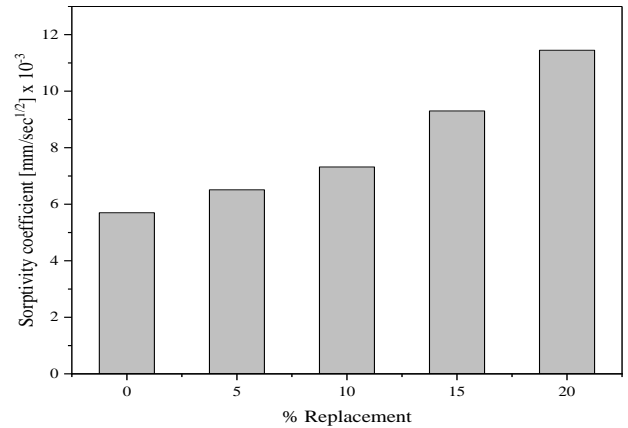


Figure 5 Sorptivity coefficients of the OPC-CTM concrete mixes at day 28

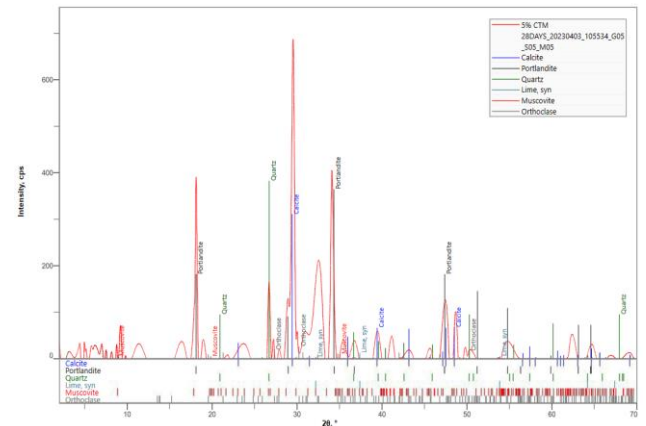


Figure 6. XRD Analysis of 5% replacement CTM concrete at day 28

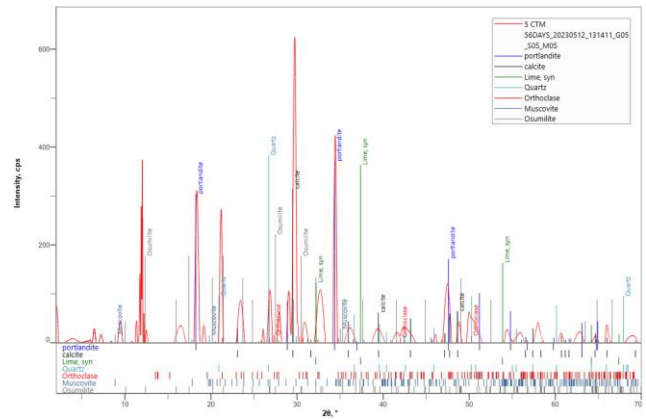


Figure 7. XRD Analysis of 5% replacement CTM concrete at day 56

The microstructure of the referenced concrete, and the 5% CTM replacement concrete at 7 and 28 days are shown in Figure 8 and Figure 9. To investigate the morphology of the test samples, the pore sizes of the samples were measured using ImageJ, and their average size was determined using Gaussian analysis on OriginPro. The larger pore sizes were observed in the control mix, compared to the 5% CTM replacement mix. However, the pore in both mixes decreased in size as the hydration days increases. At day 7, the pore sizes for the control mix and the 5% CTM replacement mix were 3.78, and 3.08 micro meter respectively. At day 28, the pore sizes of the mixes reduced by 22% (2.93 micro meter) for the control

and 43% (1.75 micro meter) for the 5% CTM replacement mix. The reduction in pore size and the densified structure in the mixes resulted from some hydration and pozzolanic activities. At the early period of hydration, it is observed that the radiating crystals of C-S-H were widely spread through the CTM blended mix. The dense structure of the mixes is evident on the compressive strength test results but not on the sorptivity. Ettringite was not observed in either mix at day 28 but there were traces of cracks; the absence of ettringite could be due to the low sulphate content in the binder which can react with the available Portlandite.

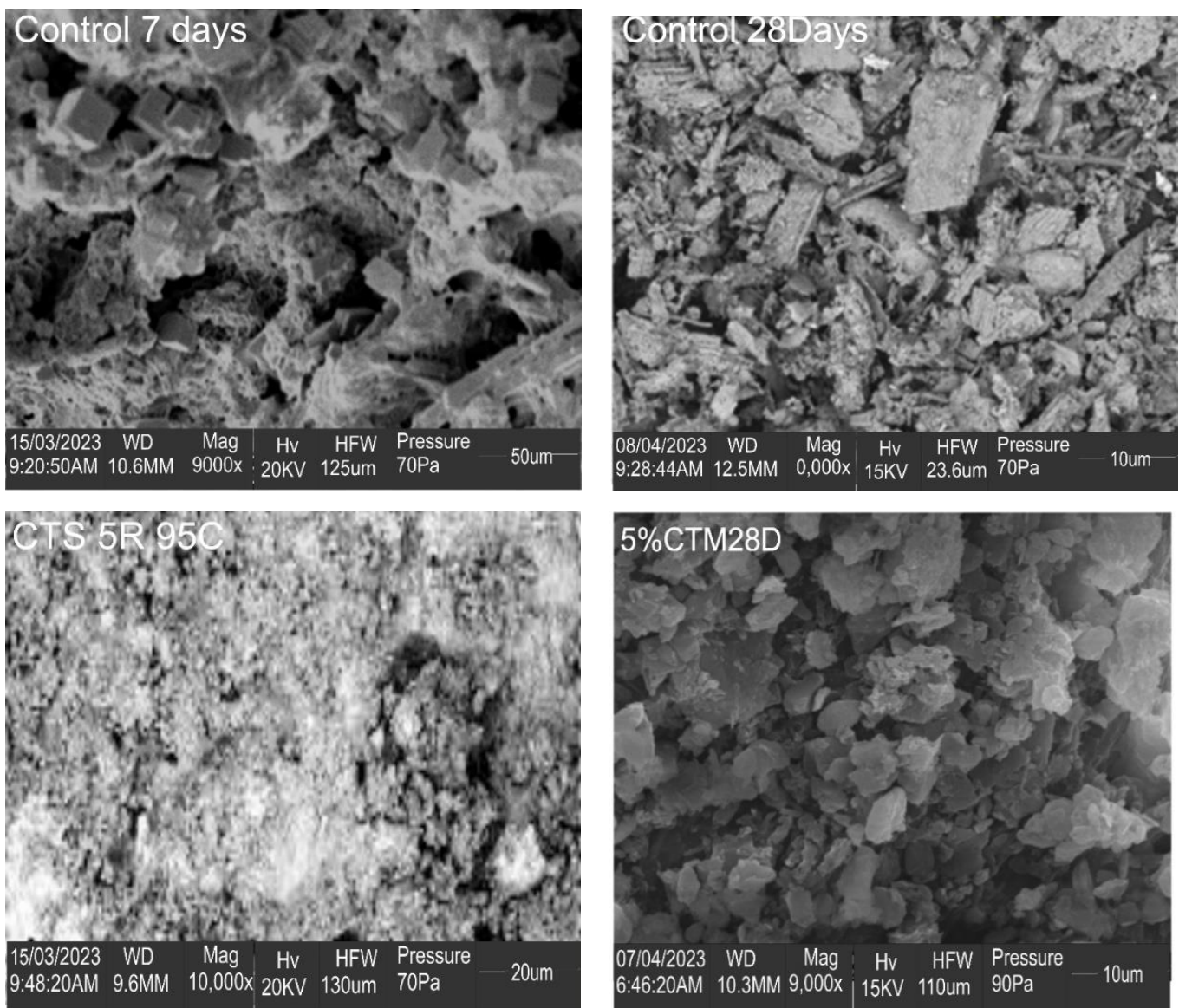


Figure 8. Scanning electron microscopy of the control specimen and 5% CTM replacement specimen at day 7 and 28

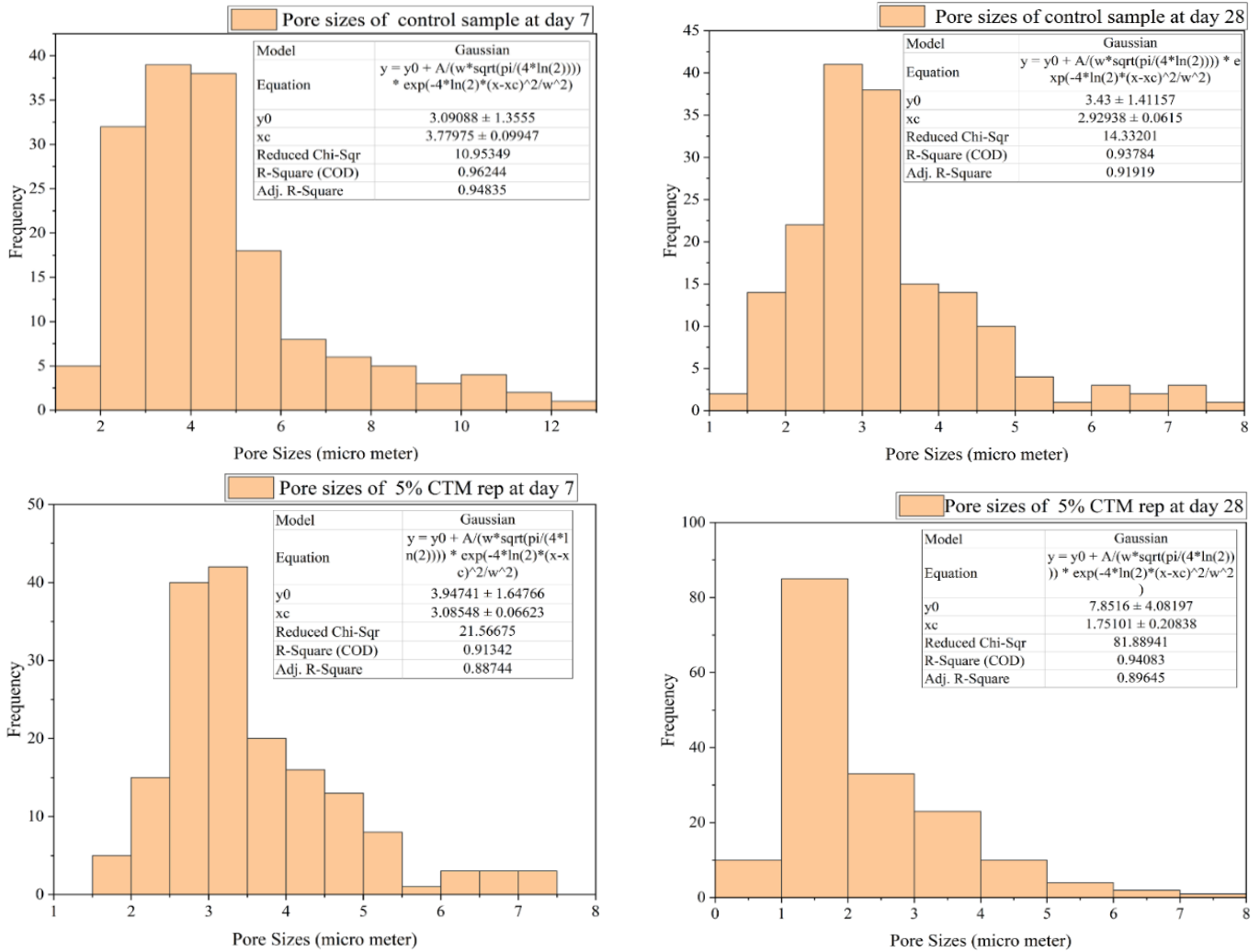


Figure 9. Pore sizes of the control specimen and 5% CTM replacement specimen at day 7 and 28

REGRESSION ANALYSIS

Linear Regression Model for Concrete Containing OPC-CTM Cement Blends:

The Linear Regression (LR) Model was constructed using a single independent variable, Calcined Termite Mound (CTM), and one dependent variable, compressive strength (CS). The mathematical model was developed to establish the relationship between the compressive strength of concrete mixes and CTM replacement levels (0%, 5%, 10%, 15%, and 20%) after 28 days of curing. The derived predictive model for the relationship between compressive strength of concrete and OPC-CTM replacement level at 28 days is as shown in Equation 2 with R^2 of 0.81 and F (12.87) considerably higher than *Significance F* (0.037) and *P-value* (0.00067501) significantly lower than 0.05.

$$y = 13.1 - 0.26CTM \quad 2$$

where:

y is the compressive strength of the concrete

CTM is Calcined Termite Mound (replacement percentage)

Multiple Linear Regression (MLR) Model Containing OPC and CTM Cement Blends:

The Multiple Linear Regression (MLR) model was constructed utilizing two distinct independent variables: Calcined Termite Mound (CTM) and Curing Age (CA), along with a dependent variable denoting compressive strength. MLR was employed to create a mathematical model aimed at predicting the compressive strength of the OPC-CTM cement blend, given specific CTM replacement levels and curing ages.

The mathematical model used for predicting the compressive strength of the CTM blended concrete samples is presented in Equation 3.

$$y = 10.592 + 0.056CA - 0.266CTM^3$$

where: y is the compressive strength of the concrete

CTM is Calcined Termite Mound (replacement percentage); CA is curing age (days)

CONCLUSION

This study evaluates the effects of CTM on the compressive strength and sorptivity properties of concrete, and the following conclusive remarks were drawn from the analyzed results and discussions:

i. the compressive strength of the test concrete mixes reduced with increase in CTM replacement while the sorptivity increased with increased in CTM replacement. In terms of compressive strength, the 5% CTM replaced concrete exhibited the optimum strength value at all curing days while the control gave best results in terms of sorptivity.

ii. the linear regression model and multiple regression model developed can be used to predict the compressive strength of OPC-CTM concrete as a function of curing age and % replacement level of OPC with CTM.

DECLARATIONS

Corresponding author

Correspondence and requests for materials should be addressed to ; cmikumapayi@futa.edu.ng; ORCID Id-0000-0002-0652-6332

Acknowledgement

The authors appreciate the Tertiary Education Trust Fund (TETFund) in Nigeria for funding this research from Institution Based Research Fund (IBRF) 2018-2019 with reference number VCPU/TETFund/155C. The host Institution, Federal University of Technology, Akure is also well appreciated

Data availability

The datasets used and/or analysed during the current study available from the corresponding author on reasonable request.

Author's contribution

C. M. Ikumapayi contributed in the area of conceptuality, statistics and editing, writing original

manuscript, review and editing, C. Arum contributed to the research in the area of statistics and editing, review and editing, V. Arum contributed to the research in the area of methodology, data analysis, and manuscript writing. M. O. Omoyajowo, contributed to the research in the area of methodology, data analysis, and manuscript writing, O.O. Omotayo, contributed to the research in the area of statistics, validation and editing, and O.J.Ohwofasa, contributed to the research in the area of statistics, data analysis, and manuscript writing.

Competing interests

The authors declare no competing interests in this research and publication.

REFERENCES

- Al-chaar GK, and Alkadi M (2013). Natural Pozzolan as a Partial Substitute for Cement in Concrete. *The Open Construction and Building Technology Journal*, 7, 33–42. DOI: [10.2174/1874836801307010033](https://doi.org/10.2174/1874836801307010033).
- Altwair NM, and Kabir S. (2010). Green concrete structures by replacing cement with pozzolanic materials to reduce greenhouse gas emissions for sustainable environment. *6th International Engineering and Construction Conference (IECC'6)*, Cairo, Egypt, 17(3), 269–279. [link](#)
- American Society for Testing and Materials Standards - ASTM C 39. (2001). Standard Test Method for Compressive Strength of Cylindrical Concrete Specimens. *ASTM International*, 04(02), 1–5. [link](#)
- American Society for Testing and Materials Standards - ASTM C150/C150M. (2012). Standard Specification for Portland Cement. *ASTM International*, 1–9. [link](#)
- American Society for Testing and Materials Standards - ASTM C1585. (2013). Standard Test Method for Measurement of Rate of Absorption of Water by Hydraulic-Cement Concretes. *ASTM International*, 41(147), 1–6. [link](#)
- American Society for Testing and Materials Standards - ASTM C618. (2019). Standard Specification for Coal Fly Ash and Raw or Calcined Natural Pozzolan for use in Concrete. *ASTM International*, 3–6. [link](#)
- British Standards - BS 1881-103. (1993). Method for determination of compacting factor. *BSI Standards Institute*. [link](#)
- British Standards - BS 882. (1992). Specification for Aggregates from natural sources for concrete. In *British Standards*. British Standards Institute. [link](#)
- BS EN, 1008. (1997). Mixing water for concrete: *British Standard*. [link](#)
- Bumanis G, Vitola L, Stipniece L, Locs J, Korjajins A., and Bajare D. (2020). Evaluation of Industrial by-products as pozzolans: A road map for use in concrete production. *Case Studies in Construction Materials*, 13, 424. <https://doi.org/10.1016/j.cscm.2020.e00424>
- Dembovska L, Bajare D, Pundiene I, and Vitola L. (2017).











- Effect of Pozzolanic Additives on the Strength Development of High Performance Concrete. *Procedia Engineering*, 172, 202–210. <https://doi.org/10.1016/j.proeng.2017.02.050>
- Elinwa AU (2006). Experimental characterization of Portland cement-calcined soldier-ant mound clay cement mortar and concrete. *Construction and Building Materials*, 20(9), 754–760. <https://doi.org/10.1016/j.conbuildmat.2005.01.053>
- Fapohunda CA, and Daramola DD (2019). Experimental study of some structural properties of concrete with fine aggregates replaced partially by pulverized termite mound (PTM). *Journal of King Saud University - Engineering Sciences*. <https://doi.org/10.1016/j.jksues.2019.05.005>
- Guyo KD, Emer TQ, and Getachew K. (2019). Calcined Termite Hill Clay Powder: As Partial Cement Replacement in Production of C-25 Grade Concrete. *American Journal of Civil Engineering and Architecture*, 7(3), 128–134. DOI: [10.12691/ajcea-7-3-2](https://doi.org/10.12691/ajcea-7-3-2)
- Ikponmwosa E, Salau M, and Mustapha S. (2019). Strength Characteristics of Concrete Beams with Cement Partially Replaced by Uncalcined Soldier-Ant Mound Clay. *Second International Conference on Advances in Engineering and Technology*, 402–408. <http://ir.unilag.edu.ng:8080/xmlui/handle/123456789/792>
- Ikumapayi CM, Arum C, Olaseinde OA, Omotayo OO, and Oniwide EO (2023). Potential of Calcined and Uncalcined Termite Mounds as Pozzolans in Concrete Mix. *FUOYE Journal of Engineering and Technology*, 8(3), 371–376. <https://doi.org/10.46792/fuoyejt.v8i3.996>
- Khan MI and Alhozaimy AM (2011). Properties of natural pozzolan and its potential utilization in environmental friendly concrete. *Canadian Journal of Civil Engineering*, 38(1), 71–78. <https://doi.org/10.1139/L10-112>
- Mohan M, Apurva A, Kumar N, and Ojha A (2020). A Review on Use of Crushed Brick Powder as a Supplementary Cementitious Material. <https://doi.org/10.1088/1757-899X/936/1/012001>
- Ohwofasa JO, Ikumapayi CM, and Arum C (2023). Effects of Fly Ash on Compressive Strength and Durability Properties of Lean Concrete. *Journal of Applied Sciences and Environmental Management*, 27(11), 2597–2610. <https://doi.org/10.4314/jasem.v27i11.32>
- Olaniyi A and Umoh AA (2014). Influence of Curing Media on the Compressive Strength of Termite Mound-Lime Blended Cement Mortar. *Malaysian Journal of Civil Engineering*, 26(3), 349–365. <https://doi.org/10.11113/mjce.v26.15896>
- Olanrewaju SB, Akinpelu S and Olaniyi A (2019). Durability of Termite Mound Lime-Blended Cement Mortar Mixtures. *International Journal of Engineering and Innovative Technology*, 9(6), 10–16. DOI: [10.17605/OSF.IO/CM9AT](https://doi.org/10.17605/OSF.IO/CM9AT)
- Sapal SS, and Wegner LD (2017). Effectiveness of a natural pozzolan from southern Saskatchewan for cement replacement in concrete. *6th International Conference on Engineering Mechanics and Materials 2017*, 1, 385–392. [link](#)

Publisher's note: [Scienceline Publication](#) Ltd. remains neutral with regard to jurisdictional claims in published maps and institutional affiliations.



Open Access: This article is licensed under a Creative Commons Attribution 4.0 International License, which permits use, sharing, adaptation, distribution and reproduction in any medium or format, as long as you give appropriate credit to the original author(s) and the source, provide a link to the Creative Commons licence, and indicate if changes were made. The images or other third party material in this article are included in the article's Creative Commons licence, unless indicated otherwise in a credit line to the material. If material is not included in the article's Creative Commons licence and your intended use is not permitted by statutory regulation or exceeds the permitted use, you will need to obtain permission directly from the copyright holder. To view a copy of this licence, visit <https://creativecommons.org/licenses/by/4.0/>.

Estimation of Water Demand for the Rural Population in the Angolan Part of the Iishana System

André M. Chiweyengue¹  , Evanilton E. Serrão Pires² , Busari, O. Afis¹ , Valentine Yato Katte¹ , Petrina Johannes¹ ,
Monique Fahrenberg³ , Christian Reinhardt-Imjela³ , Achim Schulte³  and Robert Jüpner⁴ 

¹Department of Civil and Mining Engineering, University of Namibia, Ongwediva, Namibia

²Departamento de Engenharias, Instituto Superior Politécnico Tundavala, Lubango, Angola

³Freie Universität Berlin, Institute of Geographical Science, Applied Physical Geography – Environmental Hydrology, Germany

⁴Technische Universität Kaiserslautern-Landau, Germany

✉ Corresponding author's Email: andrechiweyengue9@gmail.com

ABSTRACT

The Iishana is a shallow, low-slope channel system located in the Cuvelai basin (Southern Angola and Northern Namibia), characterised by drought and flood cycles due to erratic climate variability. The knowledge gap regarding the actual water needs in the area, the number of residents within the system, the seasonal influence of cattle migration, and poor socio-economic conditions, make the population even more vulnerable to droughts. The main objective of this study is to estimate the water demand by the rural population on the Angolan side of the Iishana system, attempting to fill the knowledge gap. To reach the demand estimates, a mathematical procedure within a GIS environment was used, in QGIS 3.32.2 software, relating population gridded and meteorological data to make the necessary calculations. In 2023, it estimated consumption for intake and personal hygiene of 4.7 Mm³, 6.3 Mm³ for 2033, 8.4 Mm³ for 2043 and 11.3 Mm³/year for 2053. In recent years there have been rainfall records throughout the Iishana system, at an average of 518 mm/annum, but high temperatures accelerate water evaporation. Due to the topographical conditions, the waters are drained by gravity to the south of the basin (Republic of Namibia), causing a greater shortage in the dry season on the Angolan side, the study targets the estimation of water demand and the concept of rainwater harvest and sustainable water infrastructure to supply safe drinking water to equalise water demand and reduce vulnerability to climate change. These early findings may provide a basis for developing sustainable water infrastructure and use plans to improve the livelihoods of the resident population within the basin.

Keywords: Water demand, Water supply, Iishana system, Cuvelai Basin, Water infrastructure.

INTRODUCTION

Water resources are finite, and their demand continues to grow alongside the rising population. Simultaneously, the increasing frequency and intensity of floods and droughts place significant pressure on livelihoods (Seckler, 2000). Effectively evaluating the water requirements of both the population and the environment within the Cuvelai Hydrographic Basin, while ensuring adequate protection against these natural events, presents a considerable challenge. The most active watercourses are confined to the Iishana area. The water in the Iishana Canal area is saline, reflecting the high rates of water evaporation in all the watercourses (Mendelsohn & Weber, 2011).

Once the main courses are reduced and then stop, large areas of water remain in the channels and gradually

dry out, leaving salts that accumulate in the substrate, it isn't easy to access water for human and animal consumption residents along the Cuvelai basin.

MATERIALS AND METHODS

Study area

Figure 1 illustrates the Iishana System, a transboundary wetland shared by Angola and Namibia, spanning approximately 18,370 km². In Angola, a significant portion of the Iishana System lies within the municipalities of Cuanhama, Cuvelai, and Namacunde, situated in the province of Cunene. This area covers roughly 8,711 km², of which 651 km² are inhabited, housing an estimated population of 521,763 individuals, according to (Bondarenko M., 2020), with the coordinates: Northern -16°.47'85N''-15°.26'34 E'', South -

RESEARCH ARTICLE
 PII: S225204302400037-14
 Received: June 25, 2024
 Revised: September 02, 2024
 Accepted: September 05, 2024

17°.37'12N''-15°.25'58E'' West -16°.94'79N''-15°.66'19E'' East -17°.01'93N''-14.78'99E'' Majority of the population lives along the drainage lines of the Iishanas in the southwest, with a mixture of sandy and clay rhinestones more suitable for agriculture than the sandy lands that cover most of the areas to the east and north of the Lishana. Many people also live around the lowlands to the southwest and along small rivers to the north, between the towns of Evale, Mupa and Cuvelai (Helge Denker et al., 2014).

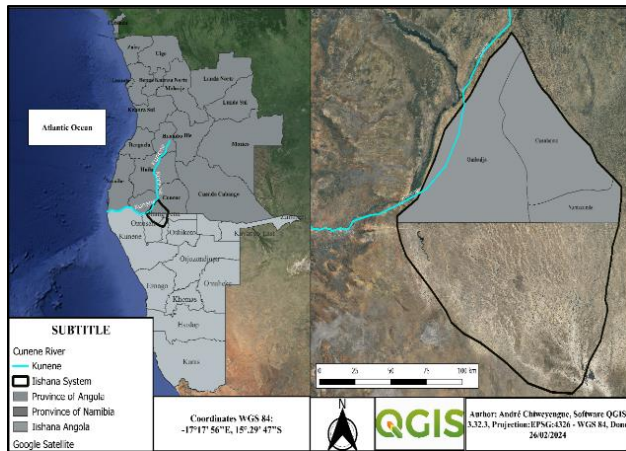


Figure 1. The Angolan part of the Iishana system.

Water demand

The unsustainable and excessive exploitation of natural resources has hindered societal growth over a short period and poses bleak prospects for the future. To address this issue, new strategies must be established that prioritize sustainable development and set clear limits on the use of natural assets, ensuring a balanced approach between utilization and environmental protection (Amaral, 2000). Water demand refers to the volume of water required to supply production and distribution systems, accounting for consumer needs, as well as losses and waste within the system (EEA, 1999).

Estimation of water consumption

The per capita water consumption of a city with a regularly functioning water supply system is determined by dividing the total volume of water distributed annually by the number of inhabitants served (Yassuda et al., 1978). This calculation is expressed mathematically in Eq. 1 and is measured in litres per inhabitant per day (L/person/day).

$$\text{Water consumption} = \frac{V}{365 P} \tag{1}$$

where V is the annual available volume; P is the population

Estimating water consumption in urban public supply systems presents significant challenges due to unreliable data from systematically conducted research. The volume of water needed to supply the basic needs of man and his socioeconomic activities has varied according to the customs and ways of life imposed by the technological transformations that have occurred in recent decades. Netto (1991) Various factors are linked to water consumption patterns, including: (i) Population Growth: Studies reveal that an increase in population typically results in higher per capita water consumption. This rise is largely due to expanded commercial and industrial activities, along with an elevated likelihood of distribution network losses; (ii) Urban Characteristics: The type of urban area significantly impacts water usage levels. For example, water consumption per capita in a tourist town differs from that in an industrial city, with the latter often having higher average consumption and greater water-related costs; (iii) Climate Conditions: Regions with warmer climates generally exhibit higher water consumption. These influences contribute to variations in daily per capita water consumption, which tend to fluctuate based on specific local factors.

Population estimation

Using the WorldPop 2020 dataset to determine the population number, QGIS software processes this data through Zonal Statistics. This algorithm calculates statistical values for a raster layer based on the features of an overlapping polygon vector layer. By applying this method, it aggregates data, such as population estimates, within the defined zones of the polygon layer, providing valuable insights into the spatial distribution of the population.

Analysis of climate data

For the analysis of the climatic data, the data provided by the ERA5 website according to (Hersbach et al., 2023), and data from the last 32 years (1992-2023) were downloaded, analyzed and processed in Python and by QGIS version 3.32.2, interpolated in the Inverse Distance Weighted (IDW) interpolation, it generates a point vector layer. Sample points are weighted during interpolation such that the influence of one point relative to the other declines with the distance from the unknown point to be created.

Calculation of water demand

CSIR (2005) states that water demand is usually based on historical consumption. Where water consumption records are not available, present consumption per capita can be estimated by administering the questionnaire. Estimating water demand requires the following algorithms: (i) Determine the size of the population in the area; (ii) Multiply the population by the average daily water usage per person; (iii) incorporate the peak demand factor to cater for fluctuations in demand and potential water waste

RESULTS AND DISCUSSION

Climate Data Precipitation

The analysis of thirty-one (31) years of data (1992-2023) gives a descriptive minimum average rainfall of 257.2 mm and a maximum of 517.6 mm. Rainfall in the north is approximately twice that of the southern region of the Basin (Figure 2). These usually occur during the wet season, specifically between November and April. This often results in large-volume storms of high frequency at short intervals. Due to the very flat nature of the terrain, the canals flow from north to south, from the southern Angolan plateau to the Etosha pan. Based on the livelihood mode (pastoralism, agriculture, and hunting) of the population residing in the Iishana system, these averages are considered below the threshold of water demand needed for survival. The Basin has a long history of floods and droughts due to the irregularity of rainfall over the last 31 years.

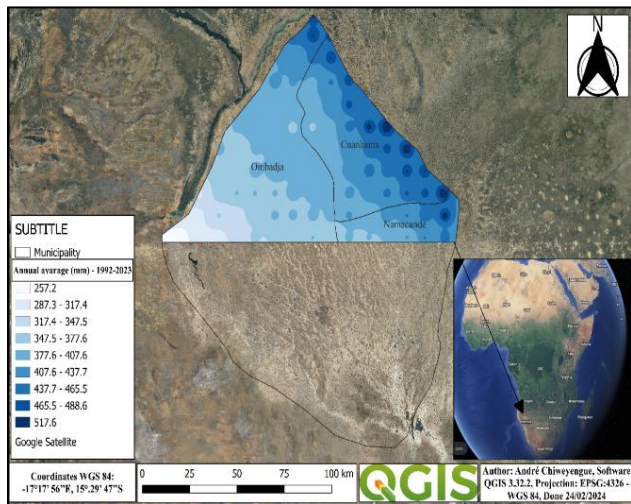


Figure 2. Average annual rainfall (1992-2023) of the Iishana system in mm

Temperature

In the last 31 years (1992-2023), an average temperature of 23° had been observed (Figure 3). The temperatures are highest in the southernmost regions of the basin. Consequently, temperature is one of the major factors that affect the amount of water consumed in the Iishana system of the Cuvelai basin. Therefore, on warmer days, it is common for water consumption to increase, for domestic activities and irrigation of plants. Climate change has an impact on water resources, affecting the water cycle. This is due to changes in precipitation patterns and the role of temperature as it accelerates the evaporation process in the Iishana system.

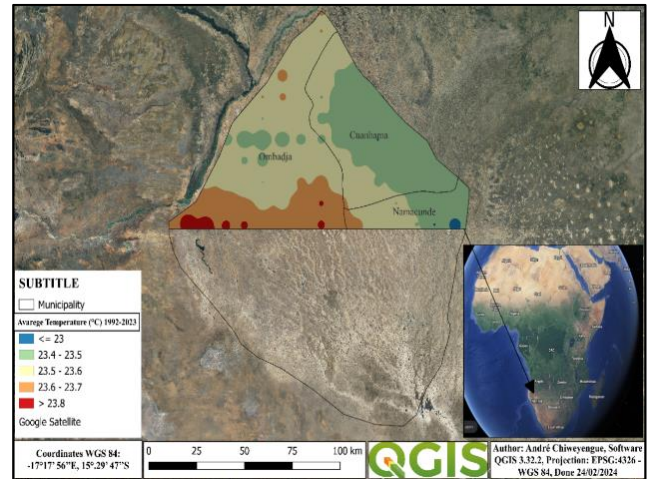


Figure 3. Average annual temperature (1992-2023)

Population Forecast

DATA:

Inhabited area: 651 km²

Rural Population: 426273 inhabitants.

Population growth of 3 % per/year (INE, 2016)

Population projection 2033 (Eq.2)

$$P_{projection} = P_{base\ year} \left(1 + \frac{Annual\ Growth\ Rate\ (\%)}{100} \right)^n \quad (2)$$

Where $P_{base\ year}$ is the base year population (2023)

$$P_{2033} = 426273 \left(1 + \frac{3\%}{100} \right)^{10} = 572875\ inhabitants.$$

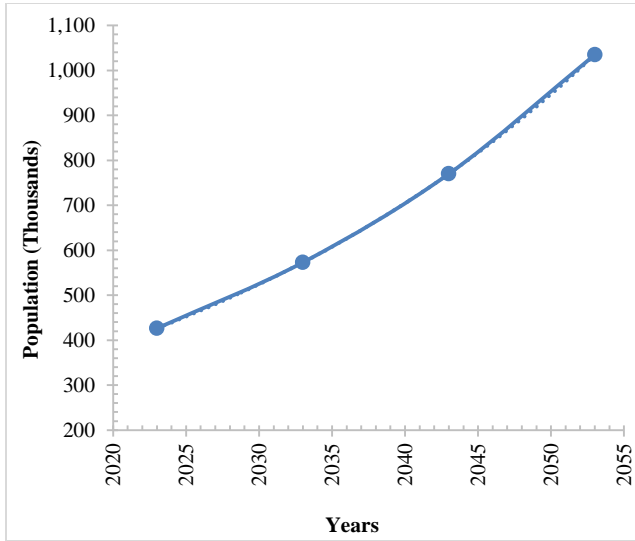


Figure 4. Probable future population (world pop 2020)

Currently, the population of the rural area is 426,273 inhabitants. Figure 4 displays the population forecast for the next three decades. Hence, the population of 572,575, 769,896 and 1,034,676 inhabitants for 2033, 2043 and 2053 respectively. This poses a threat to the available water supply in the future. Consequently, population growth has a range of effects on water consumption, from residential demand to pressure on water resources and the need for sustainable management to address these challenges. It is essential to adopt sustainable strategies to ensure access to water for future generations.

Water demand

According to the (MINEA, 2024), the per capita demand both for intake and personal hygiene, for the population of rural areas should be 30L/person/day. It can be calculated by below formula (Eq.3):

$$Water\ Demand\ (per\ day) = \left(\frac{L/person/day \times P}{1000} \right) \quad (3)$$

$$Water\ Demand\ (per\ day) = \left(\frac{30l/d \times 426273}{1000} \right) =$$

12,788.19m³/day

Annual water demand becomes:

$$f_p \times (12,788.19m^3/day) \times 365 = 4667689.35\ m^3/$$

$$year = \left(\frac{4667689}{1000000} \right) = 4.7Mm^3/year$$

f_p = 1.1 is the peak demand factor (MINEA, 2024)

From Figure 5, the year 2023 yielded a consumption for intake and personal hygiene amounting to 4.7 Mm³. The forecasted consumption for the years 2033, 2043 and 2053 are 6.3 Mm³, 8.4 Mm³ and 11.3 Mm³/year

respectively. A significant increase in future water consumption, with the impacts of climate change, can cause an increase in water scarcity in the Iishana system, which represents a great challenge for climate adaptation. The increase in water demand can have significant consequences across various domains. This includes pressure on existing water resources, competition among different sectors and users, environmental degradation, depletion of groundwater, impacts on agriculture, and economic costs. In summary, the growth in water needs can trigger complex challenges that demand careful and sustainable water resource management to mitigate its adverse effects.

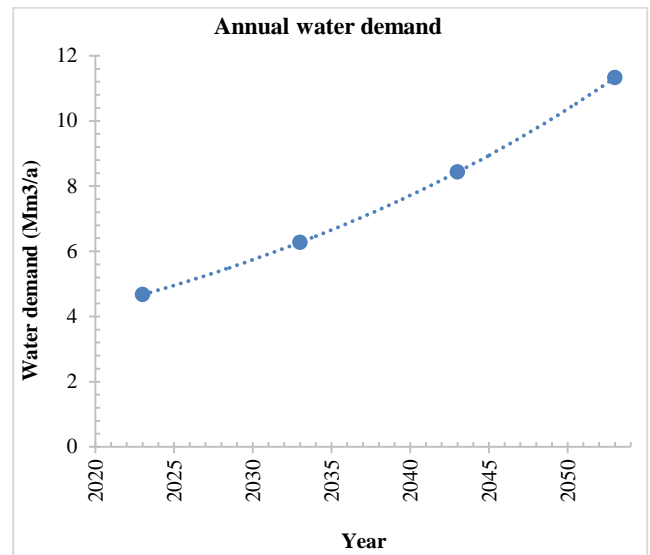


Figure 5. Projection of annual water demand

CONCLUSION AND RECOMMENDATION

The rural population of the Iishana system faces challenges related to climate change, In the last 31 years there have been records of rainfall throughout the Iishana system, but high temperatures accelerate the evaporation of water. Due to the topographical conditions, the waters are drained by gravity to the south of the basin, (Republic of Namibia), causing a greater shortage in the dry season on the Angolan side. With the population increasing, water scarcity is a significant concern in that region, to mitigate this impact and ensure a conscientious use of this valuable resource. It is recommended to reuse rainwater, retain water from the Iishna, and build water points to ensure access to drinking water (boreholes for the population and chimpaca for the animals) and reduce vulnerability to climate change.

DECLARATIONS

Corresponding author

Correspondence and requests for materials should be addressed to Mr. André Mandele Chiweyengue[✉]; E-mail: andrechiweyengue9@gmail.com; ORCID: <https://orcid.org/0009-0001-0140-7828>

Data availability

The datasets used and/or analyzed during the current study are available from the corresponding author upon reasonable request.

Acknowledgements

The authors would like to express their gratitude to SASSCAL 2.0 for its financial support. Appreciation is also extended to ISPTundavala and the University of Namibia for fostering an environment conducive to conducting this research.

Authors' contribution

First Author analysed the data obtained and wrote the manuscript. The second downloaded the climate data, the third and fourth Authors supervised, revised and approved the manuscript.

Competing interests

The authors declare no competing interests in this research and publication.

REFERENCES

- Amaral, A. M. (2000). Consumo total e residencial de água tratada: aplicação de um modelo de séries temporais em Piracicaba. São Paulo: Universidade de São Paulo; <https://doi.org/10.11606/T.11.2000.tde-20210104-170456>
- Bondarenko M., K. D. (2020). Census/projection-disaggregated gridded population datasets for 51 countries across sub-Saharan Africa in 2020 using building footprints. (U. o. Southampton, Editor). doi: <https://doi.org/10.5258/SOTON/WP00682>
- CSIR. (2000). Human settlement planning and design (Vol. II). Pretoria, South Africa: CSIR Building and Construction Technology. Available at: https://www.dhs.gov.za/sites/default/files/documents/publications/HS_Volume_1_A.pdf
- EEA. (1999). European Environmental Agency. Obtido em 20 de June de 2023, de European Environmental Agency. Available at: <https://www.eea.europa.eu/help/glossary/eea-glossary/water-demand>
- Helge Denker, J. M. (2014). Inundações e secas na Bacia do Cuvelai. Windhoek: United States Agency- Internacional Development. Available at: <https://docslib.org/doc/10291596/inunda%C3%A7%C3%B5es-e-secas-na-bacia-do-cuvelai-e-por-angola>
- Hersbach, H. B.-N. (2023). ERA5 monthly averaged data on single levels from 1940 to the present. Copernicus Climate Change Service (C3S) Climate Data Store (CDS). doi: 10.24381/CDs.f17050d7
- INE. (2016). Resultados definitivos do recenseamento geral da população e da habitação de angola 2014. Luanda, Angola: Instituto Nacional de Estatística. Available at: <https://searchworks.stanford.edu/view/11849589>
- Mendelsohn, J., & Weber, B. (2011). The Cuvelai Basin is water and people in Angola. Luanda: Development Workshop. Obtido em 15 de March de 2023. Available at: <https://docslib.org/doc/6806596/3-povos-e-%C3%A1guas-da-bacia-do-cuvelai-em-angola-e-nam%C3%ADbia-the-cuvelai>
- MINEA, M. D. (2024). Plano Director de Abastecimento de Água Ao Lubango. Workshop 2 (p. 3). Lubango
- Netto, A. &. (1991). Manual de Hidraulica (Vol. II). Sao Paulo:Eddar Blucher. Available at: https://www.academia.edu/35826793/Manual_de_hidraulica_azevedo_netto
- Seckler, D. (2000). Water Supply and Demand, 1995 to 2025. London: State University. Available at: https://www.researchgate.net/publication/264889618_Water_Supply_and_Demand_1995_to_2025
- Yassuda, E., Paulo Nogami, B. P., Martins, A., & Oliveira, W. D. (1978). Técnica de Abastecimento e Tratamento de Água (2 ed.). Sao Paulo: Cetesb. Available at: <https://repositorio.utfpr.edu.br/jspui/bitstream/1/31846/1/metodostecnicastratamento.pdf>

Publisher's note: [Scienceline Publication](#) Ltd. remains neutral with regard to jurisdictional claims in published maps and institutional affiliations.



Open Access: This article is licensed under a Creative Commons Attribution 4.0 International License, which permits use, sharing, adaptation, distribution and reproduction in any medium or format, as long as you give appropriate credit to the original author(s) and the source, provide a link to the Creative Commons licence, and indicate if changes were made. The images or other third party material in this article are included in the article's Creative Commons licence, unless indicated otherwise in a credit line to the material. If material is not included in the article's Creative Commons licence and your intended use is not permitted by statutory regulation or exceeds the permitted use, you will need to obtain permission directly from the copyright holder. To view a copy of this licence, visit <https://creativecommons.org/licenses/by/4.0/>.

© The Author(s) 2024

Instructions for Authors

 **SUBMIT AN ARTICLE**

Manuscript as Original Research Paper, Short Communication, Case Reports and Review are invited for rapid peer-review publishing in the Journal of Civil Engineering and Urbanism (ISSN 2252-0430)...[view full aims and scope](#)

[JCEU EndNote Style](#)

[Manuscript Template \(MS Word\)](#)

[Sample Articles](#)

[Declaration form](#)

[Policies and Publication Ethics](#)

Submission

The manuscript and other correspondence should be **submit online**. Please embed all figures and tables in the manuscript to become one single file for submission. Once submission is complete, the system will generate a manuscript ID and password sent to author's contact emails: editor@ojceu.com or editor.ojceu@gmail.com. All manuscripts must be checked (by English native speaker) and submitted in English for evaluation in totally confidential and impartial way.

Supplementary information

The online submission form allows supplementary information to be submitted together with the main manuscript file and covering letter. If you have more than one supplementary files, you can submit the extra ones by email after the initial [submission](#). Author guidelines are specific for each journal. Our Word template can assist you by modifying your page layout, text formatting, headings, title page, image placement, and citations/references such that they agree with the guidelines of journal. If you believe your article is fully edited per journal style, please use our [MS Word template](#) before submission.

Supplementary materials may include figures, tables, methods, videos, and other materials. They are available online linked to the original published article. Supplementary tables and figures should be labeled with a "S", e.g. "Table S1" and "Figure S1". The maximum file size for supplementary materials is 10MB each. Please keep the files as small possible to avoid the frustrations experienced by readers with downloading large files.

Submission to the Journal is on the understanding that

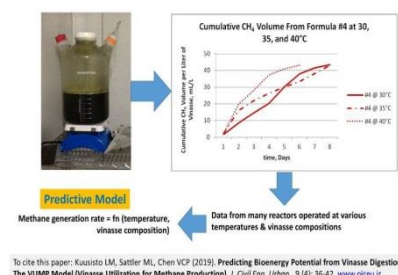
- 1.The article has not been previously published in any other form and is not under consideration for publication elsewhere;
- 2.All authors have approved the submission and have obtained permission for publish work.
- 3.If the approval of an ethics committee is required, please provide the name of the committee and the approval number obtained.

Graphical Abstract

Authors should provide a graphical abstract (a beautifully designed feature figure) to represent the paper aiming to catch the attention and interest of readers. Graphical abstract will be published online in the table of content. The graphical abstract should be colored, and kept within an area of 12 cm (width) x 6 cm (height) or with similar format. Image should have a minimum resolution of 300 dpi and line art 1200dpi.

Note: Height of the image should be no more than the width. Please avoid putting too much information into the graphical abstract as it occupies only a small space.

Authors can provide the graphical abstract in the format of PDF, Word, PowerPoint, jpg, or png, after a manuscript is accepted for publication. See more sample graphical abstracts in [archive](#).



Presentation of the article

Main Format

First page of the manuscripts must be properly identified by the title and the name(s) of the author(s). It should be typed in Times New Roman (font sizes: 17pt in capitalization for the title, 10pt for the section headings in the body of the text and the main text, double spaced, in A4 format with 2cm margins (both doc./docx formats). All pages and lines of the main text should be numbered consecutively throughout the manuscript. Abbreviations in the article title are not allowed. Manuscripts should be arranged in the following order:

1. **TITLE** (brief, attractive and targeted);
2. **Name(s) and Affiliation(s) of author(s)** (including post code and corresponding Email);
3. **ABSTRACT**;
4. **Key words** (separate by semicolons; or comma,);
5. **Abbreviations** (those used throughout the manuscript);
6. **INTRODUCTION** (clear statement of the problem, the relevant literature on the subject, and the proposed approach or solution);
7. **METHODOLOGY** (should be complete enough to allow experiments to be reproduced);
8. **RESULTS**;
9. **DISCUSSION**;
10. **CONCLUSION**;
11. **DECLARATIONS** (Acknowledgements, Consent to publish, Competing interests, Authors' contributions, and Availability of data etc.)
12. **REFERENCES**;
13. **Tables**;
14. **Figures**;
15. **Graphs**

Results and Discussion can be presented jointly.

Discussion and Conclusion can be presented jointly.

Article Sections Format

Title should be a brief phrase describing the contents of the paper. The first letter of each word in title should use upper case. The Title Page should include the author(s)'s full names and affiliations, the name of the corresponding author along with phone and e-mail information. Present address (es) of author(s) should appear as a footnote.

Abstract should be informative and completely self-explanatory, briefly present the topic, state the scope of the experiments, indicate significant data, and point out major findings and conclusions. The abstract should be 150 to 300 words in length. Complete sentences, active verbs, and the third person should be used, and the abstract should be written in the past tense. Standard nomenclature should be used and abbreviations should be avoided. No literature should be cited.

Following the abstract, about 3 to 8 **key words** that will provide indexing references should be listed.

Introduction should provide a clear statement of the problem, the relevant literature on the subject, and the proposed approach or solution. It should be understandable to colleagues from a broad range of scientific disciplines.

Methodology should be complete enough to allow experiments to be reproduced. However, only truly new procedures should be described in detail; previously published procedures should be cited, and important modifications of published procedures should be mentioned briefly. Capitalize trade names and include the manufacturer's name and address. Subheadings should be used. Methods in general use need not be described in detail.

Results should be presented with clarity and precision. The results should be written in the past tense when describing findings in the author(s)'s experiments. Previously published findings should be written in the present tense. Results should be explained, but largely without referring to the literature.

Discussion should interpret the findings in view of the results obtained in this and in past studies on this topic. State the conclusions in a few sentences at the end of the paper. The Results and Discussion sections can include subheadings, and when appropriate, both sections can be combined.

Conclusion should be brief and tight about the importance of the work or suggest the potential applications and extensions. This section should not be similar to the Abstract content.

Declarations including Acknowledgements, Authors' contributions, Competing interests, Consent to publish, and Availability of data etc.

Tables should be kept to a minimum and be designed to be as simple as possible. Tables are to be typed double-spaced throughout, including headings and footnotes. Each table should be on a separate page, numbered consecutively in Arabic numerals and supplied with a heading and a legend. Tables should be self-explanatory without reference to the text. The details of the methods used in the experiments should preferably be described in the legend instead of in the text. The same data should not be presented in both table and graph forms or repeated in the text.

Figure legends should be typed in numerical order on a separate sheet. Graphics should be prepared using applications capable of generating high resolution GIF, TIFF, JPEG or PowerPoint before pasting in the Microsoft Word manuscript file. Use Arabic numerals to designate figures and upper case letters for their parts (Figure 1). Begin each legend with a title and include sufficient description so that the figure is understandable without reading the text of the manuscript. Information given in legends should not be repeated in the text.

Declarations

Please ensure that the sections: Ethics (and consent to participate, if any), Acknowledgements, Authors' contributions, Competing interests, Consent to publish, Availability of data and materials are included at the end of your manuscript in a Declarations section.

Acknowledgements

We encourage authors to include an Acknowledgements section. Please acknowledge anyone who contributed towards the study by making substantial contributions to conception, design, acquisition of data, or analysis and interpretation of data, or who was involved in drafting the manuscript or revising it critically for important intellectual content, but who does not meet the criteria for authorship. Please also include their source(s) of funding. Please also acknowledge anyone who contributed materials essential for the study. Authors should obtain permission to acknowledge from all those mentioned in the Acknowledgements. Please list the source(s) of funding for the study, for each author, and for the manuscript preparation in the acknowledgements section. Authors must describe the role of the funding body, if any, in study design; in the collection, analysis, and interpretation of data; in the writing of the manuscript; and in the decision to submit the manuscript for publication.

Authors' Contributions

For manuscripts with more than one author, JCEU require an Authors' Contributions section to be placed after the Acknowledgementst section.

An 'author' is generally considered to be someone who has made substantive intellectual contributions to a published study. To qualify as an author one should 1) have made substantial contributions to conception and design, or acquisition of data, or analysis and interpretation of data; 2) have been involved in drafting the manuscript or revising it critically for important intellectual content; and 3) have given final approval of the version to be published. Each author should have participated sufficiently in the work to take public responsibility for appropriate portions of the content. Acquisition of funding, collection of data, or general supervision of the research group, alone, does not justify authorship.

We suggest the following format/example (please use initials to refer to each author's contribution): AB carried out the case studies, participated in the designing and drafted the manuscript. JY carried out the architectural drawing. MT participated in the design of the study and performed the statistical analysis. FG conceived of the study, and participated in its design and coordination and helped to draft the manuscript. All authors read and approved the final manuscript. For authors that equally participated in a study please write '**All/Both authors contributed equally to this work.**' Contributors who do not meet the criteria for authorship should be listed in an acknowledgements section.

Competing Interests

Competing interests that might interfere with the objective presentation of the research findings contained in the manuscript should be declared in a paragraph heading "Competing interests" (after Acknowledgment or Authors' Contributions sections). Examples of competing interests are ownership of stock in a company, commercial grants, board membership, etc. If there is no competing interest, please use the statement "**The authors declare that they have no competing interests.**".

Consent to Publish

Please include a 'Consent for publication' section in your manuscript. If your manuscript contains any individual person's data in any form (including individual details, images or videos), consent to publish must be obtained from that person, or in the case of

children, their parent or legal guardian. All presentations of case reports must have consent to publish. You can use your institutional consent form or our consent form if you prefer. You should not send the form to us on submission, but we may request to see a copy at any stage (including after publication). If your manuscript does not contain any individual persons data, please state "Not applicable" in this section.

Change in authorship

We do not allow any change in authorship after provisional acceptance. We cannot allow any addition, deletion or change in sequence of author name. We have this policy to prevent the fraud.

Data Deposition

In computational studies where the information is unacceptable for inclusion in databases because of lack of experimental validation, the information can be published as an additional file with the article.

REFERENCES

The JCEU accept the manuscripts in PDF, Word or TeX/LaTeX formats; Word files are preferred especially those are prepared using [EndNote®](#). However, our team will reformat the articles of non-EndNote users via EndNote in the galley proof stage, if accepted.

A JCEU reference style for [EndNote](#) may be found [here](#).

How to install additional styles? Please [click here](#)

How to turn on "Jumping" from a citation to the bibliography? Please [click here](#)

1. All references to publications made in the text should be presented in a list with their full bibliographical description.
2. In the text, a reference identified by means of an author's name should be followed by the date of the reference in parentheses. When there are more than two authors, only the first author's surname should be mentioned, followed by 'et al'. In the event that an author cited has had two or more works published during the same year, the reference, both in the text and in the reference list, should be identified by a lower case letter like 'a' and 'b' after the date to distinguish the works.
3. References in the text should be arranged chronologically (e.g. Kelebeni, 1983; Usman and Smith, 1992 and Agindotan et al., 2003). The list of references should be arranged alphabetically on author's surnames, and chronologically per author. If an author's name in the list is also mentioned with co-authors, the following order should be used: Publications of the single author, arranged according to publication dates - publications of the same author with one co-author - publications of the author with more than one co-author. Publications by the same author(s) in the same year should be listed as 1992a, 1992b, etc.
4. Names of authors and title of journals, published in non-latin alphabets should be transliterated in English.
5. A sample of standard reference is "1th Author surname A, 2th Author surname B , 3th Author surname C. (2020). Article title should be regular and 10 pt. Journal of Civil Engineering and Urbanism or J. Civil Eng. Urban., Volume(Issue): 00-00." "DOI: <https://dx.doi.org/10.00000/xxxx>"; "Google Scholar (<https://scholar.google.com>)"
6. Journal titles should be full in references. The titles should not be italic.
7. References with more than 10 authors should list the first 10 authors followed by 'et al.'
8. The color of [references in the text](#) of article is blue. Example: ([Preziosi et al., 2002](#); [Mills et al., 2015](#)).
- 9.

-Examples (at the text):

Abayomi (2000), Agindotan et al. (2003), (Kelebeni, 1983), (Usman and Smith, 1992), (Chege, 1998; Chukwura, 1987a,b; Tijani, 1993,1995), (Kumasi et al., 2001).

--Examples (at References section):

a) For journal:

Kuusisto LM, Sattler ML, and Chen VCP (2019). Predicting Bioenergy Potential from Vinasse Digestion: The VUMP Model (Vinasse Utilization for Methane Production). J. Civil Eng. Urban., 9 (4): 36-42. DOI: <https://dx.doi.org/10.29252/scil.2019.jceu> ; [Google Scholar](#)

Tangpagasit, J., Cheerarot, R., Jaturapitakkul, C., Kiattikomol, K. (2005). Packing Effect and Pozzolanic Reaction of Fly Ash in Mortar. Cement Concrete Research, 35: 1145– 1151. DOI: <https://doi.org/10.1016/j.cemconres.2004.09.030> ; [Google Scholar](#)

Mobasser Sh and Firoozi AA (2016). Review of nanotechnology Applications in Science and Engineering. Journal of Civil Engineering and Urbanism, 6 (4): 84-93. PII: [S225204301600011-6](#) ; [Google Scholar](#)

Najafzadeh M and Zahiri A. (2015). Neuro-fuzzy GMDH-based evolutionary algorithms to predict flow discharge in straight compound channels. Journal of Hydrologic Engineering. 20(12):04015035. DOI: [https://doi.org/10.1061/\(ASCE\)HE.1943-558.001185](https://doi.org/10.1061/(ASCE)HE.1943-558.001185) ; [Google Scholar](#)

Hernández-Cruz A, Barajas-Fernández J, Soto-Cortés G, and Rivera-Trejo F (2017). Hydraulic Analysis of an Arrangement of Groynes on a Diversion Channel. Journal of Civil Engineering and Urbanism, 7 (2): 25-29. [Article link](#)

b) For symposia reports and abstracts, special issues, conferences etc.

Hall P (1993). Toward Sustainable; Liveable and Innovative Cities for 21st Century, In Proceeding of the Third Conference of the World Capitals, Tokyo, pp. 22-28. [Google Scholar](#)

Memon NA, Unar MA, Mastorakis NE, and Khaskheli GB. (2009). Total dissolved solids (TDS) modeling by artificial neural networks in the distribution system of drinking water of Hyderabad city. cardiovascular diseases. 6: 11. [Google Scholar](#) ; [Article link](#)

c) For books:

Moghtader R (1993). 100 Years of Modernism in Iran's Architecture and Urbanism. Iran-nameh. 42: 270-259.

Garber NJ and Hoel LA (2010). Traffic and Highway Engineering" 4th Edition, Cengage Learning. [Google Scholar](#)

In referring to a personal communication the two words are followed by the year, e.g. (Brown, J. M., personal communication, 1982). In this case initials are given in the text. Papers that have not been published should be cited as "unpublished". Papers that

have been accepted for publication, but not yet specified for an issue should be cited as "to be published". Papers that have been submitted for publication should be cited as "submitted for publication".

Nomenclature and Abbreviations:

Standard abbreviations are preferable. If a new abbreviation is used, it should be defined at its first usage. Abbreviations should be presented in one paragraph, in the format: "term: definition". Please separate the items by ";".
E.g. ANN: artificial neural network; CFS: closed form solution; ...

Abbreviations of units should conform with those shown below:


Decilitre	dl	Kilogram	kg
Milligram	mg	hours	h
Micrometer	mm	Minutes	min
Percent	%		

Formulae, numbers and symbols:

1. Typewritten formulae are preferred. Subscripts and superscripts are important. Check disparities between zero (0) and the letter O, and between one (1) and the letter I.
2. Describe all symbols immediately after the equation in which they are first used.
3. For simple fractions, use the solidus (/), e.g. 10 /38.
4. Equations should be presented into parentheses on the right-hand side, in tandem.
5. Levels of statistical significance which can be used without further explanations are *P < 0.05, **P < 0.01, and ***P < 0.001
6. In the English articles, a decimal point should be used instead of a decimal comma.
7. In chemical formulae, valence of ions should be given, e.g. Ca²⁺ and CO₃²⁻, not as Ca⁺⁺ or CO₃.
8. Numbers up to 10 should be written in the text by words. Numbers above 1000 are recommended to be given as 10 powered x.
9. Greek letters should be explained in the margins with their names as follows: Αα - alpha, Ββ - beta, Γγ - gamma, Δδ - delta, Εε - epsilon, Ζζ - zeta, Ηη - eta, Θθ - theta, Ιι - iota, Κκ - kappa, Λλ - lambda, Μμ - mu, Νν - nu, Ξξ - xi, Οο - omicron, Ππ - pi, Ρρ - rho, Σσ - sigma, Ττ - tau, Υυ - ipsilon, Φφ - phi, Χχ - chi, Ψψ - psi, Ωω - omega.

Review/Decisions/Processing

Firstly, all manuscripts will be checked by one of the plagiarism finding tools ([iThenticate](#), [PlagScan](#) and or [Docol@c](#)). A double-blind reviewing model is used by JCEU for non-plagiarized papers. The manuscript is edited and reviewed by the English language editor and three reviewers selected by section editor of JCEU respectively. Also, a reviewer result form is filled by reviewer to guide authors. Possible decisions are: accept as is, minor revision, major revision, or reject. The estimated time from submission to first decision is 4.4 weeks and the estimated time from submission to final decision is 5.6 weeks. The estimated time for final publication of accepted manuscript is 6 weeks

To submit a revision please click [here](#), fill out the form, and mark  "Revised" attach the revision (MSword) and submit when completed.

After review and editing the article, a final formatted proof is sent to the corresponding author once again to apply all suggested corrections during the article process. The editor who received the final revisions from the corresponding authors shall not be hold responsible for any mistakes shown in the final publication. Manuscripts with significant results are typically reviewed and published at the highest priority.

Plagiarism

There is a zero-tolerance policy towards plagiarism (including self-plagiarism) in our journals. Manuscripts are screened for plagiarism by one of the plagiarism finding tools ([iThenticate](#), [PlagScan](#) and or [Docol@c](#)), before or during publication, and if found they will be rejected at any stage of processing. See sample of [Docol@c-Report](#).

Declaration

After manuscript accepted for publication, a [declaration form](#) will be sent to the corresponding author who that is responsible to coauthors' agreements to publication of submitted work in JCEU after any amendments arising from the peer review.

Date of issue

The journal will be issued on 25th of March, June, September and December, each year.

Publication charges

No peer-reviewing charges are required. However, the publication costs are covered through article processing charges (APCs). There is a modest APC of 100 Euro(€) editor fee for the processing of each primary accepted paper (1000-4000 words) to encourage high-quality submissions. APCs are only charged for articles that pass the pre-publication checks and are published. A surcharge will be placed on any article that is over 4000 words in length to cover the considerable additional processing costs. Payment can be made by credit card, bank transfer, money order or check. Instruction for payment is sent during publication process as soon as manuscript is accepted. Meanwhile, this journal encourages the academic institutions in low-income countries to publish high quality scientific results, free of charges.

WORD COUNT	PRICE*
1000-4000 words	€100
over 4000 words	€120

* The prices are valid until 30th June 2024.

The Waiver policy

The publication fee will be waived for invited authors, authors of hot papers, and corresponding authors who are editorial board members of the *Journal of Civil Engineering and Urbanism*. The Journal will consider requests to waive the fee for cases of financial hardship (for high quality manuscripts and upon acceptance for publication). Requests for waiver of the submission fee must be submitted via individual cover letter by the corresponding author and cosigned by an appropriate institutional official to verify that no institutional or grant funds are available for the payment of the fee. Letters including the manuscript title and manuscript ID number should be sent to: editor@ojceu.com. It is expected that waiver requests will be processed and authors will be notified within two business day.

The OA policy

Journal of World[®] Poultry Research is an open access journal which means that all content is freely available without charge to the user or his/her institution. Users are allowed to read, download, copy, distribute, print, search, or link to the full texts of the articles, or use them for any other lawful purpose, without asking prior permission from the publisher or the author. This is in accordance with the [BOAI definition of Open Access](#).

Scienceline Language Editing Services

We suggest that authors whose first language is not English have their manuscripts checked by a native English speaker before submission. This is optional, but will help to ensure that any submissions that reach peer review can be judged exclusively on academic merit. We offer a Scienceline service, and suggest that authors contact as appropriate. Please note that use of language editing services is voluntary, and at the author's own expense. Use of these services does not guarantee that the manuscript will be accepted for publication, nor does it restrict the author to submitting to Scienceline journals. You can send the article/s to the following Email: info@science-line.com

For more information about editing services please visit [here](#).

Submission Preparation Checklist

Authors are required to check off their submission's compliance with all of the following items, and submissions may be returned to authors that do not adhere to the following guidelines.

The submission has not been previously published, nor is it before another journal for consideration (or an explanation has been provided in Comments to the Editor).

The submission file is in Microsoft Word, RTF, or PDF document file format.

Where available, URLs for the references have been provided.

The text is single-spaced; uses a 12-point font; and all illustrations, figures, and tables are placed within the text at the appropriate points, rather than at the end.

The text adheres to the stylistic and bibliographic requirements outlined in the Author Guidelines.

Paper Submission Flow





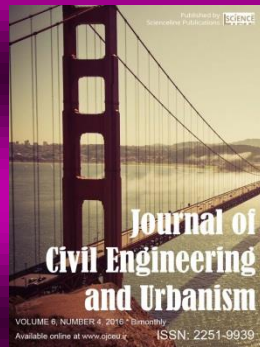
Scienceline Publication Ltd is a limited liability non-profit non-stock corporation incorporated in Turkey (Company No. 0757086921600001). Scienceline journals that concurrently belong to many societies, universities and research institutes, publishes internationally peer-reviewed open access articles and believe in sharing of new scientific knowledge and vital research in the fields of life and natural sciences, animal sciences, engineering, art, linguistic, management, social and economic sciences all over the world. Scienceline journals include:

Online Journal of Animal and Feed Research



ISSN 2228-7701; Bi-monthly
[View Journal](#) | [Editorial Board](#)
 Email: editors@ojaf.r.ir
[Submit Online >>](#)

Journal of Civil Engineering and Urbanism



ISSN 2252-0430; Bi-monthly
[View Journal](#) | [Editorial Board](#)
 Email: ojceu@ojceu.ir
[Submit Online >>](#)

Journal of Life Sciences and Biomedicine



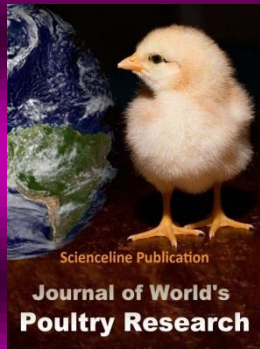
ISSN: 2251-9939; Bi-monthly
[View Journal](#) | [Editorial Board](#)
 Email: editors@jlsb.science-line.com
[Submit Online >>](#)

World's Veterinary Journal



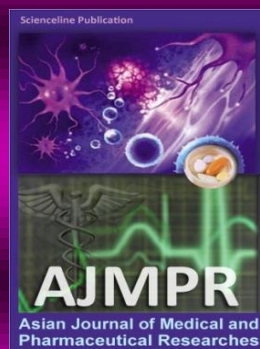
ISSN: 2322-4568; Quarterly
[View Journal](#) | [Editorial Board](#)
 Email: editor@wj.science-line.com
[Submit Online >>](#)

Journal of World's Poultry Research



ISSN: 2322-455X; Quarterly
[View Journal](#) | [Editorial Board](#)
 Email: editor@jwpr.science-line.com
[Submit Online >>](#)

Asian Journal of Medical and Pharmaceutical Researches



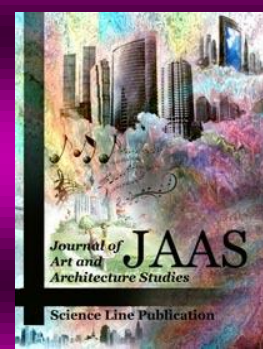
ISSN: 2322-4789; Quarterly
[View Journal](#) | [Editorial Board](#)
 Email: editor@ajmpr.science-line.com
[Submit Online >>](#)

Journal of Educational and Management Studies



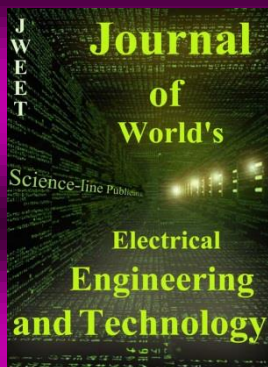
ISSN: 2322-4770; Quarterly
[View Journal](#) | [Editorial Board](#)
 Email: info@jems.science-line.com
[Submit Online >>](#)

Journal of Art and Architecture Studies



ISSN: 2383-1553; Biannually
[View Journal](#) | [Editorial Board](#)
 Email: jaas@science-line.com
[Submit Online >>](#)

Journal of World's Electrical Engineering and Technology



ISSN: 2322-5114; Irregular
[View Journal](#) | [Editorial Board](#)
 Email: editor@jweet.science-line.com
[Submit Online >>](#)

Asian Journal of Social and Economic Sciences



ISSN: 2383-0948; Quarterly
[View Journal](#) | [Editorial Board](#)
 Email: ajses@science-line.com
[Submit Online >>](#)

Journal of Applied Business and Finance Researches



ISSN: 2382-9907; Quarterly
[View Journal](#) | [Editorial Board](#)
 Email: jabfr@science-line.com
[Submit Online >>](#)

Scientific Journal of Mechanical and Industrial Engineering



ISSN: 2383-0980; Quarterly
[View Journal](#) | [Editorial Board](#)
 Email: sjmie@science-line.com
[Submit Online >>](#)

[ABOUT](#)
[AIMS AND SCOPE](#)
[LEADERSHIP TEAM](#)
[POLICIES AND PUBLICATION ETHICS](#)
[TERMS AND CONDITIONS](#)
[CONTACT US](#)

Scienceline is a non-profit organisation inspired by research funders and led by scholars. Our mission is to help researchers accelerate discovery and innovation by operating a platform for research communication that encourages and recognises the most responsible behaviours in science.

Scienceline Publications, Ltd is a limited liability non-profit non-stock corporation registered in the State of Erzurum, Turkey, with company number 0757086921600001, and branch number 18677/25379 at the address: [Scienceline Publications, Ltd.](#), Ömer Nasuhi Bilmen Road, Dönmez Apart., G/1/6, Yakutiye, Erzurum 25100, Turkey